Vicenç Méndez
Sergei Fedotov
Werner Horsthemke

Reaction-Transport Systems

Mesoscopic Foundations, Fronts, and Spatial Instabilities

Springer Complexity

Springer Complexity is an interdisciplinary program publishing the best research and academic-level teaching on both fundamental and applied aspects of complex systems – cutting across all traditional disciplines of the natural and life sciences, engineering, economics, medicine, neuroscience, social and computer science.

Complex Systems are systems that comprise many interacting parts with the ability to generate a new quality of macroscopic collective behavior the manifestations of which are the spontaneous formation of distinctive temporal, spatial or functional structures. Models of such systems can be successfully mapped onto quite diverse "real-life" situations like the climate, the coherent emission of light from lasers, chemical reaction-diffusion systems, biological cellular networks, the dynamics of stock markets and of the internet, earthquake statistics and prediction, freeway traffic, the human brain, or the formation of opinions in social systems, to name just some of the popular applications.

Although their scope and methodologies overlap somewhat, one can distinguish the following main concepts and tools: self-organization, nonlinear dynamics, synergetics, turbulence, dynamical systems, catastrophes, instabilities, stochastic processes, chaos, graphs and networks, cellular automata, adaptive systems, genetic algorithms and computational intelligence.

The two major book publication platforms of the Springer Complexity program are the monograph series "Understanding Complex Systems" focusing on the various applications of complexity, and the "Springer Series in Synergetics", which is devoted to the quantitative theoretical and methodological foundations. In addition to the books in these two core series, the program also incorporates individual titles ranging from textbooks to major reference works.

Springer Series in Synergetics

Founding Editor: H. Haken

The Springer Series in Synergetics was founded by Herman Haken in 1977. Since then, the series has evolved into a substantial reference library for the quantitative, theoretical and methodological foundations of the science of complex systems.

Through many enduring classic texts, such as Haken's *Synergetics and Information and Self-Organization*, Gardiner's *Handbook of Stochastic Methods*, Risken's *The Fokker Planck-Equation* or Haake's *Quantum Signatures of Chaos*, the series has made, and continues to make, important contributions to shaping the foundations of the field.

The series publishes monographs and graduate-level textbooks of broad and general interest, with a pronounced emphasis on the physico-mathematical approach.

Vicenç Méndez · Sergei Fedotov ·
Werner Horsthemke

Reaction–Transport Systems

Mesoscopic Foundations, Fronts,
and Spatial Instabilities

Vicenç Méndez
Universitat Autònoma de
Barcelona
Dept. de Física
Grup de Física Estadística
08193 Bellaterra Edifici Cc
Spain
vicenc.mendez@uab.cat

Sergei Fedotov
University of Manchester
School of Mathematics
Oxford Road
Manchester
United Kingdom M13 9PL
sergei.fedotov@manchester.ac.uk

Werner Horsthemke
Department of Chemistry
Southern Methodist University
Dallas TX 75275-0314
USA
whorsthe@mail.smu.edu

To Montse, Masha, and Brenda

Preface

The dynamics of reactive mixtures result from local transformation processes, chemical reactions, and transport in space, diffusion. These processes are typically modeled by a standard reaction–diffusion equation

$$\frac{\partial \boldsymbol{\rho}}{\partial t} = \mathsf{D}\frac{\partial^2 \boldsymbol{\rho}}{\partial x^2} + \mathbf{F}(\boldsymbol{\rho}),$$

where $\boldsymbol{\rho}$ is a vector of concentrations of the diffusing species, D is the diffusion matrix, and $\mathbf{F}$ is a kinetic term describing reactions or interactions between the species. Reaction–diffusion models are not limited to the field of chemistry and chemical engineering. They can describe the dynamics of nonchemical systems, and reaction–diffusion equations provide a general theoretical framework for the study of phenomena in areas such as biology, ecology, physics, and materials science.

Standard reaction–diffusion systems have been studied extensively over the last half century, and they provide a good description of the dynamics in many applications. There exist, however, a variety of situations where the standard reaction–diffusion equation fails to be an adequate model. Actual physical, chemical, biological, and ecological systems often show significant deviations from the assumptions of simple diffusive transport and spatial homogeneity inherent in the standard reaction–diffusion equation. In this monograph, we address the question how deviations from standard diffusive transport or deviations from spatial homogeneity affect the dynamics of reaction–transport systems. This represents a large area, and we selected those topics that reflect our interests.

Front propagation and Turing instabilities are two emblematic phenomena displayed by nonlinear reaction–diffusion systems. In the former, a stable state invades an unstable or less stable state. In the latter, diffusion couples with the local nonlinear transformations and drives the uniform steady state of the system unstable. We focus on the effect of deviations from standard diffusion and spatial homogeneity of the medium on these two signature phenomena.

The book is organized in three parts. Part I lays the foundation. Chapter 1 provides an introduction to rate equations and their stability analysis. It also presents several important chemical and biological models. In Chap. 2 we discuss the

standard reaction–diffusion equation and introduce two deviations from normal diffusion, namely transport with inertia and anomalous diffusion. We present a phenomenological approach of standard diffusion, transport with inertia, and anomalous diffusion. This chapter also contains a first mesoscopic description of the transport in terms of random walk models. We strongly recommend such a mesoscopic approach to ensure that the reaction–transport equations studied are physically and mathematically sound. We present a comprehensive review of the mesoscopic foundations of reaction–transport equations in Chap. 3, which is at the heart of Part I.

Part II focuses on front propagation. Chapter 4 provides an overview of front propagation in standard reaction–diffusion systems. We discuss pulled vs pushed fronts and provide tools to determine the front velocity for both cases. Chapter 5 deals with the effect of deviations from standard diffusion or Brownian motion on front propagation into unstable states. The effect of spatial heterogeneities on front propagation is studied in Chap. 6. Chapters 7 and 8 contain applications to ecology, namely human migrations, avian range expansions, and plant invasions, and biomedical systems, namely cancer invasion, virus dispersal, and propagation in spiny dendrites.

Part III focuses on spatial instabilities and patterns. We examine the simplest type of spatial pattern in standard reaction–diffusion systems in Chap. 9, namely patterns in a finite domain where the density vanishes at the boundaries. We discuss methods to determine the smallest domain size that supports a nontrivial steady state, known as the critical patch size in ecology. In Chap. 10, we provide first an overview of the Turing instability in standard reaction–diffusion systems. Then we explore how deviations from standard diffusion, namely transport with inertia and anomalous diffusion, affect the Turing instability. Chapter 11 deals with the effects of temporally or spatially varying diffusivities on the Turing instability in reaction–diffusion systems. We present applications of Turing systems to chemical reactions and biological systems in Chap. 12. Chapter 13 deals with spatial instabilities and patterns in spatially discrete systems, such as diffusively and photochemically coupled reactors.

This book can serve as a text for a special topics course for advanced undergraduate and beginning graduate students. With this purpose in mind, we have included a set of exercises at the end of each chapter. Instructors can obtain solutions by contacting the authors.

Barcelona, Spain	Vicenç Méndez
Manchester, UK	Sergei Fedotov
Dallas, TX	Werner Horsthemke
August 2009	

Contents

Acronyms

BZ	Belousov–Zhabotinsky
CDIMA	Chlorine dioxide–iodine–malonic acid
CFUR	Continuously fed unstirred reactor
CIMA	Chlorite–iodide–malonic acid
CLT	Central limit theorem
CMF	Campos–Méndez–Fort
CSTR	Continuous-flow stirred tank reactor
CTRW	Continuous-time random walk
DDRW	Direction-dependent reaction walk
DG	Delayed growth
DIRW	Direction-independent reaction walk
DTRW	Discrete-time random walk
FKPP	Fisher–Kolmogorov–Petrovskii–Piskunov
HJ	Hamilton–Jacobi
HRDE	Hyperbolic reaction–diffusion equation
IID	Independent identically distributed
IRW	Isotropic reaction walk
KISS	Kierstead–Slobodkin–Skellam
KPP	Kolmogorov–Petrovskii–Piskunov
LALI	Local auto-activation–lateral inhibition
LE	Lengyel–Epstein
LER	Lengyel–Epstein–Rabai
LVA	Local velocity analysis
MSA	Marginal stability analysis
MSD	Mean square displacement
OCN	Optimal channel network
ODE	Ordinary differential equation
PDF	Probability distribution function
PDFAA	Probability distribution function of adult ages
RD	Reaction–diffusion
RHS	Right-hand side

RRW	Reaction random walk
RT	Reaction-telegraph
SDE	Stochastic differential equation
SPA	Singular perturbation analysis
USS	Uniform steady state

Symbols

$\xrightarrow{\mathrm{d}}$	convergence in distribution
$\langle\ \rangle$	average
$\cup_{i=1}^{n}\mathcal{S}_i$	union of the sets $\mathcal{S}_i$
α	anomaly exponent of jump length PDF (CTRW)
$\boldsymbol{\alpha}_i$	eigenvector (structural mode) of Laplacian matrix
β_i	eigenvalue of Laplacian matrix
γ	speed (persistent random walk); anomaly exponent of waiting time PDF (CTRW)
$\delta(\cdot)$	Dirac delta-function
Δ	determinant of the Jacobian J
Δ_l	Hurwitz determinant
θ	ratio of diffusion coefficients
$\theta(\cdot)$	Heaviside function
λ	Poisson process transition rate
λ_i	eigenvalue of the Jacobian
$\mu(x)$	infinitesimal displacement of a diffusion process
$\nu(A)$	Lévy measure
$\xi_i(x, t, \tau)$	age distribution of particles i
$\rho, \boldsymbol{\rho}, \rho_i$	concentration or density
$\overline{\rho}$	stationary concentration
σ	measure of substrate concentration (Lengyel–Epstein model); scaling factor of stable density
σ^2	variance of jump length PDF
$\sigma^2(x)$	infinitesimal variance of a diffusion process
$\sigma(\mathsf{J})$	spectrum of J
ϕ	incident light intensity (photosensitive reaction)
$\phi(t)$	waiting time PDF
$\Phi(t)$	fundamental matrix
$\Phi_{ij}(t)$	conditional waiting time distribution
χ_A	indicator function of the set A
$\psi(k)$	characteristic exponent

$\psi(x, t)$	joint jump length and waiting time PDF of a CTRW
$\Psi(t)$	survival probability
$B(t)$	Brownian motion
c_i	coefficient of characteristic polynomial
D	diffusion coefficient
D	diffusion matrix
$D_\alpha, D_\gamma, D_{\alpha,\gamma}$	generalized diffusion coefficient
$\mathscr{D}_i$	effective diffusion coefficient (RRW)
$\mathcal{D}_t^p$	Riemann–Liouville fractional derivative
$\mathbb{E}$	expectation operator
$\mathcal{E}_\mathcal{G}$	set of edges of $\mathcal{G}$
$f(\rho)$	intrinsic reaction rate: $F(\rho) = f(\rho)\rho$
$f^+(\rho); f^-(\rho)$	intrinsic birth rate; intrinsic death rate: $f(\rho) = f^+(\rho) - f^-(\rho)$
$\tilde{f}(\boldsymbol{\rho}), \hat{f}(\boldsymbol{\rho})$	rate terms (photochemical reactions)
$F(\rho), \mathbf{F}(\boldsymbol{\rho}), F_i(\boldsymbol{\rho})$	rate term
$F_i^+; F_i^-$	production or birth term; loss or death term
$\mathcal{F}[g(x)], \tilde{g}(k)$	Fourier transform
$g_i(\boldsymbol{\rho})$	production or birth term
$g_\gamma(\tau)$	one-sided γ-stable PDF
$\mathcal{G}$	graph
h	stoichiometric factor (Oregonator)
H	Hurst exponent; Hamiltonian
$\mathsf{H} = (h_{ij})$	transition matrix
I_n	$n \times n$ identity matrix
$i(x, t)$	rate of departure of particles from the point x (CTRW)
$j(x, t)$	flow (persistent random walk); density of particles arriving at point x exactly at time t (CTRW)
J	flux
J	Jacobian matrix
$K(t)$	memory kernel
$l(s)$	Laplace exponent
L, L^*	infinitesimal generator
$\mathcal{L}[f(t)], \hat{f}(s)$	Laplace transform
L	Laplacian matrix
M	monodromy matrix
$N(t)$	counting process, renewal process, Poisson process
$\mathcal{N}_\mathcal{G}$	set of nodes of $\mathcal{G}$
$\mathbb{P}$	probability
p	momentum
$p(x, t)$	probability density function
$p(y, t|x)$	transition probability density
Q_t	transport operator

Q_{ij}	transition kernel
$S_{\alpha}(t)$	symmetric α-stable Lévy process; Lévy flight
$S_{\alpha,\gamma}(t)$	anomalous scaling limit of CTRW
$\mathbf{z}^T$	transpose of $\mathbf{z}$
T	trace of the Jacobian J
$\overline{T}$	mean waiting time
$T(t)$	random time; subordinator
$T_{\gamma}(t)$	γ-stable subordinator
T_t	transition operator
v	velocity
$w(z)$	jump length PDF; dispersal kernel
$w_{\alpha}(z)$	symmetric α-stable PDF; anomalous jump length PDF
$W(t)$	standard Wiener process
$W_i(x' \rightarrow x, \tau')$	transition rate
$X_n, X(t)$	random position of a particle
Z_i	random jump
$Z(t)$	jump process

Part I
General Concepts

Chapter 1
Reaction Kinetics

If spatial effects can be neglected, many systems in chemistry, biology, ecology, physics, and other areas can be described by rate equations, a set of ordinary differential equations. Systems may be homogeneous because the system is small enough and transport is efficient enough to eliminate spatial gradients. Or the spatial homogeneity may be imposed from the outside, for example by stirring in chemical reactors. In the following we collect some basic facts about rate equations and discuss various model schemes whose dynamics we investigate in later chapters.

1.1 Rate Equations

We consider systems consisting of individuals, e.g., microorganism or animals, or particles, e.g., molecules, of n different species. For simplicity, we generally use "particles" to refer to particles or individuals in the following. Also, we often use the language of chemical kinetics, but the concepts, tools, and results apply to any type of system whose temporal evolution can be modeled by rate equations. We assume that the system is large enough that a continuum, mean-field description is valid, i.e., that internal fluctuations due to the discrete nature of the constituents can be neglected. The evolution of the densities or concentrations is governed by kinetic equations

$$\frac{d\boldsymbol{\rho}}{dt} = \mathbf{F}(\boldsymbol{\rho}, \boldsymbol{\mu}), \tag{1.1}$$

where $\boldsymbol{\rho} \in \mathbb{R}^n$ and $\mathbf{F} : \mathbb{R}^n \to \mathbb{R}^n$. For systems of particles, the coefficients or parameters of the rate terms, $\boldsymbol{\mu}$, are real numbers. Evolution equations for systems of particles must possess certain properties to be acceptable descriptions. The densities ρ_i, $i = 1, \ldots, n$, cannot be negative. Therefore the kinetic equations must preserve positivity, i.e., $\rho_i(0) \geq 0$ at time $t = 0$ implies $\rho_i(t) \geq 0$ for all times $t > 0$. Equations (1.1) have this property if

$$F_i(\rho_1, \ldots, \rho_{i-1}, 0, \rho_{i+1}, \ldots, \rho_n) \geq 0. \tag{1.2}$$

It is sometimes convenient to split the rate function F_i into its positive and negative parts, i.e., write it in production–loss form:

$$F_i(\boldsymbol{\rho}) = F_i^+(\boldsymbol{\rho}) - F_i^-(\boldsymbol{\rho}), \tag{1.3}$$

where $F_i^+(\boldsymbol{\rho}) \geq 0$ and $F_i^-(\boldsymbol{\rho}) \geq 0$. The first term, F_i^+, is the production or birth term and captures the processes that increase the chemical concentration or population density. For simplicity of notation, we sometimes write

$$F_i^+(\boldsymbol{\rho}) = g_i(\boldsymbol{\rho}). \tag{1.4}$$

The second term, F_i^-, is the loss or death term and captures the processes that decrease the concentration or density. The rate of consumption, removal or death of particles of a given type must go to zero as the density of the particles goes to zero, $F_i^-(\boldsymbol{\rho}) \to 0$ as $\rho_i \to 0$. Otherwise, the concentration ρ_i of those particles can become negative. Introducing the per capita birth rate and loss rate, we write, where convenient,

$$F_i^+(\boldsymbol{\rho}) = f_i^+(\boldsymbol{\rho})\rho_i, \quad F_i^-(\boldsymbol{\rho}) = f_i^-(\boldsymbol{\rho})\rho_i. \tag{1.5}$$

1.2 Linear Stability Analysis

Studies of the dynamics of a system generally pay little attention to transient behavior and focus instead on the ultimate fate of the system, the asymptotic state it attains as time goes to infinity. These can be stationary states, time-dependent periodic states, or time-dependent aperiodic or chaotic states. Our interest here is the former, the stationary or steady states and their stability properties. Small fluctuations or perturbation are inevitable in any real system. If the system is in a steady state and then experiences a small perturbation, will it return to the steady state? In other words, is the state stable against small perturbations?

Let $\overline{\boldsymbol{\rho}}$ be a stationary state of (1.1):

$$\mathbf{F}(\overline{\boldsymbol{\rho}}) = 0. \tag{1.6}$$

The stationary state $\overline{\boldsymbol{\rho}}$ is stable if trajectories that start sufficiently close to it stay close to the steady state. This is more formally stated in the following definition.

Definition 1.1 The stationary state $\overline{\boldsymbol{\rho}}$ is Lyapunov stable if for any $\epsilon > 0$, there exists a $\delta > 0$ (depending on ϵ) such that for all initial conditions $\boldsymbol{\rho}(0) = \boldsymbol{\rho}_0$ with $\left|\boldsymbol{\rho}_0 - \overline{\boldsymbol{\rho}}\right| < \delta$ we have $|\boldsymbol{\rho}(t) - \overline{\boldsymbol{\rho}}| < \epsilon$ for all $t > 0$.

This does not quite answer the question we raised above. The definition states only that a stationary state is stable if the system does not wander too far away when starting close enough to the steady state. We require a stronger notion of stability,

namely that the system actually returns to the steady state after a sufficiently small perturbation. This is the content of the next definition.

Definition 1.2 The steady state $\overline{\rho}$ is asymptotically stable in the sense of Lyapunov, if there exists an η such that if $|\rho_0 - \overline{\rho}| < \eta$ then

$$\lim_{t \to \infty} |\rho(t) - \overline{\rho}| = 0. \tag{1.7}$$

The stationary state $\overline{\rho}$ is globally asymptotically stable if η can be arbitrarily large.

Since we are interested in the ultimate fate, growth or decay, of small perturbations of the steady state, it makes sense to linearize the rate equations about the steady state. Let $\delta(t) = \rho(t) - \overline{\rho}$. The evolution of the perturbations $\delta(t)$ is given by

$$\frac{d\delta}{dt} = J\delta + N(\delta), \tag{1.8}$$

where $N(\delta) = o(\delta)$ as $\delta \to 0$, i.e., $|N(\delta)| / |\delta| \to 0$ as $|\delta| \to 0$. The $n \times n$ matrix J is the Jacobian matrix of the system evaluated at the steady state $\overline{\rho}$ and is given by

$$J_{ij} = \frac{\partial F_i}{\partial \rho_j}\bigg|_{\overline{\rho}}. \tag{1.9}$$

Neglecting the small nonlinear terms $N(\delta)$, we obtain the linearized system, with respect to the steady state $\overline{\rho}$, for (1.1):

$$\frac{d\delta}{dt} = J\delta. \tag{1.10}$$

Let $\lambda_l, l = 1, \ldots, n$, be the eigenvalues of the Jacobian J and $\Phi_l, l = 1, \ldots, n$, the associated eigenvectors. For the generic case that all eigenvalues are distinct, the solution of (1.10) is given by

$$\delta(t) = \sum_{l=1}^{n} a_l \Phi_l \exp(\lambda_l t), \tag{1.11}$$

where a_l are constants determined by the initial condition $\delta(0)$. We conclude that the solution of the linearized equation (1.10) approaches 0, i.e., the perturbations decay, if all eigenvalues of the Jacobian have a negative real part, $\mathrm{Re}\,\lambda_l < 0$ for $l = 1, \ldots, n$. If there exists at least one $\lambda_{l'}$ with a positive real part, $\mathrm{Re}\,\lambda_{l'} > 0$, then the system moves away from the steady state. The perturbations grow exponentially initially until the nonlinear terms become important. This suggests that the stability of the steady state $\overline{\rho}$ is determined by the eigenvalues of the Jacobian. That is the content of the following theorem.

Theorem 1.1 (Principle of Linearized Stability)   *(a) If all the eigenvalues $\lambda_l, l = 1, \ldots, n$, of the Jacobian matrix J have a negative real part, then the steady state $\overline{\rho}$ of the nonlinear evolution equations (1.1) is asymptotically stable. (b) If at least one eigenvalue of J has a positive real part, then the steady state $\overline{\rho}$ is unstable. (c) If the Jacobian has one or more eigenvalues with zero real part and no eigenvalues with positive real part, then the steady state $\overline{\rho}$ may be stable, unstable, or asymptotically stable depending on the nonlinear terms.*

Remark 1.1 The case (c), one or more eigenvalues with zero real part and no eigenvalues with positive real part, is commonly called the case of (linear) *marginal stability*.

The eigenvalues λ_l of J are the roots of the nth order characteristic polynomial, $(-1)^n \det(\mathsf{J} - \lambda \mathsf{I}_n) = 0$, where I_n is the $n \times n$ identity matrix,

$$\lambda^n + c_1 \lambda^{n-1} + c_2 \lambda^{n-2} + \cdots + c_{n-1} \lambda + c_n = 0. \tag{1.12}$$

1.2.1 One-Variable Systems

In some applications, the system is well described by the dynamics of one species, see Sect. 1.4. In other words, the dynamics is governed by the rate equation for a single-state variable, the density ρ,

$$\frac{d\rho}{dt} = F(\rho, \boldsymbol{\mu}), \tag{1.13}$$

and the steady states are given by

$$F(\overline{\rho}(\boldsymbol{\mu}), \boldsymbol{\mu}) = 0. \tag{1.14}$$

The linearized system with respect to the steady state $\overline{\rho}$ reads, with $\delta = \rho - \overline{\rho}$,

$$\frac{d\delta}{dt} = F'(\overline{\rho}(\boldsymbol{\mu}), \boldsymbol{\mu})\delta = \lambda\delta. \tag{1.15}$$

The eigenvalue λ is real, and the steady state $\overline{\rho}$ is stable if $\lambda = F'(\overline{\rho}(\boldsymbol{\mu})) < 0$ and unstable if $\lambda = F'(\overline{\rho}(\boldsymbol{\mu})) > 0$. In one-variable systems, the steady states can undergo only one type of instability, namely a real eigenvalue passes through zero. This is known as a stationary instability or bifurcation.

While one-variable systems are easy to analyze, there are few real-world applications. Also their dynamics is simple; they can display multistability, but no oscillatory behavior. Periodic oscillations can only occur in systems with at least two species and chaos requires at least three species, see for example [421].

1.2.2 Two-Variable Systems

We will generally use the letters U and V to denote the relevant species in two-variable systems. The rate equations read

$$\frac{d\rho_u}{dt} = F_1(\rho_u, \rho_v, \boldsymbol{\mu}), \tag{1.16a}$$

$$\frac{d\rho_v}{dt} = F_2(\rho_u, \rho_v, \boldsymbol{\mu}), \tag{1.16b}$$

and the stationary states $(\overline{\rho}_u, \overline{\rho}_v)$ are given by

$$F_1(\overline{\rho}_u, \overline{\rho}_v, \boldsymbol{\mu}) = F_2(\overline{\rho}_u, \overline{\rho}_v, \boldsymbol{\mu}) = 0. \tag{1.17}$$

As discussed above, the stability of the steady states is determined by the eigenvalues of the Jacobian

$$\mathsf{J} = \begin{pmatrix} J_{11} & J_{12} \\ J_{21} & J_{22} \end{pmatrix} = \begin{pmatrix} \left.\frac{\partial F_1}{\partial \rho_u}\right|_{(\overline{\rho}_u, \overline{\rho}_v)} & \left.\frac{\partial F_1}{\partial \rho_v}\right|_{(\overline{\rho}_u, \overline{\rho}_v)} \\ \left.\frac{\partial F_2}{\partial \rho_u}\right|_{(\overline{\rho}_u, \overline{\rho}_v)} & \left.\frac{\partial F_2}{\partial \rho_v}\right|_{(\overline{\rho}_u, \overline{\rho}_v)} \end{pmatrix}. \tag{1.18}$$

The system (1.16) is said to be of the *pure activator–inhibitor* type if the Jacobian has the structure

$$\mathsf{J} = \begin{pmatrix} + & - \\ + & - \end{pmatrix}, \tag{1.19}$$

i.e.,

$$J_{11} > 0, \ J_{22} < 0, \ J_{12} < 0, \ J_{21} > 0. \tag{1.20}$$

The system (1.16) is said to be of the *cross activator–inhibitor* type if the Jacobian has the structure

$$\mathsf{J} = \begin{pmatrix} + & + \\ - & - \end{pmatrix}, \tag{1.21}$$

i.e.,

$$J_{11} > 0, \ J_{22} < 0, \ J_{12} > 0, \ J_{21} < 0. \tag{1.22}$$

Note that the type can depend on the stationary state $(\overline{\rho}_u, \overline{\rho}_v)$. If the specific type does not matter, we will refer to (1.19) and (1.21) simply as activator–inhibitor systems. In our convention, the species U is the activator and V the inhibitor. Some

authors adopt a different nomenclature and call systems of type (1.19) activator–inhibitor systems and those of type (1.21) activator-substrate-depletion systems.

The characteristic polynomial for a two-variable system is a quadratic equation

$$\lambda^2 - T\lambda + \Delta = 0, \tag{1.23}$$

where T is the trace of the Jacobian,

$$T = \operatorname{tr}\mathsf{J} = J_{11} + J_{22}, \tag{1.24}$$

and Δ is the determinant of the Jacobian,

$$\Delta = \det\mathsf{J} = J_{11}J_{22} - J_{12}J_{21}. \tag{1.25}$$

The roots of the characteristic polynomial (1.23) are given by

$$\lambda_{1,2} = \frac{1}{2}\left[T \pm \sqrt{T^2 - 4\Delta}\right]. \tag{1.26}$$

Equation (1.26) implies that for a two-variable system all eigenvalues of the Jacobian have a negative real part, i.e., the steady state is stable, if

$$T < 0, \tag{1.27a}$$
$$\Delta > 0. \tag{1.27b}$$

It is useful to analyze the behavior of the eigenvalues in more detail and distinguish the following cases which are illustrated in Fig. 1.1.

Case (I): $T < 0$, $\Delta > 0$, and the discriminant is positive, $T^2 - 4\Delta > 0$. In this case both eigenvalues are real and negative. According to (1.11), all perturbations to the steady state decay monotonically and the steady state is a *stable node*.

Case (II): $T < 0$, $\Delta > 0$, and the discriminant is negative, $T^2 - 4\Delta < 0$. In this case the eigenvalues form a pair of complex conjugate numbers, $\lambda_{1,2} = \lambda \pm i\omega$, with $\lambda = T/2$ and $\omega = \sqrt{4\Delta - T^2}/2$. The real part is negative and perturbations of the steady state still decay. However, the presence of a nonzero imaginary part implies that the perturbations no longer decrease monotonically but in an oscillatory manner. The trajectory approaches the steady state spiraling around it. The steady state is a *stable focus*.

Case (III): $T > 0$, $\Delta > 0$, and the discriminant is negative, $T^2 - 4\Delta < 0$. The eigenvalues are complex conjugate with a positive real part, $\lambda = T/2$. The steady state is unstable. Due to the presence of a nonzero imaginary part, perturbations grow in an oscillatory manner and spiral away from the steady state. The steady state is an *unstable focus*.

Case (IV): $T > 0$, $\Delta > 0$, and the discriminant is positive, $T^2 - 4\Delta > 0$. The eigenvalues are both real and positive. All perturbations grow exponentially. The steady state is an *unstable node*.

Case (V): $\Delta < 0$. In this case the discriminant is always positive, $T^2 - 4\Delta > 0$, and both eigenvalues are real. However, one is positive and the other is negative. Trajectories approach the steady state along the eigenvector corresponding to the negative eigenvalue, but move away along the eigenvector corresponding to the positive eigenvalue. The steady state has one stable and one unstable direction. It is therefore unstable and called a *saddle*.
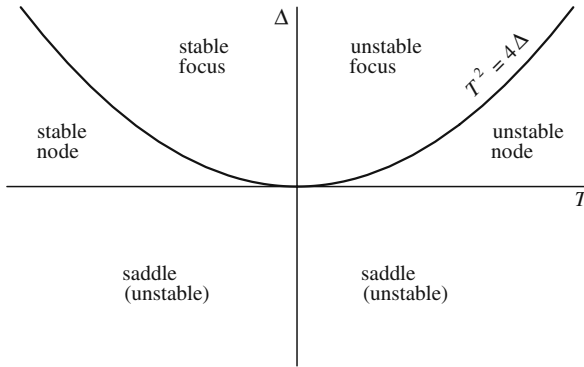
Fig. 1.1 Stability classification for two-variable systems

The preceding discussion shows that a steady state of a two-variable system can undergo an instability in two generic ways. (i) If a real eigenvalue passes through zero as a parameter μ of the system is varied, i.e, the determinant of the Jacobian changes sign, then a stationary bifurcation occurs at $\mu = \mu_{st}$:

$$\Delta = \det \mathsf{J} = 0 \quad \text{for } \mu = \mu_{st}. \tag{1.28}$$

At the instability threshold,

$$\lambda_1 = 0, \tag{1.29}$$
$$\lambda_2 = T < 0, \tag{1.30}$$

i.e., one eigenvalue vanishes, while the other is negative. (ii) If a pair of complex conjugate eigenvalues crosses the imaginary axis, as a parameter μ of the system is varied, i.e, the trace of the Jacobian changes sign, then an oscillatory or Hopf bifurcation occurs at $\mu = \mu_H$:

$$T = \text{tr } \mathsf{J} = 0 \quad \text{for } \mu = \mu_H. \tag{1.31}$$

At the instability threshold,

$$\lambda_{1,2} = \pm i\omega_H, \tag{1.32}$$

where the characteristic frequency is determined solely by the system parameters and given by

$$\omega_H = \sqrt{\Delta}. \tag{1.33}$$

The stationary bifurcation and the Hopf bifurcation typically occur as one parameter is varied and are therefore known as codimension-one bifurcations. They represent the generic ways in which a steady state of a two-variable system can become unstable. It is sometimes possible to make the stationary and Hopf instability threshold coalesce by varying two parameters. Such an instability, where $T = \Delta = 0$, is known as a Takens–Bogdanov bifurcation or a double-zero bifurcation, since $\lambda_1 = \lambda_2 = 0$ at such a point [175]. This bifurcation is a codimension-two bifurcation, since it requires the fine-tuning of two system parameters.

1.2.3 Systems with $n > 2$ Variables

A linear stability analysis of the steady states of systems with more than two variables usually employs a Routh–Hurwitz analysis, which is based on the following theorem [309, 153, 424].

Theorem 1.2 (Routh–Hurwitz)   *All roots of the characteristic polynomial* (1.12) *have a negative real part, if and only if*

$$\Delta_l = \begin{vmatrix} c_1 & c_3 & \cdot & \cdot & \cdot & \cdot \\ 1 & c_2 & c_4 & \cdot & \cdot & \cdot \\ 0 & c_1 & c_3 & \cdot & \cdot & \cdot \\ 0 & 1 & c_2 & \cdot & \cdot & \cdot \\ \cdot & \cdot & \cdot & \cdot & \cdot & \cdot \\ 0 & 0 & \cdot & \cdot & \cdot & c_l \end{vmatrix} > 0, \quad l = 1, \dots, n, \tag{1.34}$$

together with the condition

$$c_n > 0. \tag{1.35}$$

[Set $c_l = 0$ in (1.34) for $l > n$.] The generic bifurcations of steady states in n-variable systems, $n > 2$, are again the stationary bifurcation, where a real eigenvalue passes through zero, and the Hopf bifurcation, where a pair of complex conjugate eigenvalue crosses the imaginary axis. The steady state undergoes a stationary bifurcation if condition (1.35) is violated, i.e.,

$$c_n = 0. \tag{1.36}$$

Note that $c_n = (-1)^n \det \mathsf{J}$; this condition is the same as for two-variable systems. To obtain the condition for the oscillatory or Hopf bifurcation, we exploit Orlando's formula [153],

$$\Delta_{n-1} = (-1)^{n(n-1)/2} \prod_{1 \leq i < k \leq n} (\lambda_i + \lambda_k), \tag{1.37}$$

where λ_i and λ_k are roots of the characteristic polynomial (1.12). Orlando's formula implies that

$$\Delta_{n-1} = 0, \tag{1.38a}$$

$$c_n > 0, \tag{1.38b}$$

$$\Delta_l > 0, \quad l = 1, \ldots, n - 2, \tag{1.38c}$$

is a necessary and sufficient condition for a conjugate pair of purely imaginary eigenvalues [236], i.e., for a Hopf bifurcation.

The Routh–Hurwitz conditions are well known and can be used to determine, in principle, the stability properties of the steady state of any n-variable system. This advantage is, however, balanced by the fact that in practice their use is very cumbersome, even for n as small as 3 or 4. The evaluation, by hand, of all the coefficients c_l of the characteristic polynomial and the Hurwitz determinants Δ_l constitutes a rather arduous task. It is for this reason that in the past this tool of linear stability analysis could hardly be found in the literature of nonlinear dynamics. The situation changed with the advent of computer-algebra systems or symbolic computation software. Software such as MATHEMATICA (Wolfram Research, Inc., Champaign, IL) or MAPLE (Waterloo Maple Inc., Waterloo, Ontario) makes it easy to obtain exact, analytical expressions for the coefficients c_l of the characteristic polynomial (1.12) and the Hurwitz determinants Δ_l.

1.3 Chemical Kinetics

In the next section, we collect several models that we use repeatedly later on. We begin by introducing some concepts from chemical kinetics in this section. This is intended to be a very simple review of a few facts needed to discuss rate equation for chemical reactions. Consider the following (abstract) balanced chemical equation:

$$\nu_1 C_1 + \nu_2 C_2 + \cdots \longrightarrow \nu_l C_l + \nu_m C_m + \cdots . \tag{1.39}$$
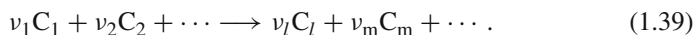
Here ν_i are the stoichiometric coefficients of the reactants, C_1, C_2, $\ldots$, and of the products, C_l, C_m, $\ldots$. They tell us, for example, that for every ν_1 moles of C_1, ν_2 moles of C_2 are simultaneously used up and ν_m moles of product C_m are formed. The chemical equation can be written in the form of an algebraic equation by

adopting the convention that the stoichiometric coefficients of products are positive and those of reactants are negative:

$$\sum_i v_i C_i = 0.$$

(1.40)

We consider only reactions that take place within a constant volume. For such reactions, the reaction velocity v of (1.40) is defined as the rate of change of the concentration of *any* species divided by its stoichiometric coefficient:

$$v = \frac{1}{v_i} \frac{d\rho_i}{dt}.$$

(1.41)

This definition results in a unique, positive reaction velocity for a given reaction. Since (1.39) is balanced, v does indeed not depend on i, and the time dependence of any reactant or product can be used. A rate law is a mathematical statement of how the reaction velocity depends on concentration:

$$v = r(\boldsymbol{\rho}).$$

(1.42)

If v depends on the concentration of some species that does not appear in the balanced chemical equation, then that species is called a *catalyst* if v increases as the concentration of that species increases. If an increase in the concentration of that species leads to a decrease of the reaction velocity v, it is called an *inhibitor*. If v depends on one or more products, then the reaction is called *autocatalytic* if the product increases the reaction velocity. If the product decreases the reaction velocity, the reaction is called *self-inhibiting*. Rate laws are determined experimentally from kinetic data. Such a rate law is called an *empirical rate law*. Rate laws are often, but not always, found to depend on simple powers of the concentrations:

$$v = k\rho_1^x \rho_2^y \rho_3^z \cdots .$$

(1.43)

The coefficient k is known as the rate constant. It depends on temperature and is, by the definition (1.41) of the reaction velocity, always a positive quantity. The exponents define the order of the reaction, and the sum of the exponents the overall order. For instance, the reaction

$$H_2 + I_2 \xrightarrow{k} 2\,HI$$

(1.44)

obeys the empirical rate law

$$v = k[H_2][I_2].$$

(1.45)

The brackets denote, as usual in chemistry, the concentration of the species enclosed. This reaction is first order in hydrogen, H_2, first order in iodine, I_2, and second order

overall. Note that the order of a reaction does *not* have to coincide with the stoichiometric coefficient in the balanced chemical equation. For example, the thermal decomposition of acetaldehyde

$$CH_3CHO \xrightarrow{k} CH_4 + CO \tag{1.46}$$

has the empirical rate law

$$v = k[CH_3CHO]^{3/2}. \tag{1.47}$$

As this example demonstrates, the order of a reaction does not need to be an integer. The next example shows that an order or overall order cannot always be defined. The reaction of hydrogen with bromine,

$$H_2 + Br_2 \xrightarrow{k} 2\,HBr, \tag{1.48}$$

has the empirical rate law

$$v = k\frac{[H_2][Br_2]^{3/2}}{[Br_2] + k'[HBr]}. \tag{1.49}$$

The reaction is first order in H_2; no order for Br_2 or HBr and no overall order can be defined. Note that v decreases as the concentration of the product HBr increases, i.e., the reaction is self-inhibiting.

Chemical equations are stoichiometric statements. For example, (1.48) means that one mole of hydrogen reacts with one mole of bromine to form two moles of hydrogen bromide. Sometimes, chemical equations can also be interpreted in terms of what happens to the molecules. If such a molecular interpretation is valid, the reaction is called *elementary*. In most cases, including reaction (1.48), the sequence of events is more complex. A molecule of hydrogen does not collide with a molecule of bromine, exchange atoms, and form two molecules of hydrogen bromide. The reaction, as is generally the case, proceeds from reactants to products involving a variety of intermediate species and elementary steps. The series of elementary reactions that constitute the stoichiometric reaction, the balanced chemical equation, is called the mechanism of the reaction. For example, the mechanism of the hydrogen–bromine reaction is given by

$$Br_2 + M \xrightarrow{k_1} 2\,Br\cdot + M, \tag{1.50}$$

$$Br\cdot + H_2 \xrightarrow{k_2} HBr + H\cdot, \tag{1.51}$$

$$H\cdot + Br_2 \xrightarrow{k_3} HBr + Br\cdot, \tag{1.52}$$

$$H \cdot + HBr \xrightarrow{k_4} H_2 + Br\cdot, \tag{1.53}$$

$$Br \cdot + Br \cdot + M \xrightarrow{k_5} Br_2 + M, \tag{1.54}$$
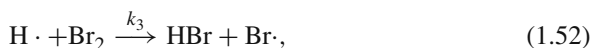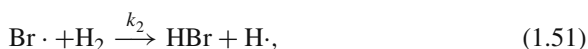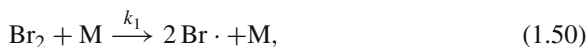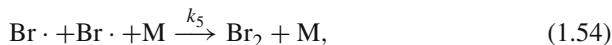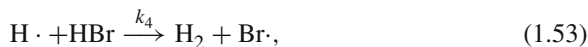
where M is an inert species. The dot on a chemical species denotes a radical, a reactive, short-lived, odd-electron species. Rate laws for elementary reactions can be read off from the chemical equation. The order of an elementary reaction is given by the stoichiometric coefficients. For instance, the rate law of reaction (1.53) is given by

$$v_4 = k_4[H][HBr]. \tag{1.55}$$

The reaction is first order in H, first order in HBr, and second order overall. This elementary reaction involves two molecules and is known as a bimolecular reaction. This is the most common type of an elementary reaction. The other two are unimolecular reactions and trimolecular (or termolecular) reactions; the latter are rare.

Most reactions are not elementary. The hydrogen–iodine reaction looks like an elementary bimolecular reaction; it is first order in H_2, first order in I_2, and second order overall. However, this reaction is not elementary [425]. Reactions that behave kinetically just like a single-step, elementary reaction are called kinetically simple. The order of each reactant in such a reaction is equal to its stoichiometric coefficients. Such reactions are also said to obey the law of mass action or to have mass-action kinetics.

1.4 Chemical and Biological Models

This section contains several models whose spatiotemporal behavior we analyze later. Nontrivial dynamical behavior requires nonequilibrium conditions. Such conditions can only be sustained in open systems. Experimental studies of nonequilibrium chemical reactions typically use so-called continuous-flow stirred tank reactors (CSTRs). As the name implies, a CSTR consists of a vessel into which fresh reactants are pumped at a constant rate and material is removed at the same rate to maintain a constant volume. The reactor is stirred to achieve a spatially homogeneous system. Most chemical models account for the flow in a simplified way, using the so-called pool chemical assumption. This idealization assumes that the concentrations of the reactants do not change. Strict time independence of the reactant concentrations cannot be achieved in practice, but the pool chemical assumption is a convenient modeling tool. It captures the essential fact that the system is open and maintained at a fixed distance from equilibrium. We will discuss one model that uses CSTR equations. All other models rely on the pool chemical assumption. We will denote pool chemicals using capital letters from the start of the alphabet, A, B, etc. Species whose concentration is allowed to vary are denoted by capital letters

from the end of the alphabet, such as U, V, etc. We will use the corresponding small letters as subscripts on the concentration variable ρ to represent the concentrations or densities of the various species.

1.4.1 Branching-Coalescence Model

We begin by discussing several models with one state variable. In the case of systems with only one relevant species, we drop the subscript and denote the concentration simply by ρ. The first specific system we consider is given by a mechanism consisting of two elementary steps:

$$A + U \xrightarrow{k_1} 2\,U, \tag{1.56}$$

$$2\,U \xrightarrow{k_2} A + U. \tag{1.57}$$

The reaction velocity for the branching step is

$$v_1 = k_1 \rho_a \rho \tag{1.58}$$

and for the coalescence step

$$v_2 = k_2 \rho^2. \tag{1.59}$$

The rate equation for the concentration of U reads

$$\frac{d\rho}{dt} = k_1 \rho_a \rho - k_2 \rho^2. \tag{1.60}$$

It is often convenient to nondimensionalize the rate equations. One way to achieve a dimensionless evolution equation for the branching-coalescence model is to introduce a dimensionless time and concentration as follows:

$$t^* = k_1 \rho_a t, \quad \rho^* = \frac{k_2}{k_1 \rho_a} \rho, \tag{1.61}$$

where the asterisk denotes dimensionless quantities. Substituting these two expressions into the rate equation (1.60) we obtain, dropping the asterisk for notational convenience,

$$\frac{d\rho}{dt} = F(\rho) = \rho - \rho^2 = \rho(1 - \rho). \tag{1.62}$$

The kinetic term of this form is commonly referred to as KPP kinetics and is used in the Fisher–Kolmogorov–Petrovskii–Piskunov (FKPP) equation, see Chap. 4. The equation has two steady states, the trivial one, $\bar{\rho}_1 = 0$, and $\bar{\rho}_2 = 1$. Since

$F'(\rho) = 1 - 2\rho$, we have $F'(0) = 1$, i.e., the trivial state is unstable, and $F'(1) = -1$, i.e., the steady state $\bar{\rho}_2 = 1$ is stable.

1.4.2 Schlögl Model I

The first Schlögl model [384] is a generalization of the branching-coalescence scheme and is defined by the mechanism

$$A + U \xrightarrow{k_1} 2\,U, \tag{1.63}$$

$$2\,U \xrightarrow{k_2} A + U, \tag{1.64}$$

$$B + U \xrightarrow{k_3} C, \tag{1.65}$$

and its rate equation is given by

$$\frac{d\rho}{dt} = (k_1\rho_a - k_3\rho_b)\rho - k_2\rho^2. \tag{1.66}$$

The original version of the first Schlögl model contains a fourth step, the back reaction $C \longrightarrow B + U$. We assume that the product C is immediately removed from the system. We consider two different ways of nondimensionalizing this rate equation. (i) Set $t^* = k_2\sqrt{\rho_a\rho_b}\,t$ and $\rho^* = k_2\rho/(k_1\rho_a - k_3\rho_b)$. This is acceptable for all situations where $k_1\rho_a > k_3\rho_b$. Then we obtain the following nondimensionalized version of (1.66):

$$\frac{d\rho}{dt} = F(\rho) = r\rho(1 - \rho). \tag{1.67}$$

We have again dropped the asterisk and will do so from now on. The parameter r is given by

$$r = \frac{k_1\rho_a - k_3\rho_b}{k_2\sqrt{\rho_a\rho_b}} = r^+ - r^- > 0. \tag{1.68}$$

The rate term of (1.67) corresponds again to KPP kinetics. (ii) Set $t^* = k_2\sqrt{\rho_a\rho_b}\,t$ and $\rho^* = \rho/\sqrt{\rho_a\rho_b}$. This works for all values of the parameters. Then

$$\frac{d\rho}{dt} = F(\rho) = \mu\rho - \rho^2, \tag{1.69}$$

where

$$\mu = \frac{k_1\rho_a - k_3\rho_b}{k_2\sqrt{\rho_a\rho_b}}. \tag{1.70}$$

The stationary states of (1.69) are the trivial steady state $\overline{\rho}_1 = 0$, which exists for all values of μ, and $\overline{\rho}_2 = \mu$, which exists only for $\mu \geq 0$. We have $F'(\rho) = \mu - 2\rho$, which implies that $F'(0) = \mu$. The steady state $\overline{\rho}_1$ is stable for $\mu < 0$, undergoes a bifurcation at $\mu_{st} = 0$, and is unstable for $\mu > 0$. Since $F'(\overline{\rho}_2) = -\mu$, the second steady state is stable for $\mu > 0$.

1.4.3 Verhulst Equation

The next system is a simple model of population dynamics. Let ρ be the density of a population. The population density will change due to births, deaths, and migration. The simplest model has no migration and the birth and death terms are simply proportional to the density:

$$\frac{\mathrm{d}\rho}{\mathrm{d}t} = b\rho - d\rho = (b - d)\rho = r\rho, \tag{1.71}$$

where b and d are positive constants and are the intrinsic birth and death rates, respectively. The parameter $r = b - d$ is the intrinsic growth rate. Equation (1.71) is known as the Malthusian growth equation. It corresponds to exponential growth, which is unrealistic. The growth must saturate eventually, and Verhulst suggested that the per capita growth rate decays linearly with population density. The resulting kinetic equation is known as the Verhulst equation or logistic equation:

$$\frac{\mathrm{d}\rho}{\mathrm{d}t} = r\rho \left(1 - \frac{\rho}{K} \right). \tag{1.72}$$

The parameter K is the carrying capacity of the system, at which the growth rate vanishes. If we nondimensionalize the system by measuring the density in terms of the carrying capacity, $\rho^* = \rho/K$, and rescale time by the intrinsic growth rate, $t^* = rt$, then we obtain again KPP kinetics:

$$\frac{\mathrm{d}\rho}{\mathrm{d}t} = \rho(1 - \rho). \tag{1.73}$$

1.4.4 Brusselator

Prigogine and Lefever introduced a simple two-variable scheme in 1968 [354, 243] that displays sustained oscillatory behavior. It was subsequently dubbed the Brusselator by Tyson [441] and consists of four steps:

$$A \xrightarrow{k_1} U, \tag{1.74}$$

$$B + U \xrightarrow{k_2} V + D, \tag{1.75}$$

$$2\,U + V \xrightarrow{k_3} 3\,U, \tag{1.76}$$

$$U \xrightarrow{k_4} E. \tag{1.77}$$

The rate equations for the Brusselator are

$$\frac{d\rho_u}{dt} = k_1 \rho_a - (k_2 \rho_b + k_4)\rho_u + k_3 \rho_u^2 \rho_v, \tag{1.78a}$$

$$\frac{d\rho_v}{dt} = k_2 \rho_b \rho_u - k_3 \rho_u^2 \rho_v. \tag{1.78b}$$

To nondimensionalize the kinetic equations we set $t^* = k_4 t$, $\rho_u^* = \sqrt{k_3/k_4}\,\rho_u$, $\rho_v^* = \sqrt{k_3/k_4}\,\rho_v$, $a = \sqrt{k_1^2 k_3/k_4^3}\,\rho_a$, and $b = (k_2/k_4)\rho_b$. Dropping again the asterisk for notational convenience, the nondimensionalized rate equations read

$$\frac{d\rho_u}{dt} = a - (b+1)\rho_u + \rho_u^2 \rho_v, \tag{1.79a}$$

$$\frac{d\rho_v}{dt} = b\rho_u - \rho_u^2 \rho_v. \tag{1.79b}$$

The Brusselator has a unique steady state,

$$\overline{\rho}_u = a, \quad \overline{\rho}_v = \frac{b}{a}, \tag{1.80}$$

and the Jacobian is given by

$$\mathsf{J} = \begin{pmatrix} b-1 & a^2 \\ -b & -a^2 \end{pmatrix}. \tag{1.81}$$

The Brusselator is a cross activator–inhibitor system if $b > 1$. The trace T and determinant Δ of the Jacobian are given by

$$T = b - 1 - a^2, \quad \Delta = a^2. \tag{1.82}$$

The determinant is always positive and the steady state of the Brusselator cannot undergo a stationary bifurcation, see (1.28). The condition for a Hopf bifurcation, $T = 0$, see (1.31), yields

$$b_H = 1 + a^2. \tag{1.83}$$

For $b < b_H$, the steady state $(a, b/a)$ is stable. For $b > b_H$, it is unstable and the asymptotic state of the Brusselator is a stable limit cycle, i.e., an attracting,

nonconstant periodic solution; see, e.g., [441]. According to (1.33), the frequency of the limit-cycle oscillations at the bifurcation point is given by

$$\omega_H = a. \tag{1.84}$$

The Brusselator provides a simple mass-action kinetic scheme that displays sustained, stable oscillatory behavior.

1.4.5 Schnakenberg Model

The Schnakenberg model is a modification of the Brusselator scheme, and its mechanism consists of the following four steps:

$$U \longrightarrow A, \tag{1.85}$$

$$A \longrightarrow U, \tag{1.86}$$

$$B \longrightarrow V, \tag{1.87}$$

$$2\,U + V \longrightarrow 3\,U. \tag{1.88}$$

The dimensionless rate equations for this scheme are given by

$$\frac{d\rho_u}{dt} = a - \rho_u + \rho_u^2 \rho_v, \tag{1.89a}$$

$$\frac{d\rho_v}{dt} = b - \rho_u^2 \rho_v. \tag{1.89b}$$

The Schnakenberg model too has a unique steady state:

$$\bar{\rho}_u = a + b, \quad \bar{\rho}_v = \frac{b}{(a+b)^2}. \tag{1.90}$$

The Jacobian is given by

$$\mathsf{J} = \begin{pmatrix} \dfrac{b-a}{a+b} & (a+b)^2 \\ -\dfrac{2b}{a+b} & -(a+b)^2 \end{pmatrix}. \tag{1.91}$$

The Schnakenberg model is a cross activator–inhibitor system if $b > a$. The determinant of the Jacobian is also always positive, $\Delta = (a+b)^2$, and no stationary bifurcation can occur. The Hopf threshold b_H is given by the cubic equation

$$b_H - a = (a + b_H)^3. \tag{1.92}$$

1.4.6 Gierer–Meinhardt Model

Gierer and Meinhardt have suggested various models to account for biological pattern formation, see for example [157, 279]. In the following we adopt a particular model and use the dimensionless version of the rate equations presented in [388, Chap. 8]:

$$\frac{d\rho_u}{dt} = 1 - \rho_u + p\frac{\rho_u^2}{\rho_v}, \tag{1.93a}$$

$$\frac{d\rho_v}{dt} = q(\rho_u^2 - \rho_v), \tag{1.93b}$$

where p and q are positive parameters. This model also has a unique steady state,

$$\overline{\rho}_u = 1 + p, \quad \overline{\rho}_v = (1 + p)^2, \tag{1.94}$$

and the Jacobian is

$$\mathsf{J} = \begin{pmatrix} \dfrac{p-1}{p+1} & -\dfrac{p}{(1+p)^2} \\ 2q(1+p) & -q \end{pmatrix}. \tag{1.95}$$

The Gierer–Meinhardt model belongs to the class of pure activator–inhibitor systems if $p > 1$. The trace T and determinant Δ of the Jacobian are given by

$$T = \frac{p-1}{p+1} - q, \quad \Delta = q. \tag{1.96}$$

For all parameter values, the determinant is positive and the steady state of the Gierer–Meinhardt model cannot undergo a stationary bifurcation. The Hopf condition, $T = 0$, is satisfied for

$$p_{\mathrm{H}} = \frac{1+q}{1-q}. \tag{1.97}$$

1.4.7 Gray–Scott Model

The second Schlögl model [384] is defined by the mechanism

$$A + 2U \underset{k_{-1}}{\overset{k_1}{\rightleftharpoons}} 3U, \tag{1.98}$$

$$B + U \underset{k_{-2}}{\overset{k_2}{\rightleftharpoons}} C, \tag{1.99}$$

and its rate equation is given by

$$\frac{d\rho}{dt} = k_{-2}\rho_c - k_2\rho_b\rho + k_1\rho_a\rho^2 - k_{-1}\rho^3. \tag{1.100}$$

As the previous models, the second Schlögl model relies on the pool chemical assumption to account for the inflow of reactants. If we assume instead that this reaction scheme occurs in a CSTR, we obtain the Gray–Scott model [170, 171]:

$$V + 2\,U \underset{k_{-1}}{\overset{k_1}{\rightleftharpoons}} 3\,U, \tag{1.101}$$

$$U \underset{k_{-2}}{\overset{k_2}{\rightleftharpoons}} W. \tag{1.102}$$

Let V be the volume of the reactor and f the volumetric flow rate. We assume that the CSTR is well mixed, i.e., we make the ideal mixing assumption. Then the average time a fluid parcel spends in the CSTR is

$$t_{\text{res}} = \frac{V}{f}. \tag{1.103}$$

Defining the flow rate q as the inverse residence time,

$$q = \frac{1}{t_{\text{res}}} = \frac{f}{V}, \tag{1.104}$$

the kinetic equations for the Gray–Scott model are given by

$$\frac{d\rho_u}{dt} = k_1\rho_v\rho_u^2 - k_{-1}\rho_u^3 - k_2\rho_u + k_{-2}\rho_w + q(\rho_{u0} - \rho_u), \tag{1.105a}$$

$$\frac{d\rho_v}{dt} = -k_1\rho_v\rho_u^2 + k_{-1}\rho_u^3 + q(\rho_{v0} - \rho_v), \tag{1.105b}$$

$$\frac{d\rho_w}{dt} = k_2\rho_u - k_{-2}\rho_w + q(\rho_{w0} - \rho_w), \tag{1.105c}$$

where the subscript 0 denotes the feed concentration. We nondimensionalize the kinetic equations by setting $\rho_u^* = \rho_u/\rho_{v0}$, $\rho_v^* = \rho_v/\rho_{v0}$, $\rho_w^* = \rho_w/\rho_{v0}$, $t^* = k_1\rho_{v0}^2 t$, $q^* = q/k_1\rho_{v0}^2$, $k_2^* = k_2/k_1\rho_{v0}^2$, $\eta_1 = k_{-1}/k_1$, and $\eta_2 = k_{-2}/k_2$. Dropping again the asterisk for notational convenience, the nondimensionalized rate equations for the Gray–Scott model read

$$\frac{d\rho_u}{dt} = \rho_v\rho_u^2 - \eta_1\rho_u^3 - k_2\rho_u + k_2\eta_2\rho_w + q(\rho_{u0} - \rho_u), \tag{1.106a}$$

$$\frac{d\rho_v}{dt} = -\rho_v\rho_u^2 + \eta_{-1}\rho_u^3 + q(1 - \rho_v), \tag{1.106b}$$

$$\frac{d\rho_w}{dt} = k_2\rho_u - k_2\eta_2\rho_w + q(\rho_{w0} - \rho_w). \tag{1.106c}$$

The Gray–Scott model has a first integral expressing the conservation of mass, namely

$$\frac{d}{dt}\left(\rho_u + \rho_v + \rho_w\right) = q\left(\rho_{u0} + 1 + \rho_{w0} - \rho_u - \rho_v - \rho_w\right). \tag{1.107}$$

Defining the total concentration $\rho \equiv \rho_u + \rho_v + \rho_w$, we obtain

$$\frac{d\rho}{dt} = q(\rho_0 - \rho). \tag{1.108}$$

This equation has the solution

$$\rho(t) = \rho(0)\exp(-qt) + \rho_0[1 - \exp(-qt)], \tag{1.109}$$

which implies that $\rho(t) \to \rho_0$ as $t \to \infty$. In other words, the total concentration relaxes to the total concentration in the feed stream. After a few residence times, the initial condition has essentially been washed out of the reactor. We assume from now on that $\rho(0) = \rho_0$ and thus $\rho(t) = \rho_0$. Then the concentration of species W can be eliminated, $\rho_w = \rho_0 - \rho_u - \rho_v$, and the Gray–Scott model reduces to a two-variable model:

$$\frac{d\rho_u}{dt} = \rho_v\rho_u^2 - \eta_1\rho_u^3 - k_2\rho_u + k_2\eta_2(\rho_0 - \rho_u - \rho_v) + q(\rho_{u0} - \rho_u), \tag{1.110a}$$

$$\frac{d\rho_v}{dt} = -\rho_v\rho_u^2 + \eta_{-1}\rho_u^3 + q(1 - \rho_v). \tag{1.110b}$$

We study the behavior of the Gray–Scott model under two simplifying assumptions. (i) The back reactions are negligible, i.e., $\eta_1 \ll 1$ and $\eta_2 \ll 1$, and we set $\eta_1 = \eta_2 = 0$ in (1.110). (ii) The autocatalytic intermediate U is *not* in the feed stream, $\rho_{u0} = 0$. Then the rate equations read

$$\frac{d\rho_u}{dt} = \rho_v\rho_u^2 - k_2\rho_u - q\rho_u, \tag{1.111a}$$

$$\frac{d\rho_v}{dt} = -\rho_v\rho_u^2 + q(1 - \rho_v). \tag{1.111b}$$

The system (1.111) has a trivial steady state:

$$(\bar{\rho}_{u1}, \bar{\rho}_{v1}) = (0, 1). \tag{1.112}$$

It is a simple consequence of the fact that no reactions occur if the reactor contains no catalyst U, since this species is not contained in the feed stream. The two other steady states,

$$(\overline{\rho}_{u2,3}, \overline{\rho}_{v2,3}) = \left(\frac{1}{2}\frac{q}{k_2 + q}\left[1 \pm \sqrt{1-\delta}\right], \frac{1}{2}\left[1 \mp \sqrt{1-\delta}\right]\right), \qquad (1.113)$$

where

$$\delta = \frac{4(k_2 + q)^2}{q}, \qquad (1.114)$$

exist for the interval (q_-, q_+) of the flow rate, where

$$q_\pm = \left(\frac{1}{8} - k_2\right) \pm \sqrt{\frac{1}{64} - \frac{k_2}{4}}, \qquad (1.115)$$

if

$$k_2 < \frac{1}{16}. \qquad (1.116)$$

Note that

$$\overline{\rho}_{u2,3}(q_\pm) = \frac{1}{2}\frac{q_\pm}{k_2 + q_\pm} \neq 0. \qquad (1.117)$$

The two branches of the nontrivial steady states are not connected to the branch of the trivial steady state. They form a so-called *isola* and appear and disappear via a saddle-node bifurcation.

The Jacobian of the Gray–Scott model (1.111) is given by

$$\mathbf{J} = \begin{pmatrix} 2\overline{\rho}_v\overline{\rho}_u - (k_2 + q) & \overline{\rho}_u^2 \\ -2\overline{\rho}_v\overline{\rho}_u & -\overline{\rho}_u^2 - q \end{pmatrix}. \qquad (1.118)$$

For the trivial steady state, $(\overline{\rho}_{u1}, \overline{\rho}_{v1}) = (0, 1)$, we find

$$\mathbf{J} = \begin{pmatrix} -(k_2 + q) & 0 \\ 0 & -q \end{pmatrix}. \qquad (1.119)$$

Since the Jacobian is a diagonal matrix for this case, the eigenvalues can be read off immediately:

$$\lambda_1 = -(k_2 + q), \quad \lambda_2 = -q. \qquad (1.120)$$

Both eigenvalues are negative and the trivial steady state is stable for all flow rates. This implies that a small initial amount of the autocatalyst U in the reactor will decay to zero.

The nontrivial steady states satisfy the relation $\bar{\rho}_v\bar{\rho}_u = k_2 + q$, which allows us to write the Jacobian in the following form:

$$J = \begin{pmatrix} k_2 + q & \bar{\rho}_u^2 \\ -2(k_2 + q) & -\bar{\rho}_u^2 - q \end{pmatrix}, \tag{1.121}$$

where $\bar{\rho}_u = \bar{\rho}_{u2}$ or $\bar{\rho}_u = \bar{\rho}_{u3}$. The trace and the determinant of the Jacobian (1.121) are given by

$$T = -\bar{\rho}_u^2 + k_2, \quad \Delta = (k_2 + q)(\bar{\rho}_u^2 - q). \tag{1.122}$$

For the steady state $(\bar{\rho}_{u3}, \bar{\rho}_{v3})$ the determinant Δ is negative for all flow rates, i.e., according to the stability classification in Sect. 1.2.2 the steady state is a saddle point. The lower branch of the isola is unstable for all flow rates for which it exists. For the upper branch of the isola, $(\bar{\rho}_{u2}, \bar{\rho}_{v2})$, the determinant Δ is always positive. The stability is determined by the trace T. For q near q_+, T is negative and the upper branch is stable. For q near q_-, T is positive and the upper branch of nontrivial steady states undergoes a Hopf bifurcation near q_- as the flow rate is decreased. For example, if $k_2 = 1/32$, then $q_+ = 0.182138$ and $q_- = 0.00536165$. The upper branch undergoes a Hopf bifurcation at $q_H = 0.00930292$.

1.4.8 Oregonator

The best known oscillating reaction is without a doubt the Belousov–Zhabotinsky (BZ) reaction, the oxidation of an organic substrate, typically malonic acid, $CH_2(COOH)_2$, by bromate, BrO_3^-, in an acidic medium in the presence of a metal-ion catalyst. It was discovered by Belousov in the early 1950s [32], and modified by Zhabotinsky [497]. The mechanism of the BZ reaction was elucidated by Field, Körös, and Noyes in 1972 [326, 130, 325] and reduced to five essential steps by Field and Noyes [131]. This model is called the Oregonator and in the version presented by Tyson and Fife [442] it is given by

$$Q + W \longrightarrow U + P, \tag{1.123}$$

$$U + W \longrightarrow 2P, \tag{1.124}$$

$$Q + U \longrightarrow 2U + 2V, \tag{1.125}$$

$$2U \longrightarrow Q + P, \tag{1.126}$$

$$B + V \longrightarrow \nu W, \tag{1.127}$$

where $Q = BrO_3^-$, $B = BrMA$ (bromomalonic acid), $P = HOBr$, $U = HBrO_2$, V is the oxidized form of the catalyst, typically Ce^{4+}, Fe^{3+}, or $Ru(bpy)_3^{3+}$, $W = Br^-$, and v is an adjustable stoichiometric parameter. The dimensionless rate equations for the scheme (1.123)–(1.127), where B, Q, and P are pool chemicals, are given by [442]

$$\epsilon \frac{d\rho_u}{dt} = q\rho_w - \rho_u\rho_w + \rho_u - \rho_u^2, \tag{1.128a}$$

$$\frac{d\rho_v}{dt} = \rho_u - \rho_v, \tag{1.128b}$$

$$\epsilon' \frac{d\rho_w}{dt} = -q\rho_w - \rho_u\rho_w + h\rho_v, \tag{1.128c}$$

with $h = 2v$. From measured rate constants for the BZ reaction, Tyson and Fife estimate the parameters in (1.128) by

$$\epsilon' \ll \epsilon \ll 1, \quad q \ll 1, \quad h \approx 1. \tag{1.129}$$

Since the variable ρ_w evolves on the fastest time scale, it can be eliminated by setting its time derivative equal to zero, and the value of ρ_w is determined by the values of ρ_u and ρ_v:

$$\rho_w = \frac{h\rho_v}{\rho_u + q}. \tag{1.130}$$

Then the three-variable Oregonator model (1.128) reduces to the two-variable Oregonator model:

$$\frac{d\rho_u}{dt} = \frac{1}{\epsilon}\left(\rho_u - \rho_u^2 - h\rho_v \frac{\rho_u - q}{\rho_u + q}\right), \tag{1.131a}$$

$$\frac{d\rho_v}{dt} = \rho_u - \rho_v. \tag{1.131b}$$

In this monograph we focus on (1.131) and refer to it for the sake of brevity as the Oregonator. The nontrivial steady state of the Oregonator is given by

$$\bar{\rho}_u = \frac{1 - h - q + \sqrt{1 - 2h + h^2 + 2q + 6hq + q^2}}{2}, \tag{1.132a}$$

$$\bar{\rho}_v = \bar{\rho}_u. \tag{1.132b}$$

The Jacobian is given by

$$
\mathsf{J} = \begin{pmatrix} \dfrac{1}{\epsilon}\left[1 - 2\overline{\rho}_u - \dfrac{2hq\overline{\rho}_u}{(\overline{\rho}_u + q)^2}\right] & -\dfrac{h}{\epsilon}\dfrac{\overline{\rho}_u - q}{\overline{\rho}_u + q} \\ 1 & -1 \end{pmatrix}. \tag{1.133}
$$

The expressions for the trace T and the determinant Δ in terms of ϵ, q, and h are somewhat lengthy and not enlightening. They are best evaluated for specific values of the parameters. The Oregonator also belongs to the class of pure activator–inhibitor systems. The autocatalytic species $HBrO_2$ is the activator and the oxidized catalyst the inhibitor.

1.4.9 Lengyel–Epstein Model

Next to the BZ reaction, the chlorite–iodide–malonic acid (CIMA) reaction has played a key role in nonlinear chemical dynamics. It belongs to the group of systematically designed chemical oscillating reactions pioneered by the Brandeis group [88, 110] and is among the very few reactions that can display transient oscillations in batch reactors. The CIMA reaction also played a crucial role in the first observation of stationary spatial chemical patterns. Most experimental studies of the CIMA reaction use starch as a visual indicator of the state of the system. Starch forms a deep blue complex with triiodide ion, I_3^-, and this color corresponds to the reduced state of the system, whereas the oxidized state has a yellow color. A major variant of the CIMA reaction is the simpler chlorine dioxide–iodine–malonic acid (CDIMA) reaction. Spectrophotometric studies show that after an initial induction period, where the chlorite, ClO_2^-, and iodide, I^-, are rapidly consumed to produce chlorine dioxide, ClO_2, and iodine, I_2, the dynamics of the CIMA reaction is given by that of the CDIMA reaction. Lengyel, Epstein, and Rabai proposed an empirical rate law description of the CDIMA reaction, which we refer to as the Lengyel–Epstein–Rabai (LRE) model [251, 252], consisting of the following reactions:

$$
MA + I_2 \longrightarrow IMA + I^- + H^+, \tag{1.134}
$$

$$
ClO_2 + I^- \longrightarrow ClO_2^- + \frac{1}{2}I_2, \tag{1.135}
$$

$$
ClO_2^- + 4\,I^- + 4\,H^+ \longrightarrow Cl^- + 2\,I_2 + 2\,H_2O, \tag{1.136}
$$

$$
S + I_2 + I^- \rightleftharpoons SI_3^-, \tag{1.137}
$$
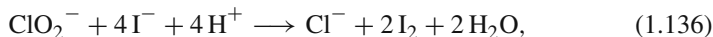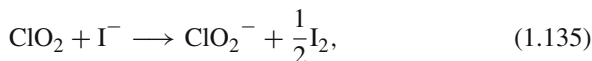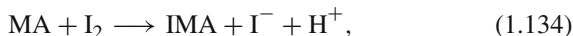
with reaction velocities given by

$$
v_1 = \frac{k_{1a}[MA][I_2]}{k_{1b} + [I_2]}, \tag{1.138}
$$

$$v_2 = k_2[\text{ClO}_2][\text{I}^-], \tag{1.139}$$

$$v_3 = k_{3a}[\text{ClO}_2{}^-][\text{I}^-][\text{H}^+] + \frac{k_{3b}[\text{ClO}_2{}^-][\text{I}_2][\text{I}^-]}{\alpha + [\text{I}^-]^2}, \tag{1.140}$$

$$v_4 = k_4[\text{S}][\text{I}_2][\text{I}^-] - k_4'[\text{SI}_3{}^-]. \tag{1.141}$$

Here MA stands for malonic acid, $\text{CH}_2(\text{COOH})_2$, IMA for iodomalonic acid, $\text{CHI}(\text{COOH})_2$, S is starch or another substrate that binds triiodide ion, and α is an empirical parameter. The independent variables are [MA], $[\text{I}_2]$, $[\text{ClO}_2]$, $[\text{I}^-]$, $[\text{ClO}_2{}^-]$, [S], and $[\text{SI}_3{}^-]$. The concentration of H^+ is considered to be constant, and Cl^- and IMA are inert products. In the absence of external feeds, the rate equations of the LER model for the CDIMA reaction in a well-stirred reactor are given by

$$\frac{d[\text{MA}]}{dt} = -v_1, \tag{1.142a}$$

$$\frac{d[\text{I}_2]}{dt} = -v_1 + \frac{1}{2}v_2 + 2v_3 - v_4, \tag{1.142b}$$

$$\frac{d[\text{ClO}_2]}{dt} = -v_2, \tag{1.142c}$$

$$\frac{d[\text{I}^-]}{dt} = v_1 - v_2 - 4v_3 - v_4, \tag{1.142d}$$

$$\frac{d[\text{ClO}_2{}^-]}{dt} = v_2 - v_3, \tag{1.142e}$$

$$\frac{d[\text{S}]}{dt} = -v_4, \tag{1.142f}$$

$$\frac{d[\text{SI}_3{}^-]}{dt} = v_4. \tag{1.142g}$$

Experimental observations show that $[\text{I}^-]$ and $[\text{ClO}_2{}^-]$ undergo much larger changes than the concentrations of the input species MA, ClO_2, and I_2. Lengyel and Epstein have simplified the LER model to reflect the behavior only of the iodide ion, U, and the chlorite ion, V [246, 247]:

$$\text{A} \longrightarrow \text{U}, \tag{1.143}$$

$$\text{U} \longrightarrow \text{V}, \tag{1.144}$$

$$4\,\text{U} + \text{V} \longrightarrow \text{D}, \tag{1.145}$$

$$\text{S} + \text{U} \rightleftharpoons \text{W}. \tag{1.146}$$

The rate equations are

$$\frac{d\rho_u}{dt} = k_1' - k_2'\rho_u - 4k_3'\frac{\rho_u\rho_v}{\alpha + \rho_u^2} - k_4'\rho_u + k_{-4}\rho_w, \tag{1.147a}$$

$$\frac{d\rho_v}{dt} = k_2'\rho_u - k_3'\frac{\rho_u\rho_v}{\alpha + \rho_u^2}, \tag{1.147b}$$

$$\frac{d\rho_w}{dt} = k_4'\rho_u - k_{-4}\rho_w, \tag{1.147c}$$

where W denotes iodide ion bound to the substrate. The rate constants are $k_1' = k_{1a}[MA]$, $k_2' = k_2[ClO_2]$, $k_3' = k_{3b}[I_2]$, and $k_4' = k_4[S][I_2]$. We have assumed that the substrate is present in large excess and that therefore [S] can be considered constant. Adding (1.147a) and (1.147c), we obtain

$$\frac{d}{dt}(\rho_u + \rho_w) = k_1' - k_2'\rho_u - 4k_3'\frac{\rho_u\rho_v}{\alpha + \rho_u^2}. \tag{1.148}$$

Assuming that the formation and dissociation of W is fast, we can eliminate ρ_w by setting its time derivative equal to zero and (1.147c) yields

$$\rho_w = \frac{k_4'}{k_{-4}}\rho_u. \tag{1.149}$$

Substituting this expression into (1.148), we find

$$\sigma\frac{d\rho_u}{dt} = k_1' - k_2'\rho_u - 4k_3'\frac{\rho_u\rho_v}{\alpha + \rho_u^2}, \tag{1.150}$$

where

$$\sigma = 1 + \frac{k_4'}{k_{-4}} = 1 + \frac{k_4}{k_{-4}}[S][I_2] = 1 + K[S][I_2]. \tag{1.151}$$

Here K is the association constant of the substrate–activator complex. Acceptable experimental values for σ lie in the range $1 \le \sigma < 1000$ [368]. Note that $\sigma = 1$ corresponds to no complexing agent. To nondimensionalize the rate equation for U and V, we set $\rho_u^* = \rho_u/\sqrt{\alpha}$, $\rho_v^* = k_3'\rho_v/k_2'\alpha$, and $t^* = k_2't$, and dropping the asterisk for notational convenience, we obtain

$$\sigma\frac{d\rho_u}{dt} = F_1(\rho_u, \rho_v) = a - \rho_u - 4\frac{\rho_u\rho_v}{1 + \rho_u^2}, \tag{1.152a}$$

$$\frac{d\rho_v}{dt} = F_2(\rho_u, \rho_v) = b\left(\rho_u - \frac{\rho_u\rho_v}{1 + \rho_u^2}\right). \tag{1.152b}$$

The parameters are given by

$$a = \frac{k_1'}{k_2'\sqrt{\alpha}}, \quad b = \frac{k_3'}{k_2'\sqrt{\alpha}}, \tag{1.153}$$

i.e., the constant a is proportional to $[CH_2COOH_2]/[ClO_2]$ and the constant b to $[I_2]/[ClO_2]$. We refer to (1.152) as the Lengyel–Epstein (LE) model.

The CDIMA reaction in a CSTR, described by the LE model, has only one steady state given by

$$\bar{\rho}_u = \frac{a}{5}, \quad \bar{\rho}_v = 1 + \frac{a^2}{25}. \tag{1.154}$$

Its stability is determined by the eigenvalues of the Jacobian matrix

$$\mathsf{J} = \begin{pmatrix} J_{11} & J_{12} \\ J_{21} & J_{22} \end{pmatrix} = \begin{pmatrix} A_{11}/\sigma & A_{12}/\sigma \\ A_{21} & A_{22} \end{pmatrix}. \tag{1.155}$$

Here

$$A_{11} = \left.\frac{\partial F_1}{\partial \rho_u}\right|_{(\bar{\rho}_u, \bar{\rho}_v)} = \frac{3a^2 - 125}{25 + a^2}, \tag{1.156a}$$

$$A_{12} = \left.\frac{\partial F_1}{\partial \rho_v}\right|_{(\bar{\rho}_u, \bar{\rho}_v)} = -\frac{20a}{25 + a^2}, \tag{1.156b}$$

$$A_{21} = \left.\frac{\partial F_2}{\partial \rho_u}\right|_{(\bar{\rho}_u, \bar{\rho}_v)} = b\frac{2a^2}{25 + a^2}, \tag{1.156c}$$

$$A_{22} = \left.\frac{\partial F_2}{\partial \rho_v}\right|_{(\bar{\rho}_u, \bar{\rho}_v)} = -b\frac{5a}{25 + a^2}. \tag{1.156d}$$

The steady state (1.154) cannot undergo a stationary bifurcation, since

$$\Delta = \frac{25ba}{\sigma(25 + a^2)} > 0 \tag{1.157}$$

for all parameter values. The condition for a Hopf bifurcation of the steady state (1.154), $T = 0$, yields

$$b_H = \frac{3a^2 - 125}{5a\sigma}. \tag{1.158}$$

Consequently, for $a > \sqrt{125/3}$ the unique steady state of the CDIMA reaction in a CSTR is stable for $b > b_H$, and for $b < b_H$ the reaction oscillates. The iodide ion is an activator, i.e., $A_{11} > 0$ for $a > a^\circ$, where

$$a^\circ = \sqrt{125/3}, \tag{1.159}$$

and the chlorite ion is the inhibitor, since $A_{22} < 0$ for all values of a and b.

To end our discussion of the LE model for the CDIMA reaction, we present an alternative, equivalent version of the rate equations used by some authors. Rescaling the dimensionless time in (1.152) by the dimensionless parameter σ, $t \to t/\sigma$, we obtain

$$\frac{d\rho_u}{dt} = a - \rho_u - 4\frac{\rho_u \rho_v}{1 + \rho_u^2}, \tag{1.160a}$$

$$\frac{d\rho_v}{dt} = \sigma b \left(\rho_u - \frac{\rho_u \rho_v}{1 + \rho_u^2} \right). \tag{1.160b}$$

Exercises

1.1 Show that a one-variable system (1.13) cannot oscillate.

1.2 Solve the kinetic equation (1.69) for the first Schlögl model. Confirm the results of the linear stability analysis for $\mu > 0$ and $\mu < 0$. Determine the stability of $\overline{\rho} = 0$ for the case of linear marginal stability $\mu = 0$.

1.3 *Cell-mediated immune surveillance.* The following model describes the interaction of tumor cells with immune cells, such as macrophages and killer cells:

$$\frac{d\rho}{dt} = a + \rho \left(1 - \frac{\rho}{K} \right) - b\frac{\rho}{1 + \rho}, \tag{1.161}$$

where ρ is the density of tumor cells per unit volume, a is the rate of conversion of healthy cells into tumor cells (usually a small number), K is the maximum number of cells per unit volume, and b is the density of killer cells. (All quantities have been nondimensionalized.) For most tissues K lies between 0.1 and 5. (a) Determine the steady-state tumor density $\overline{\rho}$ as a function of b, the density of killer cells, for fixed K, and $a = 0$, i.e., a vanishing mutation rate. Do your results depend on the value of K? (b) Determine the stability of the steady states and plot $\overline{\rho}$ vs b. Discuss any instabilities and possible medical consequences. (c) Give a qualitative discussion of the situation for $a \neq 0$.

1.4 Derive the kinetic equations for the following reaction scheme:

$$A + U \xrightarrow{k_1} 2U, \tag{1.162}$$

$$U + V \xrightarrow{k_2} 2V, \tag{1.163}$$

$$V \xrightarrow{k_3} D. \tag{1.164}$$

Find the steady states and determine their stability. How do your results change, if the following reaction step is added to the scheme:

$$2\,\mathrm{U} \xrightarrow{\epsilon} \mathrm{A} + \mathrm{U}. \tag{1.165}$$

Assume that the rate constant ϵ is small, $\epsilon \ll 1$.

1.5 Consider the following simple model for glycolysis:

$$\frac{d\rho_u}{dt} = -\rho_u + a\rho_v + \rho_u^2 \rho_v, \tag{1.166a}$$

$$\frac{d\rho_v}{dt} = b - a\rho_v - \rho_u^2 \rho_v. \tag{1.166b}$$

Here ρ_u and ρ_v are dimensionless concentrations, and a and b are positive parameters. Show that (1.166) displays a Hopf bifurcation in an appropriate region in parameter space.

1.6 The following equations,

$$\frac{d\rho_u}{dt} = 1 - \rho_u \rho_v^h, \tag{1.167a}$$

$$\frac{d\rho_v}{dt} = \alpha \rho_u \rho_v^h - \alpha \rho_v, \tag{1.167b}$$

have been proposed as another model of glycolytic oscillations. Here ρ_u and ρ_v are dimensionless concentrations, and α and h are positive parameters. The latter is known as the Hill constant. Consider the value of α to be a constant.

(a) Determine all acceptable steady states.
(b) Determine their stability as a function of h.
(c) Does the model display a Hopf bifurcation, i.e., oscillations? If so, what are the values of h for which oscillations occur?

1.7 Consider the following systems of equations which represent a simplified model of Rayleigh–Bénard convection:

$$\frac{dx}{dt} = \sigma(y - x), \tag{1.168a}$$

$$\frac{dy}{dt} = -xz + rx - y, \tag{1.168b}$$

$$\frac{dz}{dt} = xy - bz. \tag{1.168c}$$

The dimensionless variables x, y, and z do not correspond to concentrations and negative values are allowed. The constants σ, r, and b are positive. Determine the steady states of the system and their stability.

Chapter 2
Reactions and Transport: Diffusion, Inertia, and Subdiffusion

Particles, such as molecules, atoms, or ions, and individuals, such as cells or animals, move in space driven by various forces or cues. In particular, particles or individuals can move randomly, undergo velocity jump processes or spatial jump processes [333]. The steps of the random walk can be independent or correlated, unbiased or biased. The probability density function (PDF) for the jump length can decay rapidly or exhibit a heavy tail. Similarly, the PDF for the waiting time between successive jumps can decay rapidly or exhibit a heavy tail. We will discuss these various possibilities in detail in Chap. 3. Below we provide an introduction to three transport processes: standard diffusion, transport with inertia, and anomalous diffusion.

2.1 Reaction–Diffusion Equation

The classical and simplest model for spatial spread or dispersal is the diffusion equation or Fick's second law, which in spatially one-dimensional systems reads

$$\frac{\partial \rho}{\partial t} = D \frac{\partial^2 \rho}{\partial x^2}, \tag{2.1}$$

where D is the diffusion coefficient. As is well known and shown explicitly in Chap. 3, particles that perform a simple random walk or Brownian motion at the microscopic level display diffusive dispersal at the macroscopic level. The diffusion equation preserves positivity, and the fundamental solution of (2.1) with a point source at $x = 0$ and $t = 0$, $\rho(x, 0) = \delta(x)$, is given by

$$\rho(x, t) = \frac{1}{\sqrt{4\pi D t}} \exp\left(-\frac{x^2}{4Dt}\right), \qquad t > 0. \tag{2.2}$$

If the particles or individuals react or interact according to some rate law $F(\rho)$ and at the same time undergo diffusion, it is legitimate to combine the diffusion equation and the rate equation $\dot{\rho} = F(\rho)$ [178]. The result is the well-known *reaction–diffusion (RD) equation*:

$$\frac{\partial \rho}{\partial t} = D \frac{\partial^2 \rho}{\partial x^2} + F(\rho), \tag{2.3}$$

which provides a theoretical framework for the spatiotemporal dynamics not only of chemical systems but also of systems in other areas, such as biology [231, 264, 343, 393, 310], ecology [328], physics [11], and materials science [464]. In this monograph, we refer to (2.3) as the *standard reaction–diffusion equation* or simply as the reaction–diffusion equation. This equation preserves positivity, if the rate law F satisfies condition (1.2).

Besides the simple mathematical approach of combining the rate equation and the diffusion equation, two fundamental approaches exist to derive the reaction–diffusion equation (2.3), namely a phenomenological approach based on the law of conservation and a mesoscopic approach based on a description of the underlying random motion. While it is fairly straightforward to show that the standard reaction–diffusion equation preserves positivity, the problem is much harder, not to say intractable, for other reaction–transport equations. In this context, a mesoscopic approach has definite merit. If that approach is done correctly and accounts for all reaction and transport events that particles can undergo, then by construction the resulting evolution equation preserves positivity and represents a valid reaction–transport equation. For this reason, we prefer equations based on a solid mesoscopic foundation, see Chap. 3.

In the context of chemical systems, the type of reaction–transport equations we study in this monograph describe reactions in the activation-controlled or activation-limited regime. We do not consider the opposite regime of diffusion-controlled or diffusion-limited reactions. Diffusion-controlled reactions are very fast; a reactive event occurs as soon as the reactants encounter each other. The reaction rate is essentially given by the rate of transport of the reactants through the medium. In activation-controlled reactions, the reactants must overcome a substantial energy barrier after they encounter each other before a reactive event can occur. Crossing the energy barrier is the rate-limiting step for these reactions, and activation-controlled reactions are significantly slower than diffusion-controlled reactions. For the spatiotemporal dynamics of diffusion-limited reactions see for example [233, 56, 238, 255, 96, 361, 33].

2.1.1 Phenomenological Derivation of the Reaction–Diffusion Equation

Let S be an arbitrary surface enclosing a time-independent volume V. The general law of conservation for the particle density states that the rate of change of the amount of particles in V is due to the flow of particles across the surface S plus the net production of particles in the volume V:

$$\frac{\partial}{\partial t} \int_V \rho(\mathbf{x}, t) dV = - \int_S \mathbf{J} \cdot d\mathbf{S} + \int_V F(\rho, \mathbf{x}, t) dV, \qquad (2.4)$$

where $\rho(\mathbf{x}, t)$ represents the density of particles at $\mathbf{x}$ at time t, $\mathbf{J}$ the particle flux, and F the net rate of production of ρ. Application of the divergence theorem,

$$\int_S \mathbf{J} \cdot d\mathbf{S} = \int_V \boldsymbol{\nabla} \cdot \mathbf{J} dV, \qquad (2.5)$$

to (2.4) yields

$$\int_V dV \left[\frac{\partial \rho}{\partial t} + \boldsymbol{\nabla} \cdot \mathbf{J} - F \right] = 0. \qquad (2.6)$$

Since the integration volume is arbitrary, we obtain the conservation equation, or continuity equation, for ρ:

$$\frac{\partial \rho}{\partial t} = -\boldsymbol{\nabla} \cdot \mathbf{J} + F(\rho). \qquad (2.7)$$

The continuity equation (2.7) needs to be closed via a constitutive equation for the flux $\mathbf{J}$. If the transport process corresponds to classical diffusion, the constitutive equation is given by Fick's first law,

$$\mathbf{J} = -D\boldsymbol{\nabla}\rho. \qquad (2.8)$$

Substituting this expression for the flux in (2.7), we obtain

$$\frac{\partial \rho}{\partial t} = \boldsymbol{\nabla} \cdot (D\boldsymbol{\nabla}\rho) + F(\rho). \qquad (2.9)$$

If D is constant, (2.9) reduces to (2.3) in the one-dimensional case. In some models for insect populations, models for bacterial chemotaxis, or for animal grouping due to social aggregation, the diffusion coefficient can be an explicit function of the particle density or a function of other chemical components.

2.1.2 n-Variable Reaction–Diffusion Equations

The extension of (2.3) to n-variable systems is fairly straightforward:

$$\frac{\partial \boldsymbol{\rho}}{\partial t} = \frac{\partial}{\partial x} \left(\mathsf{D} \frac{\partial \boldsymbol{\rho}}{\partial x} \right) + \mathbf{F}(\boldsymbol{\rho}). \qquad (2.10)$$

In component form, (2.10) reads

$$\frac{\partial \rho_i}{\partial t} = \frac{\partial}{\partial x}\left(D_{ii}\frac{\partial \rho_i}{\partial x}\right) + \sum_{j, j \neq i}^{n} \frac{\partial}{\partial x}\left(D_{ij}\frac{\partial \rho_j}{\partial x}\right) + F_i(\boldsymbol{\rho}), \quad i = 1, \ldots, n. \quad (2.11)$$

The diagonal elements of D are called the "main-term" diffusion coefficients and the off-diagonal elements are called the "cross-term" diffusion coefficients or cross-diffusion terms. The cross-diffusion term $\frac{\partial}{\partial x}\left(D_{ij}\frac{\partial \rho_j}{\partial x}\right)$ links the gradient of species j to the flux of species i. If the cross-diffusion term is positive, $D_{ij} > 0$, then the flux of species i is directed toward decreasing values of the concentration of species j, whereas $D_{ij} < 0$ implies that the flux is directed toward increasing values of the concentration of species j. The cross-diffusion terms D_{ij} $(j \neq i)$ must go to zero as the concentration of species i goes to zero, $D_{ij}(\boldsymbol{\rho}) \to 0$ as $\rho_i \to 0$, since there can be no flux of species i if $\rho_i = 0$. For chemical systems, thermodynamics imposes the constraint that all eigenvalues of the diffusion matrix D must be real and positive, which implies that $\mathrm{tr}\,\mathsf{D} > 0$ and $\det \mathsf{D} > 0$ [454]. Some studies have investigated reaction–diffusion equations with constant cross-diffusion coefficients. Such equations represent approximations with a limited range of validity. Further, such equations do not preserve positivity [68, 69].

In this monograph, we consider only reaction–diffusion systems where the cross-diffusion terms are negligible, i.e., the diffusion matrix is a diagonal matrix, $\mathsf{D} = \mathrm{diag}(D_1, \ldots, D_n)$, and the diffusion coefficients D_i, which must be positive, do not depend on $\boldsymbol{\rho}$,

$$\frac{\partial \rho_i}{\partial t} = D_i \frac{\partial^2 \rho_i}{\partial x^2} + F_i(\boldsymbol{\rho}), \quad i = 1, \ldots, n. \quad (2.12)$$

2.2 Reaction–Transport Equations with Inertia

The diffusion equation has the well-known unrealistic feature that localized disturbances spread infinitely fast, though with heavy attenuation, through the system. To see this, consider the fundamental solution (2.2). No matter how small t and how large x, the density ρ will be nonzero, though exponentially small. In many cases, this pathology of the diffusion equation and the reaction–diffusion reaction has negligible consequences, and (2.1) and (2.3) have proven to be satisfactory descriptions in numerous circumstances and systems.

The origin of the unphysical behavior of the diffusion equation and the reaction–diffusion equation can be understood from three different viewpoints: (i) the mathematical viewpoint, (ii) the macroscopic or phenomenological viewpoint, and (iii) the mesoscopic viewpoint.

2.2.1 Hyperbolic Reaction–Diffusion Equations

From a mathematical viewpoint, the origin of the infinitely fast spreading of local disturbances in the diffusion equation can be traced to its parabolic character. This can be addressed in an ad hoc manner by adding a small term $\tau \partial_{tt} \rho$ to the diffusion equation or the reaction–diffusion equation to make it hyperbolic. From the diffusion equation (2.1) we obtain the telegraph equation, a damped wave equation,

$$\tau \frac{\partial^2 \rho}{\partial t^2} + \frac{\partial \rho}{\partial t} = D \frac{\partial^2 \rho}{\partial x^2}. \tag{2.13}$$

The fundamental solution of this equation with a point source at $x = 0$ and $t = 0$ is given by

$$\rho(x, t) = \begin{cases} \dfrac{1}{\mathcal{N}} \exp\left[-\dfrac{t}{2\tau}\right] I_0 \left[\dfrac{1}{\mathcal{N}} \sqrt{\xi}\right], & \text{for } |x| < \sqrt{\dfrac{D}{\tau}}\, t, \\ 0, & \text{otherwise,} \end{cases} \tag{2.14}$$

and converges to the solution (2.2) of the diffusion equation as $\tau \to 0$, see [494, p. 388]. Here I_0 is the modified Bessel function, $\xi = Dt^2/\tau - x^2$, and $\mathcal{N} = \sqrt{4D\tau}$. Equation (2.14) also shows explicitly that perturbations governed by the telegraph equation spread with a finite speed $\sqrt{D/\tau}$, as expected for a damped wave equation.

Adding the term $\tau \partial_{tt} \rho$ to (2.3), we obtain hyperbolic reaction–diffusion equations (HRDEs):

$$\tau \frac{\partial^2 \rho}{\partial t^2} + \frac{\partial \rho}{\partial t} = D \frac{\partial^2 \rho}{\partial x^2} + F(\rho). \tag{2.15}$$

This type of equation is also encountered in other areas, such as nonlinear waves, nucleation theory, and phase field models of phase transitions, where it is known as the damped nonlinear Klein–Gordon equation, see for example [165, 355, 366]. In the (singular) limit $\tau \to 0$, (2.15) goes to the reaction–diffusion equation (2.3). Front propagation in HRDEs has been studied analytically and numerically in [149, 150, 152, 151, 374]. The use of HRDEs in applications is problematic. Such equations are obtained indeed very much in an ad hoc manner for reacting and dispersing particle systems, and they can be derived neither from phenomenological thermodynamic equations nor from more microscopic equations, see below.

For n-variable systems, the HRDEs are given by, $i = 1, \ldots, n$,

$$\tau_i \frac{\partial^2 \rho_i}{\partial t^2} + \frac{\partial \rho_i}{\partial t} = D_i \frac{\partial^2 \rho_i}{\partial x^2} + F_i(\boldsymbol{\rho}). \tag{2.16}$$

2.2.2 Reaction-Cattaneo Systems and Reaction-Telegraph Equations

From a macroscopic or phenomenological viewpoint, the reaction–diffusion equation follows from the continuity equation

$$\frac{\partial \rho}{\partial t} = -\frac{\partial J}{\partial x} + F(\rho) \tag{2.17}$$

and the use of Fick's first law as the constitutive equation, see Sect. 2.1.1. Fick's first law implies that the flux adjusts instantaneously to the gradient of the density. This is physically unrealistic, and it gives rise to the pathological feature of infinitely fast spreading of local disturbances in the diffusion equation. Cattaneo and others, for a review see [222], have argued that the flux adjusts to the gradient with a small but nonzero relaxation time τ. Fick's first law should be replaced as the constitutive equation by the Cattaneo equation

$$\tau \frac{\partial J}{\partial t} + J = -D \frac{\partial \rho}{\partial x}. \tag{2.18}$$

We call the hyperbolic system (2.17) and (2.18) a *reaction-Cattaneo system*. Eu and Al-Ghoul have derived such systems from generalized hydrodynamic theory [9, 7, 8, 6]. Reaction-Cattaneo systems can also be obtained from extended irreversible thermodynamics [223], see for example [282]. If we differentiate (2.17) with respect to t and (2.18) with respect to x and eliminate mixed second derivatives, we obtain the so-called *reaction-telegraph equation*,

$$\tau \frac{\partial^2 \rho}{\partial t^2} + [1 - \tau F'(\rho)] \frac{\partial \rho}{\partial t} = D \frac{\partial^2 \rho}{\partial x^2} + F(\rho). \tag{2.19}$$

Remark 2.1 The reaction-telegraph equation can also be derived as the kinetic equation for a branching random evolution, see [101].

Remark 2.2 Nomenclature in this field is unfortunately not uniform, and some authors use the term hyperbolic reaction–diffusion equations for reaction-telegraph equations.

Note that the reaction-telegraph equation (2.19) differs from the ad hoc HRDE (2.15) by the additional term $-\tau F'(\rho)(\partial \rho / \partial t)$ on the left-hand side. It can be shown that solutions of (2.19) converge to solutions of the reaction–diffusion equation (2.3) as $\tau \to 0$ [494]. Traveling wave front solutions for the reaction-telegraph equation have been investigated by several authors [201, 176, 282, 291, 285, 136, 288, 137, 114, 116, 115, 117].

The hyperbolic systems derived from a mathematical or macroscopic viewpoint overcome the pathological feature of the reaction–diffusion equation, but they suffer from other drawbacks: (i) Hyperbolic equations typically do not preserve positivity.

Even if $\rho(x, 0) \geq 0$, the solution $\rho(x, t)$ of (2.19) will in general assume also negative values [178], which is unacceptable for a true density. (ii) In order to ensure the dissipative character of the reaction-telegraph equation (2.19), the damping coefficient $1 - \tau F'(\rho)$ must be positive, i.e.,

$$F'(\rho) < \frac{1}{\tau} \text{ for all } \rho. \tag{2.20}$$

This relation between the relaxation time τ of the flux and the time scale $1/F'(\rho)$ of the reaction appears to be a purely mathematical requirement. The following mesoscopic approach will shed light on the foundational problems of the reaction-Cattaneo system (2.17) and (2.18) and the reaction-telegraph equation (2.19) hinted at by points (i) and (ii).

For n-variable systems, the reaction-Cattaneo systems and reaction-telegraph equations read, $i = 1, \ldots, n$,

$$\frac{\partial \rho_i}{\partial t} = -\frac{\partial J_i}{\partial x} + F_i(\boldsymbol{\rho}), \tag{2.21}$$

$$\tau_i \frac{\partial J_i}{\partial t} + J_i = -D_i \frac{\partial \rho_i}{\partial x}, \tag{2.22}$$

and

$$\tau_i \frac{\partial^2 \rho_i}{\partial t^2} + \frac{\partial \rho_i}{\partial t} - \tau_i \sum_{j=1}^{n} \frac{\partial F_j}{\partial \rho_j} \frac{\partial \rho_j}{\partial t} = D_i \frac{\partial^2 \rho_i}{\partial x^2} + F_i(\boldsymbol{\rho}). \tag{2.23}$$

2.2.3 Persistent Random Walks and Reactions

From a mesoscopic viewpoint, the pathology of the diffusion equation can be traced to the lack of inertia of Brownian particles; their direction of motion in successive time intervals is uncorrelated. This lack of correlation has two consequences: (i) The particles move with infinite velocity. There is some probability, though exponentially small, that a dispersing particle will travel arbitrarily far from its current position in any small but nonzero amount of time. Clearly, this cannot be true for molecules or organisms. (ii) The motion of the dispersing individuals is unpredictable even on the smallest time scales. Again, this cannot be true, either for molecules or organisms. It is therefore desirable to adopt a model for dispersion that leads to more predictable motion with finite speed at smaller time scales and approaches diffusive motion on larger time scales. The natural choice is a *persistent random walk*, also known as a *correlated random walk*. It is the simplest velocity jump process and was introduced by Fürth [146] and further studied by Taylor [434] and Goldstein [163], as the simplest generalization of the ordinary random walk. In the persistent random walk the particles have a well-defined finite speed. However,

the average velocity of the particles vanishes, and no convective flow occurs in the system.

In the correlated or persistent random walk [474], a particle or individual takes steps of length Δx and duration Δt. The particle continues in its previous direction with probability $\alpha = 1 - \mu \Delta t$ and reverses direction with probability $\beta = \mu \Delta t$. In the continuum limit $\Delta x \to 0$ and $\Delta t \to 0$, such that

$$\lim_{\Delta x, \Delta t \to 0} \frac{\Delta x}{\Delta t} = \gamma = \text{constant}, \tag{2.24}$$

we obtain the following set of equations for the density of particles going to the right, $\rho_+(x, t)$, and the density of particles going to the left, $\rho_-(x, t)$:

$$\frac{\partial \rho_+}{\partial t} + \gamma \frac{\partial \rho_+}{\partial x} = \mu(\rho_- - \rho_+), \tag{2.25}$$

$$\frac{\partial \rho_-}{\partial t} - \gamma \frac{\partial \rho_-}{\partial x} = \mu(\rho_+ - \rho_-). \tag{2.26}$$

The particles travel with speed γ and turn with frequency μ. The persistent random walk is characterized by two parameters, in contrast to the ordinary random walk or Brownian motion, which is completely characterized by the diffusion coefficient D. The persistent random walk spans the whole range of dispersal, from ballistic motion, in the limit $\mu \to 0$, to diffusive motion, in the limit $\gamma \to \infty$, $\mu \to \infty$, such that $\lim \gamma^2/2\mu = D = \text{constant}$. The total density of the dispersing particles is given by

$$\rho(x, t) = \rho_+(x, t) + \rho_-(x, t), \tag{2.27}$$

and the flux J of particles is given by $J = \gamma j$, where the "flow" j is defined as

$$j(x, t) = \rho_+(x, t) - \rho_-(x, t). \tag{2.28}$$

Adding (2.25) and (2.26), we obtain the continuity equation

$$\frac{\partial \rho}{\partial t} + \gamma \frac{\partial j}{\partial x} = 0. \tag{2.29}$$

Subtracting (2.26) from (2.25), we recover the Cattaneo equation

$$\frac{\partial j}{\partial t} + \gamma \frac{\partial \rho}{\partial x} = -2\mu j. \tag{2.30}$$

Differentiating (2.29) with respect to t and (2.30) with respect to x and eliminating the mixed second derivatives, we obtain the telegraph equation

$$\tau \frac{\partial^2 \rho}{\partial t^2} + \frac{\partial \rho}{\partial t} = D \frac{\partial^2 \rho}{\partial x^2}, \qquad (2.31)$$

where

$$\tau = \frac{1}{2\mu} \qquad (2.32)$$

is the correlation time of the particle turning process, and

$$D = \frac{\gamma^2}{2\mu}. \qquad (2.33)$$

Brownian motion, or the diffusion equation, ceases to be a good model for dispersal at scales where particles or individuals have a well-defined velocity. In most physical or chemical applications, the limiting scale is determined by the mean free path. In liquids, the mean free path is a fraction of the molecular diameter, and persistence or inertia effects are negligible even on mesoscopic scales. Velocity is not a relevant variable in these situations, and the position of the particle is determined by many independent effects. Dispersal has therefore a strongly diffusive character, and reaction–diffusion equations are an appropriate description for chemical reactions in aqueous solutions. The persistent random walk provides a better description for particles dispersing in dilute gases, where the mean free path can be several orders of magnitude larger than the molecular diameter, depending on gas pressure. The McKean discrete velocity model for dilute gases is identical with a persistent random walk [273]. Turbulent diffusion and dispersal of animals, especially bacteria, are two other areas where the velocity of particles or organisms is well defined, and persistence effects are not negligible, on macroscopic scales. Section 10.6 of [303] presents the persistent random walk as a model for turbulent diffusion and discusses the inadequacy of the classical diffusion equation in this context. The persistent random walk also provides a better description for spatial spread in population dynamics than the often used diffusion equation [201, 195, 178]. Microorganisms and animals tend to continue moving in the same direction in successive time intervals. Velocity is well defined and persistence effects are important on macroscopic scales. In fact, Fürth [146] applied his theory to experiments on the motion of bacteria.

Besides these practical considerations, describing the motion of particles or individuals by a persistent random walk has several advantages from a theoretical viewpoint: (i) The persistent random walk is a generalization of Brownian motion; it contains the latter as a limiting case, see above. (ii) The persistent random walk overcomes the pathological feature of Brownian motion or the diffusion equation discussed above; it fulfills the physical requirement of bounded velocity. (iii) The persistent random walk provides a unified treatment that covers the whole range of transport, from the diffusive limit to the ballistic limit.

If the particles moving according to a persistent random walk react with each other, the evolution equations for the densities, (2.25) and (2.26), must be modified

to include a kinetic rate term. The contributions from different processes, such as reactions and transport, to the evolution of a system are additive, if all the processes are Markovian [178]. Since the persistent random walk is a Markovian process, it is legitimate to add kinetic terms to the transport equation for (ρ_+, ρ_-):

$$\frac{\partial \rho_+}{\partial t} + \gamma \frac{\partial \rho_+}{\partial x} = \mu(\rho_- - \rho_+) + F_+(\rho_+, \rho_-), \tag{2.34a}$$

$$\frac{\partial \rho_-}{\partial t} - \gamma \frac{\partial \rho_-}{\partial x} = \mu(\rho_+ - \rho_-) + F_-(\rho_+, \rho_-). \tag{2.34b}$$

Remark 2.3 If the state space is reduced from two variables, (ρ_+, ρ_-), to one variable, ρ, the process ceases to be Markovian. It is not legitimate to simply add a kinetic term to (2.31).

The problem arises as to how to "distribute" the kinetic term $F(\rho)$ of the reaction–diffusion equation to the left- and right-going densities ρ_+ and ρ_-. The choice most commonly made in the literature [201, 195, 178, 176, 177] is the so-called *isotropic reaction walk* (IRW):

$$F_+(\rho_+, \rho_-) = F_-(\rho_+, \rho_-) = \frac{1}{2} F(\rho). \tag{2.35}$$

This choice is based on the assumption that $F(\rho)$ is a source term for the particles, that the reaction does not depend on the direction of motion, and that new particles choose either direction with equal probability. With (2.35) we obtain from (2.34a) and (2.34b) the reaction-Cattaneo system

$$\frac{\partial \rho}{\partial t} + \gamma \frac{\partial j}{\partial x} = F(\rho), \tag{2.36}$$

$$\frac{\partial j}{\partial t} + \gamma \frac{\partial \rho}{\partial x} = -2\mu j. \tag{2.37}$$

Traveling waves for isotropic reaction walks have been studied in [201, 176]. However, isotropic reaction walks are unsound; they violate a basic principle of kinetics [178, 205, 204], namely that the rate of removal or death of particles of a given type must go to zero as the density of those particles goes to zero, see Sect. 1.1. Otherwise, the concentration of those particles can become negative, which is unphysical. We consider here a class of reaction random walks (RRWs) that are free from this drawback. The kinetic terms are based on the following assumptions: (i) The particles undergo a birth and death process with "fertilities" and "mortalities" that are independent of the direction of motion of the particles. (ii) The direction of "daughter" particles is correlated with that of the "mother" particle. The degree of correlation is given by κ. The value $\kappa = 1/2$ corresponds to no correlation, $\kappa = 1$ to

complete correlation, and $\kappa = 0$ to complete anticorrelation. In light of assumption
(i), it is appropriate to adopt the production–loss form for $F(\rho)$, see (1.3), (1.4), and
(1.5). Then

$$F_+(\rho_+, \rho_-) = [\kappa\rho_+ + (1-\kappa)\rho_-]f^+(\rho) - f^-(\rho)\rho_+, \qquad (2.38a)$$

$$F_-(\rho_+, \rho_-) = [(1-\kappa)\rho_+ + \kappa\rho_-]f^+(\rho) - f^-(\rho)\rho_-, \qquad (2.38b)$$

where $f^+(\rho)$ and $f^-(\rho)$ are defined by (1.5). Note that if $F^+(\rho)$ contains a constant term a, as occurs in the Brusselator, the Lengyel–Epstein model, and many
other chemical schemes, then $f^+(\rho)$ contains the term a/ρ. Other valid choices for
the kinetic terms are possible. A discussion of this aspect from the viewpoint of
chemical kinetics and population dynamics can be found in Chaps. 5 and 10.

For n-variable systems, the evolution equations for persistent random walks with
reaction read, $i = 1, \ldots, n$,

$$\frac{\partial\rho_{+,i}}{\partial t} + \gamma_i \frac{\partial\rho_{+,i}}{\partial x} = \mu_i \left(\rho_{-,i} - \rho_{+,i}\right) + F_{+,i}(\boldsymbol{\rho}_+, \boldsymbol{\rho}_-), \qquad (2.39a)$$

$$\frac{\partial\rho_{-,i}}{\partial t} - \gamma_i \frac{\partial\rho_{-,i}}{\partial x} = \mu_i \left(\rho_{+,i} - \rho_{-,i}\right) + F_{-,i}(\boldsymbol{\rho}_+, \boldsymbol{\rho}_-). \qquad (2.39b)$$

2.3 Reactions and Anomalous Diffusion

For a large variety of applications, simple Brownian motion or Fickian diffusion is
not a satisfactory model for spatial dispersal of particles or individuals. Physical,
chemical, biological, and ecological systems often display anomalous diffusion,
where the mean square displacement (MSD) of a particle does not grow linearly
with time:

$$\langle x(t)^2 \rangle \propto t^\gamma. \qquad (2.40)$$

If $0 < \gamma < 1$, the process is subdiffusive; if $\gamma > 1$, it is superdiffusive. Superdiffusion is encountered, for example, in turbulent fluids [407], in chaotic systems
[51], in rotating flows [418, 472], in oceanic gyres [44], for nanorods at viscous
interfaces [93], and for surfactant diffusion in living polymers [14]. Subdiffusion
is observed in disordered ionic chains [45], in porous systems [100], in amorphous
semiconductors [383, 174], in disordered materials [307], in subsurface hydrology
[43, 38, 23, 42, 382, 91], and for proteins and lipids in plasma membranes of various
cells [380, 477, 387], for mRNA molecules in *Escherichia coli* cells [162], and for
proteins in the nucleus [463].

Motor proteins can lead to superdiffusive transport of engulfed microbeads in
living eukaryotic cells with $\gamma = 1.47 \pm 0.07$ for short times, up to the order of

1 s, with a crossover to subdiffusive or ordinary diffusion at longer times [70]. A common cause of subdiffusive transport in living cells is macromolecular crowding, which generates an environment where diffusion is hindered by obstacles and traps. For example, in the cell cytoplasm diffusion processes with values of γ ranging from 0.5 to about 0.85, depending on the mass of the diffusing molecule, are observed [476]. Subdiffusive motion, $\gamma = 0.737 \pm 0.003$, was also observed for lipid granules in the cytoplasm of yeast cells [438]. The value of γ increased slightly to 0.755 ± 0.006, less subdiffusive behavior, when the actin filaments were disrupted.

Anomalous diffusion is often caused by memory effects and Lévy-type statistics [185, 53]. Specifically, superdiffusion is observed for random walks with heavy-tailed jump length distributions and subdiffusion for heavy-tailed waiting time distributions, see Sect. 3.4. The latter type of distribution can be caused by "traps" that have an infinite mean waiting time [185]. For reviews of anomalous diffusion see, e.g., [298, 299, 229].

2.3.1 Continuous-Time Random Walks

Anomalous diffusion is often modeled by a continuous-time random walk (CTRW) [304, 213, 298, 299, 102], though other approaches have been explored, such as stochastic switching generating superdiffusion [123], fractional Brownian motion [266, 258, 254], and generalized Langevin equations with a memory kernel [465–467]. In a CTRW, the length of a given jump and the waiting time between two successive jumps are random variables characterized by the jump probability distribution function (PDF) $\psi(x, t)$. For a more detailed discussion of CTRWs see Chap. 3. The spatial jump length PDF is given by $w(x) = \int_0^\infty \psi(x, t) \mathrm{d}t$ and the waiting time PDF by $\phi(t) = \int_{-\infty}^\infty \psi(x, t) \mathrm{d}x$. CTRWs can be characterized by the mean waiting time,

$$\overline{T} = \int_0^\infty t\phi(t)\mathrm{d}t, \tag{2.41}$$

and the second moment of the jump length PDF,

$$\sigma^2 = \int_{-\infty}^\infty x^2 w(x)\mathrm{d}x. \tag{2.42}$$

A CTRW can be described by the evolution equation for the probability density $p(x, t)$ of the particle being at site x at time t, given that it was at $x = 0$ at $t = 0$ [381]:

$$p(x, t) = \delta(x)\Psi(t) + \int_0^\infty \int_{-\infty}^\infty \psi(x - x', t - t')p(x', t')\mathrm{d}x'\mathrm{d}t', \tag{2.43}$$

where $\Psi(t)$ is the survival probability given by

$$\Psi(t) = 1 - \int_0^t \phi(t')dt'. \tag{2.44}$$

The Laplace transform of a function $f(x, t)$ is denoted either by $\mathcal{L}[f(x, t)] = \int_0^\infty dt f(x, t) \exp(-st)$ or by $\hat{f}(x, s)$. Similarly the Fourier transform of a function $f(x, t)$ is denoted either by $\mathcal{F}[f(x, t)] = \int_{-\infty}^\infty dx f(x, t) \exp(ikx)$ or by $\tilde{f}(k, t)$. Equation (2.43) can be solved in Laplace–Fourier space,

$$\hat{\tilde{p}}(k, s) = \frac{1 - \hat{\phi}(s)}{s} \frac{\tilde{p}_0(k)}{1 - \hat{\tilde{\psi}}(k, s)}, \tag{2.45}$$

where $\tilde{p}_0(k) = 1$ is the Fourier transform of the initial condition $p_0(x) = \delta(x)$. We consider the large-scale, long-time limit of CTRWs with independent jump length and waiting time PDFs, i.e., $\psi(x, t) = w(x)\phi(t)$. If the waiting time PDF does not have heavy tails, then the mean waiting time $\overline{T}$ is finite, and the long-time limit corresponds to

$$\hat{\phi}(s) \to 1 - \overline{T}s, \text{ as } s \to 0. \tag{2.46}$$

If the CTRW also has a short-range jump length PDF $w(x)$, then the variance σ^2 is finite, and the large-scale limit corresponds to

$$\tilde{w}(k) \to 1 - \frac{\sigma^2 k^2}{2}, \text{ as } k \to 0. \tag{2.47}$$

This results in

$$\hat{\tilde{p}}(k, s) = \frac{\tilde{p}_0(k)}{s + Dk^2}, \tag{2.48}$$

with $D \equiv \sigma^2/(2\overline{T})$, or

$$\left(s + Dk^2\right) \hat{\tilde{p}}(k, s) = \tilde{p}_0(k). \tag{2.49}$$

Inverse Laplace and Fourier transforming (2.49), we find that $p(x, t)$ obeys the diffusion equation (2.1) by making use of the fact that

$$\mathcal{F}\left[\frac{\partial^2 p(x, t)}{\partial x^2}\right] = -k^2 \tilde{p}(k, t) \tag{2.50}$$

and that

$$\mathcal{L}\left[\frac{\partial p(x,t)}{\partial t}\right] = s\hat{p}(x,s) - p_0(x). \tag{2.51}$$

CTRWs display subdiffusive behavior if the variance of the jump length PDF remains finite, but the waiting time PDF is heavy-tailed, such that the mean waiting time $\overline{T}$ is infinite. An example is a waiting time PDF derived from a Mittag–Leffler function for the survival probability, $\Psi(t) = E_\gamma(-t^\gamma)$ with $0 < \gamma < 1$ [381]. The asymptotic behavior of a heavy-tailed waiting time PDF is given by $\phi(t) \sim t^{-(1+\gamma)}$ as $t \to \infty$. Consequently, the long-time limit corresponds to

$$\hat{\phi}(s) \to 1 - (\tau_0 s)^\gamma, \quad \text{as } s \to 0, \tag{2.52}$$

where τ_0 is a parameter with units of time. For this type of CTRW, the long-time, large-scale limit of the evolution equation in Fourier–Laplace space reads

$$\hat{\tilde{p}}(k,s) = \frac{\tilde{p}_0(k)}{s + D_\gamma s^{1-\gamma} k^2}, \tag{2.53}$$

where

$$D_\gamma \equiv \frac{\sigma^2}{2\tau_0^\gamma} \tag{2.54}$$

is a generalized diffusion constant. To inverse Laplace transform this equation, we exploit the fact that the Grünwald–Letnikov fractional derivative, defined for $0 < p < 1$ by [353],

$$^{\mathrm{GL}}\mathcal{D}_t^p f(t) \equiv \lim_{\substack{h \to 0 \\ nh=t}} h^{-p} \sum_{r=0}^{n} (-1)^r \binom{p}{r} f(t - rh), \tag{2.55}$$

has the Laplace transform [353]:

$$\mathcal{L}\left[^{\mathrm{GL}}\mathcal{D}_t^p f(t)\right] = s^p \hat{f}(s). \tag{2.56}$$

Consequently, inverse Laplace and Fourier transforming (2.53) we find that $p(x,t)$ obeys the fractional diffusion equation

$$\frac{\partial p}{\partial t} = D_\gamma \, ^{\mathrm{GL}}\mathcal{D}_t^{1-\gamma} \frac{\partial^2 p(x,t)}{\partial x^2}. \tag{2.57}$$

Working with definition (2.55) is not very convenient. For sufficiently smooth functions $f(t)$, the Grünwald–Letnikov fractional derivative is equivalent to the Riemann–Liouville fractional derivative [353, p. 75]. The latter is defined by

$$\mathcal{D}_t^{1-\gamma} f(t) = \frac{1}{\Gamma(\gamma)} \frac{\partial}{\partial t} \int_0^t \frac{f(t')}{(t - t')^{1-\gamma}} dt', \tag{2.58}$$

for $0 < \gamma < 1$, and the fractional diffusion equation reads

$$\frac{\partial p}{\partial t} = D_\gamma \, \mathcal{D}_t^{1-\gamma} \frac{\partial^2 p(x, t)}{\partial x^2}. \tag{2.59}$$

For the mean square displacement we obtain

$$\langle x^2(t) \rangle = \frac{2}{\Gamma(1 + \gamma)} D_\gamma t^\gamma, \tag{2.60}$$

confirming that CTRWs with short-range jump length PDFs and heavy-tailed waiting time PDFs display subdiffusion. The solution of the fractional diffusion equation (2.59) can be written in terms of the Fox H-function [298]:

$$p(x, t) = \frac{1}{\sqrt{4\pi D_\gamma t^\gamma}} H_{1,2}^{2,0} \left[\frac{x^2}{4 D_\gamma t^\gamma} \,\middle|\, \begin{array}{c} (1 - \gamma/2, 2) \\ (0, 1), (1/2, 1) \end{array} \right]. \tag{2.61}$$

The mean density $\rho(x, t)$ of a system of independent particles that undergo a CTRW obeys the same equation as the PDF $p(x, t)$, which can be written in the form of a generalized Master equation. The Montroll–Weiss equation (2.45) can be rewritten for $\hat{\tilde{\rho}}(k, s)$ and rearranged as

$$s \hat{\tilde{\rho}}(k, s) - \tilde{\rho}_0(k) = \frac{s}{1 - \hat{\phi}(s)} \left(\hat{\tilde{\psi}}(k, s) - \hat{\phi}(s) \right) \hat{\tilde{\rho}}(k, s), \tag{2.62}$$

where the left-hand side is the Fourier–Laplace transform of the derivative $\partial \rho / \partial t$. If we apply the Fourier–Laplace transform inversion, then we obtain an integro-differential equation, the generalized Master equation,

$$\frac{\partial \rho}{\partial t} = \int_0^t \int_{\mathbb{R}} K(x - x', t - t') \rho(z, t') dx' dt', \tag{2.63}$$

where the kernel $K(x, t)$ is defined in terms of its Fourier–Laplace transform

$$\hat{\tilde{K}}(k, s) = \frac{s}{1 - \hat{\phi}(s)} \left(\hat{\tilde{\psi}}(k, s) - \hat{\phi}(s) \right). \tag{2.64}$$

In the uncoupled case, $\psi(x, t) = w(x)\phi(t)$, for which $\hat{\tilde{\psi}}(k, s) = \tilde{w}(k)\hat{\phi}(s)$, the generalized Master equation takes the form

$$\frac{\partial \rho}{\partial t} = \int_0^t K(t - t') \left[\int_{\mathbb{R}} \rho(x - x', t')w(x')dx' - \rho(x, t') \right] dt', \qquad (2.65)$$

where the memory kernel $K(t)$ is defined in terms of its Laplace transform

$$\hat{K}(s) = \frac{s\hat{\phi}(s)}{1 - \hat{\phi}(s)}. \qquad (2.66)$$

2.3.2 Reaction–Subdiffusion Equations

As shown above, the standard diffusion equation (2.1) has a fractional diffusion equation (2.59) as its analog in the subdiffusive case. As in the case of reaction–transport equation with inertia, see Sect. 2.2, the question arises how to combine reactions and subdiffusion in the activation-controlled regime. (For a discussion of the subdiffusion-limited case, which is outside the scope of this monograph as mentioned on page 34, see for example [491–493, 369, 391, 392, 389, 409, 410, 390, 411, 203, 187].) In some schemes, [188, 189, 186, 187], reactions terms are simply added to the fractional diffusion equation, in a manner similar to the ad hoc HRDEs (2.16), assuming at the outset that the effects of subdiffusion and reactions are separable as in the standard reaction–diffusion (2.11). However, it is easy to show that already for the simple case of linear decay, U $\xrightarrow{k}$ P,

$$\frac{\partial \rho}{\partial t} = D_\gamma \, \mathcal{D}_t^{1-\gamma} \frac{\partial^2 \rho(x, t)}{\partial x^2} - k\rho, \qquad (2.67)$$

this approach cannot be correct. Equation (2.67) does not preserve positivity [187].

The memory kernel in (2.59), recall that $\mathcal{D}_t^{1-\gamma}$ represents a nonlocal-in-time integral operator, is a clear indication that subdiffusive transport is non-Markovian. Incorporating kinetic terms into a non-Markovian transport equation requires great care and is best carried out at the mesoscopic level. We show in Sect. 3.4 how to proceed directly at the level of the mesoscopic balance equations for non-Markovian CTRWs. Here we pursue a different approach. As stated above, if all processes are Markovian, then contributions from different processes are indeed separable and simply additive. As is well known, processes often become Markovian if a sufficiently large and appropriate state space is chosen. For the case of reactions and subdiffusion, the goal of a Markovian description can be achieved by taking the age structure of the system explicitly into account as done by Vlad and Ross [460, 461]. This approach is equivalent to Model B, see Sect. 3.4.

Let $\xi_i(x, t, \tau)$ be the density of particles of type i, $i = 1, \ldots, n$, whose waiting time (age) at position x and time t lies in the range $(\tau, \tau + d\tau)$. The concentration of species i, $\rho_i(x, t)$, at position x and time t, is then given by

$$\rho_i(x, t) = \int_0^\infty \xi_i(x, t, \tau) d\tau. \tag{2.68}$$

In terms of chemical and related systems, reactions typically create and destroy particles. In terms of ecological systems and populations dynamics, individuals are born and die. In other words, kinetic events affect the waiting times of particles. We assume that new particles are created with zero age. The same holds for newborn individuals. Our assumption implies that all processes resulting in the arrival of a particle or individual at a given site x are treated equally. We do not distinguish between arrival via a jump to x from another site x' or arrival by a reactive or birth event at x. Any arrival event sets the waiting time τ at x equal to zero. We assume that locally the reactions obey classical kinetic laws, as is the case in porous media for instance, and that the local kinetics of particles or individuals can be written in production–loss form, $F_i(\boldsymbol{\rho}) = F_i^+(\boldsymbol{\rho}) - F_i^-(\boldsymbol{\rho})$, see (1.3). As discussed in Sect. 1.1, $F_i^-(\boldsymbol{\rho}) \to 0$ as $\rho_i \to 0$. To ensure the nonnegativity of the age-dependent densities $\xi_i(x, t, \tau)$, it is sufficient to require that $F_i^-(\boldsymbol{\rho})/\rho_i$ remains bounded from above as $\rho_i \to 0$. Define $W_i(x' \to x, \tau)$ to be the rate at which an individual of species i with an age between τ and $\tau + d\tau$ moves from position x' to x. The evolution of $\xi_i(x, t, \tau)$ is governed by the balance equation [461]

$$\left(\frac{\partial}{\partial t} + \frac{\partial}{\partial \tau} \right) \xi_i(x, t, \tau) = - \xi_i(x, t, \tau) \int_{x'} W_i(x \to x', \tau) dx'$$
$$- \frac{\xi_i(x, t, \tau)}{\rho_i(x, t)} F_i^-(\boldsymbol{\rho}(x, t)), \tag{2.69}$$

with the boundary condition

$$\xi_i(x, t, \tau = 0) = F_i^+(\boldsymbol{\rho}(x, t)) + \int_{x'} \int_{\tau'} \xi_i(x', t, \tau') \times W_i(x' \to x, \tau') dx' d\tau'. \tag{2.70}$$

This boundary condition implies that entities with zero age at a particular position are either created there with a rate $F_i^+(\boldsymbol{\rho}(x, t))$ or arrive there from other positions, as discussed above.

Let the jump PDF of the CTRW of species i be $\psi_i(x \to x', \tau)$, and

$$\Psi_i(x, \tau) = \int_{x'} \int_\tau^\infty \psi_i(x \to x', \tau') dx' d\tau' \tag{2.71}$$

be the survival probability of a particle of type i at position x. The connection between $W_i(x \to x', \tau')$ and $\psi_i(x \to x', \tau)$ is given by the following relation [460]:

$$\psi_i(x \to x', \tau) = \Psi_i(x, \tau) W_i(x \to x', \tau). \tag{2.72}$$

The solution to (2.69) with boundary condition (2.70) reads [461]

$$Z_i(x, t) = F_i^+(\rho(x, t)) + \int_0^t \int_{x'} Z_i(x', t - \tau') \psi_i(x' \to x, \tau')$$

$$\times \exp\left[-\int_{t-\tau'}^t \frac{F_i^-(\rho(x', t''))}{\rho_i(x', t'')} dt''\right] dx' d\tau'$$

$$+ \int_t^\infty \int_{x'} \xi_i(x', t = 0, \tau' - t) \frac{\psi_i(x' \to x, \tau')}{\Psi_i(x', \tau' - t)}$$

$$\times \exp\left[-\int_0^t \frac{F_i^-(\rho(x', t''))}{\rho_i(x', t'')} dt''\right] dx' d\tau', \qquad (2.73)$$

$$\rho_i(x, t) = \int_0^t \Psi_i(x, \tau) Z_i(x, t - \tau) \exp\left[-\int_{t-\tau}^t \frac{F_i^-(\rho(x, t''))}{\rho_i(x, t'')} dt''\right] d\tau$$

$$+ \int_t^\infty \xi_i(x, t = 0, \tau - t) \frac{\Psi_i(x, \tau)}{\Psi_i(x, \tau - t)}$$

$$\times \exp\left[-\int_0^t \frac{F_i^-(\rho(x, t''))}{\rho_i(x, t'')} dt''\right] d\tau, \qquad (2.74)$$

where $Z_i(x, t)$ is defined to be the zero-age density, $Z_i(x, t) \equiv \xi_i(x, t, \tau = 0)$. Equations (2.73) and (2.74) extend the usual linear CTRW formalism to include general nonlinear birth and death processes.

In the following, we consider the usual case of spatially homogeneous CTRWs with independent jump and waiting time PDFs, i.e., $\psi_i(x \to x', \tau) = \psi_i(x' - x, \tau) = w_i(x' - x)\phi_i(\tau)$. The survival probability then does not depend on position, $\Psi_i(x, \tau) = \Psi_i(\tau)$. We choose the initial condition as $\xi_i(x, t = 0, \tau) = \rho_i(x, 0)\delta(\tau)$, i.e., at time zero all individuals are at the beginning of a waiting period. To obtain kinetic equations for reaction–transport systems with anomalous diffusion, we need to take the long-time and the large-scale limit, i.e., $\tilde{w}_i(k) \to 1 - \sigma_i^2 k^2/2$, see (2.47). As shown in [484], in this limit (2.73) and (2.74) lead to

$$\frac{\partial \rho_i(x, t)}{\partial t} = F_i^+(\rho(x, t)) - F_i^-(\rho(x, t))$$

$$+ \frac{\sigma_i^2}{2} \nabla^2 \left\{ \int_0^t \phi_i(t - t') Z_i(x, t') \exp\left[-\int_{t'}^t \frac{F_i^-(\rho(x, t''))}{\rho_i(x, t'')} dt''\right] dt' \right\},$$

$$(2.75)$$

$$\rho_i(x,t) = \int_0^t \Psi_i(t-t')Z_i(x,t')\exp\left[-\int_{t'}^t \frac{F_i^-(\rho(x,t''))}{\rho_i(x,t'')}dt''\right]dt'. \quad (2.76)$$

We need to eliminate $Z_i(x,t)$ from the system (2.75) and (2.76). We rewrite (2.76) as

$$\rho_i(x,t)\exp\left[\int_0^t \frac{F_i^-(\rho(x,t''))}{\rho_i(x,t'')}dt''\right]$$
$$= \int_0^t \Psi_i(t-t')Z_i(x,t')\exp\left[\int_0^{t'} \frac{F_i^-(\rho(x,t''))}{\rho_i(x,t'')}dt''\right]dt'. \quad (2.77)$$

We Laplace transform this equation, use $\hat{\Psi}(s) = [1 - \hat{\phi}(s)]/s$, and obtain

$$\frac{s\hat{\phi}_i(s)}{1-\hat{\phi}_i(s)}\mathcal{L}\left[\rho_i(x,t)\exp\left(\int_0^t \frac{F_i^-(\rho(x,t''))}{\rho_i(x,t'')}dt''\right)\right]$$
$$= \hat{\phi}_i(s)\mathcal{L}\left[Z_i(x,t')\exp\left(\int_0^{t'} \frac{F_i^-(\rho(x,t''))}{\rho_i(x,t'')}dt''\right)\right]. \quad (2.78)$$

The inverse Laplace transform of (2.78) leads to

$$\int_0^t K_i(t-t')\rho_i(x,t')\exp\left[\int_0^{t'} \frac{F_i^-(\rho(x,t''))}{\rho_i(x,t'')}dt''\right]dt'$$
$$= \int_0^t \phi_i(t-t')Z_i(x,t')\exp\left[\int_0^{t'} \frac{F_i^-(\rho(x,t''))}{\rho_i(x,t'')}dt''\right]dt'. \quad (2.79)$$

We define the memory kernel $K_i(t)$ in terms of its Laplace transform as in (2.66):

$$\hat{K}_i(s) \equiv \frac{s\hat{\phi}_i(s)}{1-\hat{\phi}_i(s)}. \quad (2.80)$$

Equation (2.75) can be rewritten as

$$\frac{\partial\rho_i(x,t)}{\partial t} = F_i^+(\rho(x,t)) - F_i^-(\rho(x,t))$$
$$+ \frac{\sigma_i^2}{2}\nabla^2\left\{\exp\left[-\int_0^t \frac{F_i^-(\rho(x,t''))}{\rho_i(x,t'')}dt''\right]\right.$$
$$\left.\times \int_0^t \phi_i(t-t')Z_i(x,t')\exp\left[\int_0^{t'} \frac{F_i^-(\rho(x,t''))}{\rho_i(x,t'')}dt''\right]dt'\right\} \quad (2.81)$$

We substitute (2.79) into (2.81) and obtain

$$
\frac{\partial \rho_i(x,t)}{\partial t} = F_i^+(\boldsymbol{\rho}(x,t)) - F_i^-(\boldsymbol{\rho}(x,t))
$$
$$
+ \frac{\sigma_i^2}{2} \nabla^2 \left\{ \int_0^t K_i(t-t') \rho_i(x,t') \exp\left[-\int_{t'}^t \frac{F_i^-(\boldsymbol{\rho}(x,t''))}{\rho_i(x,t'')} dt'' \right] dt' \right\},
$$
$$
(2.82)
$$

which is the generalized reaction–diffusion equation for reacting systems with anomalous diffusion [484]. The reaction terms and the Laplacian operator in (2.82) are reminiscent of the standard reaction–diffusion equation (2.12). However, unlike in a standard reaction–diffusion equation, the Laplacian acts on a nonlocal memory term captured by a time integral. The presence of both the kernel $K_i(t-t')$, related to the waiting time PDF of the CTRW, and the death rate $F_i^-(\boldsymbol{\rho}(x,t))$ in the memory term indicates that the effects of reaction and subdiffusion are, indeed, not separable.

Remark 2.4 In the derivation of the generalized reaction–diffusion equation (2.82) we do not explicitly refer to the particular form of the waiting time PDF. Equation (2.82) is valid for *arbitrary* waiting time PDFs $\phi_i(t)$ and has much wider applicability than subdiffusive transport.

Remark 2.5 It is easy to see that (2.82) simplifies to a standard reaction–diffusion system if the CTRW is Markovian, i.e., the waiting times are exponentially distributed, $\phi_i(t) = (1/\tau_{0,i})e^{-t/\tau_{0,i}}$. In this case $\hat{K}_i(s) = 1/\tau_{0,i}$, and therefore, $K_i(t) = \delta(t)/\tau_{0,i}$.

Remark 2.6 In the derivation of (2.82) we have assumed that the spatial jump length PDF $\tilde{w}(k)$ is of the form $\tilde{w}(k) = 1 - \sigma^2 k^2/2$. It is straightforward to extend the derivation to the case of long-range jumps or Lévy flights by choosing $\tilde{w}(k) = 1 - \sigma^\alpha |k|^\alpha /2$, $1 < \alpha < 2$, see Chap. 3, and to the case of coupled jump length and waiting time PDFs.

The generalized reaction–diffusion equation (2.82) can be written in a form using fractional derivatives for subdiffusive transport, where the waiting PDF of species i is given in Laplace space by (2.52), $\hat{\phi}_i(s) \to 1 - (\tau_{0,i}s)^{\gamma_i}$. In that case

$$
\hat{K}_i(s) = \frac{s\hat{\phi}_i(s)}{1 - \hat{\phi}_i(s)} \simeq \tau_{0,i}^{-\gamma_i} s^{1-\gamma_i}, \qquad (2.83)
$$

and (2.78) reads

$$\tau_{0,i}^{-\gamma_i} s^{1-\gamma_i} \mathcal{L}\left[\rho_i(x,t)\exp\left(\int_0^t \frac{F_i^-(\boldsymbol{\rho}(x,t''))}{\rho_i(x,t'')}dt''\right)\right]$$

$$= \hat{\phi}_i(s)\mathcal{L}\left[Z_i(x,t')\exp\left(\int_0^{t'} \frac{F_i^-(\boldsymbol{\rho}(x,t''))}{\rho_i(x,t'')}dt''\right)\right]. \quad (2.84)$$

We inverse Laplace transform (2.84), using (2.56) and the equivalence of the Grünwald–Letnikov and Riemann–Liouville fractional derivatives, to obtain

$$\tau_{0,i}^{-\gamma_i}\mathcal{D}_t^{1-\gamma_i}\left(\rho_i(x,t)\exp\left[\int_0^t \frac{F_i^-(\boldsymbol{\rho}(x,t''))}{\rho_i(x,t'')}dt''\right]\right)$$

$$= \int_0^t \phi_i(t-t')Z_i(x,t')\exp\left[\int_0^{t'} \frac{F_i^-(\boldsymbol{\rho}(x,t''))}{\rho_i(x,t'')}dt''\right]dt'. \quad (2.85)$$

We substitute (2.85) into (2.81) and find [485]

$$\frac{\partial \rho_i(x,t)}{\partial t} = F_i^+(\boldsymbol{\rho}(x,t)) - F_i^-(\boldsymbol{\rho}(x,t))$$

$$+ D_{i;\gamma_i}\nabla^2\left\{\exp\left[-\int_0^t \frac{F_i^-(\boldsymbol{\rho}(x,t''))}{\rho_i(x,t'')}dt''\right]\right.$$

$$\left.\times \mathcal{D}_t^{1-\gamma_i}\left(\rho_i(x,t)\exp\left[\int_0^t \frac{F_i^-(\boldsymbol{\rho}(x,t''))}{\rho_i(x,t'')}dt''\right]\right)\right\}. \quad (2.86)$$

Exercises

2.1 Consider (2.1) with $\rho(x,0) = \delta(x)$. Define

$$\langle x(t)^m\rangle \equiv \frac{\int_{-\infty}^{\infty} x^m \rho(x,t)dx}{\int_{-\infty}^{\infty} \rho(x,t)dx}. \quad (2.87)$$

Obtain evolution equations for $\langle x(t)\rangle$ and $\langle x(t)^2\rangle$ and solve them.

2.2 Solve (2.1) with $\rho(x,0) = \delta(x)$ on the interval $[0, L]$ with no-flux boundary conditions, i.e., $(\partial\rho/\partial x)(0) = (\partial\rho/\partial x)(L) = 0$.

2.3 Solve the RD equation (2.3) for the pure death process $F(\rho) = -r\rho$ with $\rho(x,0) = \delta(x)$ on $(-\infty, \infty)$.

2.4 Consider the nonlinear diffusion equation

$$\frac{\partial \rho}{\partial t} = D \frac{\partial}{\partial x} \left[\left(\frac{\rho}{\rho_0} \right)^n \frac{\partial \rho}{\partial x} \right] \tag{2.88}$$

on $(-\infty, \infty)$ with $\rho(x, 0) = \delta(x)$, where D and ρ_0 are positive constants.

(a) Verify that

$$\rho(x, t) = \begin{cases} \dfrac{\rho_0}{A(t)} \left[1 - \left(\dfrac{x}{cA(t)} \right)^2 \right]^{1/n}, & |x| \leq cA(t), \\ 0, & |x| > cA(t), \end{cases} \tag{2.89}$$

where

$$A(t) = \left(\frac{t}{t_0} \right)^{\frac{1}{2+n}}, \quad c = \frac{\Gamma\left(\frac{1}{n} + \frac{3}{2} \right)}{\left[\pi^{1/2} \rho_0 \Gamma\left(\frac{1}{n} + 1 \right) \right]}, \quad t_0 = \frac{c^2 n}{2D(n + 2)}. \tag{2.90}$$

Here Γ is the Gamma function.

(b) Determine $\langle x(t) \rangle$ and $\langle x(t)^2 \rangle$.

Chapter 3
Random Walks and Mesoscopic Reaction–Transport Equations

As discussed in Sect. 2.1, the standard reaction–diffusion equation for the particle density $\rho(\mathbf{x}, t)$ has the form

$$\frac{\partial \rho}{\partial t} = D\Delta\rho + F(\rho), \qquad \mathbf{x} \in \mathbb{R}^3. \tag{3.1}$$

This equation is an example of a *macroscopic* reaction–transport equation that can be obtained in the long-time large-scale limit of *mesoscopic* equations. Recall that the *mesoscopic* approach is based on the idea that one can introduce mean-field equations for the particle density involving a detailed description of the movement of particles on the *microscopic* level. At the same time, random fluctuations around the mean behavior can be neglected due to a large number of individual particles. For example, we can obtain (3.1) from the mesoscopic integro-differential equation

$$\frac{\partial \rho}{\partial t} = \lambda \int_{\mathbb{R}^3} \rho(\mathbf{x} - \mathbf{z}, t) w(\mathbf{z}) d\mathbf{z} - \lambda\rho(\mathbf{x}, t) + F(\rho), \tag{3.2}$$

where λ is the intensity of particle jumps and $w(\mathbf{z})$ is the long-distance dispersal kernel. This equation arises in population theory, where the dispersal of individuals leads to population spread in space and invasion into new territories. The reaction–diffusion equation (3.1) can also be obtained from the mesoscopic balance equations

$$\rho(\mathbf{x}, t) = \rho(\mathbf{x}, 0)\Psi(t) + \int_0^t j(\mathbf{x}, t - \tau)\Psi(\tau)d\tau, \tag{3.3a}$$

$$j(\mathbf{x}, t) = F(\rho) + \int_{\mathbb{R}^3} \rho(\mathbf{x} - \mathbf{z}, 0)\psi(\mathbf{z}, t)d\mathbf{z} +$$

$$+ \int_0^t \int_{\mathbb{R}^3} j(\mathbf{x} - \mathbf{z}, t - \tau)\psi(\mathbf{z}, \tau)d\mathbf{z}d\tau. \tag{3.3b}$$

These are the mean-field equations for the density of particles that follow a continuous-time random walk (CTRW). Each random step of a particle is character-ized by a waiting time and a jump length, which are distributed according to the joint

probability density function (PDF) $\psi(\mathbf{z}, \tau)$. Here $j(\mathbf{x}, t)$ is the density of particles that are either produced with rate $F(\rho)$ at point $\mathbf{x}$ at time t or arrive there exactly at time t from other points $\mathbf{x} - \mathbf{z}$. The function

$$\Psi(t) = \int_t^\infty \int_{\mathbb{R}^3} \psi(\mathbf{z}, \tau) \mathrm{d}\mathbf{z} \mathrm{d}\tau \tag{3.4}$$

is the survival probability. Another long-time large-scale limit of (3.3) can be a fractional reaction–transport equation, such as

$$\frac{\partial \rho}{\partial t} = -D_\alpha (-\Delta)^{\frac{\alpha}{2}} \rho + F(\rho), \qquad \mathbf{x} \in \mathbb{R}^3, \tag{3.5}$$

where the Laplacian Δ is replaced by a fractional operator $-(-\Delta)^{\frac{\alpha}{2}}$ and D_α is a generalized diffusion coefficient. This replacement leads to a faster spread of particles, i.e., superdiffusion, see Sect. 3.3, than the standard reaction–diffusion equation (3.1) describes. The *microscopic* reason for the fast spread is that the jump length PDF

$$w(\mathbf{z}) = \int_0^\infty \psi(\mathbf{z}, \tau) \mathrm{d}\tau \tag{3.6}$$

has a heavy tail, so that $w(\mathbf{z}) \sim |\mathbf{z}|^{-d-\alpha}$ with $0 < \alpha < 2$ as $|\mathbf{z}| \to \infty$, where d is the dimension of space, $\mathbb{R}^d$. The fractional Laplacian can be defined as

$$(-\Delta)^{\frac{\alpha}{2}} g(\mathbf{x}) = \mathcal{F}^{-1} \left[|\mathbf{k}|^\alpha \tilde{g}(\mathbf{k}) \right], \tag{3.7}$$

where $\mathcal{F}^{-1}$ denotes the inverse Fourier transform and $\tilde{g}(\mathbf{k}) = \mathcal{F}\left[g(\mathbf{x})\right] = \int_{\mathbb{R}^3} g(\mathbf{x}) \mathrm{e}^{\mathrm{i}\mathbf{k}\cdot\mathbf{x}} \mathrm{d}\mathbf{x}$. Fractional differential equations have attracted considerable interest in past years. We believe that the approach based on random walk models, the long-time large-scale limit asymptotics of mesoscopic equations, and stable distributions often provides a deeper insight into mechanisms by which the fractional equations arise than a standard phenomenological approach.

The main objective of this chapter is to establish the relation between the *macroscopic* equations like (3.1) and (3.5), the *mesoscopic* equations (3.2) and (3.3), etc., and the underlying *microscopic* movement of particles. We will show how to derive mesoscopic reaction–transport equations like (3.2) and (3.3) from microscopic random walk models. In particular, we will discuss the scaling procedures that lead to macroscopic reaction–transport equations. As an example, let us mention that the macroscopic reaction–diffusion equation (3.1) occurs as a result of the convergence of the random microscopic movement of particles to Brownian motion, while the macroscopic fractional equation (3.5) is closely related to the convergence of random walks with heavy-tailed jump PDFs to α-stable random processes or Lévy flights.

In the following section we restrict ourselves to one-dimensional models for expository purposes. The material is presented by means of examples of random walk models and corresponding mesoscopic equations and is sometimes supported by general theory.

3.1 Discrete-Time Random Walk

We begin with a simple example of a particle performing a discrete-time random walk (DTRW) in one dimension. Assume that it is initially at point 0. The random walk can be defined by the stochastic difference equation for the particle position X_n at time n:

$$X_{n+1} = X_n + Z_{n+1}, \tag{3.8}$$

where the jumps Z_n are mutually independent, continuous random variables with the common PDF

$$w(z) = \frac{\partial}{\partial z} \mathbb{P}(Z_n \le z). \tag{3.9}$$

Equation (3.8) provides *a microscopic* description of the particle transport. After n jumps, the position of the particle is

$$X_n = \sum_{i=1}^{n} Z_i. \tag{3.10}$$

Let us define the PDF for the particle position X_n at time n:

$$p(x, n) = \frac{\partial}{\partial x} \mathbb{P}(X_n \le x). \tag{3.11}$$

It follows from (3.8) and (3.9) that the PDF $p(x, n)$ obeys the Kolmogorov forward equation

$$p(x, n + 1) = \int_{\mathbb{R}} p(x - z, n) w(z) \mathrm{d}z, \tag{3.12}$$

with $n = 0, 1, \ldots$. If Z_i has zero mean and finite variance, $\sigma^2 = \int_{\mathbb{R}} z^2 w(z) \mathrm{d}z$, the central limit theorem ensures that the PDF for the rescaled particle position $X_n/\sqrt{n}$ tends to a Gaussian as $n \to \infty$. If the jumps Z_n have a symmetric heavy-tailed PDF with power-law index $\alpha < 2$, then the variance σ^2 is infinite. According to the generalized central limit theorem, the rescaled position $X_n/n^{1/\alpha} \overset{\mathrm{d}}{\to} Z$ as $n \to \infty$,

where Z is a symmetric α-stable random variable and $\overset{d}{\rightarrow}$ means convergence in distribution [126, 377].

3.1.1 Mesoscopic Equation for the Particle Density

Let us introduce the average density of particles $\rho(x, n)$ at point x at time n. We assume that the number of particles per unit length around x is large enough that we can neglect the random fluctuations in the number density. In this case, the particle density $\rho(x, n)$ obeys the integral balance equation

$$\rho(x, n+1) = \int_{\mathbb{R}} \rho(x-z, n) w(z) \mathrm{d}z. \tag{3.13}$$

This equation states that the particle density at time $n+1$ is the sum of the densities at intermediate points $x - z$ at time n multiplied by the probability of transition from $x - z$ to x. This is a *mesoscopic* description. Although it only deals with the mean density of particles $\rho(x, n)$, it involves a detailed description of the movement of particles on the *microscopic* level. Equation (3.13) is the same as the Kolmogorov forward equation (3.12). The solution to (3.13) can be rewritten as a convolution

$$\rho(x, n) = (\rho_0 * w^{*n})(x), \tag{3.14}$$

where $\rho_0(x)$ is the initial density, the asterisk $*$ denotes convolution, and $w^{*n} = w * \cdots * w$ (n times).

If the PDF is $w(x) = \frac{1}{2}\delta(x-a) + \frac{1}{2}\delta(x+a)$, jumps Z_n can take only two values, a and $-a$, with equal probabilities. In this case we have a recurrence equation

$$\rho(x, n+1) = \frac{1}{2}\rho(x-a, n) + \frac{1}{2}\rho(x+a, n). \tag{3.15}$$

This equation can be recognized as a finite difference approximation of the diffusion equation

$$\frac{\partial \rho}{\partial t} = D \frac{\partial^2 \rho}{\partial x^2}. \tag{3.16}$$

This becomes clearer if we let the time step be of size τ instead of size 1. Then the recurrence equation (3.15) can be rewritten as

$$\frac{\rho(x, t+\tau) - \rho(x, t)}{\tau} = D \frac{\rho(x+a, t) - \rho(x, t) + \rho(x-a, t)}{a^2}, \tag{3.17}$$

where t denotes a time point of the form $n\tau$ and $D = a^2/2\tau$. We see that (3.17) is a discrete version of the standard diffusion equation (2.1). Though trivial, this

derivation clearly explains the connection between the microscopic equation for a single particle (3.8), the mesoscopic description for the particle density (3.13), and the macroscopic diffusion equation (3.16). Later we discuss how the discrete random walk (3.8) converges to Brownian motion after rescaling the time and space steps, see Sect. 3.6.

So far we have considered a homogeneous-in-space random walk for which the jump size Z_{n+1} in (3.8) is independent of the particle position X_n. The natural generalization of this situation is the case where the jumps are described by the conditional PDF

$$w(z|x) = \frac{\partial}{\partial z}\mathbb{P}(Z_n \leq z|X_{n-1} = x).$$ (3.18)

The mesoscopic density is governed by the Kolmogorov forward equation, the Master equation,

$$\rho(x, n+1) = \int_{\mathbb{R}} \rho(x-z, n)w(z|x-z)\mathrm{d}z.$$ (3.19)

The discrete model has the advantage that it can be easily generalized to include various nonlinearities such as the kinetic term $F(\rho)$ and the dependence of the jump kernel w on the density ρ. In this case we have a nonlinear recurrence equation

$$\rho(x, n+1) = \int_{\mathbb{R}} F[\rho(x-z, n)]\, w(z|x-z, \rho(x-z, n))\mathrm{d}z,$$ (3.20)

with $n = 0, 1, 2, \ldots$.

3.1.2 Random Walk with Two States and the System of Two Mesoscopic Equations

So far we have considered a single *mesoscopic* equation for the particle density and a corresponding random walk model, a Markov process with continuous states in discrete time. It is natural to extend this analysis to a system of mesoscopic equations for the densities of particles $\rho_i(x, n)$, $i = 1, 2, \ldots, m$. To describe the *microscopic* movement of particles we need a vector process (X_n, S_n), where X_n is the position of the particle at time n and S_n its state at time n. S_n is a sequence of random variables taking one of m possible values at time n. One can introduce the probability density $p_i(x, n) = \partial\mathbb{P}(X_n \leq x, S_n = i)/\partial x$ and an imbedded Markov chain with the $m \times m$ transition matrix $\mathsf{H} = (h_{ij})$, so that the matrix entry h_{ij} corresponds to the conditional probability of a transition from state i to state j.

To illustrate the idea, we derive *mesoscopic* equations for two densities $\rho_i(x, n)$, $i = 1, 2$, at point x at time n. One can think of a particle that moves along the x-axis and that can be in two different states with dispersal kernels $w_1(z)$ and

$w_2(z)$. We assume that the particles either jump or change their state. If the particle is in state 1 at time n, then the probability of being in state 2 at time $n + 1$ is h_{12}, and the probability of being in state 1 at time $n + 1$ is $h_{11} = 1 - h_{12}$. In the same way, we can define the transition probabilities for the particle if it is in state 2 at time n. We assume that these probabilities are h_{21} and $h_{22} = 1 - h_{21}$. The transition matrix H of the Markov chain with two states has the form

$$H = \begin{pmatrix} h_{11} & h_{12} \\ h_{21} & h_{22} \end{pmatrix}.$$
(3.21)

The balance equations for the two densities $\rho_i(x, n)$, $i = 1, 2$, can be written as follows:

$$\rho_1(x, n + 1) = h_{11} \int_{\mathbb{R}} \rho_1(x - z, n) w_1(z) dz + h_{21} \rho_2(x, n),$$
(3.22a)

$$\rho_2(x, n + 1) = h_{22} \int_{\mathbb{R}} \rho_2(x - z, n) w_2(z) dz + h_{12} \rho_1(x, n),$$
(3.22b)

with $n = 0, 1, 2, \ldots$. The first equation states that the density of particles $\rho_1(x, n + 1)$ in state 1 at point x at time $n + 1$ is the sum of (i) the density of particles in state 1 at intermediate points $x - z$ at time n multiplied by the probability of remaining in state 1 at the transition time $n + 1$ and the probability of transition from $x - z$ to x and (ii) the density of particles in state 2 at time n multiplied by the probability of transition from state 2 to state 1 at time $n + 1$. It is straightforward to include kinetic terms $F_1(\rho_1)$ and $F_2(\rho_2)$ and the dependence of the transition probabilities h_{ij} on densities ρ_1 and ρ_2, similar to (3.20).

3.2 Continuous-Time Random Walk

We now turn to a particle that performs a random walk in continuous time. In order to keep this section as clear as possible, we will only consider one-dimensional random walk models. As before, we assume that the jumps $Z_1, Z_2, \ldots$ are independent identically distributed (IID) random variables. However, the jumps occur at random times $T_1, T_2, \ldots$, so that the intervals between jumps $\Theta_n = T_n - T_{n-1}$ are also IID variables. In general, the time intervals Θ_n and jumps Z_n are dependent, and their statistical characteristics are completely determined by the joint PDF $\psi(z, t)$. The spatial jump length PDF is given by $w(z) = \int_0^\infty \psi(z, t) dt$ and the waiting time PDF by $\phi(t) = \int_{-\infty}^\infty \psi(z, t) dz$. If jumps and waiting times are independent of each other, the corresponding joint PDF $\psi(z, t)$ factorizes:

$$\psi(z, t) = w(z) \phi(t).$$
(3.23)

Let $X(t)$ denote the position of the particle at time t and $X(0) = 0$, then

$$X(t) = \sum_{i=1}^{N(t)} Z_i, \tag{3.24}$$

where $N(t)$ is the number of jumps up to time t. It can be defined in terms of the random time T_n as follows:

$$N(t) = \max \left\{ n \geq 0 : T_n \leq t \right\}. \tag{3.25}$$

Such a process $N(t)$ is called a *renewal* or *counting process*. The particle position $X(t)$ is called a *continuous-time random walk*. Figure 3.1 illustrates the process $X(t)$. It should be noted that the CTRW $X(t)$ defined by (3.24) can also be obtained by replacing the discrete time n in (3.10) with the "random" time $N(t)$, i.e.,

$$X(t) = X_{N(t)}. \tag{3.26}$$
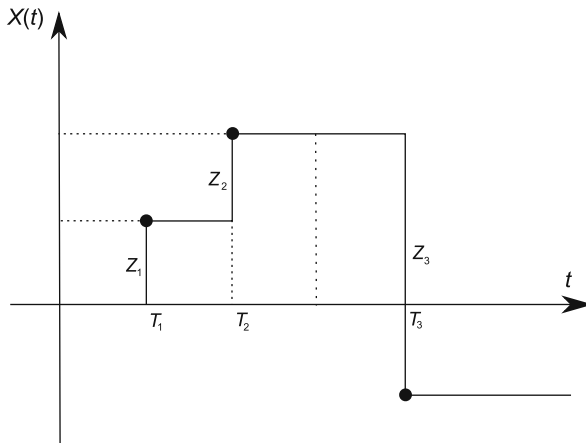
Fig. 3.1 Schematic picture of a CTRW

In the mathematical literature, $X(t)$ is called a *semi-Markov process* associated with the two-component Markov chain (X_n, T_n), a *Markov renewal process* [218]. As discussed in Sect. 2.3, the CTRW model is a standard approach for studying anomalous diffusion [298].

The *microscopic* stochastic equation for the particle position $X(t)$ can be written in the form

$$\frac{dX}{dt} = \sum_i Z_i \delta(t - T_i), \tag{3.27}$$

where the right-hand side represents the sum of the stochastic pulses at renewal times T_i with random amplitudes Z_i.

To find the PDF $p(x, t)$ for the particle position at time t we use the equation

$$p(x, t) = p_0(x)\Psi(t) + \int_0^t j(x, t - \tau)\Psi(\tau)d\tau, \qquad (3.28)$$

where $p_0(x)$ is the initial PDF, $j(x, t)$ is the probability density of reaching the point x exactly at time t, and

$$\Psi(t) = \int_t^\infty \int_\mathbb{R} \psi(z, \tau)dzd\tau \qquad (3.29)$$

is the probability that the particle does not jump in the time interval $(0, t]$, i.e., the survival probability. Equation (3.28) expresses the law of total probability. The first term on the RHS of (3.28) represents the probability of being at the point x times the probability of no jumps up to time t. The second term takes into account the probability of arriving at the point x at time $t - \tau$ and the probability of no jumps during the remaining time τ. The density $j(x, t)$ obeys the balance equation

$$j(x, t) = \int_\mathbb{R} p_0(x - z)\psi(z, t)dz + \int_0^t \int_\mathbb{R} j(x - z, t - \tau)\psi(z, \tau)dzd\tau. \quad (3.30)$$

Applying the Fourier–Laplace (F-L) transform to (3.28) and (3.30), we obtain the Fourier–Laplace transform of the PDF $p(x, t)$, the Montroll–Weiss equation,

$$\hat{\tilde{p}}(k, s) = \frac{\tilde{p}_0(k)\left[1 - \hat{\phi}(s)\right]}{s\left[1 - \hat{\tilde{\psi}}(k, s)\right]}. \qquad (3.31)$$

Here $\hat{\phi}(s)$ is the Laplace transform of the waiting time PDF $\phi(t)$, $\tilde{p}_0(k)$ is the Fourier transform of the initial PDF $p_0(x)$, and $\hat{\tilde{\psi}}(k, s)$ is the F-L transform of the joint PDF $\psi(x, t)$. In particular, (3.31) can be rearranged for the uncoupled case (3.23) as

$$s\hat{\tilde{p}}(k, s) - \tilde{p}_0(k) = \frac{s\hat{\phi}(s)}{1 - \hat{\phi}(s)}(\tilde{w}(k) - 1)\hat{\tilde{p}}(k, s), \qquad (3.32)$$

where the left-hand side is the Fourier–Laplace transform of the derivative $\partial p/\partial t$ and $\tilde{w}(k)$ is the Fourier transform of dispersal kernel $w(z)$. If we apply the F-L transform inversion, we obtain the integro-differential equation, the Master equation,

$$\frac{\partial p}{\partial t} = \int_0^t K(t-\tau)\left[\int_{\mathbb{R}} p(x-z,\tau)w(z)\mathrm{d}z - p(x,\tau)\right]\mathrm{d}\tau. \tag{3.33}$$

The memory kernel $K(t)$ is defined in terms of its Laplace transform, see (2.66),

$$\hat{K}(s) = \frac{\hat{\phi}(s)}{\hat{\Psi}(s)} = \frac{s\hat{\phi}(s)}{1-\hat{\phi}(s)}. \tag{3.34}$$

It should be emphasized that it is impossible to find an explicit expression for the memory kernel $K(t)$ for arbitrary choices of the waiting time PDF $\phi(t)$.

As we mentioned in Sect. 2.3, CTRWs can be characterized by the mean waiting time, $\overline{T} = \int_0^\infty t\phi(t)\mathrm{d}t$, and the second moment of the jump length PDF, $\sigma^2 = \int_{\mathbb{R}} z^2 w(z)\mathrm{d}z$. We assume that $w(z)$ is even, i.e., the first moment of $w(z)$ vanishes. If $\overline{T}$ and σ^2 are finite, the central limit theorem implies that the rescaled particle position $\sqrt{\varepsilon}X(t/\varepsilon)$ has a Gaussian PDF as $\varepsilon \to 0$,

$$\lim_{\varepsilon \to 0}\frac{\partial}{\partial x}\mathbb{P}\left(\sqrt{\varepsilon}X\left(\frac{t}{\varepsilon}\right) \le x\right) = \frac{1}{\sqrt{4\pi Dt}}\exp\left(-\frac{x^2}{4Dt}\right), \tag{3.35}$$

with $D = \sigma^2/2\overline{T}$. In another words, $\sqrt{\varepsilon}X(t/\varepsilon)$ converges in distribution to the Brownian motion $B(t)$ as $\varepsilon \to 0$.

The CTRW model is a standard tool for modeling subdiffusion, for which the variance of the particle position increases with time as t^γ with $0 < \gamma < 1$, see Sect. 2.3. This regime occurs if the waiting time PDF behaves like $\phi(t) \sim (\tau_0/t)^{1+\gamma}$ as $t \to \infty$. Then the mean waiting time $\overline{T}$ is infinite. The Laplace transform $\hat{\phi}(s)$ is approximated by

$$\hat{\phi}(s) \simeq 1 - (\tau_0 s)^\gamma \tag{3.36}$$

for small s and $0 < \gamma < 1$. Then $\hat{K}(s) \simeq s(\tau_0 s)^{-\gamma}$. Equation (3.32) can be written as $s^\gamma \hat{p}(k,s) - s^{\gamma-1}\tilde{p}_0(k) = \tau_0^{-\gamma}(\tilde{w}(k)-1)\hat{p}(k,s)$. We apply the F-L transform inversion and obtain the fractional Kolmogorov–Feller equation

$$\tau_0^\gamma \frac{\partial^\gamma p}{\partial t^\gamma} = \int_{\mathbb{R}} p(x-z,t)w(z)\mathrm{d}z - p(x,t), \tag{3.37}$$

where

$$\frac{\partial^\gamma p}{\partial t^\gamma} = \frac{1}{\Gamma(1-\gamma)}\frac{\partial}{\partial t}\int_0^t \frac{p(x,\tau)\mathrm{d}\tau}{(t-\tau)^\gamma} - \frac{t^{-\gamma}p_0(x)}{\Gamma(1-\gamma)} \tag{3.38}$$

is the Caputo fractional derivative, which reduces to the standard derivative for $\gamma = 1$.

3.2.1 Mesoscopic Equation for the Particle Density

Consider particles that undergo a continuous-time random walk and do not interact with each other. Then the balance equations for the mean density of particles $\rho(x, t)$ and the density of particles $j(x, t)$ arriving at the point x exactly at time t can be written as

$$\rho(x, t) = \rho_0(x)\Psi(t) + \int_0^t j(x, \tau)\Psi(t - \tau)d\tau, \qquad (3.39)$$

and

$$j(x, t) = \int_{\mathbb{R}} \rho_0(x - z)\psi(z, t)dz + \int_0^t \int_{\mathbb{R}} j(x - z, \tau)\psi(z, t - \tau)dzd\tau, \quad (3.40)$$

where $\rho_0(x)$ is the initial particle density. These two equations have the same form as (3.28) and (3.30). The two balance equations (3.39) and (3.40) can be rewritten as a single equation:

$$\rho(x, t) = \rho_0(x)\Psi(t) + \int_0^t \int_{\mathbb{R}} \rho(x - z, \tau)\psi(z, t - \tau)dzd\tau. \qquad (3.41)$$

Note that the initial distribution $\rho_0(x)$ is set up in such a way that the random walk for all particles starts from $t = 0$. Other choices of the time origin lead to aging effects [29]. In the following, we consider the uncoupled case (3.23) for simplicity. Using the Laplace–Fourier transform, we obtain from (3.39) and (3.40) the expression for $j(x, t)$ in terms of $\rho(x, t)$:

$$j(x, t) = \int_0^t \int_{\mathbb{R}} K(t - \tau)w(z)\rho(x - z, \tau)dzd\tau, \qquad (3.42)$$

where the memory kernel $K(t)$ is given by (3.34). In the uncoupled case, (3.41) can be converted into the integro-differential transport equation, the generalized Master equation,

$$\frac{\partial \rho}{\partial t} = \int_0^t K(t - \tau)\left[\int_{\mathbb{R}} \rho(x - z, \tau)w(z)dz - \rho(x, \tau)\right]d\tau. \qquad (3.43)$$

The intuitive meaning of the Master equation can be understood in terms of the density of particles $j(x, t)$ given by (3.42). If we differentiate $\rho(x, t)$ from (3.39) with respect to time, we obtain

$$\frac{\partial \rho}{\partial t} = -\rho_0(x)\phi(t) + j(x, t) - \int_0^t j(x, \tau)\phi(t - \tau)d\tau, \qquad (3.44)$$

since $\Psi'(t) = -\phi(t)$. The last equation can be written in the following form:

$$\frac{\partial \rho}{\partial t} = j(x,t) - i(x,t), \tag{3.45}$$

where $i(x,t)$ is the rate of departure of particles from the point x,

$$i(x,t) = \int_0^t K(t-\tau)\rho(x,\tau)d\tau. \tag{3.46}$$

The generalized Master equation (3.43) can be rewritten as a simple rate equation:

$$\frac{\partial \rho}{\partial t} = \int_{\mathbb{R}} i(x-z,t)w(z)dz - i(x,t). \tag{3.47}$$

It is tempting to generalize this equation by including a nonlinear reaction term $F(\rho)$ on its RHS:

$$\frac{\partial \rho}{\partial t} = \int_{\mathbb{R}} i(x-z,t)w(z)dz - i(x,t) + F(\rho). \tag{3.48}$$

It turns out that the inclusion of the kinetic term $F(\rho)$ is not a trivial procedure for non-Markovian processes. In particular, the transport term might depend on the reaction kinetics. We discuss this problem later in detail, see Sect. 3.4.

As we mentioned, the particle position $X(t)$ can be expressed in terms of a discrete random walk X_n, see (3.10), and a counting process $N(t)$ as (3.26). Therefore, the solution of the Master equation (3.43) can be written as the average value

$$\rho(x,t) = \sum_{n=0}^{\infty} \rho(x,n)\mathbb{P}(N(t) = n), \tag{3.49}$$

where the density $\rho(x,n)$ is defined by the convolution equation (3.13). Here we have assumed that the jumps and waiting times are independent. Using the formula (3.14), we can express the particle density $\rho(x,t)$ in terms of the initial density $\rho_0(x)$ and the expectation operator $\mathbb{E}$ as

$$\rho(x,t) = \mathbb{E}\left(\rho_0 * w^{*N(t)}\right)(x) = \sum_{n=0}^{\infty} (\rho_0 * w^{*n})(x)\mathbb{P}(N(t) = n). \tag{3.50}$$

Applying the Fourier–Laplace transform, we obtain

$$\hat{\tilde{\rho}}(k,s) = \tilde{\rho}_0(k)\sum_{n=0}^{\infty} \tilde{w}^n(k)\hat{P}(n,s), \tag{3.51}$$

where $\hat{P}(n, s)$ is the Laplace transform of $P(n, t) = \mathbb{P}(N(t) = n)$. It is known from renewal theory [81] that

$$\hat{P}(n, s) = \frac{\hat{\phi}^n(s)\left[1 - \hat{\phi}(s)\right]}{s}. \tag{3.52}$$

Substitution of (3.52) into (3.51) yields

$$\hat{\tilde{\rho}}(k, s) = \frac{\tilde{\rho}_0(k)\left[1 - \hat{\phi}(s)\right]}{s}\sum_{n=0}^{\infty}\tilde{w}^n(k)\hat{\phi}^n(s) = \frac{\rho_0(k)\left[1 - \hat{\phi}(s)\right]}{s\left[1 - \tilde{w}(k)\hat{\phi}(s)\right]}, \tag{3.53}$$

which is exactly the formula (3.31) for the case $\hat{\tilde{\psi}}(k, s) = \tilde{w}(k)\hat{\phi}(s)$.

3.2.2 Random Walk with Discrete States in Continuous-Time

So far we have considered the homogeneous case for which the waiting time density is independent of the position of the particles or their state. Let us formulate the general equations describing a random walk with discrete states in continuous time for which the waiting time PDF depends on the current state. (CTRWs with space-dependent waiting time PDFs have been studied in [75].) We introduce the mean density of particles $\rho_m(t)$ in state m and the density of particles $j_m(t)$ arriving in state m exactly at time t. The balance equations can be written as

$$\rho_m(t) = \rho_{m0}\Psi_m(t) + \int_0^t j_m(\tau)\Psi_m(t - \tau)d\tau \tag{3.54}$$

and

$$j_m(t) = \sum_{i\neq m}\rho_{i0}\phi_i(t)h_{im} + \sum_{i\neq m}\int_0^t j_i(\tau)\phi_i(t - \tau)h_{im}d\tau. \tag{3.55}$$

Here $\Psi_m(t) = \int_t^{\infty}\phi_m(\tau)d\tau$ is the survival probability in the state m, h_{im} is the transition probability from state i to m, and ρ_{i0} is the initial density of particles in state i. Using the Laplace transform, we obtain from (3.54) and (3.55)

$$j_m(t) = \sum_{i\neq m}\int_0^t K_i(t - \tau)\rho_i(\tau)h_{im}d\tau, \tag{3.56}$$

where the memory kernel $K_i(t)$ is defined in terms of its Laplace transform

$$\hat{K}_i(s) = \frac{\hat{\phi}_i(s)}{\hat{\Psi}_i(s)} = \frac{s\hat{\phi}_i(s)}{1 - \hat{\phi}_i(s)}. \tag{3.57}$$

The two balance equations can be rewritten as a single equation:

$$\rho_m(t) = \rho_{m0}\Psi_m(t) + \sum_{i \neq m} \int_0^t M_{im}(t - \tau)\rho_i(\tau)h_{im}d\tau, \qquad (3.58)$$

where the memory kernel $M_{im}(t)$ is defined as

$$\hat{M}_{im}(s) = \frac{\hat{\phi}_i(s)\hat{\Psi}_m(s)}{\hat{\Psi}_i(s)}. \qquad (3.59)$$

It should be noted that (3.58) cannot be written in the standard form (3.41), which makes it difficult to give its probabilistic interpretation.

The generalized Master equation is

$$\frac{\partial \rho_m(t)}{\partial t} = \sum_{i \neq m} \int_0^t K_i(t - \tau)\rho_i(\tau)h_{im}d\tau - \int_0^t K_m(t - \tau)\rho_m(\tau)d\tau. \qquad (3.60)$$

This equation can be useful for studying multi-component systems where the chemical reactions do not obey classical kinetics.

3.2.3 Semi-Markov Processes

As mentioned on page 61, CTRWs are known as semi-Markov processes in the mathematical literature. In this section we provide a brief account of semi-Markov processes. They were introduced by P. Lévy and W. L. Smith [253, 415]. Recall that for a continuous-time Markov chain, the transitions between states at random times T_n are determined by the discrete chain X_n with the transition matrix $\mathsf{H} = (h_{ij})$. The waiting time $\Theta_n = T_n - T_{n-1}$ for a given state i is exponentially distributed with the transition rate λ_i, which depends only on the current state i. The natural generalization is to allow arbitrary distributions for the waiting times. This leads to a semi-Markov process. The reason for such a name is that the underlying process is a two-component Markov chain: (X_n, T_n). Here the random sequence X_n represents the state at the nth transition, and T_n is the time of the nth transition. Obviously, $T_n = \sum_{k=1}^n \Theta_k$.

The main statistical characteristic of the two-component Markov chain (X_n, T_n) is the transition kernel

$$Q_{ij}(t) = \mathbb{P}\left\{X_{n+1} = j, \Theta_{n+1} \leq t | X_n = i\right\} \qquad (3.61)$$

for any $n \geq 0$. Here we consider only time-homogeneous chains for which the kernel $Q_{ij}(t)$ is independent of n. We use the counting process $N(t)$ (3.25) that gives the number of transitions in the time interval $(0, t]$.

Semi-Markov processes can be defined as

$$X(t) = X_{N(t)} \tag{3.62}$$

or

$$X(t) = X_n \quad \text{if} \quad T_n \le t < T_{n+1}. \tag{3.63}$$

If the process starts in the state i, then the subsequent state j is determined by the transition kernel Q so that the process remains in state i some random time before making a transition to j. One can introduce the conditional waiting time distribution $\Phi_{ij}(t)$ as

$$\Phi_{ij}(t) = \mathbb{P}\left\{ T_{n+1} - T_n \le t | X_n = i, \ X_{n+1} = j \right\}. \tag{3.64}$$

It gives us the distribution of the random time spent in state i before jumping to state j. The transition kernel $Q_{ij}(t)$ can be written as

$$Q_{ij}(t) = h_{ij}\Phi_{ij}(t), \tag{3.65}$$

where h_{ij} is the transition probability matrix of the underlying discrete Markov chain X_n. Note that $Q_{ij}(t) \to h_{ij}$ as $t \to \infty$ since $\Phi_{ij}(\infty) = 1$. In general, the waiting time distribution depends on the current state i and the next state j.

The standard continuous-time Markov chain is a special case of a semi-Markov process with the transition kernel

$$Q_{ij}(t) = h_{ij}(1 - \exp(-\lambda_i t)). \tag{3.66}$$

The transition probability

$$p_{ij}(t) = \mathbb{P}\{X(t) = j | X(0) = i\} \tag{3.67}$$

satisfies the integral backward equation

$$p_{ij}(t) = \delta_{ij} S_i(t) + \sum_k \int_0^t q_{ik}(t - \tau) p_{kj}(\tau) d\tau, \tag{3.68}$$

where

$$q_{ij}(t) = \frac{\partial Q_{ij}(t)}{\partial t} \tag{3.69}$$

is the transition density kernel and

$$S_i(t) = 1 - \sum_k Q_{ik}(t) \tag{3.70}$$

is the survival probability for state i. The first term $\delta_{ij} S_i(t)$ in (3.68) represents the probability that the process $X(t)$ does not leave the state i up to time t, given that it was in this state initially. In the Markovian case, $q_{ij}(t) = \lambda_i \exp(-\lambda_i t) h_{ij}$, this equation is equivalent to a system of backward differential equations for Markov processes. Janssen and Manca have summarized the theory of semi-Markov processes and discussed its applications in [218].

3.3 Markov CTRW Models

3.3.1 Compound Poisson Process

If the counting process $N(t)$ is a Poisson process with the transition rate λ, then the particle position

$$X(t) = \sum_{i=1}^{N(t)} Z_i \tag{3.71}$$

is a compound Poisson process [126]. The probability that n jumps occur in the time interval $[0, t]$ is given by

$$\mathbb{P}(N(t) = n) = \frac{(\lambda t)^n}{n!} e^{-\lambda t}. \tag{3.72}$$

Note that the Poisson process plays a very important role in random walk theory. It can be defined in two ways: (1) as a continuous-time Markov chain with constant intensity, i.e., as a pure birth process with constant birth rate λ; (2) as a renewal process. In the latter case, it can be represented as (3.25) with $T_n = \sum_{i=0}^{n} \Theta_i$. Here Θ_i are interarrival (waiting) times, which are independent random variables with PDF

$$\phi(t) = \lambda e^{-\lambda t}. \tag{3.73}$$

Since the waiting time PDF $\phi(t)$ is exponential, the random walk $X(t)$ is a Markov process. The jump PDF $w(z)$ is defined in (3.9).

The *mesoscopic* particle density $\rho(x, t)$ obeys the integro-differential equation

$$\frac{\partial \rho}{\partial t} = \lambda \int_{\mathbb{R}} \rho(x - z, t) w(z) \mathrm{d}z - \lambda \rho(x, t). \tag{3.74}$$

The integro-differential equation (3.74) can be derived in several ways. The following is probably the most instructive in the context of transport theory. Since a compound Poisson process is Markovian, the derivation of (3.74) is based on the idea that the particle density at time $t + h$ can be expressed in terms of the density

at time t. In other words, the balance of particles during time $(t, t + h]$ is independent of what happened during the previous time interval $(0, t]$. We assume that the probability of a jump during a small time interval of length h is $\lambda h + o(h)$ and the probability of no jumps is $1 - \lambda h + o(h)$. Thus the balance of particles at the point x can be written as

$$\rho(x, t + h) = (1 - \lambda h)\rho(x, t) + \lambda h \int_{\mathbb{R}} \rho(x - z, t)w(z)\mathrm{d}z. \tag{3.75}$$

Subtracting $\rho(x, t)$ from both sides of this equation, dividing by h, and letting $h \to 0$, we obtain (3.74). Obviously, (3.74) corresponds to a particular case of (3.43), namely where the time integral disappears, i.e., the Markov case.

Since the process is Markovian, it is easy to include chemical reactions in the above model by adding the kinetic term $F(\rho)h$ to the RHS of (3.75):

$$\frac{\partial \rho}{\partial t} = \lambda \int_{\mathbb{R}} \rho(x - z, t)w(z)\mathrm{d}z - \lambda\rho(x, t) + F(\rho). \tag{3.76}$$

We can rewrite this equation with the initial condition $\rho(x, 0) = \rho_0(x)$ in integral form. Let us look at (3.76) as a first-order inhomogeneous ODE of the form $\mathrm{d}\rho/\mathrm{d}t = -\lambda\rho(t) + g(t)$, where the function $g(t)$ combines the integral term and the kinetic term $F(\rho)$. This equation has a solution $\rho(t) = \rho(0)\mathrm{e}^{-\lambda t} + \int_0^t g(t - \tau)\mathrm{e}^{-\lambda\tau}\mathrm{d}\tau$, which implies that

$$\rho(x, t) = \rho_0(x)\mathrm{e}^{-\lambda t} + \int_0^t \int_{\mathbb{R}} \rho(x - z, t - \tau)w(z)\lambda\mathrm{e}^{-\lambda\tau}\mathrm{d}z\mathrm{d}\tau$$
$$+ \int_0^t F(\rho(x, t - \tau))\mathrm{e}^{-\lambda\tau}\mathrm{d}\tau. \tag{3.77}$$

The first term on the right-hand side represents those particles that stay at point x up to time t. The exponential factor $\mathrm{e}^{-\lambda t} = 1 - \int_0^t \phi(\tau)\mathrm{d}\tau$ is the probability that the particle makes no jump until time t. This is the survival probability $\Psi(t)$ for $\phi(t) = \lambda\mathrm{e}^{-\lambda t}$. The second term includes the contribution from the particles jumping to point x from different positions $x - z$ at time $t - \tau$ and surviving up to time t. The last term describes the contribution from the chemical reaction with the rate $F(\rho)$.

The natural generalization of a compound Poisson process is the *Markov jump process* $X(t)$ with the following statistical properties. If the position of a particle at time t is $X(t)$, then the probability of a jump during a small time interval $(t, t+h]$ is $\lambda(X(t))h + o(h)$, so that $X(t+h) = X(t) + Z(t) + o(h)$. The probability of no jump during $(t, t + h]$ is $1 - \lambda(X(t))h + o(h)$. The conditional density for a stationary jump process $Z(t)$ is

$$w(z|x) = \frac{\partial}{\partial z}\mathbb{P}\{Z(t) \le z | X(t) = x\}. \tag{3.78}$$

The balance of particles at the point x is

$$\rho(x, t + h) = \int_{\mathbb{R}} \rho(x - z, t)\lambda(x - z)hw(z|x - z)\mathrm{d}z$$
$$+ (1 - \lambda(x)h)\rho(x, t) + o(h). \tag{3.79}$$

Subtracting $\rho(x, t)$ from both sides, dividing by h, and letting $h \to 0$, we obtain the mesoscopic equation, the Master equation,

$$\frac{\partial \rho(x, t)}{\partial t} = \int_{\mathbb{R}} \rho(x - z, t)\lambda(x - z)w(z|x - z)\mathrm{d}z - \lambda(x)\rho(x, t). \tag{3.80}$$

This equation can easily be generalized to include various nonlinear effects. In particular, the jump PDF $w(z|x)$ and the jump rate $\lambda(x)$ can depend on the local density $\rho(x, t)$, due to an overcrowding effect for example. Then

$$\frac{\partial \rho(x, t)}{\partial t} = \int_{\mathbb{R}} \rho(x - z, t)\lambda(x - z, \rho(x - z, t))w(z|x - z, \rho(x - z, t))\mathrm{d}z$$
$$- \lambda(x, \rho(x, t))\rho(x, t) + F(\rho). \tag{3.81}$$

3.3.2 System of Two Mesoscopic Equations

We consider the transport of particles A and B with linear reversible reaction A $\rightleftharpoons$ B. One can introduce a two-component system of equations for the densities $\rho_1(x, t)$ and $\rho_2(x, t)$. We assume that the probability of a transition from A to B during a small time interval of length h is $\alpha_1 h + o(h)$, and the backward transformation B $\longrightarrow$ A has the probability $\alpha_2 h + o(h)$. We assume that the reaction is independent of the transport of particles. The probability of a jump during a small time interval h is $\lambda_1 h + o(h)$ for particles A and $\lambda_2 h + o(h)$ for particles B. The balance of particles A and B at the point x can be written as

$$\rho_1(x, t + h) = (1 - \lambda_1 h - \alpha_1 h)\rho_1(x, t)$$
$$+ \lambda_1 h \int_{\mathbb{R}} \rho_1(x - z, t)w_1(z)\mathrm{d}z + \alpha_2 h \rho_2(x, t) + o(h), \tag{3.82a}$$

$$\rho_2(x, t + h) = (1 - \lambda_2 h - \alpha_2 h)\rho_2(x, t)$$
$$+ \lambda_2 h \int_{\mathbb{R}} \rho_2(x - z, t)w_2(z)\mathrm{d}z + \alpha_1 h \rho_1(x, t) + o(h). \tag{3.82b}$$

These equations are the conservation laws for A and B particles. The first term on the right-hand side of (3.82a) represents the particles A that stay at location x and do not move during the time interval $(t, t + h]$ and do not become particles B. The second term corresponds to the number of particles of type A that arrive at x during $(t, t + h]$ from other points $x - z$, where the jump length z is distributed according to

the dispersal kernel or jump length PDF $w_1(z)$. The last term represents the number of particles B that turn into particles of type A.

In the limit $h \to 0$, we obtain the mesoscopic system of reaction–transport equations

$$\frac{\partial \rho_1}{\partial t} = \lambda_1 \int_{\mathbb{R}} \rho_1(x - z, t) w_1(z) \mathrm{d}z - \lambda_1 \rho_1 - \alpha_1 \rho_1 + \alpha_2 \rho_2, \qquad (3.83\mathrm{a})$$

$$\frac{\partial \rho_2}{\partial t} = \lambda_2 \int_{\mathbb{R}} \rho_2(x - z, t) w_2(z) \mathrm{d}z - \lambda_2 \rho_2 + \alpha_1 \rho_1 - \alpha_2 \rho_2. \qquad (3.83\mathrm{b})$$

The main advantage of this Markovian model is that it can be easily generalized to include various nonlinear terms. Later we consider non-Markovian models for which the inclusion of nonlinear effects is a highly nontrivial procedure, see Sect. 3.4.

3.3.3 Characteristic Function and Transport Equation for the Particle Density

Characteristic functions are very useful tools for studying random processes. It turns out that reaction–transport equations can also be effectively handled by using the characteristic function of the underlying random walks. In what follows, we will see how this function helps to define the transport operator, a pseudo-differential operator, for the mean density $\rho(x, t)$.

3.3.3.1 Compound Poisson process

For illustrative purposes we begin with the transport of particles that follow the path of the compound Poisson process (3.71), $X(t) = \sum_{i=1}^{N(t)} Z_i$. The corresponding mean-field equation for the density $\rho(x, t)$ is given by (3.74). Let us show that this equation is closely related to the characteristic function $\tilde{\rho}(k, t)$ of $X(t)$:

$$\tilde{\rho}(k, t) = \mathbb{E}\left(\mathrm{e}^{ikX(t)}\right) = \sum_{n=0}^{\infty} \mathbb{E}\left(\mathrm{e}^{ikX(t)} \middle| N(t) = n\right) \mathbb{P}(N(t) = n). \qquad (3.84)$$

Here $\mathbb{P}(N(t) = n) = \mathrm{e}^{-\lambda t} \frac{(\lambda t)^n}{n!}$, and the conditional expectation is given by

$$\mathbb{E}\left(\mathrm{e}^{ikX(t)} \middle| N(t) = n\right) = \mathbb{E}\left(\mathrm{e}^{ik \sum_{i=1}^{n} Z_i} \middle| N(t) = n\right) = \tilde{w}^n(k), \qquad (3.85)$$

where $\tilde{w}(k)$ is the characteristic function of the random jump Z_i with the density $w(z)$,

$$\tilde{w}(k) = \mathbb{E}\left(\mathrm{e}^{ikZ_i}\right) = \int_{\mathbb{R}} \mathrm{e}^{ikz} w(z) \mathrm{d}z. \qquad (3.86)$$

We obtain

$$\tilde{\rho}(k, t) = \sum_{n=0}^{\infty} e^{-\lambda t} \frac{(\lambda t \tilde{w}(k))^n}{n!} = e^{t\psi(k)}, \tag{3.87}$$

where

$$\psi(k) = \lambda(\tilde{w}(k) - 1) \tag{3.88}$$

is the characteristic exponent of the compound Poisson process $X(t)$. Note that $\psi(k) = -Dk^2$ corresponds to the Brownian motion $B(t)$ and $\psi(k) = ikv - Dk^2$ is the characteristic exponent of the Brownian motion with drift vt.

The function $\psi(k)$ plays a very important role in defining a transport operator. It follows from (3.87) that the function $\tilde{\rho}(k, t)$ satisfies the equation

$$\frac{\partial \tilde{\rho}(k, t)}{\partial t} = \psi(k)\tilde{\rho}(k, t). \tag{3.89}$$

Applying the inverse Fourier transform to (3.89) with (3.88) and the standard convolution theorem, we obtain the Kolmogorov–Feller equation (3.74). Thus the particle density $\rho(x, t)$ can be interpreted as the inverse Fourier transform of the characteristic function $\tilde{\rho}(k, t) = \mathbb{E}(e^{ikX(t)})$. Since $\tilde{\rho}(k, 0) = 1$, the initial particle density is $\rho(x, 0) = \delta(x)$. The integral operator on the RHS of the Kolmogorov–Feller equation (3.74) can be considered as a pseudo-differential operator with symbol (3.88). Recall that a pseudo-differential operator L_x acting on the variable x is defined by its Fourier transform as $\mathcal{F}[L_x \rho(x, t)] = \psi(k)\tilde{\rho}(k, t)$, where $\psi(k)$ is referred to as the symbol of L_x (see, for example, [15]).

3.3.3.2 Symmetric α-Stable Lévy Process

Let us now consider another example of a Markov process for which the characteristic exponent is

$$\psi(k) = -D_\alpha |k|^\alpha, \quad 0 < \alpha < 2. \tag{3.90}$$

This exponent corresponds to a symmetric α-stable Lévy process $S_\alpha(t)$, a Lévy flight, which is self-similar with Hurst exponent $H = 1/\alpha$. It follows from (3.89) that the mesoscopic density of particles is the solution to the space-fractional diffusion equation [371]:

$$\frac{\partial \rho(x, t)}{\partial t} = D_\alpha \frac{\partial^\alpha \rho(x, t)}{\partial |x|^\alpha}, \tag{3.91}$$

where D_α is a generalized diffusion coefficient and $\partial^\alpha \rho(x, t)/\partial |x|^\alpha$ is the symmetric Riesz fractional derivative of order α defined by the Fourier representation

$$\mathcal{F}\left[\frac{\partial^{\alpha} \rho(x,t)}{\partial |x|^{\alpha}}\right] = -|k|^{\alpha}\, \tilde{\rho}(k,t). \tag{3.92}$$

The symmetric Riesz fractional derivative (3.92) is the pseudo-differential operator with symbol $-|k|^{\alpha}$. Such a derivative describes a redistribution of particles in the whole space according to the heavy-tailed distribution of the jumps

$$\mathbb{P}\{|Z_i| > z\} \sim \frac{A}{z^{\alpha}}, \tag{3.93}$$

for large z. The symmetric Riesz derivative can be represented in explicit form as [371, 372]

$$\frac{\partial^{\alpha} \rho(x,t)}{\partial |x|^{\alpha}} = \frac{\Gamma(1+\alpha)}{\pi} \sin\left(\frac{\alpha\pi}{2}\right) \int_0^{\infty} \frac{\rho(x-z,t) - 2\rho(x,t) + \rho(x+z,t)}{z^{1+\alpha}} \mathrm{d}z. \tag{3.94}$$

The space-fractional equation (3.91) can be derived from the Kolmogorov–Feller equation (3.74) by using the assumption that the random jump Z_i has a Lévy-stable PDF $w_{\alpha}(z)$, symmetric with respect to zero, with power-law tails as $z \to \infty$. There is no general explicit form for $w_{\alpha}(z)$, but the characteristic function of $w_{\alpha}(z)$, the structure function, is

$$\tilde{w}_{\alpha}(k) = \mathrm{e}^{-\sigma^{\alpha}|k|^{\alpha}}. \tag{3.95}$$

The width of the density $w_{\alpha}(z)$ cannot be measured by the variance $\int_{\mathbb{R}} z^2 w_{\alpha}(z)dz$, which is infinite for $\alpha < 2$. The function $w_{\alpha}(z)$ looks similar to a normal density in the center, but the tails of $w_{\alpha}(z)$ are much flatter than those of a Gaussian distribution. The asymptotic expression for large $|z|$ involves power-law tails:

$$w_{\alpha}(z) \sim \frac{\sigma^{\alpha}\Gamma(1+\alpha)\sin(\alpha\pi/2)}{\pi} |z|^{-1-\alpha} \tag{3.96}$$

(see, for example, [126, 373]). We show using scaling arguments that the large-scale long-time limit for $\rho(x,t)$ is the symmetric α-stable density that decays like $t\,|x|^{-1-\alpha}$ as $x \to \infty$. It follows from (3.88) and (3.89) that $\tilde{\rho}(k,t)$ satisfies

$$\frac{\partial \tilde{\rho}(k,t)}{\partial t} = \lambda\left(\mathrm{e}^{-\sigma^{\alpha}|k|^{\alpha}} - 1\right)\tilde{\rho}(k,t). \tag{3.97}$$

Let us find a space–time scaling, $k \to \varepsilon^{H} k$ and $t \to t/\varepsilon$, for which the characteristic function

$$\tilde{\rho}^{*}(k,t) = \lim_{\varepsilon \to 0} \tilde{\rho}^{\varepsilon}(k,t) = \lim_{\varepsilon \to 0} \tilde{\rho}\left(\varepsilon^{H} k, \frac{t}{\varepsilon}\right) \tag{3.98}$$

is scale invariant. In what follows we omit the asterisk for $\tilde{\rho}^*(k, t)$. From (3.97) and (3.98) we find that

$$\tilde{\rho}(k, t) = \lim_{\varepsilon \to 0} \exp\left[\frac{\lambda t}{\varepsilon}\left(e^{-\sigma^\alpha |k|^\alpha \varepsilon^{H\alpha}} - 1\right)\right] = \exp\left(-\lambda \sigma^\alpha |k|^\alpha t\right) \qquad (3.99)$$

for the Hurst exponent $H = \alpha^{-1}$. In this case, $\rho(x, t) = \mathcal{F}^{-1}[\tilde{\rho}(k, t)]$ is the solution to the space-fractional equation (3.91) with $D_\alpha = \lambda \sigma^\alpha$. Let us find this solution by using the scaling rules for the Fourier transform: $g(x/a) \xrightarrow{\mathcal{F}} a\tilde{g}(ak)$. If we set $\lambda = 1$ and $a = t^{1/\alpha}$, then it follows from (3.99) and (3.95) that the Green's function $G(x, t)$ for the space-fractional equation (3.91) with $\rho(x, 0) = \delta(x)$ can be written in terms of the symmetric Lévy-stable PDF $w_\alpha(z)$ as

$$G(x, t) = t^{-\frac{1}{\alpha}} w_\alpha\left(x t^{-\frac{1}{\alpha}}\right). \qquad (3.100)$$

The Cauchy problem for (3.91) with $\rho(x, 0) = \rho_0(x)$ has the solution

$$\rho(x, t) = \int_{\mathbb{R}} G(x - z, t)\rho_0(z)\mathrm{d}z. \qquad (3.101)$$

Note that an asymmetric density of jump lengths leads to the Riesz–Feller space-fractional derivative of order α and skewness θ with the characteristic exponent

$$\psi(k) = -D_\alpha |k|^\alpha e^{i \operatorname{sgn}(k)\theta\pi/2}, \quad 0 < \alpha < 2, \quad |\theta| \leq \min\{\alpha, 2 - \alpha\}. \qquad (3.102)$$

The Cauchy problem involving the Riesz–Feller derivative was analyzed in [166, 260]. In the next section we discuss the general Markov random processes with independent and stationary increments, the Lévy processes, for which the characteristic function is known explicitly.

3.3.4 Lévy Processes

In the previous two sections we gave a brief account of the compound Poisson process and the symmetric α-stable Lévy process. This section is an introduction to general one-dimensional Lévy processes. The compound Poisson process and symmetric α-stable process are simply examples of Markov processes of Lévy type. Readers who are interested in this topic in greater detail are referred to the books by Applebaum [15] and Sato [378].

Recall that a Lévy process $X(t)$ is a continuous-time stochastic process that has independent and stationary increments. It represents a natural generalization of a simple random walk defined as a sum of independent identically distributed random variables. The independence of increments ensures that Lévy processes are Markov processes. The main feature of a Lévy process is that it is infinitely divisible for

any time t. It can be written as a sum of increments $X(t) = \sum_{k=1}^{n} \Delta X^k(t)$ for any $n \in N$, where $\Delta X^k(t)$ are identically distributed random variables. It is usually assumed that $X(0) = 0$. The simplest examples of Lévy processes are the Brownian motion $B(t)$, the Poisson process $N(t)$, and the compound Poisson process $X(t)$. Any Lévy process $X(t)$ can be written as the sum of a drift term at, a Brownian motion $B(t)$, and a pure jump process $Z(t)$ with a finite or infinite number of jumps in the interval $[0, t]$.

Its statistical characteristics are completely determined by the characteristic exponent $\psi(k)$, defined as

$$\mathbb{E}\left\{e^{ikX(t)}\right\} = e^{t\psi(k)}. \tag{3.103}$$

The exponent $\psi(k)$ has the Lévy–Khinchine representation

$$\psi(k) = iak - Dk^2 + \int_{z \neq 0} \left(e^{ikz} - 1 - ikz\chi_{0<|z|<1}\right) \nu(dz), \tag{3.104}$$

where a and D are constants, χ_A is the indicator function of the set A, and $\nu(dz)$ is a Lévy measure. The positive measure $\nu(A)$ is defined as the expected number of jumps of $X(t)$ per unit time, whose sizes belong to the set A. It must satisfy the integrability condition $\int_{z \neq 0} \min(1, z^2)\nu(dz) < \infty$, which means that there is a finite number of jumps whose size is $|z| \geq 1$, $\int_{|z| \geq 1} \nu(dz) < \infty$, and $\int_{0<|z|<1} z^2\nu(dz) < \infty$ because of the convergence requirement for the integral in (3.104). For example, the Lévy measure for the compound Poisson process (3.71) is $\nu(dz) = \lambda w(z)dz$. Note that instead of $z\chi_{0<|z|<1}$ one can use any bounded continuous function $g(z)$ satisfying $g(z) \to z$ as $z \to 0$. For example, $g(z) = z/(1 + z^2)$ or $g(z) = \sin z$.

It follows from the previous section that the Fourier transform $\tilde{\rho}(k, t)$ of the particle density $\rho(x, t)$ satisfies the equation

$$\frac{\partial \tilde{\rho}(k, t)}{\partial t} = \psi(k)\tilde{\rho}(k, t). \tag{3.105}$$

If we apply the inverse Fourier transform to this equation, we obtain an equation for the density $\rho(x, t)$:

$$\frac{\partial \rho}{\partial t} + a\frac{\partial \rho}{\partial x} = D\frac{\partial^2 \rho}{\partial x^2} + \int_{z \neq 0} \left(\rho(x - z, t) - \rho(x, t) + z\frac{\partial \rho}{\partial x}\chi_{0<|z|<1}\right) \nu(dz). \tag{3.106}$$

In particular, if the Lévy measure is $\nu(dz) = \lambda\delta(z - z_0)dz$ and the size of the jumps is $z_0 > 1$, then

$$\psi(k) = iak - Dk^2 + \lambda\left(e^{ikz_0} - 1\right). \tag{3.107}$$

The intuitive meaning of this formula is as follows. Let $X(t)$ be the position of a particle performing a random Lévy walk with (3.107), then $X(t) = at + B(t) + N_z(t)$. The particle starts at zero and then follows the Brownian motion $B(t)$ with the drift velocity a until the random time T_1 at which a jump of size z_0 takes place. Between random times T_1 and T_2 we have again the Brownian motion with a drift and then another jump of the same size z_0 at time T_2. The last term in (3.107) is related to a Poisson process $N_z(t)$ with the rate λ in the set of values $\{nz_0\}$ with $n = 1, 2, \ldots$. The particle position $X(t)$ is an example of a *cadlag* function. It is a *right-continuous with left limits* function for which there exist two limits, $X(t^+) = \lim_{s \to t^+} X(s)$ and $X(t^-) = \lim_{s \to t^-} X(s)$, so that $X(t) = X(t^+)$. The difference $\Delta X = X(t) - X(t^-)$ describes the jump of $X(t)$ at time t.

For example, the Lévy measure corresponding to anomalous transport is

$$\nu(dz) = \frac{C\,dz}{|z|^{1+\alpha}} \tag{3.108}$$

where $C = \text{const}$, $0 < \alpha < 2, \alpha \neq 1$ and $z \neq 0$. Let us assume that the drift a and the diffusion coefficient D are zero. Then it follows from (3.104) and (3.108) that the particle position $X(t)$ is the symmetric α-stable random process $S_\alpha(t)$, sometimes called a Lévy flight, with the anomalous diffusion coefficient $D_\alpha = 2C\alpha^{-1}\Gamma(1 - \alpha)\cos(\pi\alpha/2)$, see Sect. 3.3.3.2. It has an infinite variance which is associated with very large jumps. The mesoscopic transport equation for the particle density $\rho(x, t)$ is the space-fractional diffusion equation (3.91).

3.3.4.1 Finite and Infinite Number of Jumps

We can distinguish two cases: (1) the average number of jumps is finite, i.e., $\int_{z \neq 0} \nu(dz) < \infty$; (2) infinite number of jumps, i.e., $\int_{z \neq 0} \nu(dz) = \infty$.

The *compound Poisson process* $X(t)$, defined by (3.71), is an example of a pure jump process which has only a finite number of jumps on the finite time interval $[0, t]$. The Lévy measure $\nu(dz) = \lambda w(z)dz$ is finite on $\mathbb{R}$, that is, $\int_{z \neq 0} \nu(dz) = \lambda < \infty$. Note that ν is not a probability measure, because $\int_{\mathbb{R}} \nu(dz) = \lambda$. The characteristic function for the compound Poisson process is

$$\tilde{\rho}(k, t) = e^{t\lambda(\tilde{w}(k)-1)} = e^{t\psi(k)}, \tag{3.109}$$

where $\psi(k)$ is the characteristic exponent (see also (3.88))

$$\psi(k) = \lambda \int_{\mathbb{R}} \left(e^{ikz} - 1\right) w(z)dz. \tag{3.110}$$

The mesoscopic density of particles obeys the integro-differential equation (3.74).

The *Gamma process* is an example of a Lévy process with infinite number of jumps. The Gamma process $X_\Gamma(t)$ is a pure jump Lévy process with the intensity measure

$$\nu(dz) = \frac{\gamma_0}{z} e^{-\beta z} dz, \quad z > 0.$$ (3.111)

The jumps in $X_\Gamma(t)$ with a size in the interval $[z, z + dz]$ occur $\nu(dz)$. The parameter γ_0 determines the rate of jumps per unit time and β is the measure of jump size. Since the jumps are positive, we analyze the Gamma process by using the Laplace transform

$$\mathbb{E}\left\{ e^{-s X_\Gamma(t)} \right\} = e^{t \int_0^\infty (e^{-sz} - 1)\nu(dz)}.$$ (3.112)

Taking into account (3.112) and the integral $\int_0^\infty \left(e^{-sz} - 1 \right) \frac{1}{z} e^{-\beta z} dz = -\ln(\frac{s+\beta}{\beta})$, we obtain

$$\mathbb{E}\left\{ e^{-s X_\Gamma(t)} \right\} = \left(\frac{\beta}{s + \beta} \right)^{\gamma_0 t}.$$ (3.113)

The expression $\left[\beta/(s + \beta) \right]^{\gamma_0 t}$ is the Laplace transform of the density of the Gamma process [15]. Therefore, we can find an explicit expression for the mesoscopic density of particles for $x \geq 0$:

$$\rho(x, t) = \frac{\partial}{\partial x} \mathbb{P}(X_\Gamma(t) \leq x) = \frac{1}{\Gamma(\gamma_0 t)} \beta^{\gamma_0 t} x^{\gamma_0 t - 1} e^{-\beta x}.$$ (3.114)

Since the Lévy measure ν is infinite, i.e., $\nu(dz) = (\gamma_0/z) \exp(-\beta z) dz$ is not integrable as $z \to 0$, an infinite number of jumps occurs during a finite period of time. However, the Lévy measure ν can be approximated by

$$\nu_\delta(dz) = \begin{cases} 0, & z \leq \delta, \\ (\gamma_0/z) \exp(-\beta z) dz, & z > \delta, \end{cases}$$ (3.115)

where δ is a small number. Introducing the normalization constant $\lambda_\delta = \int_\delta^\infty (\gamma_0/z) \exp(-\beta z) dz$, we approximate the Gamma process by the compound Poisson process with intensity λ_δ that tends to infinity as $\delta \to 0$. In the limit we have an infinite number of jumps whose size distribution is given by

$$w_\delta(z) = \frac{(\gamma_0/z) e^{-\beta z}}{\int_\delta^\infty (\gamma_0/z) e^{-\beta z} dz}.$$ (3.116)

The mesoscopic density of particles obeys the integro-differential equation

$$\frac{\partial \rho}{\partial t} = \lambda_\delta \int_0^\infty \rho(x - z, t) w_\delta(z) dz - \lambda_\delta \rho(x, t).$$ (3.117)

3.4 Non-Markovian CTRW Models with Chemical Reactions

In this section we consider CTRW models for which the waiting time distribution is not exponential. The main challenge is to incorporate nonlinear kinetic terms into non-Markovian transport equations. Several approaches exist in the literature about how to include kinetic terms in reaction–transport systems with anomalous diffusion. We discuss them in detail in the following.

   We consider a one-component reaction–transport system consisting of particles that follow a CTRW. Let $\rho(x, t)$ represent the density of these particles at point x and time t. We write the reaction term in the form $F(\rho) = f(\rho)\rho$. It is also convenient to represent the nonlinear reaction rate $f(\rho)$ as the difference between the birth rate $f^+(\rho)$ and the death rate $f^-(\rho)$:

$$f(\rho) = f^+(\rho) - f^-(\rho). \tag{3.118}$$

For example, if we consider the Schlögl Model I, see (1.66), then

$$f^+(\rho) = k_1 \rho_a, \quad f^-(\rho) = k_3 \rho_b + k_2 \rho, \tag{3.119}$$

where the densities ρ_a and ρ_b are constant. Note that the birth rate $f^+(\rho)$ must allow for a constant term in $F(\rho)$, as occurs in the Brusselator, the Lengyel–Epstein model, and many other chemical schemes. In those cases, $f^+(\rho) = k\rho^{-1}$. For KPP kinetics, the birth rate is $f^+(\rho) = r$ and the death rate is $f^-(\rho) = r\rho$. The main purpose is to derive the nonlinear Master equation for the density $\rho(x, t)$ in the form $\partial\rho/\partial t = L\rho$, where the nonlinear evolution operator L has to be determined. We consider three different models for reactions and non-Markovian transport processes.

3.4.1 Model A

Non-Markovian behavior of particles performing a CTRW occurs if the particles are trapped for random times distributed according to a nonexponential distribution. The key question is how the chemical reaction influences the statistical properties of the CTRW. For Model A, we assume that the transport process associated with the CTRW and the chemical reactions are independent. We assume that the waiting time PDF $\phi(t)$ and jump length PDF $w(z)$ are independent and that the chemical reactions do not affect *at all* the waiting time PDF. This case has been considered in a series of papers [416, 143, 144, 187]. The main assumption here is that when particles are trapped, the waiting time is the same for all particles, including *newborn* particles. There are various ways to think about this assumption. In a chemical setting, the context of Sokolov and collaborators' work, the assumption implies that reactive events do not destroy or create particles, as for example in an isomerization reaction. Reactions simply change the state, label, or "color" of the particles. Such reactions are known as color-change reactions in the literature [320, 154, 271]. In

these reactions, the particles themselves survive a reactive event and their waiting time is not changed. In a population biology setting, the assumption implies that the *whole* community of individuals moves after a random time t, elapsed since the arrival of the founding members at site x, to a new site $x + z$.

Since the kinetics is of the form $f(\rho)\rho$, the change in the number of particles, of a given type, between the jumps involves the exponential factor $\exp[\int f(\rho(x, u))du]$. To explain this, let us introduce the density of particles $j(x, \tau)$ arriving at point x exactly at time τ. During time interval (τ, t), this density changes as follows:

$$j(x, \tau)e^{\int_\tau^t f(\rho(x,u))du}. \tag{3.120}$$

Let us now incorporate this nonlinear kinetic process into a non-Markovian transport process described by a CTRW. We write the equations for the densities $j(x, t)$ and $\rho(x, t)$ in the following forms:

$$j(x, t) = \int_\mathbb{R} \rho_0(x - z)e^{\int_0^t f(\rho(x-z,u))du} w(z)\phi(t)dz$$

$$+ \int_0^t \int_\mathbb{R} j(x - z, \tau)e^{\int_\tau^t f(\rho(x-z,u))du} w(z)\phi(t - \tau)dzd\tau \tag{3.121}$$

and

$$\rho(x, t) = \rho_0(x)e^{\int_0^t f(\rho(x,u))du} \Psi(t)$$

$$+ \int_0^t j(x, \tau)e^{\int_\tau^t f(\rho(x,u))du} \Psi(t - \tau)d\tau. \tag{3.122}$$

We are in position now to derive the Master equation for the density $\rho(x, t)$. Since the balance equations (3.121) and (3.122) are nonlinear, we cannot apply the standard technique of the Fourier–Laplace transforms directly. Instead we differentiate the density $\rho(x, t)$ with respect to time:

$$\frac{\partial \rho}{\partial t} = j(x, t) + f(\rho)\rho - \rho_0(x)e^{\int_0^t f(\rho(x,u))du}\phi(t)$$

$$- \int_0^t j(x, \tau)e^{\int_\tau^t f(\rho(x,u))du}\phi(t - \tau)d\tau. \tag{3.123}$$

The last two terms can be interpreted as the density of particles $i(x, t)$ leaving the point x exactly at time t:

$$i(x, t) = \rho_0(x)e^{\int_0^t f(\rho(x,u))du}\phi(t)$$

$$+ \int_0^t j(x, \tau)e^{\int_\tau^t f(\rho(x,u))du}\phi(t - \tau)d\tau. \tag{3.124}$$

It follows from (3.121) and (3.124) that $j(x, t) = \int_{\mathbb{R}} i(x-z, t)w(z)dz$. Then (3.123) can be rewritten as

$$\frac{\partial \rho}{\partial t} = \int_{\mathbb{R}} i(x - z, t)w(z)dz - i(x, t) + f(\rho)\rho. \tag{3.125}$$

This equation has a very simple meaning as the balance of particles at point x. The first term on the RHS corresponds to the number of particles arriving at x from different positions $x - z$. The second term represents the rate at which the particles leave the position x. The last term describes the rate of change due to kinetics. Note that a similar equation was used in [416]. The advantage of this equation lies in the fact that we do not need the Fourier transform to obtain a closed equation for the density $\rho(x, t)$. Let us express $i(x, t)$ in terms of $\rho(x, t)$. We divide (3.122) and (3.124) by the factor $e^{\int_0^t f(\rho(x,u))du}$ and take the Laplace transform $\mathcal{L}$ of both equations:

$$\mathcal{L}\left\{\rho(x, t)e^{-\int_0^t f(\rho(x,u))du}\right\} = \left[\rho_0(x) + \mathcal{L}\left\{j(x, t)e^{-\int_0^t f(\rho(x,u))du}\right\}\right]\hat{\Psi}(s), \tag{3.126}$$

$$\mathcal{L}\left\{i(x, t)e^{-\int_0^t f(\rho(x,u))du}\right\} = \left[\rho_0(x) + \mathcal{L}\left\{j(x, t)e^{-\int_0^t f(\rho(x,u))du}\right\}\right]\hat{\phi}(s). \tag{3.127}$$

From these two equations, we obtain

$$\mathcal{L}\left\{i(x, t)e^{-\int_0^t f(\rho(x,u))du}\right\} = \frac{\hat{\phi}(s)}{\hat{\Psi}(s)}\mathcal{L}\left\{\rho(x, t)e^{-\int_0^t f(\rho(x,u))du}\right\}. \tag{3.128}$$

The inverse Laplace transform yields the expression for $i(x, t)$:

$$i(x, t) = \int_0^t K(t - \tau)\rho(x, \tau)e^{\int_\tau^t f(\rho(x,u))du}d\tau, \tag{3.129}$$

where $K(t)$ is the standard memory kernel (3.34). Substitution of (3.129) into (3.125) results in the Master equation:

$$\frac{\partial \rho}{\partial t} = \int_0^t K(t - \tau)\left[\int_{\mathbb{R}} \rho(x - z, \tau)e^{\int_\tau^t f(\rho(x-z,u))du}w(z)dz\right.$$
$$\left. -\rho(x, \tau)e^{\int_\tau^t f(\rho(x,u))du}\right]d\tau + f(\rho)\rho. \tag{3.130}$$

Now consider the case where the reaction rate $f(\rho) = r = \text{const}$. Then the Master equation takes the form

$$\frac{\partial \rho}{\partial t} = \int_0^t K(t - \tau) e^{r(t-\tau)} \left[\int_{\mathbb{R}} \rho(x - z, \tau) w(z) dz - \rho(x, \tau) \right] d\tau + r\rho. \quad (3.131)$$

It is tempting to claim that this equation describes the coupling of chemical reaction and transport. We believe that this is misleading. In fact, this equation describes the perfect decoupling of transport with memory and linear reaction, in line with the main assumption of Model A. To show this, we make the substitution

$$\rho(x, t) = n(x, t) e^{rt}. \quad (3.132)$$

Then we obtain the following equation for $n(x, t)$,

$$\frac{\partial n}{\partial t} = \int_0^t K(t - \tau) \left[\int_{\mathbb{R}} n(x - z, \tau) w(z) dz - n(x, \tau) \right] d\tau, \quad (3.133)$$

which is independent of the reaction and describes the transport of passive particles. So we have a perfect decoupling for which the density $\rho(x, t)$ is the product of the density of passive particles $n(x, t)$ and the exponential factor e^{rt} due to reaction.

3.4.2 Model B

This model is equivalent to the Vlad–Ross approach of Sect. 2.3.2. We consider a CTRW which depends on the chemical reaction in the following way. Assume that the particles that are created with the rate $f^+(\rho)\rho$ have zero age. Note that particles also have zero age when they just arrive at some point x from which they will jump later. We interpret the density $j(x, t)$ as a zero-age density of particles arriving at the point x exactly at time t due to a jump process or a birth process with the rate $f^+(\rho)$. Equations for the densities $j(x, t)$ and $\rho(x, t)$ can be written as

$$j(x, t) = f^+(\rho)\rho + \int_{\mathbb{R}} \rho_0(x - z) e^{-\int_0^t f^-(\rho(x-z,u))du} w(z)\phi(t)dz$$
$$+ \int_0^t \int_{\mathbb{R}} j(x - z, \tau) e^{-\int_\tau^t f^-(\rho(x-z,u))du} w(z)\phi(t - \tau)dzd\tau$$

$$(3.134)$$

and

$$\rho(x, t) = \rho_0(x) e^{-\int_0^t f^-(\rho(x,u))du} \Psi(t)$$
$$+ \int_0^t j(x, \tau) e^{-\int_\tau^t f^-(\rho(x,u))du} \Psi(t - \tau)d\tau. \quad (3.135)$$

A single equation for the density $\rho(x, t)$ can be derived in the same way as for Model A. It takes the form

$$\frac{\partial \rho}{\partial t} = \int_0^t K(t-\tau)\left[\int_{\mathbb{R}} \rho(x-z,\tau)e^{-\int_\tau^t f^-(\rho(x-z,u))du}w(z)dz\right.$$

$$\left. -\rho(x,\tau)e^{-\int_\tau^t f^-(\rho(x,u))du}\right]d\tau + f^+(\rho)\rho - f^-(\rho)\rho. \qquad (3.136)$$

If we expand the expression in brackets for small z and truncate the Taylor series at the second moment, we obtain

$$\frac{\partial \rho}{\partial t} = \frac{\sigma^2}{2}\frac{\partial^2}{\partial x^2}\int_0^t K(t-\tau)\rho(x,\tau)e^{-\int_\tau^t f^-(\rho(x,u))du}d\tau$$

$$+f^+(\rho)\rho - f^-(\rho)\rho, \qquad (3.137)$$

which is identical with (2.82). Model B describes the situation where reactant parti- cles are destroyed and product particles are created during a reactive event, the com- mon situation in a chemical context, and where consequently the newborn product particles are endowed a new waiting time. This model does not distinguish between arrival of a particle at site x by reaction (birth) or by transport (jump); it treats both processes on the same footing. Model B is expected to describe chemical reactions in static porous or disordered media. Age on page 82 refers to the waiting time of particles at a given point. Note that we do not consider aging effects of the system as stated on page 64.

Models A and B result in the same reaction–transport equation, if the CTRW is Markovian. In that case, $K(t-\tau) = \delta(t-\tau)/\tau_0$, see Remark 2.5, and the Master equations (3.130) and (3.136) are identical:

$$\frac{\partial \rho}{\partial t} = \frac{1}{\tau_0}\left[\int_{\mathbb{R}} \rho(x-z,t)w(z)dz - \rho(x,t)\right] + f(\rho)\rho. \qquad (3.138)$$

3.4.3 Model C

This is a very simple model. It assumes that the reaction is a pure birth process. It corresponds to the case where the reaction term is $F(\rho) = f^+(\rho)\rho$. This model was considered in [188, 189, 121]. The balance equations are

$$j(x,t) = f^+(\rho)\rho + \int_{\mathbb{R}} \rho_0(x-z)\psi(z,t)dz$$

$$+ \int_0^t \int_{\mathbb{R}} j(x-z,t-\tau)\psi(z,\tau)dzd\tau \qquad (3.139)$$

and

$$\rho(x,t) = \rho_0(x)\Psi(t) + \int_0^t j(x,t-\tau)\Psi(\tau)d\tau. \qquad (3.140)$$

This system of equations can be written as a single equation for the density

$$\rho(x,t) = \rho_0(x)\Psi(t) + \int_0^t \int_{\mathbb{R}} \rho(x-z,t-\tau)\psi(z,\tau)dzd\tau$$

$$+ \int_0^t f^+(\rho(x,t-\tau))\rho(x,t-\tau)\Psi(\tau)d\tau. \tag{3.141}$$

Thus the simplest way to take into account the chemical reaction is to add the term $\int_0^t F(\rho(x,t-\tau))\Psi(\tau)d\tau$ to the RHS of the balance equation (3.41). The reaction term $F(\rho) = f^+(\rho)\rho$ is a pure birth process for which all newborn particles are given zero age.

Equation (3.141) takes the following form in Fourier–Laplace space:

$$\hat{\tilde{\rho}}(k,s) = \tilde{\rho}_0(k)\hat{\Psi}(s) + \hat{\tilde{\rho}}(k,s)\hat{\tilde{\psi}}(k,s) + \hat{\tilde{F}}(k,s)\hat{\Psi}(s). \tag{3.142}$$

We assume that the random jumps and the waiting times are independent, i.e., $\hat{\tilde{\psi}}(k,s) = \tilde{w}(k)\hat{\phi}(s)$, and divide (3.142) by $\hat{\phi}(s)$ to separate temporal and spatial variables:

$$\frac{\hat{\tilde{\rho}}(k,s)}{\hat{\phi}(s)} - \frac{\tilde{\rho}_0(k)\hat{\Psi}(s)}{\hat{\phi}(s)} = \hat{\tilde{\rho}}(k,s)\tilde{w}(k) + \frac{\hat{\tilde{F}}(k,s)\hat{\Psi}(s)}{\hat{\phi}(s)}. \tag{3.143}$$

If the waiting time PDF and the jump length PDF do not possess heavy tails, then the mean waiting time and the variance of the jump length PDF are finite, and we have the following results in the large-time and large-scale limit, see Sect. 3.2. First, the Fourier transform of the even dispersal kernel can be written as

$$\tilde{w}(k) = 1 - \sigma^2 k^2/2 + o(k^2), \tag{3.144}$$

since

$$\tilde{w}(0) = \int_{-\infty}^{\infty} w(x)dx = 1, \quad \tilde{w}'(0) = 0, \quad \sigma^2 = -\tilde{w}''(0) = \int_{-\infty}^{\infty} x^2 w(x)dx. \tag{3.145}$$

Second, $1/\hat{\phi}(s)$ can be written as

$$\frac{1}{\hat{\phi}(s)} \simeq 1 + \langle t\rangle s, \tag{3.146}$$

up to first order in s, or

$$\frac{1}{\hat{\phi}(s)} \simeq 1 + \langle t\rangle s + \left(\langle t\rangle^2 - \frac{\langle t^2\rangle}{2}\right)s^2 \tag{3.147}$$

up to second order, since

$$\hat{\phi}(0) = \int_0^\infty \phi(t)\mathrm{d}t = 1, \quad \langle t \rangle = -\hat{\phi}'(0) = \int_0^\infty t\phi(t)\mathrm{d}t, \tag{3.148}$$

$$\langle t^2 \rangle = \hat{\phi}''(0) = \int_0^\infty t^2 \phi(t)\mathrm{d}t. \tag{3.149}$$

Substituting (3.144) into (3.143) and using that $\hat{\Psi}(s) = [1 - \hat{\phi}(s)]/s$, we obtain

$$\frac{1 - \hat{\phi}(s)}{\hat{\phi}(s)} \left[\hat{\tilde{\rho}}(k, s) - \frac{\tilde{\rho}(k, 0)}{s} \right] = -\frac{\sigma^2 k^2}{2} \hat{\tilde{\rho}}(k, s) + \frac{1 - \hat{\phi}(s)}{s\hat{\phi}(s)} \hat{\tilde{F}}(k, s). \tag{3.150}$$

Substitution of (3.146) into (3.150) and inversion of the Fourier and Laplace transforms leads to the RD equation (2.3) with $D = \sigma^2/2 \langle t \rangle$. If we substitute (3.147) into (3.150) and invert the Fourier and Laplace transforms, we obtain the reaction-telegraph equation:

$$\left(\langle t \rangle - \frac{\langle t^2 \rangle}{2\langle t \rangle} \right) \frac{\partial^2 \rho}{\partial t^2} + \frac{\partial \rho}{\partial t} = \frac{\sigma^2}{2\langle t \rangle} \frac{\partial^2 \rho}{\partial x^2} + F + \left(\langle t \rangle - \frac{\langle t^2 \rangle}{2\langle t \rangle} \right) \frac{\partial F}{\partial t}. \tag{3.151}$$

A comparison of (2.19) and (3.151) leads to the relation between the macroscopic parameters τ (relaxation time) and D (diffusion coefficient) and the mesoscopic quantities, namely

$$\tau = \langle t \rangle - \frac{\langle t^2 \rangle}{2\langle t \rangle} \quad \text{and} \quad D = \frac{\sigma^2}{2\langle t \rangle}. \tag{3.152}$$

3.5 Random Walk in Random Time and Subordination

In this section we consider a random walk in random time. In this case the particle position X depends on the random time $T(t)$, $X(T(t))$, rather than on the conventional time t. An insight into this model can be obtained by considering a particle moving in a nonstationary random environment for which the intensity of jumps is random. We use the standard formula for the particle position as the sum of IID random jumps Z_i,

$$X(t) = \sum_{i=1}^{N(t)} Z_i, \tag{3.153}$$

in which the number of jumps $N(t)$ is a nonhomogeneous Poisson process with the random intensity $\lambda(t) \geq 0$. For example, one can think of a particle moving in a random turbulent flow. The process $X(t)$ is called a *compound Cox process* and $N(t)$ is a *doubly stochastic Poisson process*. The probability of n jumps up to time t is

$$\mathbb{P}(N(t) = n) = \mathbb{E}_\lambda \left\{ \frac{\left(\int_0^t \lambda(s) \mathrm{d}s \right)^n}{n!} \exp\left(-\int_0^t \lambda(s) \mathrm{d}s \right) \right\}, \qquad (3.154)$$

where the expectation $\mathbb{E}_\lambda$ is taken over the random process $\lambda(t)$. If we introduce the random time $T(t) = \lambda^{-1} \int_0^t \lambda(s) \mathrm{d}s$, then the Cox process $N(t)$ can be rewritten in terms of a homogeneous Poisson process $N_h(t)$ with intensity λ and random time $T(t)$ as

$$N(t) = N_h(T(t)). \qquad (3.155)$$

It follows from (3.153) and (3.155) that the particle position depends on $T(t)$:

$$X(T(t)) = \sum_{i=1}^{N_h(T(t))} Z_i. \qquad (3.156)$$

In what follows we put the intensity of the Poisson process $\lambda = 1$ and treat both t and $T(t)$ as dimensionless.

Let us now consider the random time $T(t)$ which is assumed to have nonnegative stationary and independent increments, an increasing Lévy process, such that $T(t) \geq 0$, $T(0) = 0$, and $T(t) \leq T(s)$ whenever $t \leq s$. It is often referred to as a *subordinator* or *operational time* (we assume that $T(t)$ and $N_h(t)$ are independent). If $X(t)$ is a Markov process, then the process $X(T(t))$ is Markovian too. The later process is said to be subordinate to $X(t)$ [15, 126].

Our goal is to find an equation for the density of particles that follow the random walk (3.156). First, let us find the characteristic function

$$\tilde{\rho}(k,t) = \mathbb{E}\left(e^{ikX(t)} \right) = \sum_{n=0}^{\infty} \mathbb{E}\left(e^{ikX(t)} \big| N(t) = n \right) \mathbb{P}(N(t) = n). \qquad (3.157)$$

Recall that we interpret this function as the Fourier transform of the density $\rho(x,t)$ with $\rho(x,0) = \delta(x)$. The conditional expectation is given by $\mathbb{E}\left(e^{ikX(t)} \big| N(t) = n \right) = \tilde{w}^n(k)$, where $\tilde{w}(k) = \mathbb{E}\left(e^{ikZ_i} \right)$ is the characteristic function of the random jumps Z_i. Using $N(t) = N_h(T(t))$ with $\lambda = 1$, we find

$$\mathbb{P}(N(t) = n) = \int_0^\infty \mathbb{P}(N_h(\tau) = n) p_T(\tau, t) \mathrm{d}\tau = \int_0^\infty \frac{\tau^n e^{-\tau}}{n!} p_T(\tau, t) \mathrm{d}\tau, \qquad (3.158)$$

where $p_T(\tau, t)$ is the PDF of the random time $T(t)$, defined as

$$p_T(\tau, t) = \frac{\partial}{\partial \tau} \mathbb{P}(T(t) \leq \tau). \qquad (3.159)$$

Substitution of (3.158) into (3.157) yields

$$\tilde{\rho}(k, t) = \sum_{n=0}^{\infty} \int_{0}^{\infty} \tilde{w}^n(k) \frac{(\tau)^n e^{-\tau}}{n!} p_T(\tau, t) d\tau$$

$$= \int_{0}^{\infty} e^{\tau(\tilde{w}(k)-1)} p_T(\tau, t) d\tau = \mathbb{E}\left(e^{T(t)(\tilde{w}(k)-1)} \right). \tag{3.160}$$

Since $T(t) \geq 0$ is a Lévy process, its Laplace transform, the moment generating function can be written as

$$\mathbb{E}\left(e^{-sT(t)} \right) = e^{-tl(s)}, \tag{3.161}$$

where $l(s)$ is the Laplace exponent of the random time $T(t)$. Using (3.160) and (3.161), we obtain

$$\tilde{\rho}(k, t) = e^{-tl(-(\tilde{w}(k)-1))}. \tag{3.162}$$

This implies that the characteristic exponent $\psi(k)$ for the particle position $X(t)$ is

$$\psi(k) = -l(-(\tilde{w}(k) - 1)). \tag{3.163}$$

For example, if the random time $T(t)$ is the Poisson process $N(t)$ with $\lambda = 1$, then the Laplace transform $\mathbb{E}\left(e^{-sN(t)} \right) = \sum_{n=0}^{\infty} e^{-sn} \mathbb{P}(N(t) = n) = e^{-t\left(1-e^{-s}\right)}$, therefore $l(s) = \left(1 - e^{-s} \right)$. In the long-time limit, $l(s) = s + o(s)$ as $s \to 0$. This limit corresponds to the Kolmogorov–Feller equation.

It follows from (3.89) that the mesoscopic transport equation for the density of particles is

$$\frac{\partial \rho}{\partial t} = L\rho, \tag{3.164}$$

where L is a pseudo-differential operator with symbol given by (3.163), $\mathcal{F}[L\rho] = \psi(k)\tilde{\rho}(k, t)$. When the random time $T(t)$ is deterministic $T(t) = t$, then the Laplace exponent is $l(s) = s$, the characteristic exponent defined in (3.161) is $\psi(k) = \tilde{w}(k) - 1$ and Eq. (3.164) becomes the Kolmogorov–Feller equation.

3.5.1 Space-Fractional Transport Equation

In this section we use the idea of subordination to obtain the space-fractional transport equation. Since $T(t)$ is a nonnegative Lévy process, the Laplace exponent $l(s)$ defined in (3.161) can be written as

$$l(s) = as + \int_{0}^{\infty} \left(1 - e^{-sz} \right) \nu(dz), \tag{3.165}$$

where $a \geq 0$ and $\nu(A) \geq 0$ is a Lévy measure satisfying $\int_{(0,\infty)} \min(1, z)\nu(dz) < \infty$ [15].

γ-*stable subordinator*. As an example, consider a strictly γ-stable random time $T_\gamma(t)$, the stable subordinator, for which $a = 0$ and the Lévy measure is

$$\nu(dz) = \frac{\gamma dz}{\Gamma(1 - \gamma)z^{1+\gamma}} \tag{3.166}$$

with $0 < \gamma < 1$. Let us find the Laplace exponent $l(s)$ of the γ-stable random time $T_\gamma(t)$. Integration by parts in (3.165) shows that $l(s) = s^\gamma$. Thus

$$\mathbb{E}\left(e^{-sT_\gamma(t)}\right) = \int_0^\infty e^{-s\tau} p_T(\tau, t)d\tau = e^{-ts^\gamma}, \tag{3.167}$$

which implies that $\mathbb{E}\left[T_\gamma(t)\right] = \infty$. The PDF $p_T(\tau, t)$ can be written in terms of the strictly γ-stable PDF $g_\gamma(\tau)$ with the Laplace transform

$$\hat{g}_\gamma(s) = e^{-s^\gamma}, \ 0 < \gamma < 1. \tag{3.168}$$

The strictly stable process $T_\gamma(t)$ has a nice scaling property: $T_\gamma(t) \stackrel{d}{=} t^{1/\gamma}T_\gamma(1)$ for all t. Scaling arguments lead to

$$p_T(\tau, t) = \frac{1}{t^{1/\gamma}} g_\gamma\left(\tau/t^{1/\gamma}\right). \tag{3.169}$$

Since the asymptotic decay of the tail of $g_\gamma(\tau)$ is $\tau^{-(1+\gamma)}$ as $\tau \to \infty$, we conclude that $p_T(\tau, t)$ has a power-law tail

$$p_T(\tau, t) \sim \frac{t}{\tau^{1+\gamma}} \tag{3.170}$$

as $\tau \to \infty$. The density $p_T(\tau, t)$ admits an explicit representation for $\gamma = \frac{1}{2}$ in terms of the Lévy–Smirnov density $g_{1/2}(\tau) = \left(4\pi\tau^3\right)^{-1/2} \exp(-1/4\tau)$:

$$p_T(\tau, t) = t^{-2}g_{1/2}\left(\tau/t^2\right) = \frac{t}{2\sqrt{\pi\tau^3}} \exp\left(-\frac{t^2}{4\tau}\right). \tag{3.171}$$

It follows from (3.163) that $\psi(k) = -[-(\tilde{w}(k) - 1)]^\gamma$. The governing equation for the particle density is the mesoscopic transport equation

$$\frac{\partial \rho}{\partial t} = \mathcal{I}_\gamma \rho(x, t), \tag{3.172}$$

where the right-hand side is the fractional integral operator, defined as

$$\mathcal{I}_\gamma g(x) = \mathcal{F}^{-1}\left[-(-(\tilde{w}(k) - 1))^\gamma \tilde{g}(k)\right], \tag{3.173}$$

and $\mathcal{F}^{-1}$ denotes the inverse Fourier transform. This operator can be considered as a generalization of the fractional Laplace operator. In the large-scale limit, $\tilde{w}(k) - 1 = -\sigma^2 k^2/2 + o(k^2)$ as $k \to 0$, the transport equation (3.172) can be approximated by the standard space-fractional diffusion equation

$$\frac{\partial \rho}{\partial t} = \frac{\sigma^\alpha}{\sqrt{2^\alpha}} \frac{\partial^\alpha \rho}{\partial |x|^\alpha} \tag{3.174}$$

with $\alpha = 2\gamma$.

If the density of particles following the Lévy process $X(t)$ is $\rho_X(x, t)$, then the density of particles performing the random walk $Y(t) = X(T(t))$ can be defined as

$$\rho_Y(x, t) = \int_0^\infty \rho_X(x, \tau) p_T(\tau, t) \mathrm{d}\tau, \tag{3.175}$$

where $p_T(\tau, t) = \frac{\partial}{\partial \tau} \mathbb{P}(T(t) \leq \tau)$ is the density of the random time $T(t)$. Note that the random process $Y(t)$ is a Lévy process too. In order to illustrate how the formula can be used, we consider the particles following the diffusion process $X(t)$ for which

$$\rho_X(x, \tau) = \frac{1}{\sqrt{2\pi\sigma^2\tau}} \exp\left(-\frac{x^2}{2\sigma^2\tau}\right). \tag{3.176}$$

Substitution of (3.176) and (3.171) into (3.175) yields the Cauchy density

$$\rho_Y(x, t) = \frac{\sigma t}{\sqrt{2\pi}\left(x^2 + \sigma^2 t^2/2\right)}. \tag{3.177}$$

This density is the Green function for the space-fractional equation (3.174) with $\alpha = 1$. The characteristic exponent $\psi_Y(k)$ of the new process $Y(t)$ can be obtained as a composition of the Laplace exponent $l(s)$ with the characteristic exponent $\psi_X(k)$, i.e.,

$$\mathbb{E}\left\{\mathrm{e}^{ikY(t)}\right\} = \mathrm{e}^{-t\psi_Y(k)} = \mathrm{e}^{-tl(-\psi_X(k))}. \tag{3.178}$$

We find

$$\mathbb{E}\left\{\mathrm{e}^{ikY(t)}\right\} = \int_0^\infty \mathbb{E}\left\{\mathrm{e}^{ikX(T(s))}\right\} p_T(s, t) \mathrm{d}s$$
$$= \int_0^\infty \mathrm{e}^{T(s)\psi_X(k)} p_T(s, t) \mathrm{d}s = \mathrm{e}^{-tl(-\psi_X(k))}. \tag{3.179}$$

Hougaard subordinator (tempered stable subordinator). Another example of a random time is the Hougaard subordinator $T(t)$ with the Lévy measure

$$v(\mathrm{d}z) = \frac{\gamma \xi e^{-kz}}{\Gamma(1-\gamma)z^{1+\gamma}}\mathrm{d}z, \quad z > 0, \tag{3.180}$$

where $k \geq 0, \xi > 0$, and $0 < \gamma < 1$. This density is obtained from the γ-stable density if we multiply it by the factor ξe^{-kz}. The Laplace transform for the Hougaard process is

$$\mathbb{E}\left\{e^{-sT(t)}\right\} = \exp\left[t\int_0^\infty (1-e^{-sz})v(\mathrm{d}z)\right] = e^{-t\xi\left[(k+s)^\gamma - k^\gamma\right]}, \quad s \geq 0. \tag{3.181}$$

The Laplace exponent is $l(s) = \xi\left[(k+s)^\gamma - k^\gamma\right]$. For $\gamma = 1$ we have a deterministic process $T(t) = \xi t$. If $k = 0$ and $\xi = 1$ we have a γ-stable subordinator. In particular, the mean value is

$$\mathbb{E}\left\{T(t)\right\} = -\frac{\partial}{\partial s}\mathbb{E}\left\{e^{-sT(t)}\right\}_{s=0} = \frac{\gamma\xi t}{k^{1-\gamma}} \tag{3.182}$$

and it is finite. It is clear that $\mathbb{E}\left\{T(t)\right\} \to \infty$ as $k \to 0$ for $0 < \gamma < 1$. So the Hougaard subordinator is useful when we consider transport processes with both normal and anomalous behaviour.

3.5.2 Inverse Subordination and Time-Fractional Transport Equation

In this section we show how to obtain subdiffusive transport by using the idea of inverse subordination [278, 371]. Assume that the density $\rho_X(x, t)$ obeys the Kolmogorov–Feller equation

$$\frac{\partial\rho_X}{\partial t} = \int_\mathbb{R} \rho_X(x - z, t)w(z)\mathrm{d}z - \rho_X(x, t) \tag{3.183}$$

with the initial condition

$$\rho_X(x, 0) = \rho_0(x). \tag{3.184}$$

We define the particle density $\rho(x, t)$ as follows:

$$\rho(x, t) = \int_0^\infty \rho_X\left(x, \left(\frac{t}{\tau}\right)^\gamma\right)g_\gamma(\tau)\mathrm{d}\tau, \tag{3.185}$$

where $g_\gamma(\tau)$ is the density of the γ-stable variable with $0 < \gamma < 1$ defined by the Laplace transform (3.168). Then $\rho(x, t)$ satisfies the time-fractional Kolmogorov–Feller equation

$$\frac{\partial^\gamma\rho}{\partial t^\gamma} = \int_\mathbb{R} \rho(x - z, t)w(z)\mathrm{d}z - \rho(x, t), \tag{3.186}$$

where $\partial^\gamma \rho / \partial t^\gamma$ is the Caputo fractional derivative and time t is dimensionless. The main idea here is the introduction of the subordinated process, the position of particles $X(N_\gamma(t))$, whose mesoscopic density is $\rho(x, t)$. The parent process $X(t)$ is the compound Poisson process with the density $\rho_X(x, t)$ and the random time $N_\gamma(t)$ is the inverse γ-stable subordinator defined as the hitting time $N_\gamma(t) = \inf(\tau : T_\gamma(\tau) > t)$ for γ-stable subordinator $T_\gamma(\tau)$ with the Laplace exponent $l(s) = s^\gamma$. The non-Markovian behavior of the inverse subordinator $N_\gamma(t)$ leads to subdiffusion of $X(N_\gamma(t))$. The details of the derivation of (3.186) can be found in [278]. Note that as the parent process $X(t)$ one can use any Lévy process with the transport operator L, so the time-fractional equation is of the form $\partial^\gamma \rho / \partial t^\gamma = L\rho$.

3.6 Macroscopic Description

The term *macroscopic* description refers to the long-time and large-scale limit, $t \to \infty$ and $x \to \infty$, of mesoscopic equations where the details of the *microscopic* movement are irrelevant. In particular, it refers to the *diffusive limit* where balance equations such as (3.13), (3.41), and (3.74) are approximated by the diffusion equation (2.1). The standard derivation of the diffusion equation involves the assumption that the typical microscopic jumps and times are small compared to the characteristic macroscopic space and time scales. Let us illustrate this using the mesoscopic transport equation (3.74). If the jump density $w(z)$ is a rapidly decaying function for large z, one can expand $\rho(x - z, t)$ in z and truncate the Taylor series at the second moment:

$$\rho(x - z, t) = \rho(x, t) - \frac{\partial \rho}{\partial x} z + \frac{1}{2} \frac{\partial^2 \rho}{\partial x^2} z^2 + o(z^2). \tag{3.187}$$

Substitution of (3.187) into (3.74) yields

$$\frac{\partial \rho}{\partial t} + v \frac{\partial \rho}{\partial x} = D \frac{\partial^2 \rho}{\partial x^2}, \tag{3.188}$$

where

$$v = \lambda \int_{\mathbb{R}} z w(z) \mathrm{d}z, \quad D = \frac{\lambda}{2} \int_{\mathbb{R}} z^2 w(z) \mathrm{d}z. \tag{3.189}$$

This truncation is a well-defined procedure, if the higher moments become progressively smaller. If the jump density $w(z)$ is even, then we obtain the standard diffusion equation. However, this "naive" Taylor series expansion is not valid for "heavy-tailed" probability density functions, such as a Cauchy PDF,

$$w(z) = \frac{\sigma}{\pi \left(\sigma^2 + z^2 \right)}, \tag{3.190}$$

for which the second moment, $\int_{\mathbb{R}} z^2 w(z) dz$, diverges. A jump PDF is said to have a power-law tail if

$$w(z) \sim \frac{1}{|z|^{1+\alpha}}, \quad z \to \infty, \tag{3.191}$$

for which the nth moment exists if $n < \alpha$. The question arises for which values of the power-law exponent α the diffusion approximation (2.1) is not valid.

3.6.1 Scaling Procedure

In this section we use a scaling procedure to derive *macroscopic* equation. This allows us to understand the connection between *macroscopic* and *microscopic* descriptions. We introduce the *macroscopic* variables (x^*, t^*) as follows:

$$x^* = \varepsilon^H x, \quad t^* = \varepsilon t, \tag{3.192}$$

where ε is a small parameter and H is a scaling exponent that has to be determined. It is convenient to introduce such a small parameter, so that instead of taking the limits $t \to \infty$ and $x \to \infty$, we can consider $\varepsilon \to 0$ for fixed values of the *macroscopic* space–time variables (x^*, t^*). We now drop the asterisk for *macroscopic* variables and adopt the following notation for rescaling:

$$x \to \frac{x}{\varepsilon^H}, \quad t \to \frac{t}{\varepsilon}. \tag{3.193}$$

To illustrate the method, we derive the diffusion equation corresponding to the discrete balance equation (3.13). For simplicity, we assume that the jump density is an even function, $w(z) = w(-z)$. We introduce the continuous-time variable t so that $n = [t]$, where $[\cdot]$ denotes the integer part of a real number. Using (3.193), we obtain the rescaled density

$$\rho^\varepsilon(x, t) = \rho\left(\frac{x}{\varepsilon^H}, \left[\frac{t}{\varepsilon}\right]\right). \tag{3.194}$$

Note that $[t/\varepsilon] \approx t/\varepsilon$ as $\varepsilon \to 0$. From (3.13) we obtain the equation

$$\rho^\varepsilon(x, t + \varepsilon) = \int_{\mathbb{R}} \rho^\varepsilon\left(x - \varepsilon^H z, t\right) w(z) dz. \tag{3.195}$$

It is clear that after rescaling the time step, $\varepsilon \ll 1$, the jump size is proportional to ε^H. In the limit $\varepsilon \to 0$, we expand both sides of the rescaled equation (3.195) in a Taylor series as

$$\rho^\varepsilon(x,t) + \frac{\partial \rho^\varepsilon}{\partial t}\varepsilon + o(\varepsilon) = \rho^\varepsilon(x,t) + \frac{\sigma^2}{2}\frac{\partial^2 \rho^\varepsilon}{\partial x^2}\varepsilon^{2H} + o\left(\varepsilon^{2H}\right), \qquad (3.196)$$

where $\sigma^2 = \int_{\mathbb{R}} z^2 w(z)\mathrm{d}z$. To obtain the *macroscopic* diffusion equation for the density $\rho(x,t) = \lim_{\varepsilon\to 0}\rho^\varepsilon(x,t)$, we must choose $H = 1/2$. Then (3.196) turns into (2.1) with the diffusion coefficient $D = \sigma^2/2$. This limit has a very nice probabilistic interpretation. First let us consider the discrete case. It follows from the central limit theorem (CLT) that if the number of steps n is large, the rescaled particle position $X_n/n^{\frac{1}{2}}$ tends to a Gaussian variable with zero mean and variance σ^2. The random position X_n is defined in (3.10). In particular $\mathbb{E}X_n^2 = \sigma^2 n$. The functional CLT states that if Z_i is a sequence of IID random variables with zero mean and variance $\sigma^2 = \mathbb{E}\left(Z_i^2\right)$, then

$$\frac{X_{[nt]}}{n^{\frac{1}{2}}} = \frac{1}{n^{\frac{1}{2}}}\sum_{i=1}^{[nt]}Z_i \xrightarrow{\mathrm{d}} B(t) \text{ as } n \to \infty, \qquad (3.197)$$

where $\xrightarrow{\mathrm{d}}$ means convergence in distribution. Here $B(t)$ is the Brownian motion with the PDF

$$\frac{\mathrm{d}}{\mathrm{d}x}\mathbb{P}(B(t) \le x) = \frac{1}{\sqrt{4\pi Dt}}\exp\left(-\frac{x^2}{4Dt}\right), \qquad (3.198)$$

which is the Green's function for the diffusion equation (2.1) with $D = \sigma^2/2$.

Using the rescaling $t \to t/\varepsilon$ with a small parameter $\varepsilon = n^{-1}$ and fixed time t, we write a rescaled particle position $X^\varepsilon(t)$ in terms of X_n:

$$X^\varepsilon(t) = \varepsilon^{\frac{1}{2}}X_{[t/\varepsilon]} = \varepsilon^{\frac{1}{2}}\sum_{i=1}^{[t/\varepsilon]}Z_i. \qquad (3.199)$$

The functional CLT ensures that as $\varepsilon \to 0$, the random process $X^\varepsilon(t)$ converges to the Brownian motion $B(t)$. The PDF $p^\varepsilon(x,t)$ for the particle position $X^\varepsilon(t)$, starting at $x = 0$, satisfies

$$\lim_{\varepsilon\to 0}\frac{1}{\varepsilon}p^\varepsilon(x,t) = \lim_{\varepsilon\to 0}\frac{1}{\varepsilon}p\left(\frac{x}{\varepsilon^{\frac{1}{2}}},\left[\frac{t}{\varepsilon}\right]\right) = \frac{1}{\sqrt{2\pi\sigma^2 t}}\left(-\frac{x^2}{2\sigma^2 t}\right) \qquad (3.200)$$

where $p(x,t)$ is defined in (3.11).

It is instructive to show that $X^\varepsilon(t) \xrightarrow{\mathrm{d}} B(t)$ as $\varepsilon \to 0$. Let us use the characteristic function

$$\mathbb{E}\left\{\exp(ikX^{\varepsilon}(t))\right\} = \mathbb{E}\left\{\exp\left(ik\varepsilon^{\frac{1}{2}}\sum_{i=1}^{[t/\varepsilon]}Z_i\right)\right\} = \left(\mathbb{E}\left\{\exp\left(ik\varepsilon^{\frac{1}{2}}Z_i\right)\right\}\right)^{[t/\varepsilon]}.$$

(3.201)

In the limit $\varepsilon \to 0$, we have $[t/\varepsilon] \approx t/\varepsilon$, and $\mathbb{E}\left\{\exp(ikX^{\varepsilon}(t))\right\} = (1 - k^2\varepsilon\sigma^2/2 + o(\varepsilon))^{t/\varepsilon} \to \exp(-k^2\sigma^2 t/2)$. That is

$$\lim_{\varepsilon\to 0}\mathbb{E}\left\{\exp\left(ikX^{\varepsilon}(t)\right)\right\} = \exp\left(-Dk^2 t\right),$$

(3.202)

which is a characteristic function of the Brownian motion with $D = \sigma^2/2$. In the next section we consider the case where the random variables Z_i have infinite second moments, which leads to the anomalous scaling $x \to x/\varepsilon^{1/\alpha}$, $t \to t/\varepsilon$, and $\lim_{\varepsilon\to 0}\mathbb{E}\left\{\exp(ikX^{\varepsilon}(t))\right\} = \exp(-D_{\alpha}|k|^{\alpha}t)$ with $0 < \alpha < 2$. This corresponds to the convergence of the discrete random walk X_n (3.10) to the symmetric α-stable Lévy process (Lévy flight).

If we rescale the compound Poisson process $X(t)$ as

$$X^{\varepsilon}(t) = \varepsilon^{\frac{1}{2}}X(t/\varepsilon) = \varepsilon^{\frac{1}{2}}\sum_{i=1}^{N(t/\varepsilon)}Z_i,$$

(3.203)

one can show that the random process $X^{\varepsilon}(t)$ converges to the Brownian motion $B(t)$ as well. This is the probabilistic explanation why the integral equation (3.74) can be approximated by the diffusion equation. However, if the second moment $\mathbb{E}(Z_i^2) = \infty$, then $X^{\varepsilon}(t)$ has other limiting processes, depending on the counting process $N(t)$.

3.6.2 Anomalous Scaling

So far we have discussed random walks with a finite mean waiting time and a finite variance of the jump length. These models lead to the classical parabolic scaling: $x \to x/\varepsilon^{1/2}$, $t \to t/\varepsilon$. The governing macroscopic equation for the density ρ becomes the standard diffusion equation. Let us now consider two cases for which the scaling is anomalous and the mean-field equations for ρ are fractional diffusion equations.

3.6.2.1 Finite Mean Waiting Time and Infinite Variance

Suppose that the jump PDF $w(z)$ is an even function and decreases as

$$w(z) \sim \frac{1}{|z|^{1+\alpha}}, \quad 0 < \alpha < 2,$$

(3.204)

for large z. It is clear that the second moment diverges for $0 < \alpha < 2$. The key question is how the rescaled process $X^\varepsilon(t) = \varepsilon^H X(t/\varepsilon)$ behaves as $\varepsilon \to 0$. Note that we rescale $X(t)$ by using a nontrivial scaling exponent H, the Hurst exponent. As before, we assume that the particle position $X(t)$ at time t is given by a CTRW

$$X(t) = \sum_{i=1}^{N(t)} Z_i, \tag{3.205}$$

where $N(t)$ is the Poisson process and the Z_i are random jumps with a heavy-tailed density (3.204). For simplicity, the jumps are assumed to be independent of the counting process $N(t)$. The waiting times between jumps are exponentially distributed with the mean value λ^{-1}. The generalized CLT ensures that

$$X^\varepsilon(t) = \varepsilon^H X(t/\varepsilon) = \varepsilon^H \sum_{i=1}^{N(t/\varepsilon)} Z_i \tag{3.206}$$

converges in distribution to a symmetric α-stable Lévy process, that is, $X^\varepsilon(t) \xrightarrow{d} S_\alpha(t)$ as $\varepsilon \to 0$ [126] (see Sect. 3.3.3.2). The density of particles obeys the fractional diffusion equation

$$\frac{\partial \rho}{\partial t} = D_\alpha \frac{\partial^\alpha \rho}{\partial |x|^\alpha} \tag{3.207}$$

with $0 < \alpha < 2$. We conclude that stable Lévy processes are important for transport theory because they provide the macroscopic description of particles with heavy-tailed jumps in the hydrodynamic limit, $t \to \infty$ and $x \to \infty$.

From a probabilistic point of view, $S_\alpha(t)$ is the attractor for the rescaled particle position $X^\varepsilon(t)$. To understand this, consider first a discrete random walk. The rescaled position of a particle with jumps Z_i that are symmetric with respect to zero is $Y_n = n^{-1/\alpha} \sum_{i=1}^n Z_i$ with $0 < \alpha < 2$. We are interested in the limit $n \to \infty$, such that the sequence Y_n converges toward a "new" random variable Z in distribution, i.e., $Y_n \xrightarrow{d} Z$ as $n \to \infty$ or $\lim_{n\to\infty} \mathbb{P}(Y_n < x) = \mathbb{P}(Z < x)$. The random variable Z is referred to as a symmetric *stable variable*. Since the parameter α plays a very important role, the random variable Z is said to be a symmetric α-stable random variable.

Recall that, in general, the stable random variable Z involves four parameters: the exponent (stable index) $0 < \alpha \leq 2$, the skewness $-1 \leq \beta \leq 1$, the shift $a \in \mathbb{R}$, and the scale $\sigma \geq 0$. It is well known that the stable probability density function

$$w(z|\alpha, \beta, \sigma, a) = \frac{\partial}{\partial z} \mathbb{P}(Z < z) \tag{3.208}$$

cannot be written in an explicit form, but its Fourier transform, the characteristic function has the following representation:

$$\tilde{w}(k|\alpha, \beta, \sigma, a) = \exp\left[ika - \sigma^{\alpha}|k|^{\alpha}(1 - i\beta\, \text{sgn}(k)\Omega)\right], \tag{3.209}$$

where $\Omega = \tan(\pi\alpha/2)$ for $\alpha \neq 1$ and $\Omega = -2/\pi \log|k|$ for $\alpha = 1$. The value $\beta = 0$ corresponds to a symmetric PDF. For example, the Cauchy distribution is

$$w(x|1, 0, \sigma, a) = \frac{\sigma}{\pi\left[(x-a)^2 + \sigma^2\right]}, \tag{3.210}$$

for which $\alpha = 1$. We refer to Feller's book [126] for further details on stable random variables.

The generalized CLT states that if the jumps Z_i are symmetric around zero and distributed with heavy tails like $|z|^{-1-\alpha}$ for $z \to \infty$, then for a large number of steps n, the rescaled particle position $X_n/n^{1/\alpha}$ can be described by a symmetric α-stable distribution with $a = \beta = 0$. So if we choose $H = 1/\alpha$, then the rescaled particle position

$$X^{\varepsilon}(t) = \varepsilon^H \sum_{i=1}^{N(t/\varepsilon)} Z_i \tag{3.211}$$

tends to the symmetric α-stable Lévy process $S_\alpha(t)$ with the characteristic function $\mathbb{E}\left(e^{ikS_\alpha(t)}\right) = e^{-D_\alpha|k|^\alpha t}$ and $D_\alpha = \lambda\sigma^\alpha$ (see (3.99)). The parameter D_α is referred to as a scale factor, which is a measure of the width of the density $\rho(x, t)$.

We conclude that as long as the mean waiting time and the variance of the jumps are finite, parabolic scaling leads to the Brownian motion in the limit $\varepsilon \to 0$. The *macroscopic* equation for the density of particles is a scale-invariant diffusion equation. Infinite variance of jumps in the domain of attraction of a stable law leads to Lévy processes, Lévy flights. In the limit $\varepsilon \to 0$, the particle position $X^{\varepsilon}(t)$ becomes self-similar with exponent $1/\alpha$. Recall that the random process $X(t)$ is *self-similar*, if there exists a scaling exponent H such that $X(t)$ and $\varepsilon^H X(t/\varepsilon)$ have the same distributions for any scaling parameter ε. In this case we write $X(t) \stackrel{\text{d}}{=} \varepsilon^H X(t/\varepsilon)$. For a symmetric Lévy process with the characteristic function $\mathbb{E}\{\exp(ikX(t))\} = \exp(-D_\alpha|k|^\alpha t)$, the scaling exponent is $H = 1/\alpha$. For the Brownian motion, $H = 1/2$. The main feature of a symmetric α-stable Lévy process is that it has independent heavy-tailed increments. The asymptotic behavior of the density of particles $\rho(x, t)$ for large x is

$$\rho(x, t) \sim \frac{D_\alpha t}{|x|^{1+\alpha}}. \tag{3.212}$$

In the three-dimensional case, the fractional diffusion equation in the long-time large-scale limit has the form

$$\frac{\partial \rho}{\partial t} = -D_\alpha (-\Delta)^{\frac{\alpha}{2}} \rho, \qquad \mathbf{x} \in \mathbb{R}^3, \tag{3.213}$$

in which the standard Laplacian Δ is replaced by a fractional Riesz operator. This replacement leads to a faster spread of particles, than the standard diffusion equation describes, i.e., superdiffusion, see Sect. 2.3. This is due to the heavy tails of the dispersal kernel $w(\mathbf{z}) \sim |\mathbf{z}|^{-d-\alpha}$ with $0 < \alpha < 2$ as $\mathbf{z} \to \infty$ where d is the dimension of space, $\mathbb{R}^d$. The underlying stochastic process is the rotationally invariant α-stable process [15]. A careful discussion of stable distributions and corresponding random processes is provided in [373, 444].

3.6.2.2 Infinite Mean Waiting Time and Infinite Variance of Jumps

Assume that the PDF of the waiting time $\phi(t)$ decreases like $t^{-1-\gamma}$ as $t \to \infty$, and particles have a dispersal kernel $w(z)$ with heavy tails $|z|^{-1-\alpha}$. What is the scale-invariant *macroscopic* equation for the particles density in this case? It turns out that the infinite variance of jumps leads to a fractional space derivative, and the infinite mean waiting time leads to the fractional Caputo derivative. The density of particles obeys the time–space fractional diffusion equation

$$\frac{\partial^\gamma \rho}{\partial t^\gamma} = D_{\alpha,\gamma} \frac{\partial^\alpha \rho}{\partial |x|^\alpha} \tag{3.214}$$

and the scale invariance relation

$$\rho(x, t) = \frac{1}{\varepsilon^{\frac{\gamma}{\alpha}}} \rho \left(\frac{x}{\varepsilon^{\frac{\gamma}{\alpha}}}, \frac{t}{\varepsilon} \right). \tag{3.215}$$

Note that the underlying stochastic process $S_{\alpha,\gamma}$ is not Markovian ($0 < \gamma < 1$) [371].

Let us show how the standard diffusion equation (3.16) and anomalous diffusion equation (3.214) emerge as a result of long-time large-scale limit of a CTRW described by (3.53). If we use the Dirac delta-function as the initial condition, then $\tilde{\rho}_0(k) = 1$, and the Fourier–Laplace transform of $\rho(x, t)$, (3.53), is given by

$$\hat{\tilde{\rho}}(k, s) = \frac{1 - \hat{\phi}(s)}{s \left[1 - \tilde{w}(k)\hat{\phi}(s) \right]}. \tag{3.216}$$

First we rescale $\hat{\tilde{\rho}}(k, s)$ as $\rho^\varepsilon(k, s) = \hat{\tilde{\rho}} \left(\varepsilon^H k, \varepsilon s \right)$ and use the standard expansions

$$\tilde{w} \left(\varepsilon^H k \right) = 1 - \frac{\sigma^2 \varepsilon^{2H} k^2}{2} + o \left(\varepsilon^{2H} \right), \tag{3.217}$$

$$\hat{\phi}(\varepsilon s) = 1 - \overline{T}\varepsilon s + o(\varepsilon). \tag{3.218}$$

If we choose scaling exponent $H = 1/2$, we obtain

$$\lim_{\varepsilon \to 0} \rho^\varepsilon(k, s) = \frac{1}{s + Dk^2}, \tag{3.219}$$

with $D = \sigma^2/2\overline{T}$. This corresponds to the standard diffusion equation; in the long-time large-scale limit all details of the random walk become irrelevant.

Consider now the anomalous case with the following scaling behavior:

$$\tilde{w}\left(\varepsilon^H k\right) = 1 - \frac{\sigma^\alpha \varepsilon^{H\alpha} |k|^\alpha}{2} + o\left(\varepsilon^{\alpha H}\right), \tag{3.220a}$$

$$\hat{\phi}(\varepsilon s) = 1 - \tau_0^\gamma (\varepsilon s)^\gamma + o\left(\varepsilon^\gamma\right). \tag{3.220b}$$

Substitution of these expressions into (3.216) yields the rescaled density $\rho^\varepsilon(k, s) = \hat{\tilde{\rho}}\left(\varepsilon^H k, \varepsilon s\right)$. To obtain a nontrivial limit $\lim_{\varepsilon \to 0} \rho^\varepsilon(k, s)$, we have to choose

$$H = \frac{\gamma}{\alpha} \tag{3.221}$$

such that

$$\lim_{\varepsilon \to 0} \rho^\varepsilon(k, s) = \frac{s^{\gamma-1}}{s^\gamma + D_{\alpha,\gamma} k^\alpha}, \tag{3.222}$$

which is the Fourier–Laplace transform of the fundamental solution of the time–space fractional equation (3.214) with

$$D_{\alpha,\gamma} = \frac{\sigma^\alpha}{2\tau_0^\gamma}. \tag{3.223}$$

Further details on the Cauchy problem for the time–space fractional diffusion equation (3.214) and its extension for the asymmetric case can be found in [371, 260].

Let us examine more closely the nature of the underlying stochastic process $S_{\alpha,\gamma}(t)$ for the time–space fractional equation (3.214). The latter is the long-time large-scale limit of the generalized Master equation (3.43) under the conditions that the symmetric jumps have a heavy-tailed density (3.204) with infinite variance and the waiting time PDF $\phi(t)$ decreases like $t^{-1-\gamma}$ with the index $0 < \gamma < 1$ as $t \to \infty$. Let us find the long-time large-scale limit of the CTRW under these conditions. We have introduced the CTRW as a subordinated stochastic process $X(t) = X_{N(t)}$ in which the parent process X_n is the position of a particle (3.10) in the discrete-time random walk (DTRW) model and the counting process $N(t)$ plays the role of the randomized time or operational time (see (3.26)). We have shown that

under the anomalous scaling $x \rightarrow x/\varepsilon^{1/\alpha}$, $t \rightarrow t/\varepsilon$, the discrete random walk X_n (3.10) converges to the symmetric α-stable Lévy process $S_\alpha(t)$, i.e.,

$$\varepsilon^{1/\alpha} X_{[t/\varepsilon]} \xrightarrow{d} S_\alpha(t) \tag{3.224}$$

as $\varepsilon \rightarrow 0$. It can be shown that the rescaled counting process converges as

$$\varepsilon^\gamma N\left(\frac{t}{\varepsilon}\right) \xrightarrow{d} N_\gamma(t) \tag{3.225}$$

If we compose these two processes, we obtain the subordinated process

$$S_{\alpha,\gamma}(t) = S_\alpha(N_\gamma(t)), \tag{3.226}$$

which is the scaling limit of the CTRW we are looking for. Note that $N_\gamma(t)$ is the hitting time: $N_\gamma(t) = \inf(\tau : T_\gamma(\tau) > t)$ for the γ-stable subordinator $T_\gamma(\tau)$. The latter is the scaling limit of the time of the nth jump T_n,

$$\varepsilon^{1/\gamma} T_{[t/\varepsilon]} = \varepsilon^{1/\gamma} \sum_{i=1}^{[t/\varepsilon]} \Theta_i \xrightarrow{d} T_\gamma(t), \tag{3.227}$$

as $\varepsilon \rightarrow 0$. Here $\Theta_i = T_i - T_{i-1}$ is the interval between jumps. The non-Markovian behavior of the inverse subordinator $N_\gamma(t)$ leads to the non-Markovian behavior of $S_{\alpha,\gamma}(t)$. Of course, the scaling limit $S_{\alpha,\gamma}(t)$ is a self-similar process: $S_{\alpha,\gamma}(t) \stackrel{d}{=} \varepsilon^{\gamma/\alpha} S_{\alpha,\gamma}(t/\varepsilon)$. For further details and the statistical analysis of the relation between rescaled CTRWs and fractional equations, we refer to the series of papers by Meerschaert and his colleagues [39, 275, 277, 276, 278, 22, 25].

In Fig. 3.2 we present a schematic picture of the convergence from microscopic to macroscopic levels of description for different scalings and processes.

3.6.3 Scaling and Convergence to the Diffusion Process

We have seen how the scaling procedure can be used to obtain a *macroscopic* standard or fractional diffusion equation. We now describe the method for obtaining *macroscopic* equations without deriving *mesoscopic* balance equations like (3.13), (3.41), or (3.74). Let us explain the usefulness of the rescaling procedure. When *mesoscopic* balance equations are derived from some underlying *microscopic* random walk models, certain simplifying assumptions are made regarding the statistical characteristics of random movements. However, if the assumptions are less restrictive, we might have some problems deriving closed balance equations for the particle density. In fact, in many cases we will not be able to do so.

Consider the *microscopic* stochastic equation for the particle position $X(t)$,
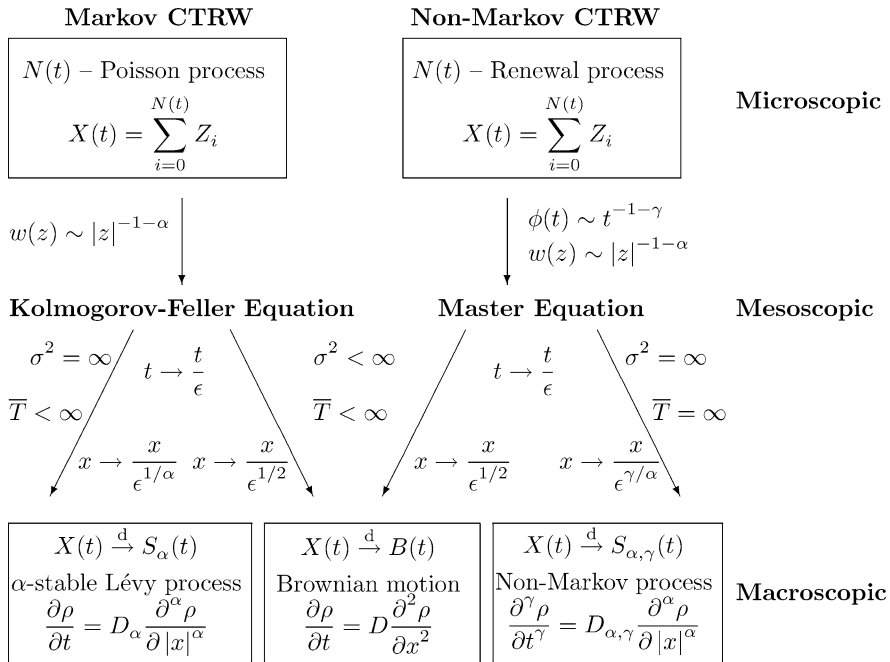
Fig. 3.2 Schematic picture for transition from microscopic to macroscopic equations

$$\frac{\mathrm{d}X}{\mathrm{d}t} = v\left(\varepsilon^{1/2}X(t), \xi(t)\right), \tag{3.228}$$

where the velocity v is a slowly varying function of the space coordinate x; $\varepsilon^{1/2}$ is a small parameter. We assume that v depends on some stationary random process $\xi(t)$ with zero mean. Under quite general conditions, the rescaled particle position, $X^{\varepsilon}(t) = \varepsilon^{\frac{1}{2}} X(t/\varepsilon)$, tends to a diffusion process as $\varepsilon \to 0$. The key question is how to find the effective velocity and diffusivity in the corresponding Fokker–Planck equation.

Before dealing with the general stochastic equation (3.228), it is useful for fixing the basic ideas to discuss a relatively simple example. Consider the equation for the particle position $X(t)$:

$$\frac{\mathrm{d}X}{\mathrm{d}t} = v(t), \tag{3.229}$$

where the random velocity $v(t)$ has zero mean and takes a finite number of values at random times T_n. We define the discrete Markov process (v_n, T_n), where v_n represents the velocity of the particle at the nth transition and T_n represents the random time at which the nth transition occurs. We assume that successive waiting times $T_n - T_{n-1}$ are independent identically distributed positive random variables. Even

under these assumptions, it is impossible to derive a closed equation for the PDF for the particle position or the mean density $\rho(x, t)$. To solve this problem, we need to make further simplifying assumptions regarding the velocity $v(t)$. Obviously, if $v(t)$ is Gaussian white noise, then $X(t)$ is the Brownian motion.

Let us apply the scaling idea and determine the behavior of the rescaled particle position $X^\varepsilon(t) = \varepsilon^{\frac{1}{2}} X(t/\varepsilon)$ in the long-time limit $\varepsilon \to 0$. It follows from (3.229) that $X^\varepsilon(t)$ with $X^\varepsilon(0) = 0$ can be written as

$$X^\varepsilon(t) = \varepsilon^{\frac{1}{2}} \int_0^{t/\varepsilon} v(s)\mathrm{d}s \approx \varepsilon^{\frac{1}{2}} \sum_{i=1}^{N(t/\varepsilon)} Y_i, \tag{3.230}$$

where $N(t) = \max\left\{n : T_n \leq t\right\}$ is the random number of jumps in particle's velocity up to time t, $Y_i = v_{i-1}(T_i - T_{i-1})$ are IID random variables with zero mean and variance $\sigma_Y^2 = \mathbb{E}\{v_{i-1}^2(T_i - T_{i-1})^2\}$, and $T_0 = 0$. Our goal is to show that $X^\varepsilon(t)$ converges in distribution to the Brownian motion $B(t)$ as $\varepsilon \to 0$. The important question is how the rescaled process $\varepsilon N(t/\varepsilon)$ behaves as $\varepsilon \to 0$. The renewal theorem states that if the mean waiting time between jumps $\overline{T} = \mathbb{E}\left\{T_i - T_{i-1}\right\}$ is finite, then $\varepsilon N(t/\varepsilon) \to t/\overline{T}$ as $\varepsilon \to 0$ [81]. The characteristic function $\mathbb{E}\left\{\exp\left(ik X^\varepsilon(t)\right)\right\}$ can be written as $\mathbb{E}\left\{\exp\left(ik\varepsilon^{\frac{1}{2}} \sum_{i=1}^{N(t/\varepsilon)} Y_i\right)\right\} \approx \left(\mathbb{E}\left\{\exp\left(ik\varepsilon^{\frac{1}{2}} Y_i\right)\right\}\right)^{t/\varepsilon\overline{T}}$. Since $\mathbb{E}\left\{Y_i\right\} = 0$, we can write $\mathbb{E}\left\{\exp\left(ik X^\varepsilon(t)\right)\right\} = \left(1 - k^2\varepsilon\sigma_Y^2/2 + o(\varepsilon)\right)^{t/\varepsilon\overline{T}} \to \exp\left(-Dk^2t\right)$ as $\varepsilon \to 0$. So $X^\varepsilon(t)$ converges in distribution to $B(t)$ with the diffusion coefficient $D = \sigma_Y^2/2\overline{T}$.

For the general stochastic equation (3.228), the rescaled particle position $X^\varepsilon(t) = \varepsilon^{\frac{1}{2}} X(t/\varepsilon)$ tends to a diffusion process, in the limit $\varepsilon \to 0$, with the probability density function $p(x, t)$. The latter obeys the Fokker–Planck equation

$$\frac{\partial p}{\partial t} = -\frac{\partial}{\partial x}(\mu(x)p) + \frac{1}{2}\frac{\partial^2}{\partial x^2}\left(\sigma^2(x)p\right), \tag{3.231}$$

with infinitesimal displacement

$$\mu(x) = \lim_{\varepsilon \to 0} \int_0^{1/\varepsilon} \int_0^{1/\varepsilon} \mathbb{E}_\xi\left[\frac{\partial v(x, \xi(s))}{\partial x} v(x, \xi(t))\right] \mathrm{d}s\mathrm{d}t \tag{3.232}$$

and infinitesimal variance $\sigma^2(x)$,

$$\sigma^2(x) = \lim_{\varepsilon \to 0} \int_0^{1/\varepsilon} \int_0^{1/\varepsilon} \mathbb{E}_\xi\left[v(x, \xi(s))v(x, \xi(t))\right] \mathrm{d}s\mathrm{d}t. \tag{3.233}$$

The details of the derivation can be found in [142].

3.7 Transport Equations and Underlying Stochastic Processes

In this section we remind the reader of the Kolmogorov forward and backward equations, infinitesimal generators, stochastic differential equations, and functional integrals and then consider how the basic transport equations are related to underlying Markov stochastic processes [141, 142].

3.7.1 Brownian Motion, Lévy Flight, and the Diffusion Equations

We start with a very simple one-dimensional diffusion equation

$$\frac{\partial \rho}{\partial t} = D \frac{\partial^2 \rho}{\partial x^2}, \quad x \in \mathbb{R}, \tag{3.234}$$

with the initial condition

$$\rho(x, 0) = \rho_0(x). \tag{3.235}$$

The solution of the initial value problem (3.234) and (3.235) can be written as

$$\rho(x, t) = \int_{\mathbb{R}} \rho_0(y) p(y, t | x) dy, \tag{3.236}$$

where the Green's function, the propagator, is

$$p(y, t | x) = \frac{1}{\sqrt{4Dt}} \exp\left(-\frac{(y - x)^2}{4Dt}\right). \tag{3.237}$$

It should be noted that we integrate with respect to the "forward" variable y in (3.236). In this case, (3.236) has a very nice probabilistic interpretation. Consider the Brownian motion $B(t)$, which is a stochastic process with independent increments, such that $B(t + s) - B(s)$ is normally distributed with zero mean and variance $2Dt$. The corresponding transition probability density function $p(y, t | x)$ is given by (3.237). Therefore the solution (3.236) has a probabilistic representation

$$\rho(x, t) = \mathbb{E}_x \rho_0(B(t)), \tag{3.238}$$

where $\mathbb{E}_x$ is the expectation operator with respect to the random process $B(t)$ starting at point x. At first glance, (3.238) appears to provide the connection between the *microscopic* Brownian motion $B(t)$ and the *macroscopic* diffusion equation for the density of particles that all follow the Brownian motion. This is not quite true. Since we integrate with respect to the "forward" variable y, we treat (3.234) as the Kolmogorov backward equation which does not represent the transport equation. If

we integrate with respect to the "backward" variable x, then

$$\rho(y, t) = \int_{\mathbb{R}} \rho_0(x) p(y, t|x) \mathrm{d}x \tag{3.239}$$

is the solution to the Kolmogorov forward equation,

$$\frac{\partial \rho}{\partial t} = D \frac{\partial^2 \rho}{\partial y^2}, \quad y \in \mathbb{R}, \tag{3.240}$$

with $\rho(y, 0) = \rho_0(y)$.

Of course (3.234) and (3.240) are identical in form, but only the forward equation (3.240) has the physical meaning of a transport equation for particles. We will discuss the difference between forward and backward equations in the next section. It turns out that, it is more convenient to deal with the backward equation (3.234). Let us give an example. The Brownian motion $B(t)$ starting at x can be rewritten in terms of the standard Wiener process $W(t)$ as

$$B(t) = x + \sqrt{2D} W(t). \tag{3.241}$$

Recall that $W(0) = 0$, $\mathbb{E}W(t) = 0$, and $\mathbb{E}W^2(t) = t$. The solution to (3.234) and (3.235) can be written as

$$\rho(x, t) = \mathbb{E}\rho_0\left(x + \sqrt{2D}W(t)\right), \tag{3.242}$$

where $\mathbb{E}$ is the expectation operator with respect to $W(t)$. The main advantage of the probabilistic representation (3.242) is that we can use a Monte Carlo approach to estimate $\rho(x, t)$:

$$\rho(x, t) \approx \frac{1}{N} \sum_{i=1}^{N} \rho_0\left(x + \sqrt{2Dt}\xi_i\right), \tag{3.243}$$

where the sample ξ_i is computed from the standard normal distribution $\mathcal{N}(0, 1)$ with zero mean and unit variance and N is the sample size [300]. The generalization of these ideas to a Brownian particle moving in three dimensions is straightforward. The solution of the Cauchy problem

$$\frac{\partial u}{\partial t} = D \Delta u, \quad u(\mathbf{x}, 0) = u_0(\mathbf{x}), \quad \mathbf{x} \in \mathbb{R}^3, \tag{3.244}$$

can be written as

$$u(\mathbf{x}, t) = \mathbb{E}u_0\left(\mathbf{x} + \sqrt{2D}\mathbf{W}(t)\right), \tag{3.245}$$

where $\mathbf{W}(t)$ is the standard three-dimensional Wiener process.

The probabilistic solution to the space-fractional Cauchy problem

$$\frac{\partial u}{\partial t} = D_\alpha \frac{\partial^\alpha u}{\partial |x|^\alpha}, \quad u(x, 0) = u_0(x), \quad x \in \mathbb{R}, \tag{3.246}$$

can be written in terms of the symmetric α-stable Lévy motion $S_\alpha(t)$ (Lévy flight) as

$$u(x, t) = \mathbb{E} u_0\big(x + S_\alpha(t)\big), \tag{3.247}$$

where $S_\alpha(t)$ is defined in Sect. 3.3.3.2. Of course, for the simple transport problem (3.234) and (3.235) we have an explicit solution (3.236). In most cases, explicit solutions to the transport equations are not available, but we still can write down the solution in the form of the functional integral (3.238). In fact, this formula can be easily coded to obtain numerical solutions; it provides a powerful alternative to standard finite difference methods [300].

3.7.2 Transport Equations: Forward vs Backward

Consider a collection of particles that move independently of each other in three-dimensional space $\mathbb{R}^3$. We assume that the position of a particle $\mathbf{X}(t)$ is a time-homogeneous Markov process with transition density $p(\mathbf{y}, t|\mathbf{x})$.

The density of particles $\rho(\mathbf{y}, t)$ at point $\mathbf{y}$ at time t can be expressed in terms of the initial density of particles $\rho_0(\mathbf{x})$ as

$$\rho(\mathbf{y}, t) = \int_{\mathbb{R}^3} \rho_0(\mathbf{x}) p(\mathbf{y}, t|\mathbf{x}) d\mathbf{x}, \tag{3.248}$$

where the integration is performed with respect to the "initial" or "backward" variable $\mathbf{x}$. This equation has a very simple meaning as the balance of particles arriving at point $\mathbf{y}$ from various initial positions $\mathbf{x}$. The probabilistic meaning of this equation is the law of total probability: the probability density $\rho(\mathbf{y}, t)$ is the sum (integral) of the probability density $p(\mathbf{y}, t|\mathbf{x})$ to be at point $\mathbf{y}$ at time t conditional on being at point $\mathbf{x}$ at $t = 0$ multiplied by the probability density $\rho_0(\mathbf{x})$ to be at point $\mathbf{x}$ at time 0.

We define a transport operator Q_t as follows:

$$\rho(\mathbf{y}, t) = Q_t \rho_0(\mathbf{y}) \equiv \int_{\mathbb{R}^3} \rho_0(\mathbf{x}) p(\mathbf{y}, t|\mathbf{x}) d\mathbf{x}, \tag{3.249}$$

so the density of particles $\rho(\mathbf{y}, t)$ is the solution of a transport equation written in terms of the "forward" variable $\mathbf{y}$. The key question is what equation does $\rho(\mathbf{y}, t) = Q_t \rho_0(\mathbf{y})$ satisfy. In what follows, we derive several transport equations

corresponding to various random processes $\mathbf{X}(t)$ and probability density functions $p(\mathbf{y}, t|\mathbf{x})$, Green's functions.

As we have mentioned in the previous section, it is convenient to integrate with respect to the "forward" variable $\mathbf{y}$. We define the transition operator T_t and the new function $u(\mathbf{x}, t)$ as

$$u(\mathbf{x}, t) = T_t u_0(\mathbf{x}) \equiv \int_{\mathbb{R}^3} u_0(\mathbf{y}) p(\mathbf{y}, t|\mathbf{x}) d\mathbf{y}, \qquad (3.250)$$

where $u(\mathbf{x}, 0) = u_0(\mathbf{x})$. We use the notation u instead of ρ to emphasize that the function $u(\mathbf{x}, t)$ is formal and does not generally represent the particle density.

It follows from (3.250) that the operator T_t, associated with the transition probability $p(\mathbf{y}, t|\mathbf{x})$, can be written in terms of a conditional expectation $\mathbb{E}_\mathbf{x}$ over the particle position $\mathbf{X}(t)$ at time t, provided $\mathbf{X}(0) = \mathbf{x}$:

$$T_t f(\mathbf{x}) = \mathbb{E}_\mathbf{x} f(\mathbf{X}(t)). \qquad (3.251)$$

We always write the expectation $\mathbb{E}_\mathbf{x}$ with the index $\mathbf{x}$ when we want to emphasize that the process $\mathbf{X}(t)$ starts at point $\mathbf{x}$, i.e., $\mathbf{X}(0) = \mathbf{x}$:

$$\mathbb{E}_\mathbf{x}\{f(\mathbf{X}(t))\} = \mathbb{E}\{f(\mathbf{X}(t))|\mathbf{X}(0) = \mathbf{x}\}. \qquad (3.252)$$

The operator T_t has the semigroup property, $T_t T_s f = T_{t+s} f$. It is easy to check that T_t is the adjoint of Q_t:

$$\int_{\mathbb{R}^3} T_t f(\mathbf{x})\varphi(\mathbf{x})d\mathbf{x} = \int_{\mathbb{R}^3} f(\mathbf{x})Q_t\varphi(\mathbf{x})d\mathbf{x}. \qquad (3.253)$$

We conclude that if the operator T_t is self-adjoint, i.e., $T_t = Q_t$, then it can be used as a transport operator. If the random position $\mathbf{X}(t)$ of a particle starting at $\mathbf{x} = 0$ is a symmetric process for which $\mathbb{P}(\mathbf{X}(t) = \mathbf{x}) = \mathbb{P}(\mathbf{X}(t) = -\mathbf{x})$, then the operator T_t is self-adjoint. For example, the Brownian motion $B(t)$ is a symmetric process. Note that if a stationary distribution $\overline{\rho}(\mathbf{y})$ exists, it satisfies $\overline{\rho}(\mathbf{y}) = Q_t\overline{\rho}(\mathbf{y})$.

Let us define two evolution operators L and L^* for the Markov process $\mathbf{X}(t)$:

$$Lf(\mathbf{x}) = \lim_{h\to 0} \frac{T_h f(\mathbf{x}) - f(\mathbf{x})}{h} = \lim_{h\to 0} \frac{\int_{\mathbb{R}^3} f(\mathbf{y})p(\mathbf{y}, h|\mathbf{x})d\mathbf{y} - f(\mathbf{x})}{h}, \qquad (3.254)$$

where L acts only on the "backward" variable $\mathbf{x}$, and

$$L^* f(\mathbf{y}) = \lim_{h\to 0} \frac{Q_h f(\mathbf{y}) - f(\mathbf{y})}{h} = \lim_{h\to 0} \frac{\int_{\mathbb{R}^3} f(\mathbf{x})p(\mathbf{y}, h|\mathbf{x})d\mathbf{x} - f(\mathbf{y})}{h}, \qquad (3.255)$$

where L^* acts on the "forward" variable $\mathbf{y}$. The operators L and L^* are called the infinitesimal generators of the semigroups T_t and Q_t, respectively [142]. The operator L^* is the adjoint of L:

$$\int_{\mathbb{R}^3} L^* f(\mathbf{x}) \varphi(\mathbf{x}) d\mathbf{x} = \int_{\mathbb{R}^3} f(\mathbf{x}) L \varphi(\mathbf{x}) d\mathbf{x}. \tag{3.256}$$

One can show that $u(\mathbf{x}, t)$ given by (3.250) is the unique solution of the initial-value problem:

$$\frac{\partial u}{\partial t} = Lu, \quad u(\mathbf{x}, 0) = u_0(\mathbf{x}), \quad \mathbf{x} \in \mathbb{R}^3. \tag{3.257}$$

The function $\rho(\mathbf{y}, t)$ given by (3.248) obeys the following initial-value problem:

$$\frac{\partial \rho}{\partial t} = L^* \rho, \quad \rho(\mathbf{y}, 0) = \rho_0(\mathbf{y}), \quad \mathbf{y} \in \mathbb{R}^3. \tag{3.258}$$

Note that some authors have used these operators interchangeably for the description of the mesoscopic transport process. It is clear that if L is self-adjoint, then it can be used as a transport operator and the function $u(\mathbf{x}, t)$ can represent the particle density. For example, the one-dimensional Brownian motion $B(t)$ has the infinitesimal generator $L = \partial^2 / \partial x^2$ which is self-adjoint. A symmetric α-stable Lévy process on $\mathbb{R}$ has the generator $L = \partial^\alpha / \partial |x|^\alpha$, which is self-adjoint too. In the next section we obtain L and L^* from the Chapman–Kolmogorov equation.

3.7.3 Chapman–Kolmogorov Equation and Infinitesimal Generators

Let us consider the Chapman–Kolmogorov equation for the transition density $p(\mathbf{y}, t|\mathbf{x})$:

$$p(\mathbf{y}, t + s|\mathbf{x}) = \int_{\mathbb{R}^3} p(\mathbf{z}, t|\mathbf{x}) p(\mathbf{y}, s|\mathbf{z}) d\mathbf{z}. \tag{3.259}$$

Our goal is to derive the Kolmogorov forward and backward equations and to discuss the main difference between them. The forward equation deals with the events during the small time interval $(t, t + h]$ and gives us the answer for how those events define the probability density $p(\mathbf{y}, t+h|\mathbf{x})$ at time $t+h$, while the backward equation is concerned with events just after the time $t = 0$.

Let us replace s with small h in (3.259) and rewrite this equation for the density $\rho(\mathbf{y}, t)$:

$$\rho(\mathbf{y}, t + h) = \int_{\mathbb{R}^3} \rho(\mathbf{z}, t) p(\mathbf{y}, h|\mathbf{z}) d\mathbf{z}, \tag{3.260}$$

where $p(\mathbf{y}, h|\mathbf{z})$ represents the probability of the transitions from $\mathbf{z}$ to $\mathbf{y}$ occurring during short time interval $(t, t + h]$. The meaning of this equation is very simple. It gives the balance of particles at point $\mathbf{y}$ at time $t + h$. Subtracting $\rho(\mathbf{y}, t)$ from both sides and dividing by h, we find

$$\frac{\rho(\mathbf{y}, t+h) - \rho(\mathbf{y}, t)}{h} = \frac{\int_{\mathbb{R}^3} \rho(\mathbf{z}, t) p(\mathbf{y}, h|\mathbf{z})d\mathbf{z} - \rho(\mathbf{y}, t)}{h}. \tag{3.261}$$

Letting $h \to 0$, we obtain the Kolmogorov forward equation, the Master equation,

$$\frac{\partial \rho(\mathbf{y}, t)}{\partial t} = L^* \rho(\mathbf{y}, t), \tag{3.262}$$

where L^* is defined by (3.255). The transition probability $p(\mathbf{y}, t|\mathbf{x})$ obeys the same equation with respect to the forward variable $\mathbf{y}$. The main idea in the derivation of (3.262) is to split the time interval $(0, t+h]$ into a long interval $(0, t]$ and a short interval $(t, t+h]$, so that the particle density at time $t+h$ is the result of transitions during the short time interval $(t, t+h]$.

To derive the backward equation, we consider the events just after the time $t = 0$ during the short time interval $(0, h]$. The Chapman–Kolmogorov equation is

$$p(\mathbf{y}, h+t|\mathbf{x}) = \int_{\mathbb{R}^3} p(\mathbf{z}, h|\mathbf{x}) p(\mathbf{y}, t|\mathbf{z}) d\mathbf{z}. \tag{3.263}$$

We cannot write a similar equation for the density $\rho(\mathbf{x}, h+t)$. Rewriting (3.263) as

$$\frac{p(\mathbf{y}, h+t|\mathbf{x}) - p(\mathbf{y}, t|\mathbf{x})}{h} = \frac{\int_{\mathbb{R}^3} p(\mathbf{z}, h|\mathbf{x}) p(\mathbf{y}, t|\mathbf{z}) d\mathbf{z} - p(\mathbf{y}, t|\mathbf{x})}{h}, \tag{3.264}$$

we obtain, in the limit $h \to 0$, the Kolmogorov backward equation

$$\frac{\partial p(\mathbf{y}, t|\mathbf{x})}{\partial t} = L p(\mathbf{y}, t|\mathbf{x}). \tag{3.265}$$

This equation is written for two variables, the time t and the initial position $\mathbf{x}$. The final position $\mathbf{y}$ plays the role of a parameter. The function $u(x, t)$ defined in (3.250) obeys the Kolmogorov backward equation:

$$\frac{\partial u(\mathbf{x}, t)}{\partial t} = L u(\mathbf{x}, t). \tag{3.266}$$

The natural question arises whether this equation represents the mesoscopic transport of particles. The answer in general is negative. In what follows we illustrate a general technique, using several examples of Markov processes.

3.7.3.1 Poisson Process

As a first illustration, consider the Poisson process $N_a(t)$ with intensity λ and jump size a. We assume that the process starts at the point x. Then

$$Lf(x) = \lim_{h \to 0} \frac{\mathbb{E}_x f(N_a(h)) - f(x)}{h} = \lambda(f(x+a) - f(x)). \tag{3.267}$$

Referring to (3.250) and (3.257), we conclude that the solution to the finite difference backward equation

$$\frac{\partial u}{\partial t} = Lu = \lambda(u(x+a,t) - u(x,t)), \quad x \in \mathbb{R}, \tag{3.268}$$

with the initial condition $u(x,0) = u_0(x)$, can be written as

$$u(x,t) = T_t u_0(x) = \mathbb{E}_x u_0(N_a(t)) = \sum_{k=0}^{\infty} u_0(x+ak) \frac{e^{-\lambda t}(\lambda t)^k}{k!}. \tag{3.269}$$

As usual we use the notation $\mathbb{E}_x$ to emphasize that the expectation is taken with respect to the process $N_a(t)$ starting at x.

The forward equation follows from the balance equation (3.74) with $w(z) = \delta(z-a)$, i.e.,

$$\frac{\partial \rho}{\partial t} = L^*\rho = \lambda(\rho(y-a,t) - \rho(y,t)), \quad y \in \mathbb{R}. \tag{3.270}$$

The advantage of having a probabilistic solution (3.269) is that it helps us to find an explicit solution of the Cauchy problem for the transport equation (3.270) by changing the sign $a \to -a$:

$$\rho(y,t) = Q_t \rho_0(y) = \sum_{k=0}^{\infty} \rho_0(y-ak) \frac{e^{-\lambda t}(\lambda t)^k}{k!}. \tag{3.271}$$

3.7.3.2 Three-Dimensional Brownian motion

As another illustration, consider the Brownian motion $\mathbf{B}(t)$ in three dimensions starting at point $\mathbf{x}$. The operator L is the Laplacian, i.e.,

$$Lf(\mathbf{x}) = \lim_{h \to 0} \frac{\mathbb{E}_\mathbf{x} f(\mathbf{B}(h)) - f(\mathbf{x})}{h} = D\Delta f. \tag{3.272}$$

The solution of the Kolmogorov backward diffusion equation

$$\frac{\partial u(\mathbf{x},t)}{\partial t} = D\Delta u(\mathbf{x},t), \quad \mathbf{x} \in \mathbb{R}^3, \tag{3.273}$$

with the initial condition $u(\mathbf{x},0) = u_0(\mathbf{x})$, can be written as

$$u(\mathbf{x},t) = T_t u_0(\mathbf{x}) = \mathbb{E}_\mathbf{x} u_0(\mathbf{B}(t)) = \int_{\mathbb{R}^3} \rho_0(\mathbf{x}+\mathbf{z}) \frac{e^{-\mathbf{z}\cdot\mathbf{z}/(4Dt)}}{(4\pi Dt)^{3/2}} d\mathbf{z}. \tag{3.274}$$

The operator L is self-adjoint, and the transport equation for the density is of the form

$$\frac{\partial \rho(\mathbf{y}, t)}{\partial t} = D \Delta \rho(\mathbf{y}, t), \quad \mathbf{y} \in \mathbb{R}^3. \tag{3.275}$$

The solution to this equation with the initial condition $\rho(\mathbf{y}, 0) = \rho_0(\mathbf{y})$ is $\rho(\mathbf{y}, t) = \mathbb{E}_{\mathbf{y}} \rho_0(\mathbf{B}(t))$. In this case $\mathbf{B}(t)$ starts at point $\mathbf{y}$.

3.7.3.3 Deterministic Motion

Consider the case where the particles move with deterministic velocity $\mathbf{v}(\mathbf{x})$:

$$\frac{d\mathbf{X}(t)}{dt} = \mathbf{v}(\mathbf{X}(t)), \quad \mathbf{X}(0) = \mathbf{x}, \quad \mathbf{x} \in \mathbb{R}^3. \tag{3.276}$$

Then

$$Lf(\mathbf{x}) = \lim_{h \to 0} \frac{f(\mathbf{X}(h)) - f(\mathbf{x})}{h} = \mathbf{v}(\mathbf{x}) \cdot \nabla f = \sum_i v_i(\mathbf{x}) \frac{\partial f}{\partial x_i}. \tag{3.277}$$

The initial value problem

$$\frac{\partial u}{\partial t} = Lu = \mathbf{v}(\mathbf{x}) \cdot \nabla u, \quad u(\mathbf{x}, 0) = u_0(\mathbf{x}) \tag{3.278}$$

has the solution

$$u(\mathbf{x}, t) = T_t u_0(\mathbf{x}) = u_0(\mathbf{X}(t)). \tag{3.279}$$

The backward equation, Liouville's equation, for the particle density takes the form

$$\frac{\partial \rho}{\partial t} = L^* \rho = -\sum_i \frac{\partial}{\partial y_i} (v_i(\mathbf{y}) \rho). \tag{3.280}$$

For incompressible flow where $\nabla \cdot \mathbf{v} = 0$ we obtain the transport equation

$$\frac{\partial \rho}{\partial t} + \mathbf{v}(\mathbf{y}) \cdot \nabla \rho = 0. \tag{3.281}$$

This equation, together with the initial condition $\rho(\mathbf{y}, 0) = \rho_0(\mathbf{y})$, is identical to (3.278) if we change the direction of velocity field $\mathbf{v} \to -\mathbf{v}$. That is why we can write

$$\rho(\mathbf{y}, t) = \rho_0(\mathbf{X}(t)), \tag{3.282}$$

where $\mathbf{X}(t)$ is the solution of the initial value problem

$$\frac{d\mathbf{X}(t)}{dt} = -\mathbf{v}(\mathbf{X}(t)), \quad \mathbf{X}(0) = \mathbf{y}. \tag{3.283}$$

Later we will see how the deterministic theory above can be extended to the convection–diffusion equation of the form

$$\frac{\partial \rho}{\partial t} + \mathbf{v}(\mathbf{y}) \cdot \nabla \rho = D\Delta \rho. \tag{3.284}$$

3.7.3.4 Discrete-in-Space Random Walk

Let $X(t)$ be the position of a particle performing a random walk on the x-axis. If the particle is at point x at time t, then the probability that it will jump to the right, to the point $x + a$, during $(t, t + h]$ is $\alpha(x)h + o(h)$. The probability of a jump to the left to $x - a$ at time $t + h$ is $\beta(x)h + o(h)$. The probability of no jumps is $1 - \alpha(x)h - \beta(x)h + o(h)$. These transition probabilities allow us to find the infinitesimal operator L:

$$Lf(x) = \lim_{h \to 0} \frac{\mathbb{E}_x f(X(h)) - f(x)}{h} = \alpha(x)(f(x + a) - f(x))$$
$$+ \beta(x)(f(x - a) - f(x)). \tag{3.285}$$

So the Kolmogorov backward equation is

$$\frac{\partial u}{\partial t} = Lu = \alpha(x)\left[u(x + a, t) - u(x)\right] + \beta(x)\left[u(x - a, t) - u(x, t)\right]. \tag{3.286}$$

For the initial condition $u(x, 0) = u_0(x)$, it has the solution $u(x, t) = \mathbb{E}_x u_0(X(t))$. The forward equation for the density of particles takes the form

$$\frac{\partial \rho}{\partial t} = L^* \rho = \alpha(y - a)\rho(y - a, t)$$
$$- \alpha(y)\rho(y) + \beta(y + a)\rho(y + a, t) - \beta(y)\rho(y, t). \tag{3.287}$$

If the transition rates $\alpha = \beta = \text{const}$, then the forward and backward equations are identical. In particular, the mesoscopic equation for the density ρ is

$$\frac{\partial \rho}{\partial t} = \alpha(\rho(x + a, t) - 2\rho(x, t) + \rho(x - a, t)). \tag{3.288}$$

We see that (3.288) is simply a discrete-in-space version of the diffusion equation (3.234). On the right-hand side we have a symmetric central-difference approximation for the second derivative $D\partial^2\rho/\partial x^2$ with the diffusion coefficient $D = \alpha a^2$.

This suggests that if we let the step size $a \to 0$ and the rate $\alpha \to \infty$ such that $D = \alpha a^2 =$ const, the density $\rho(x, t)$ converges to the function that obeys the diffusion equation. The function $\rho(x, t) = \mathbb{E}_x \rho_0(X(t))$ represents a solution of the difference equation (3.288) with $\rho(x, 0) = \rho_0(x)$ as an expectation with respect to the position of the random walk $X(t)$.

3.7.3.5 Markov Process with Jumps

Consider a particle that moves with a velocity $v(x)$ on $\mathbb{R}$ and jumps at random times so that the rate of jumps depends on the position of the particle. The one-dimensional microscopic movement can be represented as follows. If the position of the particle at time t is $X(t)$, then at time $t + h$ the position is

$$X(t + h) = X(t) + v(X(t))h + Z(t) + o(h), \tag{3.289}$$

with probability $\lambda(X(t))h + o(h)$, and

$$X(t + h) = X(t) + v(X(t))h + o(h) \tag{3.290}$$

with probability $1 - \lambda(X(t))h + o(h)$. The stationary random process $Z(t)$ has the conditional jump density

$$w(z|x) = \frac{\partial}{\partial z} \mathbb{P}\{Z(t) \le z | X(t) = x\}. \tag{3.291}$$

The Kolmogorov backward equation is

$$\frac{\partial u(x, t)}{\partial t} = Lu(x, t) = v(x)\frac{\partial u}{\partial x}$$
$$+ \lambda(x) \int_{\mathbb{R}} u(x + z, t)w(z|x)dz - \lambda(x)u(x, t). \tag{3.292}$$

The Kolmogorov forward equation, the Master equation, for the density $\rho(y, t)$ is

$$\frac{\partial \rho(y, t)}{\partial t} = L^* \rho(y, t) = -\frac{\partial(v(y)\rho)}{\partial y}$$
$$+ \int_{\mathbb{R}} \lambda(y - z)\rho(y - z, t)w(z|y - z)dz - \lambda(y)\rho(y, t). \tag{3.293}$$

If $\lambda =$ const, $w(z)$ does not depend on x, and $v(x) = 0$, we obtain the Kolmogorov–Feller equation (3.74), for which the underlying microscopic random movement is a compound Poisson process.

3.7.3.6 Integral-Difference Equation and Discrete Random Walk

Consider the discrete-time random walk model for the particle position X_n,

$$X_{n+1} = X_n + Z_{n+1}, \qquad (3.294)$$

where the sequence of independent random jumps Z_n is defined by the conditional density

$$w(z|x) = \frac{\partial}{\partial z} \mathbb{P}(Z_n \le z | X_{n-1} = x). \qquad (3.295)$$

The transition probability density function

$$p(y, n|x) = \frac{\partial}{\partial y} \mathbb{P}(X_n \le y | X_0 = x) \qquad (3.296)$$

obeys two equations [126]. The Kolmogorov forward equation involves the last jump that takes place at time $n - 1$:

$$p(y, n|x) = \int_{\mathbb{R}} p(y - z, n - 1|x) w(z | y - z) \mathrm{d}z \qquad (3.297)$$

with $n = 1, 2, 3, \ldots$. The Kolmogorov backward equation deals with the first jump at time 1:

$$p(y, n|x) = \int_{\mathbb{R}} w(z|x) p(y, n - 1 | x + z) \mathrm{d}z. \qquad (3.298)$$

The Master equation for the density is

$$\rho(y, n) = \int_{\mathbb{R}} \rho(y - z, n - 1) w(z | y - z) \mathrm{d}z. \qquad (3.299)$$

The backward equation for the function u takes the form

$$u(x, n) = \int_{\mathbb{R}} w(z|x) u(z, n - 1) \mathrm{d}z. \qquad (3.300)$$

For even jump PDFs, i.e., $w(x) = w(-x)$, the backward and forward equations are identical in form.

3.7.3.7 One-Dimensional Diffusion Process

We have seen that an appropriate rescaling of time and renormalizing the stochastic process leads to the Brownian motion. Here we define the homogeneous-in-time

diffusion process $X(t)$, which has two basic statistical characteristics, the infinitesimal displacement (or drift) $\mu(x)$ and the infinitesimal variance $\sigma^2(x)$:

$$\mu(x) = \lim_{h \to 0} \frac{1}{h} \mathbb{E}\{X(t+h) - X(t)|X(t) = x\}, \tag{3.301}$$

$$\sigma^2(x) = \lim_{h \to 0} \frac{1}{h} \mathbb{E}\left\{[X(t+h) - X(t)]^2 |X(t) = x\right\}. \tag{3.302}$$

The diffusion process $X(t)$ can also be defined by the Itô stochastic differential equation (SDE)

$$dX = \mu(X)dt + \sigma(X)dW, \tag{3.303}$$

where $W(t)$ is the standard Wiener process [141, 142]. It is clear that $W(t)$ can be defined as a diffusion process with $\mu(x) = 0$ and $\sigma^2(x) = 1$.

The conditional probability density function

$$p(y, t|x) = \frac{\partial}{\partial y} \mathbb{P}\{X(t) \leq y|X(0) = x\} \tag{3.304}$$

satisfies the forward equation, the Fokker–Planck equation,

$$\frac{\partial p}{\partial t} = L^* p = -\frac{\partial}{\partial y}(\mu(y)p) + \frac{1}{2}\frac{\partial^2}{\partial y^2}\left(\sigma^2(y)p\right) \tag{3.305}$$

and the backward equation

$$\frac{\partial p}{\partial t} = Lp = \mu(x)\frac{\partial p}{\partial x} + \frac{\sigma^2(x)}{2}\frac{\partial^2 p}{\partial x^2}. \tag{3.306}$$

So the initial value problem

$$\frac{\partial u}{\partial t} = Lu, \quad u(x, 0) = u_0(x), \tag{3.307}$$

has the solution

$$u(x, t) = \mathbb{E}_x u_0(X(t)). \tag{3.308}$$

As we discussed earlier, the backward equation (3.307) does not describe the average transport process of particles that follow the process $X(t)$. The transport equation for the density $\rho(y, t)$ with the convection–diffusion flux $J = v(y)\rho - D(y)\partial\rho/\partial y$ can be written as

$$\frac{\partial \rho}{\partial t} = -\frac{\partial}{\partial y}(v(y)\rho) + \frac{\partial}{\partial y}\left(D(y)\frac{\partial \rho}{\partial y}\right). \tag{3.309}$$

The convection–diffusion equation (3.309) has the form of a forward equation, $\partial \rho / \partial t = L^* \rho$, if

$$D(y) = \frac{\sigma^2(y)}{2}, \quad v(y) = \mu(y) - \sigma(y)\frac{\partial \sigma(y)}{\partial y}. \tag{3.310}$$

3.7.3.8 Diffusion Process in Three Dimensions

We discuss the diffusion process in three dimensions in the context of an anisotropic convection–diffusion equation for the density of particles. Our goal is to obtain the probabilistic solution to the initial value problem

$$\frac{\partial \rho}{\partial t} + \sum_{i=1}^{3} v_i(\mathbf{x})\frac{\partial \rho}{\partial x_i} = \sum_{i,j=1}^{3} \frac{\partial}{\partial x_i}\left(D_{ij}(\mathbf{x})\frac{\partial \rho}{\partial x_j}\right), \quad \rho(\mathbf{x}, 0) = \rho_0(\mathbf{x}). \tag{3.311}$$

Let us assume that the particle position $\mathbf{X}(t)$ is the solution to the Itô SDE

$$d\mathbf{X}(s) = b(\mathbf{X}(s))ds + \sigma(\mathbf{X}(s))d\mathbf{W}(s), \quad \mathbf{X}(0) = \mathbf{x}, \quad 0 \le s \le t, \tag{3.312}$$

where $\mathbf{W}(s)$ is the standard three-dimensional Wiener process, and σ is the matrix of infinitesimal variances [141]. Using coordinate notation, we rewrite the SDE (3.312) in the integral form as

$$X_i(t) = x_i + \int_0^t b_i(\mathbf{X}(s))ds + \int_0^t \sum_{j=1}^{3} \sigma_{ij}(\mathbf{X}(s))dW_j(s), \quad i = 1, 2, 3. \tag{3.313}$$

This formula allows us to find the generator

$$Lf(\mathbf{x}) = \lim_{h \to 0} \frac{\mathbb{E}_{\mathbf{x}} f(\mathbf{X}(h)) - f(\mathbf{x})}{h}$$

$$= \sum_{i=1}^{3} b_i(\mathbf{x})\frac{\partial f(\mathbf{x})}{\partial x_i} + \sum_{i,j=1}^{3} D_{ij}(\mathbf{x})\frac{\partial f(\mathbf{x})}{\partial x_i \partial x_j}, \tag{3.314}$$

where the diffusion matrix $D(\mathbf{x})$ is given by

$$D_{ij}(\mathbf{x}) = \frac{1}{2}\sum_{k=1}^{3} \sigma_{ik}(\mathbf{x})\sigma_{kj}(\mathbf{x}). \tag{3.315}$$

The anisotropic convection–diffusion equation (3.311) can be written in the form of a backward equation, $\partial \rho / \partial t = L\rho$, if

$$b_i(\mathbf{x}) = -v_i(\mathbf{x}) + \sum_{k=1}^{3} \frac{\partial D_{ki}(\mathbf{x})}{\partial x_k}. \tag{3.316}$$

We know that the Cauchy problem

$$\frac{\partial u}{\partial t} = Lu, \quad u(\mathbf{x}, 0) = u_0(\mathbf{x}), \quad \mathbf{x} \in \mathbb{R}^3, \tag{3.317}$$

has the solution $u(\mathbf{x}, t) = \mathbb{E}_{\mathbf{x}} u_0(\mathbf{X}(t))$. Thus we conclude that the probabilistic solution to the initial value problem (3.311) is

$$\rho(\mathbf{x}, t) = \mathbb{E}_{\mathbf{x}} \rho_0(\mathbf{X}(t)), \tag{3.318}$$

where the random process $\mathbf{X}(t)$ is defined by the SDE (3.312) with (3.315) and (3.316).

It is instructive to show how the Itô formula can be used to obtain the probabilistic solution to (3.317) [141]. We consider a "new" Markov process $(\mathbf{X}(s), T(s))$, where the first component $\mathbf{X}(s)$ obeys (3.312) and the effective time $T(s)$ is defined as

$$T(s) = t - s, \quad 0 \le s \le t. \tag{3.319}$$

We apply the Itô formula to the smooth function $u(\mathbf{x}, t)$:

$$du(\mathbf{X}(s), T(s)) = \left[-\frac{\partial u}{\partial t}(\mathbf{X}(s), T(s)) + Lu(\mathbf{X}(s), T(s)) \right] ds$$
$$+ \nabla_{\mathbf{x}} u(\mathbf{X}(s), T(s)) \cdot \sigma(\mathbf{X}(s)) d\mathbf{W}(s). \tag{3.320}$$

This equation can be rewritten in the integral form as

$$u(\mathbf{X}(t), 0) - u(\mathbf{x}, t) = \int_0^t \left[-\frac{\partial u}{\partial t}(\mathbf{X}(s), t - s) + Lu(\mathbf{X}(s), t - s) \right] ds$$
$$+ \int_0^t \nabla_{\mathbf{x}} u(\mathbf{X}(s), t - s) \cdot \sigma(\mathbf{X}(s)) d\mathbf{W}(s). \tag{3.321}$$

If we average both sides and take into account (3.317), we obtain

$$u(\mathbf{x}, t) = \mathbb{E}_{\mathbf{x}} u_0(\mathbf{X}(t)). \tag{3.322}$$

3.7.4 Convection–Diffusion Equation with Reactions

This section is devoted to probabilistic solutions of reaction–diffusion equations in terms of functional integrals. We will not attempt to cover the general theory and all relevant equations. Our purpose is to discuss the main ideas and principal results and give illustrating examples involving typical equations. The reader interested in the general theory and all mathematical details will find a comprehensive treatment of the subject in Freidlin's book [141].

So far we have discussed the probabilistic solution of the convection–diffusion equation only. There are various directions in which a probabilistic approach to PDEs can be extended and generalized. The first direction is to extend it to the case where chemical reactions are taken into account. The next direction would be to allow the velocity field $\mathbf{v}$ and the diffusion matrix D to depend on both space $\mathbf{x}$ and time t. Another direction for generalization is to analyze initial-boundary problems.

3.7.4.1 Path-Integral and Feynman–Kac Formula

We start with the one-dimensional reaction–diffusion equation

$$\frac{\partial \rho}{\partial t} = D \frac{\partial^2 \rho}{\partial x^2} + r(x)\rho, \quad x \in \mathbb{R}, \tag{3.323}$$

where the function $r(x)$ represents the intrinsic growth rate. The solution to the reaction–diffusion equation (3.323) with $\rho(x, 0) = \rho_0(x)$ can be written as the Feynman path integral, a functional integral,

$$\rho(x, t) = \int_{x(0)=x} \rho_0(x(t)) \exp\left\{ -\int_0^t \left[\frac{\dot{x}^2(s)}{4D} - r(x(s)) \right] ds \right\} \mathcal{D}x(s), \tag{3.324}$$

where the integration is performed over all trajectories $x(s)$ starting at point x. The propagator, $p(y, t|x)$ can be written as

$$p(y, t|x) = \int_{\substack{x(0)=x \\ x(t)=y}} \exp\left\{ -\int_0^t \left[\frac{\dot{x}^2(s)}{4D} \right] ds \right\} \mathcal{D}x(s), \tag{3.325}$$

which is the transition probability density function for the Brownian motion: $p(y, t|x) = \frac{\partial}{\partial y} \mathbb{P}(B(t) \leq y | B(0) = x)$. So the path-integral (3.324) can be rewritten in terms of the expectation operator, the Feynman–Kac formula,

$$\rho(x, t) = \mathbb{E}_x \rho_0(B(t)) \exp\left(\int_0^t r(B(s)) ds \right), \tag{3.326}$$

where $B(t)$ is the Brownian motion starting at point x [141].

If the mesoscopic density of particles obeys the integro-differential equation

$$\frac{\partial \rho}{\partial t} = \lambda \int_{\mathbb{R}} \rho(x - z, t) w(z) dz - \lambda \rho(x, t) + r(x)\rho, \tag{3.327}$$

then the underlying random process is a compound Poisson process $X(t)$ given by

$$X(t) = \sum_{i=1}^{N(t)} Z_i, \tag{3.328}$$

where $N(t)$ is a Poisson process with the transition rate λ and Z_i is a sequence of IID jumps with density function $w(z)$. The solution to the integro-differential equation (3.327) with the initial condition $\rho(x, 0) = \rho_0(x)$ can be written as

$$\rho(x, t) = \mathbb{E}_x \rho_0(X(t)) \exp\left(\int_0^t r(X(s)) ds\right). \tag{3.329}$$

If the process $X(t)$ is a symmetric α-stable Lévy motion $S_\alpha(t)$ on $\mathbb{R}$, then the formula (3.329) provides the solution to the Cauchy problem

$$\frac{\partial \rho}{\partial t} = D_\alpha \frac{\partial^\alpha \rho}{\partial |x|^\alpha} + r(x)\rho, \quad \rho(x, 0) = \rho_0(x), \quad x \in \mathbb{R}. \tag{3.330}$$

In the same way we can obtain the probabilistic representation for the density that obeys the nonlinear Cauchy problem

$$\frac{\partial \rho}{\partial t} = D\Delta \rho + r(x, \rho)\rho, \quad \rho(\mathbf{x}, 0) = \rho_0(\mathbf{x}), \quad \mathbf{x} \in \mathbb{R}^3. \tag{3.331}$$

We have

$$\rho(\mathbf{x}, t) = \mathbb{E}_{\mathbf{x}} \rho_0(\mathbf{B}(t)) \exp\left[\int_0^t r(\mathbf{B}(s), \rho(\mathbf{B}(s), t - s)) ds\right]. \tag{3.332}$$

3.7.4.2 Nonstationary Convection–Diffusion Equation with Reactions

So far the velocity field $\mathbf{v}$ and the growth rate r have been functions of the space coordinate only. The goal now is to allow both $\mathbf{v}$ and r to depend on time t as well. Consider a transport problem involving a nonstationary incompressible fluid flow with the velocity field $\mathbf{v}(\mathbf{x}, t)$, standard diffusion with the constant diffusivity D, and reactions with rate $r(x, t)\rho$. The equation for the density of particles takes the form

$$\frac{\partial \rho}{\partial t} + \mathbf{v}(\mathbf{x}, t) \cdot \nabla \rho = D\Delta \rho + r(\mathbf{x}, t)\rho, \quad \mathbf{x} \in \mathbb{R}^3, \tag{3.333}$$

with the initial condition

$$\rho(\mathbf{x}, t) = \rho_0(\mathbf{x}). \tag{3.334}$$

The solution of this problem can be written as the functional integral

$$\rho(\mathbf{x}, t) = \mathbb{E}_{\mathbf{x}} \rho_0(\mathbf{X}(t)) \exp\left[\int_0^t r(\mathbf{X}(s), t - s) ds\right], \qquad (3.335)$$

where the random process $\mathbf{X}(s)$ is the solution of the SDE

$$d\mathbf{X}(s) = -\mathbf{v}(\mathbf{X}(s), t - s) ds + \sqrt{2D} d\mathbf{W}(s), \quad 0 \leq s \leq t, \qquad (3.336)$$

with the initial condition $\mathbf{X}(0) = \mathbf{x}$. Here $\mathbf{W}(t)$ is the standard three-dimensional Wiener process.

In particular, the solution of the convection–diffusion equation ($r = 0$) is

$$\rho(\mathbf{x}, t) = \mathbb{E}_{\mathbf{x}} \rho_0(\mathbf{X}(t)). \qquad (3.337)$$

In the next section we show why the velocity in (3.336) has arguments $(\mathbf{X}(s), t - s)$ and why there is a minus sign for this velocity.

3.7.4.3 Convection–Transport Equation

Consider a convection–transport equation without diffusion,

$$\frac{\partial \rho(\mathbf{x}, t)}{\partial t} + \mathbf{v}(\mathbf{x}, t) \cdot \nabla \rho(\mathbf{x}, t) = 0, \quad \mathbf{x} \in \mathbb{R}^3, \qquad (3.338)$$

with the initial condition $\rho(\mathbf{x}, 0) = \rho_0(\mathbf{x})$. The solution to this Cauchy problem can be written as follows:

$$\rho(\mathbf{x}, t) = \rho_0(\mathbf{X}(t)), \qquad (3.339)$$

where $\mathbf{X}(t)$ is the solution of the characteristic equation

$$d\mathbf{X}(s) = -\mathbf{v}(\mathbf{X}(s), t - s) ds, \quad \mathbf{X}(0) = \mathbf{x}, \quad 0 \leq s \leq t. \qquad (3.340)$$

The formula (3.339) tells us that the value of the density at point $\mathbf{x}$ at time t is the value of the initial density at the point $\mathbf{X}(t)$. The main idea is that we release the underlying process $\mathbf{X}(s)$ from the point $\mathbf{x}$ so that s varies from 0 up to t. So we allow the particle to move backward in time, such that the velocity field has a value $-\mathbf{v}(\mathbf{x}, t)$ at time $s = 0$ and $-\mathbf{v}(\mathbf{X}(t), 0)$ at time $s = t$. We have

$$\frac{d\rho(\mathbf{X}(s), t - s)}{ds} = \frac{d\mathbf{X}(s)}{ds} \cdot \nabla \rho(\mathbf{X}(s), t - s) - \frac{\partial \rho(\mathbf{X}(s), t - s)}{\partial t}. \qquad (3.341)$$

We integrate both sides and find

$$
\rho_0(\mathbf{X}(t)) - \rho(\mathbf{x}, t) =
$$
$$
- \int_0^t \left(\mathbf{v}(\mathbf{X}(s), t - s) \cdot \nabla \rho(\mathbf{X}(s), t - s) + \frac{\partial \rho(\mathbf{X}(s), t - s)}{\partial t} \right) ds. \quad (3.342)
$$

Because of (3.338) the RHS of the last equation is zero, and therefore $\rho(\mathbf{x}, t) = \rho_0(\mathbf{X}(t))$.

3.7.4.4 Boundary Reaction–Diffusion Problem

So far we have found probabilistic solutions to PDEs on the whole space. In fact Itô's formula allows us to represent the solutions to these equations in a bounded domain, $\Omega \in \mathbb{R}^3$, with appropriate boundary conditions. For example, let us consider the stationary reaction–diffusion problem

$$
D\Delta\rho(\mathbf{x}) + r(\mathbf{x})\rho = 0, \quad \mathbf{x} \in \Omega, \quad \rho(\mathbf{x})_{\mathbf{x} \in \partial\Omega} = g(\mathbf{x}). \quad (3.343)
$$

Then

$$
\rho(\mathbf{x}) = \mathbb{E}_\mathbf{x} g(\mathbf{B}(\tau)) \exp\left\{ \int_0^\tau r(\mathbf{B}(s))ds \right\}, \quad (3.344)
$$

where $\mathbf{B}(t)$ is the Brownian motion starting at point $\mathbf{x}$ and τ is the first exit time for Brownian motion to reach the boundary $\partial\Omega$, i.e., $\tau = \min(t : \mathbf{B}(t) \notin \Omega)$. Freidlin's book [141] is an excellent reference for more details on initial-boundary problems similar to (3.343) and corresponding diffusion processes.

Exercises

3.1 Show that the Laplace transform of the Caputo derivative defined in (3.38) is

$$
\mathcal{L}\left(\frac{\partial^\gamma p(x, t)}{\partial t^\gamma} \right) = s^\gamma \hat{p}(x, s) - s^{\gamma - 1} p_0(x). \quad (3.345)
$$

Hint: Use the definition of the Gamma function $\Gamma(1 - \gamma) = \int_0^\infty e^{-t} t^{-\gamma} dt$ and the fact that the integral in (3.38) is the convolution of the functions $f(t)$ and $t^{-\gamma}$.

3.2 Using the Montroll–Weiss equation (3.31) for the uncoupled case (3.23), derive the equation for $\rho(x, t)$ in the form

$$\int_0^t M(t - \tau) \frac{\partial \rho(x, \tau)}{\partial \tau} d\tau = \int_{\mathbb{R}} \rho(x - z, t) w(z) dz - \rho(x, t), \qquad (3.346)$$

where $M(t)$ is defined by its Laplace transform $\hat{M}(s) = [1 - \hat{\phi}(s)]/[s\hat{\phi}(s)]$. Note that this is an alternative equation to the Master equation (3.31).

3.3 Obtain (3.141) from (3.139) and (3.140).

3.4 Assume that the waiting time PDF $\phi(t)$ corresponds to the family of Gamma distributions with parameters $m = 2$ and λ:

$$\phi(t) = \frac{\lambda^2 t e^{-\lambda t}}{\Gamma(2)}. \qquad (3.347)$$

If the kinetic term is linear, show that the solution to (3.130) is $\rho(x, t) = e^{rt} n(x, t)$, where $n(x, t)$ is the solution to

$$\frac{1}{2\lambda} \frac{\partial^2 \rho}{\partial t^2} + \frac{\partial \rho}{\partial t} = \frac{\lambda}{2} \left[\int_{\mathbb{R}} \rho(x - z, \tau) w(z) dz - \rho(x, \tau) \right]. \qquad (3.348)$$

3.5 If the survival probability is

$$\Psi(t) = E_\gamma \left[-\left(\frac{t}{\tau_0} \right)^\gamma \right], \quad 0 < \gamma \le 1, \qquad (3.349)$$

where $E_\gamma[x] = \sum_0^\infty x^n / \Gamma(\gamma n + 1)$ is the Mittag–Leffler function, show that (3.130) can be written as the fractional reaction–transport equation

$$\frac{\partial \rho}{\partial t} = \frac{e^{\int_0^t f(\rho(x-z,u)) du}}{\tau_0^\gamma} \mathcal{D}_t^{1-\gamma} \left(\int_{\mathbb{R}} \rho(x - z, t) e^{-\int_0^t f(\rho(x-z,u)) du} w(z) dz \right)$$

$$- \frac{e^{\int_0^t f(\rho(x,u)) du}}{\tau_0^\gamma} \mathcal{D}_t^{1-\gamma} \left(\rho(x, t) e^{-\int_0^t f(\rho(x,u)) du} \right) + f(\rho)\rho, \quad (3.350)$$

where $\mathcal{D}_t^{1-\gamma}$ is the Riemann–Liouville fractional derivative defined by (2.58).

Part II
Front Propagation

Chapter 4
Reaction–Diffusion Fronts

Traveling waves are typical nonequilibrium phenomena encountered in numerous instances in physics, chemistry, biology, and other areas [129, 82, 309, 310]. React- ing and diffusing systems described by the RD equation (2.3) represent a particular well-studied class of applications. Equation (2.3) is known as Fisher's equation, if the reaction term has the logistic form $F(\rho) = r\rho(1 - \rho)$:

$$\frac{\partial \rho}{\partial t} = D\frac{\partial^2 \rho}{\partial x^2} + r\rho(1 - \rho). \tag{4.1}$$

It was introduced in 1937 in the seminal contributions of R. A. Fisher [132] and A. N. Kolmogorov, together with I. G. Petrovskii and N. S. Piskunov [232] as a model for the spreading of an advantageous gene. Consequently, we will refer to (4.1) also as the FKPP equation. It is the simplest and most well-known equation that has traveling wave solutions.

4.1 Propagating Fronts

A *front* corresponds to a traveling wave solution, which maintains its shape, travels with a constant velocity v^*, $\rho(x, t) = \rho(x - v^*t)$, and joins two steady states of the system. The latter are uniform stationary states, $\rho(x, t) = \overline{\rho}$, where $F(\overline{\rho}) = 0$. For the logistic kinetics, the steady states are $\overline{\rho}_1 = 0$ and $\overline{\rho}_2 = 1$. While the logistic kinetics has only two steady states, three or more stationary states can exist for a broad class of systems in nonlinear chemistry and population dynamics with Allee effect, but a front can only connect two of them. To determine the propagation direction of the front, we need to evaluate the stability of the stationary states, see Sect. 1.2. The steady state $\overline{\rho}$ is stable if $F'(\overline{\rho}) < 0$ and unstable if $F'(\overline{\rho}) > 0$. Let the initial particle density $\rho(x, 0)$ be such that on a certain finite interval, $\rho(x, 0)$ is different from 0 and 1, and to the left of this interval $\rho(x, 0) = 1$, while to the right $\rho(x, 0) = 0$. In this case, the initial condition is said to have compact support. Kolmogorov et al. [232] showed for Fisher's equation that due to the combined effects of diffusion and reaction, the region of density close to 1 expands to the

right. There exists a front that connects the stable steady state to the unstable steady state and that propagates to the right; the stable state invades the unstable state.

Consider a general reaction term that satisfies $F(0) = F(1) = 0$. If F vanishes at $\rho = c > 0$ with $c \neq 1$, ρ can be renormalized by defining a new field ρ/c for which the above condition is satisfied. Aronson and Weinberger [18] showed that any positive, sufficiently localized (this means decaying faster than exponentially for $|x| \to \infty$) initial condition $\rho(x, 0)$, with $\rho(x, 0) \in [0, 1]$, evolves into a front propagating with velocity v^*, i.e., for large t, $\rho(x, t)$ behaves as $\rho(x - v^* t)$. The shape of the front is determined by the boundary value problem

$$D\rho_{zz} + v\rho_z + F(\rho) = 0 \tag{4.2}$$

with

$$\lim_{z \to -\infty} \rho(z) = 1 \quad \text{and} \quad \lim_{z \to +\infty} \rho(z) = 0. \tag{4.3}$$

Here $z \equiv x - vt$, and (4.2) is obtained by transforming (2.3) to the frame co-moving with the front, since $\partial_x \rho \to d\rho/dz \equiv \rho_z$ and $\partial_t \rho \to -vd\rho/dz \equiv -v\rho_z$. Aronson and Weinberger [18] characterized the asymptotic velocity v^* as the minimum value of the parameter v in (4.2) for which the solution $\rho(z)$ is monotonic. This poses the problem of how to determine the value of v^* for different reaction terms. We will consider two types of reaction terms.

Case A: $F'(0) > 0$, $F(\rho) > 0$, $\rho \in (0, 1)$. This case is known as heterozygote intermediate in population dynamics or as KPP kinetics.

Case B: $F(\rho) > 0$ for all $\rho \in (b, 1)$ and $F(\rho) < 0$ for all $\rho \in (0, b)$ with $b \in (0, 1)$, $\int_0^1 F(\rho)d\rho > 0$, and $F'(0) < 0$. This case is known as heterozygote inferior in population dynamics or as bistable kinetics.

In both cases, (4.2) can be viewed as Newton's equation for a particle moving in one dimension under the action of the force $-F(\rho) - v\rho_z$; the variable z plays the role of time. The force $-F(\rho)$ is conservative and derives from the potential $V(\rho) = \int_0^\rho F(s)ds$.

If the kinetic term $F(\rho)$ belongs to Case A, the potential has a minimum at the point $\rho = 0$ and a maximum at $\rho = 1$. The second term, $-v\rho_z$, in (4.2) represents a damping force, where v represents the viscosity. Then (4.2) describes the motion of a particle rolling down from the top of the potential at $\rho = 1$ to the bottom of the potential well, $\rho = 0$, in the presence of a viscous force. If v is small, i.e., the viscosity is small, the particle oscillates near the bottom of the well before it settles down at the minimum $\rho = 0$. If v increases, there exists a threshold value at which the oscillations cease. In other words, the particle rolls down monotonically from $\rho = 1$ to $\rho = 0$; in mechanics this is known as critical damping. If v increases even further, the particle continues to roll down monotonically and has less and less velocity at every point of its trajectory. Consequently, there exists a critical value of v, which we denote by v^*, such that for $v \geq v^*$, there will be monotonically decreasing solutions to (4.2). The front is said to be *propagating into the*

unstable state. This result was proven rigorously by Aronson and Weinberger, who also showed that the critical value v^* is the front velocity for the RD equation in Case A, if the front evolves from an initial condition with compact support.

If $F(\rho)$ belongs to Case B, the potential has two maxima, at $\rho = 1$ and $\rho = 0$, and a minimum at $\rho = b$. The particle starts at $\rho = 1$, $z = -\infty$, and needs to arrive at $\rho = 0$, $z = +\infty$, with zero velocity. Energy conservation requires that the height of the maximum at $\rho = 0$ must be smaller than the height of the maximum at $\rho = 1$. Otherwise the particle never reaches $\rho = 0$. This condition is precisely $\int_0^1 F(\rho)d\rho > 0$. In this case, the front connects two stable states and is said to be *propagating into a metastable state*; $\rho = 0$ is less stable than $\rho = 1$. It should be clear intuitively that there is only one value of v^* for which the particle rolls down from $\rho = 1$ to the bottom of the valley at $\rho = b$ and then climbs up to the top at $\rho = 0$ to stop there with zero velocity. If $v < v^*$, the particle overshoots at $\rho = 0$, leading to an unphysical front. If $v > v^*$, the particle becomes trapped forever at $\rho = b$, representing again a front propagating into an unstable state. We represent schematically this discussion in Fig. 4.1.

A phase plane analysis represents a useful alternative to the mechanical analogy discussed above. The phase plane is constructed by the standard technique of converting the second-order ordinary differential equation (4.2) into a system of two first-order differential equations:
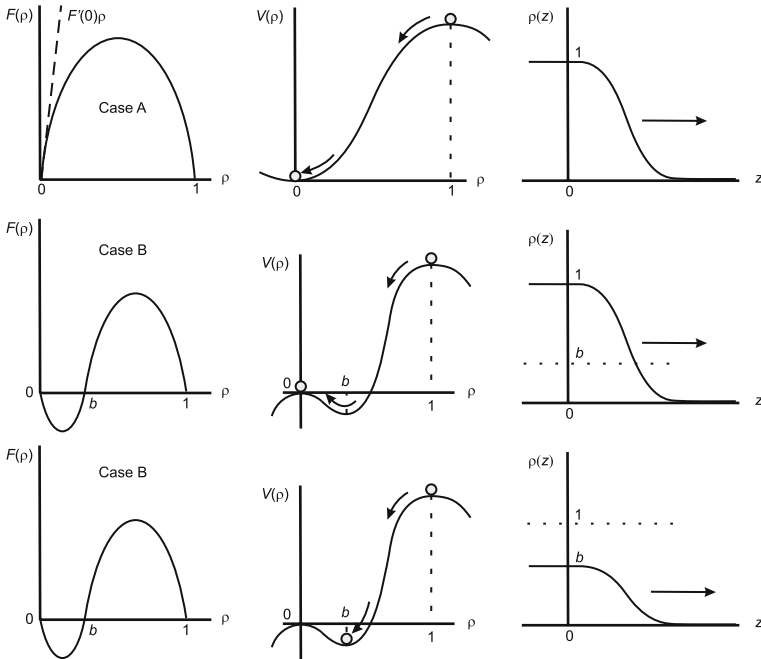

Fig. 4.1 Schematic picture for Cases A and B. We plot the reaction term, its corresponding potential, and the front profile

$$\rho_z = -q, \tag{4.4a}$$

$$q_z = -\frac{v}{D}q - \frac{r}{D}F(\rho). \tag{4.4b}$$

In the phase plane (ρ, q), a front corresponds to trajectory that connects two steady states of (4.4). Such a trajectory is know as a *heteroclinic orbit* or a heteroclinic connection. The steady states of (4.4) are given by $(\overline{\rho}, 0)$, where $F(\overline{\rho}) = 0$. The phase plane trajectories or orbits of (4.4) are the solutions of

$$\frac{d\rho}{dq} = \frac{vq + rF(\rho)}{Dq}. \tag{4.5}$$

To be specific, we consider logistic kinetics and Nagumo kinetics [274], $F(\rho) = r\rho(1-\rho)(\rho-b)$, as examples for cases A and B, respectively. For the logistic case, a linear stability analysis of the stationary states $(0, 0)$ and $(1, 0)$ provides their eigenvalues $\lambda_\pm(0, 0) = -v/2 \pm \sqrt{v^2 - 4Dr}/2$ and $\lambda_\pm(1, 0) = -v/2 \pm \sqrt{v^2 + 4Dr}/2$, respectively. The state $(0, 0)$ is a stable node if $v > 2\sqrt{Dr}$ and a stable focus if $v < 2\sqrt{Dr}$. The state $(1, 0)$ is always a saddle point. To be physically acceptable, a front must always be nonnegative. Consequently, only nonnegative heteroclinic orbits are acceptable. Such orbits can only exist if $(0, 0)$ is a stable node. In other words, fronts only exist for $v > 2\sqrt{Dr}$. Since there exists a heteroclinic connection or front for each value of v with $v > 2\sqrt{Dr}$, this analysis does not yield a unique propagating velocity. In fact, the front velocity v depends on the initial condition, specifically on the tail of the initial condition.

For bistable kinetics there exist three steady states: $(0, 0)$, $(b, 0)$, and $(1, 0)$. Both $(0, 0)$ and $(1, 0)$ are saddle points, while $(b, 0)$ is stable. A heteroclinic connection between $(1, 0)$ and $(b, 0)$ requires $(b, 0)$ to be stable node, which is satisfied for $v > 2\sqrt{b(1 - b)}$. This case is equivalent to the logistic case. The heteroclinic orbit corresponding to a front connecting $(0, 0)$ and $(1, 0)$ must be a saddle–saddle connection. If one fixes b and varies v, one finds that for low values of v the phase plane trajectories undershoot the state $(1, 0)$, while for large values of v, the phase plane trajectories overshoot the state $(1, 0)$. There is a unique saddle–saddle connection, the separatrix, which is uniquely determined by a specific value of v. In contrast to the logistic case, where an infinite number of fronts exist if v is larger than $2\sqrt{Dr}$, only a single front with a unique velocity exists in the bistable case. In Fig. 4.2 we depict the phase portrait for both the logistic and the bistable cases. In the next two sections, we present quantitative methods to characterize front propagation for both cases A and B.

4.1.1 Fronts Propagating into Unstable States. Pulled vs Pushed Fronts

Consider the RD equation (2.3). Without specifying the shape of $F(\rho)$, we assume two steady states such that
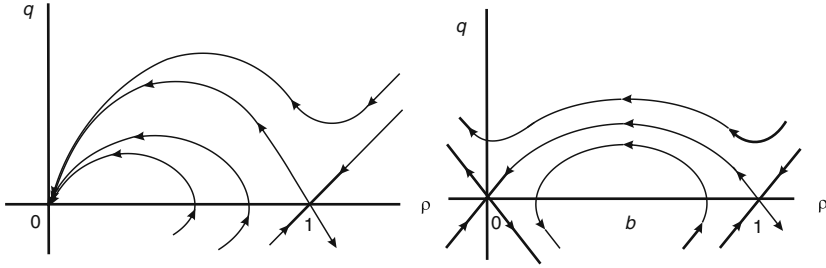
Fig. 4.2 Phase portrait for logistic and bistable reaction terms. The front is a heteroclinic saddle–node connection for the logistic case. The front is a saddle–saddle connection for the bistable case

$$F(0) = F(1) = 0 \quad \text{and} \quad F(\rho) > 0, \text{ if } 0 < \rho < 1, \tag{4.6}$$

i.e., $\overline{\rho} = 0$ is an unstable steady state and $\overline{\rho} = 1$ a stable steady state. We linearize the RD equation in the frame comoving with the front around the unstable steady state:

$$D\rho_{zz} + v\rho_z + F'(0)\rho = 0. \tag{4.7}$$

Looking for exponential solutions, we find $\rho(z) \sim Ae^{-\lambda_+ z} + Be^{-\lambda_- z}$, where

$$\lambda_{\pm} = \frac{v}{2} \pm \frac{1}{2}\sqrt{v^2 - 4DF'(0)}. \tag{4.8}$$

The solutions are physically acceptable if

$$v \geq 2\sqrt{DF'(0)}. \tag{4.9}$$

Otherwise the solution oscillates around the state $\rho = 0$, resulting in negative values for the particle density. The linear analysis establishes the existence of a minimum value for the front velocity. We can also obtain the minimum value by substituting $\rho(z) \sim e^{-\lambda z}$ in (4.7), writing the characteristic equation in the form

$$v(\lambda) = D\lambda + \frac{F'(0)}{\lambda}, \tag{4.10}$$

and calculating

$$v^* = \min_{\lambda}[v(\lambda)] = 2\sqrt{DF'(0)}. \tag{4.11}$$

Aronson and Weinberger [18] obtained the condition

$$2\sqrt{DF'(0)} \leq v^* < 2\sqrt{D \sup_{\rho}\left[\frac{F(\rho)}{\rho}\right]}, \tag{4.12}$$

for fronts evolving from initial conditions with compact support. This result provides both a lower and an upper bound for the front velocity. For any concave kinetic term, i.e., $F(\rho) \leq \rho F'(0)$, the lower and the upper bounds in (4.12) coincide, and the front velocity can be predicted with certainty:

$$v^* = 2\sqrt{DF'(0)}. \tag{4.13}$$

It equals the minimum velocity obtained by linearizing around the unstable state, the linear velocity. In this case the front dynamics is determined by the $\rho(x, t) \approx 0$ region. The front is called a *pulled* front, since it is pulled by its leading edge. The lower and upper bounds do *not* coincide for convex kinetic terms, and the front velocity is larger than the linear velocity. In this case, the nonlinear part of the kinetic term plays an important role in determining the value of the front velocity; the front dynamics is *pushed* by its interior part.

We consider the Ginzburg–Landau reaction term $F(\rho) = \rho(1 - \rho)(1 + \alpha\rho)$, with $\alpha > 0$, in (2.3) to illustrate the existence of pulled and pushed regimes. This RD equation has two steady states, $\overline{\rho} = 0$ (unstable) and $\overline{\rho} = 1$ (stable). The front connecting both states propagates into the unstable state, which resembles the situation in the FKPP case. However, Ben-Jacob et al. [37] show that when the front emerges from initial conditions with compact support, the velocity is given by

$$v = \begin{cases} 2\sqrt{D}, & \alpha \leq 2, \\ \left(\sqrt{\alpha} + 2/\sqrt{\alpha}\right)\sqrt{D/2}, & \alpha > 2. \end{cases} \tag{4.14}$$

The linear velocity $2\sqrt{D}$ is selected by the front only if $\alpha \leq 2$. The front is pulled in this case. However, if $\alpha > 2$, the selected velocity is $\left(\sqrt{\alpha} + 2/\sqrt{\alpha}\right)\sqrt{D/2}$, and the front is pushed. The value $\alpha = 2$ corresponds to the transition between pulled and pushed regimes.

The asymptotic velocity depends explicitly on the shape of the initial conditions, if they do not have compact support. An adaptation of the Hamilton–Jacobi theory from classical mechanics is a useful technique to deal with this problem in a very general way, see below. The prototypical example of a concave reaction term is the KPP or logistic term $F(\rho) = r\rho(1 - \rho)$. Equation (4.13) implies that $v = 2\sqrt{rD}$. Examples for convex reaction functions typically occur in combustion theory, where $F(\rho) = e^{-\rho_c/\rho}(1 - \rho)$ is referred to as the Arrhenius reaction term, or $F(\rho) = \rho^m(1 - \rho)$ for forest fire models. In these cases, as well as for Case B, generally the variational characterization is the only tool that can provide analytical expressions for the front velocity. Other types of reaction terms are a combination of Cases A and B, such that the kinetic term is convex for a range of values of ρ, while elsewhere it is concave.

4.1.2 Transient Dynamics of Pulled Fronts

Pushed fronts, such as fronts propagating into a metastable state, converge exponentially to the asymptotic front profile $\rho(x - vt)$. Both the profile and velocity of pulled fronts converge algebraically. It was proven rigorously by Bramson [57] that the solution of the Fisher equation with a KPP reaction term relaxes to a unique front profile $\rho(x - 2t)$, where the velocity converges asymptotically as $v(t) = 2 - \frac{3}{2t}$. (Here and in the remainder of this section, we consider the case that space and time have been scaled such that $D = r = 1$.) More recently, Ebert and van Saarloos [103, 104] found universal behavior in the relaxation to the asymptotic regime for fronts emerging from initial conditions with compact support or with exponential decay. We summarize their main results for the first case. We consider the shape of the transient front as a small perturbation η about the asymptotic shape, $\rho^*[x - v(t)t]$, where $v(t) = v^* + \dot{X}(t)$. Then, written in the frame $\xi = x - v^* t - X(t)$, the Fisher equation (2.3) with logistic growth reads

$$\rho(\xi, t) = \rho^*(\xi) + \eta(\xi, t) = \rho^*(\xi) + \dot{X}(t)\eta_s(\xi) \qquad (4.15)$$

for the interior region of the front, $\xi \ll 2\sqrt{t}$. Here $\eta(\xi, t)$ obeys the equation

$$\frac{\partial \eta}{\partial t} = \mathcal{L}^* \eta + \dot{X}(t)\frac{\partial}{\partial \xi}\left[\eta + \rho^*(\xi)\right] + \frac{\eta^2}{2}F''(\rho^*) + O(\eta^3), \qquad (4.16)$$

with $\mathcal{L}^* = \partial_\xi^2 + v^* \partial_\xi + F'(\rho^*)$. The fact that $\dot{X}(t)$ is $O(t^{-1})$ suggests the asymptotic expansion

$$\dot{X}(t) = \frac{c_1}{t} + \frac{c_{3/2}}{t^{3/2}} + \cdots, \qquad (4.17)$$

$$\eta(\xi, t) = \frac{\eta_1}{t} + \frac{\eta_{3/2}}{t^{3/2}} + \cdots. \qquad (4.18)$$

Substitution of this expansion into (4.16) yields the hierarchy of ordinary differential equations:

$$\mathcal{L}^* \eta_1 = -c_1 \partial_\xi \rho^*, \quad \mathcal{L}^* \eta_{3/2} = -c_{3/2}\partial_\xi \rho^*, \ldots. \qquad (4.19)$$

Each η_i is determined by its differential equation, the requirement $\eta_i(0) = 0$, and the appropriate boundary conditions. The equations for η_1/c_1 and $\eta_{3/2}/c_{3/2}$ are precisely the differential equations for $\eta_s(\xi)$ in (4.16).

In the far edge, where $\xi \geq O(\sqrt{t}) \gg 1$, a different expansion is needed, as the transient profile falls off faster than ρ^*, so that $\eta \approx -\rho^*$. Linearizing about $\rho = 0$ one finds

$$\rho(\xi, t) = e^{-\xi - \xi^2/(4t)} \left[\sqrt{t} g_{-1/2}\left(\frac{\xi^2}{4t}\right) + g_0\left(\frac{\xi^2}{4t}\right) + \frac{g_{1/2}\left(\frac{\xi^2}{4t}\right)}{\sqrt{t}} + \cdots \right],$$

$$(4.20)$$

where the functions g_i obey a new hierarchy of ordinary differential equations that can also be integrated with the appropriate boundary conditions. Finally, matching this solution to the one for the interior region, we determine the parameters c_1 and $c_{3/2}$, and the front velocity is found to be

$$v(t) = v^* - \frac{3}{2t} + \frac{3\sqrt{\pi}}{2t^{3/2}} + \cdots .$$

$$(4.21)$$

4.1.3 Front Propagation into Metastable States

As explained above, the shape and velocity of a front propagating into a metastable state is governed by the nonlinear (interior) part, and the nonlinear term in the reaction function plays an important role. When a front propagates into a metastable state, only one velocity is possible, in contrast to a front propagating into an unstable state. In the latter case, there exists an infinite number of possible velocities, namely all velocities larger than the linear velocity. To obtain the unique velocity of a front propagating into a metastable state, one has to solve the differential equation in the frame co-moving with the front and find the front shape. Since the differential equation is nonlinear, this is not an easy task. Often, one has to resort to some trial parametric solution and substitute it into the differential equation to calculate the parameter values. As a typical example we consider the reaction term $F(\rho) = r(\rho - \rho_1)(\rho_2 - \rho)(\rho - \rho_3)$, where $\rho_1 < \rho_2 < \rho_3$. This kinetic term has the steady states $\overline{\rho} = \rho_i$, with $i = 1, 2, 3$. The states ρ_1 and ρ_3 are stable, while ρ_2 is unstable. To obtain the front profile and velocity, we need to solve the differential equation

$$D\rho_{zz} + v\rho_z + r(\rho - \rho_1)(\rho_2 - \rho)(\rho - \rho_3) = 0.$$

$$(4.22)$$

Since the front joins the two stable states and propagates into the metastable state, the boundary conditions are given by

$$\lim_{z \to -\infty} \rho(z) = \rho_3 \quad \text{and} \quad \lim_{z \to +\infty} \rho(z) = \rho_1.$$

$$(4.23)$$

The derivative ρ_z must vanish at $\rho = \rho_3$ and at $\rho = \rho_1$. A possible candidate for the front solution is $\rho_z = b(\rho - \rho_1)(\rho - \rho_3)$, where b is a constant to be determined. Substituting this solution into (4.22), we obtain a cubic polynomial in ρ. Setting the coefficients to 0 provides a system of four algebraic equations. The equation for the coefficient of ρ^3 yields $b = \sqrt{r/2D}$. With this value, the equations for the

coefficient of ρ^2 and ρ^0 are satisfied, and only one equation remains to be solved. The equation for the coefficient of ρ provides the relation for the velocity:

$$v = \sqrt{\frac{rD}{2}} \left(\rho_1 - 2\rho_2 + \rho_3 \right). \tag{4.24}$$

Finally, we calculate the front profile by integrating

$$\rho_z = \sqrt{r/2D}(\rho - \rho_1)(\rho - \rho_3) \tag{4.25}$$

and imposing the boundary conditions. The result is

$$\rho(z) = \frac{\rho_3 + K\rho_1 e^{\sqrt{r/2D}(\rho_3 - \rho_1)z}}{1 + K e^{\sqrt{r/2D}(\rho_3 - \rho_1)z}}, \tag{4.26}$$

where K is an arbitrary constant that can be determined, e.g, by imposing a value for $\rho(z = 0)$. Equation (4.24) implies that $v > 0$ if $\rho_2 < (\rho_1 + \rho_3)/2$, and it is negative otherwise. This means that we can change the direction of front propagation for fixed values of ρ_1 and ρ_3 by varying the value of ρ_2. Changing ρ_2 affects the relative stability of the stable states ρ_1 and ρ_3, i.e., which one is the stable and the metastable state, and thus the direction of front motion. This can be easily understood by invoking the dynamical picture introduced in Sect. 4.1. The potential difference between states ρ_1 and ρ_3 is given by

$$\Delta V = V(\rho_3) - V(\rho_1) = \int_{\rho_1}^{\rho_3} F(\rho) d\rho = \frac{(\rho_3 - \rho_1)^3}{12} \left(\rho_1 - 2\rho_2 + \rho_3 \right). \tag{4.27}$$

If $\rho_2 < (\rho_1 + \rho_3)/2$, $V(\rho_3) > V(\rho_1)$, and ρ_3 is stable, while ρ_1 is metastable. In this case, the front travels to the right, $v > 0$, by invading ρ_1 (remember that $\rho_1 < \rho_3$). Otherwise, if $\rho_2 > (\rho_1 + \rho_3)/2$, $V(\rho_1) > V(\rho_3)$, and ρ_1 is stable, while ρ_3 is metastable; the front propagates to the left. This is depicted in Fig. 4.3. The sign of the front velocity, i.e., the direction of propagation, can be determined for a general kinetic term $F(\rho)$. We multiply (4.2) by ρ_z and integrate over z to obtain

$$\int_{-\infty}^{\infty} \rho_{zz} \rho_z dz + v \int_{-\infty}^{\infty} \rho_z^2 dz + \int_{-\infty}^{\infty} F(\rho) \rho_z dz = 0. \tag{4.28}$$

The first integral is

$$\int_{-\infty}^{\infty} \rho_{zz} \rho_z dz = \frac{1}{2} \left[\rho_z^2 \right]_{-\infty}^{+\infty} = 0, \tag{4.29}$$

and the third one is

$$\int_{-\infty}^{\infty} F(\rho) \rho_z dz = \int_{\rho_1}^{\rho_3} F(\rho) d\rho, \tag{4.30}$$
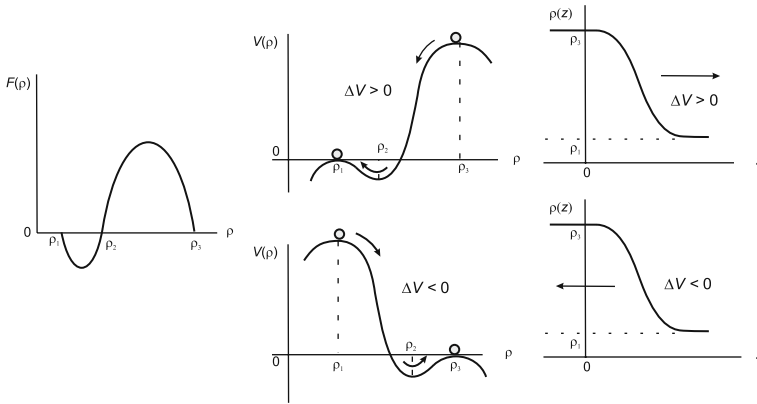
Fig. 4.3 The potential difference between the stable steady states changes their relative stability and changes the direction of front propagation

so that

$$v = \frac{\int_{\rho_1}^{\rho_3} F(\rho)\mathrm{d}\rho}{\int_{-\infty}^{\infty} \rho_z^2 \mathrm{d}z} \qquad (4.31)$$

and

$$\mathrm{sgn}(v) = \mathrm{sgn}\left(\int_{\rho_1}^{\rho_3} F(\rho)\mathrm{d}\rho\right). \qquad (4.32)$$

For the case (4.22), $\mathrm{sgn}(v) = \mathrm{sgn}\left(\rho_1 - 2\rho_2 + \rho_3\right)$, in agreement with (4.24).

4.2 Front Velocity Selection

The fact that an infinity of front velocities occurs for pulled fronts gives rise to the problem of velocity selection. In this section we present two methods to tackle this problem. The first method employs the Hamilton–Jacobi theory to analyze the dynamics of the front position. It is equivalent to the marginal stability analysis (MSA) [448] and applies only to pulled fronts propagating into unstable states. However, in contrast to the MSA method, the Hamilton–Jacobi approach can also deal with pulled fronts propagating in heterogeneous media, see Chap. 6. The second method is a variational principle that works both for pulled and pushed fronts propagating into unstable states as well as for those propagating into metastable states. This principle can deal with the problem of velocity selection, if it is possible to find the proper trial function. Otherwise, it provides only lower and upper bounds for the front velocity.

4.2.1 Hamilton–Jacobi Formalism

4.2.1.1 Hyperbolic Scaling and Hamilton–Jacobi Equation for the Front Position

This method consists in finding the Hamilton–Jacobi equation for an RD equation with a KPP reaction term and was originally introduced by Freidlin [140]. The first step consists in performing the hyperbolic scaling on the RD equation (2.3):

$$x \to \frac{x}{\varepsilon} \quad \text{and} \quad t \to \frac{t}{\varepsilon}, \quad \varepsilon \ll 1. \tag{4.33}$$

The second step consists in analyzing the behavior of solutions of (2.3) for large times, of order ε^{-1}, and determine whether or not a front exists in the limit $t \to \infty$ ($\varepsilon \to 0$). We expect that after the hyperbolic scaling the new field $\rho^\varepsilon(x, t) = \rho(x/\varepsilon, t/\varepsilon)$ takes only two values, 0 and 1, as $\varepsilon \to 0$, which means that the solution of (2.3) converges to the indicator function of the set whose boundary can be considered as the position of a moving front that separates the stable and unstable states. In fact any initial condition with compact support will ensure a front propagating with the minimal velocity. After the hyperbolic scaling, (2.3) reads

$$\varepsilon \frac{\partial \rho^\varepsilon}{\partial t} = D\varepsilon^2 \frac{\partial^2 \rho^\varepsilon}{\partial x^2} + r F(\rho^\varepsilon). \tag{4.34}$$

Since $\rho^\varepsilon(x, t) \geq 0$, we can make use of the transformation

$$\rho^\varepsilon(x, t) = \exp\left[-G^\varepsilon(x, t)/\varepsilon\right], \tag{4.35}$$

where $G^\varepsilon(x, t) \geq 0$. The new function $G^\varepsilon(x, t)$ determines the location of the front in the limit $\varepsilon \to 0$. If $F(\rho) = \rho(1 - \rho)$, straightforward calculations show that $G^\varepsilon(x, t)$ obeys the equation

$$-\frac{\partial G^\varepsilon}{\partial t} = -D\varepsilon \frac{\partial^2 G^\varepsilon}{\partial x^2} + D\left(\frac{\partial G^\varepsilon}{\partial x}\right)^2 + r\left[1 - e^{-G^\varepsilon(x,t)/\varepsilon}\right]. \tag{4.36}$$

Since $\exp\left[-G^\varepsilon/\varepsilon\right] \to 0$ as $\varepsilon \to 0$ for $G^\varepsilon > 0$, we conclude that the limiting function $G(x, t) = \lim_{\varepsilon \to 0} G^\varepsilon(x, t)$ obeys the classical Hamilton–Jacobi equation

$$-\frac{\partial G}{\partial t} = D\left(\frac{\partial G}{\partial x}\right)^2 + r. \tag{4.37}$$

Indeed, we obtain the classical Hamiltonian, $H = Dp^2 + r$, if we define

$$H = -\frac{\partial G}{\partial t} \quad \text{and} \quad p = \frac{\partial G}{\partial x}. \tag{4.38}$$

4.2.1.2 Propagation Velocity

The hyperbolic scaling (4.33) and the transformation (4.35) of the field allows us to obtain, in the asymptotic limit $\varepsilon \to 0$, a Hamilton–Jacobi equation for any given reaction–transport equation. In this chapter we focus only on RD equations, but in Chap. 5 we deal with other models. Regardless of the specific form of the Hamilton–Jacobi equation, its solution can be written as

$$G(x, t) = \inf_{x(0)=0, x(t)=x} \left[\int_0^t L(x, s)\mathrm{d}s \right], \qquad (4.39)$$

where

$$L(x, s) = p(s)\frac{\mathrm{d}x(s)}{\mathrm{d}s} - H(x, s) \qquad (4.40)$$

is the Lagrangian and s the temporal coordinate. $x(s)$ and $p(s)$ satisfy the Hamilton equations

$$\frac{\mathrm{d}x}{\mathrm{d}s} = \frac{\partial H}{\partial p}, \quad \frac{\mathrm{d}p}{\mathrm{d}s} = -\frac{\partial H}{\partial x}, \qquad (4.41)$$

with the conditions $x(0) = 0$, $x(t) = x$. The location of the front position is determined by the equation $G(x(t), t) = 0$, and the propagation velocity can be found as follows. Differentiating $G(x(t), t) = 0$ and taking into account $v = \mathrm{d}x/\mathrm{d}t$, one writes

$$\frac{\partial G}{\partial t} + v\frac{\partial G}{\partial x} = 0 \qquad (4.42)$$

or using (4.38)

$$v = \frac{H}{p}. \qquad (4.43)$$

If the reaction–transport equations are homogeneous, i.e., there is no explicit dependence on time or space coordinates, then the Hamilton–Jacobi equation is of the form $H = H(p)$. (The case with spatial or temporal heterogeneities is dealt with in Chap. 6.) The Hamilton equations (4.41) imply that p is constant and that

$$x(s) = \frac{\partial H}{\partial p}s, \quad \frac{\partial H}{\partial p} = \frac{x}{t}, \qquad (4.44)$$

where we have made use of the boundary conditions. From (4.39) and (4.44)

$$G(x, t) = px - H(p)t, \tag{4.45}$$

and the front position evolves according to $x/t = H/p$, which combined with the second equation in (4.44) and (4.43) yields a closed system of algebraic equation to calculate the front velocity,

$$v = \frac{\partial H}{\partial p}, \quad \text{and} \quad \frac{\partial H}{\partial p} = \frac{H}{p}. \tag{4.46}$$

This system of equations can be summarized in the single equation

$$v = \min_{p>0} \left[\frac{H(p)}{p} \right]. \tag{4.47}$$

In the case of the RD equation,

$$v = \min_{p>0} \left[\frac{Dp^2 + r}{p} \right] = 2\sqrt{rD}, \tag{4.48}$$

which is known as the Fisher velocity.

4.2.2 Variational Characterization

We follow here the derivation by Benguria and Depassier [34, 35]. The starting point for the variational principle is the ordinary differential equation for the RD equation in the frame comoving with the front (4.2). Without loss of generality, we assume that the front connects the states $\rho = 0$ and $\rho = 1$, i.e., $\lim_{z\to\infty} \rho = 0$ and $\lim_{z\to-\infty} \rho = 1$. Since the front is monotonic, we define $q(\rho) = -\rho_z > 0$. Monotonic fronts are solutions of

$$Dq(\rho) \frac{dq}{d\rho} - vq(\rho) + F(\rho) = 0, \tag{4.49}$$

with

$$q(0) = 0, \quad q(1) = 0, \tag{4.50}$$

and $q > 0$ in $(0, 1)$.

Let $g(\rho)$ be any positive function on $(0, 1)$, such that $h = -dg/d\rho > 0$. Multiplying (4.49) by g/q and integrating with respect to ρ, we obtain

$$\int_0^1 \left(Dhq + \frac{F(\rho)}{q} g \right) d\rho = v \int_0^1 g \, d\rho, \tag{4.51}$$

where the first term is obtained after integration by parts. For fixed ρ, the functional

$$\Phi[q] \equiv Dhq + \frac{F(\rho)}{q}g \tag{4.52}$$

has a minimum at $q_{\min} = \sqrt{Fg/(Dh)}$, since v, q, g, and h are positive. Consequently, $\Phi[q] \geq \Phi[q_{\min}] = 2\sqrt{DFgh}$ and

$$\int_0^1 \Phi[q]\mathrm{d}\rho = v \int_0^1 g\mathrm{d}\rho \geq 2\sqrt{D} \int_0^1 \sqrt{Fgh}\mathrm{d}\rho, \tag{4.53}$$

that is,

$$v \geq 2\sqrt{D}\frac{\int_0^1 \sqrt{Fgh}\mathrm{d}\rho}{\int_0^1 g\mathrm{d}\rho}. \tag{4.54}$$

This lower bound for the front velocity is valid for any $F(\rho) > 0$ on $(0,1)$ and $F(0) = F(1) = 0$, i.e., for a front propagating into unstable states (reaction terms of Case A) [34]. To show that (4.54) represents indeed a variational principle, we must establish that there exists a function, namely $\check{g}$, for which the equality holds in (4.54). Equality holds if $\check{g}$ satisfies $hq = F\check{g}/(Dq)$, i.e.,

$$-\frac{\mathrm{d}(\ln \check{g})}{\mathrm{d}\rho} = \frac{v}{Dq} - \frac{\mathrm{d}(\ln q)}{\mathrm{d}\rho}, \tag{4.55}$$

where we have made use of (4.49). This equation can be integrated to yield

$$\check{g}(\rho) = q(\rho)\exp\left(\int_\rho^{\rho_0} \frac{v}{Dq}\mathrm{d}\rho\right) \tag{4.56}$$

for some fixed ρ_0, $0 < \rho_0 < 1$. Obviously, $\check{g}(\rho)$ is a continuous, positive, and decreasing function on $(0,1)$ and $\check{g}(1) = 0$. However, for $\rho \to 0$, a singularity occurs that needs to be handled carefully. We must ensure that the integrals in (4.54) exist for this value. We linearize (4.2) near $\rho = 0$ and find that if $\rho \sim \exp(-\lambda z)$ then $q \sim \lambda_+\rho$. Here $\lambda_+ = \left[v + \sqrt{v^2 - 4DF'(0)}\right]/2D$ is the largest root of the characteristic equation for λ. From (4.56)

$$\sqrt{F\check{g}h} \sim \check{g}(\rho) \sim \rho^{1-v/(\lambda_+ D)} \quad \text{near } \rho = 0. \tag{4.57}$$

Therefore, if $v > 2\sqrt{DF'(0)}$, we have $\int_0^1 g\mathrm{d}\rho < \infty$ and $\int_0^1 \sqrt{Fgh}\mathrm{d}\rho < \infty$. In summary, we have proven that there exists a positive, continuous, and monotonically decreasing function g, for which the integrals in (4.54) exist and which maximizes the lower bound in (4.54) in such a way that the equality holds. In summary,

$$v = \max_{g} \left(2\sqrt{D} \frac{\int_0^1 \sqrt{Fgh}\,d\rho}{\int_0^1 g\,d\rho} \right), \tag{4.58}$$

if $v > 2\sqrt{DF'(0)}$ which is a lower bound for the front velocity. We can obtain from (4.58) also the upper bound derived by Aronson and Weinberger [18]:

$$v = \max_{g} \left(2\sqrt{D} \frac{\int_0^1 \sqrt{Fgh}\,d\rho}{\int_0^1 g\,d\rho} \right) = \max_{g} \left(2\sqrt{D} \frac{\int_0^1 g\sqrt{Fh/g}\,d\rho}{\int_0^1 g\,d\rho} \right)$$

$$\leq 2\sqrt{D} \max_{g} \sqrt{\frac{\int_0^1 Fh\,d\rho}{\int_0^1 g\,d\rho}}, \tag{4.59}$$

where the inequality follows from Jensen's inequality. Since $h > 0$, we have

$$\frac{\int_0^1 Fh\,d\rho}{\int_0^1 g\,d\rho} = \frac{\int_0^1 (F/\rho)h\rho\,d\rho}{\int_0^1 g\,d\rho} \leq \frac{\int_0^1 h\rho\,d\rho}{\int_0^1 g\,d\rho} \sup_{\rho} \left(\frac{F}{\rho} \right) = \sup_{\rho} \left(\frac{F}{\rho} \right). \tag{4.60}$$

We have used $\int_0^1 h\rho\,d\rho = \int_0^1 g\,d\rho$, which follows from integration by parts. Finally, we obtain

$$2\sqrt{DF'(0)} < v \leq 2\sqrt{D} \sqrt{\sup_{\rho} \left(\frac{F}{\rho} \right)}, \tag{4.61}$$

which is the result given in (4.12).

Note that the variational characterization given in (4.58) only holds if $F > 0$ on $(0,1)$ and for fronts propagating into unstable states. To derive a variational result valid if $F < 0$ for some values of ρ, we need to extend these results [35]. To do so, we multiply (4.49) by g. Integrating between $\rho = 0$ and $\rho = 1$, we obtain after integration by parts

$$\int_0^1 F(\rho)g\,d\rho = v \int_0^1 qg\,d\rho - \frac{1}{2} D \int_0^1 hq^2\,d\rho. \tag{4.62}$$

For fixed ρ, the functional

$$\Phi[q] \equiv vqg - \frac{1}{2}Dhq^2 \tag{4.63}$$

has a maximum at $q_{max} = vg/(Dh)$, since v, q, g, and h are positive. Therefore $\Phi[q] \leq \Phi[q_{max}] = v^2g^2/(2Dh)$ for any value of ρ. It follows that

$$v^2 \geq 2D \frac{\int_0^1 Fg\,d\rho}{\int_0^1 (g^2/h)\,d\rho}, \tag{4.64}$$

which holds for any $F(\rho)$ for which a monotonic front exists. The equality in (4.64) holds if $\check{g}$ satisfies

$$-\frac{d(\ln \check{g})}{d\rho} = \frac{v}{Dq}, \tag{4.65}$$

which can be integrated to yield

$$\check{g}(\rho) = \exp\left(\int_\rho^{\rho_0} \frac{v}{Dq}\,d\rho\right). \tag{4.66}$$

Obviously, $\check{g}(\rho)$ is again a continuous, positive, and decreasing function on $(0,1)$ with $\check{g}(1) = 0$. Near $\rho = 0$, $\check{g}$ diverges. We linearize (4.2) to find from (4.66)

$$\check{g}(\rho) \sim \rho^{-v/(\lambda_+ D)} \quad \text{near } \rho = 0, \tag{4.67}$$

and $f\check{g} \sim (\check{g})^2/h \sim \rho^{1-v/(\lambda_+ D)}$. The integrals in (4.64) exist if $\lambda_+ D/v > 1/2$. This condition is always satisfied if $F'(0) \leq 0$, i.e., for Case B (front propagating into metastable states). However, it is also satisfied for Case A (fronts propagating into unstable states) provided that $v > 2\sqrt{DF'(0)}$. The asymptotic front velocity is given for both cases A and B by

$$v^2 = \max_g \left[2D \frac{\int_0^1 Fg\,d\rho}{\int_0^1 (g^2/h)\,d\rho}\right], \tag{4.68}$$

where the maximum is taken over all positive, decreasing trial functions on $(0,1)$ for which the integrals exist.

We illustrate the power of the variational characterization (4.68) by solving some examples for cases A and B. To do so, we will consider the trial function

$$g(\rho) = \rho^{-\mu}(1-\rho)^\mu \quad \text{with} \quad \mu > 0. \tag{4.69}$$

We maximize over all possible values of μ for which the integrals in the variational formula exist:

$$v^2 = \max_{0<\mu\leq 2} 2D \left[\frac{\mu\Gamma(4)}{\Gamma(2-\mu)\Gamma(2+\mu)} \int_0^1 F(\rho)\rho^{-\mu}(1-\rho)^\mu\,d\rho\right]. \tag{4.70}$$

KPP reaction term. With $F(\rho) = \rho(1 - \rho)$ (4.70) yields

$$v^2 = 2D \max_{0 < \mu \leq 2} \mu, \tag{4.71}$$

i.e., $v = 2\sqrt{D}$.

Pulled–Pushed transition. The variational characterization can account for the pulled–pushed transition for fronts propagating into unstable states. We consider the Ben-Jacob case [37], where $F(\rho) = \rho(1 - \rho)(1 + \alpha\rho)$ with $\alpha > 0$. Equation (4.70) yields

$$v^2 = \max_{0 < \mu \leq 2} 2D\mu \left[1 + \frac{\alpha}{4}(2 - \mu) \right]. \tag{4.72}$$

The maximum must be evaluated carefully for this case. For $\alpha \leq 2$, the maximum occurs at $\mu = 2$ and for $\alpha \geq 2$ at $\mu = (\alpha + 2)/\alpha$,

$$v = \begin{cases} 2\sqrt{D}, & \alpha \leq 2, \\ \sqrt{D/2}\left(\sqrt{\alpha} + 2/\sqrt{\alpha}\right), & \alpha \geq 2, \end{cases} \tag{4.73}$$

which coincides with Ben-Jacob's result.

Cubic reaction term. We deal again with the case considered in (4.22) for a front propagating into a metastable state, i.e., connecting ρ_1 and ρ_3. To apply (4.70), where it is assumed that the front connects 0 and 1, we rescale (4.22) by defining the new field $u = (\rho - \rho_1)/(\rho_3 - \rho_1)$. Equation (4.22) then reads

$$Du_{zz} + vu_z + rau(1 - u)(u - b), \tag{4.74}$$

where

$$a \equiv (\rho_3 - \rho_1)^2 \quad \text{and} \quad b \equiv \frac{\rho_2 - \rho_1}{\rho_3 - \rho_1} > 0. \tag{4.75}$$

Substitute the reaction term $F(u) = rau(1 - u)(u - b)$ into (4.70). Then

$$v^2 = \max_{0 < \mu \leq 2} D\mu ar \left[1 - \frac{\mu}{2} - 2b \right]. \tag{4.76}$$

In this case, the maximum occurs at $\mu = 1 - 2b$,

$$v = \sqrt{\frac{raD}{2}}(1 - 2b) = \sqrt{r\frac{D}{2}}(\rho_3 - 2\rho_2 + \rho_1), \tag{4.77}$$

which is exactly the same result as in (4.24). Furthermore, we can also obtain the front profile from the variational characterization. The selected front is the one that satisfies the equality in (4.64), and the front profile is given by $q = vg/(Dh)$:

$$-\frac{du}{dz} = \frac{vg}{Dh} = \sqrt{\frac{r}{2D}}(\rho_3 - \rho_1)u(1 - u). \tag{4.78}$$

Since $u = (\rho - \rho_1)/(\rho_3 - \rho_1)$, the above equation turns into

$$\frac{d\rho}{dz} = \sqrt{\frac{r}{2D}}(\rho - \rho_1)(\rho - \rho_3), \tag{4.79}$$

which coincides with (4.25) for the front profile.

4.3 Effect of Low Concentrations

The sensitivity of fronts to the dynamics of small perturbations about the unstable or metastable states has been studied by Brunet and Derrida [61] for pulled fronts and Kessler et al. [227] for pulled and pushed fronts. The mean-field description of reacting and diffusing systems ceases to be valid for low values of the particle density ρ, values that correspond to less than one particle. This fact can be incorporated into the RD equation by introducing a cutoff for the reaction term. Such a cutoff strongly affects the front velocity. Throughout this section we consider for simplicity that space and time have been rescaled such that $D = r = 1$.

4.3.1 Effect on Pulled Fronts

The starting point of Brunet and Derrida's approach is to replace the kinetic term in the FKPP equation by $F(\rho) = \theta(\rho - \epsilon)\rho(1 - \rho)$. Here $\theta(\cdot)$ denotes the Heaviside function, and $\epsilon = 1/N$ is the cutoff, where N is the average number of particles in the state $\rho = 1$. In the frame comoving with the front, the RD equation

$$\rho_{zz} + v_\epsilon \rho_z + \theta(\rho - \epsilon)\rho(1 - \rho) = 0 \tag{4.80}$$

can be divided into three regions. In region II, $\epsilon < \rho \ll 1$, the nonlinear terms in the reaction function can be ignored. In region III, $\rho < \epsilon$, the kinetic term vanishes. In region I, ρ is not small compared to 1, and one has to consider the full nonlinear equation without cutoff. These considerations lead to the system of equations:

$$\rho_{zz} + v_\epsilon \rho_z + \rho(1 - \rho) = 0, \quad \text{in region I}, \tag{4.81a}$$
$$\rho_{zz} + v_\epsilon \rho_z + \rho \simeq 0, \quad \text{in region II}, \tag{4.81b}$$
$$\rho_{zz} + v_\epsilon \rho_z = 0, \quad \text{in region III}. \tag{4.81c}$$

At the boundary between regions I and II and the boundary between II and III, the particle density ρ, as well as its comoving derivative ρ_z, must be continuous. Since $\epsilon \ll 1$, the solutions of (4.81) are given to leading order by

$$\rho(z) = \epsilon e^{-v_\epsilon(z-z_0)}, \quad \text{in region III, and} \tag{4.82a}$$

$$\rho(z) \sim \sin\left(\frac{\pi z}{|\ln \epsilon|}\right) e^{-z}, \quad \text{in region II,} \tag{4.82b}$$

where $z_0 \simeq |\ln \epsilon|$ marks the boundary between regions II and III. The continuity conditions at the boundary between both regions lead to

$$v_\epsilon \simeq 2 - \frac{\pi^2}{(\ln \epsilon)^2}. \tag{4.83}$$

The velocity converges to 2 as $(\ln \epsilon)^{-2}$ or $(\ln N)^{-2}$.

4.3.2 Effect on Pushed Fronts

For fronts propagating into metastable states and pushed fronts propagating into unstable states, Kessler et al. [227] showed that the velocity shift introduced by the cutoff depends on a power of ϵ. Consider a RD equation with a cutoff around the state $\rho = 0$, where the linear part of the growth term is ρ. In the nonreacting region III, i.e., $z > z_0$, and the region corresponding to large z with $z < z_0$, the solutions of the RD equation are

$$\rho(z) = \epsilon e^{-v_\epsilon(z-z_0)}, \quad \text{for } z > z_0, \tag{4.84a}$$

$$\rho(z) = A_1 e^{-\lambda_+ z} + \delta v A_2 e^{-\lambda_- z}, \quad \text{for large } z \text{ with } z < z_0. \tag{4.84b}$$

Here

$$\lambda_\pm = \frac{v_0 \pm \sqrt{v_0^2 - 4}}{2}, \tag{4.85}$$

and v_0 is the front velocity in the absence of a cutoff, i.e., $v_\epsilon = v_0 + \delta v$. The integration constants A_1 and A_2 do not depend on ϵ and can be obtained by matching the solutions at the boundary, treating δv as a small parameter. At $z = z_0$, the two terms in (4.84b) must be of the same order, $e^{-\lambda_+ z_0} \sim \delta v e^{-\lambda_- z_0}$, or $\delta v \sim e^{z_0(\lambda_- - \lambda_+)}$. The matching condition implies that $e^{-\lambda_+ z_0} \sim \epsilon$, or $z_0 \sim -\ln \epsilon / \lambda_+$, and

$$\delta v \sim \epsilon^{1 - \frac{\lambda_-}{\lambda_+}} = \epsilon^{1 + \frac{\sqrt{1-4/v_0^2}-1}{\sqrt{1-4/v_0^2}+1}}. \tag{4.86}$$

We consider first an example of a pushed front propagating into an unstable state, namely Ben-Jacob's case with a cutoff, $F(\rho) = \theta(\rho - \epsilon)\rho(1 - \rho)(1 + \alpha\rho)$. A pushed front occurs for $\alpha > 2$ and $v_0 = (\sqrt{\alpha} + 2/\sqrt{\alpha})/\sqrt{2}$, see (4.14). In this

case, $\delta v \sim \epsilon^{(\alpha-2)/\alpha}$, i.e., a sublinear dependence of the shift in the front velocity on the cutoff.

We consider next a front propagating into a metastable state for the Nagumo equation, $F(\rho) = \theta(\rho - \epsilon)\rho(1 - \rho)(\rho - a)$. The front velocity in the absence of a cutoff is $v_0 = 1/\sqrt{2} - a\sqrt{2}$. Equation (4.86) yields $\delta v \sim \epsilon^{1+2a}$. Exact analytical results for the front solutions can be obtained if the reaction term $F(\rho)$ with a cutoff is replaced by a piecewise linear approximation. The dependence of the velocity shift on the cutoff displays good agreement with the results by Brunet and Derrida and Kessler et al. [495].

4.3.3 Variational Principles and the Cutoff Problem

Recent studies have applied improved variational principles to deal with the velocity shift due to a cutoff in the reaction term, both for fronts propagating into unstable and metastable states [284, 36]. They confirm the results by Brunet and Derrida and improve the results by Kessler et al. The variational principle given in (4.68) implies that for any admissible trial function a lower bound for the velocity can be found by (4.64). The trial function for which equality in (4.64) holds diverges at $\rho = 0$, and it is convenient to consider trial functions that in addition to the requirements $g > 0$ and $g' < 0$ also satisfy $g(0) \to \infty$. Such trial functions allow us to obtain accurate lower bounds for the front velocity. We perform a change of variables $\rho = \rho(s)$, where $s = 1/g$, and consider s as the independent variable in (4.68). With this change of variables, the variational principle reads

$$v^2 = \max_{\rho(s)} 2 \frac{V(1)/s_0 + \int_0^{s_0} \left(V[\rho(s)]/s^2\right) ds}{\int_0^{s_0} (d\rho/ds)^2 ds}. \tag{4.87}$$

Here $s_0 = 1/g(\rho = 1)$, $V(\rho) = \int_0^\rho F(u)du$, and the maximum is taken over positive increasing functions $\rho(s)$, such that $\rho(0) = 0$ and for which the integrals in (4.87) converge. Consider the reaction term $F(\rho) = \theta(\rho - \epsilon)\rho(1 - \rho^2)$ and the trial function

$$\rho(s) = \begin{cases} s, & \text{if } 0 \leq s \leq \epsilon, \\ \sqrt{\epsilon s}\sqrt{1 + \frac{(\ln \epsilon)^2}{4\phi^2}} \cos\left[\frac{\phi}{|\ln \epsilon|} \ln(s/\epsilon) - \phi\right], & \text{if } \epsilon \leq s \leq \epsilon^{-1}, \end{cases} \tag{4.88}$$

where ϕ is the solution of the equation $\phi \tan \phi - |\ln \epsilon|/2 = 0$. Substituting this trial function into (4.87), we find the lower bound

$$v^2 \geq 4\left(1 - \frac{\pi^2}{|\ln \epsilon|^2} + \cdots\right) \tag{4.89}$$

after expanding for small ϵ. For pushed fronts, the existence of a variational principle allows one to use the Feynman–Hellman theorem to calculate the dependence of the velocity on parameters of the reaction term [36]. If the reaction term is of the form $F(\rho) = F(\rho, \alpha)$ then

$$\frac{\partial v^2}{\partial \alpha} = 2 \frac{\int_0^1 \frac{\partial F(\rho,\alpha)}{\partial \alpha} \breve{g}(\rho, \alpha) d\rho}{\int_0^1 \left(-\breve{g}^2 / \breve{g}' \right) d\rho}, \tag{4.90}$$

where $\breve{g}$ is the trial function, unique up to a multiplicative constant, that produces the maximum in (4.68) for the given parameter α. Note that the Feynman–Hellman theorem only holds, if the maximum is actually realized, which is not the case for pulled fronts. Consider the reaction term $F(\rho) = \theta(\rho - \epsilon) f(\rho)$ and $\alpha \equiv \epsilon$. The Feynman–Hellman theorem (4.90) implies that

$$\frac{\partial v^2}{\partial \epsilon} = 2 \frac{\int_0^1 \breve{g}(\rho, \epsilon) \frac{\partial}{\partial \epsilon} \left[\theta(\rho - \epsilon) f(\rho) \right] d\rho}{\int_0^1 \left(-\breve{g}^2 / \breve{g}' \right) d\rho} = -2 \frac{\breve{g}(\epsilon, \epsilon) f(\epsilon)}{\int_0^1 \left(-\breve{g}^2 / \breve{g}' \right) d\rho}. \tag{4.91}$$

For small ϵ, the leading order of the trial function $\breve{g}(\rho, \epsilon)$ is $\breve{g}(\rho, 0) \equiv \breve{g}_0(\rho)$, which is exactly the optimizing function for the case without a cutoff. On the other hand, for small ϵ we can write $v(\epsilon) = v_0 + \epsilon \, (\partial v / \partial \epsilon)_{\epsilon=0} + \cdots$, so that

$$\delta v = \epsilon \left. \frac{\partial v}{\partial \epsilon} \right|_{\epsilon=0} = -\frac{1}{v_0 \int_0^1 \left(-\breve{g}_0^2 / \breve{g}_0' \right) d\rho} \epsilon f(\epsilon) \breve{g}_0(\epsilon), \tag{4.92}$$

where we have made use of the variational result for the case without cutoff:

$$v_0^2 = 2 \frac{\int_0^1 f(\rho) \breve{g}_0(\rho) d\rho}{\int_0^1 \left(-\breve{g}_0^2 / \breve{g}_0' \right) d\rho}. \tag{4.93}$$

From (4.67) we know that $\breve{g}_0(\rho) \sim \rho^{-v_0/\lambda_+}$ near $\rho = 0$, with

$$\lambda_+ = \frac{1}{2} \left[v_0 + \sqrt{v_0^2 - 4f'(0)} \right], \tag{4.94}$$

and $\breve{g}_0(\epsilon) \sim \epsilon^{-v_0/\lambda_+}$. Since the denominator in (4.92) is a positive constant and does not depend on ϵ, we conclude that

$$\delta v \sim \begin{cases} -f(\epsilon), & \text{if } f'(0) = 0, \\ -f'(0)\epsilon^{2-v_0/\lambda_+}, & \text{if } f'(0) \neq 0. \end{cases} \tag{4.95}$$

These results are in agreement with the previous results obtained from a different variational principle and also with the results obtained by Kessler et al. The dependence of the second result is exactly that given in (4.86).

4.4 Effect of External Noise

In this section we explore the systematic effect of an external noise on the front velocity. Consider a reaction term $F(\rho, \alpha)$ that depends not only on the density but also on a parameter α that fluctuates. Assuming small fluctuations around its mean value, we can write $\alpha(x, t) = \alpha_m - \epsilon^{1/2} \eta(x, t)$, where α_m is the mean value, ϵ is a small parameter governing the noise amplitude, and $\eta(x, t)$ is a Gaussian noise with zero mean and correlation given by

$$\left\langle \eta(x, t) \eta(x', t') \right\rangle = 2C(x - x') \delta(t - t'), \tag{4.96}$$

where $\delta(\cdot)$ is the Dirac delta-function and $\langle \cdot \rangle$ denotes averaging. The role of spatiotemporal structured noise has been discussed in [377]. For simplicity, we consider here noise that is white in time and correlated in space [376]. This is an excellent approximation if the time scale of the noise is much shorter than the characteristic time of the kinetics. We assume that the fluctuations have a small amplitude, $F(\rho, \alpha) = F(\rho, \alpha_m) - \frac{\partial F}{\partial \alpha} \epsilon^{1/2} \eta(x, t) + O(\epsilon)$. Then the RD equation can be written as the following stochastic partial differential equation:

$$\frac{\partial \rho}{\partial t} = \frac{\partial^2 \rho}{\partial x^2} + f(\rho) + \epsilon^{1/2} g(\rho) \eta(x, t), \tag{4.97}$$

where $f(\rho) = F(\rho, \alpha_m)$ and $g(\rho) = -\frac{\partial F}{\partial \alpha}(\rho, \alpha_m)$. The noise appears in the RD equation (4.97) in a multiplicative way. An additive noise source can also be included to account for fluctuations due to internal noise. Additive noise does not modify the front velocity for the invasion of either metastable or unstable states, and the front itself exists only during a short transient period. We consider here only the case of a multiplicative noise. The effects on front propagation are twofold: First, multiplicative noise produces a random meandering of the front position with respect to its mean position [17, 16]. Second, multiplicative noise induces a shift in the mean front velocity. We focus on the second effect; the problem reduces to an analogous deterministic problem with renormalized coefficients.

A crucial feature of the multiplicative noise case is that the noise term in (4.97) has a nonzero mean value. Using Novikov's theorem [324] for Gaussian noise in the Stratonovich interpretation, we find that

$$\epsilon^{1/2} \langle g(\rho) \eta(x, t) \rangle = \epsilon C(0) \left\langle g(\rho) g'(\rho) \right\rangle. \tag{4.98}$$

According to this result, (4.97) can be rewritten as

$$\frac{\partial \rho}{\partial t} = \frac{\partial^2 \rho}{\partial x^2} + h(\rho) + \epsilon^{1/2} R(\rho, x, t), \tag{4.99}$$

where

$$h(\rho) \equiv f(\rho) + \epsilon C(0) g(\rho) g'(\rho) \tag{4.100}$$

and

$$R(\rho, x, t) \equiv g(\rho) \eta(x, t) - \epsilon^{1/2} C(0) g(\rho) g'(\rho). \tag{4.101}$$

The stochastic term in (4.99) has zero mean, $\langle R(\rho, x, t) \rangle = 0$, and correlation

$$\Big\langle R(\rho, x, t) R(\rho, x', t') \Big\rangle = \Big\langle g(\rho(x, t)) \eta(x, t) g(\rho(x', t')) \eta(x', t') \Big\rangle + O(\epsilon^{1/2}). \tag{4.102}$$

This rearrangement allows us to distinguish explicitly between the systematic contribution from the noise term and a residual stochastic one. Since the noise is white in time, the average of the noise term has no explicit time dependence. Writing $\rho(x, t) = \rho_0(x, t) + \delta\rho$, where $\rho_0(x, t) = \langle \rho(x, t) \rangle$ and the perturbative fluctuation is $\delta\rho \sim O(\epsilon^{1/2})$, we obtain to lowest order

$$\frac{\partial \rho_0}{\partial t} = \frac{\partial^2 \rho_0}{\partial x^2} + f(\rho_0) + \epsilon C(0) g(\rho_0) g'(\rho_0), \tag{4.103}$$

which is the RD equation for the mean front profile. The methods developed in Sect. 4.2 allow us to study fronts connecting the steady states of (4.103) and to obtain the mean velocity in terms of the noise intensity $\epsilon(0) \equiv \epsilon C(0)$.

To illustrate our approach, we consider the Ginzburg–Landau reaction term $F(\rho) = \rho(1 - \rho)(\alpha + \rho)$, where $\alpha \rightarrow \alpha_m - \epsilon^{1/2} \eta(x, t)$. Then $f(\rho_0) = \rho_0(1 - \rho_0)(\alpha_m + \rho_0)$ and $g(\rho_0) = -\rho_0(1 - \rho_0)$. In the absence of noise, the velocity of the front propagating into the unstable state 0 is given by

$$v = \begin{cases} (1 + 2\alpha)/\sqrt{2}, & -1/2 < \alpha < 1/2 \text{ (nonlinear)}, \\ 2\sqrt{\alpha}, & 1/2 \leq \alpha \text{ (linear)}, \end{cases} \tag{4.104}$$

a result that can be obtained directly from (4.70). In the presence of multiplicative noise, the mean front profile is governed by (4.103), which reads in this case

$$\frac{\partial \rho_0}{\partial t} = \frac{\partial^2 \rho_0}{\partial x^2} + \rho_0(1 - \rho_0)(\alpha'_m + \beta\rho_0), \tag{4.105}$$

with $\alpha'_m = \alpha_m + \epsilon(0)$ and $\beta = 1 - 2\epsilon(0)$. Applying the variational formula (4.70) to the RD equation (4.105), we obtain the velocity for the front propagating, in the presence of noise, into the unstable state 0:

$$v = \begin{cases} (1 + 2\alpha_m)/\sqrt{2[1 - 2\epsilon(0)]}, & -1/2 \leq \alpha_m < 1/2 - 2\epsilon(0) \text{ (nonlinear)}, \\ 2\sqrt{\alpha_m + \epsilon(0)}, & 1/2 - 2\epsilon(0) \leq \alpha_m < 1 \text{ (linear)}. \end{cases}$$

(4.106)

An important condition for propagating fronts to exist is that $\epsilon(0) < 1/2$, otherwise the above result does not hold and the presence of noise can destroy the front formation. This result shows that multiplicative noise, which is white in time, can modify the mean front velocity as well as the transition point from the linear to the nonlinear regime of propagation.

4.5 Effect of Time Delay and Age Structure

The inclusion of age structure in RD equations has its origin in the generalization of population growth models. Age-structured models take explicitly into account that population growth is due only to adult individuals. The oldest such model is described by the McKendrick–von Foerster equation [447]:

$$\frac{\partial \rho(a, t)}{\partial t} + \frac{\partial \rho(a, t)}{\partial a} = -\mu(a, t)\rho(a, t),$$

(4.107)

where $\rho(a, t)$ is the age distribution density of the population. Let $\rho(a, t)\mathrm{d}a$ be the density of individuals with an age in the interval $(a, a + \mathrm{d}a)$ at time t. The rate of change of the number of individuals in a given age interval Δa is due to the rate of entry at age a minus the rate of departure at age $a + \mathrm{d}a$ minus the deaths, which yields the balance equation

$$\frac{\partial \rho(a, t)}{\partial t}\Delta a = J(a, t) - J(a + \Delta a, t) - \mu(a, t)\rho(a, t)\Delta a.$$

(4.108)

Here $\mu(a, t)$ is the per capita mortality rate for individuals of age a at time t, and $J(a, t)$ is the flux of individuals of age a at time t. Dividing by Δa and taking the limit $\Delta a \to 0$, we obtain the conservation equation for the density of individuals:

$$\frac{\partial \rho(a, t)}{\partial t} + \frac{\partial J(a, t)}{\partial a} = -\mu(a, t)\rho(a, t).$$

(4.109)

The flux J is not a flux in space, but rather the "movement" of individuals in age. We assume that it is proportional to the density of individuals and some characteristic velocity of aging, $J(a, t) = \rho(a, t)v(a, t)$. Aging is simply the passage of time $v = \mathrm{d}a/\mathrm{d}t = 1$, and we obtain (4.107). If we also include the flux in the space due to the motion of individuals, then we obtain Metz–Diekman model [295]:

$$\frac{\partial \rho(x, a, t)}{\partial t} + \frac{\partial \rho(x, a, t)}{\partial a} = D \frac{\partial^2 \rho(x, a, t)}{\partial x^2} - \mu(a, t)\rho(x, a, t). \qquad (4.110)$$

Almost parallel to McKendrick, Hutchinson [215], a well-known ecologist, proposed a time-delayed version for the logistic growth equation, where the nonlinear term was delayed in time. The diffusive Hutchinson equation, also known as the delayed Fisher equation,

$$\frac{\partial \rho(x, t)}{\partial t} = D \frac{\partial^2 \rho(x, t)}{\partial x^2} + \rho(x, t)\left[1 - \rho(x, t - \tau)\right], \qquad (4.111)$$

has front solutions. When the delay τ is large, the traveling wave solution oscillates around the state $\rho = 1$, which can be driven unstable for still larger τ [482]. A generalization of (4.111) consists in incorporating distributed delays in an ad hoc manner by multiplying the second term on the right-hand side of (4.111) by a kernel $k(\tau)$ and integrating over τ. Many other delayed RD equations have appeared in the ecological literature. A particularly well-known one is the Nicholson's blowflies equation:

$$\frac{\partial \rho(x, t)}{\partial t} = D \frac{\partial^2 \rho(x, t)}{\partial x^2} - \delta \rho(x, t) + p\rho(x, t - \tau)e^{-\beta \rho(x, t - \tau)}. \qquad (4.112)$$

Under certain conditions, this equation has front solutions. However, as for (4.111), loss of monotonicity occurs as the delay is increased and the front develops a prominent hump [167].

There exists a connection between age-structured and time-delayed RD models [169]. From (4.110) we can obtain an equation for the total mature population density $w(x, t)$. Let $f(a)$ be the probability density function of maturation ages, i.e., $f(a)\mathrm{d}a$ is the probability of maturing between the ages a and $a + \mathrm{d}a$. Then the probability of maturing before age a is $F(a) = \int_0^a f(a')\mathrm{d}a'$. The total density of mature individuals is

$$w(x, t) = \int_0^\infty \mathrm{d}a f(a) \int_a^\infty \rho(x, t, a')\mathrm{d}a' = \int_0^\infty \mathrm{d}a F(a)\rho(x, t, a). \qquad (4.113)$$

Differentiating (4.113) with respect to time and using (4.110), we obtain

$$\frac{\partial w}{\partial t} = D \frac{\partial^2 w}{\partial x^2} - \mu w + \int_0^\infty \mathrm{d}a f(a)\rho(x, t, a), \qquad (4.114)$$

where the diffusion coefficient D and the death rate μ for immature population are assumed to be constants. The solution of (4.110) is given by

$$\rho(x, t, a) = \frac{e^{-\mu a}}{2\sqrt{\pi Da}} \int_{-\infty}^{\infty} b\left[w(y, t - a)\right] e^{-(x-y)^2/4Da} dy, \qquad (4.115)$$

where $\rho(x, t = 0, a) \equiv b[w(x, t)]$ is the birth function. Inserting this expression into (4.114), we obtain the equation

$$\frac{\partial w}{\partial t} = D\frac{\partial^2 w}{\partial x^2} - \mu w + \int_0^{\infty} da f(a) \frac{e^{-\mu a}}{2\sqrt{\pi Da}} \int_{-\infty}^{\infty} b\left[w(y, t - a)\right] e^{-(x-y)^2/4Da} dy.$$
$$(4.116)$$

If the diffusion coefficient for immature individuals is very small ($D \to 0$), then the Gaussian function in the integrand can be approximated by a Dirac-delta-function,

$$\frac{\partial w}{\partial t} = D\frac{\partial^2 w}{\partial x^2} - \mu w + \int_0^{\infty} da f(a) e^{-\mu a} b\left[w(x, t - a)\right]. \qquad (4.117)$$

If there exists only a unique maturation age τ, then $f(a) = \delta(a - \tau)$. Assuming that $b(w) = we^{-w}$ we recover Nicholson's equation. Recently, a model consisting of two subpopulations, mature and immature, with an age-dependent disperser–nondisperser transition has been studied analytically and applied to the Neolithic transition in Europe. This model shows good agreement with observational data [292]. This example will be analyzed in detail in Chapter 7.

4.6 Multi-Component Reaction–Diffusion Systems

The reaction–diffusion equations for a system of n species in one-dimensional space read, see Sect. 2.1.2,

$$\frac{\partial \boldsymbol{\rho}}{\partial t} = D\frac{\partial^2 \boldsymbol{\rho}}{\partial x^2} + \mathbf{F}(\boldsymbol{\rho}), \qquad (4.118)$$

where $\boldsymbol{\rho} \in \mathbb{R}^n$, $\mathbf{F} : \mathbb{R}^n \to \mathbb{R}^n$, and D is the $n \times n$ diffusion matrix. We focus on front solutions and illustrate how to determine the front velocity for KPP kinetics. Let us write, for simplicity,

$$F_j(\boldsymbol{\rho}) = c_{jj}(\boldsymbol{\rho})\rho_j + \sum_{m \neq j} \gamma_{jm}\rho_m, \qquad (4.119)$$

where $\gamma_{jm} > 0$ for $j \neq m$. The kinetic terms in (4.118) must satisfy the following conditions:

(i) In $\mathbb{R}_+^n = \{(\rho_1, \ldots, \rho_n) \,|\, \rho_j > 0\}$, the vector field $(F_1(\boldsymbol{\rho}), \ldots, F_n(\boldsymbol{\rho}))$ has an unstable stationary state at $\mathbf{0} = (0, \ldots, 0)$ and an asymptotically stable one at $\mathbf{A} = (A_1, \ldots, A_n)$ with $A_j > 0$ for $j = 1, \ldots, n$.

(ii) The coefficients

$$r_j = c_{jj}(\mathbf{0}) = \sup_{0 \leq \rho_i \leq A_i; \forall i=1,\ldots,n} \left[c_{jj}(\boldsymbol{\rho}) \right] \tag{4.120}$$

must be finite.

4.6.1 Two-Component RD system

In this section we show how to compute the front velocity for a reaction–diffusion system of two components. The calculations can be extended easily to three or more components. Define $\gamma_{12} = \gamma_1$ and $\gamma_{21} = \gamma_2$ for simplicity. Consider the system

$$\frac{\partial \rho_1}{\partial t} = D_1 \frac{\partial^2 \rho_1}{\partial x^2} + f_1(\rho_1, \rho_2)\rho_1 + \gamma_1 \rho_2, \tag{4.121a}$$

$$\frac{\partial \rho_2}{\partial t} = D_2 \frac{\partial^2 \rho_2}{\partial x^2} + f_2(\rho_1, \rho_2)\rho_2 + \gamma_2 \rho_1. \tag{4.121b}$$

We assume that the interaction terms $f_i(\rho_1, \rho_2)$, $i = 1, 2$, are of KPP type. The dynamical behavior of the front is governed by the linear part of the system and we can use the Hamilton–Jacobi formalism, see Sect. 4.2.1. Under the hyperbolic scaling (4.33), the fields $\rho_i^\varepsilon(x, t) = \rho_i(x/\varepsilon, t/\varepsilon)$ satisfy

$$\varepsilon \frac{\partial \rho_1^\varepsilon}{\partial t} = \varepsilon^2 D_1 \frac{\partial^2 \rho_1^\varepsilon}{\partial x^2} + r_1 \rho_1^\varepsilon + \gamma_1 \rho_2^\varepsilon, \tag{4.122a}$$

$$\varepsilon \frac{\partial \rho_2^\varepsilon}{\partial t} = \varepsilon^2 D_2 \frac{\partial^2 \rho_2^\varepsilon}{\partial x^2} + r_2 \rho_2^\varepsilon + \gamma_2 \rho_1^\varepsilon. \tag{4.122b}$$

This system of equations can be rewritten as

$$-A_1 \frac{\partial G^\varepsilon}{\partial t} = D_1 A_1 \left(\frac{\partial G^\varepsilon}{\partial x} \right)^2 - D_1 A_1 \varepsilon \frac{\partial^2 G^\varepsilon}{\partial x^2} + r_1 A_1 + \gamma_1 A_2, \tag{4.123a}$$

$$-A_2 \frac{\partial G^\varepsilon}{\partial t} = D_2 A_2 \left(\frac{\partial G^\varepsilon}{\partial x} \right)^2 - D_2 A_2 \varepsilon \frac{\partial^2 G^\varepsilon}{\partial x^2} + r_2 A_2 + \gamma_2 A_1, \tag{4.123b}$$

after taking into account the nonlinear transformation

$$\rho_i^\varepsilon(x, t) = A_i \exp\left[-\frac{G^\varepsilon(x, t)}{\varepsilon} \right]. \tag{4.124}$$

For simplicity we suppose that the initial conditions for (4.121) have the form

$$\rho_i(x, 0) = \begin{cases} A_i, & x < 0, \\ 0, & x \geq 0, \end{cases} \tag{4.125}$$

which will give rise to a front with the minimal propagation velocity. Taking the limit $\varepsilon \to 0$, i.e., the long-time and large-spatial scale limit, we obtain the equation for the action functional $G(x, t)$. Introduction of the definitions (4.38) turns the system (4.123) into an eigenvalue problem $\mathbf{MA} = H\mathbf{A}$, where

$$\mathbf{M} = \begin{pmatrix} D_1 p^2 + r_1 & \gamma_1 \\ \gamma_2 & D_2 p^2 + r_2 \end{pmatrix}. \tag{4.126}$$

This system of algebraic equations for A_1 and A_2 has a nontrivial solution if $\det(\mathbf{M} - H\mathbf{I}) = 0$:

$$H^2 - H\left(D_1 p^2 + D_2 p^2 + r_1 + r_2\right) + (D_1 p^2 + r_1)(D_2 p^2 + r_2) - \gamma_1 \gamma_2 = 0. \tag{4.127}$$

To ensure the positivity of A_1 and A_2, we need to choose the largest eigenvalue $H(p)$, i.e., the largest solution of equation (4.127),

$$H(p) = \frac{D_1 + D_2}{2} p^2 + \frac{r_1 + r_2}{2}$$
$$+ \frac{1}{2}\sqrt{\left[(D_1 - D_2)p^2 + r_1 - r_2\right]^2 + 4\gamma_1 \gamma_2}. \tag{4.128}$$

The front velocity can be determined from (4.128) and (4.47). One of the exercises below deals with a particular case where an analytical solution for the front velocity can be obtained.

Exercises

4.1 Find exact solutions for the RD equation with the reaction term $F(\rho) = \rho^{q+1}(1 - \rho^q)$ by looking for solution in the form $\rho(z) = (1 + ae^{bz})^{-s}$ with $z = x - vt$. Determine the unique values for v, b, and s in terms of q. Consider D, a, b, s as positive parameters.

4.2 Consider the RD equation with the piecewise linear emulation for the KPP reaction term

$$F(\rho) = \begin{cases} \alpha\rho, & 0 \leq \rho < a, \\ \beta(1 - \rho), & a < \rho \leq 1, \end{cases} \tag{4.129}$$

with $\beta > 0$. Shift to the traveling wave coordinate and solve the corresponding ordinary differential equation to determine the front profile that satisfies $\rho(-\infty) = 1$ and $\rho(+\infty) = 0$. By matching the derivative of the front profile at $\rho = a$ obtain the front velocity.

4.3 Consider the RD equation with the initial condition

$$\rho(x, 0) = \begin{cases} 1, & x < 0, \\ e^{-h(x)}, & x > 0. \end{cases} \tag{4.130}$$

The Hamilton–Jacobi formalism can be extended to incorporate initial condition without compact support by considering

$$G(x, t) = \min_{y \geq 0} \left\{ \varepsilon h(y/\varepsilon) + \int_0^t L(x, s) ds, \ x(t) = x, \ x(0) = y \right\}. \tag{4.131}$$

Prove that for $h(x) = \alpha x$ the front velocity is

$$v = \begin{cases} 1/\alpha + \alpha, & \alpha < 1, \\ 2, & \alpha > 1. \end{cases} \tag{4.132}$$

4.4 The equation

$$\frac{\partial \rho}{\partial t} = \frac{\partial^2 (\rho^m)}{\partial x^2} + F(\rho) \tag{4.133}$$

with $F(0) = F(1) = 0$ and $m > 1$ is known as the reaction–diffusion equation in porous media. Transform to the traveling wave coordinate and consider the boundary conditions $\lim_{z \to -\infty} \rho = 1$ and $\lim_{z \to +\infty} \rho = 0$. By defining $q = -\rho^{m-1} \rho_z$ construct a variational principle as in Sect. (4.2.2) to show that

$$v = \max_g 2\sqrt{m} \frac{\int_0^1 \sqrt{\rho^{m-1} F(\rho) g h} d\rho}{\int_0^1 g d\rho}. \tag{4.134}$$

Show that the fronts of the equation (4.133) and those of the equation

$$\frac{\partial \rho}{\partial t} = \frac{\partial^2 \rho}{\partial x^2} + m\rho^{m-1} F(\rho) \tag{4.135}$$

travel with the same velocity.

4.5 The evolution of iodide, I^-, in the iodate–arsenous acid reaction with arsenous acid in stoichiometric excess is well described by the RD equation

$$\frac{\partial \rho}{\partial t} = D \frac{\partial^2 \rho}{\partial x^2} + (a + b\rho)\rho(c - \rho). \tag{4.136}$$

Here ρ is the concentration of I^-, in M=mol/L, $a = k_a[H^+]^2$, $b = k_b[H^+]^2$, and c is the initial concentration of iodate, IO_3^-. The experimental values are $k_a = 4.50 \times 10^3 /M^3$ s, $k_b = 4.36 \times 10^8 /M^4$ s, $D = 2.0 \times 10^{-3} mm^2/s$, $[H^+] = 7.1 \times 10^{-3}$ M, and $c = 5.0 \times 10^{-3}$ M. Find the chemically acceptable stationary states of the kinetic term in (4.136) and determine their stability. Show that (4.136) has a propagating front solution connecting the stable to the unstable steady state and determine the propagation velocity v. Compare your value with the experimental value $v_{exp} = 2.3 \times 10^{-2}$ mm/s.

4.6 Use the variational principle

$$v = \max_g 2\alpha \frac{\int_0^1 \frac{Fg}{\rho(1-\rho)} d\rho}{\int_0^1 g d\rho} \tag{4.137}$$

with the trial function $g(\rho) = \exp\left[-\alpha^2 \int \frac{F}{\rho^2(1-\rho)^2} d\rho\right]$ to calculate the front velocity, connecting 0 and 1, for RD equations with reaction terms given by (a) $b^{-1}\rho(1-\rho)(\rho+b)$, (b) $\rho(1-\rho)(\rho-a)$, and (c) $\rho(1-\rho)$.

4.7 Determine the shift in the front velocity for the RD equation with a Ginzburg–Landau reaction term $F(\rho) = (1 - \rho^2)(\rho + a)$ with $0 < a < 1$, when a cutoff is imposed at the metastable state $\rho = -1$.

4.8 Determine the shift in the front velocity for the RD equation with a Nagumo reaction term, when a cutoff is imposed at the state $\rho = 0$. Use the variational principle to show that

$$\delta v = \frac{\sqrt{2}\Gamma(4)a}{\Gamma(1 + 2a)\Gamma(3 - 2a)} \varepsilon^{1+2a}. \tag{4.138}$$

4.9 Find the shift in the front velocity for a reaction–diffusion equation where the diffusion coefficient $D(\rho)$ depends on ρ, with $D(0) = 0$, $D'(\rho) > 0$, and the cutoff is imposed at the state $\rho = 0$ of the KPP reaction term.

4.10 Consider the RD equation with the reaction term $F(\rho) = -\rho(\alpha + \rho)$. Since it is always negative, the RD equation cannot have propagating front solutions. Consider that the control parameter α fluctuates around its mean value α_m with a Gaussian noise of zero mean and correlation given by (4.96). Show that if the noise intensity is larger than α_m, the state 0 becomes unstable and can be invaded by a front propagating with the linear velocity.

4.11 Consider the system given in (4.121) with $D_1 = D_2 = D$. Calculate the Hamiltonian and show that it coincides with the Hamiltonian for a single-component RD equation with an effective reaction rate $r = \left(r_1 + r_2 + \sqrt{(r_1 - r_2)^2 + 4\gamma_1\gamma_2} \right)/2$.

Chapter 5
Reaction–Transport Fronts Propagating into Unstable States

In this chapter we consider the problem of propagating fronts traveling into an unstable state of a reaction–transport system. The purpose is to present the general formalism for the asymptotic analysis of traveling fronts. The method relies on the hyperbolic scaling procedure, the theory of large deviations, and the Hamilton–Jacobi technique. A generic model that describes phenomena of this type is the RD equation (2.3) with appropriate kinetics, such as the FKPP equation (4.1). The propagation velocity of fronts of this equation has been studied in Chap. 4. The RD equation involves implicitly a long-time large-scale *parabolic scaling*, while as far as propagating fronts are concerned, the appropriate scaling must be a *hyperbolic* one. The macroscopic transport process arises from the overall effect of many particles performing complex random movements. Classical diffusion is simply an approximation for this transport in the long-time large-scale parabolic limit. In general, this approximation is not appropriate for problems involving propagating fronts. The basic idea is that the kinetic term in the RD equation with KPP kinetics is very sensitive to the tails of a density profile. These tails are typically "non-universal," "non-diffusional," and dependent on the *microscopic* details of the underlying random walk. The purpose of this chapter is to demonstrate that the macroscopic dynamics of the front for a reaction–transport system are dependent on the choice of the underlying random walk model for the transport process. To illustrate the idea of an alternative description of front propagation into an unstable state of reaction–transport system, we consider several models including discrete-in-time or continuous-in-time Markov models with long-distance dispersal kernels, non-Markovian models with memory effects, etc., instead of the RD equation. Let us give a few examples of such models.

The discrete-time model

$$\rho(x, t + \tau) = \int_{\mathbb{R}} \rho(x - z, t) w(z) \mathrm{d}z + r\tau\rho(1 - \rho) \tag{5.1}$$

is the extension of the mesoscopic equation for the DTRW, see (3.13), with KPP kinetics, if the reaction and transport processes are independent. The continuous-time model with long-range dispersal, see (3.76),

$$\frac{\partial \rho}{\partial t} = \lambda \int_{\mathbb{R}} \rho(x - z, t) w(z) \mathrm{d}z - \lambda \rho(x, t) + r\rho(1 - \rho), \tag{5.2}$$

is the result of combining the Kolmogorov–Feller equation with KPP kinetics, if both reaction and transport are independent processes. The equation with memory effects

$$\frac{\partial \rho}{\partial t} = \int_0^t K(t - \tau) \frac{\partial^2 \rho(x, \tau)}{\partial x^2} \mathrm{d}\tau + r\rho(1 - \rho) \tag{5.3}$$

is obtained phenomenologically by combining the continuity equation for particle density with a nonlocal Fick's first law. Equations (5.1) and (5.2) provide a suitable coarse-grained description of reaction–transport processes with long-range interaction modeled by the kernel $w(z)$ [310]. It is natural to assume that $w(z) \to 0$ as $z \to \infty$ and $w(z) = w(-z) \geq 0$.

Since exact solutions of the integro-differential equations (5.1), (5.2), and (5.3) are not known, some sort of approximation is needed. The conventional way to simplify the problem consists in approximating the integral term in these equations by the second derivative of ρ with respect to the spatial coordinate x, which results in the FKPP equation (4.1), see for example [310]. In the following we show that, in general, this approximation for a propagating front problem is not appropriate and can lead to unphysical results. To illustrate the idea, consider the kernel $w(z)$ given by

$$w(z) = \frac{1}{2}\delta(z - a) + \frac{1}{2}\delta(z + a). \tag{5.4}$$

This case corresponds to the random walk model where the jumps Z_i can only take two values, $-a$ or a, with equal probability $1/2$, see Sect. 3.1.1. Then (5.1) takes the form

$$\rho(x, t + \tau) = \frac{1}{2}\rho(x + a, t) + \frac{1}{2}\rho(x - a, t) + r\tau\rho(1 - \rho). \tag{5.5}$$

This is a typical example of a coupled map lattice describing a logistic map and spatial diffusion. It has been extensively used in modeling traveling fronts and spatiotemporal chaos [65, 67]. In the limit $a \to 0$ and $\tau \to 0$, such that $D = a^2/2\tau = $ const, we recover the FKPP equation (4.1) from (5.5). This diffusion approximation corresponds to the replacement of the random walk by the Brownian motion. As far as traveling waves are concerned, the diffusion approximation is not adequate, since in the limit $a \to 0$ and $\tau \to 0$ we should keep the velocity $v = a/\tau$ constant, rather than $D = a^2/2\tau$. It is clear that the velocity $v = a/\tau$ must be the maximum possible velocity of front propagation. The theory of front propagation in reaction–transport systems with nondiffusive transport and its applications have been reviewed in [139].

5.1 Hyperbolic Scaling and Hamilton–Jacobi Equation for the Front Position

In this section we explore some examples to derive the Hamilton–Jacobi equation for a reaction–transport equation. We follow the same procedure as illustrated in Chap. 4.

5.1.1 Discrete-Time Model

We consider here the discrete-time transport process corresponding to (5.1). After the hyperbolic scaling (4.33), the equation governing the rescaled field $\rho^\varepsilon(x, t)$ reads

$$\rho^\varepsilon(x, t + \varepsilon\tau) = \int_\mathbb{R} \rho^\varepsilon(x - \varepsilon z, t) w(z) \mathrm{d}z + r\tau\rho^\varepsilon(1 - \rho^\varepsilon), \qquad (5.6)$$

with initial condition with compact support.

We seek a solution in the exponential form (4.35), so that $G(x, t)$ obeys, to leading order in ε, the following equation:

$$\exp\left(-\tau\frac{\partial G}{\partial t}\right) = \int_\mathbb{R} \exp\left(z\frac{\partial G}{\partial x}\right) w(z)\mathrm{d}z + r\tau. \qquad (5.7)$$

Taking logarithms of both sides, we find that $G(x, t)$ satisfies the nonlinear partial differential equation

$$\frac{\partial G}{\partial t} + \frac{1}{\tau}\ln\left[\int_\mathbb{R} \exp\left(z\frac{\partial G}{\partial x}\right) w(z)\mathrm{d}z + r\tau\right] = 0, \qquad (5.8)$$

which is the Hamilton–Jacobi equation with the Hamiltonian

$$H(p) = \frac{1}{\tau}\ln\left[\int_\mathbb{R} \exp(zp)w(z)\mathrm{d}z + r\tau\right]. \qquad (5.9)$$

This result is of particular importance. It shows that the front dynamics for (5.1) must be different from that of the classical RD equation. This follows from the fact that the Hamiltonian (5.9), governing the evolution of the action functional G and thereby the dynamics of traveling front, differs from $H(p) = Dp^2 + r$, see (4.37), corresponding to the RD equation. We conclude that an understanding of the relevant Hamiltonians H, combined with the appropriate action functional G, provides the basis for understanding traveling fronts in reaction–transport systems.

If the jumps can only take the values a or $-a$ with the same probability, i.e., the kernel $w(z)$ is a superposition of two delta-functions as in (5.4), the Hamilton–Jacobi equation takes the form

$$\frac{\partial G}{\partial t} + \frac{1}{\tau} \ln\left[\cosh\left(a\frac{\partial G}{\partial x}\right) + r\tau\right] = 0, \tag{5.10}$$

with the Hamiltonian

$$H(p) = \frac{1}{\tau} \ln\left[\cosh(ap) + r\tau\right]. \tag{5.11}$$

If we expand the expression in square brackets in powers of ap, take logarithms, and let $a \to 0$ and $\tau \to 0$ such that $a^2/\tau = \text{const}$, we easily find that G obeys the classical Hamilton–Jacobi equation:

$$\frac{\partial G}{\partial t} + \frac{a^2}{2\tau}\left(\frac{\partial G}{\partial x}\right)^2 + r = 0. \tag{5.12}$$

This corresponds to a limiting procedure for a random walk model where the jumps and the time intervals in which they occur are considered to be very small, such that $a^2/\tau = \text{const}$. The front velocity for the case of the dispersal kernel given by (5.4) can be calculated from (4.47) and (5.11):

$$v = \min_{p>0} \frac{\ln[\cosh(ap) + r\tau]}{\tau p}. \tag{5.13}$$

It is easy to see that the function to be minimized tends to $+\infty$ as $p \to 0^+$, whereas this function tends to the constant value a/τ for $p \to \infty$. This implies that somewhere in the middle exists a value of p, namely p^*, that satisfies $dv/dp = 0$, i.e.,

$$\frac{ap\sinh(ap)}{\cosh(ap) + r\tau} = \ln[\cosh(ap) + r\tau]. \tag{5.14}$$

For this value, $p = p^*$, the front velocity (5.13) reads

$$v = \frac{a}{\tau}\frac{\sinh(ap^*)}{\cosh(ap^*) + r\tau} \le \frac{a}{\tau}. \tag{5.15}$$

As expected, the front velocity is always smaller than a/τ, in contrast to the RD equation for which the front velocity grows without bound in the fast reaction limit $r\tau \gg 1$.

If we assume that the PDF $w(z)$ corresponds to a normal distribution,

$$w(z) = \frac{1}{\sigma\sqrt{2\pi}}\exp\left(-\frac{z^2}{2\sigma^2}\right), \tag{5.16}$$

then the Hamiltonian takes the form

$$H(p) = \frac{1}{\tau} \ln \left[\exp\left(\sigma^2 p^2/2\right) + r\tau \right].$$ (5.17)

The front velocity is now

$$v = \min_{p>0} \frac{\ln \left[\exp\left(\sigma^2 p^2/2\right) + r\tau \right]}{\tau p}.$$ (5.18)

As $p \to 0^+$, $v \to \infty$, and as $p \to \infty$, v grows linearly with p. This ensures the existence of a minimum velocity but does not guarantee a maximum velocity. In fact, in this case, no maximum velocity exists, and the front velocity grows without bound in the fast reaction limit, as for the RD equation.

5.2 Continuous-Time Model with Long-Range Dispersal

Consider particles that follow a CTRW, such that the random time T between jumps is exponentially distributed with rate λ, $\mathbb{P}(T > t) = \exp(-\lambda t)$. The mean-field equation for the particle density is the Master equation for the compound Poisson process with logistic growth (5.2). Hyperbolic scaling yields

$$\frac{\partial \rho^\varepsilon}{\partial t} = \frac{\lambda}{\varepsilon} \left[\int_\mathbb{R} \rho^\varepsilon(x + \varepsilon z, t) w(z) \mathrm{d}z - \rho^\varepsilon(x, t) \right] + \frac{1}{\varepsilon} r \rho^\varepsilon (1 - \rho^\varepsilon).$$ (5.19)

The corresponding Hamiltonian is given by

$$H(p) = \lambda \left[\int_\mathbb{R} \exp(zp) w(z) \mathrm{d}z - 1 \right] + r.$$ (5.20)

For a simple random walk with dispersal kernel $w(z) = \frac{1}{2}\delta(z - a) + \frac{1}{2}\delta(z + a)$, we obtain

$$H(p) = \lambda \left[\cosh(ap) - 1 \right] + r.$$ (5.21)

Both Hamiltonians (5.11) and (5.21) involve the maximum velocities a/τ and $a\lambda$, respectively. The front velocities tend to infinity in the fast reaction limit when the diffusion approximation is considered. This means that $H(p)$ depends quadratically on ap for ap small. The two models (5.11) and (5.20) differ fundamentally with respect to propagating fronts; discreteness in time leads to a finite propagation rate, while the continuous-in-time model leads to an infinite velocity of propagation in the limit of fast reaction, $r \to \infty$. The front velocity for model (5.21) is

$$v = \min_{p>0} \frac{\lambda \ln\left[\cosh(ap) - 1\right] + r}{p}. \tag{5.22}$$

As $p \to 0^+$, $v \to \infty$, and as $p \to \infty$, v saturates toward the value $a\lambda$. This also ensures the existence of a minimum velocity and the maximum velocity $a\lambda$, in contrast to the RD equation. If we assume that the density function $w(z)$ has the normal distribution (5.16), then the Hamiltonian takes the form

$$H(p) = \lambda \left[\exp\left(\frac{\sigma^2 p^2}{2}\right) - 1 \right] + r. \tag{5.23}$$

It is clear from (5.11) and (5.23) that for arbitrary values of the parameters a, λ, τ, σ, and r, these Hamiltonians are different from the classical Hamiltonian $H(p) = Dp^2 + r$. However, we obtain the latter if we expand (5.11) and (5.23) in terms of small values of ap and $r\tau$. From this expansion we identify

$$D = \frac{1}{2\tau} \int_{\mathbb{R}} z^2 w(z) \mathrm{d}z \quad \text{and} \quad D = \frac{\lambda}{2} \int_{\mathbb{R}} z^2 w(z) \mathrm{d}z, \tag{5.24}$$

for the two models with discrete and normally distributed kernels $w(z)$, respectively. The front velocity for the case of a normally distributed PDF $w(z)$ reads

$$v = \min_{p>0} \frac{\lambda \left[\exp(\sigma^2 p^2/2) - 1 \right] + r}{p}. \tag{5.25}$$

As $p \to 0^+$, we have $v \to \infty$, and as $p \to \infty$, we find that v grows with p. In consequence, a minimum velocity exists, but no maximum velocity. In the previous section we considered the cases when the microscopic transport processes are described by Markovian random walks. The great advantage of the Hamilton–Jacobi formulation of the front propagation problem in general, and the formulas (4.46) in particular, is that they allow us to study quite complicated transport operators for the evolution of the scalar field ρ and the underlying random walk model, including non-Markovian processes [118, 121, 125].

5.3 CTRW Models and Front Propagation

In this section we present a geometric approach to the problem of propagating fronts into an unstable state, valid for an *arbitrary* CTRW with a KPP reaction rate. We derive an integral Hamilton–Jacobi type equation determining the position of the front and its velocity. The essential feature of the method is that it does not rely on the explicit derivation of an evolution equation for the particle density. In particular,

we obtain an *explicit* formula for the propagation velocity for the case of anomalous transport involving non-Markovian random processes.

In previous sections we showed that the *macroscopic* dynamics of propagating fronts depend on the statistical characteristics of the underlying random walk model for the *mesoscopic* transport process. Since the dynamics of fronts are nonuniversal, it is an important problem to find *universal* rules relating both levels of description. The goal of this section is to address this problem. We are interested in exploring the physical properties of systems of particles that disperse according to a general CTRW.

As usual we introduce the *mesoscopic* concentration $\rho(x, t)$ of particles performing a CTRW. The complete description of the *mesoscopic* transport processes is given by the joint probability density $\psi(\tau, z)$ of making a jump of length z in the time interval $(\tau, \tau + d\tau)$, see Sect. 3.2. We assume that the local growth rate has the KPP form:

$$F(\rho) = r\rho(1 - \rho). \tag{5.26}$$

We start with Model C given by (3.141) and the above kinetics. The governing equation for $\rho(x, t)$ can be written in the form

$$\rho(x, t) = \rho_0(x)\Psi(t) + \int_0^t \int_{\mathbb{R}} \psi(\tau, z)\rho(x - z, t - \tau,)dzd\tau$$

$$+r \int_0^t \Psi(\tau)\rho(x, t - \tau)\left[1 - \rho(x, t - \tau)\right]d\tau. \tag{5.27}$$

This equation describes the balance of particles at the position x at time t. The first term on the RHS of (5.27) represents the number of particles remaining at their initial position x up to time t. The second term corresponds to the number of particles arriving at x up to time t from position $x - z$ and time $t - \tau$, and the last term is a production term due to growth (5.26).

For reaction–transport process with a linear kinetic term $F(\rho) = r\rho$, an alternative description has been suggested in [187], namely

$$\rho(x, t) = \Psi(t)e^{rt}\rho_0(x) + \int_0^t \int_{\mathbb{R}} \psi(\tau, z)e^{r\tau}\rho(x - z, t - \tau)dzd\tau, \tag{5.28}$$

where the exponential growth e^{rt} has been taken into account. For the case of linear kinetics, (3.121) and (3.122) of Model A can be reduced to (5.28).

Proceeding as in the previous section, and taking into account the definitions of the moment-generating functions,

$$\check{\psi}(p, H) = \int_0^\infty \int_{\mathbb{R}} \psi(\tau, z)e^{-H\tau}e^{px}dzd\tau, \quad \hat{\Psi}(H) = \int_0^\infty \Psi(\tau)e^{-H\tau}d\tau, \tag{5.29}$$

we can rewrite (5.27) as an equation for the Hamiltonian function H:

$$1 - \check{\psi}(p, H) - r\hat{\Psi}(H) = 0. \tag{5.30}$$

It turns out that for (5.28) one can obtain a very simple equation for the Hamiltonian:

$$\check{\psi}(p, H - r) = 1. \tag{5.31}$$

If the jump length and waiting time are independent random variables, we can write down the moment-generating function $\check{\psi}(p, H)$ in the decoupled form

$$\check{\psi}(p, H) = \hat{\phi}(H)\check{w}(p), \tag{5.32}$$

where

$$\check{w}(p) = \int_{\mathbb{R}} e^{pz} w(z)\mathrm{d}z. \tag{5.33}$$

Note that our approach applies only to situations where the moment-generating function $\check{w}(p)$ is finite, which excludes heavy-tailed jump length PDFs.

Consider a power-law waiting time distribution $\phi(t)$ with Laplace transform

$$\hat{\phi}(H) = \frac{1}{1 + (H\tau_0)^\gamma}, \qquad 0 < \gamma < 1. \tag{5.34}$$

The waiting time PDF $\phi(t)$ behaves like $t^{-(\gamma+1)}$ for large t, and its expectation diverges if $0 < \gamma < 1$. If the moment-generating function for the jump length PDF is $\check{w}(p) \simeq 1 + \sigma^2 p^2/2$, then (5.30) takes the form of the anomalous Hamilton–Jacobi equation

$$(H\tau_0)^\gamma - r\tau_0 (H\tau_0)^{\gamma-1} = \frac{\sigma^2 p^2}{2}. \tag{5.35}$$

In a similar fashion, one can write down the time-fractional Hamilton–Jacobi equation for the case where the waiting time PDF $\phi(t)$ is stable with the index of stability γ. The corresponding Laplace transform is $\hat{\phi}(H) = \exp\left[-(H\tau_0)^\gamma\right]$.

From (5.35) we obtain the momentum p in terms of the Hamiltonian, $p = f(H)$, where $f(H) = \left[2\tau_0(H - r)(H\tau_0)^{\gamma-1}\right]^{1/2}\sigma^{-1}$. This, together with (4.46), provides the equation for H, namely $1 = H\,\mathrm{d}\ln f(H)/\mathrm{d}H$, which has the solution $H = r(3 - \gamma)(2 - \gamma)^{-1}$, and an explicit expression for v,

$$v = \frac{\sigma}{\tau_0\sqrt{2}} (r\tau_0)^{1-\gamma/2} (3 - \gamma)^{(3-\gamma)/2}(2 - \gamma)^{-1+\gamma/2}. \tag{5.36}$$

For the case $\gamma = 1$, (5.36) agrees with the corresponding Fisher velocity, with the diffusion coefficient $D = \sigma^2/2\tau_0$. In the absence of reaction, $r = 0$, the mean squared displacement (MSD) of particles grows as t^γ, so that the physical meaning of the exponent γ is clear. For a fixed time, the MSD grows monotonically with γ, which means that the intensity of the transport increases with γ. One can think of γ as a measure of the tail length of the waiting time distribution $\phi(t)$ (5.34). When the waiting time PDF has a heavy tail, we expect that the mean rate of jumps is smaller than normal. In other words, a heavy-tailed waiting time PDF decreases the rate of the spread of the particles and therefore the velocity of the front, because some particles have long sojourns before starting the next jump. As a result, the velocity of the front, when reaction is present, should also be a monotonically increasing function of γ, that is $dv/d\gamma > 0$. This physical requirement, applied to (5.36), yields $r < r_{\max} = \tau_0^{-1}(2-\gamma)/(3-\gamma)$ and therefore the reaction rate cannot be arbitrarily large. Moreover

$$v < v_{\max} = \sqrt{\frac{D}{\tau_0}}\sqrt{\frac{3-\gamma}{2}}. \tag{5.37}$$

If we consider (5.31) with (5.34) and the diffusion approximation for the jump length PDF, then the Hamilton–Jacobi equation for Model A reads

$$\sigma^2 p^2 = 2\tau_0^\gamma (H - r)^\gamma, \tag{5.38}$$

and the minimum value of H/p is attained at $H^* = 2r/(2-\gamma)$. The front velocity is given by

$$v = \sqrt{\frac{2r^{2-\gamma}\sigma^2}{\tau_0^\gamma(2-\gamma)^{2-\gamma}\gamma^\gamma}}. \tag{5.39}$$

Following the same reasoning as before, the criterion $dv/d\gamma > 0$ leads to $r < r_{\max} = \tau_0^{-1}(2-\gamma)/\gamma$ and $v < v_{\max} = \sigma\sqrt{2}/\gamma\tau_0$. The front velocities (5.36) and (5.39) have been derived assuming diffusive transport which is attained if the chemical time r^{-1} is large compared to the transport time scale τ_0, i.e., $r\tau_0$ is small. This condition reflects the fact that diffusive behavior results from the accumulation of many jumps of the random walk on a time scale much larger than τ_0. Therefore, large reaction rates r require corresponding small values of τ_0. For subdiffusive transport, the condition that $r\tau_0$ is small ensures that there exists a maximum front velocity. Front propagation in reaction–superdiffusion systems has been considered in [265, 90, 60, 89].

5.4 Memory Effects in RD Equation

To account for memory effects in the transport, one is tempted to replace the standard Fick's first law form of the constitutive equation by a nonlocal phenomenological relation between the flux and the density gradient:

$$J(x, t) = - \int_0^t K(t - \tau) \frac{\partial \rho(x, \tau)}{\partial x} d\tau, \qquad (5.40)$$

where $K(t)$ is a memory kernel. This form of the constitutive equation captures the physical fact that the particle flux does not instantaneously adjust to the particle density gradient. If $K(t) = D\delta(t)$, then (5.40) corresponds to Fick's first law, while the exponential kernel $K(t) = \frac{D}{\tau_0} \exp(-t/\tau_0)$ leads to the Cattaneo equation (2.18) for the flux.

Combining the constitutive equation for the flux (5.40) with the continuity equation for the particle density, we obtain the nonlocal RD equation

$$\frac{\partial \rho}{\partial t} = \int_0^t K(t - \tau) \frac{\partial^2 \rho(x, \tau)}{\partial x^2} d\tau + F(\rho). \qquad (5.41)$$

If one considers the exponential memory kernel in (5.41) and takes the temporal derivative, the reaction-telegraph equation (2.19) is recovered.

We assume that the reaction term is of the KPP type, $F(\rho) = r\rho(1 - \rho)$. Our main goal is to find the front velocity for a general memory kernel in terms of its Laplace transform, $\hat{K}$, and to show that fronts travel with a finite velocity in the fast reaction limit only if the initial value of the memory kernel is positive definite. This general result will be applied to some specific memory kernels.

We proceed as in the previous sections and find that the Hamilton–Jacobi equation for (5.41) can be written as

$$H = \hat{K}(H)p^2 + r. \qquad (5.42)$$

From (4.46) and (5.41) we obtain

$$v(H) = H\sqrt{\frac{\hat{K}(H)}{H - r}}, \qquad \frac{\partial p}{\partial H} = \frac{p}{H}. \qquad (5.43)$$

The front velocity is given by $v(H^*)$, where H^* is the solution to

$$\frac{d}{dH^*}\left(\frac{H^* - r}{\hat{K}(H^*)}\right) = \frac{2(H^* - r)}{H^*\hat{K}(H^*)}. \qquad (5.44)$$

The existence of the front and the value of the minimal velocity depend crucially on the behavior of $v(H)$ as $H \to \infty$. To see this, note that $v(H) \to \infty$ as $H \to r^+$.

Therefore, if $v(H)$ is a monotonically decreasing function in the limit $H \to \infty$, then the minimum value is 0 and no propagating front exists. If, on the other hand, $v(H)$ is monotonically increasing with H, then a minimum velocity exists. We assume that $K(t)$ is a smooth function. The limit $H \to \infty$ is equivalent to the limit $t \to 0$. We write $K(t) = K(0) + K'(0)t + K''(0)t^2/2 + \cdots$, which has the Laplace transform $\hat{K}(H) = K(0)H^{-1} + K'(0)H^{-2} + K''(0)H^{-3} + \cdots$, where the prime denotes the derivative with respect to time. Then, in the limit $H \to \infty$, $\hat{K}(H) \simeq K(0)H^{-1}$ and $v(H \to \infty) = \sqrt{K(0)}$. This velocity value can be selected by the front because it fulfills the condition $\partial_H p = p/H$, if $K(0) > 0$, as can be easily shown. We conclude that

$$
v = \begin{cases} H^* \sqrt{\dfrac{\hat{K}(H^*)}{H^* - r}}, & K(0) = 0, \\[3mm] \min\left[H^* \sqrt{\dfrac{\hat{K}(H^*)}{H^* - r}}, \sqrt{K(0)} \right], & K(0) > 0, \end{cases} \tag{5.45}
$$

where H^* is the solution of (5.44). It is interesting to note that v is a monotonically increasing function of the reaction rate, $\partial v/\partial r > 0$. However, if $K(0) > 0$, this growth saturates at $\sqrt{K(0)}$, a value that is not affected at all by the reaction process and depends only on the characteristics of the transport through the memory kernel. Equation (5.45) implies that the memory kernel contains all the physical information we need to determine the propagation velocity. Indeed, the upper bound for the front velocity equals the velocity of propagation of periodic disturbances in the high-frequency limit for the pure transport equation, i.e., (5.41) with $F = 0$ [223]. Equation (5.45) demonstrates that for an infinitely differentiable memory kernel with $K(0) > 0$, the front velocity is bounded from above by the transport process, even if the reaction process is very fast. The flux at time t is a weighted average of the particle density gradients at previous times, see (5.40). The weight of the gradient at time t, $\partial_x \rho(x, t)$, is given by $K(0)$. If $K(0) = 0$, the instantaneous particle gradient at time t does not contribute to the particle flux at time t and the front velocity is unbounded. We illustrate these results for some typical memory kernels.

(a) Consider first the case $K(t) = D\delta(t)$. In this case, (5.45) cannot be applied because $\delta(t)$ is not differentiable near $t = 0$. However, the velocity can be calculated from (5.43) to yield $v = 2\sqrt{rD}$ as expected.

(b) For the exponential kernel $K(t) = D\tau_0^{-1}e^{-t/\tau_0}$, one has $K(0) = D/\tau_0 > 0$, and the front velocity reads

$$
v = \min_{z > b} \sqrt{\frac{D}{\tau_0}} \left[1, \frac{z}{\sqrt{z+1}\sqrt{z-b}} \right] = \begin{cases} 2\sqrt{\dfrac{D}{\tau_0}}\dfrac{\sqrt{b}}{1+b}, & b \le 1, \\[3mm] \sqrt{\dfrac{D}{\tau_0}}, & b > 1, \end{cases} \tag{5.46}
$$

where $z \equiv H\tau_0$ and $b = r\tau_0$. Note that the front velocity is bounded from above by the limiting velocity of the transport process $\sqrt{D/\tau_0}$.

(c) Let us consider the power-law kernel

$$K(t) = \frac{D(\gamma - 1)}{\tau_0} \left(1 + \frac{t}{\tau_0}\right)^{-\gamma} \tag{5.47}$$

with $\gamma > 1$ and finite moments. Since $K(0) = D(\gamma - 1)/\tau_0 > 0$, (5.45) implies that the front velocity is bounded by $\sqrt{D(\gamma - 1)/\tau_0}$. The Laplace transform of the kernel is $\hat{K}(H) = D(\gamma - 1)(H\tau_0)^{\gamma - 1} e^{H\tau_0} \Gamma(1 - \gamma, H\tau_0)$, where $\Gamma(\cdot, \cdot)$ is the incomplete Gamma function. The front velocity has to be calculated numerically from (5.44) and (5.45).

In Fig. 5.1 we plot the front velocity vs $r\tau_0$ for different values of γ. The saturation effect at $\sqrt{D(\gamma - 1)/\tau_0}$ is observed. Note that when γ increases, the front velocity also increases due to the faster decay of the memory kernel tail.
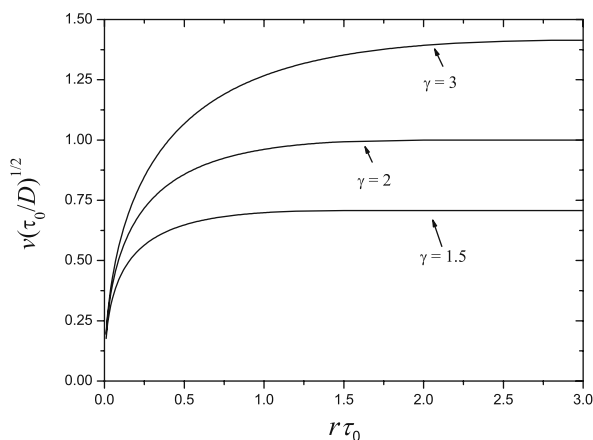
Fig. 5.1 Dimensionless front velocity vs $r\tau_0$ for the kernel given in (5.47). In this case, the dimensionless front velocity is bounded by $\sqrt{\gamma - 1}$. For higher values of the index γ the kernel tail decays faster than for low γ and this generates faster fronts. Reprinted with permission from [287]. Copyright 2007, EPL

5.5 Front Propagation in the Reaction-Telegraph Equation

In this section we consider the problem of front propagation for the three-dimensional reaction-telegraph equation involving KPP kinetics. The goal is to derive the equation governing the evolution of the front in the long-time large-scale limit as in the previous sections and to show that this equation is identical in form to the relativistic Hamilton–Jacobi equation.

Consider the reaction-telegraph equation (2.19) in three dimensions,

$$\tau_0 \frac{\partial^2 \rho}{\partial t^2} + \left[1 - \tau_0 r \left(1 - 2\rho\right)\right] \frac{\partial \rho}{\partial t} = D\Delta\rho + r\rho(1 - \rho), \quad \mathbf{x} \in \mathbb{R}^3, \tag{5.48}$$

with an initial condition with compact support. Applying the hyperbolic scaling to (5.48), we obtain the equation for ρ^ε in the form

$$\varepsilon\tau_0\frac{\partial^2\rho^\varepsilon}{\partial t^2} + \left(1 - \tau_0 r + 2\tau_0 r\rho^\varepsilon\right)\frac{\partial\rho^\varepsilon}{\partial t} = \varepsilon D\Delta\rho^\varepsilon + \frac{r}{\varepsilon}\rho^\varepsilon\left(1 - \rho^\varepsilon\right). \tag{5.49}$$

The limiting function $G(t, x)$ obeys the first-order nonlinear PDE:

$$-\tau_0\left(\frac{\partial G}{\partial t}\right)^2 + \left(1 - \tau_0 r\right)\frac{\partial G}{\partial t} + D(\nabla G)^2 + r = 0. \tag{5.50}$$

The location of the reaction front can be determined as the boundary of the set

$$S = \left\{\mathbf{x} \in \mathbb{R}^3 : G(x, t) \geq 0\right\}. \tag{5.51}$$

5.5.1 Relativistic Hamilton–Jacobi Equation

The basic idea is that equation (5.50) is identical in form to an equation arising in classical relativity theory. If we introduce the new parameters

$$\varphi = \frac{1}{2}\left(r - \frac{1}{\tau_0}\right), \quad m = \frac{\tau_0}{2D}\left(r + \frac{1}{\tau_0}\right), \quad c^2 = \frac{D}{\tau_0}, \tag{5.52}$$

then (5.50) can be rewritten in the form of the relativistic Hamilton–Jacobi equation for a particle with a mass m moving in the potential field φ:

$$\left(\frac{\partial G}{\partial t} + \varphi\right)^2 - m^2 c^4 - c^2(\nabla G)^2 = 0, \quad \mathbf{x} \in \mathbb{R}^3, \tag{5.53}$$

where c is the speed of light. The Hamiltonian associated with this equation is

$$H(p) = \sqrt{m^2 c^4 + c^2 p^2} + \varphi, \tag{5.54}$$

and the Lagrangian L has the form

$$L = -mc^2\sqrt{1 - \frac{1}{c^2}\left(\frac{d\mathbf{x}}{ds}\right)^2} - \varphi, \tag{5.55}$$

that is,

$$L = -\frac{1}{2}\left(r + \frac{1}{\tau_0}\right)\sqrt{1 - \frac{\tau_0}{D}\left(\frac{d\mathbf{x}}{ds}\right)^2} - \frac{1}{2}\left(r - \frac{1}{\tau_0}\right). \tag{5.56}$$

The analogy with the relativistic mechanics allows us to derive the explicit expression for the function $G(x, t)$ and thereby to find the reaction front position and its velocity.

5.5.2 Exact Formula for Front Velocity

The optimal trajectory is that of a free particle, i.e., the straight line connecting the points $\mathbf{x}$ and $\mathbf{y} \in \Omega_0$, where Ω_0 is the support of the initial condition:

$$\mathbf{x}(s) = \left(\frac{\mathbf{y} - \mathbf{x}}{t} \right) s + \mathbf{x}, \quad 0 \leq s \leq t. \tag{5.57}$$

The action integral can be written as

$$G(\mathbf{x}, t) = \inf_{\mathbf{y} \in \Omega_0} \left\{ -mc^2 t \sqrt{1 - \frac{1}{c^2} \left(\frac{\mathbf{y} - \mathbf{x}}{t} \right)^2} - \varphi t \right\}. \tag{5.58}$$

Let $l(\mathbf{x}, \Omega_0)$ denote the minimal distance between the point $\mathbf{x}$ and the set Ω_0. Then, in terms of the phenomenological parameters τ_0, D, and r, the action functional $G(\mathbf{x}, t)$ can be rewritten as

$$G(\mathbf{x}, t) = -\frac{t}{2} \left(r + \frac{1}{\tau_0} \right) \sqrt{1 - \frac{\tau}{D} \left(\frac{l(\mathbf{x}, \Omega_0)}{t} \right)^2} + \frac{t}{2} \left(\frac{1}{\tau_0} - r \right). \tag{5.59}$$

We are now in a position to determine the exact formula for the reaction front propagation velocity. The set $S = \left\{ \mathbf{x} \in \mathbb{R}^3 : G(\mathbf{x}, t) \geq 0 \right\}$, where $\rho^\varepsilon(\mathbf{x}, t) \to 0$ as $\varepsilon \to 0$, can be represented as $S = \left\{ \mathbf{x} \in \mathbb{R}^3 : l(\mathbf{x}, \Omega_0) > vt \right\}$, where

$$v = c \sqrt{1 - \left(\frac{1 - \tau_0 r}{1 + \tau_0 r} \right)^2} = \frac{\sqrt{4Dr}}{1 + \tau_0 r}, \quad \tau_0 r \leq 1. \tag{5.60}$$

The effect of diffusion with finite velocity, $\tau_0 r \neq 0$, is to decrease the propagation rate corresponding to the RD equation. The last restriction $\tau_0 r \leq 1$ arises from the fact that the speed of light $c = \sqrt{D/\tau_0}$ is the maximal velocity of propagation. In other words, front motion with a velocity greater than the speed of light c is impossible.

In the limiting case, where the relaxation time τ_0 is small compared with the chemical time r^{-1}, i.e., $\tau_0 r \ll 1$, we can neglect the effect that the velocity of the transport mechanism is finite.

5.6 Front Propagation in Persistent Random Walks with Reactions

As discussed in Sect. 2.2, persistent random walks provide a mesoscopic description of reaction–transport systems with inertia. This approach provides another opportunity to explore the effects of a finite velocity in the transport mechanism on propagating fronts. We consider two cases. The first corresponds to reaction walks where the kinetic terms do not depend on the direction of the particles. This corresponds to choosing $\kappa = 1/2$ in (2.38), and persistent random walks with such kinetics are called *direction-independent reaction walks* (DIRW). The second case corresponds to walks where reactions occur only between particles with opposite velocities. We call such systems direction-dependent reaction walks (DDRWs).

5.6.1 Fronts in Direction-Independent Reaction Walks

We consider RRWs with KPP kinetics [204]. Specifically we choose the branching-coalescence kinetic scheme, see Sect. 1.4.1. A DIRW with such kinetics obeys the following nondimensionalized evolution equations:

$$\frac{\partial \rho_+}{\partial t} + \gamma \frac{\partial \rho_+}{\partial x} = \mu(\rho_- - \rho_+) + \frac{1}{2}\rho - \rho\rho_+, \tag{5.61a}$$

$$\frac{\partial \rho_-}{\partial t} - \gamma \frac{\partial \rho_-}{\partial x} = \mu(\rho_+ - \rho_-) + \frac{1}{2}\rho - \rho\rho_-, \tag{5.61b}$$

where $\rho = \rho_+ + \rho_-$ again denotes the total particle density. We consider (5.61) on $(-\infty, +\infty)$. The uniform steady states of the Fisher DIRW (5.61) are given by $(\overline{\rho}_+(x), \overline{\rho}_-(x)) = (0, 0)$ and $(\overline{\rho}_+(x), \overline{\rho}_-(x)) = (1/2, 1/2)$. It is easily verified that the former is unstable, while the latter is stable. If the system is prepared such that $\lim_{x \to -\infty}(\rho_+(x, 0), \rho_-(x, 0)) = (1/2, 1/2)$ and $\lim_{x \to +\infty}(\rho_+(x, 0), \rho_-(x, 0)) = (0, 0)$, the stable state invades the unstable state in the form of propagating front. We employ phase plane analysis, see Sect. 4.1, to show this. We look for solutions of (5.61) of the form

$$\rho_+(x, t) = u_+(z), \quad \rho_-(x, t) = u_-(z), \tag{5.62}$$

where $z = x - vt$, $v > 0$, and

$$\lim_{z \to -\infty} u_\pm(z) = \frac{1}{2}, \quad \lim_{z \to \infty} u_\pm(z) = 0. \tag{5.63}$$

Substituting (5.62) into (5.61), we obtain

$$u'_+ = \frac{1}{\gamma - v}\left[\mu(u_- - u_+) + \frac{1}{2}u - uu_+\right], \quad \gamma \neq v, \tag{5.64a}$$

$$0 = \mu(u_- - u_+) + \frac{1}{2}u - uu_+, \quad \gamma = v, \tag{5.64b}$$

$$u'_- = -\frac{1}{\gamma + v}\left[\mu(u_+ - u_-) + \frac{1}{2}u - uu_-\right]. \tag{5.64c}$$

The prime denotes the derivative with respect to the argument of the function and $u = u_+ + u_-$. The fixed points of (5.64) are $(0, 0)$ and $(1/2, 1/2)$, and a front corresponds to a nonnegative heteroclinic orbit in the u_-–u_+ phase plane connecting the two fixed points. Such an orbit exists if $(1/2, 1/2)$ is a saddle point and $(0, 0)$ a stable node, see Sect. 4.1. The nullcline of the density u_+, i.e., the curve $u'_+ = 0$, in the u_-–u_+ phase plane is given by (5.64b), of which only the positive root is acceptable:

$$u_+ = N(u^-) = -\frac{1}{2}\left(u_- + \mu - \frac{1}{2}\right) + \sqrt{\frac{1}{4}\left(u_- + \mu - \frac{1}{2}\right)^2 + \left(\mu + \frac{1}{2}\right)u_-}. \tag{5.65}$$

For $v > \gamma$, the vector field of (5.64a) and (5.64c) points away from the nullcline $N(u^-)$, and a stable heteroclinic orbit does not exist. For $v < \gamma$, the vector field points toward the nullcline, and for front velocities close to γ, i.e., $0 < \gamma - v = \epsilon \ll 1$, the density u_+ is a fast variable and follows the evolution of u_- adiabatically. The system (5.64a) and (5.64c) is then well approximated by (5.65) and

$$u'_- = -\frac{1}{2\gamma}\left[\mu(u_+ - u_-) + \frac{1}{2}u - uu_-\right] = -\frac{1}{2\gamma}R^-(u_+, u_-). \tag{5.66}$$

This approximation becomes exact in the limit $v \to \gamma$. The trajectory in the phase plane is then given by the nullcline $N(u^-)$. Substituting (5.65) into (5.66), we obtain

$$u'_- = -\frac{1}{2\gamma}R^-(N(u_-), u_-) = R(u_-). \tag{5.67}$$

For $2\mu > 1$, the nullcline $N(u^-)$ runs from the fixed point $(0, 0)$ to the fixed point $(1/2, 1/2)$. It is nonnegative, and straightforward calculations show that $R'(0) < 0$ and $R'(1/2) > 0$. In other words, for $0 \leq \gamma - v \ll 1$ a nonnegative heteroclinic orbit exists and is well approximated by the u_+-nullcline $N(u^-)$ in the u_-–u_+ phase plane.

The condition

$$2\mu > 1 \tag{5.68}$$

implies that the DIRW is in the diffusive regime. The correlation time of the particle turning process is $\tau_{\text{corr}} = 1/(2\mu)$, see (2.32), and the typical time scale of the kinetics is $\tau_{\text{chem}} = 1$, due to nondimensionalization. If the condition (5.68) is fulfilled, the time scale of the transport process is faster than the time scale of the kinetics; the RRW is in the diffusive regime. The ballistic regime, i.e., slow turning compared to the kinetics, corresponds to $2\mu < 1$.

The nonnegative heteroclinic orbit will persist as v decreases, as long as no bifurcation occurs in the vector field of (5.64a) and (5.64c) and $(1/2, 1/2)$ remains a saddle point and $(0, 0)$ a stable node, whose eigenvectors lie strictly within the positive quadrant. For $v < \gamma$, the eigenvalues for the fixed point $(0, 0)$ are

$$\lambda_{\pm}(0) = -\frac{1}{2}\frac{v(1 - 2\mu)}{v^2 - \gamma^2} \pm \sqrt{\frac{1}{4}\frac{v^2(1 - 2\mu)^2}{\left(v^2 - \gamma^2\right)^2} + \frac{2\mu}{v^2 - \gamma^2}}, \qquad (5.69)$$

and for the fixed point $(1/2, 1/2)$,

$$\lambda_{\pm}(1/2) = \frac{v(1 + \mu)}{v^2 - \gamma^2} \pm \sqrt{\frac{v^2(1 + \mu)^2}{\left(v^2 - \gamma^2\right)^2} - \frac{(1 + 2\mu)}{v^2 - \gamma^2}}. \qquad (5.70)$$

It is easily verified that the fixed point $(1/2, 1/2)$ is a saddle point, i.e., λ_+ is real and positive and λ_- is real and negative, for all values of μ. The fixed point $(0, 0)$ undergoes a Hopf bifurcation at $\mu_{\text{H}} = 1/2$. Condition (5.68) ensures that $(0, 0)$ is a stable fixed point. It is a node, if the discriminant is positive, see Sect. 1.2.2, which implies that

$$v \geq v_{\text{DIRW}} = \frac{2\sqrt{2\mu}}{1 + 2\mu}\gamma. \qquad (5.71)$$

The eigenvectors of the stable node $(0, 0)$ are given by

$$\begin{pmatrix} e_+^{\pm} \\ e_-^{\pm} \end{pmatrix} = \begin{pmatrix} -\alpha_{\pm}/n \\ 1/n \end{pmatrix}, \qquad (5.72)$$

where

$$\alpha_{\pm} = \frac{\frac{1}{2} - \mu + (v + \gamma)\lambda_{\pm}}{\frac{1}{2} + \mu}, \quad n = \sqrt{\alpha_{\pm}^2 + 1}. \qquad (5.73)$$

They lie strictly in the positive quadrant for $\mu > 1/2$ and $\gamma > v \geq v_{\text{DIRW}}$.

We have established the following result: If the reaction walk is in the diffusive regime, i.e., if $2\mu > 1$, then the stable state $(1/2, 1/2)$ invades the unstable state

$(0, 0)$ in the Fisher DIRW in the form of a propagating front. The front travels at constant velocity v with $v \in [v_{\mathrm{DIRW}}, \gamma)$.

Recall that the diffusive limit corresponds to $\gamma \to \infty$ and $\mu \to \infty$ such that $\gamma = \sqrt{2\mu D}$. Therefore we have as $\mu \to \infty$,

$$v_{\mathrm{DIRW}} = \frac{4\mu\sqrt{D}}{1 + 2\mu} \to 2\sqrt{D}. \tag{5.74}$$

Adding (5.64a) and (5.64c) and integrating the resulting equation over z from $-\infty$ to $+\infty$, we find that

$$v = \int_{-\infty}^{\infty} \mathrm{d}z \, \left[u(z) - u^2(z) \right]. \tag{5.75}$$

The integrand is appreciably different from zero only in the front region of the wave; a smaller value of v corresponds to a narrower, i.e., steeper front. As for the Fisher equation (4.1), the steepness of the wave front depends inversely on the wave velocity v, and "natural" initial conditions, i.e., initial conditions that are localized or that decay faster than exponentially, relax to the front with the minimal front velocity. The minimal front velocity for the Fisher DIRW is smaller than the minimal front velocity for the Fisher equation, $v_{\mathrm{RD}} = 2\sqrt{D}$, see Sect. 4.1.1, and approaches the latter in the diffusive limit.

5.6.2 Fronts in Direction-Dependent Reaction Walks

If we replace Brownian motion by its simplest generalization, the persistent random walk, we obtain direction-independent reaction walks as the simplest generalization of reaction–diffusion equations. Both describe chemical reactions in the reaction-limited or activation-controlled regime. However, the activation barrier is only implicitly taken into account; it is incorporated into the kinetic coefficients
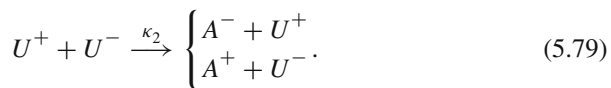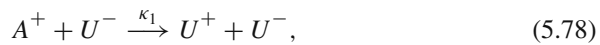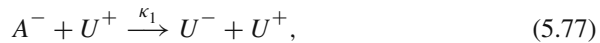
$$k_i = A_i \exp(-E_i/RT), \tag{5.76}$$

where E_i is the activation energy, R the gas constant, T the temperature, and A_i the preexponential factor [350]. The Boltzmann factor in (5.76) reflects the requirement that molecules must possess sufficient energy to overcome an activation barrier for a reaction to occur. In condensed phase reactions, this energy can be acquired from the surroundings, and a description in terms of direction-independent kinetics is satisfactory. In population dynamics, birth and death rates typically depend on the total density, and again a reaction random walk with direction-independent kinetics is an appropriate description.

In gas-phase reactions, molecules must collide with sufficient kinetic energy to overcome the activation barrier. Since velocity is not defined for Brownian motion, this requirement cannot be taken into account explicitly in a reaction–diffusion

equation. Velocity is, however, defined for persistent random walks, and they offer an opportunity to incorporate the existence of an energy requirement for reactive collisions into the formalism. Of course, the persistent random walk retains velocity only in a simplified, namely a dichotomous, way. Within this limitation we can model the energy requirement by allowing reactions only between particles with opposite velocities.

For the branching-coalescence kinetics, this amounts to replacing the kinetic scheme (1.56) and (1.57) by

$$A^- + U^+ \xrightarrow{\kappa_1} U^- + U^+, \tag{5.77}$$

$$A^+ + U^- \xrightarrow{\kappa_1} U^+ + U^-, \tag{5.78}$$

$$U^+ + U^- \xrightarrow{\kappa_2} \begin{cases} A^- + U^+ \\ A^+ + U^- \end{cases}. \tag{5.79}$$

Here $\kappa_i = A_i = P_i Z_i$, and P_i is the steric factor and Z_i the collision frequency factor [350]. We will consider only situations where the steric factor ensures that the kinetics are reaction-limited. We assume that the pool species A is in equilibrium, i.e., $\rho_{+,a} = \rho_{-,a} = \frac{1}{2}\rho_a$. In dimensionless variables we obtain the following evolution equations for the kinetic scheme (5.77), (5.78), and (5.79):

$$\frac{\partial \rho_+}{\partial t} + \gamma \frac{\partial \rho_+}{\partial x} = \mu(\rho_- - \rho_+) + \rho_- - 2\rho_+\rho_-, \tag{5.80a}$$

$$\frac{\partial \rho_-}{\partial t} - \gamma \frac{\partial \rho_-}{\partial x} = \mu(\rho_+ - \rho_-) + \rho_+ - 2\rho_+\rho_-. \tag{5.80b}$$

The uniform steady states of the Fisher DDRW (5.80) and their stability properties are identical to those of the Fisher DIRW (5.61). We again look for propagating front solutions of (5.80a) and (5.80b), i.e., solutions of the form (5.62) and (5.63), and we obtain

$$u'_+ = \frac{1}{\gamma - v} \left[\mu(u_- - u_+) + u_- - 2u_+u_- \right], \quad \gamma \neq v, \tag{5.81a}$$

$$0 = \mu(u_- - u_+) + u_- - 2u_+u_-, \quad \gamma = v, \tag{5.81b}$$

$$u'_- = -\frac{1}{\gamma + v} \left[\mu(u_+ - u_-) + u_+ - 2u_+u_- \right]. \tag{5.81c}$$

The u_+-nullcline is given by

$$u_+(u_-) = \bar{N}(u_-) = \frac{(\mu + 1)u_-}{\mu + 2u_-}, \tag{5.82}$$

and for $v = \gamma$ we obtain from (5.81c)

$$u'_- = \bar{R}(u_-) = -\frac{1}{2\gamma}\left[\mu(\bar{N}(u_-) - u_-) + \bar{N}(u_-) - 2\bar{N}(u_-)u_-\right]. \qquad (5.83)$$

For all values of μ, the nullcline $\bar{N}(u_-)$ runs from the fixed point $(0, 0)$ to the fixed point $(1/2, 1/2)$. It is nonnegative, and straightforward calculations show that $\bar{R}'(0) < 0$ and $\bar{R}'(1/2) > 0$. For $v \neq \gamma$, the eigenvalues of the fixed point $(1/2, 1/2)$ are identical to those of the DIRW case, (5.70), and the eigenvalues for $(0, 0)$ are given by

$$\lambda_\pm = \frac{v\mu}{v^2 - \gamma^2} \pm \sqrt{\frac{v^2\mu^2}{\left(v^2 - \gamma^2\right)^2} + \frac{1 + 2\mu}{v^2 - \gamma^2}}. \qquad (5.84)$$

For

$$\gamma > v \geq v_{\text{DDRW}} = \frac{\sqrt{1 + 2\mu}}{1 + \mu}\gamma, \qquad (5.85)$$

$(0, 0)$ is a stable node, and its eigenvectors

$$\begin{pmatrix} \bar{e}_+^\pm \\ \bar{e}_-^\pm \end{pmatrix} = \begin{pmatrix} \beta_\pm/n \\ 1/n \end{pmatrix}, \qquad (5.86)$$

where

$$\beta_\pm = \frac{\mu - (v + \gamma)\lambda_\pm}{\mu + 1}, \quad n = \sqrt{\beta_\pm^2 + 1}, \qquad (5.87)$$

lie strictly in the positive quadrant. No Hopf bifurcation occurs for the DDRW.

Reasoning along the same lines as for the DIRW case, we obtain the following result: In the diffusive as well as the ballistic regime, the stable state $(1/2, 1/2)$ invades the unstable state $(0, 0)$ in the Fisher DDRW in the form of a propagating front. The front travels at constant velocity v with $v \in [v_{\text{DDRW}}, \gamma)$.

In the diffusive limit, $\mu \to \infty$, with $\gamma = \sqrt{2\mu D}$, we have

$$v_{\text{DDRW}} = \frac{2\mu\sqrt{1 + 1/(2\mu)}}{1 + \mu}\sqrt{D} \to 2\sqrt{D} = v_{\text{RD}}. \qquad (5.88)$$

It is also easily verified that $v_{\text{DDRW}} < v_{\text{RD}}$, and that in the diffusive regime, $2\mu > 1$, where propagating fronts exist in both the Fisher DIRW and the Fisher DDRW,

$$v_{\text{DDRW}} < v_{\text{DIRW}}. \qquad (5.89)$$

5.7 Reaction-Biased Random Walks. Propagation Failure

An interesting question arises when the dispersal is biased in a direction away from the region occupied by the unstable state [286]. What are the conditions on the reaction rate and bias that will result in a stalled front? Or phrased differently, what is the critical (minimal) value of the reaction rate to sustain front propagation when the underlying random walk has a bias in the opposite direction? The goal of this section is to show the following: (i) The standard diffusion approximation of the transport process always provides an inaccurate value for the critical reaction rate. (ii) If the reaction rate exceeds the jump frequency of the random walk, then the front cannot stall and will always propagate into the unstable state, independently of the values of the other statistical parameters of the random walk.

We choose the initial conditions to be $\rho(x, 0) = 1$ for $x \leq 0$ and $\rho(x, 0) = 0$ for $x > 0$. This initial condition describes, for example, a territory divided into an invaded zone, $x \leq 0$, and a noninvaded zone, $x > 0$, separated by a frontier at $x = 0$. If particles disperse according to an isotropic random walk with KPP kinetics, this initial condition turns into a front propagating from left to right, i.e., the invasion starts. Since the particle jumps are isotropic, the reaction is responsible for the motion of the front from left to right. It is the reaction process that starts and maintains a successful invasion. A bias to the left in the random walk will hinder the invasion. Therefore we expect that the critical reaction rate is given by a balance between the factor favoring the invasion, the reaction process, and the factor opposing the invasion, the bias in the transport process.

We use Model C, given by (5.27), for the mean-field equation for $\rho(x, t)$ with $\psi(t, z) = \phi(t)w(z)$. The standard diffusion approximation of (5.27), i.e., taking the limit of small jump lengths and small waiting times, yields the reaction–diffusion–advection equation

$$\frac{\partial \rho}{\partial t} - c\frac{\partial \rho}{\partial x} = D\frac{\partial^2 \rho}{\partial x^2} + r\rho(1 - \rho), \tag{5.90}$$

where

$$c = \frac{\langle z \rangle}{\overline{T}}, \quad D = \frac{\langle z^2 \rangle}{2\overline{T}}, \quad \overline{T} = \int_0^\infty t\phi(t)\mathrm{d}t, \quad \text{and} \quad \langle z^j \rangle = \int_{\mathbb{R}} z^j w(z)\mathrm{d}z. \tag{5.91}$$

The propagation velocity is obtained from (4.46), involving H and p. The critical condition, i.e., a stalled front, $v = 0$, is realized if $H(p^*) = 0$ with $p^* > 0$. Writing the Laplace transform $\hat{\phi}(H)$ as a power series of H, $\hat{\phi}(H) = 1 - \overline{T}H + \cdots$, and taking the limit $H \to 0$ in (5.30), we obtain $1 - \check{\psi}(0, p) - \overline{T}r^* = 0$, where $\check{\psi}$ is defined by (5.29). Differentiating (5.30) with respect to p and taking into account that $v = 0$ in (4.46), we find that the critical value of the momentum p is the solution of $\mathrm{d}\check{\psi}(0, p)/\mathrm{d}p = 0$. This results in the following simple form for the critical reaction rate,

$$r^* = \frac{1 - \check{w}(p^*)}{\overline{T}}, \tag{5.92}$$

with p^* such that

$$\left.\frac{\mathrm{d}\check{w}(p)}{\mathrm{d}p}\right|_{p=p^*} = 0, \tag{5.93}$$

and $\check{w}(p)$ is defined by (5.33). Note that the critical value r^* depends on the shape of the dispersal kernel and on the mean waiting time $\overline{T}$ only. This implies that two systems with identical dispersal kernels and different waiting times PDFs, but the same mean waiting time $\overline{T}$, will have the same r^*. Since $\check{w}(p) > 0$, the maximum value for r^* is $1/\overline{T}$. If $r = r^*$, front propagation fails. The front velocity is 0 due to the opposing effects of the reaction and jump processes. If $r > r^*$, $v > 0$ and the front moves from left to right. If $r < r^*$, $v < 0$ and the front moves from right to left. An interesting way to interpret (5.92) is as a balance or an equilibrium condition between parameters favorable (left-hand side) and unfavorable (right-hand side) to the invasion. However, there is another way to look at this relation. The product $\overline{T}r$ is a dimensionless quantity, namely the reaction–diffusion number. Equation (5.92) implies that $r > r^*$ is equivalent to $N_{\mathrm{GRD}} \equiv \overline{T}r + \check{w}(p^*) > 1$, where we have defined the generalized reaction–diffusion number N_{GRD}. If $N_{\mathrm{GRD}} > 1$, the front travels from left to right, $v > 0$. If $N_{\mathrm{GRD}} < 1$, the front travels from right to left, and if $N_{\mathrm{GRD}} = 1$ the front stalls and turns into a stationary spatial pattern, $v = 0$. If r is larger than the maximum possible value of r^*, then $v > 0$ and invasion always succeeds, no matter how large the opposing bias in the transport process. From (5.92), $\max(r^*) = 1/\overline{T}$, and we conclude that if $r > 1/\overline{T}$, i.e., the reaction rate is larger than the jump frequency, the front *always* propagates to the right, completely independent of the other statistical properties of the random walk.

We now prove that the diffusion approximation always underestimates r^*, $r^*_{\mathrm{dif}} < r^*$. To do so, it is sufficient to consider a small bias to the left such that

$$\int_{-\infty}^{0} w(x)\mathrm{d}x - \int_{0}^{\infty} w(x)\mathrm{d}x \equiv \epsilon, \tag{5.94}$$

and $0 < \epsilon \ll 1$. The normalization condition implies

$$\int_{-\infty}^{0} w(x)\mathrm{d}x + \int_{0}^{\infty} w(x)\mathrm{d}x = 1. \tag{5.95}$$

First, we determine the order of magnitude of the moments of $w(x)$. For $j = 1, 2, \ldots$ we can write

$$\langle x^j \rangle = \lim_{\ell \to \infty} \left[\int_{-\ell}^{0} x^j w(x) dx + \int_{0}^{\ell} x^j w(x) dx \right]$$

$$= \lim_{\ell \to \infty} \int_{0}^{\ell} x^j \left[w(x) + (-1)^j w(-x) \right] dx. \tag{5.96}$$

Using of the Mean Value Theorem for integrals and (5.95), we find

$$\langle x^{2j} \rangle = \lim_{\ell \to \infty} \int_{0}^{\ell} x^{2j} \left[w(x) + w(-x) \right] dx$$

$$= \xi_1^{2j} \lim_{\ell \to \infty} \int_{0}^{\ell} \left[w(x) + w(-x) \right] dx = \xi_1^{2j} \sim O(1), \tag{5.97}$$

and

$$\langle x^{2j-1} \rangle = \lim_{\ell \to \infty} \int_{0}^{\ell} x^{2j-1} \left[w(x) - w(-x) \right] dx$$

$$= \xi_2^{2j} \lim_{\ell \to \infty} \int_{0}^{\ell} \left[w(x) - w(-x) \right] dx$$

$$= -\xi_2^{2j-1} \epsilon \sim O(\epsilon), \tag{5.98}$$

for some ξ_1 and ξ_2 in $[0, \ell]$. The minus sign in (5.98) implies $\langle x^{2j-1} \rangle < 0$ and reflects that the random walk is biased to the left. As a result we can write

$$\check{w}(p) = \sum_{j=0}^{\infty} \frac{\langle x^j \rangle p^j}{j!}. \tag{5.99}$$

We break off the expansion at order $j = 3$, i.e., a small correction to the diffusion approximation, order $j = 2$,

$$\check{w}(p) = 1 + p\langle x \rangle + \frac{1}{2} p^2 \langle x^2 \rangle + \frac{1}{6} p^3 \langle x^3 \rangle, \tag{5.100}$$

and find

$$p^* = \frac{\langle x^2 \rangle}{\langle x^3 \rangle} \left(-1 + \sqrt{1 - 2 \frac{\langle x \rangle \langle x^3 \rangle}{\langle x^2 \rangle^2}} \right)$$

$$\simeq -\frac{\langle x \rangle}{\langle x^2 \rangle} \left(1 + \frac{1}{2} \frac{\langle x \rangle \langle x^3 \rangle}{\langle x^2 \rangle^2} \right) + O\left(\epsilon^4 \right), \tag{5.101}$$

where we have made use of (5.97) and (5.98) to calculate the series expansion. Substituting (5.101) into (5.100) and expanding according to (5.97) and (5.98), we obtain

$$\check{w}(p^*) = 1 - \frac{1}{2}\frac{\langle x \rangle^2}{\langle x^2 \rangle} - \frac{1}{6}\frac{\langle x \rangle^3 \langle x^3 \rangle}{\langle x^2 \rangle^3}. \tag{5.102}$$

As the condition for the critical reaction rate is $\overline{T}r^* = 1 - \check{w}(p^*)$, one has for the diffusion approximation

$$\overline{T}r_{\text{dif}}^* = \frac{1}{2}\frac{\langle x \rangle^2}{\langle x^2 \rangle} \tag{5.103}$$

and finally

$$\overline{T}r^* - \overline{T}r_{\text{dif}}^* = \frac{1}{6}\frac{\langle x \rangle^3 \langle x^3 \rangle}{\langle x^2 \rangle^3} > 0. \tag{5.104}$$

The last inequality results from the fact that the odd moments are negative. In conclusion, $r^* > r_{\text{dif}}^*$, i.e., the diffusion approach always *underestimates* the critical reaction rate.

We illustrate the theoretical results by considering a simple dispersal kernel $w(x)$ with an effective drift from right to left. There are two simple ways to introduce such a drift: (i) the probability of a jump to the left is greater than the probability of the same jump to the right or (ii) jumps to the right and left have the same probability but are of different length. Consider first a Dirac delta kernel, i.e., a dispersal kernel with fixed jump length, $w(x) = q\delta(x - a) + (1 - q)\delta(x + a), 0 < q < 1/2$. Using (5.92) and (5.103), we obtain

$$\overline{T}r^* = 1 - 2\sqrt{q(1 - q)}, \quad \overline{T}r_{\text{dif}}^* = \frac{1}{2}(1 - 2q)^2. \tag{5.105}$$

If $w(x) = \frac{1}{2}\delta(x - a_R) + \frac{1}{2}\delta(x + a_L)$, then

$$\overline{T}r^* = 1 - \frac{1}{2}\left[y^{-\frac{y}{1+y}} + y^{\frac{1}{1+y}}\right], \quad \overline{T}r_{\text{dif}}^* = \frac{(1 - y)^2}{4(1 + y^2)}, \tag{5.106}$$

where $0 < y = a_R/a_L < 1$. Next we consider an exponential distribution with different statistical characteristics for $x \geq 0$ and $x < 0$. Let $w(x)$ be $qe^{-x/a}/a$ for $x \geq 0$ and $(1 - q)e^{x/a}/a$ for $x < 0$. Then,

$$\overline{T}r^* = 1 - \frac{(1 - 2q)^2}{2 - 4\sqrt{q(1 - q)}}, \quad \overline{T}r_{\text{dif}}^* = \frac{1}{4}(1 - 2q)^2. \tag{5.107}$$

If $w(x)$ is $e^{-x/a_R}/(a_R + a_L)$ for $x \geq 0$ and $e^{x/a_L}/(a_R + a_L)$ for $x < 0$ then

$$\overline{T}r^* = \left(\frac{1-y}{1+y}\right)^2, \quad \overline{T}r^*_{\text{dif}} = \frac{(1-y)^2}{4\left(1-y+y^2\right)}. \quad (5.108)$$

To check these analytical results, one can perform numerical simulations that mimic the dispersal–reaction processes microscopically, for every biased form of $w(x)$ considered above, and find the critical value r^* at which wave propagation stalls. One can consider a one-dimensional lattice where dispersal and reaction processes take place starting from step-like initial conditions as in [67]. Instead of studying the evolution of a large number of individual particles, as is usually done, one can consider a continuous density of particles $\rho(x, t)$ for every cell in the lattice. For the case $w(x) = q\delta(x - a) + (1 - q)\delta(x + a)$ dispersal works in this way: a fraction q of the density $\rho(x, t)$ in a certain cell goes to the cell at $x + a$ and a fraction $1 - q$ goes to the cell at $x - a$. (For nondiscrete forms of $w(x)$ one must discretize the corresponding function.) After that, the reaction function is applied to each cell in the lattice. The time between successive steps in this scheme is equal to $\overline{T}$.

Panels in Fig. 5.2 show that the numerical simulations (open circles) are in excellent agreement with the analytical predictions (solid curves) given by (5.105),
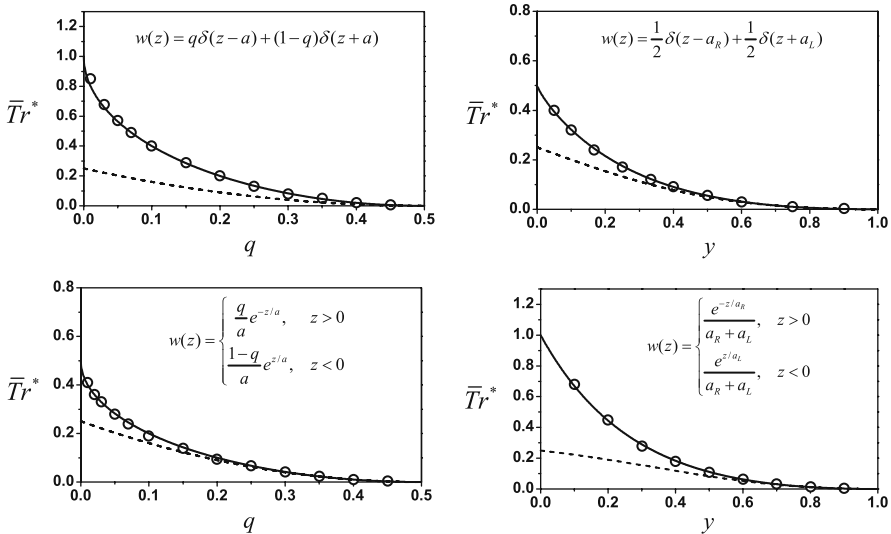
Fig. 5.2 The dimensionless critical reaction rate, calculated analytically (*solid lines*), obtained numerically (*circles*), and obtained from the diffusion approach, is plotted vs the dimensionless parameters q or y. Reprinted with permission from [286]. Copyright 2007 by the American Physical Society

(5.106), (5.107), and (5.108) for Dirac delta and exponential kernels. Moreover, the dashed curves correspond to the diffusion approximation and lie below the solid curves, in agreement with the general result given by (5.104).

In summary, the critical reaction rate r^* depends on the dispersal kernel and on the mean waiting time only, i.e., r^* does not depend on the shape of the waiting time PDF. If the reaction rate is larger than the jump frequency, the invasion front never fails, independent of the shape of the waiting time PDF, even if the dispersal kernel is maximally biased. Finally, the diffusion approximation always underestimates r^*.

Exercises

5.1 Consider the Lévy kernel

$$\hat{K}(H) = D\left[1 + (H\tau_0)^\gamma\right]^{-1} \tag{5.109}$$

with $0 < \gamma \leq 1$ for an RD equation with memory as given by (5.41). Calculate the front velocity invading the unstable state in terms of the Hamiltonian and show that there is no upper bound for the front velocity in the fast reaction limit.

5.2 Consider the waiting time PDF in Laplace space

$$\hat{\phi}(H) = e^{-(H\tau_0)^\gamma} \tag{5.110}$$

and the diffusion approximation for the jump PDF $\check{w}(p) \simeq 1 + \sigma^2 p^2/2$ in (5.27). Using the hyperbolic scaling and the Hamilton–Jacobi formalism show that the front velocity is given by

$$v = \frac{\sigma}{\sqrt{2\tau_0}} \min_{y>b} \frac{y^{3/2}}{\sqrt{y-b}\sqrt{e^{y^\gamma} - 1}}, \tag{5.111}$$

where $y = H\tau_0$ and $b = r\tau_0$. Study the behavior of this expression and show that $v = 0$, i.e., no propagating front invades the unstable state. In [283] the conditions for propagation failure in Model C with KPP kinetics are studied in detail.

5.3 The Laplace dispersal jump PDF

$$w(x) = \frac{1}{2\alpha_0} e^{-|x|/\alpha_0} \tag{5.112}$$

is widely used in ecological models for animal invasions. Consider the continuous-time model with long-range dispersal (5.2) and show that the velocity of the front invading the unstable state is given by the exact formula

$$v = \frac{\alpha_0 \sqrt{2}}{\tau_0} \frac{(1-b)^{3/2}}{\left(\sqrt{1+8b} - 1 - 2b\right)^{1/2}} \frac{\sqrt{1+8b} - 1}{3 - \sqrt{1+8b}}, \qquad (5.113)$$

where $\tau_0 = \lambda^{-1}$ and $b = \tau_0 r$.

5.4 Consider the reaction-telegraph equation (5.48) in one dimension. Show that the Hamilton–Jacobi equation is given by

$$\tau_0 H^2 + (1 - r\tau_0)H = Dp^2 + r, \qquad (5.114)$$

and show that the velocity of the front invading the unstable state is given by

$$v = \begin{cases} 2\sqrt{rD}/\left(1 + r\tau_0\right), & r\tau_0 < 1, \\ \sqrt{D/\tau_0}, & r\tau_0 \geq 1. \end{cases} \qquad (5.115)$$

5.5 Consider (3.137) for Model B with branching-coalescence kinetics, where the birth rate is $f^+(\rho) = r$ and the death rate is $f^-(\rho) = r\rho$. Show that the Hamilton–Jacobi equation is given by

$$H = \sigma^2 p^2 \hat{K}(H) + r. \qquad (5.116)$$

Chapter 6
Reaction–Diffusion Fronts in Complex Structures

Most systems in nature are heterogeneous. Porous media, fractals, random or fluctuating environments, and ecological patchiness are only a few examples. Homogeneous media are, in fact, an idealization. In this chapter we discuss how fronts propagate in these more complex structures. Our main goal is to present various techniques that allow us to calculate the front velocity. When the heterogeneity is weak, we can employ perturbative methods, but in most cases only the Hamilton–Jacobi method works effectively in the large-time limit.

6.1 Diffusion on Fractals

Fractals can be defined in two different ways. The first definition considers a fractal to be a structure that is self-similar at any scale. The second definition considers a fractal to be a structure with a noninteger Hausdorff dimension. Let M be the fractal mass, i.e., the number of points of the fractal. If the mass density is constant, the mass is proportional to the fractal volume. The latter is proportional to L^{d_f}, where L is the fractal length and d_f the Hausdorff, or fractal, dimension. Both definitions are equivalent; the power-law relation for the fractal mass $M \sim L^{d_f}$ satisfies the self-similarity condition, as is easily verified.

As far as transport properties of a fractal structure are concerned, the mean square displacement (MSD) of a particle follows a power law, $\langle r^2 \rangle \sim t^{2/d_w}$, where r is the distance from the origin of the random walk and d_w is known as the random walk dimension. In other words, diffusion on fractals is anomalous, see Sect. 2.3. Recall that for normal diffusion in three-dimensional space the MSD is given by $\langle r^2 \rangle = 6Dt$. For fractals, $d_w \geq 2$, and the exponent of t in the MSD is smaller than 1. We introduce a dimensionless distance by dividing r by the typical diffusive length $\sqrt{\langle r^2 \rangle}$ and find $r/\sqrt{\langle r^2 \rangle} \sim rt^{-1/d_w}$. Diffusive transport on fractals displays two different regimes. The first one corresponds to the asymptotic regime, where the particles are at large distances from the origin, i.e., $r \gg \sqrt{\langle r^2 \rangle}$ and $rt^{-1/d_w} \gg 1$. The second one corresponds to the opposite limit, where the particles are very

close to the origin compared to the typical diffusive length scale, $r \ll \sqrt{\langle r^2 \rangle}$ and $rt^{-1/d_w} \ll 1$. Bunde and Dräger pointed out that the relevant physical length for diffusive transport is the chemical distance [62]. Given two points on the fractal structure, the chemical distance l is defined as the shortest distance on the fractal from one point to the other. We illustrate this idea in Fig. 6.1 for the Sierpinski gasket. The Euclidean or radial distance between the points a and a' is r, while the chemical distance is $l = l_1 + l_2 + l_3$.
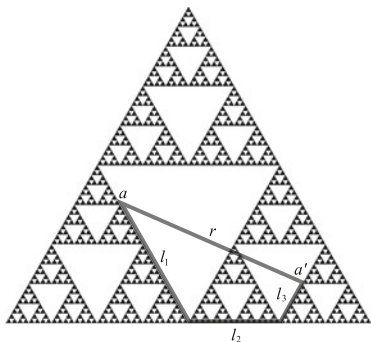
Fig. 6.1 Comparison between the chemical distance l and the Euclidean distance r for a Sierpinski gasket

The chemical and Euclidean distances are related by

$$l \sim r^{d_{\min}}, \tag{6.1}$$

where $d_{\min}$ is the fractal dimension of the shortest path between two given points in the fractal.

The derivation of the functional form for the probability distribution function (PDF) $P(r, t)$ for diffusion on fractals, i.e., the probability that a particle or individual is at a distance r from the origin at time t, has been a challenge. The geometry of fractals causes local and global diffusion to behave in different ways. For most applications we need to know only how the particles move at global scales. Here the homogenization properties of fractals become important. Due to the "restoration of isotropy," the averaged global diffusion behaves like Brownian motion, which allows us to define a proper averaged PDF in the asymptotic regime. Scaling arguments and computer simulations lead to the following form for this averaged PDF:

$$P(r, t) \sim t^{-d_f/d_w} \exp\left[-c \left(\frac{r}{t^{1/d_w}} \right)^{\frac{d_w}{d_w - 1}} \right], \tag{6.2}$$

where c is a constant. Mosco considered an alternative approach and introduced an intrinsic metric for fractals, defined by the relation

$$s \equiv r^{d_w/2}, \tag{6.3}$$

where s and r are the intrinsic and Euclidean distances, respectively [306]. The importance of this formalism lies in the fact that it incorporates the anomalous dynamics of fractals into the metric and therefore provides an ideal framework to describe phenomena that occur in the usual Euclidean space for nonfractal systems. Mosco [306] obtained the following expression for the PDF:

$$P(r, t) \sim t^{-d_f/d_w} \exp\left[-c \left(\frac{r}{t^{1/d_w}} \right)^{\frac{d_w d_{\min}}{d_w - d_{\min}}} \right]. \tag{6.4}$$

Equation (6.4) is a generalization of the usual form (6.2), which is recovered in the case $d_{\min} = 1$ or by averaging in the appropriate regime, as shown both theoretically and by simulations.

We have left an important question open at this point. What is the appropriate diffusion equation for transport on a fractal? One of the first attempts at an answer was due to O'Shaughnessy and Procaccia [331], before (6.2) and (6.4) had been derived. They based their derivation on the continuity equation

$$\frac{\partial P(r, t)}{\partial t} + \frac{1}{r^{d_f-1}} \frac{\partial J(r, t)}{\partial r} = 0 \tag{6.5}$$

and the constitutive equation for the particle flux

$$J(r, t) = -D(r) r^{d_f-1} \frac{\partial P(r, t)}{\partial r} \tag{6.6}$$

and obtained

$$\frac{\partial P}{\partial t} = \frac{1}{r^{d_f-1}} \frac{\partial}{\partial r} \left[D(r) r^{d_f-1} \frac{\partial P}{\partial r} \right], \tag{6.7}$$

where $D(r) = D^* r^{2-d_w}$ is the diffusion coefficient, or conductivity, on fractals. The exact solution for this equation is known. Its second moment behaves like t^{2/d_w}, but lacks the scaling (6.4).

To address this issue, generalizations were proposed by different authors. For example, Giona and Roman took into account memory effects [161]. They replaced (6.5) and (6.6) by

$$\int_0^t dt' \Omega(t - t') P(r, t') = \frac{1}{r^{d_f-1}} \int_0^t dt' J(r, t') \tag{6.8}$$

for the continuity equation and

$$J(r, t) = -D(r) \left[\frac{\partial P}{\partial r} + \frac{d_f - 1}{2} P(r, t) \right] \tag{6.9}$$

for the constitutive equation for the flux. Equation (6.8) implies that the particle density flux J at position r is equal to the probability of being at this point at a prior time t' multiplied by the probability Ω of moving for a period $t - t'$ and integrated over the whole history. Assuming a power law for the memory kernel, $\Omega(t) \sim t^{-1/d_w}$, and the diffusion coefficient, $D(r) \sim r^{d_f - 1}$, and combining (6.8) and (6.9), we obtain

$$\mathcal{D}_t^{1/d_w} P(r, t) = -A \left[\frac{\partial P}{\partial r} + \frac{d_f - 1}{2} P(r, t) \right], \tag{6.10}$$

where A is a constant. The left-hand side of (6.10) contains a fractional derivative as defined in (2.58). The exact solution of (6.10) is also known and yields again the behavior $\langle r^2 \rangle \sim t^{2/d_w}$. However, it also lacks the scaling of (6.4), except for $d_{\min} = 1$.

The idea of introducing fractional derivatives in diffusion equations to account for long-range memory effects has given rise to a large number of publications. In this context, the work by Metzler, Glöckle, and Nonnenmacher is noteworthy [297]. They realized that (6.10) suffers from a pathological defect: For $d_f = 1$ and $d_w = 2$ one should recover the standard diffusion equation; however, this is not the case. To overcome this difficulty they propose

$$\mathcal{D}_t^{2/d_w} P(r, t) = \frac{1}{r^{d_f - 1}} \frac{\partial}{\partial r} \left(D(r) r^{d_f - 1} \frac{\partial P}{\partial r} \right) \tag{6.11}$$

with $D(r)$ as in (6.7). However, as in the previous case, the solution still lacks the scaling of (6.4), except for the case $d_{\min} = 1$.

Recently Campos, Méndez, and Fort (CMF) have proposed a new equation that overcomes all these difficulties and is derived without the need to introduce ad hoc fractional derivative operators to obtain anomalous diffusion [66]. The authors assume that the procedure by O'Shaughnessy and Procaccia can be adapted directly to the intrinsic metric of the fractal by writing the equation in terms of s and d_S instead of r and d_f:

$$\frac{\partial P(s, t)}{\partial t} = \frac{1}{s^{d_S - 1}} \frac{\partial}{\partial s} \left[D(s) s^{d_S - 1} \frac{\partial P(s, t)}{\partial s} \right], \tag{6.12}$$

where $d_S = 2 d_f / d_w$ is the mass scaling exponent in the intrinsic metric. (See [306] for the equivalence relation between the Euclidean and intrinsic metric.) This approach has the advantage that the undesirable dynamical consequences from the fractal nature, which prevented previous models from producing the

expected results, are now absorbed into the intrinsic metric [306]. The approach by O'Shaugnessy and Procaccia [331] can account for the fractional geometric properties of fractals, but not completely for their fractional dynamic properties, since the parameter d_w does not appear there. Mosco's idea of an intrinsic metric provides an alternative that is more suitable to deal with diffusion processes on fractals.

Equation (6.12) faces one main difficulty, namely the determination of the explicit functional form of $D(s)$. It is important to stress that $D(s)$ does not have exactly the same properties as the classical diffusion coefficient, and we refer to it here as the conductivity. Likewise, we define the resistivity of the medium as $R = 1/D$. We expect the resistivity to be proportional to the number of steps of the particle, and arguments from random walks on fractals should be useful to determine R. Walks on fractals are characterized by the existence of two scales. Divide the medium into small blocks of size ξ, such that the diffusion is normal within the small blocks, $\xi^2 \sim t$. At scales larger than ξ, the effect of the heterogeneities becomes important, and motion depends on the fractal parameters. The self-invariance properties of the fractal are not valid at short distances. Similarly, the idealized concept of self-similarity at all scales does not hold for fractals in practice.

For large scales s, the number of blocks n crossed by walkers increases as $n \sim (s^2/t)^\gamma$, where $\gamma = d_{min}^S/(2 - d_{min}^S)$ and $d_{min}^S = 2d_{min}/d_w$ is the equivalent of d_{min} for the intrinsic metric [306]. In the asymptotic regime, the number of steps executed by the walker is proportional to the number n of blocks crossed, and we expect that $R \sim n$. This result must be renormalized to recover the limiting case of constant resistivity for homogeneous media. We have to divide n by the number of blocks n_{hom} for diffusion in homogeneous media. Therefore $R \sim n/n_{hom} \sim (s^2/t)^\gamma/(s^2/t) = (s^2/t)^{\gamma-1}$, and

$$D(s) = D_0(s^2/t)^{1-\gamma} \tag{6.13}$$

for the conductivity, where D_0 is a constant. The time dependence of D arises from the existence of two separate scales and the relation between them. Brownian random walks, namely normal diffusion, take place for small scales. We are concerned with the transport behavior on large, asymptotic scales and must take into account the dual behavior. The idea of a time-dependent conductivity was proposed previously for specific systems involving heterogeneous media [190]. To confirm the validity of (6.13), numerical simulations for random walks on two-dimensional percolation clusters were performed [66]. To keep r and s fixed, a circle of a certain radius from the origin of the walk was chosen, and the flux of particles and the spatial derivative of the density at that radius were measured as a function of time. The results of the simulations are shown in Fig. 6.2. They yield $D \sim t^{-0.33\pm0.04}$, in good agreement with the known exponent of the power law for percolation clusters, $\gamma - 1 = \frac{d_{min}}{d_w-d_{min}} - 1 = -0.35 \pm 0.01$. The results obtained for simulations in homogeneous media (solid circles) show that the diffusion coefficient is constant as expected. The small discrepancy, and the error estimate given above, is due to
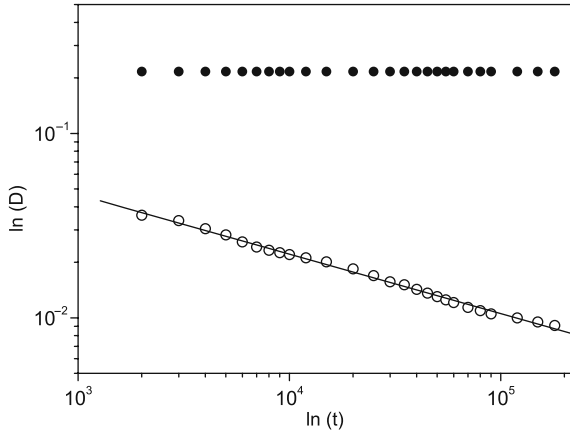
Fig. 6.2 Time dependence of the diffusion coefficient for a percolation cluster on a square lattice (*open circles*). The slope of the linear fit is -0.33 ± 0.04. *Solid circles* represent the diffusion coefficient for homogeneous media. Reprinted with permission from [66]. Copyright 2004 by the American Physical Society

the fact that the spatial derivative is difficult to estimate exactly from discretized simulations. We substitute (6.13) into (6.12) and find the point-source solution for the PDF:

$$P(s,t) \sim t^{-\frac{d_S}{2}} \exp\left[-c\left(\frac{s^2}{t}\right)^{\gamma}\right], \tag{6.14}$$

where we have used the normalization condition $\int P(s,t) \mathrm{d}(s^{d_s}) = 1$. This expression is exactly the same as (6.4), the expression which Mosco obtained using only scaling arguments. Since $r \equiv s^{2/d_w}$, the corresponding equation in Euclidean space for the diffusive flux is

$$J(r,t) = \frac{4D_0}{d_w^2}\left(\frac{r}{t^{1/d_w}}\right)^{d_w - u} r^{d_f - d_w + 1} \frac{\partial P(r,t)}{\partial r}. \tag{6.15}$$

Combining this constitutive equation with the continuity equation (6.5), we obtain the CMF equation:

$$\frac{\partial P(r,t)}{\partial t} = \frac{4D_0}{d_w^2 r^{d_f - 1}} \frac{\partial}{\partial r}\left[\left(\frac{r}{t^{1/d_w}}\right)^{d_w - u} r^{d_f - d_w + 1} \frac{\partial P(r,t)}{\partial r}\right], \tag{6.16}$$

where $u = d_w d_{min}/(d_w - d_{min})$. The exact solution of (6.16) in the asymptotic limit is (6.4). The MSD is given by

$$\langle r^2 \rangle (t) = \int r^2 \mathrm{d}(r^{d_f}) P(r,t) = \frac{\Gamma\left(\frac{2+d_f}{u}\right)}{\Gamma\left(\frac{d_f}{u}\right)} \left(\frac{4u D_0}{d_w}\right)^{2/u} t^{2/d_w}, \qquad (6.17)$$

i.e., the transport is subdiffusive.

6.2 Reaction–Diffusion Fronts on Fractals

In the previous section we presented some of the equations proposed in the literature for describing diffusion on fractal structures. These equations must meet three requirements to be considered valid. First, the MSD must display subdiffusion, $\langle r^2 \rangle \sim t^{2/d_w}$. Second, the PDF $P(r,t)$ must agree with the scaling form (6.4). Third, the equation has to recover the form of the standard diffusion equation for $d_w = 2$, $d_f = 1$, and $d_{\min} = 1$. We have shown that only the CMF equation (6.16) meets all three requirements. As expected, this result remains true for the description of front propagation on fractals.

Following the argument by Bunde and Dräger [62], front propagation is well defined in the chemical distance space. The front has to propagate with constant velocity, i.e., the front position in the chemical distance space behaves like $l \sim t$. Euclidean and chemical distances are related by (6.1). The front position in real (Euclidean) space behaves like $r \sim l^{1/d_{\min}} \sim t^{1/d_{\min}}$ and [33]

$$v = \frac{\mathrm{d}r}{\mathrm{d}t} \sim t^{\frac{1}{d_{\min}} - 1}. \qquad (6.18)$$

Since $d_{\min} \geq 1$, the front is always decelerated. Clearly, the models that do not explicitly consider $d_{\min}$ cannot fulfill the scaling law (6.18) for the front velocity on a fractal; only the CMF equation can satisfy (6.18). To obtain the CMF equation with reaction, we combine the constitutive equation for the flux (6.15) with the conservation equation for the particle density ρ:

$$\frac{\partial \rho}{\partial t} + \frac{1}{r^{d_f - 1}} \frac{\partial J}{\partial r} = F(\rho), \qquad (6.19)$$

where $F(\rho)$ is a particle source term. The phenomenological reaction-CMF equation with KPP kinetics, $F(\rho) = a\rho(1 - \rho)$, reads

$$\frac{\partial \rho}{\partial t} = \frac{4D_0}{d_w^2 r^{d_f - 1}} \frac{\partial}{\partial r} \left[\left(\frac{r}{t^{1/d_w}}\right)^{d_w - u} r^{d_f - d_w + 1} \frac{\partial \rho}{\partial r} \right] + a\rho(1 - \rho), \qquad (6.20)$$

where a denotes, in this section, the reaction rate. We employ the Hamilton–Jacobi formalism introduced in Sect. 4.2.1 for homogeneous media. Performing the hyperbolic scaling (4.33) and introducing the field $G^\varepsilon(r,t) = -\varepsilon \ln \rho(r/\varepsilon, t/\varepsilon)$, we obtain the Hamilton–Jacobi equation for (6.20),

$$\frac{\partial G}{\partial t} + \frac{4D_0}{d_w^2}\varepsilon^{-\frac{u}{d_w}+u-1}t^{\frac{u}{d_w}-1}r^{-u+2}\left(\frac{\partial G}{\partial r}\right)^2 + a = 0 \qquad (6.21)$$

in the limit $\varepsilon \to 0$. Equation (6.21) can be solved by using the Hamilton equations

$$\frac{dr(\tau)}{d\tau} = \frac{8D_0}{d_w^2}\varepsilon^{-\frac{u}{d_w}+u-1}\tau^{\frac{u}{d_w}-1}r(\tau)^{-u+2}p(\tau), \qquad (6.22a)$$

$$\frac{dp(\tau)}{d\tau} = -\frac{4D_0}{d_w^2}(2-u)\varepsilon^{-\frac{u}{d_w}+u-1}\tau^{\frac{u}{d_w}-1}r(\tau)^{-u+1}p^2(\tau). \qquad (6.22b)$$

Integrating the system (6.22) with the boundary conditions $r(0) = 0$ and $r(t) = x$, we find $r(\tau) = x(\tau/t)^{2/d_w}$, and the Lagrangian is given by

$$L(x,\tau) = \frac{1}{4D_0}\varepsilon^{\frac{u}{d_w}-u+1}x^u\tau^{\frac{u}{d_w}-1}t^{-\frac{2u}{d_w}} - a. \qquad (6.23)$$

From (4.39) we obtain

$$G(x,t) = \frac{d_w\varepsilon^{\frac{u}{d_w}-u+1}x^u t^{-\frac{u}{d_w}}}{4D_0 u} - at. \qquad (6.24)$$

Inverting the hyperbolic scaling in (6.24), by taking $x \to \varepsilon x$ and $t \to \varepsilon t$, and solving $G(x,t) = 0$, we arrive at

$$v(t) = \frac{dx}{dt} = \left(\frac{1}{u} + \frac{1}{d_w}\right)\left(\frac{u}{d_w}\right)^{1/u}(4rD_0)^{\frac{1}{u}}t^{\frac{1}{d_w}-1+\frac{1}{u}} \sim t^{\frac{1}{d_{\min}}-1}. \qquad (6.25)$$

The reaction-CMF equation predicts a front velocity with the appropriate scaling (6.18).

6.3 Reaction–Transport Fronts on Comb Structures

Lattice models and other discrete models are used to describe a wide variety of dynamical systems [270, 77]. In this section we study the propagation of reaction-random walk wavefronts on heterogeneous lattices that consist of a main backbone with a regular distribution of secondary branches. An example is comb-like structures, see Fig. 6.3 [53].

6.3.1 Comb-Like Structures

We first consider the case of a discrete one-dimensional chain where the nearest neighbors are separated by a distance a. A random walk, where each walker moves
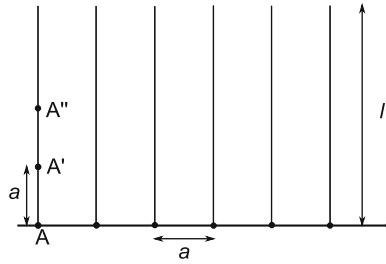
Fig. 6.3 Sketch of a comb structure with a nearest neighbor distance a and secondary branches of length l. The symbols $A, A', A'', \ldots$ denote sites on the lattice (see text)

only to one of its nearest neighbors with equal probability after a fixed waiting time τ, is characterized by the following PDFs for the waiting times and jump lengths, respectively:

$$\phi(t) = \delta(t - \tau), \tag{6.26}$$

$$w(x) = \frac{1}{2}\left[\delta(x - a) + \delta(x + a)\right]. \tag{6.27}$$

In this way, systems with discrete time and space can be analyzed in terms of CTRWs.

Next, we add to every site of the backbone a secondary branch of length l, to produce a comb-like structure (see Fig. 6.3). On such a structure, a walker that is at a given site of the backbone can spend a certain amount of time in the secondary branch before jumping to one of the nearest neighbor sites on the backbone. If we are only interested in the behavior of the system in the direction of the backbone, then the secondary branches introduce a delay time for jumps between the neighboring sites on the backbone. The random walk on the comb structure can be modeled as a CTRW with (6.27) and a new waiting PDF $\phi(t)$ that includes the effect of the delay due to the secondary branches.

To determine analytically the effect of the branches, we invoke convolution rules that were introduced in [446] for the case of homogeneous lattices:

(i) Consider a walker that is initially at a certain site within the secondary branch. If the walker proceeds further into the secondary branch, i.e., moves away from the backbone, its probability to return to the initial site after a time t is a convolution of factors, i.e., a product in the Laplace space.

(ii) The total probability for that walker to return to the initial site is determined by summing over all t from 0 to ∞.

(iii) When the walker reaches a crossing, where it can choose between different directions, the total probability is the sum of the probabilities for each possible direction.

The secondary branches have no crossings for comb structures such as the one shown in Fig. 6.3, and rule (iii) does not apply. For the sake of generality, we consider the case that when the walker is at a site on the backbone it can jump to another site on the backbone with probability α or move onto the secondary branch with probability $1 - \alpha$. This generalization allows us to analyze, for example, structures as those shown in Fig. 6.4, treating them as equivalent to that in Fig. 6.3 by choosing an appropriate value for α.
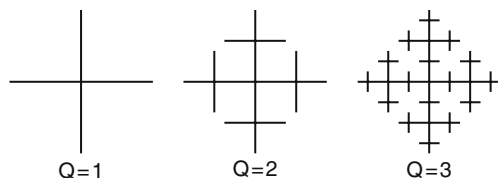
Fig. 6.4 The first three construction levels of the Peano fractal basin

Without loss of generality, we assume that initially the walker is located on the backbone and we apply the rules (i)–(iii) to determine $\phi(t)$. We study three specific cases.

(a) *Comb structure with $l = a$.* In this case there is only one site on the secondary branch, A'. The walker can only jump in the direction of the backbone with probability α or move onto the branch with probability $1 - \alpha$ and then return to the initial site at the next jump. The time it takes to reach one of the nearest neighbors on the backbone is $t = \tau$ with probability α, $t = 3\tau$ with probability $(1 - \alpha) \times 1 \times \alpha$, $t = 5\tau$ with probability $(1 - \alpha)^2 \times 1^2 \times \alpha$, and so on. We can write intuitively the general form $\phi(t)$ as

$$\phi(t) = \sum_{j=1}^{\infty} \alpha (1 - \alpha)^{j-1} \delta \left[t - (2j - 1)\,\tau \right]. \tag{6.28}$$

The rules listed above for $\phi(t)$ should reproduce this behavior. For this purpose we need to work in the Laplace space. Let $\hat{\phi}(s)$ be the Laplace transform of $\phi(t)$. The rules (i)–(iii) lead to the expression

$$\hat{\phi}(s) = \alpha \hat{\phi}_0 \sum_{j=0}^{\infty} \left[(1 - \alpha) \hat{\phi}_0^2 \right]^j = \frac{\alpha \hat{\phi}_0}{1 - (1 - \alpha) \hat{\phi}_0^2}, \tag{6.29}$$

where $\hat{\phi}_0$ is the probability distribution for a single jump, $\hat{\phi}_0 = e^{-\tau s}$, which is the Laplace transform of (6.26).

Equation (6.29) is derived as follows. The term $(1 - \alpha) \hat{\phi}_0^2$ in the sum represents, according to rule (i), the probability function for each occurrence of the walker moving onto the secondary branch. This expression must be summed up to infinity, rule (ii), to take into account that the walker can move onto the secondary branch

$1, 2, \ldots, \infty$ times. The factor $\alpha\hat{\phi}_0$ accounts for the final jump to the nearest neighbor on the backbone.

It is easy to see that the expression (6.29) may be written as a Taylor series,

$$\hat{\phi}(s) = \sum_{j=1}^{\infty} \alpha(1-\alpha)^{j-1} \left(\hat{\phi}_0\right)^{2j-1}, \tag{6.30}$$

which is the Laplace transform of (6.28). The method for determining $\hat{\phi}(s)$ is shown to be valid in this case.

(b) *Comb structure with $l = 2a$.* The secondary branch is two-sites long, A' and A''. Similar to the previous case we can write the distribution for the time probabilities as

$$\hat{\phi}(s) = \alpha\hat{\phi}_0 \sum_{j=0}^{\infty} \left[\frac{(1-\alpha)}{2} \hat{\phi}_0^2 \sum_{k=0}^{\infty} \left(\frac{1}{2}\hat{\phi}_0^2 \right)^k \right]^j = \frac{\alpha\hat{\phi}_0(2 - \hat{\phi}_0^2)}{2 - (2-\alpha)\hat{\phi}_0^2}. \tag{6.31}$$

In this equation a new sum over the index k appears, because the walker can move away from the backbone twice. For each such occurrence we must apply rule (i). We also assume that jumps to the nearest neighbor occur with probability $1/2$ on the linear secondary branch.

(c) *Comb structure with $l \to \infty$.* Each time the walker moves away from the backbone, a new convolution factor appears in $\hat{\phi}(s)$. For the case $l \to \infty$, we have in principle infinitely many convolution factors in the expression for $\hat{\phi}(s)$. Fortunately, we can simplify this situation considerably. Assume that the walker is at the first site on the secondary branch, point A' in Fig. 6.3, and moves away from the backbone. Let $\eta_{A'}$ be the probability distribution of returning for the first time to the point A' after a time t. Now imagine the same situation but for the initial point A''. It is easy to see that as $l \to \infty$ the limit $\eta_{A''} \to \eta_{A'}$ has to hold, and we can again use the rules (i)–(iii) to determine $\eta_{A'}$. Doing so, we obtain the expression

$$\eta_{A'} = \frac{1}{2}\hat{\phi}_0 \sum_{j=0}^{\infty} \left(\frac{1}{2}\hat{\phi}_0\eta_{A''} \right)^j. \tag{6.32}$$

This expression is equivalent to the form (6.29) with $\alpha = 1/2$; on the secondary branch every jump to a nearest neighbor occurs with probability $1/2$. Introducing the condition $\eta_{A''} = \eta_{A'}$, which is strictly correct for $l = \infty$, and solving (6.32), we find

$$\eta_{A'} = \frac{1 - \sqrt{1 - \hat{\phi}_0^2}}{\hat{\phi}_0}. \tag{6.33}$$

With this result, the distribution $\hat{\phi}(s)$ is obtained straightforwardly from the three rules (i)–(iii):

$$\hat{\phi}(s) = \alpha\hat{\phi}_0 \sum_{j=0}^{\infty}\left[(1-\alpha)\hat{\phi}_0\eta_{A'}\right]^j = \frac{\alpha\hat{\phi}_0}{\alpha + (1-\alpha)\sqrt{1-\hat{\phi}_0^2}}. \tag{6.34}$$

In finding the waiting time PDF associated with the comb structures, we assumed that we are only interested in the dynamical behavior along the backbone and considered the rest of the structure as secondary. Another interesting structure, the well-known Peano basin, shown in Fig. 6.4 as a function of the construction level Q, has been used to model fractal river basins [64]. Again, if we are only interested in the behavior in the direction of the backbone, then for $Q = 1$ the waiting time distribution function is given by

$$\hat{\phi}(s) = \frac{1}{2}\hat{\phi}_0 \sum_{j=0}^{\infty}\left(\frac{1}{2}\hat{\phi}_0^2\right)^j = \frac{\hat{\phi}_0}{2 - \hat{\phi}_0^2}. \tag{6.35}$$

Similarly, for $Q = 2$ we find

$$\hat{\phi}(s) = \frac{1}{2}\hat{\phi}_0 \sum_{j=0}^{\infty}\left[\frac{1}{2}\frac{\hat{\phi}_0^2}{4}\sum_{k=0}^{\infty}\left(\frac{\hat{\phi}_0^2}{2} + \frac{\hat{\phi}_0^2}{4}\right)^k\right]^j = \frac{4\hat{\phi}_0 - 3\hat{\phi}_0^3}{8 - 7\hat{\phi}_0^2}, \tag{6.36}$$

where we have used $\alpha = 1/2$, i.e., the same jump probability in all directions.

6.3.2 Diffusion and Front Propagation

6.3.2.1 Diffusion

To characterize diffusion on these structures, we calculate the MSD using the CTRW formalism with the waiting time PDFs (6.29), (6.31), (6.34), (6.36), and the dispersal PDF (6.27). In Laplace–Fourier space, the MSD reads

$$\widehat{\langle x^2\rangle}(s) = -\left.\frac{d^2\hat{\bar{\rho}}(k,s)}{dk^2}\right|_{k=0} = \frac{\hat{\phi}(s)a^2}{s\left[1 - \hat{\phi}(s)\right]}. \tag{6.37}$$

Substituting (6.29) and (6.31) into (6.37), we find for cases (a) and (b) $\langle x^2\rangle(t) = 2D_{(a),(b)}t$ in the limit $t \to \infty$, with

$$D_{(a)} = \frac{\alpha a^2}{2\tau(2-\alpha)}, \quad D_{(b)} = \frac{\alpha a^2}{2\tau(4-3\alpha)}. \tag{6.38}$$

Introducing (6.34) into (6.37), we find anomalous diffusion in the limit $t \to \infty$ for case (c):

$$\langle x^2 \rangle (t) = \sqrt{\frac{2}{\pi} \frac{\alpha a^2}{1 - \alpha}} \left(\frac{t}{\tau} \right)^{1/2}. \tag{6.39}$$

6.3.2.2 Front Propagation

Front propagation in heterogeneous media has recently received much attention due to the potential applications. Some examples are reaction–diffusion equations in periodic and random media [483], spatial heterogeneities [290], temporal heterogeneities [289], and biological invasions in ecological patchy environments [403–405]. Computer simulations of heterogeneous models have also been used to describe the dynamics of brain tumors [427], the formation of Alzheimer's disease senile plaques [105], and calcium release waves [225, 367]. In Chap. 5 we obtained the Hamilton–Jacobi equation for reaction–transport equations, derived from the CTRW formalism, with a KPP reaction term such as $F(\rho) = r\rho(1-\rho)$. Introducing the bilateral transform of the dispersal kernel (6.27), $\breve{w}(p) = \cosh(ap)$, into (5.30), we obtain from (4.46) the following expression for the front velocity across the comb structure:

$$v = \min_{H > r} \frac{H}{\cosh^{-1} \left[\frac{1}{\breve{\phi}(H)} \left(1 - \frac{r}{H} \right) + \frac{r}{H} \right]}. \tag{6.40}$$

We plot in Fig. 6.5 the dimensionless front velocity $v\tau/a$ vs the reaction rate r on a log–log scale. The front velocity increases with r. For the cases $l = a$ and $l = 2a$, the slope is very similar, but for $l = \infty$ it is steeper. In all cases the front velocity increases as a power law of r, straight line in a log–log plot, for small and moderate values of r and saturates to 1 for larger values, the slope in the log–log plot tends to 0. This behavior is due to the fact that an increase of the reaction rate r leads to an increase of the front velocity. However, the front cannot travel faster than the jump velocity of the particles if all of them jump in the backbone direction, i.e., $v \le a/\tau$. For $l = a$ and $l = 2a$ the transport is diffusive, and the diffusion coefficient is properly defined. If this transport is combined with a KPP reaction, a Fisher velocity is expected, i.e., in both cases $v \sim \sqrt{r}$. Computing numerically the slope from a linear fit in Fig. 6.5 we obtain $r^{0.48}$ and $r^{0.51}$ for $l = a$ and $l = 2a$, respectively. The case $l \to \infty$ is quite different, because the transport is anomalous. Equation (5.36) with $\gamma = 1/2$ yields $v \sim r^{3/4}$, while the linear fit of the numerical results yields $r^{0.71}$. Numerical and analytical results are in good agreement.
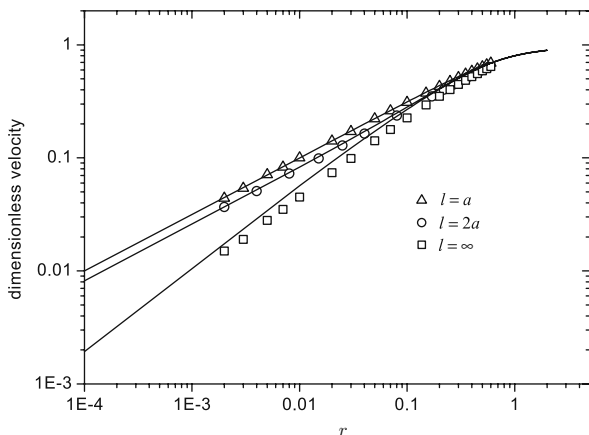
Fig. 6.5 Comparison of the front velocity across the comb structure obtained from (6.40) (*lines*) and from the simulations within the comb structures (*symbols*) as function of the reaction parameter r for the three cases studied here. $\alpha = 2/3$

6.3.3 Front Propagation on Oriented Graphs

Oriented graphs are graphs where the edges connecting the nodes have a direction, so-called directed graphs that have no symmetric pair of directed edges. Reaction-random walks on such structures were studied recently and applied to describe migration fronts through river networks [46]. In this section we outline how to calculate the front velocity on Peano networks from CTRWs with reactions. The walker sojourns for a time τ at a node. Then the walker jumps from that node to one of its adjacent nodes with a certain probability. The adjacent nodes are comprised of all the nodes that are connected to a node by an inward or outward edge. Let P_{out} (P_{in}) be the probability that a particle moves from a node to an adjacent node along an outward (inward) edge. We assume that all particles move at each time step, $P_{\text{out}} + P_{\text{in}} = 1$. If each node has d_{out} outward edges and d_{in} inward edges, then the probability P_{ij} for a particle to jump from the node i to one of its neighbors j can be expressed as

$$P_{ij} = \frac{P_{\text{out}}}{d_{\text{out}}(i) P_{\text{out}} + d_{\text{in}}(i) P_{\text{in}}}, \quad i \to j, \tag{6.41a}$$

$$P_{ij} = \frac{P_{\text{in}}}{d_{\text{out}}(i) P_{\text{out}} + d_{\text{in}}(i) P_{\text{in}}}, \quad j \to i, \tag{6.41b}$$

with

$$\sum_{j=1}^{d_{\text{out}}(i) + d_{\text{in}}(i)} P_{ij} = 1. \tag{6.42}$$

The bias of the transport through the network can be defined as $b = P_{out} - P_{in} = 2P_{out} - 1$. We focus on an oriented Peano network at the first level of construction. Figure 6.6 shows this network, where the segment AB is the backbone direction.
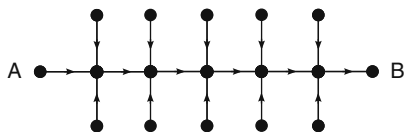
Fig. 6.6 Peano network at the first level of its construction process. The *arrows* show the edge direction. The *line* indicated as *AB* is the backbone direction

The probabilities that a particle, starting from any node on the backbone, jumps to its downstream neighbor or to one of its three upstream neighbors are, respectively,

$$P_+ = \frac{P_{out}}{P_{out} + 3P_{in}}, \quad P_- = \frac{P_{in}}{P_{out} + 3P_{in}}. \tag{6.43}$$

To obtain the expression for the waiting time PDF we proceed as in Sect. 6.3, see the part corresponding to the comb structure with $l = a$. The Laplace transform of the waiting time PDF is given by

$$\hat{\phi}(s) = (P_+ + P_-)\hat{\phi}_0 \sum_{j=0}^{\infty} \left(2P_-\hat{\phi}_0^2\right)^j = \frac{(P_+ + P_-)\hat{\phi}_0}{1 - 2P_-\hat{\phi}_0^2}. \tag{6.44}$$

The jump length distribution for a walker moving along the backbone of the network, segment AB in Fig. 6.6, is $w(x) = P_{out}\delta(x - l) + P_{in}\delta(x + l)$, where l is the distance between two consecutive nodes. Equations (5.30) and (4.46) yield the following expression for the front velocity:

$$v = \frac{l}{\tau} \min_{y > r\tau} \frac{y}{\ln\left[\zeta(y) + \sqrt{\zeta(y)^2 - 1 + b^2}\right] - \ln(1 + b)}, \tag{6.45}$$

where

$$\zeta(y) = \left[(2 - b)e^y - (1 - b)e^{-y}\right]\left(1 - \frac{r\tau}{y}\right) + \frac{r\tau}{y}. \tag{6.46}$$

Results for the front velocity, determined numerically from (6.45), are shown in Fig. 6.7, where the dimensionless front velocity is plotted as a function of the dimensionless growth rate $r\tau$.

The front velocity is a monotonically increasing function of $r\tau$. As expected, it approaches asymptotically the advection velocity along the backbone l/τ, since the front velocity cannot exceed the maximum particle velocity. The inset shows that the front velocity does not depend linearly on the bias b, which implies that the front
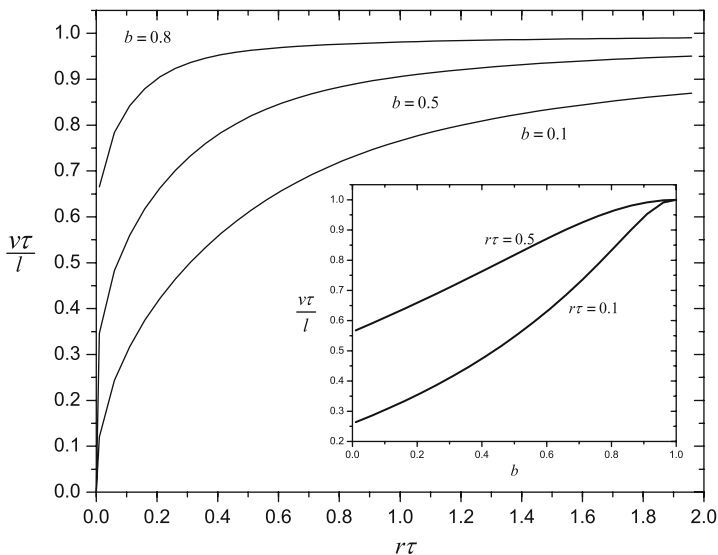
Fig. 6.7 Dimensionless front velocity as a function of $r\tau$ (*main figure*) and as a function of b (*inset*)

velocity on this network is not simply given by the sum of the advection velocity in the backbone plus the front velocity for the unbiased case.

6.4 Reaction–Diffusion Fronts in General Heterogeneous Media

In this section we present three different analytical tools that can be used to calculate the velocity of a front propagating in nonuniform media, if the heterogeneities are small. Methods such as the marginal (linear) stability analysis, Sect. 4.1.1, and variational analysis, Sect. 4.2.2, have been widely used to find the asymptotic velocity of a front. Both methods do not work or at least need to be appropriately generalized, if the reaction–diffusion equation depends explicitly on the spatial or temporal coordinate. Instead, we employ well-known analytical techniques such as singular perturbation analysis and the local velocity approach, both valid for weak heterogeneities, and the Hamilton–Jacobi formalism, Sect. 4.2.1, valid for general heterogeneities, to study how heterogeneities introduce corrections to the asymptotic front velocity, both for pulled and pushed (but monostable) fronts. We will compare the analytical results and numerical solutions.

These methods have some limitations. Singular perturbation analysis is an effective tool if the solution is known to the leading order and if the reaction term is not given by KPP kinetics. The solution to the lowest order can be found for some particular non-KPP kinetic terms, but it is not known in general. This method requires, of course, that a small parameter is present in the model. It is necessary to assume that the spatial heterogeneities in the system introduce a small variation in the reaction

rate or the diffusion coefficient, *weak heterogeneities*, and the characteristic length of the heterogeneities must be greater than the characteristic width of the front, *smooth heterogeneities*. To illustrate this, consider the problem

$$\frac{\partial \rho}{\partial t} = D\frac{\partial^2 \rho}{\partial x^2} + rg(x/l)f(\rho), \tag{6.47}$$

where $g(x)$ is the heterogeneity function and l the characteristic length of the spatial heterogeneities. If we define the dimensionless variables $x^* = x\sqrt{r/D}$ and $t^* = tr$, we find that, omitting the asterisk for notational simplicity, (6.47) takes the form

$$\frac{\partial \rho}{\partial t} = \frac{\partial^2 \rho}{\partial x^2} + g(\varepsilon x)f(\rho), \tag{6.48}$$

where $\varepsilon \equiv l^{-1}\sqrt{D/r}$. The width of the front

$$L \sim \left(\frac{\partial \rho}{\partial x}\right)^{-1} = \sqrt{D/r}\left(\frac{\partial \rho}{\partial x^*}\right)^{-1} \tag{6.49}$$

is $O(\sqrt{D/r})$, which implies ε is $O(L/l)$. If $L \ll l$, then $\varepsilon \ll 1$.

The Hamilton–Jacobi formalism, on the other hand, only holds for KPP kinetics, but in contrast to singular perturbation analysis there is no need to assume either weak or smooth heterogeneities. The local velocity approach is based on the assumption that for weak and smooth heterogeneities the velocity of the front is given by the local value of the reaction rate r and the diffusion coefficient D at each spatial point, i.e., the front velocity coincides with the instantaneous Fisher velocity: $v \simeq 2\sqrt{r(x)D(x)}$. In general, this simple-minded approach is not consistent with results from the other analytical methods or with numerical solutions.

In this section we study the smooth heterogeneous problem

$$\frac{\partial \rho}{\partial t} = \frac{\partial^2 \rho}{\partial x^2} + r(\varepsilon x)f(\rho), \tag{6.50}$$

i.e., an RD equation with a nonuniform reaction term. The function f satisfies $f(0) = f(1) = 0$ and $\rho(x, 0) = \tilde{\theta}(x)$ where $\tilde{\theta}(x)$ is an initial condition that can range from the Heaviside step function to a fully developed front. Here r is the dimensionless reaction rate, and ε is a small parameter. Space has been scaled such that $D = 1$. Since we are interested in solutions that behave like fully developed fronts, we consider the asymptotic regime, i.e., the large-scale and large-time limit, and employ the hyperbolic scaling $t \rightarrow t/\varepsilon$ and $x \rightarrow x/\varepsilon$. Equation (6.50) then reads

$$\varepsilon \frac{\partial \rho}{\partial t} = \varepsilon^2 \frac{\partial^2 \rho}{\partial x^2} + r(x) f(\rho), \tag{6.51}$$

$$r(x) \equiv 1 + \delta \eta_u(x), \tag{6.52}$$

where δ is the amplitude of the heterogeneities and $\eta_u(x)$ is the reactive hetero-geneity. Consistent with the initial condition and the existence of a front, we require the solution to satisfy $\lim_{x \to -\infty} \rho = 1$ and $\lim_{x \to \infty} \rho = 0$. To calculate the front velocity we make use of the singular perturbation analysis (SPA), the local velocity approach (LVA), and the Hamilton–Jacobi (HJ) formalism.

6.4.1 Singular Perturbation Analysis

Singular perturbation analysis was employed to study the velocity of pulled fronts, and it was shown that the solvability integrals diverge [103, 104, 448]. Therefore we will use this method only for non-KPP kinetics. We assume $\delta = O(\varepsilon)$, weak heterogeneities, i.e., $\delta \equiv \sigma \varepsilon$ in (6.51) with $\sigma = O(1)$. Equation (6.51), together with the corresponding boundary conditions, becomes

$$\varepsilon \frac{\partial \rho}{\partial t} = \varepsilon^2 \frac{\partial^2 \rho}{\partial x^2} + \left[1 + \sigma \varepsilon \eta_u(x)\right] f(\rho), \tag{6.53a}$$

$$\lim_{x \to -\infty} \rho = 1, \qquad \lim_{x \to \infty} \rho = 0. \tag{6.53b}$$

To study (6.53) we carry out a nonrigorous asymptotic analysis. We assume that the domain is divided into two regions, an interior or boundary layer region, whose width is $O(\varepsilon)$, where ρ varies rapidly, and an outer region where ρ is almost constant. In other words, either $\rho = O(\varepsilon^{n_1})$ or $\rho = 1 + O(\varepsilon^{n_2})$, where n_1 and n_2 are positive real numbers. To solve (6.53) in the outer region we expand ρ as follows:

$$\rho(x, t; \varepsilon) = \Phi_0(x, t) + \varepsilon \Phi_1(x, t) + \varepsilon^2 \Phi_2(x, t) + O(\varepsilon^3). \tag{6.54}$$

By substituting (6.54) into (6.53) and equating terms of equal power in ε, we obtain

$$f(\Phi_0) = 0, \quad \lim_{x \to -\infty} \Phi_0 = 1, \quad \lim_{x \to \infty} \Phi_0 = 0, \tag{6.55}$$

$$\frac{\partial \Phi_0}{\partial t} = f'(\Phi_0)\Phi_1 + \sigma \eta_u(x) f(\Phi_0), \quad \lim_{x \to \pm\infty} \Phi_1 = 0, \tag{6.56}$$

$$\frac{\partial \Phi_1}{\partial t} = \frac{\partial^2 \Phi_0}{\partial x^2} + \frac{1}{2} f''(\Phi_0)\Phi_1^2 + f'(\Phi_0)\Phi_2 + \sigma \eta_u(x) f'(\Phi_0)\Phi_1, \quad \lim_{x \to \pm\infty} \Phi_2 = 0. \tag{6.57}$$

The solution of (6.55) is $\Phi_0 = 1$ to the left of the boundary layer and $\Phi_0 = 0$ to the right of the boundary layer. The solutions of (6.56) and (6.57) are $\Phi_1 \equiv 0$ and $\Phi_2 \equiv 0$, respectively. This implies that $\rho(x, t; \varepsilon) = O(\varepsilon^3)$ to the left of the boundary layer and $\rho(x, t; \varepsilon) = 1 + O(\varepsilon^3)$ to the right of the boundary layer. To the order of the expansion considered here, the homogeneous and heterogeneous cases are identical, and there is no difference in the shape of the front.

To study the dynamics in the interior of the boundary layer we transform (6.53) to the reference frame of the front, i.e., we define the new variable $z = [x - S(t)]/\varepsilon$, where $S(t)$ represents the position of the front. The derivatives in (6.51) transform according to

$$\frac{\partial}{\partial t} \rightarrow -\frac{\dot{S}}{\varepsilon}\frac{\partial}{\partial z} + \frac{\partial}{\partial t}, \qquad \frac{\partial^2}{\partial x^2} \rightarrow \frac{1}{\varepsilon^2}\frac{\partial^2}{\partial z^2}, \tag{6.58}$$

where the dot denotes the time derivative. We expand ρ and S in powers of ε,

$$\rho(z, t) = \phi_0(z) + \varepsilon\phi_1(z, t) + \varepsilon^2\phi_2(z, t) + \cdots , \tag{6.59}$$

$$S(t) = S_0(t) + \varepsilon S_1(t) + \varepsilon^2 S_2(t) + \cdots , \tag{6.60}$$

and consequently

$$\eta_u(x) = \eta_u(S_0 + z\varepsilon + S_1\varepsilon + \cdots) \simeq \eta_u(S_0) + \eta_u'(S_0)(z + S_1)\varepsilon + \cdots , \tag{6.61}$$

$$f(\phi) = f(\phi_0) + f'(\phi_0)\phi_1\varepsilon + \frac{1}{2}f''(\phi_0)\phi_1^2\varepsilon^2 + f'(\phi_0)\phi_2\varepsilon^2 + \cdots , \tag{6.62}$$

where $\eta_u'(S_0) = d\eta_u(x)/dx\big|_{x=S_0}$ and $f'(\phi_0) = df(\rho)/d\rho\big|_{\rho=\phi_0}$. Substituting (6.60) and (6.62) into (6.53) and taking account of (6.58), and equating terms with equal powers of ε we obtain at orders ε^0, ε, and ε^2, respectively,

$$\mathcal{L}\phi_0 = 0, \tag{6.63}$$

$$\mathcal{L}_1\phi_1 = -\sigma f(\phi_0)\eta_u(S_0) - \dot{S}_1\frac{\partial\phi_0}{\partial z}, \tag{6.64}$$

$$\mathcal{L}_1\phi_2 = -\dot{S}_2\frac{\partial\phi_0}{\partial z} - \dot{S}_1\frac{\partial\phi_1}{\partial z} - \frac{1}{2}f''(\phi_0)\phi_1^2 - \sigma\eta_u(S_0)f'(\phi_0)\phi_1$$
$$- \sigma f(\phi_0)\eta_u'(S_0)(z + S_1) + \frac{\partial\phi_1}{\partial t}, \tag{6.65}$$

where $\mathcal{L} = \partial_{zz} + \dot{S}_0\partial_z + f(\phi_0)$ and $\mathcal{L}_1 = \partial_{zz} + \dot{S}_0\partial_z + f'(\phi_0)$.

Since we assumed $\phi_0 = \phi_0(z)$ in (6.59), the first equation (6.63) is equivalent to the homogeneous ($\varepsilon = 0$) reaction–diffusion equation transformed to the front reference frame, $z = x - \dot{S}_0t$, which travels with constant velocity $\dot{S}_0$. We set $\dot{S}_0 \equiv c$, and $S_0 = ct$ with $S(0) = 0$. Since $\mathcal{L}_1$ has a zero eigenvalue, $\mathcal{L}_1 d\phi_0/dz = 0$, it cannot be inverted to obtain the solutions of (6.64) and (6.65). Instead those equations have

to fulfill a solvability condition, which determines the corrections to the velocity of the front. The solvability condition of (6.64) is $\int_{-\infty}^{\infty} \psi \mathcal{L}_1 \phi_1 dz = 0$, where ψ is the zero eigenfunction of the adjoint operator $\mathcal{L}_1^{\dagger} = \partial_{zz} - \dot{S}_0 \partial_z + f'(\phi_0)$, i.e., $\mathcal{L}_1^{\dagger} \psi = 0$. It is easy to show that $\psi = e^{cz} d\phi_0/dz$ is an eigenfunction of $\mathcal{L}_1^{\dagger}$ with zero eigenvalue. The solvability condition for (6.64) yields

$$\dot{S}_1 = -\frac{\sigma \eta_u(ct) \int_{-\infty}^{\infty} e^{cz} \frac{d\phi_0}{dz} f(\phi_0) dz}{\int_{-\infty}^{\infty} e^{cz} \left(\frac{d\phi_0}{dz}\right)^2 dz} = \frac{1}{2}\sigma c \eta_u(ct). \tag{6.66}$$

Note that $\dot{S}_1$ depends only on the function η_u and not on the solution of ϕ_0. Inverting the hyperbolic scaling, we find that the velocity of the front is given by

$$v(t) = c + \frac{1}{2} c \eta_u(ct\varepsilon)\delta + O(\delta^2). \tag{6.67}$$

Before proceeding to the next order in the expansion, we need to solve (6.64). Since $\mathcal{L}_1 d\phi_0/dz = 0$, we look for a solution of the form $\phi_1(z, t) = \frac{d\phi_0}{dz} + \frac{d\phi_0}{dz} z F(t)$. Substituting this ansatz into (6.64), we find $F(t) = \frac{1}{2}\sigma \eta_u(ct)$ and

$$\phi_1(z, t) = \frac{d\phi_0}{dz}\left[1 + \frac{1}{2}\sigma \eta_u(ct)z\right]. \tag{6.68}$$

After substituting $S_0 = ct$, (6.66), and (6.68) into (6.65) and applying the solvability condition $\int_{-\infty}^{\infty} e^{cz} \frac{d\phi_0}{dz} \mathcal{L}_1 \phi_2 dz = 0$ for (6.65), we obtain

$$\dot{S}_2 = -\frac{c\sigma^2}{8}\eta_u(ct)^2 + \alpha\sigma \eta_u'(ct) + \frac{c\sigma}{2}\eta_u'(ct)S_1(t), \tag{6.69}$$

where $\eta_u'(ct) \equiv d\eta_u(x)/dx\big|_{x=ct}$, $S_1(t) = \frac{1}{2}\sigma \int^{ct} \eta_u(x)dx$ with $S(0) = 0$, and

$$\alpha \equiv -\frac{1}{2} + c\frac{\int_{-\infty}^{\infty} z e^{cz} \left(\frac{d\phi_0}{dz}\right)^2 dz}{\int_{-\infty}^{\infty} e^{cz} \left(\frac{d\phi_0}{dz}\right)^2 dz}. \tag{6.70}$$

Note that $\dot{S}_2$ depends explicitly on the solution of ϕ_0. To calculate analytically the second-order correction of the velocity it is necessary to have an analytical expression for the zeroth order solution $\phi_0(z)$. Some exact solutions are known in the literature for reaction terms of the form $f(\rho) = \rho^{q+1}(1 - \rho^q)$ for $q \geq 1$ (see Exercise 4.1). In this case, the solution for the homogeneous case takes the form

$$\phi_0(z) = \frac{1}{\left(1 + e^{bz}\right)^a}, \quad c = \frac{1}{\sqrt{1+q}}, \quad b = qc, \quad a = \frac{1}{q}. \tag{6.71}$$

It is easy to check that the integrals involved in (6.66) and (6.70) converge for any q. For example, for $q = 1$ we have $f(\rho) = \rho^2(1 - \rho)$, $\alpha = 1$, and the velocity of the front is given by

$$v(t) = \dot{S}(t) = \frac{1}{\sqrt{2}} + \frac{\sigma}{2\sqrt{2}}\eta_u\left(\frac{t}{\sqrt{2}}\right)\varepsilon +$$

$$\left\{-\frac{\sigma^2}{8\sqrt{2}}\eta_u\left(\frac{t}{\sqrt{2}}\right)^2 + \sigma\eta'_u\left(\frac{t}{\sqrt{2}}\right) + \frac{\sigma^2}{4\sqrt{2}}\eta'_u\left(\frac{t}{\sqrt{2}}\right)\int^{t/\sqrt{2}}\eta_u(x)\mathrm{d}x\right\}\varepsilon^2$$

$$+ O(\varepsilon^3). \tag{6.72}$$

For the sake of mathematical and numerical simplicity we illustrate the results for the case where $\eta_u(x) = x$ is linear. Taking $\sigma = 1$, we find from (6.72) that $v(t) = 1/\sqrt{2} + t\varepsilon/4 + \varepsilon^2$, and inverting the hyperbolic scaling we obtain

$$v(t) = \frac{1}{\sqrt{2}} + \left(1 + \frac{t}{4}\right)\varepsilon^2 + O(\varepsilon^3), \tag{6.73}$$

which is valid for $t \ll O(\varepsilon^{-2})$. For any non-KPP $f(\rho)$ one has the general result

$$v(t) = c + \left(\frac{c^2 t}{2} + \alpha\right)\varepsilon^2 + O(\varepsilon^3). \tag{6.74}$$

6.4.2 Local Velocity Approach

The local velocity approach assumes that the front position changes adiabatically in time as the front moves into a region where the characteristic parameters D and r change. For (6.50) with a source term $f(\rho) = \rho^2(1 - \rho)$ the velocity of the front is locally given by $v = \sqrt{r(\varepsilon x_f)/2}$, where x_f is the position of the front. To be more specific, let us also assume $\eta_u(x) = x$ and $\sigma = 1$. The temporal dependence of the front velocity is obtained by integrating the differential equation

$$\frac{\mathrm{d}x_f}{\mathrm{d}t} = \sqrt{\frac{1 + \varepsilon^2 x_f}{2}} \tag{6.75}$$

for the front position. With the initial condition $x_f(0) = 0$, the local velocity approach yields

$$v(t) = \frac{1}{\sqrt{2}} + \frac{t\varepsilon^2}{4}. \tag{6.76}$$

In Fig. 6.8 we compare the numerical results for the front velocity of (6.50) for $r(\varepsilon x) = 1 + \delta\eta_u(\varepsilon x)$, $\eta_u(x) = x$, and $\rho(x, 0)$ a Heaviside function, with the analytical solutions (6.73) and (6.76) for different values of ε. We observe that the velocity calculated from the SPA is in better agreement with numerical solutions than that calculated from the LVA.
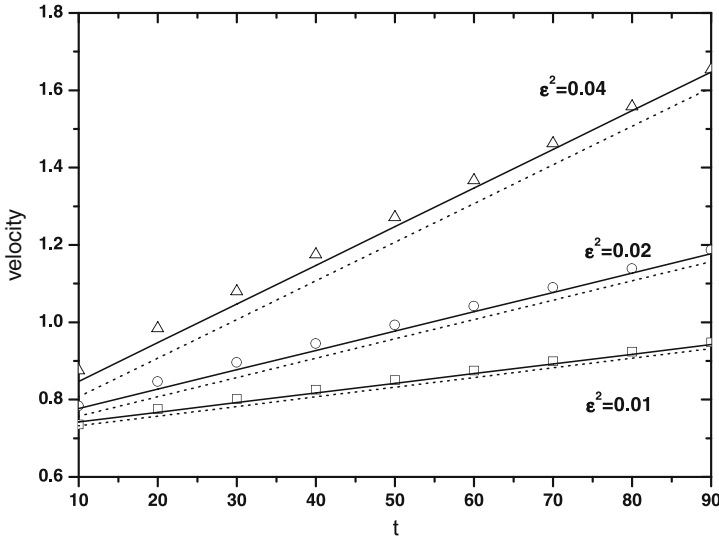

Fig. 6.8 Comparison of the temporal evolution of the velocity of fronts (in dimensionless units) between the singular perturbation analysis result given by (6.73) (*solid lines*), the local velocity approach (6.76) (*dashed lines*), and numerical results (*symbols*) for different values of ε. Here $\eta_u(x) = x$ and $f = \rho^2(1 - \rho)$. Reprinted with permission from [290]. Copyright 2003 by the American Physical Society

6.4.3 Hamilton–Jacobi Formalism

Singular perturbation analysis does not provide a fully analytical result for the very important case of KPP kinetics. It is not possible to go beyond the first order in δ, because the exact unperturbed solution is not known and the integrals in the solvability condition diverge. Proceeding as in Sect. 4.2.1 for (6.50) with KPP kinetics, we obtain to leading order the following equation for the action functional ($\varepsilon = 0$):

$$\partial_t G + (\partial_x G)^2 + r(\delta, x) = 0, \tag{6.77}$$

where $r(\delta, x) = 1 + \delta\eta_u(x)$. The Hamilton equations

$$\frac{dx}{ds} = 2p,$$
(6.78)

$$\frac{dp}{ds} = -\delta \frac{d\eta_u}{dx}$$
(6.79)

yield the differential equation for $x(s)$,

$$\ddot{x}(s) + 2\delta \frac{d\eta_u[x(s)]}{dx} = 0,$$
(6.80)

for the boundary conditions $x(s = 0) = x$ and $x(s = t) = 0$. The solution for the action functional $G(x, t)$ is given by (4.39). Since the Hamiltonian does not depend explicitly on the time s, the energy integral

$$E = \frac{\dot{x}(s)^2}{4} + 1 + \delta\eta[x(s)]$$
(6.81)

exists, and

$$G(x, t) = -Et + \frac{1}{2}\int_0^t \dot{x}(s)^2 ds.$$
(6.82)

We carry out the calculations explicitly for two simple choices of η_u, where (6.80) has an exact solution. The first one is $\eta_u(x) = x$ as in the previous section. In this case, (6.80) yields, together with the boundary conditions,

$$x(s) = x - \delta s^2 - \frac{sx}{t} + \delta st, \text{ for } 0 \le s \le t,$$
(6.83)

and

$$E = 1 + \frac{1}{2}x\delta + \frac{1}{4}\delta^2 t^2 + \frac{x^2}{4t^2}.$$
(6.84)

Equation (6.82) implies that $G(x, t) = -t - \delta^2 t^3/12 - xt\delta/2 + x^2/4t$. The position of the front, given by $G(x, t) = 0$, is

$$x(t) = \delta t^2 + 2t\sqrt{1 + \frac{1}{3}\delta^2 t^2}.$$
(6.85)

The *exact* expression for the velocity, after inverting the hyperbolic scaling, is given by

$$v(t) = \frac{dx}{dt} = 2\delta\varepsilon t + \frac{4\varepsilon^2\delta^2 t^2 + 6}{\sqrt{3\varepsilon^2\delta^2 t^2 + 9}}$$
(6.86)

for any δ. For weak heterogeneities ($\delta \ll 1$) and for $\sigma = 1$, (6.86) reduces to

$$v(t) \simeq 2 + 2t\varepsilon^2 + t^2\varepsilon^4 + O(\varepsilon^8), \tag{6.87}$$

which holds only for $t \ll O(\varepsilon^{-2})$. The HJ formalism can provide a general solution for any $\eta_u(x)$ if $\delta \ll 1$. In this case, see Exercise 6.5,

$$v(t) = 2 + \delta\eta_u(2t\varepsilon) + O(\delta^2). \tag{6.88}$$

The local velocity approach for KPP kinetics yields $v = 2\sqrt{r(\varepsilon x_f)}$. The differential equation for the front position is

$$\frac{dx_f}{dt} = 2\sqrt{1 + \varepsilon^2 x_f}, \tag{6.89}$$

and integrating with the initial condition $x_f(0) = 0$, we find

$$v(t) = 2 + 2t\varepsilon^2. \tag{6.90}$$

In Fig. 6.9 we compare (6.86) and (6.90) with the numerical solution of (6.50) for different values of ε. We observe in general good agreement after an initial transient. However, the front velocity (6.87) is in better agreement with numerical solutions
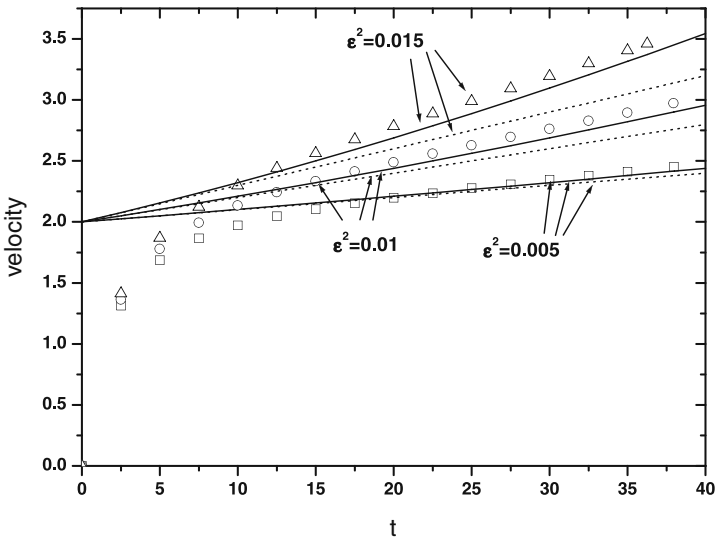
Fig. 6.9 Comparison of the temporal evolution of the velocity of fronts (in dimensionless units) between the HJ analytical result given by (6.86) (*solid lines*), the LVA (6.90) (*dashed lines*), and numerical results (*symbols*) for different values of ε. Here $\eta_u(x) = x$ for nonuniform KPP kinetics. Reprinted with permission from [290]. Copyright 2003 by the American Physical Society

than (6.90), as is the case for a comparison between SPA and LVA. In Exercises 6.6, 6.7, and 6.8 we propose to study the case of a nonuniform diffusion coefficient. From their results and from (6.72) and (6.88) we deduce the following general result:

Theorem 6.1 *For the equations*

$$\frac{\partial \rho}{\partial t} = \frac{\partial^2 \rho}{\partial x^2} + \left[1 + \delta \eta_u(\varepsilon x)\right] f(\rho) \tag{6.91}$$

and

$$\frac{\partial \rho}{\partial t} = \frac{\partial}{\partial x} \left\{ \left[1 + \delta \eta_D(\varepsilon x)\right] \frac{\partial \rho}{\partial x} \right\} + f(\rho), \tag{6.92}$$

with $f(\rho)$ such that $f(0) = f(1) = 0$, δ, $\varepsilon \ll 1$ (weak and smooth heterogeneities), and $\eta_{u,D}(x)$ a continuous and differentiable function, the front velocity has the form

$$v(t) = c + \frac{1}{2} c \eta_{u,D}(ct\varepsilon)\delta + O(\delta^2), \tag{6.93}$$

for $t \ll O(\varepsilon^{-1})$. Here c is the asymptotic (constant) velocity for the homogeneous system.

Remark 6.1 If η is an increasing (decreasing) function of space, the front is accelerated (decelerated).

Exercises

6.1 Apply the Hamilton–Jacobi formalism to the O'Shaughnessy–Procaccia equation (6.7) and show that the front velocity behaves like $v \sim t^{2/d_w - 1}$.

6.2 Apply the Hamilton–Jacobi formalism to the Giona–Roman equation (6.10) and show that the front velocity is constant.

6.3 Find the waiting time PDF for the Peano basin with $Q = 3$. Calculate $\langle x^2 \rangle(t)$ when $t \to \infty$.

6.4 Consider $\eta_u(x) = x^2$ and KPP kinetics in the equation (6.51) and find the front position. Obtain the front velocity up to $O(\delta^3)$.

6.5 Consider (6.51) with a general $\eta_u(x)$ and KPP kinetics but now assume $\delta \ll 1$. Obtain the front velocity up to $O(\delta^3)$.

6.6 Consider the RD equation with a nonuniform diffusion coefficient

$$\frac{\partial \rho}{\partial t} = \frac{\partial}{\partial x}\left[D(\varepsilon x)\frac{\partial \rho}{\partial x}\right] + f(\rho), \tag{6.94}$$

with $D(x) = 1 + \delta \eta_D(x)$. Assume that $\delta = \sigma \varepsilon$ and make use of the SPA to calculate the front velocity up to $O(\varepsilon^3)$.

6.7 Consider (6.94). Assume KPP kinetics and $\eta_D(x) = x$. Find the exact front velocity for any δ by using the HJ formalism.

6.8 Find the front velocity for the equation (6.94) for any $\eta_D(x)$ and KPP kinetics up to $O(\delta^3)$.

6.9 Consider the RD equation with a time-dependent reaction rate given by

$$\frac{\partial \rho}{\partial t} = \frac{\partial^2 \rho}{\partial x^2} + [1 + \varepsilon \eta(\varepsilon t)]\rho^2(1 - \rho). \tag{6.95}$$

Calculate the front velocity up to $O(\varepsilon^3)$.

6.10 The RD equations with a time-dependent reaction rate or diffusion coefficient and KPP kinetics are given by

$$\frac{\partial \rho}{\partial t} = \frac{\partial^2 \rho}{\partial x^2} + g(\varepsilon t)\rho(1 - \rho), \tag{6.96}$$

$$\frac{\partial \rho}{\partial t} = g(\varepsilon t)\frac{\partial^2 \rho}{\partial x^2} + \rho(1 - \rho), \tag{6.97}$$

respectively. Show that both equations have fronts propagating with the same velocity. Show that this velocity is given by

$$v(t) = \frac{\varepsilon t g(\varepsilon t) + \int_0^{\varepsilon t} g(s)\mathrm{d}s}{\left[\varepsilon t \int_0^{\varepsilon t} g(s)\mathrm{d}s\right]^{1/2}}. \tag{6.98}$$

Chapter 7
Ecological Applications

Reaction–transport equations allow us to model the spread of invading populations. Traveling front solutions describe the invasive process, and their velocity is a quantity that can be obtained from observational data. In this chapter we review some recent reaction–transport models and compare the theoretical predictions with the observed values for the rate of population invasions.

7.1 Human Migrations

7.1.1 Neolithic Transition: Single-Species Models

An interesting, direct application of the RD equation (2.3) arose after archaeological data led to the conclusion that European farming originated in the Near East, from where it spread across Europe. The rate of this spread was measured [12], and a mathematical model was proposed according to which early farming expanded in the form of an RD wave of advance [13]. Such a model provides a consistent explanation for the origin of Indo-European languages [94] and also finds remarkable support from the observed gene frequencies [73]. However, this RD model predicts a velocity for the spread of agriculture that is higher than that inferred from archaeological evidence, provided that one accepts those values for the parameters in the model that have been measured in independent observations [13].

In order to make a comparison with archaeological data possible for this process, one needs a more detailed microscopic model than the RD model. Such a model should (i) apply to two-dimensional (2D) spaces and (ii) relate the macroscopic parameters of the evolution equation to the microscopic properties of the system [87]. We consider here the RT model and compare its predictions with observations [137]. The RT equation in 2D reads

$$\tau \frac{\partial^2 \rho}{\partial t^2} + \frac{\partial \rho}{\partial t} = D\nabla^2 \rho + rF(\rho) + r\tau \frac{\partial F(\rho)}{\partial t}, \qquad (7.1)$$

where ∇^2 is the Laplacian. Note that (7.1) is the RT equation (3.151) in 2D, with relaxation time given by (3.152), that is,

$$\tau = \langle t \rangle - \frac{\langle t^2 \rangle}{2 \langle t \rangle}. \tag{7.2}$$

If the waiting time is the same for all individuals and equal to T, then $\phi(t) = \delta(t - T)$ and (7.2) yields

$$\tau = T/2. \tag{7.3}$$

If the space is assumed to be a 2D regular lattice of spacing σ and individuals can perform isotropic jumps only to their nearest neighbors, the jump length PDF reads $w(x, y) = [\delta(x - \sigma) + \delta(x + \sigma) + \delta(y - \sigma) + \delta(y + \sigma)]/4$. The 2D extension of (3.152) with $\phi(t) = \delta(t - T)$,

$$D = \frac{1}{4T} \int_{-\infty}^{\infty} \int_{-\infty}^{\infty} \left(x^2 + y^2 \right) w(x, y) \mathrm{d}x \mathrm{d}y, \tag{7.4}$$

leads to the diffusion coefficient

$$D = \frac{1}{4} \frac{\sigma^2}{T}, \tag{7.5}$$

a well-known result for two-dimensional diffusion.

The time T is estimated as the time of travel, on the order of days or weeks, plus the time of "residence," i.e., the time interval between the arrival of a family and the subsequent migration, on the order of a generation [358]. This implies that in our case T is approximately the time of residence or the waiting time during the rest phase of the population.

We assume that the population growth can be described by the logistic growth function $F(\rho) = \rho \left(1 - \rho/\rho_{\max} \right)$, where $\rho_{\max}$ is the saturation density or carrying capacity. This growth function compares favorably with a wealth of experimental results [256]. Equation (7.1) leads to wavefronts with asymptotic velocity, see (5.60),

$$v = \begin{cases} \dfrac{2\sqrt{rD}}{1 + \dfrac{rT}{2}}, & rT < 2, \\[6mm] \sqrt{\dfrac{2D}{T}}, & rT > 2. \end{cases} \tag{7.6}$$

In the limit $T \to 0$, (7.6) becomes

$$v_{T \to 0} = 2\sqrt{rD}, \tag{7.7}$$

which is the basis of the classical wave-of-advance theory of the Neolithic transition in Europe [13]. Equation (7.6) implies that the waiting time T slows down the wavefront, as it should.

Here σ^2/T is the invaded area during the time interval T that separates two successive migrations. Previous approaches did not take the factor 1/4 in (7.5) into account but relied on the approximation $D \approx \sigma^2/T$ [13].

The front velocity for the expansion of agriculture can be predicted from (7.6), provided that independent estimates for the values of T, r, and D are available. As in [13], we assume 25 yr for the average generation, $T = 25$ yr. Let us assume, for the moment, an initial growth rate of 3%, i.e., $r = 0.032$ yr^{-1} [73], and $\sigma^2/T = 1700$ km^2/generation [13]. Using these values in the approximation $D \approx \sigma^2/T$ and (7.7), we obtain a front velocity of $v_{T \to 0} = 2.86$ km/yr. In contrast, (7.7) with (7.5) yields a velocity of 1.43 km/yr. The dashed-dotted and dashed lines in Fig. 7.1, which reproduces the archaeological data for the spread of the Neolithic transition in Europe found in [13], are the best fits with these slopes, respectively. The front velocity implied by $D \approx \sigma^2/T$ is much higher than that inferred from the data. The prediction with D given by (7.5), on the other hand, shows the usefulness of the wave-of-advance theory, provided that the factor 1/4 in (7.5) is included, which corresponds to 2D diffusion. Still, the data clearly imply a lower front velocity. This can also be seen from the regression (full line) in Fig. 7.1 [12, 13]: its slope yields a velocity of 1.0 km/yr. When the same values for the parameters as above are introduced into (7.6) and (7.5), we obtain a front velocity of $v = 1.04$ km/yr. The prediction from (7.1) agrees very well with observations, see the values of χ^2 in Fig. 7.1.

Changing the value of the average length of a generation has little effect. For example, (7.6) and (7.5) yield $v = 0.95$ km/yr with $T = 28$ yr [13]. In Figs. 7.2 and 7.3, the curves labeled with the number 1 give the possible values of r and σ^2/T that are compatible, according to each one of the three models, with the observed velocity of 1 km/yr [12, 13]. It is interesting to note that this invasion velocity was estimated using a data set of 53 archaeological sites. Over the years, a much larger data set has become available and recently the 95% confidence-level (CL) velocity was estimated as 0.95±0.35 km/yr using a data set of 735 sites [351]. In Figs. 7.2 and 7.3 we also include curves corresponding to these velocities. The hatched regions in these figures correspond to likely ranges of the parameters and have been obtained as follows. Birdsell [47] was able to collect detailed evolution data of two human populations which settled in virgin territory. A fit of these data, either to an exponential or to a logistic curve, yields $r = 0.032 \pm 0.003$ yr^{-1}, with an 80% confidence level. Values for σ^2/T have been derived [13, 357] from observations of Ethiopian shifting agriculturalists and Australian aborigines. A statistical analysis of these values yields $\sigma^2/T = 1544\pm368$ km^2/generation (80% C.L. interval). As we have stressed, (7.5) should replace the approximation $D \approx \sigma^2/T$ in
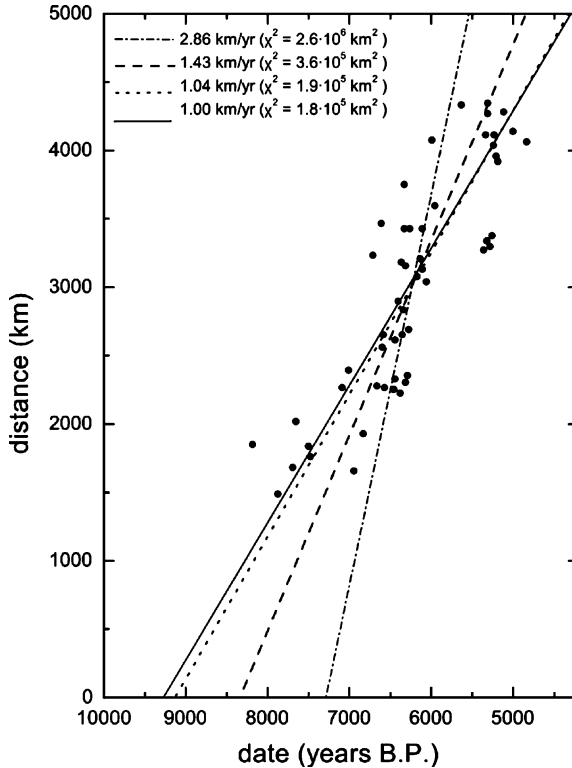
Fig. 7.1 Comparison between empirical evidence and theoretical models for the spread of agriculture in Europe [137]. The *points* are the data already analyzed in [13], distances being measured as great circle routes from Jericho (the presumed center of diffusion). Dates are conventional radiocarbon ages in years Before Present (B.P.). The *full line* is the regression by Ammerman and Cavalli-Sforza (correlation coefficient 0.89) [13]. The other three lines are least-square fits with slopes calculated from the classical wave-of-advance model with $D \approx \sigma^2/T$ (*dashed-dotted line*), D (*dashed line*) given by (7.5), and from the RT model with D as in (7.5) (*dotted line*). Here $T = 25$ yr, $r = 0.03$ yr^{-1}, and $\sigma^2/T = 1700$ km^2/generation. Reprinted with permission from [137]. Copyright 1999 by the American Physical Society

two-dimensional situations. This does not rely on any assumption. Figure 7.2 shows that use of this correction (three upper curves), instead of the classical approach (lower curves), makes the nondelayed model marginally consistent with the experimental range of r and σ^2/T values (hatched rectangle). In other words, the RD approach is compatible with the demographic data, but only assuming extreme values for the parameters. The RT model leads to (7.6) and Fig. 7.3. From this figure we conclude that the agreement between the available empirical data and the RT model is very satisfactory, in spite of the simplicity of the latter. This shows that it is not necessary to assume extreme values of the measured parameters, provided that one is willing to accept the hypothesis that a time interval T of about one generation separates successive migrations.
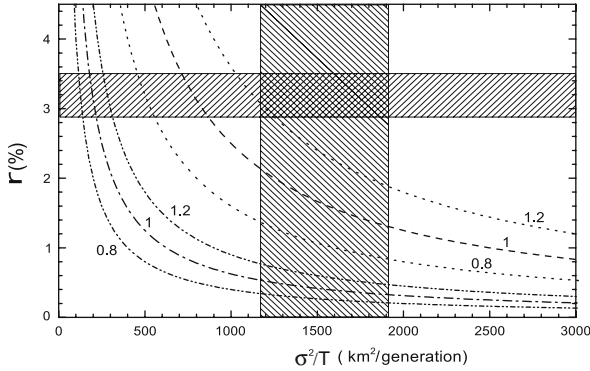
Fig. 7.2 Predictions of the classical wave-of-advance model (7.7) [137]. The *hatched regions* correspond to the range of allowed values for r and σ^2/T, according to the available empirical evidence. Each *curve* is labeled with a *number*, which corresponds to the front velocity in km/yr. The three lower curves correspond to the $D \approx \sigma^2/T$ approximation, which was used in [13]. The three upper curves correspond to the same model, but taking into account (7.5) for two-dimensional diffusion. Reprinted with permission from [137]. Copyright 1999 by the American Physical Society
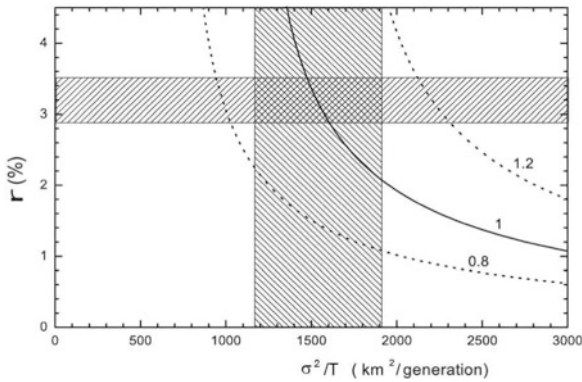
Fig. 7.3 The same as Fig. 7.2, but for the hyperbolic wave-of-advance model (7.6) and an average generation of $T = 25$ yr [137]. For almost all of the likely values of the parameters r and σ^2/T (*hatched rectangle*), the predictions of the model are consistent with the observed front velocity (1.0±0.2 km/yr). Reprinted with permission from [137]. Copyright 1999 by the American Physical Society

Simulations of the Neolithic transition in Europe with the values $r = 0.02$ yr^{-1} and $\sigma^2/T = 973.4$ km^2/generation yield a front velocity of $v = 1.09$ km/yr [357]. Making use of (7.7), the two-dimensional result (7.5), and the above values for r and σ^2/T, we obtain $v_{T \to 0} = 0.88$ km/yr. In [357] an irregular lattice was considered. Since (7.5) can be easily generalized to $D = \frac{1}{2d}\frac{\sigma^2}{T}$, where d is the number of dimensions and $2d$ is the number of nearest neighbors of a point on the lattice, we

note that a decrease in the number of neighbors corresponds to an enhancement of diffusion, as expected intuitively. If we take into account that for the irregular lattice used in [357] the mean number of neighbors was 3.4, we estimate from (7.7) that $v_{T \to 0} = 0.96$ km/yr, which is closer to the value 1.09 km/yr observed in the simulations. Since the simulations in [357] included corrections due to the acculturation of hunter-gatherers by farmers, which leads to a more rapid agricultural expansion as will be shown in the following subsection, one can conclude that there is reasonable agreement between analytical predictions and simulations.

7.1.1.1 Neolithic Transition in Oceania

For the Neolithic transition in Oceania, there also exist enough archaeological data so that a front velocity can be inferred [135]. The theory in the previous subsection assumes a continuous description, in the sense that all areas of two-dimensional space are equally suitable in principle for the settlement of human populations. This can be an adequate approximation to a large-scale, space-averaged description of the observed clustered distribution of sites. A continuous description does not mean that all land areas are occupied by individuals; this is obviously impossible at small enough scales, no matter what habitat and biological population one wishes to consider. From this perspective, it is reasonable to apply the same model to island expansions. In this case, settlements cluster on islands, whereas large sea areas are unsettled. Similarly, in mainland expansions settlements are clustered near water resources, whereas large forest areas remain unsettled. However, the diffusion coefficient has now a different value, which can again be inferred from anthropological observations, leading to good agreement with the observed velocity of about 5 km/yr [135], which is much faster than that for the Neolithic transition in Europe previously discussed.

Another application refers to mass extinctions. Simulations using RD models (limit $T \to 0$) and realistic parameter values for the diffusion of hunter-gatherers predict that it took humans about $\Delta t_{T \to 0} = 1200$ yr to colonize North America, leading to the extinction of some 30 species of herbivores [10]. This is basically consistent with the archaeological evidence. However, this approach neglects the waiting time in the diffusion process. In the approximate, single-species description above, we obtain from (7.6) and (7.7)

$$\frac{\Delta t}{\Delta t_{T \to 0}} = \frac{v_{T \to 0}}{v} = 1 + r\frac{T}{2}, \tag{7.8}$$

which, using as a first approximation the same parameter values as above, yields about 1700 yr, i.e., a correction of about 40% relative to the RD value $\Delta t_{T \to 0} = 1200$ yr.

7.1.2 Hunter-Gatherers Interaction: Indo-European Neolithic Transition

Consider a two-component RT system with densities ρ_1 and ρ_2:

$$\tau_1 \frac{\partial^2 \rho_1}{\partial t^2} + \frac{\partial \rho_1}{\partial t} = D_1 \frac{\partial^2 \rho_1}{\partial x^2} + F_1(\rho_1) + \tau_1 F_1'(\rho_1) \frac{\partial \rho_1}{\partial t} + \gamma_1 \rho_1 \rho_2, \qquad (7.9a)$$

$$\tau_2 \frac{\partial^2 \rho_2}{\partial t^2} + \frac{\partial \rho_2}{\partial t} = D_2 \frac{\partial^2 \rho_2}{\partial x^2} + F_2(\rho_2) + \tau_2 F_2'(\rho_2) \frac{\partial \rho_2}{\partial t} - \gamma_2 \rho_1 \rho_2. \qquad (7.9b)$$

This model describes a reaction–diffusion process with a sedentary phase where interactions between species are reduced to a switch between species and are not included in the reproduction process. In terms of a predator–prey system, the last term means that predators increase their population density ρ_1 because of their inter-action with preys, which in turn experience a decrease in their population density ρ_2. We assume that the interaction term $\rho_1 \rho_2$ is small compared to the other terms, since otherwise higher-order terms such as $\rho_1^2 \rho_2$ might be important in the description of the interaction between both species. For $\tau_1 = \tau_2 = 0$, one recovers the usual RD Lotka–Volterra system. In the Neolithic transition, the population invasion of farmers, with number density ρ_1, traveled into areas where they encountered a population of preexisting hunter-gatherers with a number density ρ_2 that is usually assumed to be approximately uniform, say ρ_2^0 [13, 357]. This approximation will be valid for sufficiently small values of the interaction term $\rho_1 \rho_2$. Both populations mixed to some extent, and this interaction is regarded as the cause of the gradients observed in the present spatial distribution of human genes [13]. With $\rho_2(x) = \rho_2^0$, (7.9) can be reduced to the single RT equation

$$\tau_1 \frac{\partial^2 \rho_1}{\partial t^2} + \frac{\partial \rho_1}{\partial t} = D_1 \frac{\partial^2 \rho_1}{\partial x^2} + r_1 \rho_1 (1 - \rho_1) + r_1 \tau_1 (1 - 2\rho_1) \frac{\partial \rho_1}{\partial t} + \gamma_1 \rho_2^0 \rho_1, \quad (7.10)$$

where we have assumed logistic growth with rate r_1. It is not difficult to show that the front velocity for (7.10) is

$$v = \begin{cases} 2\sqrt{\dfrac{D\left(r_1 + \gamma_1 \rho_2^0\right)}{\left(1 + r_1 \tau_1\right)^2 + 4\gamma_1 \rho_2^0 \tau_1}}, & r_1 \tau_1 < 1, \\[20pt] \sqrt{\dfrac{D}{\tau_1}}, & r_1 \tau_1 > 1. \end{cases} \qquad (7.11)$$

In order to obtain numerical predictions from (7.11), we need values for the parameters appropriate to the Neolithic transition. As explained in Sect. 7.1.1, such values have been obtained from independent observations of the Neolithic expansion and their mean values are $r_1 = 0.032$ yr^{-1}, $D = 15.44$ km^2/yr, and $\tau_1 = T/2 = 12.5$ yr. The latter value follows from the mean generation time $T = 25$ yr. On the other hand, from the observations in [357] we have the mean values for the other two parameters, $\rho_2^0 = 0.04$ hunters/km and $\gamma_1 = 5.84$ km^2/(hunter yr). Using these values for the RD case ($\tau_1 \to 0$) we find 1.6 km/yr, which is much higher than the velocity derived from the archaeological record. In contrast, (7.11) yields $v = 1.1$ km/yr, which lies entirely within the experimental range, namely 1.0±0.2 km/yr.

7.1.3 Model for Human Settlements

Despite the interest in the establishment of farming communities in Europe during the Neolithic transition, there are few models explaining the spatial pattern formed behind the wave of advance. We present a model [124] that provides an explanation for the formation of human settlements and the tendency of the population distribution to form clusters. We show that this large-scale pattern is a transient phenomenon which disappears as an extinction wave due to land degradation.

We assume that the population consists of semisedentary foragers and sedentary farmers who share the same territory. The semisedentary foragers are the population of individuals who randomly move along a river valley and search for food and other resources. An implicit consequence of this behavior is the foundation of new settlements—large localized values of population density and an interchange between farming and foraging populations. The sedentary farmers are individuals who do not migrate. They live in small villages scattered near cultivated land in the valley of a major river. We define the total density as $\rho(x, t) = \rho_1(x, t) + \rho_2(x, t)$, where $\rho_1(x, t)$ is the density of semisedentary foragers and $\rho_2(x, t)$ the density of sedentary farmers. We assume that there are transitions from a sedentary to a foraging way of life and vice versa and that these transitions depend strongly on the local food supply. The key feature of the movement of semisedentary foragers is that they do not move from place to place completely randomly, i.e., their movements cannot be modeled by a standard diffusion law. We adopt a biased random walk whose statistical characteristics depend on the local food supply. In this model, the probability of a random migration event resulting in a jump of length x' in the time interval $[t, t + \Delta t]$ is $\mu \Delta t$, the probability of a transition from a foraging lifestyle to farming is $\alpha_1 \Delta t$, and the probability of the conversion of farmers to semisedentary foragers is $\alpha_2 \Delta t$. We consider that the local crop production per individual per year is $q(x, t)$ and the frequencies μ, α_1, and α_2 depend explicitly on the crop production: $\mu = \mu(q)$ and $\alpha_i = \alpha_i(q)$ for $i = 1, 2$. The balance equations for semisedentary forager and sedentary farmers are, respectively,

$$\rho_1(x, t + \Delta t) = \left\{1 - \mu[q(x, t)]\Delta t - \alpha_1[q(x, t)]\Delta t\right\} \rho_1(x, t)$$
$$+ \alpha_2[q(x, t)]\rho_2(x, t)\Delta t$$
$$+ \Delta t \int_{\mathbb{R}} \mu[q(x - x', t)]\rho_1(x - x', t)w(x')dx', \qquad (7.12a)$$

$$\rho_2(x, t + \Delta t) = \left\{1 - \alpha_2[q(x, t)]\Delta t\right\} \rho_2(x, t) + \alpha_1[q(x, t)]\rho_1(x, t)\Delta t$$
$$+ r\Delta t \rho_2(x, t) \left[1 - \frac{\rho(x, t)}{K}\right]. \qquad (7.12b)$$

The first term on the right-hand side of (7.12a) represents those foragers who stay at location x and do not move during the period Δt and do not become sedentary farmers. The second term corresponds to the number of sedentary farmers who become semisedentary foragers during the period Δt, and the last term accounts for foragers who arrive at x during the period Δt from different places $x - x'$, where the jump distance x' is distributed by a dispersal kernel $w(x')$. The first term on the right-hand side of (7.12b) represents those sedentary farmers who do not become foragers during the period Δt. The second term corresponds to the number of foragers who become farmers during the period Δt, and the last term accounts for the new sedentary farmers born during the period Δt. The parameters r and K are the intrinsic reproduction rate and the carrying capacity, respectively. In the limit $\Delta t \to 0$, we obtain from (7.12a) and (7.12b)

$$\frac{\partial \rho}{\partial t} = \int_{\mathbb{R}} \mu[q(x - x', t)]p[q(x - x', t)]\rho(x - x', t)w(x')dx'$$
$$- p(q)\mu(q)\rho + r[1 - p(q)]\rho\left[1 - \frac{\rho}{K}\right], \qquad (7.13)$$

where we have introduced the fraction of foragers p as $\rho_1 = p\rho$ and $\rho_2 = (1 - p)\rho$. This fraction depends on the crop production $p(q)$. To obtain a closed system of equations, we assume that $p(q)$ is given by

$$p(q) = \begin{cases} p_{\max}, & q \leq q_{\min}, \\ \dfrac{p_{\max} - p_{\min}}{q_{\max} - q_{\min}}q + \dfrac{p_{\max} + p_{\min}}{2}, & q_{\min} < q < q_{\max}, \\ p_{\min}, & q \geq q_{\max}, \end{cases} \qquad (7.14)$$

and the local food production by

$$q(x, t) = \alpha \frac{\rho(x, t)}{\rho_0 + \rho(x, t)} \left[1 - e^{-\beta F(x, t)}\right], \qquad (7.15)$$

where $F(x, t)$ is the density of soil nutrients, ρ_0 is a constant, and β determines how the yield depends on the nutrients. The factor $1 - e^{-\beta F(x, t)}$ describes the land

degradation, and $\rho/(\rho_0 + \rho)$ represents a tendency toward group solidarity that increases efficiency of food production. The equation for the soil nutrients has the form

$$\frac{\partial F}{\partial t} = \xi_1 - \xi_2 F(x, t) - \gamma q(x, t)\rho(x, t), \tag{7.16}$$

where ξ_1 is the rate at which soil nutrients regenerate naturally, ξ_2 the rate of nutrient depletion due to environmental reasons, such as erosion and flooding, and γ the rate at which nutrients are depleted due to harvests. Finally, the dispersal kernel is assumed to be of the Laplace type: $w(x) \sim e^{-|x|/l}$, where l is a characteristic length. The system of equations (7.13), (7.14), (7.15), and (7.16) is now closed and can be solved numerically.

We chose the following values for the parameters: $q_{min} = 300$ and $q_{max} = 736$ kg per person and per year, $p_{max} = 0.95$, and $p_{min} = 0.05$. Data indicate that the annual production of food per unit area was up to 0.0736 kg/m^2. If the area cultivated by a person per year is about 10^4 m^2, then $\alpha \simeq 736$ kg per person and per year. For corn cultivation $\beta \simeq 890$ m^2/kg, and this parameter is in general of the order of 10^2. The rate of nutrient depletion $\gamma \simeq 5.43 \times 10^{-3}$ kg$_P$/kg, where kg$_P$ denotes kilograms of phosphorous in the soil. Numerical solutions of (7.13), (7.14), (7.15), and (7.16) reveal the emergence of a large-scale pattern in the population density. This phenomenon can be interpreted as the formation of human settlements along a river valley. The individual farmers have a tendency toward aggregation and clustering as a result of nonlinear random migration. The results also show the decay of these clusters or settlements due to land degradation. This is shown in Fig. 7.4, where a sequence of total population densities for different times is plotted.

7.1.4 Models with Dispersive Variability

RD models have certain limitations in applications to the real world. For example, members of a population do not necessarily disperse in the same way, there is always some variability. To take this fact into account, Cook considered that the population explicitly consists of distinct subpopulations, namely dispersers with density ρ_1 and nondispersers with density ρ_2. These subpopulations are allowed to have different birth rates. They interbreed fully, and all newborns have the same probability of being a disperser [309]. The evolution equations for the RD system are given by

$$\frac{\partial \rho_1}{\partial t} = D \frac{\partial^2 \rho_1}{\partial x^2} + r_1(\rho_1 + \rho_2)\left[1 - \frac{\rho_1 + \rho_2}{K}\right], \tag{7.17a}$$

$$\frac{\partial \rho_2}{\partial t} = r_2(\rho_1 + \rho_2)\left[1 - \frac{\rho_1 + \rho_2}{K}\right]. \tag{7.17b}$$
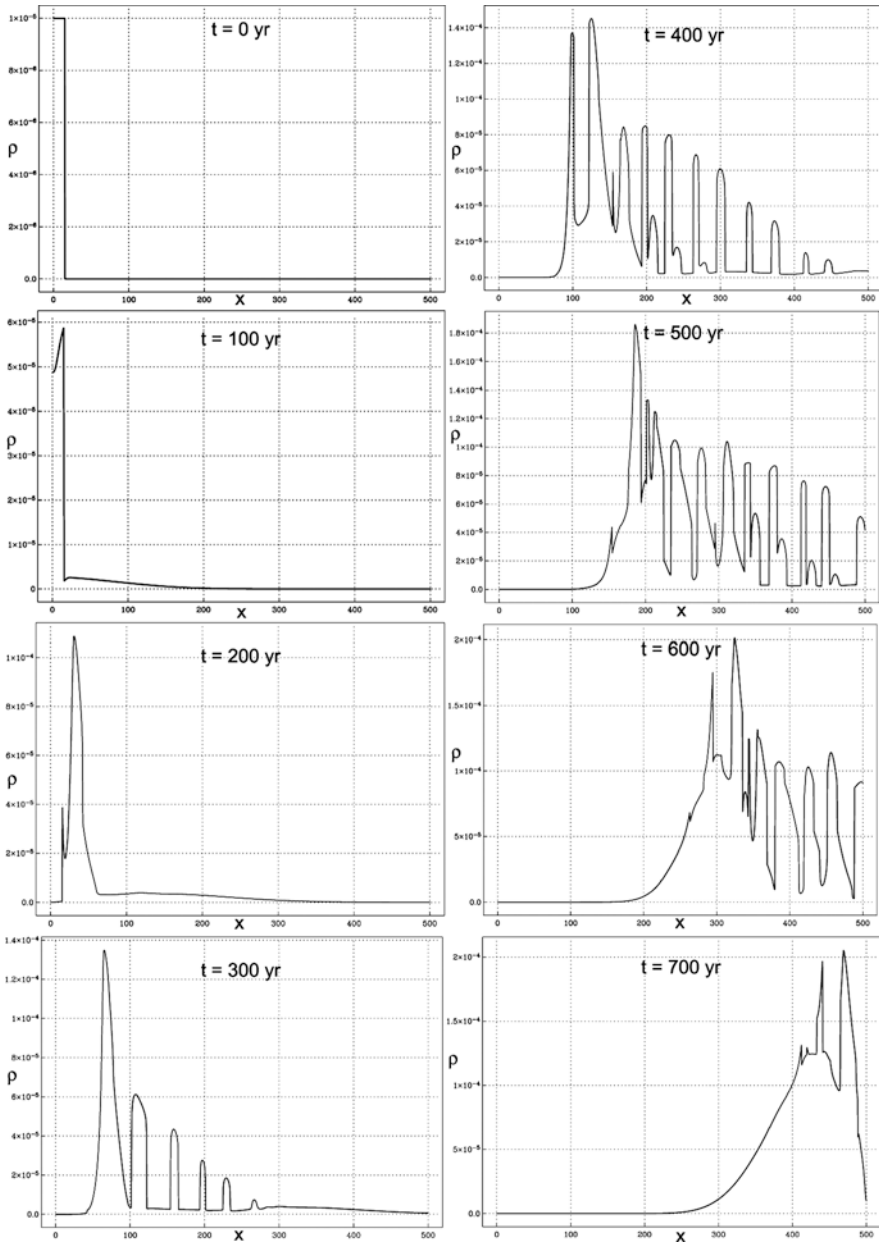
Fig. 7.4 Total density $\rho(x,t)$ for the system (7.13), (7.14), (7.15), and (7.16) with $\mu = 0.1$, $l = 10$, $\xi_1 = 10^{-4}$, $\xi_2 = 0$, $r = 0.03$ yr^{-1}, $\beta = 200$ m^2/kg, $\gamma = 0.01$ m^2/kg, $K = 10^{-4}$, and the other parameters as in the text. The initial condition is $\rho = 0.1K$ for $0 < x < 15$ km and $\rho = 0$ elsewhere. Reprinted with permission from [124]. Copyright 2008 by the American Physical Society

We have assumed logistic population growth, with K being the carrying capacity of the environment. The probability of a newborn being a disperser is $\mu = r_1/(r_1+r_2)$. Note that if $r_2 \to 0$, the whole population disperses and (7.17) becomes the standard RD equation. Since the kinetics satisfy the KPP criteria, we can calculate the front velocity from the Hamilton–Jacobi formalism. The corresponding Hamiltonian is

$$H^2 - (r + Dp^2)H + (1 - \mu)p^2 = 0, \tag{7.18}$$

where $r = r_1 + r_2$. The front velocity is, see Sect. 4.6,

$$v = \min_{p>0} \frac{H(p)}{p} = \min_{p>0} \frac{\sqrt{(r - Dp^2)^2 + 4Dr\mu p^2} + r + Dp^2}{2p}$$
$$= \sqrt{rD}\left(1 + \sqrt{\mu}\right). \tag{7.19}$$

7.1.4.1 Cook's Model with Delayed Growth

Consider the evolution equations for both populations in the general form [292]

$$\frac{\partial \rho_1}{\partial t} = \mathcal{L}[\rho_1] + R_1(\rho_1, \rho_2, x, t), \tag{7.20a}$$

$$\frac{\partial \rho_2}{\partial t} = \mathcal{L}[\rho_2] + R_2(\rho_1, \rho_2, x, t), \tag{7.20b}$$

where $\mathcal{L}$ is the transport operator and R_1 and R_2 the reproduction contribution to the change in ρ_1 and ρ_2, respectively. If the population with density ρ_1 disperses by diffusion and the subpopulation with ρ_2 is sedentary, then $\mathcal{L}[\rho_1] = D\partial^2\rho_1/\partial x^2$ and $\mathcal{L}[\rho_2] = 0$. To include a delay between dispersal and reproduction, which accounts for the time of newborns to mature and reach adulthood, we consider reproduction terms that are nonlocal in time. The contribution of these terms to the change in the densities ρ_1 and ρ_2 at time t depends on their values at preceding times. If $\rho(1-\rho/K)$ is the number of new individuals born at time t, where $\rho = \rho_1+\rho_2$, then this quantity evaluated at $t-t'$, i.e., $\rho(x, t-t')\left[1 - \rho(x, t - t')/K\right]$, represents the number of new individuals born at time t' earlier and which reach adulthood now, at time t, i.e., become members of both subpopulations. If the population displays variability in the time to reach adulthood, the fraction of new individuals born at t' and which mature at time t is $\varphi(t')\rho(x, t - t')\left[1 - \rho(x, t - t')/K\right]$. Here $\varphi(t')$ represents the fraction of individuals that mature at time t', i.e., a probability distribution function of the age at onset of adulthood (PDFAA). To determine the contributions of all the possible maturation ages, one has to integrate the above quantity over the whole range of t'. The number of individuals which reach adulthood and become dispersers (or nondispersers) at time t is a fraction μ (or $1 - \mu$) of those individuals born at time t' earlier, summed over all the possible values of t'. New individuals do

not affect the dynamical process of migration during the period of maturation. With all this in mind, our model system is given by

$$\frac{\partial \rho_1}{\partial t} = D\frac{\partial^2 \rho_1}{\partial x^2} + r_1 \int_0^\infty dt'\varphi(t')\Big[\rho_1(x, t - t') + \rho_2(x, t - t')\Big] \times$$

$$\left[1 - \frac{\rho_1(x, t - t') + \rho_2(x, t - t')}{K}\right], \tag{7.21a}$$

$$\frac{\partial \rho_2}{\partial t} = r_2 \int_0^\infty dt'\varphi(t')\Big[\rho_1(x, t - t') + \rho_2(x, t - t')\Big] \times$$

$$\left[1 - \frac{\rho_1(x, t - t') + \rho_2(x, t - t')}{K}\right]. \tag{7.21b}$$

To calculate the front velocity for (7.21) we reduce the system to a Hamilton–Jacobi equation. To do so, we employ the hyperbolic scaling (4.33), the exponential transformation (4.35), the large scale limit $\varepsilon \to 0$, and the definitions in (4.38) to obtain the Hamilton–Jacobi equation

$$H^2 - H\Big[Dp^2 + r\hat{\varphi}(H)\Big] + (1 - \mu)Drp^2\hat{\varphi}(H) = 0, \tag{7.22}$$

where $\hat{\varphi}(H)$ is the Laplace transform of $\varphi(t)$ with argument H. Equation (4.46) yields

$$v = \sqrt{D} \min_{H > H^*} \sqrt{H\frac{r(1 - \mu)\hat{\varphi}(H) - H}{r\hat{\varphi}(H) - H}}, \tag{7.23}$$

where H^* is the solution to $r\hat{\varphi}(H^*) = H^*$. Equation (7.23) implies that the front velocity depends on the statistical properties of the PDFAA.

The hyperbolic extension to Cook's models was proposed in [181]. The system of RT equations is

$$\tau_{\text{eff}}\frac{\partial^2 \rho_1}{\partial t^2} + \frac{\partial \rho_1}{\partial t} = D\frac{\partial^2 \rho_1}{\partial x^2} + r_1(\rho_1 + \rho_2)(1 - \rho_1 - \rho_2)$$

$$+ \tau_{\text{eff}}r_1\frac{\partial}{\partial t}\Big[(\rho_1 + \rho_2)(1 - \rho_1 - \rho_2)\Big], \tag{7.24a}$$

$$\frac{\partial \rho_2}{\partial t} = r_2(\rho_1 + \rho_2)(1 - \rho_1 - \rho_2). \tag{7.24b}$$

Reducing this system to a Hamilton–Jacobi equation, we find the front velocity

$$v = \frac{\sqrt{rD}}{1 + b}\Big[b(1 - \mu) + 1 + \mu + 2\sqrt{b\mu(1 - \mu) + \mu}\Big]^{1/2}, \tag{7.25}$$

where

$$b = r\tau_{\text{eff}} = \frac{r\langle t \rangle}{2}\left(2 - \frac{\langle t^2 \rangle}{\langle t \rangle^2}\right) \tag{7.26}$$

and $\langle t \rangle$ is the mean maturation age. We compare the invasion velocity for Cook's model (7.19) with the RT extension (7.24) and the numerical solution obtained from (7.23) for different forms of the PDFAA, but with the same mean value for the onset of adulthood. In Table 7.1 we present values for the model parameters obtained from the literature.

From a practical point of view, the dependence of the front velocity on characteristic parameters related to the shape of the PDFAA is an important issue. The observational data available for the Neolithic transition in Europe typically provide the mean maturation age $\langle t \rangle$ but not the complete form of the PDFAA. The question arises as to how the shape of different PDFAAs with the same mean value affects the velocity of the migratory fronts. To address this question, we consider three different PDFAAs. The simplest one is the Dirac delta form which corresponds to a unique maturation age for the whole population. Second, we consider a Gamma family of PDFAAs that allows us to determine the dependence of the migratory front velocity on the probability of maturation ages larger than the mean one. Third, we consider a Gamma PDFAA where the tail is truncated to analyze the effect of the tail length.

(i) *Dirac delta.* The PDFAA $\varphi(t) = \delta(t - \tau)$ yields $\widehat{\varphi}(H) = e^{-H\tau}$. For the delayed growth model (7.23) leads to

$$v = \sqrt{D}\,\min_{H>H^*}\sqrt{H\frac{r(1-\mu)e^{-H\tau} - H}{re^{-H\tau} - H}}, \tag{7.27}$$

which has to be evaluated numerically. For the hyperbolic model the velocity is given by (7.25) with $b = r\tau/2$. Using the data of Table 7.1, we display in Fig. 7.5 the velocity of migratory fronts in terms of μ. As expected, the velocity is an increasing function of μ in both models. Symbols in Fig. 7.5 represent the calculated values of the velocity for both models with the observational values of μ in Table 7.1. Table 7.2 provides the values for the velocity calculated for the RD model (7.19), the delayed growth [DG, (7.23)] and hyperbolic [RT, (7.25)] models for the whole population (wp), Gilishi with 15 yr of mean adult age (g15), Gilishi with 20 yr of mean adult age (g20), and Shiri with 15 yr of mean adult age (s15). For both DG

Table 7.1 Observational data for the Neolithic transition in Europe. Reprinted from [292]. Copyright 2006, with permission from Elsevier

Population	μ	$\langle t \rangle$ (yr)	D (km^2/yr)	r (yr^{-1})
wp	1	25	15.44	0.032
g15	0.46	15	11.57	0.032
g20	0.52	20	12.24	0.032
s15	0.81	15	21.53	0.032
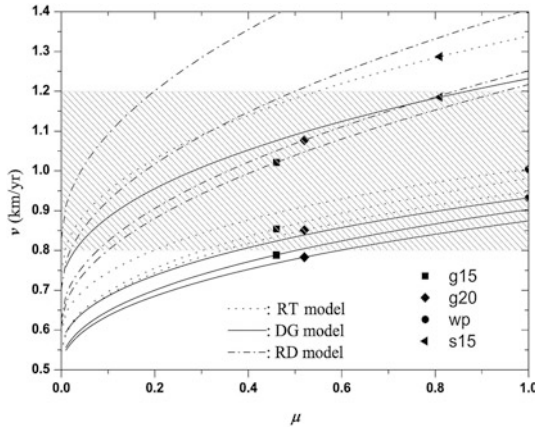
Fig. 7.5 Graph of the migratory front velocity in terms of the disperser fraction μ for a Dirac delta PDFAA. *Symbols* are the calculated velocities from the RD, DG, and RT models for the values of μ in Table 7.1. The *shaded area* corresponds to the observational range. Reprinted from [292]. Copyright 2006, with permission from Elsevier

Table 7.2 Results for the migratory fronts velocity in km/yr for the Dirac delta and Gamma-family PDFAAs for the RD, DG, and RT models. Reprinted from [292]. Copyright 2006, with permission from Elsevier

Population		Dirac delta		Gamma family	
	v_{RD}	v_{RT}	v_{DG}	v_{RT}	v_{DG}
wp	1.41	1.00	0.93	1.19–1.66	0.93–1.01
g15	1.02	0.85	0.79	0.85–1.02	0.79–0.82
g20	1.08	0.85	0.78	0.85–1.08	0.78–0.83
s15	1.58	1.29	1.18	1.29–1.58	1.18–1.24

and RT models and for the four populations we obtain values for the migratory front velocity very close to its observational range 1.0 ± 0.2 km/yr.

(ii) *Gamma family*. We consider now a more realistic situation: There exists a wide range of maturation ages, each one with a certain probability, obeying the Gamma PDF

$$\varphi(t) = \frac{1}{\tau \Gamma(m+1)} \left(\frac{t}{\tau}\right)^m e^{-t/\tau}, \quad m \in (0, \infty], \tag{7.28}$$

with $\langle t \rangle = (m+1)\tau, \widehat{\varphi}(H) = (1+H\tau)^{-m-1}$. From (7.23)

$$v = \sqrt{D} \min_{H > H^*} \sqrt{H \frac{H(1+H\tau)^{m+1} - r(1-\mu)}{H(1+H\tau)^{m+1} - r}}, \tag{7.29}$$

which has to be solved numerically. The velocity for the RT model is given by (7.25) with

$$b = \frac{r \langle t \rangle m}{2(m+1)}. \tag{7.30}$$

We analyze now how the velocity of migratory fronts depends on the probability of having a maturation age larger than the mean value

$$P\left(t > \langle t \rangle\right) = \int_{\langle t \rangle}^{\infty} \varphi(t) \mathrm{d}t = \frac{\Gamma\left(m+1, m+1\right)}{\Gamma\left(m+1\right)}, \tag{7.31}$$

where $\Gamma(\cdot, \cdot)$ is the incomplete Gamma function. We have calculated the range of values for the migratory front velocity from DG and RT models for $m \in (0, \infty]$, see Table 7.2. These results show how strongly the migratory front velocity depends on the parameter m when it goes from 0 to infinity.

This parameter controls the shape of the PDFAA, as shown in Fig. 7.6, because it is related to its kurtosis β_2 by the relation $m = (9 - \beta_2)/(\beta_2 - 3)$. The range $m \in (0, \infty]$ is equivalent to $3 < \beta_2 \le 9$, and the Gamma family PDFAA is always leptokurtic.

In Fig. 7.7 we plot the results of the velocity of migratory fronts in terms of $P\left(t > \langle t \rangle\right)$. As expected, the velocity decreases as $P\left(t > \langle t \rangle\right)$ increases. Figure 7.7 shows that the details of the shape of the PDFAA affect the velocity of migratory fronts in both models, yielding in some cases values that fall outside the observational range.

(iii) *Gamma family with cutoff.* The previous PDFAAs have an infinite tail. In other words, the probability that individuals have an extremely large maturation age is small but not zero. Such a situation is unrealistic, and the tail should be truncated at a maximum age $t_{\max}$, so that there are no individuals with a maturation age larger than $t_{\max}$. To study the effect of the tail length on the velocity of migratory fronts,
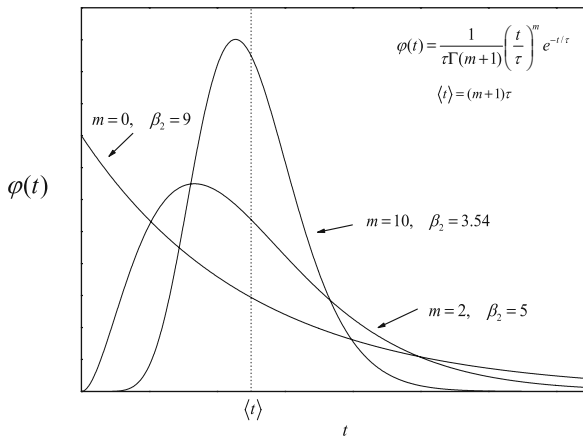
Fig. 7.6 Graph of the Gamma family of PDFAAs for different values of m. All the PDFAAs depicted have the same mean maturation age. Reprinted from [292]. Copyright 2006, with permission from Elsevier
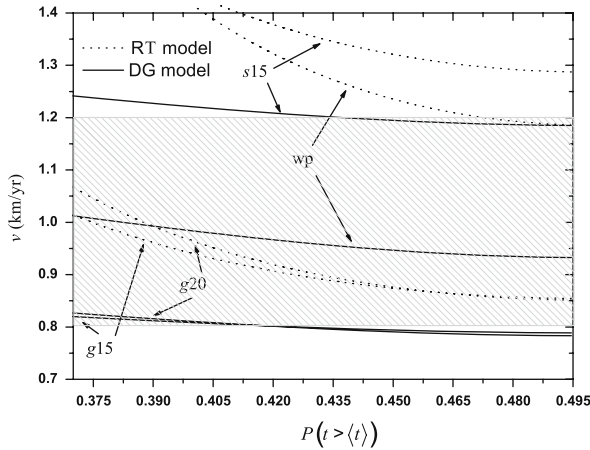
Fig. 7.7 Migratory fronts velocity in terms of the probability $P(t > \langle t \rangle)$. The velocity is a monotonically decreasing function for both the DG and RT models. The *shaded area* corresponds to the observational range. Reprinted from [292]. Copyright 2006, with permission from Elsevier

we consider the Gamma PDFAA with a truncated tail:

$$\varphi(t) = \frac{1}{\tau \left(1 - e^{-t_{\max}/\tau} - \frac{t_{\max}}{\tau} e^{-t_{\max}/\tau}\right)} \frac{t}{\tau} e^{-t/\tau} \theta \left(t_{\max} - t\right), \tag{7.32}$$

where $\theta(\cdot)$ is the Heaviside step function. The PDFAA in (7.32) has a mean maturation age of

$$\langle t \rangle = \int_0^\infty t\varphi(t)\mathrm{d}t = \tau \frac{2e^{t_{\max}/\tau} - \left(t_{\max}/\tau\right)^2 - 2 - 2\left(t_{\max}/\tau\right)}{e^{t_{\max}/\tau} - 1 - t_{\max}/\tau}. \tag{7.33}$$

To characterize the tail length, we define $t_{\max}$ as n times the mean maturation age, i.e., $t_{\max} \equiv n \langle t \rangle$ with n a positive integer number. With the definition of the dimensionless quantity $y \equiv \langle t \rangle /\tau$, (7.33) turns into

$$y = \frac{2e^{ny} - n^2 y^2 - 2 - 2ny}{e^{ny} - 1 - ny}. \tag{7.34}$$

Once the tail length is established, i.e., n is fixed, (7.34) can be solved numerically to yield y. Since $\langle t \rangle$ is known from observational data, the values of τ and $t_{\max}$ can be obtained. It is easy to check that (7.34) has a solution only if $n \in (3/2, \infty)$, i.e., $t_{\max} > 3 \langle t \rangle /2$. After some algebra we obtain from (7.32)

$$\widehat{\varphi}(H) = \frac{e^\alpha - e^{-H\tau\alpha} \left[1 + (1 + H\tau) \alpha\right]}{(1 + H\tau)^2 \left(e^\alpha - 1 - \alpha\right)} \tag{7.35}$$

and $b = r \langle t \rangle F(\alpha)/(2y)$, with

$$F(\alpha) = \frac{2e^{2\alpha} + e^{\alpha}\left(\alpha^3 - 5\alpha^2 - 4\alpha - 4\right) + \alpha^4 + 4\alpha^3 + 7\alpha^2 + 4\alpha + 2}{\left(e^{\alpha} - 1 - \alpha\right)\left(2e^{\alpha} - \alpha^2 - 2 - 2\alpha\right)} \tag{7.36}$$

and $\alpha = ny$. The velocity of migratory fronts for both models can now be calculated. Before doing so, it is interesting to analyze how the dimensionless delay $a = r\tau$ and b for the DG and RT models, respectively, depends on the tail length. This is depicted in Fig. 7.8.

Both dimensionless delays decrease as the tail length increases, contrary to expectations; the existence of individuals with a large maturation age should increase the delay effect. This counterintuitive behavior is due to the fact of maintaining the mean maturation age fixed independently of the tail length. It is expected that the velocity of migratory fronts increases with the tail length. In Fig. 7.9 this behavior is observed and we find, as in Fig. 7.7, that the tail length also affects the velocity, yielding in some cases values outside of the observational range.
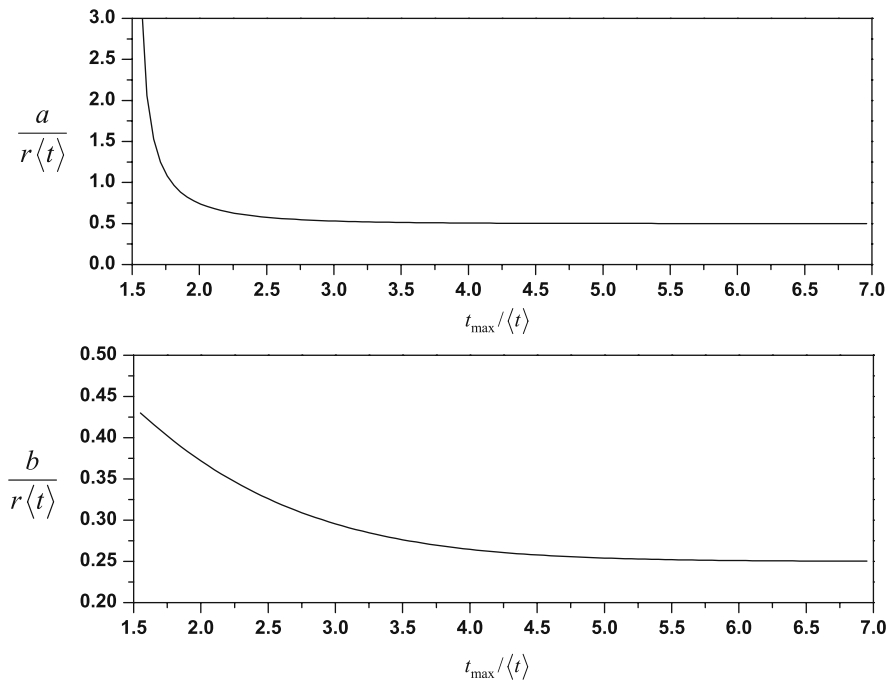
Fig. 7.8 Plot of the dimensionless delay a and b vs the dimensionless tail length. A monotonically decreasing behavior is observed. Reprinted from [292]. Copyright 2006, with permission from Elsevier
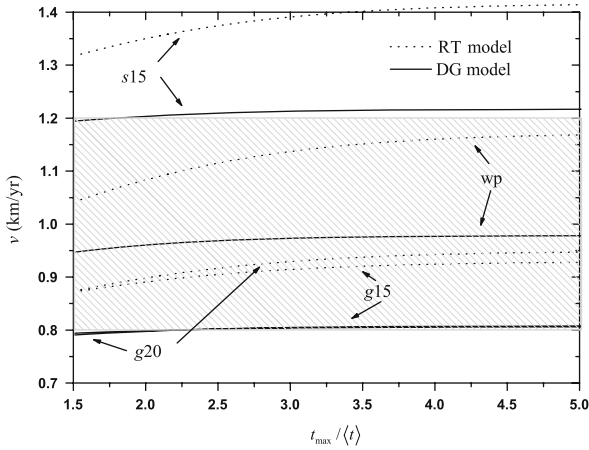
Fig. 7.9 Behavior of the speed of migratory fronts in terms of the dimensionless tail length. The *shaded area* corresponds to the observational range of the speed. Reprinted from [292]. Copyright 2006, with permission from Elsevier

7.1.5 Neanderthal Extinction

Neanderthal populations were very stable in Europe for more than 60,000 yr; nevertheless, 40,000 yr before our epoch, they were replaced by Early Modern Men. Although it remains unclear whether the interaction was direct or not, we consider here the case where both species compete for the same ecological niche composed by limited resources and territory [134]. Let ρ_n express the density of Neanderthal individuals and ρ_m the density of Early Modern Men. If we assume that the Neanderthals are sedentary, the reaction–diffusion system reads

$$\frac{\partial \rho_n}{\partial t} = \rho_n f(\rho_n, \rho_m) - \beta \rho_n, \tag{7.37a}$$

$$\frac{\partial \rho_m}{\partial t} = D \frac{\partial^2 \rho_m}{\partial x^2} + \rho_m f(\rho_n, \rho_m) - \beta s \rho_m, \tag{7.37b}$$

where $f(\rho_n, \rho_m)$ is the birth rate for both species and β is the mortality rate. We assume that Early Modern Men are better adapted to survive and the parameter s varies between 0 and 1. It indicates the similarity between both species, with $s = 1$ corresponding to complete similarity. The limited resources are included in f which has the form $f(\rho_n, \rho_m) = r - \epsilon(\rho_n + \rho_m)$, where r is the reproduction rate and ϵ is an interaction parameter.

A stability analysis of the uniform steady states $(\bar{\rho}_n, \bar{\rho}_m)$ of the system yields

$$(0, 0), \qquad \text{unstable node}, \tag{7.38a}$$

$$\left(\frac{r - \beta}{\epsilon}, 0 \right), \qquad \text{saddle point}, \tag{7.38b}$$

$$\left(0, \frac{r - s\beta}{\epsilon} \right), \qquad \text{stable node}. \tag{7.38c}$$

The steady state (7.38c) represents the final state of the evolution of the invasion process and the extinction of the Neanderthal individuals. A linear stability analysis around (7.38c) shows that the Neanderthal population decays like $e^{-t/\tau}$, with

$$\tau = \frac{1}{\beta(1 - s)} \tag{7.39}$$

the time of extinction. Paleontological data yield an extinction time between 5000 and 10,000 yr and a lifetime $1/\beta$ between 30 and 40 yr, which implies that $0.992 < s < 0.997$. Using the Hamilton–Jacobi formalism we calculate the propagation velocity for the invasion front and find $v = 2\sqrt{D(r - s\beta)}$. For a successful invasion, i.e., for the Neanderthal extinction, the condition $r > s\beta$ has to be fulfilled. This inequality leads to $r_{\min} = 0.029$ yr^{-1} for the upper value $s = 0.997$ and $\beta = 1/35$ yr^{-1}, which agrees with the value 0.032 yr^{-1} for the Neolithic transition [47].

7.1.6 US Colonization: Invasions Through Fractal River Networks

One of the best-known modern range expansions is the colonization across the United States in the 19th century. In 1790, the North American population of European origin was concentrated in the Atlantic region, but during the following decades internal migrations resulted in a displacement of the established population westwards. According to the data and atlases, the average expansion rate for this transition between 1790 and 1910 was approximately 13.5 ± 0.8 km/yr [133].

An essential characteristic of the US transition westwards was the fact that settlers did not occupy all of the territory, as homogeneous models assume [137], but followed the course of the major rivers and lakes and settled near them to make use of their resources [113, 133]. Therefore, landscape heterogeneities should have played an essential role in the process of migration. This situation is similar to the case of dispersion of biological species along the margins of rivers and streams [220, 63].

Great efforts have been undertaken to describe the intricate geometry of river networks [363]. In Chap. 6 we illustrated some models, such as the Peano network, which resembles fractal river basins. Another well-known structure that was proposed to describe better the evolution and formation of river basins and that agrees with most of the observations is the *Optimal Channels Network* (OCN) model, based on some optimization principles that minimize the energy expenditure by the net-
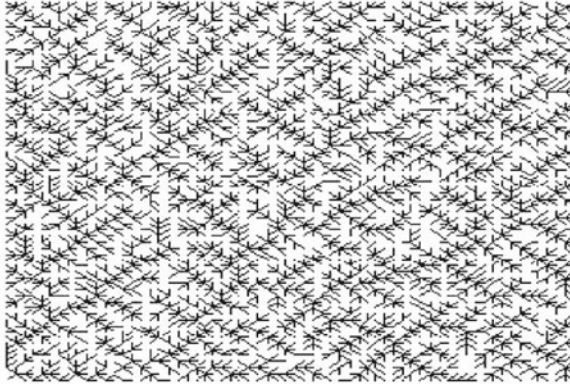
Fig. 7.10 River basin modeled by an OCN network

work [364, 360]. The evolution rules of this model lead to fractal structures like that shown in Fig. 7.10. The properties of the OCN have been shown to be similar to those of Peano network [80], and we can employ the results (6.35) and (6.36) for the waiting time distributions $\phi(t)$ for first and second degrees of constructions, respectively.

The jump distance distribution $w(x)$ for an isotropic random walk across the backbone is $w(x) = \frac{1}{2}\delta(x + l) + \frac{1}{2}\delta(x - l)$. Equation (5.30) yields the Hamilton–Jacobi equation for the CTRW model:

$$\frac{1}{\hat{\phi}(H)} = \cosh(lp) + \frac{r}{H}\left(\frac{1}{\hat{\phi}(H)} - 1\right). \tag{7.40}$$

Let us first consider the asymptotic regime, $\tau \ll t$ and $l \ll x$, where τ is the time spent by the walker at a node and l is the distance between two consecutive nodes. This is equivalent to $lp \ll 1$ and $H\tau \ll 1$ in (7.40). Expanding up to first order, i.e., $O(H\tau)$ and $O(l^2 p^2)$, we obtain the Hamilton–Jacobi equation for the RD equation: $H = Dp^2 + r$ with $D = l^2/2\langle t\rangle$, where $\langle t\rangle = \int_0^\infty t\phi(t)\mathrm{d}t = -\hat{\phi}'(0)$ is the mean waiting time. Equations (6.35) and (6.36) yield $\langle t\rangle = 3\tau$ for $Q = 1$ and $\langle t\rangle = 9\tau$ for $Q = 2$, respectively. The front velocity is given by the Fisher equation

$$v = \sqrt{\frac{2l^2 r}{\langle t\rangle}}. \tag{7.41}$$

In general, from (4.47) and (7.40) the front velocity is given by

$$v = l \min_{H} \frac{H}{\cosh^{-1}\left[\frac{1}{\hat{\phi}(H)}\left(1 - \frac{r}{H}\right) + \frac{r}{H}\right]}. \tag{7.42}$$
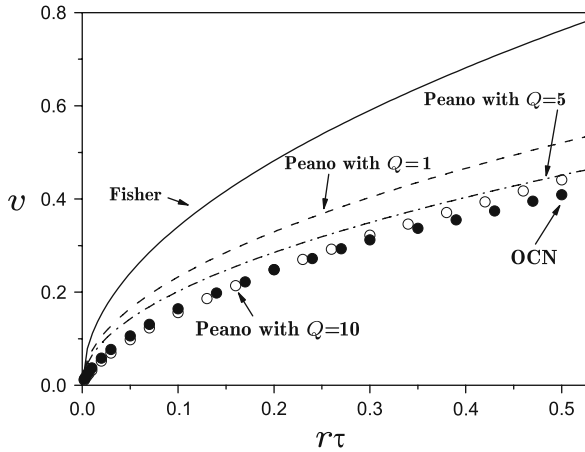
Fig. 7.11 Plot of the results for the front velocity vs the parameter $r\tau$. The *points* are obtained from simulations of the stochastic process on the OCNs (*full circles*) and the Peano basin (*open circles*). The *lines* correspond to theoretical values from the Fisher equation (*solid*) and for the Peano basin (*dotted* and *dotted-dashed*). Reprinted from [64]. Copyright 2006, with permission from Elsevier

Figure 7.11 summarizes the results obtained from (7.42) (lines) and compares it with random walk simulations on the Peano basin up to order $Q = 10$ (open circles) and OCNs (full circles). In the simulations, all the walkers were initially on the left side of the lattice and the front advanced to the right. A logistic growth $r\rho(1 - \rho)$ was introduced at every site at every time step to simulate the reaction process. For the OCNs, we averaged over 10 different 200×200 networks.

We observe that simulations on the Peano lattice and the OCN network lead to very similar results. Although these structures show some topological differences, their dynamical similarities are due to the fact that the front velocity in fractals is mainly determined by d_{min}, see (6.18) and (6.25), and the existence of loops in the structure. Both Peano and OCN networks are loopless structures with $d_{min} = 1$, which explains the results. Figure 7.11 also shows that a higher level of construction Q for the Peano network in (7.42) leads to better agreement with simulations on OCN.

To estimate the velocity of human migration one can consider τ to be the time between successive generations. A value of $\tau = 25$ yr is usually assumed [137]. The growth parameter r can be obtained directly from [256], where the population vs time plot for the United States in the 19th century was fitted to a logistic curve, obtaining $r = 0.031 \pm 0.001$ yr^{-1}.

Regarding the distribution of jump lengths, we know that the settlers did not always cover the same distance, and the distribution $w(x)$ should include the possibility of different jump lengths. This can be done by fitting the observed data to a continuous distribution. In [64], the jump distances covered by settlers were estimated from individual records obtained from the "migrations.org project" database, available at `http://www.migrations.org`. The authors collected 400 individual

records from the database and measured the distance covered by colonizers from their birthplace to the place they were 25 yr later, i.e., after a time τ. Only the distances in the E–W direction were considered, in keeping with the one-dimensional nature of our model. The jump length distribution obtained in this way is represented in Fig. 7.12.

This approach does not take into account the fraction f of people who remained at their birthplace after 25 yr without migrating. Ferrie's works [127], based on the censuses of the 19th century, allow us to estimate $f = 0.3 \pm 0.05$. Taking all these aspects into account, the best fit corresponds to an exponentially decaying distribution of the form $w(x) = Ae^{-|x|/x_0}$, where A is a normalization factor and $x_0 = 640 \pm 23 \text{ km}^{-1}$, and the mean distance is $l = 810 \pm 93$ km. By introducing these distributions and parameters into (7.40), we obtain the results for the velocity listed in Table 7.3.

Table 7.3 includes results for different values of Q, because the settlers moved mainly following the major river valleys according to historical reports. One might conclude therefore that small details in the structure of the Peano basin, namely tertiary, quaternary, and higher-order channels, do not affect the dynamics of the migration process, and a low order in Q should be chosen.
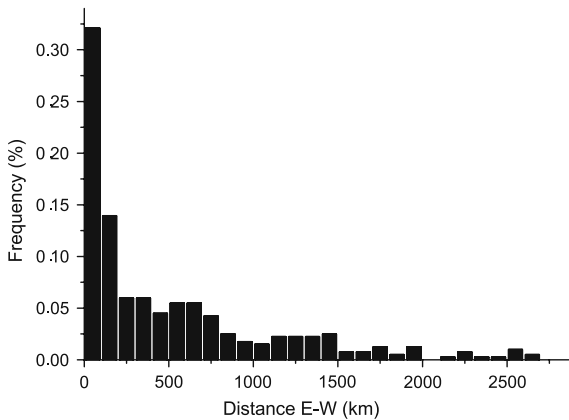
Fig. 7.12 Plot of the distribution of distances covered by migrants in the E–W direction during the 19th century, obtained from 400 individual records. Reprinted from [64]. Copyright 2006, with permission from Elsevier

Table 7.3 Observed front velocity and predictions obtained from theory and simulations on fractal basins for the case of the US colonization. Reprinted from [64]. Copyright 2006, with permission from Elsevier

Observed velocity	13.5±0.8 km/yr
Fisher's prediction	40.3±2.9 km/yr
Exponential $w(x)$ and Peano with $Q = 2$	19.4±3.2 km/yr
Exponential $w(x)$ and Peano with $Q = 5$	18.9±3.1 km/yr
Simulations on Peano with $Q = 10$	14.5±0.1 km/yr
Simulation on OCN	14.4±0.1 km/yr

In any case, we observe from Table 7.3 that the geometrical constraints of the networks significantly affect the velocity of the fronts. The classical prediction by Fisher clearly overestimates the observed velocity of the migration front, while the results obtained from simulations for the Peano and the OCN and the theoretical predictions agree reasonably well with the observations. This leads us to the hypothesis that colonization of the United States during the 19th century was significantly influenced by the landscape constraints and that heterogeneities reduced the propagation rate substantially. This specific example illustrates the importance of analyzing transport through river networks and heterogenous media in general.

7.2 Avian Range Expansions

We consider two avian range expansions, Collared Dove and House Finch, and compare their observed range expansion rates with the predictions of RD and RT models with $\phi(t) = \delta(t - T)$ [329]:

$$v_{\text{RD}} = 2\sqrt{rD}, \tag{7.43a}$$

$$v_{\text{RT}} = \begin{cases} \dfrac{2\sqrt{rD}}{1 + \dfrac{rT}{2}}, & rT < 2, \\[4mm] \sqrt{\dfrac{2D}{T}}, & rT > 2. \end{cases} \tag{7.43b}$$

To compare the predictions from (7.43) with the observed values, we need to estimate the parameters T, D, and r. As in previous sections, T is the mean time elapsed between two successive migrations, i.e., the generation time. It can be estimated as the time needed for a newborn individual to grow into an adult and reproduce. When the adult age is reached, individuals leave the paternal territory and fly to new places. Since the available data for the dispersal process correspond to a histogram of frequencies of jump distances, the diffusion coefficient can be calculated from the discrete version of (7.4):

$$D = \frac{1}{4T} \sum_j z_j^2 f_j, \tag{7.44}$$

where z_j are the radial observed distances and f_j their respective observed frequencies, $\sum_j f_j = 1$. For these birds, reproduction does not occur throughout the year; it is episodic and relatively synchronous. Therefore, one way to model their spread would be to employ a discrete-time model. This would be necessary if the time scale of measurements were of the order of, or smaller than, the typical reproduction time, about a year. Measurements of population invasion velocities usually span several decades. The use of a continuous model is a reasonable approximation for the bird

reproductive dynamics which is assumed to be logistic. If P is the population size and it is small, or at the initial phase of growth, the logistic equation can written as $dP/dt \approx rP$, where r is the intrinsic growth rate. Note the whole survey data for the population size should be used and not only those of a restricted range.

7.2.1 House Finch

The range expansion of the House Finch (*Carpodacus mexicanus*) in Northern America has been taking place since 1940. From the observed population size, Fig. 7.13 inset, we can estimate r by fitting a straight line to the logarithms of the observed data for the total population vs time. The slope of the fitted line yields $r = 0.020 \pm 0.003$ yr^{-1}.

To calculate T, note that when the adult age is reached, individuals leave the paternal territory and fly to new places. The value of this time has been estimated from observations to fall between 1.5 and 2 years [196]; we choose 1.75 yr as a typical value. In fact, values of T between 1.5 and 2 yr do not change the results we derive below. From Fig. 7.13 (main figure) and (7.44) we obtain $D = (10.1 \pm 2.4) \times 10^3$ km^2/yr. From (7.43) one finds that both RD and RT models yield an invasion velocity of 28 ± 4 km/yr with a relative difference $(v_{RD} - v_{RT})/v_{RT}$ of 1.8 ± 0.4. The observed velocity is 28 ± 1 km/yr and can be estimated from experimental
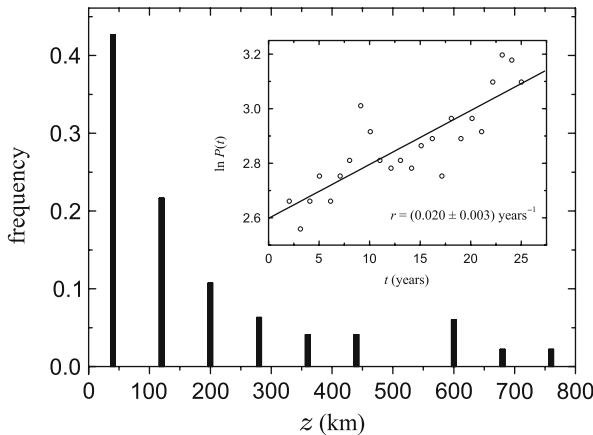
Fig. 7.13 *Inset*: House Finch survey-wide population size (P, measured in counts per party hour) vs time (The North American Breeding Bird Survey. Graph of survey-wide yearly indices from CBC. USGS Patuxent Wildlife Research Center, Laurel, Maryland, USA). In order to estimate r we used a logarithmic plot and removed points far away from the exponential phase (large times), which implied a decrease in the regression coefficient of the linear fits. *Main figure*: House Finch annual dispersal histogram (from [457]). Note that a time interval of 1 yr, which is the value for the data shown, corresponds roughly to the time required by a newborn individual to turn into an adult, i.e., roughly to T in the RT model. Reprinted from [329]
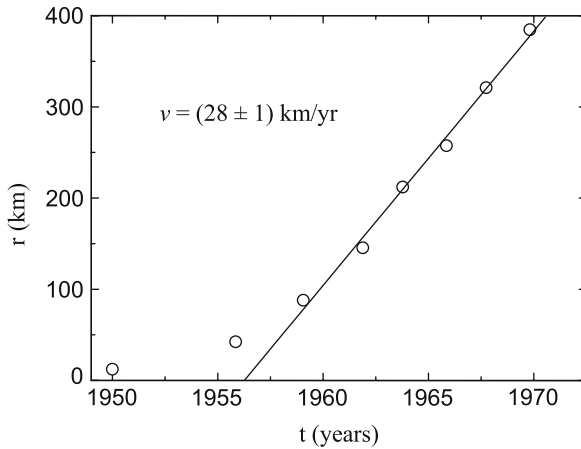
Fig. 7.14 Linear fit of experimental data to estimate the velocity of the range expansion of the House Finch. The two first data points were removed because they correspond to early times, when the population invasions had not yet reached the saturation (constant) velocity. Reprinted from [329]

data obtained from [327] illustrated in Fig. 7.14. Excellent agreement is observed between both RD and RT models and observational data.

7.2.2 Eurasian Collared Dove

We now turn our attention to the range expansion of the Collared Dove (*Streptopelia decaocto* Friv.) into Europe. Using the same method as for the House Finch, the graph of survey-wide data for the Collared Dove, see Fig. 7.15, allows us to calculate $r = 0.29 \pm 0.02$ yr^{-1}. From Tables 3 and 4 in [445] we obtain $T = 1.81 \pm 0.73$ yr and $D = 5026 \pm 2400$ km^2/yr. With these values we find $v_{RT} = 60 \pm 19$ km/yr, whereas $v_{RD} = 76 \pm 19$ km/yr. Reference [445] reports a migration velocity of 44 ± 3 km/yr. Note that the RT model provides a range for the front speed compatible with observations, whereas the Fisher model does not.

7.3 Plant Invasions

We focus on a version of the CTRW model adapted for the description of plant invasions. Further modifications of the model for applications to animal invasions or more complex situations are straightforward. Although these models are rather complex at first sight, the results and expressions in most cases are simple and have a clear ecological meaning. This makes the models attractive tools for management purposes. One of our main results consists of a threshold condition to predict if a species will show invasive behavior or not in terms of their specific life cycle. This
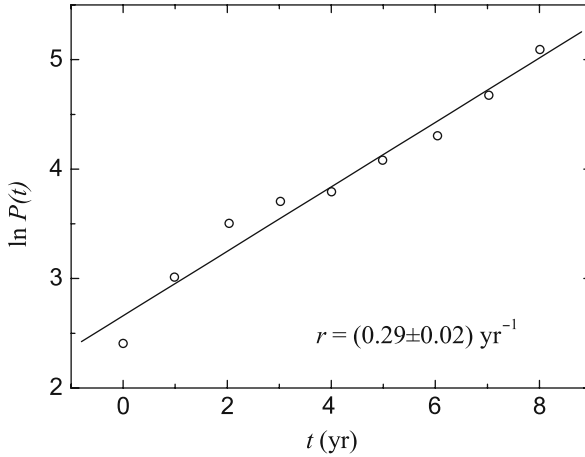
Fig. 7.15 Eurasian Collared-Dove survey-wide population size (P) vs time (USGS 2001). To estimate r we used the logarithmic plot and removed points far away from the exponential phase (large times), which implied a decrease in the regression coefficient of the linear fits. Reprinted from [329]

condition can be an alternative to Caswell's models [72] based on projected population matrices. In those models, a value of the population growth parameter, usually labeled λ, above or below unity determines if a population increases or decreases with time.

To demonstrate the applicability of the mathematical approach we compare our model with population data taken from the literature for different invasive plants. Data from the native and exotic ranges of *Echium plantagineum*, *Cytisus scoparius*, and *Carduus nutans* [172, 344, 397, 398, 479] were used to establish that the model predicts their invasive behavior when the fecundity of these species in their exotic ranges is considered. Finally, the invasion rates recently found experimentally [221] for *Carduus acanthoides* are shown to fit closely the analytical predictions of the model.

We present a stage-structured model where each process is governed by temporal or spatial probability distributions to obtain as detailed and realistic a description of the process as possible. We assume a spatially homogeneous medium. To capture the essential dynamics of an invasion process, it is necessary to account for only three life stages: unripe seeds on the plant (called seeds of type 1), mature seeds (dispersible seeds, called seeds of type 2), and adult plants. Figure 7.16 describes the plant invasion life cycle, including mature seed germination, death or growth, the ripening phase of unripe seeds, and dispersal of the mature seeds.

When a mature seed has dispersed, germination begins. After a random time interval distributed according to the PDF $\beta_1(t)$, a plant germinates with probability α_0. This plant grows, over a random time interval distributed according to the PDF $\beta_2(t)$, to maturity (i.e., able to produce seeds), unless it first dies within a random time distributed according to the PDF $\beta_3(t)$. When a plant matures, it produces Y
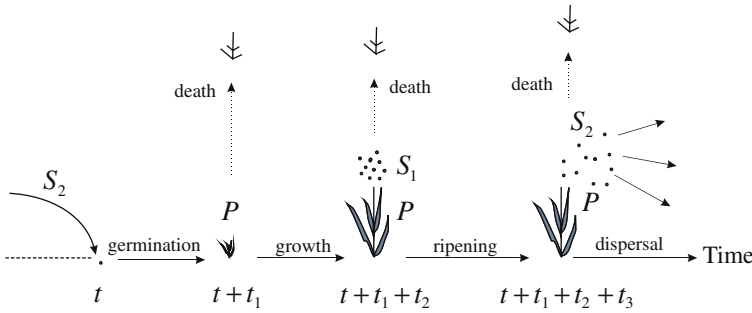
Fig. 7.16 The life cycle graph. The random times t_1, t_2, and t_3 of germination, growth, and waiting are distributed according to the PDFs $\beta_1(t)$, $\beta_2(t)$, and $\varphi(t)$, respectively

unripe seeds. Unripe seeds become mature seeds after a ripening period distributed according to the PDF $\varphi(t)$. Mature seeds disperse to repeat the cycle. We have not accounted explicitly for seed death, since mortality effects are implicitly taken into account through every seed generating a new plant with probability α_0.

7.3.1 The Model. Invasion Threshold

The two-dimensional continuous-time mesoscopic equations for each stage are

$$P(\mathbf{x}, t) = \int_0^t \beta_3(t') p(\mathbf{x}, t - t') dt', \tag{7.45}$$

$$p(\mathbf{x}, t) = p_0(\mathbf{x}, 0)\delta(t) + \alpha_0 \int_0^t \beta_1(t') s_2(\mathbf{x}, t - t') \left[1 - \frac{P(\mathbf{x}, t - t')}{K} \right] dt', \tag{7.46}$$

$$S_1(\mathbf{x}, t) = \int_0^t \varphi^*(t') s_1(\mathbf{x}, t - t') dt', \tag{7.47}$$

$$s_1(\mathbf{x}, t) = s_1(\mathbf{x}, 0)\delta(t) + Y \int_0^t \beta_2(t') \beta_3^*(t') p(\mathbf{x}, t - t') dt', \tag{7.48}$$

$$S_2(\mathbf{x}, t) = \int_0^t \beta_1^*(t') s_2(\mathbf{x}, t - t') dt', \tag{7.49}$$

$$s_2(\mathbf{x}, t) = s_2(\mathbf{x}, 0)\delta(t) + \int_0^t \varphi(t') dt' \int w(\mathbf{x}') s_1(\mathbf{x} - \mathbf{x}', t - t') d\mathbf{x}'. \tag{7.50}$$

Here $P(\mathbf{x}, t)$, $S_1(\mathbf{x}, t)$, and $S_2(\mathbf{x}, t)$ are the number density of plants, unripe seeds, and mature seeds *located* at point $\mathbf{x}$ at time t, respectively, while $p(\mathbf{x}, t)$, $s_1(\mathbf{x}, t)$, and $s_2(\mathbf{x}, t)$ are the number density of plants, unripe and dispersible seeds *arriving* at point $\mathbf{x}$ at time t, respectively. The distribution functions $\beta_3^*(t)$, $\beta_1^*(t)$, and $\varphi^*(t)$ are the survival probabilities for plant death, germination, and seed ripening, respectively, and are defined by

$$\beta_3^*(t) = \int_t^\infty \beta_3(t')dt', \quad \beta_1^*(t) = \int_t^\infty \beta_1(t')dt', \quad \varphi^*(t) = \int_t^\infty \varphi(t')dt'. \quad (7.51)$$

Equation (7.45) describes the number of plants present at point $\mathbf{x}$ at time t and is the sum of plants that arrived at $\mathbf{x}$ at time t' earlier and of those that have survived during the interval $t - t'$. Equation (7.46) describes the number of plants that appear at point $\mathbf{x}$ at time t and is the sum of the initial distribution plus the type 2 seeds which fall and germinate at point $\mathbf{x}$ by time t. The factor $1 - P/K$ provides a form of density dependence by describing growth saturation due to the limited resources of the environment; K stands for the carrying capacity. Equation (7.47) describes the number of unripe seeds at point $\mathbf{x}$ at time t and is the accumulated number of unripe seeds produced on the plants. Equation (7.48) describes the number of unripe seeds that arrive at point $\mathbf{x}$ at time t and is the sum of unripe seeds already present at $t = 0$ plus those seeds, produced by adult plants, that survived since their germination at time $t - t'$. The number of mature seeds at point $\mathbf{x}$ at time t are those that arrived at point $\mathbf{x}$ at time $t - t'$ and have not germinated during this period and are described by (7.49). Equation (7.50) expresses the number of mature seeds that arrive at point $\mathbf{x}$ at time t as those that arrived at $t = 0$ plus those unripe seeds that appeared at $\mathbf{x}'$ at t' and waited a time $t - t'$ before dispersing to $\mathbf{x}$.

The steady states of the system (7.45), (7.46), (7.47), (7.48), (7.49), and (7.50), $(\overline{P}, \overline{S}_1, \overline{S}_2)$, fulfill the conditions

$$\overline{P} = \alpha_0 Y a_0 \overline{P}(1 - \overline{P}/K), \quad (7.52a)$$

$$\overline{S}_1 = \tau Y a_0 \overline{P}/\tau_m, \quad (7.52b)$$

$$\overline{S}_2 = \tau_1 \overline{S}_1/\tau, \quad (7.52c)$$

where

$$a_0 \equiv \int_0^\infty \beta_2(t)\beta_3^*(t)dt, \quad (7.53)$$

and τ, τ_1, and τ_m are the average seed ripening, seed germination, and plant mortality times, respectively. Since $\int_0^\infty \beta_2(t)dt = 1$ and $\beta_3^*(t) < 1$ for $t > 0$,

$$a_0 \equiv \int_0^\infty \beta_2(t)\beta_3^*(t)dt \leq \sup_{t \in [0,\infty)} [\beta_3^*(t)] \int_0^\infty \beta_2(t)dt = 1, \quad (7.54)$$

and the condition $a_0 < 1$ is always fulfilled. Equations (7.52) have two solutions:

$$(\overline{P}, \overline{S}_1, \overline{S}_2)_1 = (0, 0, 0) \quad (7.55)$$

and

$$(\bar{P}, \bar{S}_1, \bar{S}_2)_2 =$$

$$\left(K\left[1 - \frac{1}{\alpha_0 Y a_0}\right], K\frac{\tau}{\tau_m} Y a_0\left[1 - \frac{1}{\alpha_0 Y a_0}\right], K\frac{\tau_1}{\tau_m} Y a_0\left[1 - \frac{1}{\alpha_0 Y a_0}\right]\right). \quad (7.56)$$

For the steady state to be biologically meaningful, the population density must be positive, which requires

$$Y > Y_{\min} \equiv \frac{1}{\alpha_0 a_0}. \quad (7.57)$$

Equation (7.57) represents a threshold condition for invasion success in terms of the number of fertile unripe seeds released per plant. It depends only on the parameter α_0 and through a_0 on how the random times for death, $\beta_3^*(t)$, and maturity, $\beta_2(t)$, are distributed. The threshold satisfies the inequality $Y_{\min} > 1$, since both $a_0 < 1$ and $\alpha_0 < 1$. Expression (7.57) is equivalent to Lotka's equation [256] for growth in age-structured populations. In the present model, Lotka's result arises as a natural consequence, without the need for phenomenological arguments as in the original derivation [256, 445]. Equation (7.57) implies that the number of seeds giving rise to new plants at each life cycle, $\alpha_0 Y$, must be larger than the number of adult plants that died within a life cycle. We have presented first a three-stage model, because the life cycle is implemented more intuitively that way. The model can be nicely written as a closed and simple expression, which makes it more manageable. Equations (7.45), (7.46), (7.47), (7.48), (7.49), and (7.50) can be reduced to the following equation for $P(\mathbf{x}, t)$:

$$P(\mathbf{x}, t) = f(\mathbf{x}, t) + \frac{Y}{Y_{\min}} \int_0^t \beta(t') \int_{\mathbb{R}^2} w(\mathbf{x}') P(\mathbf{x} - \mathbf{x}', t - t') d\mathbf{x}' dt'. \quad (7.58)$$

Here $f(\mathbf{x}, t)$ incorporates all the terms where initial conditions appear, and $\beta(t)$ can be regarded as the PDF of times between successive generations. It is defined as

$$\beta(t) = \frac{1}{a_0} \int_0^t \beta_1(t_1) \int_0^{t-t_1} \beta_2(t_2) \beta_3^*(t_2) \varphi(t - t_1 - t_2) dt_2 dt_1. \quad (7.59)$$

The roles of the PDFs $\beta_1, \beta_2, \beta_3$, and φ are encapsulated in $\beta(t)$. Given a PDF for the generation of seeds and plant mortality we can calculate from (7.57) the minimum number of seeds that need to be produced by a plant to invade successfully. This outcome can sometimes be an alternative to the well-known model by Caswell [72] based on population matrices for predicting the population growth characteristics. The product $Y\alpha_0$ is approximately equivalent to the parameter λ of Caswell's model, which usually represents the population growth in the matrix formalism. Compared with Caswell's approach, where the condition $\lambda \gtrsim 1$ determines the invasive character of a species, we find that the threshold depends on the distributions of plant survival $\beta_3^*(t)$ and seed production $\beta_2(t)$. Therefore, this model can be seen as a generalization of Caswell's result for the case where temporal PDFs for every

process are considered. Let us now discuss some specific examples to show how simple expressions for $Y_{\min}$ can be obtained for different situations:

(a) Seed production and plant mortality are exponentially distributed, $\beta_2(t) = \tau_2^{-1} e^{-t/\tau_2}$ and $\beta_3(t) = \tau_m^{-1} e^{-t/\tau_m}$, where τ_i accounts for the typical time scale of the processes. In this case condition (7.57) leads to

$$Y_{\min} = \frac{1}{\alpha_0} \left(1 + \frac{\tau_2}{\tau_m} \right). \tag{7.60}$$

(b) Seed production occurs at a fixed time τ_2 after germination, $\beta_2(t) = \delta(t - \tau_2)$, and mortality is as in case (a). This matches plants producing seeds at approximately a fixed age, e.g., an annual species. This case leads to

$$Y_{\min} = \frac{1}{\alpha_0} e^{\tau_2/\tau_m}. \tag{7.61}$$

(c) Seed production occurs periodically with a period given by τ_2, $\beta_2(t) = \delta(t - \tau_2) + \delta(t - 2\tau_2) + \delta(t - 3\tau_2) + \cdots$, and mortality over time is again exponentially distributed. This choice for $\beta_2(t)$ allows us to take into account that a given plant can generate seeds many times, i.e., many generations, before dying and a seasonal behavior is introduced. Condition (7.57) leads to

$$Y_{\min} = \frac{1}{\alpha_0} (e^{\tau_2/\tau_m} - 1), \tag{7.62}$$

where the periodic behavior of $\beta_2(t)$ renders the condition (7.57) less restrictive compared to case (b).

(d) Seed production occurs periodically, as in (c), and the life span is fixed at τ_m, so $\beta_3(t) = \delta(t - \tau_m)$. We introduce a parameter n, defined as $n \equiv \text{Int}\left[\tau_2/\tau_m\right]$, to define the number of times that plants produce seeds before they die. ("Int" denotes the integer part of a number.) Condition (7.57) has the form

$$Y_{\min} = \frac{1}{\alpha_0 n}. \tag{7.63}$$

7.3.2 Applications to the Invasion Success of Weeds

To illustrate the applicability (7.57), we compare it with published data of three different invasive weed species in their native and exotic ranges. In the exotic range, species can exhibit invasive behavior. The model should show that predicted $Y_{\min}$ values are higher than the actual plant fecundities in the native range and lower than actual plant fecundities in the exotic range. Although the three species studied show

important differences in their life cycle, the model can account for these differences easily by introducing suitable PDFs.

7.3.2.1 E. plantagineum

This is an annual plant native to the western Mediterranean basin which was introduced and became invasive in pastures in Australia. In [172] the authors compared its population dynamics in Evora, Portugal, where this plant is native, with Canberra, Australia, where this plant is exotic. From the published data we accurately estimated the parameters needed to evaluate Y_{min}. As *E. plantagineum* is an annual, all surviving plants produce seed once at age 1 yr and die. This presents the case in (7.63) with $n = 1$. To estimate the parameters Y and α_0, we average the data published in [172] over all the populations considered. If one assumes that seeds produced can survive in the seedbank up to 6 yr [172], then

$$\alpha_0 = G S_i h \left[1 + \sum_{j=1}^{5} (S_b)^j \right], \tag{7.64}$$

where G is the seedling establishment fraction, S_i is the seedbank incorporation rate, h is the fraction of the seedbank germinating every year, and S_b is the seedbank survival rate. The averaged results obtained from our analysis are given in Table 7.4. The theoretical prediction for Y_{min} holds, as only those populations where $Y > Y_{min}$ exhibit invasive behavior.

7.3.2.2 C. scoparius

This leguminous shrub is native to western Europe and has become an invasive weed in some Australian ecosystems, suppressing native species and increasing fire risk [212]. We compare the population dynamics of this species in a native habitat in southern France [344] with those from an invasive population in Australia [396].

Table 7.4 Parameter estimates from our model of the invasiveness of *E. plantagineum*, *C. scoparius*, and *C. nutans* in their native and exotic range. (1) Portugal, (2) France, (3) Australia

Plant	Range	α_0	a_0	Y_{min}	Actual Y
E. Plantagineum	Native[1]	7.1×10^{-3}	0.18	783	322
	Exotic[3]	1.2×10^{-2}	0.66	124	261
C. scoparius	Native[2]	0.0314	0.06	531	81.6
	Native (SC)	0.0314	2.27	14.0	81.6
	Exotic[3]	0.023	0.16	272	300
C. nutans	Native[2]	0.01	0.109	917	125
	Exotic[3]	0.12	7.2×10^{-3}	1161	1950

In the native range, the parameters can be estimated as follows. The average percentage seed germination was used to estimate α_0, see Fig. 2 in [344]. Fecundity was estimated from average seed production per unit area (38.3 seeds per m^2), taken from the total study area (400 m^2) and that 7% of plants produced any seeds by the end of the experiment ($Y = 81.6$ seeds per plant). The survival distribution is taken from Fig. 4 in [344], where from the second-year sampling, survival decay is approximately a linear function of time. One of the treated subpopulations, labeled single-cultivated (SC) in the original work, see also Table 7.4, had very different survival behavior from the others. This subpopulation has to be studied separately.

Finally, one can estimate the germination distribution $\beta_2(t)$ using that 18% of the flowering plants produced seeds in their first flowering year (at 3 yr of age), as noted in [396]. Assuming that after the second flowering year all surviving plants (they can survive up to 20 yr) could produce seeds, we obtain a PDF for seed production over time of the form

$$\beta_2(t) = \sum_{j=t_i}^{t_f} \gamma_j \delta(t - j), \tag{7.65}$$

where $t_i = 3$ yr, $t_f = 20$ yr, $\gamma_3 = 0.18$, and $\gamma_{l>3} = 1$. Estimation of the parameters for *C. scoparius* in the exotic range was carried out in a similar way as for the native range, since the published data are very similar. The averaged value $\alpha_0 = 0.023$ is already given in the text in [396] and fecundity data are also presented in graphical form. The age at the first seed production is also studied in the original work, and from that we estimated $\beta_2(t)$ as in (7.65), but with $t_i = 2$ yr, $t_f = 20$ yr, $\gamma_2 = 0.003$, $\gamma_3 = 0.068$, $\gamma_4 = 0.706$, $\gamma_5 = 0.990$, and $\gamma_{j>5} = 1$. Finally, the survival data showed the best fit to a power law of the form

$$\beta_3^*(t) \approx \frac{1}{1.607 + 0.844 t^{2.37}}. \tag{7.66}$$

The estimated values of Y and $Y_{\min}$ for the native and exotic range in Table 7.4 are as expected for noninvasive and invasive populations, respectively, except for the SC subpopulation in the native range, which our Y and $Y_{\min}$ estimates suggest should exhibit invasive behavior. However, the SC subpopulation relates to a disturbed treatment, and survival was very different from that found in other subpopulations in the same study. We conclude that this case is not representative of the characteristic behavior of *C. scoparius* in its native range.

7.3.2.3 C. nutans

This thistle of European origin has become a weed in many parts of the world. Demographic data of *C. nutans* for some native populations in France, studied over more than 2 yr reported at intervals of 3 months, were published in [397]. The parameters corresponding to the exotic range have been extracted from analogous

published data for one site in Australia [479]. Fecundity Y was estimated from seed density and flowering plant density. The probability α_0 was estimated from the product of the proportion of surviving mature seeds entering the seedbank and the proportion of the seedbank recruited. The values are listed in Table 7.4, where lower α_0 values in the native range reflect the important effect of predispersal predation [396]. *C. nutans* is monocarpic, i.e., it dies after seed production. Since the age at flowering can vary among individuals, we made the same assumption as used for *E. plantagineum*. In this case we needed to produce a survival distribution, which could be done accurately from the published demographic data and leads to

$$\text{Native:} \quad \beta_3^*(t) \approx \frac{1}{1 + 9t^{1.47}}, \tag{7.67a}$$

$$\text{Exotic:} \quad \beta_3^*(t) \approx \frac{1}{1 + 106t^{2.69}}. \tag{7.67b}$$

The data indicate individual survival is greater in the native range than in the exotic habitat, as is also evident from a_0 values in Table 7.4. Nevertheless, the importance of the predispersal predation on the seedbank and the great differences in fecundity between the two ranges are the factors that determine the invasive behavior of *C. nutans* in Australia [479], as confirmed by comparing Y and $Y_{\min}$ parameters in Table 7.4.

7.3.3 Invasion Velocity of Weeds

Recent experimental work [221] for another invasive thistle, *C. acanthoides*, was used to test our theoretical predictions for the invasion rate. Rosettes of *C. acanthoides* were introduced into uninvaded plots in Maryland (USA), where each rosette was considered as a founder individual for new invasive thistle populations. The cumulative probability distribution for jump lengths $W(r)$ was measured for different years and different treatments, named 0x, 1x, and 2x clippings. The relation between $W(r)$ and $w(r)$ is given by $W(r) = 2\pi \int_0^r r' w(r') \mathrm{d}r'$ or

$$w(r) = \frac{1}{2\pi r} \frac{\mathrm{d}W(r)}{\mathrm{d}r}. \tag{7.68}$$

The Hamilton–Jacobi equation corresponding to (7.58) reads

$$1 = \frac{Y}{Y_{\min}} \widehat{\beta}(H) \check{w}(p), \tag{7.69}$$

where $\widehat{\beta}(H)$ is the Laplace transform of $\beta(t)$ with argument H and

$$\check{w}(p) = 2\pi \int_\Omega r w(r) I_0(pr) \mathrm{d}r. \tag{7.70}$$

We have assumed isotropic dispersal, Ω is the spatial dispersal domain, and $I_0(\cdot)$ is the modified Bessel function of order 0. One can consider 1 year as the fixed time between two successive generations, i.e., $\beta(t) = \delta(t - \tau_g)$ with $\tau_g = 1$ yr [221]. The invasion velocity is, from (4.47) and (7.69),

$$v = \frac{1}{\tau_g} \min_{p>0} \frac{1}{p} \ln \left[\frac{Y}{Y_{\min}} \breve{w}(p) \right]. \tag{7.71}$$

To compare the theoretical prediction (7.71) with the observed results in [221], it is necessary to know the value for the quotient $Y/Y_{\min}$. The field data are not on a fine enough spatial scale. However, it is possible to make this comparison with a desirable accuracy for the case of the invasion in 1995, where the number of seeds released per plot was approximately 1111 seeds per plot for any treatment.

Since $Y_{\min}$ is not known, we have estimated it by fitting the theoretical prediction with the observed value. Fitting the cumulative distribution $W(r)$ to the experimental data for 0x clipping in 1995 one can estimate, with a correlation coefficient $R^2 = 0.961$, the dispersal kernel to be of the form

$$w(r) = \frac{k}{2\pi r} \frac{e^{-kr}}{e^{-kr_{\min}} - e^{-kr_{\max}}}. \tag{7.72}$$

Here $k = 4.63$ m^{-1} is the inverse of the characteristic jump length, and $r_{\min} = 0.04$ m and $r_{\max} = 0.44$ m are the minimum and maximum jump lengths. The dispersal domain is $\Omega = \{r : r \in [r_{\min}, r_{\max}]\}$. Substituting (7.72) into (7.70) and integrating from $r_{\min}$ to $r_{\max}$, we find $Y_{\min} = 44.4$, which will be used for comparing with 1x and 2x clippings.

Fitting the dispersal kernel to the data from the 1x clipping for 1995, we obtain the same kernel as in (7.72), but with $R^2 = 0.977$, $k = 3.57$ m^{-1}, $r_{\min} = 0.036$ m, and $r_{\max} = 0.55$ m. Substituting these values into (7.72) and (7.70), we can calculate the invasion rate from (7.71) and obtain 0.45 m/yr, which is very close to the observed result of 0.49 m/yr in [221].

By fitting the dispersal kernel to the data for 2x clipping in 1995 we obtain, $R^2 = 0.982$,

$$w(r) = \frac{kr + k_1}{2\pi r}, \tag{7.73}$$

with $k = 2.87$ m^{-1}, $k_1 = 0.14$, $r_{\min} = 0$, and $r_{\max} = 0.30$ m, with a dispersal domain $\Omega = \{r : r \in [0, r_{\max}]\}$. In this case the invasion velocity is 0.26 m/yr, which is again in agreement with the observed result of 0.27 m/yr in [221].

These results can be discussed in light of those obtained in [413], where the invasion velocities for *C. acanthoides* and *C. nutans* were also studied. In that work, the authors obtained some predictions for the front velocities by using nonparametric [78] and mechanistic estimates of the dispersal kernel. Their work was specially

focused on the role of the dispersal patterns and the influence of long-distance dispersal on the invasion velocity, while in the present approach we have instead highlighted the importance of the PDFs governing the life cycle of individuals. The present results are restricted to local dispersal. The work by Jongegans, which we used as a reference, was restricted to dispersal distances up to 4 m, and we have introduced the thresholds $r_{\min}$ and $r_{\max}$ to remove the problem of data extrapolation [78, 79]. These differences prevent us from performing a direct comparison between both works. We stress, however, that they both agree with the idea that models based on PDFs can fit quite well the behavior of weed invasions, if the dispersal kernel can be implemented accurately.

Exercises

7.1 Consider the RT model for the hunter-gatherer interaction of Sect. 7.1.2. Obtain (7.11) for the migration front velocity.

7.2 Find the steady states given by (7.55) and (7.56) for the system (7.45), (7.46), (7.47), (7.48), (7.49), and (7.50). Study their temporal stability.

7.3 Obtain (7.58) from the system (7.45), (7.46), (7.47), (7.48), (7.49), and (7.50).

7.4 Calculate the Hamilton–Jacobi equation (7.69) corresponding to (7.58).

Chapter 8
Biomedical Applications

Reaction–transport equations have found many applications to biological processes of interest in medicine and microbiology. Examples range from cancer invasion to virus dispersal and transport in spiny dendrites.

8.1 Cancer Invasion

Cancer arises essentially from mutations of single somatic cells that are able to divide uncontrollably, invade adjacent normal tissues, and give rise to secondary cell clusters, tumors, at sites different from their primary origin, metastasis. Numerous mathematical models have been constructed to describe the competition between tumor cells and surrounding normal cells. These include reaction–diffusion equations that describe the dispersal behavior of tumor cell growth together with the interaction between normal and cancer cells [155, 156, 402]. Other models deal with cancer evolution and its interaction with the immune system [399, 31], the motility of gliomas [427, 428], and their dichotomy between proliferation and migration [119, 120].

8.1.1 Tumor–Host Interaction

Reaction–diffusion models have very successfully accounted for the interaction between normal and tumor cells. The diffusion terms in these models can be broadly divided into two categories, linear and nonlinear diffusion. In linear diffusion models, the flux of one cell type depends only on the concentration of cells of the same type. In nonlinear diffusion models, the presence of one cell type affects the diffusion of cells of a different type. Models with nonlinear diffusion have described the spatial dispersal and temporal development of tumor tissue, normal tissue, and excess H^+ ion concentration [155]. They assume that transformation-induced reversion of neoplastic tissue creates a microenvironment around the tumor where tumor cells survive and proliferate, whereas normal cells do not remain viable. These conditions, favorable for tumor cells and unfavorable for normal cells, are due to

increased production of H^+ ions, i.e., the presence of a pH gradient, and the diffusion of those ions into surrounding normal tissue. Model results are consistent with tumor growth rates in vivo. Other models with nonlinear diffusion describe tumor encapsulation. Solid tumors typically undergo an initial period of avascular growth, after which they become quiescent for a long time. The first steps in the metastatic cascade end the dormant phase. A significant feature of the quiescent phase is the presence, in some cases, of capsules of dense and fibrous extracellular matrix around the solid tumor. The formation of a capsule is a key prognostic indicator in a wide range of cancers. However, the mechanisms responsible for capsule formation remain unclear. Two competing hypotheses have been advanced: the expansive growth hypothesis, which holds that remodeling of existing extracellular matrix without any new matrix production generates the capsule, and the foreign body hypothesis which assumes that de novo cellular secretion of collagen plays a key role. Mathematical models have been developed to study the implications of the expansive growth hypothesis [349, 401]. The model in [349] exhibits traveling wave solutions where a pulse of extracellular matrix, corresponding to a capsule, moves in parallel with the invasive tumor front. In [401], saturation in the extent of matrix rearrangement per cell is included, and the existence of stable solutions for a pulse of extracellular matrix, corresponding to a capsule, moving ahead of the growing tumor is established. Moreover, the author shows that the predicted density of matrix in the capsule correlates with the rate of local matrix movement and remodeling per cell. This implies that the capsule density is not correlated with either the velocity at which the tumor grows or its size. This explains the wide discrepancies between studies attempting to correlate tumor size and capsule incidence or thickness and argues against the conventional intuition that these should be correlated if the capsule forms without matrix production.

A simple model for the interaction between tumor and normal cells with linear diffusion has been analyzed as an inverse problem [156]. The stability of the invasion front imposes constraints on the model parameters, which demonstrate the limitations of traditional therapeutic strategies that focus solely on killing tumor cells or reducing their proliferation rate. The model assumes that the tumor–host interface of an invasive cancer is morphologically a traveling wave, where the tumor edge represents a plane wave front propagating into, and replacing, the surrounding normal tissue. If $\rho_N(x, t)$ and $\rho_T(x, t)$ denote normal and tumor cell densities, respectively, at time t and spatial position x, then the reaction–diffusion system takes the form

$$\frac{\partial \rho_N}{\partial t} = D_N \frac{\partial^2 \rho_N}{\partial x^2} + r_N \rho_N \left(1 - \frac{\rho_N}{K_N} - \frac{b_{NT} \rho_T}{K_N} \right), \tag{8.1a}$$

$$\frac{\partial \rho_T}{\partial t} = D_T \frac{\partial^2 \rho_T}{\partial x^2} + r_T \rho_T \left(1 - \frac{\rho_T}{K_T} - \frac{b_{TN} \rho_N}{K_T} \right). \tag{8.1b}$$

We assumed Lotka–Volterra kinetics between tumor and normal cells in (8.1). The maximum growth rates of normal and tumor cells, i.e., the net result of tumor cell doubling minus tumor cells loss from apoptosis or necrosis, are r_N and r_T,

respectively. K_N and K_T denote the maximal normal and tumor cell densities, b_{NT} and b_{TN} are the lumped competition terms, and D_N and D_T are the cellular diffusion coefficients. Note that b_{NT} represents the negative effects of a tumor on normal tissue, such as tumor-induced extracellular matrix breakdown and microenvironmental changes, and b_{TN} includes a variety of host defenses, such as immune response. The steady states of (8.1) are

$$\text{state I:} \quad (\overline{\rho}_N, \overline{\rho}_T) = (0, 0), \tag{8.2}$$

$$\text{state II:} \quad (\overline{\rho}_N, \overline{\rho}_T) = (K_N, 0), \tag{8.3}$$

$$\text{state III:} \quad (\overline{\rho}_N, \overline{\rho}_T) = (0, K_T), \tag{8.4}$$

$$\text{state IV:} \quad (\overline{\rho}_N, \overline{\rho}_T) = \left(\frac{K_N - b_{NT} K_T}{1 - b_{NT} b_{TN}}, \frac{K_T - b_{TN} K_N}{1 - b_{NT} b_{TN}} \right). \tag{8.5}$$

State I is the trivial solution; it is unstable and biologically irrelevant. State II corresponds to normal, healthy tissue without tumor cells. The system evolves to this state, regardless of the initial state, if $b_{NT} K_T < K_N$ and $b_{TN} K_N > K_T$. If the initial state is sufficiently close to State II, only the second condition needs to be satisfied. State III corresponds to complete tumor invasion with total destruction of normal tissue. The system evolves to this state, regardless of the initial state, if $b_{NT} K_T > K_N$ and $b_{TN} K_N < K_T$. If the initial state is sufficiently close to State III, only the first condition is needed. State IV corresponds to a state of coexistence between tumor and normal cells. The system evolves to this state, if $b_{NT} K_T < K_N$ and $b_{TN} K_N < K_T$.

In this model, an invasive cancer, where the tumor edge advances as a propagating front into normal tissue, corresponds to a transition to a stable state containing tumor cells, state III or IV. The Hamilton–Jacobi formalism provides the propagation velocity of a front connecting state II to state III, an invasive tumor front,

$$v = 2 \left[r_T D_T \left(1 - \frac{b_{TN} K_N}{K_T} \right) \right]^{1/2}, \tag{8.6}$$

if the front evolves from an initial condition with compact support. In order to stop or reverse the cancer invasion, one needs to alter the stability of the states II and III. Sufficient conditions are, for example, b_{NT} large and b_{TN} small. The most obvious contribution to b_{NT} comes from the fact that tumor cells consume much more resources than do normal cells. Another possibly significant contribution is the acidic intercellular pH in tumors as a result of the glycolytic metabolic pathways. Other factors could be extracellular matrix breakdown by tumor-produced proteinases or normal cell crowding by increased interstitial pressure in tumors.

A recovery front, where the invasive front travels in the opposite direction and ensures the complete eradication of the tumor, requires state II to be stable and state III unstable. To this end, the conditions $b_{NT} K_T < K_N$ and $b_{TN} K_N > K_T$ must be met, and the velocity of the recovery front is given by

$$v = 2 \left[r_N D_N \left(1 - \frac{b_{NT} K_T}{K_N} \right) \right]^{1/2}. \tag{8.7}$$

Consequently, therapeutic strategies should include the following aspects: (i) Reduce K_T, which can be achieved by decreasing vascularity. (ii) Reduce b_{NT} and increase b_{TN}, which can be achieved by therapy oriented toward decreasing the uptake and utilization of substrate by tumor cells, increasing the avidity of substrate uptake by normal cells, or reducing the production of protease and tumor acid. (iii) Increase K_N, which can be achieved by therapy directed toward normal cells. The model predicts that therapy that decreases contact inhibition in normal cells by increasing K_N could result in a tumor regression.

8.1.2 Tumor–Host Interaction with Contact Inhibition

Linear diffusion satisfactorily describes the transport mechanism for a single popu-lation. For interacting populations, linear diffusion terms imply that the populations are able to mix completely, with the movement of one cell type unaffected by the presence of cells of the other type. The reality is exactly the opposite. Cell move-ment is typically halted by contact with another cell. This phenomenon is known as *contact inhibition* and is very well documented for many types of cells. Sherratt introduced a phenomenological model to account for contact inhibition [402]. Con-sider the interaction between normal and tumor cells with concentrations $\rho_N(x, t)$ and $\rho_T(x, t)$, respectively. The overall cell flux of both populations is given by $-\partial_x(\rho_N + \rho_T)$. A fraction $\rho_N/(\rho_N + \rho_T)$ of this flux corresponds to normal cells, so that the flux of normal cells is $-\left[\rho_N/(\rho_N + \rho_T)\right]\partial_x(\rho_N + \rho_T)$, and a similar expression for the flux of tumor cells. These expressions indicate that the movement of one population is inhibited by the presence of the other. The system of dimen-sionless reaction–diffusion equations reads [402]

$$\frac{\partial \rho_N}{\partial t} = \frac{\partial}{\partial x} \left[\frac{\rho_N}{\rho_N + \rho_T} \frac{\partial}{\partial x} (\rho_N + \rho_T) \right] + \rho_N \left(1 - \rho_N - \rho_T \right), \tag{8.8a}$$

$$\frac{\partial \rho_T}{\partial t} = \frac{\partial}{\partial x} \left[\frac{\rho_T}{\rho_N + \rho_T} \frac{\partial}{\partial x} (\rho_N + \rho_T) \right] + \rho_T \left(\gamma - \rho_N - \rho_T \right). \tag{8.8b}$$

The term $-\rho_N - \rho_T$ in the kinetics of (8.8) represents the decrease in the cell division rate due to crowding. The constant γ (> 1) expresses the proliferative advantage of the tumor cell population. Note that the model is in one-dimensional space and that the kinetic terms are of Lotka–Volterra competition type.

Consider front-like initial conditions, such that the density of normal cells travels to the left connecting $\rho_N = 0$ to $\rho_N = 1$ and the density of tumor cells travels to the right connecting $\rho_T = 0$ to $\rho_T = \gamma$ [402]. If $\gamma > 1$, fronts of normal and tumor cells move toward one another. As they approach each other, the tumor front continues

to advance, but more slowly, while the normal cell density changes direction and moves in parallel with that of tumor cells.

This change in the dynamics when the fronts meet and interact is due to the contact inhibition, since this behavior does not occur in the case of linear diffusion. Biologically, the front dynamics correspond to a tumor invasion and is exactly the behavior seen in the very early stages of a carcinoma. The tumor cells proliferate very fast and develop a dense ball that replaces surrounding tissue. Numerical experiments suggest that for $\gamma > 1$ a family of fronts exists, whose velocity depends on the width of the initial density of tumor cells but not on the width of the initial density of the normal cells. Figure 8.1 depicts the front profiles for the densities of normal and cancer cells for $\gamma = 2$. Analysis [402] shows that the use of simple
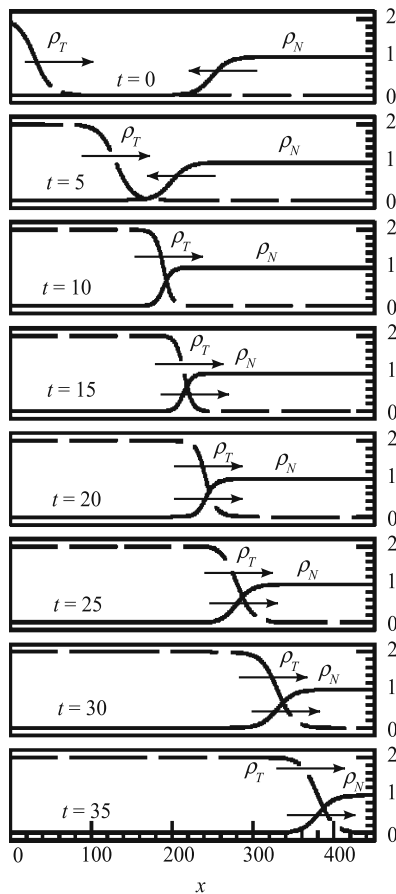
Fig. 8.1 Typical solutions of (8.8) for $\gamma = 2$. The initial condition are $\rho_N(x, 0) = [1 + \exp(-0.1(x - 250))]^{-1}$ and $\rho_T(x, 0) = [1 + \exp(0.1(x - 30))]^{-1}$. The front for ρ_T continues to advance in parallel with the receding front for ρ_N. Reprinted from [402]. Copyright 2000 with permission from The Royal Society

linear diffusion in (8.8) leads to an overestimate of the front velocity of interfaces between normal and tumor cell populations by a factor that is at least 2.4, and very much larger when the competitive advantage is small.

8.1.3 Glioma Invasion

The mathematical models discussed above and many others in the literature were designed mainly to describe solid tumors. The understanding of malignant gliomas is much less complete. Gliomas are intracranial neoplasms of glial cells, neural cells capable of division, and usually occur in the upper cerebral hemisphere. However, gliomas can be found throughout the brain due to their highly diffuse behavior. Experimental results indicate that within 7 days of tumor implantation in rat brains, gliomas can be identified throughout the central nervous system. Progress in diagnostic techniques and detection capabilities, such as computer tomography and magnetic resonance imaging, has resulted in earlier detection of gliomas and their geometric patterns. Despite this progress, the benefits of early treatments remain minimal. For example, even with extensive surgical excision well beyond the visible tumor boundary, regeneration near the edge of resection ultimately results. This indicates a potential failing point of the treatment. Most glioma treatments are directed locally to the bulk mass when, in fact, the action of the tumor growth and invasion is elsewhere.

Mathematical modeling has been used as a theoretical framework to describe the invasive nature of gliomas [439, 480, 427, 184] by isolating two characteristics: proliferation and migration (invasion). Experimental studies show a lower proliferation rate of mobile gliomas in comparison with the tumor core. This indicates an inverse correlation between mobility and proliferation of gliomas, supported by numerous experimental data obtained in vitro and clinical data obtained in vivo [158]. This phenomenon was dubbed the migration–proliferation dichotomy by Giese and Westphal [160]. Diffusive transport was considered to represent the active mobility of gliomas. Since malignant gliomas implanted in the brain of rats disperse more quickly along the white matter than along the grey matter, some mathematical models proposed heterogeneous reaction–diffusion equations with a spatially varying diffusion coefficient [427]. These models include linear reaction terms instead of logistic growth. Although logistic growth would be more accurate, the differences in calculated survival times are so slight as to be negligible on the time scale considered [439, 480]. An excellent review of these mathematical models can be found in Chap. 11 of the second volume of Murray's book [310]. In this section we focus on an alternative way to model the dichotomy between proliferation and migration of gliomas. The molecular basis for this dichotomy has been established [478]. It forms the foundation for numerical models of brain tumors and their fractal topologies [267, 268]. These models focus primarily on the effect of cell fission on transport properties of cells. An essential decrease in cell mobility during fission time is determined by the interaction of cells with their environment. In vitro experiments of cell

dispersal confirm the essential decrease in cell dispersal during cell proliferation. An agent-based model was developed recently where glioma transport is described in terms of a local-search mechanism. The purpose of this *conscious search* is to find and then invade the most permissive location in extracellular matrix [267]. A simplified scheme of migration–proliferation dichotomy in terms of a CTRW was studied in [216, 217, 119]. It involves two random processes, cell fission with characteristic time $\mathcal{T}_f$ and cell migration with characteristic duration $\mathcal{T}_t$. On the time scale $\mathcal{T}_f$, the cells interact strongly and motility of cells is small. On the time scale $\mathcal{T}_t$, interaction between cells is weak and motility of cells is determined by a characteristic jump length proportional to $\mathcal{T}_t$. Moreover, the CTRW can deal with chemotaxis or haptotaxis by considering biased random walks and matrix cell adhesions by using heavy-tailed waiting time distributions.

Experimental observations of *migration–proliferation dichotomy* suggest that the process of tumor cell invasion consists of two states. In state 1, the migratory phenotype, the cells move randomly, but there is no cell proliferation. In state 2, the proliferating phenotype, the cancer cells do not migrate and only proliferation takes place. To describe the random switching between the two phenotypes, we employ a two-state Markov chain model. A cell of type 1 remains in state 1 during a waiting time τ_1 and then switches to a cell of type 2. After a waiting time τ_2, spent in state 2, it switches back to a cell of type 1. Both waiting times τ_1 and τ_2 are mutually independent random variables, distributed exponentially with parameters β_1 and β_2,

$$\mathcal{P}(\tau_k) = \beta_k \exp\left(-\beta_k \tau_k\right) \tag{8.9}$$

with $k = 1, 2$. The parameters β_k are the switching rates, namely, β_1 is the rate of switching from state 1 to 2, while β_2 determines the transition rate $2 \rightarrow 1$. We assume that the growing tumor is a spheroid consisting of the tumor core with a high density of cells and the outer invasive zone where the cell density is much smaller. To describe the cancer cells of the two phenotypes, we introduce the density of the cells of migrating phenotype, $\rho_1(\mathbf{x}, t)$, and the density of the cells of proliferating phenotype, $\rho_2(\mathbf{x}, t)$. The balance equations for the densities are

$$\rho_1(\mathbf{x}, t) = \rho_1(\mathbf{x}, 0)\Psi(t)e^{-\beta_1 t} + \int_0^t \int_{\mathbb{R}^d} \rho_1(\mathbf{x} - \mathbf{x}', t - t')\psi(\mathbf{x}', t')e^{-\beta_1 t'}\, d\mathbf{x}'dt'$$

$$+ \beta_2 \int_0^t \rho_2(\mathbf{x}, t - t')\Psi(t')e^{-\beta_1 t'}\, dt', \tag{8.10a}$$

$$\rho_2(\mathbf{x}, t) = \rho_2(\mathbf{x}, 0)e^{-\beta_2 t} + \int_0^t f\left[\rho_1(\mathbf{x}, t - t'), \rho_2(\mathbf{x}, t - t')\right]e^{-\beta_2 t'}\, dt'$$

$$+ \beta_1 \int_0^t \rho_1(\mathbf{x}, t - t')e^{-\beta_2 t'}\, dt', \tag{8.10b}$$

where $\psi(\mathbf{x}, t)$ is the joint probability density function of making a jump $\mathbf{x}$ in the time interval $(t', t' + dt')$, and $\mathbb{R}^d$ indicates that integration is over d-dimensional space. Cell migration, random jumps, involves a receptor-mediated adhesion to

matrix proteins, matrix degradation by proteases, detachment from adhesion sites, active invasion into "new" intercellular space formed by degradation, etc. It would be extremely difficult, not to say impossible, to formulate a rigorous deterministic model for this process. Since so many factors are involved, a random walk with memory effects represents a good alternative. The active mechanism of migration of tumor cells involves small random jumps and waiting times between jumps. The latter are expected to be of the same order as the proliferation time. The dynamics is obviously random, and its distribution is given by the PDF $\phi(t)$. Equation (8.10a) is the conservation law for cells of type 1 at time t at position $\mathbf{x}$. The first term on the right-hand side $\rho_1(\mathbf{x}, 0)\Psi(t)e^{-\beta_1 t}$ represents cells of type 1 that remain up to time t at position $\mathbf{x}$, such that no jump occurred and no switch in phenotype occurred. This term involves the survival probability $\Psi(t)$, the probability that a cell of type 1 makes no jump until time t. The exponential factor $e^{-\beta_k t} = 1 - \int_0^t \mathcal{P}(\tau_k)d\tau_k$ is the probability that cells of phenotypes k do not switch until time t. The independence of the random jumps and switching leads to the probability $\Psi(t)e^{-\beta_1 t}$, while the first factor $\rho_1(\mathbf{x}, 0)$ is the initial density of cells of type 1 at $\mathbf{x}$. The second term,

$$\int_0^t \int_{\mathbb{R}^d} \rho_1(\mathbf{x} - \mathbf{x}', t - t')\psi(\mathbf{x}', t')e^{-\beta_1 s}d\mathbf{x}'dt', \qquad (8.11)$$

represents the number of cells of type 1 arriving at $\mathbf{x}$ up to time t. We assume the following random mechanism of migration: a cell of type 1 at time $t - t'$ at position $\mathbf{x} - \mathbf{x}'$ waits a random time t' before jumping to position $\mathbf{x}$ and remains a cell of type 1. The last term $\beta_2 \int_0^t \rho_2(\mathbf{x}, t - t')\Psi(t')e^{-\beta_1 t'}dt'$ represents the number of cells of type 2 that switch to cells of type 1 up to time t and remain the cells of type 1, the factor $e^{-\beta_1 t'}$. It also takes into account the fact that if the transition $2 \to 1$ occurs at time $t - t'$, then no jump takes place during the remaining time t', the factor $\Psi(t')$.

Equation (8.10b) describes the balance of cells of proliferating phenotype, which do undergo spatial jumps. The first term on the right-hand side, $\rho_2(\mathbf{x}, 0)e^{-\beta_2 t}$, represents the density of cells of type 2 that remain up to time t at position $\mathbf{x}$ such that no switch $2 \to 1$ takes place. The second term on the right-hand side $\int_0^t f\left[\rho_1(\mathbf{x}, t - t'), \rho_2(\mathbf{x}, t - t')\right]e^{-\beta_2 t'}dt'$ represents the proliferation of cells of type 2, which occurs providing that no switch takes place up to time t. The last term $\beta_1 \int_0^t \rho_1(\mathbf{x}, t - t')e^{-\beta_2 t'}dt'$ represents the number of cells of type 1 switching to state 2 during the time interval $(0, t)$.

The PDF $\psi(\mathbf{x}, t)$ can be written in decoupled form $\psi(\mathbf{x}, t) = w(\mathbf{x})\phi(t)$, where $\phi(t)$ is the waiting time PDF and $w(\mathbf{x})$ is the PDF of cell jumps. The balance equations (8.10a) and (8.10b) can be rewritten as a system of integro-differential equations:

$$\frac{\partial \rho_1}{\partial t} = \int_0^t K(t - t') \int_{\mathbb{R}^d} \left[\rho_1(\mathbf{x} - \mathbf{x}', t') - \rho_1(\mathbf{x}, t') \right] w(\mathbf{x}') d\mathbf{x}' dt' - \beta_1 \rho_1 + \beta_2 \rho_2,$$

$$(8.12a)$$

$$\frac{\partial \rho_2}{\partial t} = f(\rho_1, \rho_2) + \beta_1 \rho_1 - \beta_2 \rho_2. \tag{8.12b}$$

The memory kernel $K(t)$ is, in terms of its Laplace transform,

$$\hat{K}(s) = \frac{(s + \beta_1) \hat{\phi}(s + \beta_1)}{1 - \hat{\phi}(s + \beta_1)}. \tag{8.13}$$

The cells of the migrating phenotype are biased to migrate away from the tumor spheroid core. The reasons for this asymmetrical motion are the nonuniform nutrient concentration (chemotaxis), the gradient of cell adhesion sites (haptotaxis), etc. Experimental observations suggest that cell jumps are controlled by adhesion of tumor cells to extracellular matrix and that jump lengths are very small [159]. Therefore $w(\mathbf{x})$ is a rapidly decaying function for large $|\mathbf{x}|$. We can use a Taylor series in (8.12a), expand $\rho_1(\mathbf{x} - \mathbf{x}', t - t')$ in $\mathbf{x}$, and truncate the series at the second moment. This truncation is a well-defined procedure, since the higher moments become progressively smaller. We have

$$\int_{\mathbb{R}^d} \rho_1(\mathbf{x} - \mathbf{x}', t - t') w(\mathbf{x}') d\mathbf{x}' = \rho_1(\mathbf{x}, t - t') - \sum_{i=1}^d \langle x_i \rangle \frac{\partial \rho_1}{\partial x_i} +$$

$$+ \frac{1}{2} \sum_{i=1}^d \langle x_i x_j \rangle \frac{\partial^2 \rho_1}{\partial x_i \partial x_j} + \cdots, \tag{8.14}$$

where

$$\langle x_i \rangle = \int_{\mathbb{R}^d} x_i w(\mathbf{x}) d\mathbf{x}, \tag{8.15}$$

$$\langle x_i x_j \rangle = \int_{\mathbb{R}^d} x_i x_j w(\mathbf{x}) d\mathbf{x}. \tag{8.16}$$

If the cell jumps are normally distributed, the characteristic function of $w(\mathbf{x})$ is $\tilde{w}(\mathbf{k}) = \exp\left(i a_i k_i - \frac{1}{2} \sigma_{ij} k_i k_j \right)$. The positive definite matrix σ_{ij} can be written in terms of the first two moments

$$\sigma_{ij} = \langle x_i x_j \rangle - \langle x_i \rangle \langle x_j \rangle. \tag{8.17}$$

The PDF $w(\mathbf{x})$ is given by

$$w(\mathbf{x}) = \frac{1}{(2\pi)^{d/2} (\det \sigma)^{1/2}} \exp\left[-\frac{1}{2} \left(\sigma^{-1} \right)_{ij} (x_i - \langle x_i \rangle)(x_j - \langle x_j \rangle) \right]. \quad (8.18)$$

We assume that the characteristic length scale for the tumor front is much smaller than the radius of the initial tumor spheroid and that the bias acts in the radial direction. These assumptions allow us to neglect all curvature effects and to consider the propagation as that of an effective plane front in the radial direction. Then (8.14) reads

$$\int_{\mathbb{R}^d} \rho_1(\mathbf{x} - \mathbf{x}', t - t') w(\mathbf{x}') d\mathbf{x}' = \rho_1(r, t - t') - m_1 \frac{\partial \rho_1}{\partial r} + \frac{1}{2} m_2 \frac{\partial^2 \rho_1}{\partial r^2} + \cdots, \quad (8.19)$$

which can be substituted into (8.12a):

$$\frac{\partial \rho_1}{\partial t} + m_1 \int_0^t K(t') \frac{\partial \rho_1(r, t - t')}{\partial r} dt'$$

$$= \frac{m_2}{2} \int_0^t K(t') \frac{\partial^2 \rho_1(r, t - t')}{\partial r^2} dt' - \beta_1 \rho_1 + \beta_2 \rho_2, \quad (8.20a)$$

$$\frac{\partial \rho_2}{\partial t} = r\rho_2 \left(1 - \frac{\rho_1 + \rho_2}{\rho^*} \right) + \beta_1 \rho_1 - \beta_2 \rho_2. \quad (8.20b)$$

We have used the logistic growth for cell proliferation, and the first two moments of the dispersal kernel are $m_1 = \int r w(r) dr$ and $m_2 = \int r^2 w(r) dr$.

We assume that the initial tumor is a sphere of radius R_0 with the following distribution:

$$\rho_k(r, 0) = \begin{cases} A_k, & r \le R_0, \\ 0, & r > R_0, \end{cases} \quad k = 1, 2. \quad (8.21)$$

where the positive constants A_1 and A_2 represent the stable uniform stationary values of the densities ρ_1 and ρ_2, respectively. For the system (8.20) these are given by

$$A_1 = \rho^* \frac{\beta_2}{\beta_1 + \beta_2}, \quad A_2 = \rho^* \frac{\beta_1}{\beta_1 + \beta_2}. \quad (8.22)$$

Using the Hamilton–Jacobi formalism, we obtain the Hamilton–Jacobi equation

$$m_1 p + \frac{m_2}{2} p^2 - \frac{H + \beta_1}{\hat{K}(H)} \left[1 - \frac{\beta_1 \beta_2}{(H + \beta_2 - r)(H + \beta_1)} \right] = 0. \quad (8.23)$$

The invasion velocity is given by (4.46):

$$v = \frac{m_2}{m_1} \min_{H \in (H^*, \infty)} \frac{H}{\sqrt{1 + 2\frac{m_2}{m_1}\xi(H)} - 1},$$ (8.24)

where

$$\xi(H) = \frac{H + \beta_1}{\hat{K}(H)} \left[1 - \frac{\beta_1 \beta_2}{(H + \beta_2 - r)(H + \beta_1)} \right],$$ (8.25)

and H^* is such that $\xi(H^*) = 0$, i.e.,

$$H^* = \frac{1}{2}\sqrt{(\beta_1 + \beta_2)^2 + r^2 + 2r(\beta_1 - \beta_2)} - \frac{1}{2}(\beta_1 + \beta_2 - r).$$ (8.26)

An alternative description for the two phenotypes of glioma cells is the following balance equations obtained directly from Chap. 3:

$$\rho_1(x, n+1) = h_{11} \int_{\mathbb{R}} \rho_1(x - z, n) w_1(z) \, dz + h_{21}\rho_2(x, n),$$ (8.27a)

$$\rho_2(x, n+1) = h_{22} f_2(\rho_2(x, n)) + h_{12}\rho_1(x, n).$$ (8.27b)

Here the mechanism of switching between the two phenotypes is described by the transition matrix $\mathsf{H} = (h_{ij})$ given in (3.21). One can easily take into account asymmetrical motion of cells due to nonuniform nutrient concentration (chemotaxis) and the gradient of cell adhesion sites (haptotaxis), etc., by allowing both w_1 and H to depend on the nutrient concentration $c(x, n)$ and $\rho_i(x, n)$.

8.2 Virus Dispersal in Bacterial Colonies

The space–time dynamics of bacteriophages in bacterial colonies can be described by considering two mechanisms: (i) virus dispersal through the heterogeneous medium composed of the bacterial colony and the substrate and (ii) interactions between viruses and bacteria [487, 489, 138]. The life cycle of bacteriophages is a well-established topic in microbiology. Viruses are very simple molecular structures that are not able to reproduce by themselves. They need to hijack the reproductive machinery of bacteria to replicate their own genetic material. If the cycle ends with the destruction of bacteria, it is known as a lytic cycle, which is the case we analyze here. From a biological point of view, the lytic cycle is very complex and involves a large number of biochemical reactions. For our purposes it suffices to lump them together in two main reactions: adsorption, with rate k_1, and replication, with rate k_2,

$$V + B \xrightarrow{k_1} I, \tag{8.28}$$

$$I \xrightarrow{k_2} Y\, V. \tag{8.29}$$

Here V, B, and I denote virus, host bacteria, and infected bacteria, respectively. Y is the production or yield of new viruses per host. We focus on the relevant factors by excluding negligible reactions, such as virus desorption and their adsorption to infected hosts. Consider a homogeneous medium composed initially of host bacteria and a few free viruses. The adsorption process can be described by the classical kinetic equations

$$\frac{d\rho_V}{dt} = -k_1 \rho_V \rho_B, \tag{8.30a}$$

$$\frac{d\rho_B}{dt} = -k_1 \rho_V \rho_B, \tag{8.30b}$$

where ρ_V and ρ_B are the number densities of virus and host bacteria at time t. One virus is removed for each adsorbed bacterium, i.e., $d\rho_V/dt = d\rho_B/dt$, which can be integrated to yield $\rho_V(t) - \rho_V(0) = \rho_B(t) - \rho_B(0)$. This relation can be substituted into (8.30), and integration leads to

$$g(\rho_V) \equiv \ln\left(\frac{\rho_V + C}{\rho_V}\right) - \ln\left(\frac{\rho_V(0) + C}{\rho_V(0)}\right) = C k_1 t, \tag{8.31}$$

where $C = \rho_B(0) - \rho_V(0)$. Both parameters C and k_1 can be estimated from experimental data for adsorption between virus and bacteria.

The replication process begins when the virus injects its DNA into the bacterium. The latter replicates the viral DNA and new viruses are formed. They are released into the medium by bursting the bacteria and the lytic cycle ends. Replication phenomena match very well a logistic growth of viruses, and we assume

$$\frac{d\rho_V}{dt} = k_2 \rho_V \left(1 - \frac{\rho_V}{\rho_V^{\text{max}}}\right). \tag{8.32}$$

If replication begins at $t = 0$ and if we define τ as the time elapsed from the adsorption to the replication of $\rho_V^{\text{max}}/2$ viruses, the solution of (8.32) reads

$$\rho_V(t) = \frac{\rho_V^{\text{max}}}{1 + e^{-k_2(t-\tau)}}, \tag{8.33}$$

where k_2 is the rate of release of the new viruses. The time τ is a measure of the lag time between the beginning of replication and the viruses' release and coincides with the characteristic time spent by viruses between two successive jumps. The conservation of the number of viruses and infected bacteria implies $\rho_V + Y\rho_I = \rho_V^{\text{max}} = Y\rho_I^{\text{max}}$, which can be substituted into (8.32) to yield

$$\frac{d\rho_V}{dt} = Yk_2\rho_I\left(1 - \frac{\rho_I}{\rho_I^{max}}\right), \tag{8.34a}$$

$$\frac{d\rho_I}{dt} = -k_2\rho_I\left(1 - \frac{\rho_I}{\rho_I^{max}}\right). \tag{8.34b}$$

We illustrate how to estimate the above parameters. The specific case we consider here is the interaction between the virus T7 and the bacterium *Escherichia coli*. The adsorption rate k_1 can be obtained by fitting $g(\rho_V)$ to experimental data [406] as shown in the inset of Fig. 8.2. The fit yields $C = 1.39 \times 10^8$ ml^{-1} and $k_1 = (1.29 \pm 0.59) \times 10^{-9}$ ml/min. The function (8.33) is called the one-step growth and is fitted to the experimental results [486] for replication of T7 inside *E. coli*. The fit, illustrated in the main part of Fig. 8.2, provides $Y = 34.5$, $\tau = 18.4$ min, and $k_2 = 1.39$ min^{-1}. The kinetic equations for viruses, host bacteria, and infected bacteria can be written as

$$\frac{d\rho_V}{dt} = F_V \equiv -k_1\rho_V\rho_B + Yk_2\rho_I\left(1 - \frac{\rho_I}{\rho_I^{max}}\right), \tag{8.35a}$$

$$\frac{d\rho_B}{dt} = F_B \equiv -k_1\rho_V\rho_B, \tag{8.35b}$$

$$\frac{d\rho_I}{dt} = F_I \equiv k_1\rho_V\rho_B - k_2\rho_I\left(1 - \frac{\rho_I}{\rho_I^{max}}\right). \tag{8.35c}$$

The system (8.35) has four steady states; we are interested in only two of them. The state $(\overline{\rho}_V, \overline{\rho}_B, \overline{\rho}_I) = (0, \rho_B^*, 0)$ is the infection-free state which could represent an initial state, $\rho_B(0) = \rho_B^*$. Provided that $Y > 1$, this state is always unstable.
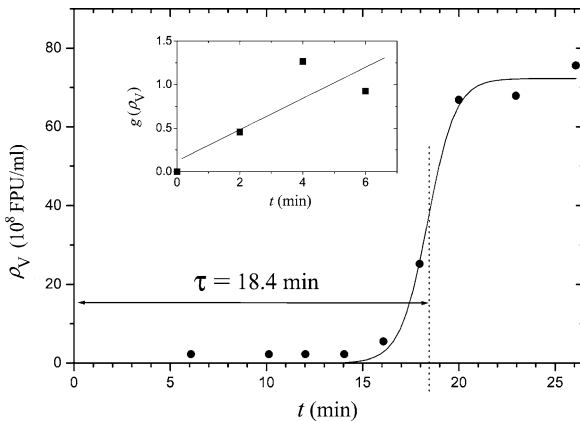
Fig. 8.2 Experimental results (*symbols*) and theoretical predictions (*solid curves*) for adsorption and replication processes between T7 and *E. coli*. The *inset* depicts the adsorption process and the *main part of the figure* corresponds to virus release after adsorption. Reprinted with permission from [138]. Copyright 2002 by the American Physical Society

The state $(\bar{\rho}_V, \bar{\rho}_B, \bar{\rho}_I) = (\rho_V^*, 0, 0)$ is the final state, is stable, and represents a completely invaded state where all the host cells were killed producing new viruses. We are interested in studying a front of invasion connecting both states. Since lysis of bacteria results in a precipitous decline in the culture turbidity, virus population growth produces circular clearings called plaques. The growth of these plaques in size is not only a result of the kinetics but also due to the dispersal movement of the viruses within the bacterial culture. To derive an equation for virus dispersal in agar, we start with the mesoscopic balance equation for the virus density at point $\mathbf{x}$ at time t obtained from Model C (see Sect. 3.4.3) [121]:

$$
\rho_V(\mathbf{x}, t) = \rho_V(\mathbf{x}, 0)\Psi(t) + \int_0^t \int_{\mathbb{R}^2} \rho_V(\mathbf{x} - \mathbf{x}', t - t')\psi(\mathbf{x}', t')\mathrm{d}\mathbf{x}'\mathrm{d}t'
$$
$$
+ \int_0^t F_V(\mathbf{x}, t - t')\Psi(t')\mathrm{d}t', \tag{8.36}
$$

where, as above, $\psi(\mathbf{x}, t)$ is the PDF of performing a jump of length $|\mathbf{x}|$ after waiting a time t, $\phi(t)$ is the waiting time PDF, and $\Psi(t)$ is its survival probability. The function $F_V(\mathbf{x}, t)$ takes into account the kinetics of viruses at point $\mathbf{x}$ and is the right-hand side of (8.35a). We assume again that the jump length PDF is given by a 2D Gaussian distribution. The one-step growth curve, or more precisely its derivative, suggests that the waiting time PDF should be of the form $\phi(t) = (t/\tau^2)\mathrm{e}^{-t/\tau}$, where τ denotes the characteristic waiting time between jumps. Note that we intentionally employ the same notation for this time as for the half reproduction time for viruses. This reflects the fact that viruses reproduce only in the sedentary stage. With these assumptions, (8.36) yields, after Fourier–Laplace transformation and rearrangement of terms, the following RT equation:

$$
\frac{\tau}{2}\frac{\partial^2 \rho_V}{\partial t^2} + \frac{\partial \rho_V}{\partial t} = D\frac{\partial^2 \rho_V}{\partial r^2} + F_V + \frac{\tau}{2}\frac{\partial F_V}{\partial t}, \tag{8.37}
$$

where r the radial coordinate. The diffusion coefficient D has to take into account that virus dispersal takes place in a medium where movement is hindered by the presence of a suspension of spheroids, the host bacteria. The effect of host bacteria on the movement of viruses is twofold. They constitute impenetrable obstacles and they are centers of adsorption. We employ Fricke's formula to account for these effects:

$$
D = D^*\frac{1 - f}{1 + f/\varsigma}, \tag{8.38}
$$

where $f = \rho_B(0)/\rho_B^{\text{max}}$ is the concentration of bacteria relative to the maximum possible value for a fixed nutrient concentration, and $\rho_B(0) = \rho_B^*$ is the initial concentration of host bacteria, previous to the arrival of viruses. The diffusion coefficient in the absence of host bacteria is denoted by D^*, which is approximately

4×10^{-8} cm^2/s for T7 in agar, and ς is a parameter that accounts for the shape of bacteria and is equal to 1.67 for *E. coli*.

The set of partial differential equations (8.37), $\partial \rho_B / \partial t = F_B$, and $\partial \rho_I / \partial t = F_I$ form a closed system. We calculate the velocity of a propagating front, connecting the state $(0, \rho_B^*, 0)$ to $(\rho_V^*, 0, 0)$ from initial conditions with compact support, from the Hamilton–Jacobi equation in dimensionless units:

$$\left[\frac{\tau k_2}{2} H^2 + H \left(1 + \frac{\tau k_2}{2} \kappa \right) - p^2 + \kappa \right] (H + 1) - Y \kappa \left(1 + \frac{\tau k_2}{2} H \right) = 0, \quad (8.39)$$

with $\kappa = k_1 f \rho_B^{\max} / k_2$. To obtain the velocity in dimensioned units, we must multiply the velocity given by (4.46) by the factor $\sqrt{Dk_2}$. We plot the results obtained from (4.46) and (8.39) for the two extreme values of k_1 (solid and dashed lines) together with the parabolic case where $\tau = 0$ in Fig. 8.3. Symbols represent the experimental results [487] for $\rho_B^{\max} = 10^7$ ml^{-1} and $\rho_B^{\max} = 10^8$ ml^{-1}. Figure 8.3 shows that the hyperbolic model agrees considerably better with the experimental data than the parabolic model. This result demonstrates the importance of a non-Markovian waiting time PDF in the model. Approximate solutions for the front velocity were also obtained by considering the small parameter $\varepsilon = k_1 \rho_B^{\max} / k_2 \sim 10^{-3} - 10^{-2}$ [330]. These results can be useful as an alternative way to characterize mutant virus strains in terms of its front velocities [1, 2].

8.3 Propagation in Spiny Dendrites

Spiny dendrites are essential elements of most brain regions because they form a surface for receiving synaptic inputs. For the Purkinje cells of the cerebellar cortex, over 90% of their excitatory synapses are located on dendritic spines. The latter play a very important role in regulating neuronal activity [179, 321]. The heads of spines have an active membrane, and as a consequence, spiny dendrites can sustain the propagation of an action potential with a rate that depends on the spatial distribution of spines. Abnormalities in dendritic spine populations, e.g., decreased spine density, can result in cognitive disorders, such as autism, mental retardation, and fragile X syndrome [321]. A significant amount of theoretical work has been devoted to study the interaction of spines with dendrites on the *macroscopic* level with so-called cable models. Baer and Rinzel [21] proposed a cable theory for excitable spiny dendrites and found that the spread of local excitation depends strongly on the spine-stem resistance. Other extensions of that work take into account the dynamic structure of the spines and their changes in response to synaptic activity [481].

The development of confocal microscopies and other techniques rendered feasible the study of transport and biochemical reactions on the *microscopic* level of a single spine and a parent dendrite [426, 370, 80]. Several models exist for particle transport and chemical reactions inside biological microdomains [386, 200, 199, 59, 85].
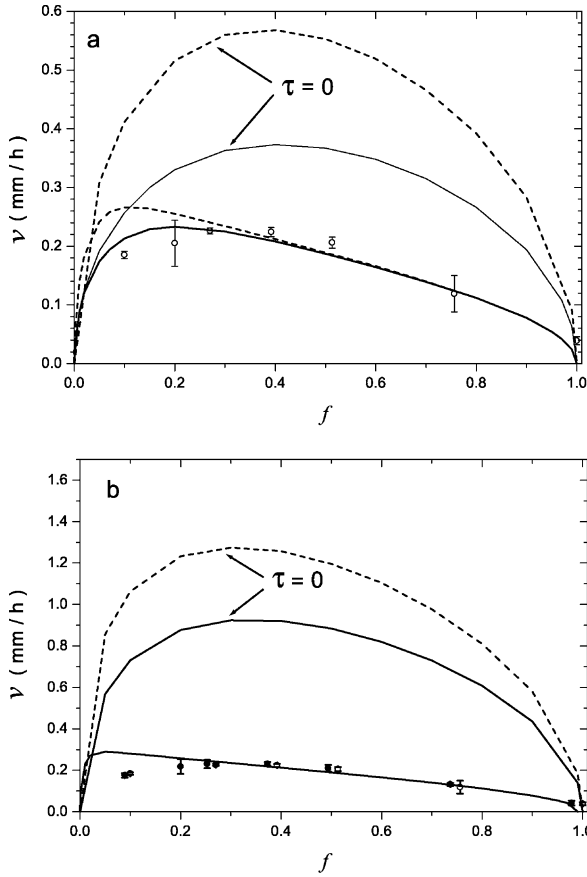
Fig. 8.3 Plaque growth velocity as a function of the relative bacteria concentration for $\rho_B^{max} = 10^7 ml^{-1}$ (panel a) and $\rho_B^{max} = 10^8 ml^{-1}$ (panel b). The solid curves correspond to $k_1 = 0.70 \times 10^{-9}$ ml/min and the dashed curves to $k_1 = 1.88 \times 10^{-9}$ ml/min. In panel b, the two lower curves are not distinguishable from each other at the present scale, implying that the uncertainty in the value of k_1 has a little effect on the predicted velocity. Reprinted with permission from [138]. Copyright 2002 by the American Physical Society

Santamaria et al. [375] found that the transport of biologically inert particles, fluorescein dextran, in spiny dendrites is very slow compared with standard diffusion. The mean-square displacement is $\langle x^2(t) \rangle \sim t^\gamma$ with $\gamma < 1$ [298, 379]. The anomalous diffusion appears to be caused by the dendritic spines acting as the traps for the particles. We present here a *mesoscopic* model for the transport and biochemical reactions inside a population of spines and dendrites [122]. The morphology of spiny dendrites is very complex; the distances between the spines and their sizes and shapes are randomly distributed [179, 362]. The model allows us to deal with the morphological diversity of dendritic spines via the transparent formalism of waiting time distributions.

8.3.1 Mesoscopic Model

The main ingredients of the model are as follows. Inside a dendrite with a uniform surface spine density n_s, particles perform Brownian motion with a constant drift v along the dendrite and a diffusion coefficient D. This describes, e.g., the motion of an overdamped ion under the action of an electric field E such that $v = \mu E$, where μ is the ion mobility. After a random time τ_d, distributed according to the PDF $\phi_1(\tau)$, the particle hits the neck of a spine on the surface of the dendrite. It is then trapped inside the spine for a random time τ_s. The PDF for the sojourn time τ_s is $\phi_2(\tau)$. During this time, an irreversible chemical reaction $C \xrightarrow{\beta} C_b$ takes place, where β is the rate of removing particles by buffers and pumps inside spines. After the random time τ_s, the particle is released back into the parent dendrite through the spine neck. Measurements of the Ca^{2+} flux out of spines show that spine necks slow down the transport of ions up to a factor 10^2 compared with free diffusion [370]. Therefore it is reasonable to assume a power-law distribution for the waiting time PDF $\phi_2(\tau)$, which also accounts for heterogeneous spine–dendrite transport coupling [49]. The PDF $\phi_1(\tau)$ for the random time τ_d can be derived from the escape problem for diffusion in bounded domain with absorbing sites, spines, on the surface [386]. If a cylindrical dendrite of length L and radius R has just one spine with a neck radius $a \ll R$, then the survival probability $\int_t^\infty \phi_1(s)\mathrm{d}s$ is exponentially distributed for large t and the mean escape time $\langle \tau_d \rangle$ is $\pi R^2 L / 4aD$ [386, 85]. To be specific, we consider two distributions, the exponential distribution, $\phi_1(t) = \mu_1 \exp(-\mu_1 t)$, which implies Markovian behavior, and the Gamma distribution, $\phi_1(t) = v_1^2 t \exp(-v_1 t)$, which corresponds to non-Markovian behavior. For both cases we assume that the parameters μ_1 and v_1 are functions of the linear spine density $n_l = 2\pi R n_s$, that is $\mu_1 = n_l \mu_1^0$ and $v_1 = n_l v_1^0$.

We derive the balance equations for the density of particles inside a single dendrite ρ_1 and the density of particles inside a single spine ρ_2 starting with the stochastic model for a single particle delineated above. Let ρ_1^0 and ρ_2^0 be the initial densities of particles in the dendrite and the spine. If $j_1(x, t)$ denotes the number of particles arriving at point x in a dendrite at time t through a single spine stem and $j_2(x, t)$ is the number of particles arriving at point x in a single spine at time t, see Fig. 8.4, the balance equations for the densities ρ_1 and ρ_2 can be written as follows:

for a dendrite:

$$\rho_1(x, t) = \Psi_1(t) Q_t \rho_1^0(x) + n_l \int_0^t \Psi_1(t - t') Q_{t-t'} j_1(x, t')\mathrm{d}t', \qquad (8.40a)$$

for a single spine:

$$\rho_2(x, t) = \Psi_2(t)\mathrm{e}^{-\beta t} \rho_2^0(x) + \int_0^t \Psi_2(t - t')\mathrm{e}^{-\beta(t-t')} j_2(x, t')\mathrm{d}t'. \qquad (8.40b)$$

Here we introduced the transport operator Q_t, see also (3.248),
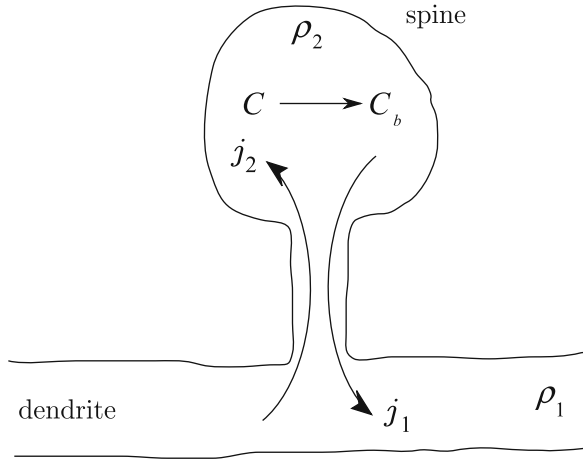
Fig. 8.4 Spine–dendrite interaction. Reprinted with permission from [122]. Copyright 2008 by the American Physical Society

$$Q_t \rho_1^0(x) = \int_{\mathbb{R}} p(x, t|x') \rho_1^0(x') \mathrm{d}x', \tag{8.41a}$$

$$Q_{t-t'} j_1(x, t') = \int_{\mathbb{R}} p(x, t - t'|x') j_1(x', t') \mathrm{d}x', \tag{8.41b}$$

where $p(x, t|x')$ is the transition PDF for a particle that starts at point x' in a dendrite and ends up at point x at time t. Equation (8.40a) expresses the density of particles at point x in a dendrite at time t as a sum of two terms. The first term $\Psi_1(t) Q_t \rho_1^0(x)$ is the contribution of those particles that are initially located inside the dendrite and diffuse along it from $t = 0$ up to time t without moving into spines. The second term represents those particles that arrived in the dendrite from spines at point x' at time t' and diffuse to reach point x without switching to spines. The functions $\Psi_1(t)$ and $\Psi_2(t)$ are the survival probabilities of particles inside dendrites and spines, respectively. Equation (8.40b) is the particle balance equation in a single spine. The function $\mathrm{e}^{-\beta t}$ represents the fraction of free particles. The first term $\Psi_2(t) \mathrm{e}^{-\beta t} \rho_2^0(x)$ is the contribution from particles initially located in a spine that remain free up to time t without moving into the dendrite.

We also need the balance equations for $j_1(x, t)$ and $j_2(x, t)$:

for a dendrite:

$$j_1(x, t) = \phi_2(t) \mathrm{e}^{-\beta t} \rho_2^0(x) + \int_0^t \phi_2(t - t') \mathrm{e}^{-\beta(t-t')} j_2(x, t') \mathrm{d}t', \tag{8.42a}$$

for a single spine:

$$j_2(x, t) = \phi_1(t) Q_t \rho_1^0 / n_l + \int_0^t \phi_1(t - t') Q_{t-t'} j_1(x, t') \mathrm{d}t'. \tag{8.42b}$$

The first term in (8.42a) corresponds to the number of particles initially located in the spine that arrive at the dendrite at time t due to transport through the spine neck. The second term represents those particles that arrived at spines at point x at time t' and spent time $t - t'$ there before moving into the dendrite at time t. Equation (8.42b) is derived in a similar manner, but we must take into account the motion of particles along the dendrite. We consider $v = \text{const}$ in the following. For this linear problem, we can obtain an explicit expression for the PDF:

$$p(x, t|x') = (4\pi Dt)^{-1/2} \exp\left[-(x - x' - vt)^2/4Dt\right].\tag{8.43}$$

Using the Fourier–Laplace transforms $(x, t) \to (k, s)$, we derive from the balance equations (8.40) and (8.42) expressions for $s\hat{\tilde{\rho}}_i(k, s) - \tilde{\rho}_i^0(k)$. Using the Fourier–Laplace inversion formula, we obtain a system of integro-differential equations,

$$\frac{\partial \rho_1}{\partial t} + v\frac{\partial \rho_1}{\partial x} = D\frac{\partial^2 \rho_1}{\partial x^2} - n_l J[\rho_1, \rho_2],\tag{8.44a}$$

$$\frac{\partial \rho_2}{\partial t} = J[\rho_1, \rho_2] - \beta\rho_2,\tag{8.44b}$$

with the spine–dendrite interaction term

$$
\begin{aligned}
J[\rho_1, \rho_2] = &-\int_0^t e^{-\beta t'} a_2(t')\rho_2(x, t - t')dt' \\
&+ n_l^{-1}\int_{-\infty}^{\infty}\int_0^t p(x', t'|z)a_1(t')\rho_1(x - x', t - t')dt'dx'.
\end{aligned}\tag{8.45}
$$

The Laplace transforms of the kernels are given by $\hat{a}_i(s) = \hat{\phi}_i(s)/\hat{\Psi}_i(s)$, $i = 1, 2$. Note that this model involves two equations, one for the freely moving particles and one for the particles trapped in the spines, whereas the standard CTRW model describes the trapping as a temporal memory of the moving particles. $J[\rho_1, \rho_2]$ is the number of particles per unit time flowing between the dendrite and a single spine. The first term on the RHS of (8.45) describes the flux of particles from a single spine through the spine neck into a parent dendrite. The second term represents the flux of particles from the dendrite into the spine. The spine–dendrite coupling is crucial for the propagation of an action potential along spiny dendrites, since there is no direct communication between neighboring spines. It turns out that this interaction is far from trivial and cannot be easily found using a phenomenological approach. In general, both terms in (8.45) are nonlocal in time. Equations (8.45) implies that the effective memory kernel in the first term depends on the chemical reaction in spines with decay rate β. The second term of (8.45) is nonlocal in space. Note that this effect is *not* due to long-range jumps of particles inside the dendrite. This nonlocal behavior can lead to anomalous transport of particles in dendrites as we show below. If the probability density functions $\phi_1(t)$ and $\phi_2(t)$ are exponential

with the rates $\mu_1 = \langle \tau_d \rangle^{-1}$ and $\mu_2 = \langle \tau_s \rangle^{-1}$, then the memory kernels $a_i(t)$ are delta functions and the system (8.44) reduces to standard reaction–diffusion equations with the interaction term

$$J[\rho_1, \rho_2] = \mu_1^0 \rho_1 - \mu_2 \rho_2, \tag{8.46}$$

where $\mu_1^0 = \mu_1/n_l$. This Markovian model corresponds to the phenomenological approach for spine–dendrite interaction [59]. Consider now the *non-Markovian* case where both waiting time PDFs ϕ_i are Gamma distributions $\phi_i(t) = v_i^2 t e^{-v_i t}$. Then the interaction memory kernels are $a_i(t) = v_i^2 e^{-2v_i t}$, $i = 1, 2$. This formula shows that the effective memory kernel in the first term of (8.45) is $e^{-(2v_1 + \beta)t}$, with an effective delay time $(2v_1 + \beta)^{-1}$. When the drift is zero, the second term can be written in Fourier space as $v_1^2 \int_0^t e^{-(2v_1 + Dk^2)t'} \tilde{\rho}_1(k, t - t') dt'$. This implies that the effective delay time $(2v_1 + Dk^2)^{-1}$ depends on the diffusion in the dendrites and the density of spines, since $v_1 = n_l v_1^0$.

8.3.2 Biologically Inert Particles: Anomalous Diffusion

The transport of inert particles, fluorescein dextran, in spiny dendrites of cerebellar Purkinje cells is subdiffusive [375], i.e., $\langle x^2(t) \rangle \sim t^\gamma$, where $0 < \gamma < 1$. The model formulated in Sect. 8.3.1 predicts this subdiffusive behavior. For simplicity we assume that the waiting time PDF for the dendrite $\phi_1(t)$ is exponential. Experimental evidence suggests a power-law distribution for the waiting time PDF $\phi_2(t) \sim (t/\tau)^{-1-\gamma}$ as $t \to \infty$, which reads in Laplace space $\hat{\phi}_2(s) = 1 - (\tau s)^\gamma$ [298, 379]. The Laplace transform of the mean squared displacement is given by

$$\widehat{\langle x^2 \rangle}(s) = - \left. \frac{d^2 \hat{\tilde{\rho}}}{dk^2}(k, s) \right|_{k=0}. \tag{8.47}$$

Here $\hat{\tilde{\rho}}(k, s) = \hat{\tilde{\rho}}_1(k, s) + n_l \hat{\tilde{\rho}}_2(k, s)$ is the Laplace–Fourier transform of the total density of particles. We obtain from (8.40), (8.41), and (8.42)

$$\hat{\tilde{\rho}}(k, s) = \tilde{\rho}_1^0(k) \frac{\hat{\Psi}_1^k(s) + \hat{\Psi}_2(s + \beta) \hat{\phi}_1^k(s)}{1 - \hat{\varphi}_2(s + \beta) \hat{\phi}_1^k(s)}$$

$$+ n_l \tilde{\rho}_2^0(k) \frac{\hat{\Psi}_2(s + \beta) + \hat{\phi}_2(s + \beta) \hat{\Psi}_1^k(s)}{1 - \hat{\phi}_2(s + \beta) \hat{\phi}_1^k(s)}, \tag{8.48}$$

where $\hat{\Psi}_1^k(s) = \Psi_1(s + ikv + Dk^2)$ and $\hat{\phi}_1^k(s) = \hat{\phi}_1(s + ikv + Dk^2)$. In particular, when $\beta = 0$, $v = 0$ and $\rho_2^0(x) = 0$, the mean squared displacement is found to be

$$\langle x^2(t) \rangle = \frac{2}{\Gamma(1+\gamma)} D \langle \tau_d \rangle \left(\frac{t}{\tau} \right)^\gamma, \tag{8.49}$$

as $t \to \infty$. In the Markovian case with PDFs $\phi_i(t) = \mu_i \exp(-\mu_i t)$, we obtain the standard behavior, $\langle x^2(t) \rangle = 2D_{eq}t$ with the effective diffusivity $D_{eq} = D\gamma_2$ $(\mu_1 + \mu_2)^{-1}$. In the anomalous case, (8.49) implies that the effective diffusion coefficient goes to zero.

8.3.3 Kinetics of Particle Decay in Spiny Dendrites

While anomalous switching slows down the transport of particles in dendrites (8.49), it leads to a higher rate of particle decay than in the Markovian case. This is illustrated in Fig. 8.5, where the decay of particles in the anomalous case ($\gamma = 0.1$) is compared with that in the non-Markovian case (Gamma distribution) and the standard Markovian case ($\gamma = 1$). One can see that the decrease of diffusion of particles toward the parent dendrite, decrease of the exponent γ, leads to a faster decay of the total number of particles $\rho(t) = \int (\rho_1 + n_l \rho_2) \, dx$. From (8.48), $\rho(t) \sim t^{-\gamma} e^{-\beta t}$ as $t \to \infty$. This explains the effect of limited diffusion of Ca^{2+} along dendrites
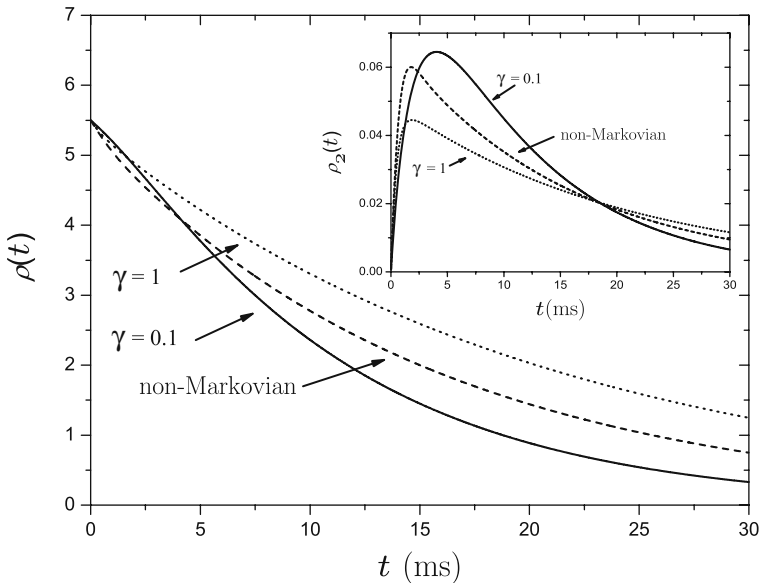
Fig. 8.5 Kinetics of particles decaying in the spine–dendrite system $\rho(t)$ (*main figure*) and in spines $\rho_2(t)$ (*inset*). $D = 0.2 \ \mu m^2/ms$, $\langle \tau_s \rangle = \langle \tau_d \rangle = 1$ ms, $\beta = 0.1$ ms^{-1}, $n_l = 10 \ \mu m^{-1}$. The initial conditions are $\rho_i(x, 0) = \delta(x)/2$, $i = 1, 2$. Reprinted with permission from [122]. Copyright 2008 by the American Physical Society

observed in experiments [375]. The decay of ρ_2 is also depicted in Fig. 8.5. It shows that transport equilibration is slow, which is important for the accumulation of plasticity-inducing signals inside spines [49]. The phenomenological models for spine–dendrite interaction assume that the ion current I passing through the spine necks is proportional to current voltage difference between the spines and dendrite [21]. This model shows that particles flux through the spine's neck is nonlocal in time and space, see (8.45).

Exercises

8.1 Obtain the velocity of the invasion front (8.6) and the recovery front (8.7) for the tumor–host interaction model given by (8.1).

8.2 Obtain the integro-differential equations for glioma invasion (8.12) from the balance equations (8.10).

8.3 Find the Hamilton–Jacobi equation for the glioma invasion front (8.23) from (8.20) following the same procedure as in Sect. 4.6.1.

8.4 Find the Hamilton–Jacobi equation for the plaque growth (8.39) from the equations (8.37) and

$$\frac{\partial \rho_B}{\partial t} = -k_1 \rho_B \rho_V, \tag{8.50a}$$

$$\frac{\partial \rho_I}{\partial t} = k_1 \rho_B \rho_V - k_2 \rho_I \left(1 - \frac{\rho_I}{\rho_I^{\max}} \right), \tag{8.50b}$$

for the densities of viruses, host bacteria, and infected bacteria.

Part III
Spatial Instabilities and Patterns

Chapter 9
Persistence and Extinction of Populations in Finite Domains

We now turn our attention to steady states of reaction–transport systems. We focus first on steady states that arise in RD models on finite domains. Such models are important from an ecological point of view, since they describe population dynamics in island habitats. The main problem consists in determining the critical patch size, i.e., the smallest patch that can minimally sustain a population. As expected intuitively, the critical patch size depends on a number of factors, such as the population dynamics in the patch, on the nature of the boundaries, the patch geometry, and the reproduction kinetics of the population. The first critical patch model was studied by Kierstead and Slobodkin [228] and Skellam [414] and is now called the KISS problem. A significant amount of work has focused on systems with partially hostile boundaries, where individuals can cross the boundary at some times but not at others, or systems where individuals readily cross the boundary but the region outside the patch is partially hostile, or a combination of the above. In this chapter we deal with completely hostile boundaries and calculate the critical patch size for different geometries, reproduction processes, and dynamics.

9.1 Critical Patch Size

Let L be the patch size. Throughout this chapter we consider the RD equation on the interval $[0, L]$ with Dirichlet boundary conditions:

$$\frac{\partial \rho}{\partial t} = D \frac{\partial^2 \rho}{\partial x^2} + r F(\rho), \tag{9.1a}$$

$$\rho(0, t) = \rho(L, t) = 0, \tag{9.1b}$$

$$\rho(x, 0) = \rho_0(x), \quad F'(0) > 0. \tag{9.1c}$$

Since the critical patch size corresponds to the borderline between population extinction and survival, the population density ρ is small and we can linearize (9.1) about $\rho(x) \equiv 0$, the state of extinction. If $\rho = 0$ is stable, the population goes to extinction. If $\rho = 0$ is unstable, the population persists or survives. Near $\rho = 0$

there are two competing effects, growth and loss from the boundaries. Linearizing (9.1) about $\rho(x) = 0$, we obtain

$$\frac{\partial \rho}{\partial t} = D \frac{\partial^2 \rho}{\partial x^2} + r F'(0)\rho, \tag{9.2a}$$

$$\rho(0, t) = \rho(L, t) = 0, \tag{9.2b}$$

$$\rho(x, 0) = \rho_0(x), \quad F'(0) > 0. \tag{9.2c}$$

Since the problem is linear, it is reasonable to look for solutions of the form $\rho(x, t) = e^{r F'(0)t} u(x, t)$. We substitute this ansatz into (9.2) and find that the $u(x, t)$ obeys

$$\frac{\partial u}{\partial t} = D \frac{\partial^2 u}{\partial x^2}, \tag{9.3a}$$

$$u(0, t) = u(L, t) = 0, \tag{9.3b}$$

$$u(x, 0) = \rho_0(x). \tag{9.3c}$$

Equation (9.3) is the heat equation with homogeneous Dirichlet boundary conditions. Its solution is well known, and the solution of (9.2) is given by

$$\rho(x, t) = \sum_{k=1}^{\infty} A_k \exp \left\{ \left[r F'(0) - D \left(\frac{\pi k}{L} \right)^2 \right] t \right\} \sin \left(\frac{\pi k x}{L} \right), \tag{9.4}$$

where the coefficients A_k are determined by the Fourier series expansion of the initial condition $\rho_0(x)$.

The trivial solution $\rho(x) \equiv 0$ is unstable, i.e., the population grows, if $\lambda_k \equiv r F'(0) - D (\pi k/L)^2 > 0$ for some k. Since the "growth" rates λ_k decrease monotonically with k, the dominant mode is the long-wavelength mode $k = 1$. It determines the fate of the population, and the condition $\lambda_1 < 0$, i.e., $L < \pi \sqrt{D/r F'(0)}$, ensures extinction of the population. The critical patch size, commonly referred to as the KISS size, is then given by

$$L_c = \pi \sqrt{\frac{D}{r F'(0)}}. \tag{9.5}$$

If the patch size L is less than L_c, $\rho(x, t) \to 0$ as $t \to \infty$. No nontrivial steady state develops, and the population collapses from its initial condition. Increasing the patch size leads to a bifurcation. The state $\rho(x) = 0$ loses its stability at the bifurcation point L_c (a detailed analysis of the bifurcation diagram can be found in the next section) and ρ starts to grow with time. The growth saturates due to

nonlinear effects, and $\rho(x, t)$ tends to a steady state, a spatially nonuniform solution $\overline{\rho}(x)$, that according to (9.1) is determined by

$$D\frac{d^2\overline{\rho}}{dx^2} + rF(\overline{\rho}) = 0, \tag{9.6a}$$

$$\overline{\rho}(0) = \overline{\rho}(L) = 0. \tag{9.6b}$$

We are interested only in those solutions for which $\overline{\rho}(x) \geq 0$. The trivial solution $\overline{\rho}(x) \equiv 0$ satisfies (9.6) for any value of L. Due to the spatial symmetry of (9.1) and (9.6), we expect the solutions to be symmetric in x about the midpoint $x = L/2$. Since $\overline{\rho} = 0$ at the boundaries, we can assume that the population density of nontrivial steady states reaches its maximum value ρ_m at the midpoint, $[d\overline{\rho}(x)/dx](L/2) = 0$.
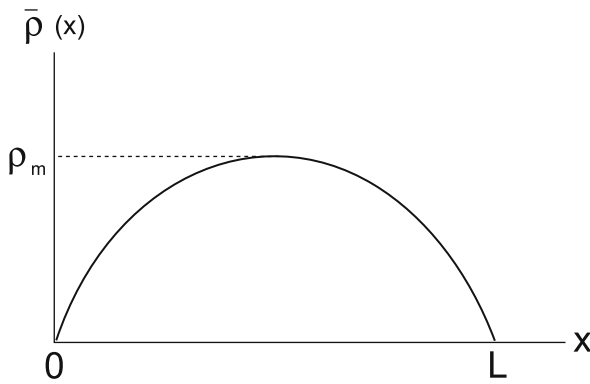
Fig. 9.1 Sketch of a typical nontrivial steady state

In Fig. 9.1 we plot a typical nontrivial steady state. Multiplying (9.6) by $d\overline{\rho}/dx$ and integrating with respect to x from 0 to L, we obtain

$$\frac{D}{2}\left(\frac{d\overline{\rho}}{dx}\right)^2 + r\varphi(\overline{\rho}) = r\varphi(\rho_m), \tag{9.7}$$

where $\varphi(\overline{\rho}) = \int_0^{\overline{\rho}} F(s)ds$. We separate the variables in (9.7) and integrate with respect to x from 0 to $L/2$ and find

$$L = \sqrt{\frac{2D}{r}} \int_0^{\rho_m} \frac{d\overline{\rho}}{\sqrt{\varphi(\rho_m) - \varphi(\overline{\rho})}}, \tag{9.8}$$

which can be rewritten in a more suitable form by making the substitution $z = \overline{\rho}/\rho_m$:

$$L = \sqrt{\frac{2D}{r}} \rho_m \int_0^1 \frac{dz}{\sqrt{\varphi(\rho_m) - \varphi(z\rho_m)}}. \tag{9.9}$$

This formula is usually referred to as a time map and allows us to determine, implicitly, ρ_m as a function of L. The critical patch size can be recovered from (9.9) by taking the limit $L_c = \lim_{\rho_m \to 0} L$. To do so, we carry out a Taylor expansion around $\rho_m = 0$. We write

$$\varphi(\rho_m) - \varphi(z\rho_m) = \frac{1}{2} F'(0)\rho_m^2(1 - z^2) + O(\rho_m^3). \tag{9.10}$$

Equations (9.9) and (9.10) yield

$$L_c = 2\sqrt{\frac{D}{rF'(0)}} \int_0^1 \frac{dz}{\sqrt{1 - z^2}} = \pi\sqrt{\frac{D}{rF'(0)}}, \tag{9.11}$$

recovering (9.5).

We now formulate a variational characterization of the critical patch size to determine the relation between L and ρ_m. To this end, it is convenient to change the origin to $L/2$, i.e., we set $x \to x - L/2$. Let $y = 2x/L - 1$, then

$$D\frac{d^2\overline{\rho}}{dy^2} + \lambda F(\overline{\rho}) = 0, \tag{9.12a}$$

$$\overline{\rho}(0) = \rho_m, \quad \overline{\rho}(1) = 0, \tag{9.12b}$$

$$\left.\frac{d\overline{\rho}}{dy}\right|_{y=0} = 0, \tag{9.12c}$$

where the eigenvalue λ, $\lambda = L^2 r/4D$, has to be determined. Let $g(\overline{\rho})$ be an arbitrary, nonnegative function such that $g(0) = 0$ and $g'(\overline{\rho}) > 0$, and $q \equiv -\overline{\rho}'(y) > 0$ for $y \in (0, 1)$. Here and below, the prime denotes the derivative with respect to the argument of the function. Then (9.12) reads

$$q\frac{dq}{d\overline{\rho}} + \lambda F(\overline{\rho}) = 0, \quad q(\rho_m) = 0, \quad \text{and } q(0) > 0. \tag{9.13}$$

Multiplying (9.13) by g and integrating with respect to $\overline{\rho}$, we obtain

$$\frac{1}{2}\int_0^{\rho_m} q^2(\overline{\rho})g'(\overline{\rho})d\overline{\rho} = \lambda \int_0^{\rho_m} g(\overline{\rho})F(\overline{\rho})d\overline{\rho}. \tag{9.14}$$

For fixed $g(\overline{\rho})$, we consider the functional

$$J_g[\overline{\rho}] \equiv \frac{1}{2} \int_0^{\rho_m} q^2(\overline{\rho}) g'(\overline{\rho}) d\overline{\rho} = \frac{1}{2} \int_0^1 \phi(\overline{\rho}, \overline{\rho}') dy, \qquad (9.15)$$

where $\phi(\overline{\rho}, \overline{\rho}') \equiv -[\overline{\rho}'(y)]^3 g'(\overline{\rho})$. The Euler–Lagrange equation

$$\frac{d}{dz}\left(\frac{\partial \phi}{\partial \overline{\rho}'}\right) - \frac{\partial \phi}{\partial \overline{\rho}} = 0 \qquad (9.16)$$

yields $3dq/q = -[g''(\overline{\rho})/g'(\overline{\rho})]d\overline{\rho}$. Integration results in

$$q^3 g'(\overline{\rho}) = K, \qquad (9.17)$$

where K is an integration constant to be determined. We substitute (9.17) into (9.15) to obtain $J_g[\overline{\rho}] \geq \min J_g[\overline{\rho}] = K/2$ and finally

$$\lambda \geq \frac{K/2}{\int_0^{\rho_m} g(\overline{\rho}) F(\overline{\rho}) d\overline{\rho}}. \qquad (9.18)$$

Once the trial function $g(\overline{\rho})$ is selected according to the conditions $g(\overline{\rho}) \geq 0$, $g(0) = 0$, and $g'(\overline{\rho}) > 0$, we calculate K by integrating (9.17) and obtain from (9.18)

$$\lambda = \max_{g(\overline{\rho})} \frac{\left[\int_0^{\rho_m} g'(\overline{\rho})^{1/3} d\overline{\rho}\right]^3}{\int_0^{\rho_m} g(\overline{\rho}) F(\overline{\rho}) d\overline{\rho}}. \qquad (9.19)$$

We omit here the proof that there exists a function g that maximizes the above quantity, i.e., for which the equality in (9.18) holds, and refer the reader to [35] and [281] for details.

If the nonlinear terms of the reaction function are small, we can choose the g that corresponds to the linear case where $F(\overline{\rho}) = \overline{\rho}$. In this case, (9.12) reads $\overline{\rho}'' + \lambda \overline{\rho} = 0$, with $\overline{\rho}(0) = \rho_m$ and $\overline{\rho}'(0) = 0$. This is exactly the equation for a linear oscillator, with $\sqrt{\lambda}$ as the frequency and y as the time. This equation is easily solved, $\overline{\rho}(y) = \rho_m \cos(y\sqrt{\lambda})$. The third boundary condition $\overline{\rho}(1) = 0$ implies $\sqrt{\lambda} = \pi/2$. We now determine which $g(\overline{\rho})$ provides the correct result for λ. Since $q \equiv -\overline{\rho}'(y) = (\rho_m \pi/2)\sqrt{1 - (\overline{\rho}/\rho_m)^2}$, (9.17) yields $g'(\overline{\rho}) \sim q^{-3} \sim \left[1 - (\overline{\rho}/\rho_m)^2\right]^{-3/2}$, so that for the linear case

$$g(\overline{\rho}) = \frac{\overline{\rho}}{\sqrt{1 - (\overline{\rho}/\rho_m)^2}}. \qquad (9.20)$$

Choosing this form (9.20) of g for the nonlinear system (9.12) and integrating (9.17), we find $K = \left(\pi\rho_m/2\right)^3$. Inserting the latter result into (9.18), we obtain the relation $L(\rho_m)$ from the variational principle:

$$L^2 \approx \frac{D}{4r}\left(\pi\rho_m\right)^3 \left[\int_0^{\rho_m} \frac{\overline{\rho}F(\overline{\rho})\mathrm{d}\overline{\rho}}{\sqrt{1-\left(\overline{\rho}/\rho_m\right)^2}}\right]^{-1}, \tag{9.21}$$

and with $z = \overline{\rho}/\rho_m$,

$$L^2 \approx \frac{D}{4r}\pi^3\rho_m \left[\int_0^1 \frac{zF(z\rho_m)\mathrm{d}z}{\sqrt{1-z^2}}\right]^{-1}. \tag{9.22}$$

The critical patch size is obtained by taking the limit $\rho_m \to 0$ in (9.22):

$$L_c^2 \approx \lim_{\rho_m \to 0} L^2 = \frac{D\pi^3}{4rF'(0)} \left[\int_0^1 \frac{z^2\mathrm{d}z}{\sqrt{1-z^2}}\right]^{-1} = \frac{D\pi^2}{rF'(0)}, \tag{9.23}$$

which is identical with (9.5). In summary, there exists a nonuniform stationary solution of the RD equation (9.1) if $L > L_c$. This solution coexists with the trivial solution $\overline{\rho}(x) \equiv 0$. What are the stability properties of these solutions? The stability of the trivial solution was analyzed at the beginning of this section. The stability analysis of the nontrivial steady state is more difficult.

9.2 Bifurcation Diagrams: Stability of Spatial Patterns

Some authors used subsolutions, supersolutions, and comparison theorems to analyze the stability of the nontrivial steady state $\overline{\rho}(x)$ [257]. For the Fisher equation, Skellam's linear stability analysis about $\overline{\rho}(x)$ can be used [414]. If we set $\rho(x, t) = \overline{\rho}(x) + \delta\rho(x, t)$ and consider the linearization of (9.1) about $\overline{\rho}(x)$, we obtain

$$\frac{\partial \delta\rho}{\partial t} = rF'(\overline{\rho})\delta\rho + D\frac{\partial^2 \delta\rho}{\partial x^2}, \tag{9.24a}$$

$$\delta\rho(0, t) = \delta\rho(L, t) = 0, \tag{9.24b}$$

for perturbations with appropriate initial conditions. Equation (9.24) can be solved via separation of variables, $\delta\rho(x, t) = S(x)T(t)$. The temporal equation reads

$$\frac{\mathrm{d}T}{\mathrm{d}t} = -\mu_n DT, \tag{9.25}$$

where $-\mu_n$ is the separation constant. The spatial equation reads

$$\frac{d^2 S}{dx^2} + \left[\mu_n + \frac{r}{D} F'(\bar{\rho})\right] S = 0, \tag{9.26a}$$

$$S(0) = S(L) = 0. \tag{9.26b}$$

The explicit form of the nontrivial steady state $\bar{\rho}(x)$ is generally not known, which presents a difficulty in dealing with (9.26). However, (9.26) forms a regular Sturm–Liouville problem, and the generic properties of its solutions are well known. The spectrum of (9.26) consists of a discrete set of real eigenvalues μ_n, which form an infinite ordered sequence $\mu_1 < \mu_2 < \mu_3 < \cdots$ with $\mu_n \to \infty$ as $n \to \infty$. The eigenfunction corresponding to the eigenvalue μ_1, denoted by $S_1(x)$, has no zeros in $[0, L]$, i.e., does not change sign on $[0, L]$. Setting $\mu_n = \mu_1$ and $S = S_1$, multiplying (9.26a) by $\bar{\rho}(x)$, integrating by parts, and using (9.6), we obtain

$$\mu_1 = \frac{r}{D} \frac{\int_0^L S_1(x) Q(\bar{\rho}) dx}{\int_0^L S_1(x) \bar{\rho}(x) dx}, \tag{9.27}$$

where $Q(\bar{\rho}) \equiv F(\bar{\rho}) - \bar{\rho} F'(\bar{\rho})$. For the logistic kinetic term, $F(\rho) = \rho(1 - \rho)$ and $Q(\bar{\rho}) = \bar{\rho}^2$. Since $\bar{\rho}(x) > 0$ and S_1 does not change sign on $(0, L)$, it follows that μ_1 and all of the other eigenvalues are positive which guarantees the stability of the nonuniform steady state, see (9.25).

This conclusion is not quite as straightforward for other kinetic terms. For example, if $F(\rho) = \rho(1-\rho)(\rho-a)$, then $Q(\bar{\rho}) = \bar{\rho}^2(2\bar{\rho}-1-a)$, which does not have a definite sign on $[0, L]$. If $Q(\bar{\rho}) > 0$ on $[0, L]$, the nonuniform steady state is stable. If $Q(\bar{\rho}) < 0$ on $[0, L]$, the nonuniform steady state is unstable. If $Q(\bar{\rho})$ changes sign on $[0, L]$, no conclusion can be drawn and one has to resort to other tools. The bifurcation diagram that emerges for the logistic case is that of a simple forward or supercritical bifurcation at L_c as illustrated in Fig. 9.2. Below L_c the trivial steady state is stable and the population dies out. Above L_c, the nonuniform steady state is stable, the trivial state is unstable, and the population persists or survives.
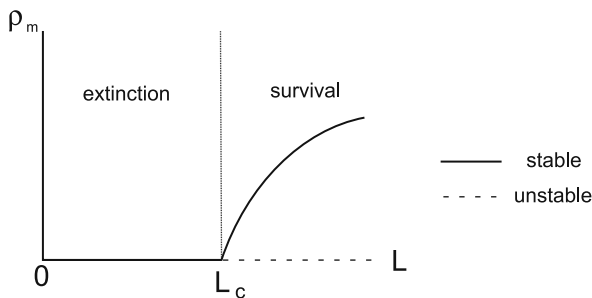
Fig. 9.2 Schematic bifurcation diagram (L, ρ_m) for the logistic case

9.3 Normal Solution Expansion

The method of the normal solution expansion provides a means to obtain the critical patch size if $F'(0) > 0$, the saddle–node bifurcation point if $F'(0) \leq 0$, and the stability of the steady states. An analytical expression for the steady state can also be obtained, but it is an approximate solution since we truncate the expansion. The normal solution expansion is a well-known method to obtain solutions of the nonlinear Boltzmann equation [180, 359]. It assumes that the distribution function $f(x, v, t)$, describing the density of atoms or structureless molecules at position x with velocity v at time t depends on time only through the velocity moments $\rho(x, t)$, $u(x, t)$, $P_{ij}(x, t)$, i.e., $f(x, v, t) \rightarrow f(x, v, \rho(x, t), u(x, t), P_{ij}(x, t))$, where ρ, u, P_{ij} are found by integrating f, $f v$, and $f v_i v_j$, respectively, over the full velocity space. We express the solution of (9.1) in terms of an appropriate complete set of orthogonal spatial basis functions:

$$\rho(x, t) = \sum_{k=1}^{\infty} \varphi_k(t) \sin\left(\frac{k\pi x}{L}\right). \tag{9.28}$$

The normal solution ansatz consists in the assumption that all the coefficients $\varphi_k(t)$ with $k > 1$ depend on time only through their functional dependence on $\varphi_1(t)$, i.e.,

$$\varphi_k(t) = \varphi_k\left[\varphi_1(t)\right] = \alpha_k \varphi_1(t) + \beta_k \varphi_1(t)^2 + \cdots, \quad k > 1. \tag{9.29}$$

As is the case with the normal solutions of the Boltzmann equation, the initial conditions may be such that the solution obtained is not accurate for early times (initial slip [180]). The validity of the normal solution method requires that $\lim_{\varphi_1 \to 0} \varphi_{k>1}/\varphi_1 = 0$. We show below that this condition is satisfied. Since we focus on the critical patch size, i.e., the size of the habitat where a transition from population extinction to persistence occurs, we deal with the case where ρ is a small quantity. We expect therefore that the solution will be well approximated outside an initial time layer by $\varphi_1(t)$. The equations for $\varphi_j(t)$, with $j = 1, 2, \ldots$, can be found by substituting (9.28) into (9.1), multiplying by $\sin(j\pi x/L)$, and integrating over the spatial domain.

We assume the kinetic term has the general form

$$F(\rho) = a_1 \rho + a_2 \rho^2 + a_3 \rho^3. \tag{9.30}$$

Kinetic functions of especial interest in population dynamics are logistic growth, $a_1 = 1$, $a_2 = -1$, $a_3 = 0$, depensation growth, $a_1 = a$, $a_2 = 1 - a$, $a_3 = -1$, and critical depensation growth, also known as Nagumo reaction or Allee effect, $a_1 = -a$, $a_2 = 1 + a$, $a_3 = -1$. The equation for $\varphi_1(t)$ is given by

$$\frac{d\varphi_1}{dt} + \left(\frac{D\pi^2}{L^2} - ra_1\right)\varphi_1 = \frac{8ra_2}{3\pi}\varphi_1^2 + \frac{3ra_3}{4}\varphi_1^3, \tag{9.31}$$

where we have neglected higher order terms, such as $\varphi_1\varphi_2$, $\varphi_1\varphi_3,\ldots$, $\varphi_2\varphi_3$, $\ldots$, $\varphi_2^2,\ldots$. The equation for $\varphi_j(t)$, with $j = 2, 3, \ldots$, reads

$$\frac{d\varphi_j}{dt} + \left(\frac{Dj^2\pi^2}{L^2} - ra_1\right)\varphi_j = M_j ra_2\varphi_1^2 + N_j ra_3\varphi_1^3, \tag{9.32}$$

where

$$M_j = \frac{4}{j\pi}\frac{\cos(\pi j) - 1}{j^2 - 4}, \quad N_j = \frac{12}{\pi}\frac{\sin(\pi j)}{(j^2 - 9)(j^2 - 1)}. \tag{9.33}$$

Substituting the expansion $\varphi_{j>1}(t) = \varphi_{j>1}[\varphi_1(t)] \equiv \alpha_j\varphi_1(t) + \beta_j\varphi_1(t)^2 + \gamma_j\varphi_1(t)^3 + \cdots$ (by construction $\beta_1 = \gamma_1 = 0$) into (9.32) and using (9.31), we find $\alpha_{j>1} = 0$ and

$$\beta_j = \frac{M_j ra_2}{\left(j^2 - 2\right)\frac{D\pi^2}{L^2} + ra_1}, \tag{9.34}$$

$$\gamma_j = r\frac{N_j a_3 - 2\beta_j M_1 a_2}{\left(j^2 - 3\right)\frac{D\pi^2}{L^2} + 2ra_1}, \tag{9.35}$$

by equating the coefficients of φ_1, φ_1^2, φ_1^3, $\ldots$ on each side of (9.32). Then, $\varphi_{k>1}(t) = \beta_k\varphi_1(t)^2 + \gamma_k\varphi_1(t)^3 + \cdots$, which implies $\varphi_{k>1}/\varphi_1 \to 0$ as $\varphi_1 \to 0$, and the approximate solution of (9.1) reads

$$\rho(x, t) \simeq \varphi_1(t)\sin\frac{\pi x}{L} + \varphi_1(t)^2\sum_{m=2}\beta_m\sin\frac{m\pi x}{L}$$

$$+ \varphi_1(t)^3\sum_{m=2}\gamma_m\sin\frac{m\pi x}{L}. \tag{9.36}$$

To find the stationary states, we set $\varphi_1(t) = \varphi^* = $ constant in (9.31). The solutions are

$$\varphi_1^* = 0 \quad \text{(extinction)}, \tag{9.37a}$$

$$\varphi_\pm^* = \frac{-M_1 a_2 \pm \sqrt{M_1^2 a_2^2 - 4N_1 a_3\left(a_1 - \frac{D\pi^2}{rL^2}\right)}}{2N_1 a_3} \quad \text{(survival)}, \tag{9.37b}$$

if $a_3 \neq 0$. If $a_3 = 0$, then $\varphi_1^* = 0$ and $\varphi_\pm^* = -\left(a_1 - \frac{D\pi^2}{rL^2}\right)\frac{1}{M_1 a_2}$. The stationary state of (9.1) is given by

$$\overline{\rho}(x) \simeq \varphi^* \sin\frac{\pi x}{L} + (\varphi^*)^2 \sum_{m=2} \beta_m \sin\frac{m\pi x}{L} + (\varphi^*)^3 \sum_{m=2} \gamma_m \sin\frac{m\pi x}{L}. \quad (9.38)$$

Since the maximum population density ρ_m occurs at the midpoint, $x = L/2$, the branches of the bifurcation diagram (L, ρ_m) correspond to

$$\rho_m \simeq \varphi^* + (\varphi^*)^2 \sum_{m=2} \beta_m \sin\frac{m\pi}{2} + (\varphi^*)^3 \sum_{m=2} \gamma_m \sin\frac{m\pi}{2}. \quad (9.39)$$

To determine the stability of the stationary state, we set $\varphi_1(t) = \varphi^* + \epsilon(t)$ with $\epsilon(t) \ll 1$. Substituting this expression into (9.31) and linearizing the equation, we obtain

$$\frac{d\epsilon}{dt} = -\left[\frac{D\pi^2}{L^2} - ra_1 - 2M_1 ra_2 \varphi^* - 3N_1 ra_3(\varphi^*)^2\right]\epsilon(t). \quad (9.40)$$

The steady state is stable if the term in brackets is positive, and unstable if it is negative. To be specific, we consider explicitly some examples of ecological interest, namely compensation and depensation population growth. In Fig. 9.3 we plot typical growth functions.
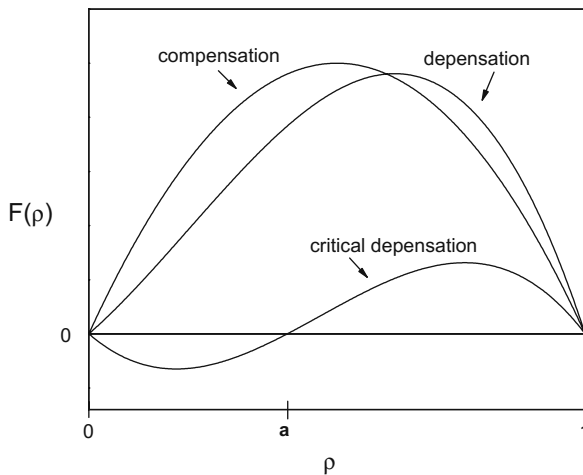
Fig. 9.3 Sketch of typical growth functions in ecology

9.3.1 Compensation Growth

Compensation growth corresponds to a logistic term, that is (9.30) with $a_1 = 1$, $a_2 = -1$, and $a_3 = 0$. In this case (9.37) turns into

$$\varphi_1^* = 0 \quad \text{(extinction)}, \tag{9.41a}$$

$$\varphi_\pm^* = \frac{3\pi}{8}\left(1 - \frac{D\pi^2}{rL^2}\right) \quad \text{(survival)}. \tag{9.41b}$$

The state (9.41a) is stable if $\frac{D\pi^2}{L^2} - r > 0$, i.e., if $L < L_c$ with L_c given by (9.5) and it is unstable if $L > L_c$. The value of ρ_m in the survival state (9.41b) is

$$\rho_m \simeq \frac{3\pi}{8}\left(1 - \frac{D\pi^2}{rL^2}\right) + \frac{9\pi^2}{64}\left(1 - \frac{D\pi^2}{rL^2}\right)^2 \sum_{m=3}\beta_m \sin\frac{m\pi}{2}. \tag{9.42}$$
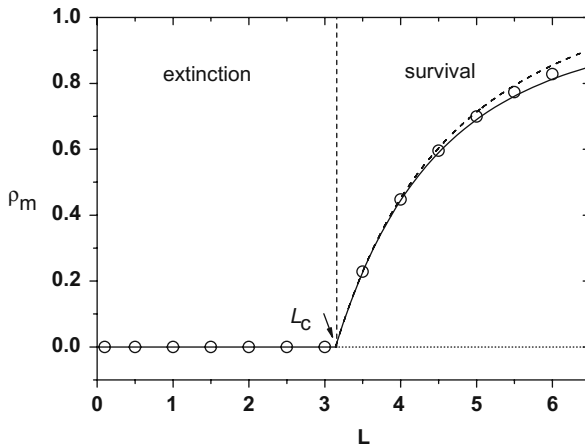
Fig. 9.4 Bifurcation diagram for compensation growth for $D = r = 1$

In Fig. 9.4 we plot the corresponding bifurcation diagram. A forward or super-critical bifurcation occurs at $L = L_c$. We depict with symbols the values obtained by integrating (9.1) numerically using an explicit finite difference method with a time step of 10^{-3} units and a mesh size of 5×10^{-2}. The system reaches the steady state after a time of 90 units. Solid curves correspond to (9.42). The dashed line corresponds to the result obtained from the variational principle (9.22):

$$L^2 = \frac{D\pi^2}{r}\left(1 - \frac{8\rho_m}{3\pi}\right)^{-1}. \tag{9.43}$$

Equation (9.40) implies that the survival state (9.41b) is stable for $L > L_c$.

9.3.2 Depensation Growth

Depensation growth corresponds to a kinetic term $F(\rho) = \rho(1 - \rho)(\rho + a)$ with $0 < a \leq 1$, i.e., to setting $a_1 = a$, $a_2 = 1 - a$, and $a_3 = -1$. From (9.37) we can find the three branches of steady states:

$$\varphi_1^* = 0 \quad \text{(extinction)}, \tag{9.44a}$$

$$\varphi_\pm^* = \frac{16(1 - a)}{9\pi} \pm \frac{2}{3}\sqrt{\Delta(L)} \text{ (survival)}, \tag{9.44b}$$

where

$$\Delta(L) = \frac{64(1 - a)^2}{9\pi^2} + 3a\left[1 - \left(\frac{L_c}{L}\right)^2\right], \quad \text{with} \quad L_c = \pi\sqrt{\frac{D}{ra}}. \tag{9.45}$$

In this case there exists a critical patch size. In the following we truncate the expansion in (9.39) at the first order for simplicity, $\rho_m \simeq \varphi^*$ with φ^* given by (9.44). The nontrivial branches collide at a saddle–node bifurcation point or turning point that has the following coordinates:

$$(\rho_{\text{bif}}, L_{\text{bif}}) = \left(\frac{16(1 - a)}{9\pi}, \frac{L_c}{\sqrt{1 + \frac{64(1-a)^2}{27a\pi^2}}}\right). \tag{9.46}$$

Equation (9.40) implies that the trivial solution is stable if $L < L_c$ with L_c given by (9.45); otherwise it is unstable. Equation (9.40) implies that stability of the nontrivial branches requires $\varphi_\pm^* > 16(1 - a)/9\pi$, which is satisfied only by φ_+^*. The branch $\rho_m^+ \simeq \varphi_+^*$ is stable, and the branch $\rho_m^- \simeq \varphi_-^*$ is unstable. We represent the bifurcation diagram in Fig. 9.5a. A backward or subcritical bifurcation occurs at $L = L_c$. Branches are calculated from (9.39), and symbols correspond to numerical solutions. For $L < L_{\text{bif}}$, only the trivial solution exists, and the population always dies out, the region of absolute extinction. Within the intermediate region $L_{\text{bif}} < L < L_c$, the system is bistable; both $\rho_m = 0$ and ρ_m^+ are stable branches. The system selects one of them, i.e., the population dies out or survives, depending on the value of the initial condition. For $L > L_c$, only ρ_m^+ is stable and the population survives independently of the initial condition, the region of absolute survival. In the phase diagram $d\varphi_1/dt$ vs φ_1, given by (9.31), φ_-^* is a repellor, while $\varphi_1^* = 0$ and φ_+^* are attractors. If the initial condition $\varphi_1(0)$ lies between 0 and φ_-^*, the asymptotic state of the system is $\rho_m = 0$; otherwise it is ρ_m^+. In summary, there exists a critical
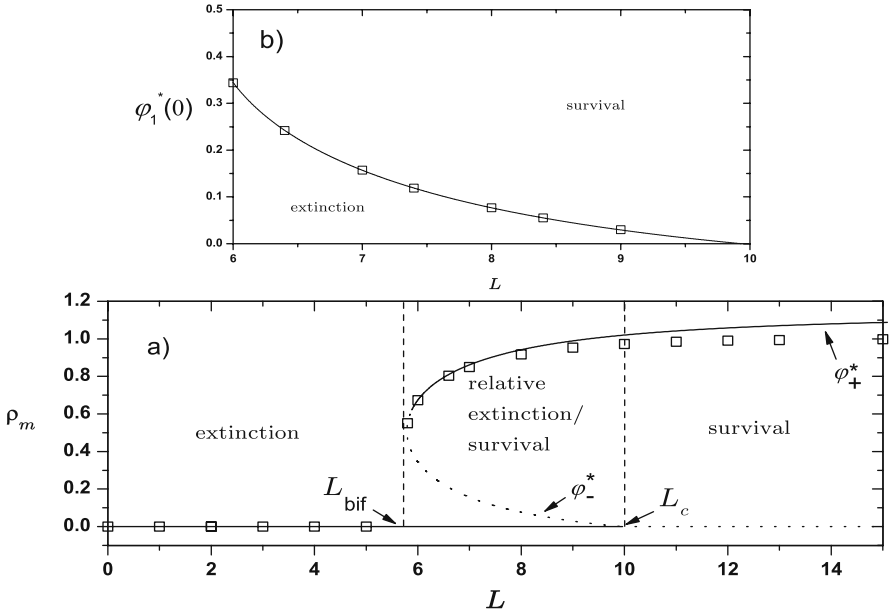
Fig. 9.5 (**a**) Bifurcation diagram for depensation growth for $a = 0.1$ and $D = r = 1$. *Solid lines* correspond to stable branches and the *dotted lines* to unstable branches. *Symbols* depict numerical results. *Vertical dashed lines* separate the extinction, relative extinction/survival, and survival regions. (**b**) Plot of the critical initial density vs the patch size for the relative extinction/survival region

value for the initial condition $\varphi_1^*(0) = \varphi_-^*$, such that for $\varphi_1(0) < \varphi_-^*$ the population dies out, while for $\varphi_1(0) > \varphi_-^*$ it survives. ρ_m^- plays the role of the separatrix between the basins of attraction for the states $\rho_m = 0$ and ρ_m^+. We have plotted this result in Fig. 9.5b, where we also compare it with the numerical solutions. Fixing the parameter values and varying $\varphi_1(0)$ from 1 to 0, we have determined numerically the value at which the steady state collapses to 0. Figure 9.5b shows that the critical value of the initial condition ρ_m^- decreases as L increases, as expected intuitively.

9.3.3 Critical Depensation

We consider the case of a strong Allee effect which corresponds to a growth term of the form $F(\rho) = \rho(1 - \rho)(\rho - a)$ with $0 < a < 1/2$, i.e., $a_1 = -a$, $a_2 = 1 + a$, and $a_3 = -1$. The three branches of the bifurcation diagram are

$$\varphi_1^* = 0 \quad \text{(extinction)}, \tag{9.47a}$$

$$\varphi_\pm^* = \frac{16(1 + a)}{9\pi} \pm \frac{2}{3}\sqrt{\Delta(L)} \quad \text{(survival)}, \tag{9.47b}$$

with

$$\Delta(L) = 64(1 + a)^2/9\pi^2 - 3a \left[1 + D\,(\pi/L)^2\,/ra\right].   \tag{9.48}$$

The coordinates of the saddle–node bifurcation point are

$$\left(\rho_{\mathrm{bif}}, L_{\mathrm{bif}}\right) = \left(\frac{16(1 + a)}{9\pi}, \pi^2\sqrt{\frac{D}{r}}\,\frac{3\sqrt{3}}{\sqrt{64(1 + a)^2 - 27a\pi^2}}\right).   \tag{9.49}$$

The trivial steady state, extinction, satisfies the stability condition for any L, while φ_+^* is stable and φ_-^* is unstable, as in the depensation growth case. Again, for $0 < L < L_{\mathrm{bif}}$, only the trivial solution exists and the population dies out. However, there is an important difference. The trivial steady state does not undergo a bifurcation and no critical patch size exists. The relative extinction/survival region extends indefinitely for $L > L_{\mathrm{bif}}$; there is no absolute survival region. In Fig. 9.6a we plot the corresponding bifurcation diagram. Figure 9.6b corresponds, as in the previous case, to the critical initial condition $\varphi_1^*(0) = \varphi_-^*$ with φ_-^* given by (9.47). The reason for the stability of the trivial state, extinction, and the absence of a critical patch size, does not simply stem from the fact that the growth term $F(\rho)$ is negative for low values of the density ρ, see Fig. 9.3. Note that the unstable branch is given by the value φ_-^* and not by the Allee parameter a alone. As we showed for
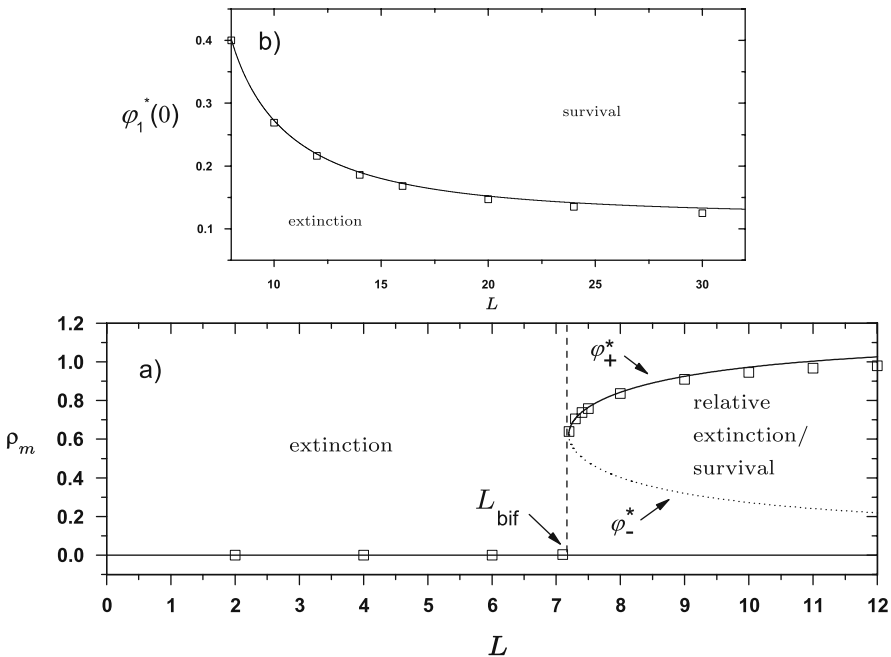
Fig. 9.6 The same as Fig. 9.5 but for critical depensation

depensation growth, a region of relative survival/extinction exists even for a strictly positive function $F(\rho)$.

9.4 Exact Solutions

Equation (9.6) can be solved exactly in terms of Jacobi elliptic functions if $F(\rho) = \rho(1 - \rho)$ [226]. Define $\xi = x/L - 1/2$; then $\rho(\xi = 1/2) = \rho(\xi = -1/2) = 0$. Consider the ansatz $\rho(\xi, k) = A + B\,\mathrm{cd}(C\xi, k)^2$, where k is a positive parameter and $\mathrm{cd}(u) = \mathrm{cn}(u)/\mathrm{dn}(u)$. Substituting this ansatz into (9.6), we find the values of the coefficients A, B, and C in terms of k. Making use of the relations between Jacobi elliptic functions, we can write the derivative $d^2\rho/dx^2$ in terms of the function $\mathrm{sn}(\cdot)$ only. Collecting terms with the same powers of $\mathrm{sn}(\cdot)$, we obtain three algebraic equations that provide the values of the coefficients A, B, and C in terms of k:

$$A = \frac{1}{2}\left(1 - \frac{k^2 + 1}{\sqrt{k^4 - k^2 + 1}}\right),\tag{9.50a}$$

$$B = \frac{3}{2}\frac{k^2}{\sqrt{k^4 - k^2 + 1}},\tag{9.50b}$$

$$C = \frac{L\sqrt{r/D}}{2\left(k^4 - k^2 + 1\right)^{1/4}}.\tag{9.50c}$$

The boundary conditions, $\rho(\xi = 1/2, k) = \rho(\xi = -1/2, k) = A + B\,\mathrm{cd}(C/2, k)^2 = 0$, imply that

$$3k^2\,\mathrm{cd}\left[\frac{L\sqrt{r/D}}{4\left(k^4 - k^2 + 1\right)^{1/4}}, k\right]^2 + \sqrt{k^4 - k^2 + 1} - 1 - k^2 = 0.\tag{9.51}$$

Substitution of the constants (9.50) into the ansatz yields the parametric equation for the pattern:

$$\bar\rho(x) = \frac{1}{2}\left(1 - \frac{k^2 + 1}{\sqrt{k^4 - k^2 + 1}}\right)$$
$$+ \frac{3}{2}\frac{k^2}{\sqrt{k^4 - k^2 + 1}}\,\mathrm{cd}\left[\frac{L\sqrt{r/D}\left(\frac{x}{L} - \frac{1}{2}\right)}{4\left(k^4 - k^2 + 1\right)^{1/4}}, k\right]^2,\tag{9.52}$$
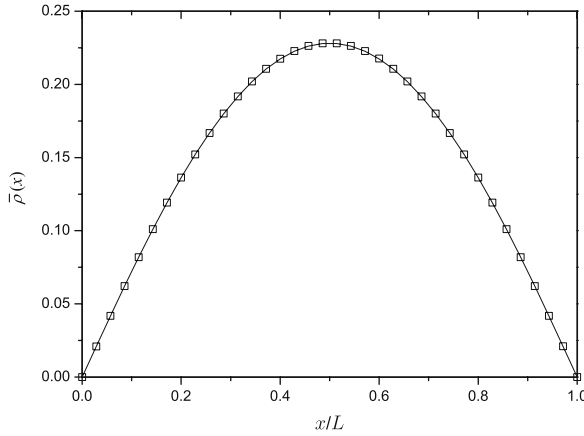
Fig. 9.7 Nontrivial steady state. *Solid curve* corresponds to (9.52) and *symbols* to numerical solutions. In both cases we have taken $r = D = 1$ and $L = 3.5$. To plot (9.52), we solved first (9.51) for k to obtain $k = 0.505$

where k is given in terms of L by the relation (9.51). The pattern is shown in Fig. 9.7.

The bifurcation diagram can be obtained by noting that $\rho_m(k) = \rho(\xi = 0, k) = A + B$, and the curve ρ_m vs L is, in parametric form,

$$\rho_m(k) = \frac{1}{2}\left(1 + \frac{2k^2 - 1}{\sqrt{k^4 - k^2 + 1}}\right), \tag{9.53}$$

where again k is given in terms of L by the relation (9.51) with $0 < k < 1$. It is easy to check that $\rho_m(k = 0) = 0$, and the critical patch size is obtained by taking the limit $k \to 0$ in (9.51). Since $\mathrm{cd}(x, 0) = \cos(x)$, the limit yields $L_c = \pi\sqrt{D/r}$.
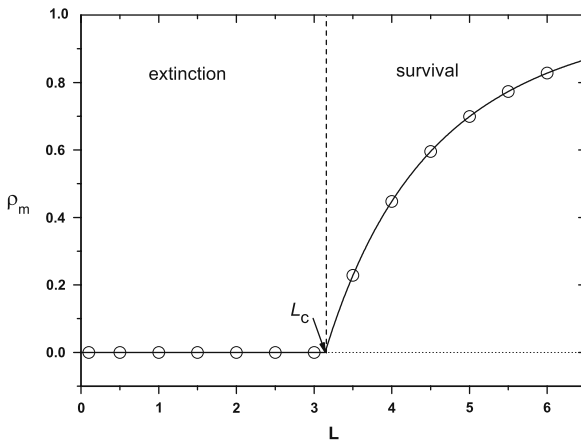
Fig. 9.8 Bifurcation diagram for the maximum central density vs the patch size for $r = D = 1$

In Fig. 9.8 we compare the analytical predictions obtained from (9.53) (solid curve) with the numerical results (circles) for the bifurcation diagram. As expected, the agreement is perfect.

Exercises

9.1 Consider the RD equation with a cutoff in the reaction term, i.e., $F(\rho) = \theta(\rho - \epsilon) f(\rho)$. As we saw in Sect. 4.3, the cutoff takes into account that a successful reaction requires a minimum value of the particle density, ϵ. If $\epsilon \ll 1$, derive the relation between L and ρ_m up to terms of order ϵ^3 from (9.8).

9.2 Consider $F(\rho) = \theta(\rho - \epsilon)\rho(1 - \rho)$ and determine the coordinates of the bifurcation point $(\rho_{\text{bif}}, L_{\text{bif}})$ from the variational characterization (9.22).

9.3 Find the critical patch size for the RD equation with Robin boundary conditions

$$\frac{\partial \rho}{\partial t} = D \frac{\partial^2 \rho}{\partial x^2} + r F(\rho), \tag{9.54a}$$

$$\left. \frac{\partial \rho}{\partial x} \right|_{x=0} = \alpha \rho(0, t), \qquad \left. \frac{\partial \rho}{\partial x} \right|_{x=L} = -\alpha \rho(L, t), \tag{9.54b}$$

$$\rho(x, 0) = \rho_0(x). \tag{9.54c}$$

9.4 Find the critical patch size for the radially symmetric problem

$$\frac{\partial \rho}{\partial t} = \frac{D}{r} \frac{\partial}{\partial r} \left(r \frac{\partial \rho}{\partial r} \right) + \alpha F(\rho), \tag{9.55a}$$

$$\rho(r \geq R, t) = 0. \tag{9.55b}$$

Note that we use α rather than r as the intrinsic growth rate.

9.5 Consider a linear stream ecosystem. The RD equation contains now a drift term, so that

$$\frac{\partial \rho}{\partial t} + v \frac{\partial \rho}{\partial x} = D \frac{\partial^2 \rho}{\partial x^2} + r F(\rho). \tag{9.56}$$

Typical streams have an upstream source and then empty into a larger body of water. Reasonable boundary conditions are zero flux at the upstream end, $x = 0$, because population cannot leave, and hostile at the downstream end, $x = L$, where environmental condition may dramatically change:

$$v\rho(0, t) - D \left(\frac{\partial \rho}{\partial x} \right)_{x=0} = 0, \qquad\qquad (9.57a)$$

$$\rho(L, t) = 0, \qquad\qquad (9.57b)$$

respectively. Linearize the RD-advection equation (9.56) about the state $\rho = 0$ and show that the critical patch size is

$$L_c = \sqrt{\frac{D/r}{1 - \frac{v^2}{4rD}}} \arctan \left[-\frac{2\sqrt{rD}}{v} \left(1 - \frac{v^2}{4rD} \right) \right]. \qquad (9.58)$$

Chapter 10
Turing Instabilities in Homogeneous Systems

Alan Turing's paper entitled "The Chemical Basis of Morphogenesis" [440] ranks without doubt among the most important papers of the last century. In that seminal work Turing laid the foundation for the theory of chemical pattern formation. Turing showed that diffusion can have nontrivial effects in nonequilibrium systems. The interplay of diffusion with nonlinear kinetics can destabilize the uniform steady state of reaction–diffusion systems and generate stable, stationary concentration patterns. To quote from the abstract,

> It is suggested that a system of chemical substances, called morphogens, reacting together and diffusing through a tissue, is adequate to account for the main phenomena of morphogenesis. Such a system, although it may originally be quite homogeneous, may later develop a pattern or structure due to an instability of the homogeneous equilibrium, which is triggered off by random disturbances.

The diffusion-induced instability of the uniform steady state is now called a Turing instability or Turing bifurcation. The stationary patterns to which it gives rise are called Turing patterns. Turing patterns posses the important feature of an intrinsic length. The typical length scale of these stationary patterns is solely determined by the diffusion coefficients and the rate coefficients and not by geometrical parameters of the system. In this chapter we review first the theory of Turing instabilities in standard reaction–diffusion systems. We then present results on transport-induced instabilities in reacting systems with nonstandard diffusive transport, namely transport with inertia and anomalous diffusion. These results address the question of how the characteristics of the transport process affect spatial instabilities and the formation of stationary spatial patterns in reaction–transport systems. To quote once more from the abstract of Turing's paper, "The investigation is chiefly concerned with the onset of instability," and this is also the main concern of this chapter.

10.1 Turing Instabilities in Standard Reaction–Diffusion Systems

We begin the discussion of Turing instabilities by presenting some general results for n-variable systems. We focus particularly on properties of the diffusion matrix D that facilitate or hinder the onset of spatial instabilities.

10.1.1 n-Variable Reaction–Diffusion Systems

We consider the general n-variable reaction–diffusion system (2.12),

$$\frac{\partial \rho_i}{\partial t} = D_i \frac{\partial^2 \rho_i}{\partial x^2} + F_i(\boldsymbol{\rho}, \boldsymbol{\mu}), \quad i = 1, \ldots, n, \tag{10.1}$$

with three possible boundary conditions:

(1) infinite system: $x \in (-\infty, \infty)$; $\qquad\qquad\qquad\qquad\qquad\quad$ (10.2a)

(2) finite system: $x \in [0, L]$, $\quad \dfrac{\partial \rho_i}{\partial x}(0, t) = \dfrac{\partial \rho_i}{\partial x}(L, t) = 0, \quad i = 1, \ldots, n,$

   no-flux (Neumann) boundary condition; $\qquad\qquad\qquad\qquad$ (10.2b)

(3) finite system: $x \in [0, L]$, $\quad \boldsymbol{\rho}(0, t) = \boldsymbol{\rho}(L, t) = \boldsymbol{\rho}_b, \quad i = 1, \ldots, n,$

   fixed concentration (Dirichlet) boundary condition. $\qquad\qquad$ (10.2c)

The spatially uniform solution $\overline{\boldsymbol{\rho}}(x) = \overline{\boldsymbol{\rho}}$, where $\mathbf{F}(\overline{\boldsymbol{\rho}}, \boldsymbol{\mu}) = 0$, is a stationary state of (10.1) with boundary conditions (10.2a) or (10.2b). For Dirichlet boundary conditions, uniform steady states of (10.1) are only possible if

$$\boldsymbol{\rho}_b = \overline{\boldsymbol{\rho}}. \tag{10.3}$$

The uniform steady state $\overline{\boldsymbol{\rho}}(x)$ is stable against uniform perturbations, if $\overline{\boldsymbol{\rho}}$ is a stable steady state of the homogeneous or well-mixed system:

$$\frac{\mathrm{d}\boldsymbol{\rho}}{\mathrm{d}t} = \mathbf{F}(\boldsymbol{\rho}, \boldsymbol{\mu}), \tag{10.4}$$

i.e., if all eigenvalues of the Jacobian matrix $\mathbf{J}$ have a negative real part, see Sect. 1.2. A Turing instability corresponds to a diffusion-driven instability where a stable uniform steady state becomes unstable to a small nonuniform spatial perturbation with wavenumber $k_{\mathrm{T}} \neq 0$. A small inhomogeneity about $\overline{\boldsymbol{\rho}}(x) = \overline{\boldsymbol{\rho}}$ can be written as

$$\delta\boldsymbol{\rho}(x, t) = \boldsymbol{\rho}(x, t) - \overline{\boldsymbol{\rho}} = \sum \mathbf{a}_k \phi_k(x) \exp(\lambda_k t), \tag{10.5}$$

where the spatial modes $\phi_k(x)$ satisfy

$$\frac{\partial^2 \phi_k(x)}{\partial x^2} = -k^2 \phi_k(x) \tag{10.6}$$

and the boundary conditions. Substituting (10.5) into (10.1) and linearizing with respect to the uniform steady state, we find that the λ_k, which determine the stability of the uniform steady to infinitesimal perturbations of the form $\phi_k(x)$, are

the eigenvalues of the matrix $\widehat{J}(k^2) \equiv J - Dk^2$, i.e., the roots of the characteristic polynomial $(-1)^n \det[\widehat{J}(k^2) - I_n \lambda_k] = 0$. A Turing instability occurs when for the first time a single real λ_k, for some nonzero k, passes through zero as a control parameter μ is varied, while the real part of all other eigenvalues of $\widehat{J}(k^2)$ remains negative. In other words, as the control parameter is changed, the uniform steady state of the reaction–diffusion system becomes unstable at $\mu = \mu_T$ to perturbations with a nonzero wavenumber k_T, and the spatial mode $\phi_{k_T}(x)$ grows into a stationary spatially nonuniform solution of (10.1) beyond the Turing threshold μ_T, i.e., a time-independent concentration pattern. The final pattern is determined by the nonlinear terms of the kinetic rate functions and can differ qualitatively from the unstable Turing mode $\phi_{k_T}(x)$.

If all diffusion coefficients are equal, $D_i = D$, that is $D = DI_n$ is a scalar times the identity, known as a scalar matrix, then the characteristic polynomial reads $(-1)^n \det[J - (Dk^2 + \lambda_k)I_n] = 0$. This implies that $Dk^2 + \lambda_k$ must equal the eigenvalues of J. The latter all have a negative real part, since $\overline{\rho}$ is a stable steady state of the well-mixed system. Consequently, the eigenvalues λ_k all have a negative real part, and $\mathrm{Re}\,\lambda_k < \mathrm{Re}\,\lambda_0$ for $k \neq 0$ [455]. These results imply the following theorem and corollary.

Theorem 10.1 *If* $D = DI_n$, *then* $\overline{\rho}(x) = \overline{\rho}$ *is a stable solution of* (10.1). *If all diffusion coefficients of the reaction–diffusion system* (10.1) *are equal, no Turing instability can occur.*

Corollary 10.1 *No Turing bifurcation can occur in a one-variable reaction–diffusion system.*

Remark 10.1 Since $\mathrm{Re}\,\lambda_k < \mathrm{Re}\,\lambda_0$, diffusion is always stabilizing in one-variable reaction–diffusion systems and in n-variable reaction–diffusion systems with equal diffusion coefficients. The initial bifurcation from the uniform steady state $\overline{\rho}(x) = \overline{\rho}$ of (10.1), as the parameter μ is varied, must always be the eigenfunction $\phi_k(x)$ corresponding to the lowest wavenumber. For infinite systems and systems with Neumann boundary conditions, the initial bifurcation is thus a wavenumber-zero bifurcation, i.e., a homogenous bifurcation. For finite systems with Dirichlet boundary conditions a wavenumber-zero mode is not possible. The lowest wavenumber is given by $k = \pi/L$. The length scale of this inhomogeneity is determined by the boundary conditions. There is no intrinsic length scale and this is not a chemical pattern. In systems with equal diffusion coefficients the initial bifurcation does not give rise to steady chemical patterns.

To obtain the threshold criterion for the onset of a Turing instability, we set $\lambda_k = 0$ and analyze the determinant

$$\Delta(k^2) = \det(J - Dk^2). \tag{10.7}$$

For (10.2a), the spectrum of possible wavenumber is continuous, $k \geq 0$. For (10.2b) and (10.2c), the spectrum of possible wavenumbers is given by $k = m\pi/L$, where

$m = 0, 1, 2, \ldots$ for Neumann boundary conditions and $m = 1, 2, \ldots$ for Dirichlet boundary conditions. To simplify the presentation, we treat k as a continuous variable also for finite systems and assume that the system can accommodate a pattern with intrinsic wavenumber k_T. This represents no restriction of generality, since one can ensure that any given k is in the spectrum by an appropriate choice of the system size L. A Turing instability occurs when $\Delta(k^2)$ has a degenerate, strictly positive, root k_T^2, i.e., when

$$\Delta(k^2)\big|_{\mu_T, k_T^2 > 0} = 0, \tag{10.8a}$$

$$\frac{d\Delta(k^2)}{d(k^2)}\bigg|_{\mu_T, k_T^2 > 0} = 0, \tag{10.8b}$$

$$\mathrm{sgn}\left(\frac{d^2\Delta(k^2)}{d(k^2)^2}\bigg|_{\mu_T, k_T^2 > 0}\right) = -1^n. \tag{10.8c}$$

Theorem 10.1 raises the question how unequal the diffusion coefficients must be in order for a Turing instability to occur. The answer was given in [348]: Turing instabilities can occur in generic systems with nearly scalar diffusion matrices if and only if J has at least two eigenvalues that are sufficiently close to zero. Generically, it is necessary to vary two control parameters of the well-mixed system, say μ_1 and μ_2, to find such a point. We define without loss of generality the double-zero condition as $\mu_1 = \mu_2 = 0$. Before stating the results more precisely, we briefly discuss the double-zero bifurcation. The generic case corresponds to a coalescence of a Hopf and a saddle–node bifurcation, the Takens–Bogdanov bifurcation [175], see Sect. 1.2.2. The linear part in Jordan–Arnold normal form is given by

$$\begin{pmatrix} 0 & 1 \\ -a_1 & -a_2 \end{pmatrix}, \tag{10.9}$$

where a_1 and a_2 are positive functions of the control parameters. The double-zero bifurcation occurs for $a_1 = a_2 = 0$. The line of Hopf bifurcations corresponds to $a_2 = 0$ and the line of saddle–node bifurcations to $a_1 = 0$. Along the line of Hopf bifurcations the frequency of the limit-cycle oscillations is given by $\omega_H = \sqrt{a_1}$. The second type of double-zero bifurcation corresponds to the Lotka–Volterra system and has the linear part

$$\begin{pmatrix} -a & 0 \\ 0 & -b \end{pmatrix} \tag{10.10}$$

near the double zero. Such systems are nongeneric; small perturbations destroy the diagonal character of the linearized system. Lotka–Volterra systems are structurally unstable; the Lotka–Volterra double zero occurs only in systems with symmetries. In

general, chemical systems have no such symmetries. The matrix (10.9) is the generic form for matrices with two eigenvalues near zero. Therefore, when we refer to double-zero bifurcations we mean Takens–Bogdanov points. To find a double-zero bifurcation in chemical systems, one needs to locate a branch of Hopf bifurcations and track it in the direction of decreasing frequency.

Let us define a smallness parameter ϵ that measures the deviation of the diffusion matrix D from a scalar matrix. Define the mean diagonal coefficient D as

$$D = \det(\mathsf{D})^{1/n}. \tag{10.11}$$

If the diffusion matrix is a diagonal matrix, $\mathsf{D} = \mathrm{diag}(D_1, \ldots, D_n)$, then D is just the geometric mean of the n diffusion coefficients. We write D as

$$\mathsf{D} = D\mathsf{I}_n + \bar{\mathsf{d}} \tag{10.12}$$

and define ϵ as

$$\epsilon = \max_{i,j} \frac{|\bar{d}_{ij}|}{D}. \tag{10.13}$$

We define the deviations d_{ij} by

$$D_{ij} = D(\delta_{ij} + \epsilon d_{ij}), \tag{10.14}$$

where δ_{ij} is the Kronecker delta.

Theorem 10.2 *If a set of d_{ij} exists such that a Turing bifurcation occurs for arbitrarily small but nonzero ϵ and the eigenvalues of J remain bounded in modulus, then*

$$\lim_{\epsilon \to 0} \mu_{1,\mathrm{T}} = \lim_{\epsilon \to 0} \mu_{2,\mathrm{T}} = 0. \tag{10.15}$$

This limit corresponds to a small wavenumber limit:

$$\lim_{\epsilon \to 0} Dk_{\mathrm{T}}^2 = 0. \tag{10.16}$$

The preceding theorem establishes that the well-mixed system being in the vicinity of a double-zero point is a necessary condition for a Turing bifurcation to occur in (10.1) with nearly equal diffusion coefficients. The next theorem establishes that this is also a sufficient condition.

Theorem 10.3 *If the well-mixed system is sufficiently close to a Takens–Bogdanov point, then there exists a set of d_{ij} such that a Turing bifurcation occurs for arbitrarily small ϵ.*

Theorem 10.4 *The critical wavenumber k_T of the Turing instability near a double-zero point is given by*

$$k_T^2 = \frac{\sqrt{a_1}}{D}.$$

(10.17)

The proofs of Theorems 10.2, 10.3, and 10.4 are found in [348]. Equation (10.17) is of particular interest. Near the Takens–Bogdanov point, the frequency of the limit-cycle oscillations along the line of Hopf bifurcations, $a_2 = 0$, is given by $\omega_H = \sqrt{a_1}$, see above. On the line of saddle–node bifurcations we have $a_1 = 0$. An equation like (10.17) is expected from simple dimensional arguments. The only intrinsic length scales in reaction–diffusion systems come from the diffusion coefficients. The inverse time $\sqrt{a_1}$ is determined by the rate coefficients of the reaction kinetics. Thus (10.17) provides an estimate of the intrinsic length of the Turing pattern near a double-zero point:

$$l_T \approx \sqrt{\frac{2\pi D}{\omega_H}}.$$

(10.18)

10.1.2 Two-Variable Reaction–Diffusion Systems

In this section we study the onset of Turing instabilities in more detail for two-variable systems. We will focus on systems with Neumann boundary conditions, which are most relevant for experimental systems,

$$\frac{\partial \rho_u}{\partial t} = D_u \frac{\partial^2 \rho_u}{\partial x^2} + F_1(\rho_u, \rho_v),$$

(10.19a)

$$\frac{\partial \rho_v}{\partial t} = D_v \frac{\partial^2 \rho_v}{\partial x^2} + F_2(\rho_u, \rho_v),$$

(10.19b)

with no-flow boundary conditions on the interval $[0, L]$:

$$\frac{\partial \rho_u}{\partial x}(0, t) = \frac{\partial \rho_u}{\partial x}(L, t) = 0,$$

(10.20a)

$$\frac{\partial \rho_v}{\partial x}(0, t) = \frac{\partial \rho_v}{\partial x}(L, t) = 0.$$

(10.20b)

Let $(\bar{\rho}_u, \bar{\rho}_v)$ be a stable steady state of the homogeneous system

$$\frac{d\rho_u}{dt} = F_1(\rho_u, \rho_v),$$

(10.21a)

$$\frac{d\rho_v}{dt} = F_2(\rho_u, \rho_v), \tag{10.21b}$$

namely

$$F_1(\overline{\rho}_u, \overline{\rho}_v) = F_2(\overline{\rho}_u, \overline{\rho}_v) = 0. \tag{10.22}$$

Then, see (1.27),

$$T = J_{11} + J_{22} < 0, \tag{10.23a}$$

$$\Delta = J_{11}J_{22} - J_{12}J_{21} > 0. \tag{10.23b}$$

To assess the stability of the uniform steady state $(\overline{\rho}_u(x), \overline{\rho}_v(x)) = (\overline{\rho}_u, \overline{\rho}_v)$, we carry out a linear stability analysis as in Sect. 10.1.1:

$$\rho_u(x, t) = \overline{\rho}_u + u_0 \cos(kx) \exp(\lambda_k t), \tag{10.24a}$$

$$\rho_v(x, t) = \overline{\rho}_v + v_0 \cos(kx) \exp(\lambda_k t). \tag{10.24b}$$

The "growth" rates λ_k of the spatial modes $\cos(kx)$ are the roots of the characteristic polynomial

$$\det(\mathsf{J} - \mathsf{D}k^2 - \mathsf{I}_n\lambda_k) = \begin{vmatrix} J_{11} - D_u k^2 - \lambda_k & J_{12} \\ J_{21} & J_{22} - D_v k^2 - \lambda_k \end{vmatrix} = 0. \tag{10.25}$$

This is a second-order polynomial

$$\lambda_k^2 + c_1\lambda_k + c_2 = 0, \tag{10.26}$$

where

$$c_2 = (J_{11} - D_u k^2)(J_{22} - D_v k^2) - J_{12}J_{21}$$
$$= D_u D_v k^4 - (D_v J_{11} + D_u J_{22})k^2 + \Delta, \tag{10.27}$$

$$c_1 = (D_u + D_v)k^2 - T. \tag{10.28}$$

Equation (10.26) is called the dispersion relation; it relates the growth rates of the spatial modes to the parameter values of the system.

A spatial Hopf bifurcation, commonly called a wave bifurcation, corresponds to a pair of purely imaginary eigenvalues for some $k_H \neq 0$, i.e., $c_1 = 0$ and $c_2 > 0$. According to the stability conditions (10.23), $T < 0$, and therefore

$$c_1 = (D_u + D_v)k^2 - T > 0 \tag{10.29}$$

for all k. In other words, the uniform steady state of a two-variable reaction–diffusion system cannot undergo a wave bifurcation, i.e., an oscillatory instability to a standing wave pattern.

A Turing bifurcation corresponds to $\lambda_{k_T} = 0$ for $k_T \neq 0$, i.e., $c_2 = 0$, which leads to

$$\left(J_{11} - D_u k^2\right)\left(J_{22} - D_v k^2\right) - J_{12} J_{21} = 0 \tag{10.30}$$

or

$$K^2 - \left(\frac{J_{11}}{D_u} + \frac{J_{22}}{D_v}\right) K + \frac{\Delta}{D_u D_v} = 0, \tag{10.31}$$

where $K = k^2$. Since the roots of (10.31) have to be positive,

$$D_v J_{11} + D_u J_{22} > 0 \tag{10.32}$$

is a necessary but not sufficient condition for a Turing bifurcation. In light of (10.23), a Turing bifurcation can therefore occur only if (i) the coefficients J_{11} and J_{22} do not have the same sign and (ii) if the diffusion coefficients are not equal, see Theorem 10.1. In other words, Turing instabilities can occur only in pure or cross activator–inhibitor systems, (1.19) or (1.21). For such systems

$$J_{11} > 0, \; J_{22} < 0, \tag{10.33}$$

which together with (10.32) implies that Turing bifurcations can only occur if $\left|J_{22}\right| > J_{11}$ since $T < 0$ and $J_{12} J_{21} < 0$ since $\Delta > 0$. Defining

$$\theta_{RD} = \frac{D_v}{D_u}, \tag{10.34}$$

we obtain from (10.32)

$$\theta_{RD} > \frac{-J_{22}}{J_{11}} > 1. \tag{10.35}$$

In other words, for a Turing instability to occur, the activator must diffuse slower than the inhibitor. This is known as the principle of "short-range activation and long-range inhibition." It is also known as "local autocatalysis with lateral inhibition" or "local auto-activation–lateral inhibition" (LALI), see for example [332, 319], "local self-activation and lateral inhibition" [280], or "self-enhancement and lateral inhibition" (SELI) [315] and has been applied to mechanisms other than reaction–diffusion.

Rewriting (10.31) in the form

$$k^4 + \hat{c}_2 k^2 + \hat{c}_4 = 0, \tag{10.36}$$

with

$$\hat{c}_2 = -\left(\frac{J_{11}}{D_u} + \frac{J_{22}}{D_v}\right), \tag{10.37}$$

$$\hat{c}_4 = \frac{\Delta}{D_u D_v}, \tag{10.38}$$

we find that the roots of (10.31) are given by

$$k_{\pm}^2 = \frac{1}{2}\left(-\hat{c}_2 \pm \sqrt{\hat{c}_2^2 - 4\hat{c}_4}\right), \tag{10.39}$$

provided $\hat{c}_2 < 0$, i.e., (10.32) is satisfied. As discussed in Sect. 10.1.1, a Turing instability occurs when (10.31) has a degenerate or double root, i.e., if $\hat{c}_2^2 - 4\hat{c}_4 = 0$. The stable uniform steady state undergoes a Turing bifurcation for parameter values μ of the system such that

$$D_v J_{11} + D_u J_{22} = \sqrt{4 D_u D_v \Delta} \tag{10.40}$$

or equivalently at the critical ratio of diffusion coefficients

$$\theta_{RD,c} = \left[\frac{1}{J_{11}}\left(\sqrt{\Delta} + \sqrt{-J_{12} J_{21}}\right)\right]^2. \tag{10.41}$$

The critical wavenumber is given by

$$k_{T,RD}^2 = -\frac{\hat{c}_2}{2} = \sqrt{\frac{\Delta}{D_u D_v}}. \tag{10.42}$$

In conclusion, the uniform steady state of (10.19), $(\overline{\rho}_u(x), \overline{\rho}_v(x)) = (\overline{\rho}_u, \overline{\rho}_v)$, satisfying the stability conditions (10.23), will be driven unstable by diffusion if and only if

$$\hat{c}_2 < 0, \quad \text{i.e.,} \quad D_v J_{11} + D_u J_{22} > 0, \tag{10.43a}$$

$$\hat{c}_2^2 - 4\hat{c}_4 > 0, \quad \text{i.e.,} \quad [D_v J_{11} + D_u J_{22}]^2 > 4 D_u D_v \Delta, \tag{10.43b}$$

and the band of unstable modes is given by

$$\frac{1}{2}\left(-\hat{c}_2 - \sqrt{\hat{c}_2^2 - 4\hat{c}_4}\right) < k^2 < \frac{1}{2}\left(-\hat{c}_2 + \sqrt{\hat{c}_2^2 - 4\hat{c}_4}\right). \tag{10.44}$$

10.1.3 Turing Instability in the Standard Brusselator Reaction–Diffusion System

We use the Brusselator, see Sect. 1.4.4, to illustrate these results. The steady state of the well-mixed system is stable if $b < b_H = 1 + a^2$, see (1.83). Condition (10.35) implies that

$$\theta_{RD} > \frac{a^2}{b-1} > 1. \tag{10.45}$$

The second inequality is satisfied if the uniform steady state $(\overline{\rho}_u(x), \overline{\rho}_v(x)) = (a, b/a)$ is stable against uniform perturbation, that is $b < b_H$. The Turing condition (10.40) reads

$$D_v(b-1) + D_u(-a^2) = \sqrt{4D_u D_v a^2}, \tag{10.46}$$

and the critical ratio of diffusion coefficients is given by

$$\theta_{RD,c} = \frac{a^2}{(b-1)^2} \left(1 + \sqrt{b}\right)^2. \tag{10.47}$$

If we consider b to be the control parameter, then the threshold for the Turing instability is given by

$$b_{T,RD} = \left(1 + a\sqrt{\frac{D_u}{D_v}}\right)^2 = \left(1 + a\theta_{RD}^{-1/2}\right)^2. \tag{10.48}$$

From (10.42) we find the critical wavenumber to be

$$k_{T,RD}^2 = \frac{a}{\sqrt{D_u D_v}}. \tag{10.49}$$

In order for the Turing bifurcation to occur first, the Turing threshold must lie below the Hopf threshold of the well-mixed system, $b_T < b_H$:

$$\left(1 + \frac{1}{\sqrt{\theta_{RD}}} a\right)^2 < 1 + a^2 \tag{10.50}$$

or

$$a > \frac{2\sqrt{\theta_{RD}}}{\theta_{RD} - 1}. \tag{10.51}$$

Note that the Brusselator does not have a Takens–Bogdanov point. Theorems 10.2 and 10.3 are not applicable in this case, and the Brusselator displays somewhat pathological behavior as θ_{RD} decreases toward unity. Equation (10.51) implies that a becomes arbitrarily large as $\theta_{RD} \to 1$. Infinite a corresponds to an infinite Hopf frequency ω_H and an infinite wavenumber of the Turing instability k_T.

10.2   Turing Instabilities in Reaction–Transport Systems with Inertia: HRDEs and Reaction-Cattaneo Systems

As discussed in Sect. 2.2 the diffusion equation has the well-known unrealistic feature that localized disturbances spread infinitely fast, though with heavy attenuation, through the system. In that section we described three approaches to address the unphysical behavior of the diffusion equation and reaction–diffusion equation. Since the Turing instability is a diffusion-driven instability, it is of particular interest to explore how this bifurcation depends on the characteristics of the transport process. In this section, we address the effects of inertia in the dispersal of particles or individuals on the Turing instability. Does the finite speed of propagation of perturbations in such systems affect Turing instabilities? We determine the stability properties of the uniform steady state for the three approaches presented in Sect. 2.2.

10.2.1   Turing Instabilities in Hyperbolic Reaction–Diffusion Equations

We first use hyperbolic reaction–diffusion equations, see Sect. 2.2.1, to study the effect of inertia on Turing instabilities [206]. Specifically, we consider two-variable HRDEs,

$$\tau_u \frac{\partial^2 \rho_u}{\partial t^2} + \frac{\partial \rho_u}{\partial t} = D_u \frac{\partial^2 \rho_u}{\partial x^2} + F_1(\rho_u, \rho_v), \qquad (10.52a)$$

$$\tau_v \frac{\partial^2 \rho_v}{\partial t^2} + \frac{\partial \rho_v}{\partial t} = D_v \frac{\partial^2 \rho_v}{\partial x^2} + F_2(\rho_u, \rho_v), \qquad (10.52b)$$

with no-flow boundary conditions on the interval $[0, L]$:

$$\frac{\partial \rho_u}{\partial x}(0, t) = \frac{\partial \rho_u}{\partial x}(L, t) = 0, \qquad (10.53a)$$

$$\frac{\partial \rho_v}{\partial x}(0, t) = \frac{\partial \rho_v}{\partial x}(L, t) = 0. \qquad (10.53b)$$

Let $(\overline{\rho}_u(x), \overline{\rho}_v(x)) = (\overline{\rho}_u, \overline{\rho}_v)$ be a uniform steady state (USS) of (10.52), where $(\overline{\rho}_u, \overline{\rho}_v)$ is again a stable steady state of the well-mixed system (10.21), i.e., the stability conditions (10.23) are satisfied. To determine the stability of the USS, we consider as usual the evolution of small, spatially nonuniform perturbations,

$$\rho_u(x, t) = \overline{\rho}_u + u_0 \cos(kx) \exp(\lambda_k t), \tag{10.54a}$$

$$\rho_v(x, t) = \overline{\rho}_v + v_0 \cos(kx) \exp(\lambda_k t), \tag{10.54b}$$

and determine their "growth" rate by linearizing (10.52) about the uniform steady state. This procedure leads to the following characteristic equation for λ_k:

$$\det \begin{pmatrix} \dfrac{J_{11}}{\tau_u} - \lambda_k^2 - \dfrac{\lambda_k}{\tau_u} - \dfrac{k^2}{\tau_u} D_u & \dfrac{J_{12}}{\tau_u} \\[2ex] \dfrac{J_{21}}{\tau_v} & \dfrac{J_{22}}{\tau_v} - \lambda_k^2 - \dfrac{\lambda_k}{\tau_v} - \dfrac{k^2}{\tau_v} D_v \end{pmatrix} = 0, \tag{10.55}$$

which, as for all two-variable hyperbolic descriptions considered in this section, is a fourth-order polynomial in λ_k:

$$\lambda_k^4 + c_1 \lambda_k^3 + c_2 \lambda_k^2 + c_3 \lambda_k + c_4 = 0. \tag{10.56}$$

The uniform steady state is stable if all roots have a negative real part for all k. The necessary and sufficient conditions for this to hold are the Routh–Hurwitz conditions, see Theorem 1.2. The Turing bifurcation corresponds to a real root λ_k crossing the imaginary axis for some nonzero k_T, i.e., $\lambda_{k_T} = 0$. This occurs if condition (1.35) is violated, i.e., $c_4 = 0$ for some $k_T \neq 0$. A bifurcation to oscillatory patterns, i.e., a spatial Hopf bifurcation, corresponds to a pair of complex conjugate roots $\lambda_k^{\pm} = \overline{\lambda}_k \pm i\omega_k$ crossing the imaginary axis for some nonzero k_H, i.e., $\overline{\lambda}_{k_H} = 0$. According to (1.38), a Hopf bifurcation occurs if the Hurwitz determinant Δ_3 vanishes, $\Delta_3 = 0$.

The Turing condition $c_4 = 0$ for hyperbolic reaction–diffusion equations leads to exactly the same conditions as for the standard reaction–diffusion equation, namely (10.42) and (10.40). In other words, the Turing condition is independent of τ_u and τ_v. If inertia in the transport is modeled by HRDEs, then the inertia has no effect whatsoever on the Turing instability to stationary patterns.

In contrast to standard two-species reaction–diffusion systems, the uniform steady state of the hyperbolic reaction–diffusion system can undergo a spatial Hopf bifurcation to oscillatory spatial pattern, if $\Delta_3 = 0$ can be fulfilled for some $k_H \neq 0$. This condition gives rise to a second-order polynomial in k^2:

$$a_0 k^4 + a_1 k^2 + a_2 = 0. \tag{10.57}$$

The coefficients a_i are complicated expressions of the parameters of the system, and an exact evaluation of the Hopf condition is a very involved and tedious task. However, for the physically relevant regime of small inertia, i.e., τ_u and τ_v small, all the coefficients a_i are positive if (10.23) is satisfied, and consequently (10.57) has no physically acceptable solution. The spatial Hopf bifurcation to oscillatory patterns cannot occur in hyperbolic reaction–diffusion systems with small inertia.

10.2.2 Turing Instabilities in Reaction-Cattaneo Systems

As a second approach, we use reaction-Cattaneo equations, see Sect. 2.2.2, to study the effect of inertia on Turing instabilities [206]. The uniform steady state of the two-species reaction-Cattaneo system,

$$\frac{\partial \rho_u}{\partial t} = -\frac{\partial J_u}{\partial x} + F_1(\rho_u, \rho_v), \quad \frac{\partial \rho_v}{\partial t} = -\frac{\partial J_v}{\partial x} + F_2(\rho_u, \rho_v), \tag{10.58a}$$

$$\tau_u \frac{\partial J_u}{\partial t} + J_u = -D_u \frac{\partial \rho_u}{\partial x}, \quad \tau_v \frac{\partial J_v}{\partial t} + J_v = -D_v \frac{\partial \rho_v}{\partial x}, \tag{10.58b}$$

with zero-flow boundary conditions

$$J_u(0, t) = J_u(L, t) = 0, \quad J_v(0, t) = J_v(L, t) = 0, \tag{10.59}$$

is given by

$$(\overline{\rho}_u, \overline{\rho}_v) = (\overline{\rho}_u, \overline{\rho}_v), \quad (\overline{J}_u(x), \overline{J}_v(x)) = (0, 0). \tag{10.60}$$

We assume again that $(\overline{\rho}_u, \overline{\rho}_v)$ satisfies the stability conditions (10.23). To determine the stability of (10.60) against spatially inhomogeneous perturbations, we set

$$\rho_u(x, t) = \overline{\rho}_u + \delta\rho_u(x)\exp(\lambda t), \quad \rho_v(x, t) = \overline{\rho}_v + \delta\rho_v(x)\exp(\lambda t), \tag{10.61a}$$

$$J_u(x, t) = \delta J_u(x)\exp(\lambda t), \quad J_v(x, t) = \delta J_v(x)\exp(\lambda t). \tag{10.61b}$$

Linearizing (10.58a) and (10.58b) about the uniform steady state, we obtain

$$\lambda\delta\rho_u(x) = -\delta J_u'(x) + J_{11}\delta\rho_u(x) + J_{12}\delta\rho_v(x), \tag{10.62a}$$

$$\lambda\delta\rho_v(x) = -\delta J_v'(x) + J_{21}\delta\rho_u(x) + J_{22}\delta\rho_v(x), \tag{10.62b}$$

$$\tau_u\lambda\delta J_u(x) + \delta J_u(x) = -D_u\delta\rho_u'(x), \tag{10.62c}$$

$$\tau_v\lambda\delta J_v(x) + \delta J_v(x) = -D_v\delta\rho_v'(x), \tag{10.62d}$$

where the prime denotes derivative with respect to x. We differentiate (10.62a) and (10.62b) with respect to x and use (10.62c) and (10.62d) to eliminate $\delta\rho_u'$ and $\delta\rho_v'$:

$$-\frac{\lambda(\tau_u\lambda+1)}{D_u}\delta J_u = -\delta J_u'' + J_{11}\left(-\frac{\tau_u\lambda+1}{D_u}\right)\delta J_u + J_{12}\left(-\frac{\tau_v\lambda+1}{D_v}\right)\delta J_v,$$
$$(10.63a)$$

$$-\frac{\lambda(\tau_v\lambda+1)}{D_v}\delta J_v = -\delta J_v'' + J_{21}\left(-\frac{\tau_u\lambda+1}{D_u}\right)\delta J_u + J_{22}\left(-\frac{\tau_v\lambda+1}{D_v}\right)\delta J_v.$$
$$(10.63b)$$

The appropriate spatial modes for the fluxes δJ_u and δJ_v are $\sin(kx)$, and we obtain the characteristic equation for the reaction-Cattaneo system, $\det \widehat{J} = 0$, where

$$\widehat{J}_{11} = \frac{\tau_u\lambda_k+1}{\tau_u}J_{11} - \left(\lambda_k^2 + \frac{\lambda_k}{\tau_u}\right) - \frac{D_u k^2}{\tau_u}, \qquad (10.64a)$$

$$\widehat{J}_{12} = \frac{D_u}{D_v}\frac{\tau_v\lambda_k+1}{\tau_u}J_{12}, \qquad (10.64b)$$

$$\widehat{J}_{21} = \frac{D_v}{D_u}\frac{\tau_u\lambda_k+1}{\tau_v}J_{21}, \qquad (10.64c)$$

$$\widehat{J}_{22} = \frac{\tau_v\lambda_k+1}{\tau_v}J_{22} - \left(\lambda_k^2 + \frac{\lambda_k}{\tau_v}\right) - \frac{D_v k^2}{\tau_v}. \qquad (10.64d)$$

The characteristic equation is again a fourth-order polynomial:

$$\lambda_k^4 + c_1\lambda_k^3 + c_2\lambda_k^2 + c_3\lambda_k + c_4 = 0. \qquad (10.65)$$

As for HRDEs, the Turing condition $c_4 = 0$ for the reaction-Cattaneo system leads to exactly the same conditions as for the standard reaction–diffusion equation, namely (10.42) and (10.40); the Turing condition is independent of τ_u and τ_v for reaction-Cattaneo equations. As for HRDEs, the spatial Hopf bifurcation cannot occur in the regime of small inertia, if (10.23) is satisfied.

10.3 Turing Instabilities in Reaction–Transport Systems with Inertia: Persistent Random Walks with Reactions

As a third approach, we use persistent random walks with reactions, see Sect. 2.2.3, to study the effect of inertia on Turing instabilities [205, 206]. This is our preferred approach to describe reaction–transport systems with inertia, since it has a solid mesoscopic foundation. We consider Turing instabilities for two classes of reaction random walks, DIRWs and DDRWs, see Sect. 5.6.

10.3.1 Turing Instabilities in Direction-Independent Reaction Walks

We consider two-species DIRWs:

$$\frac{\partial \rho_{+,u}}{\partial t} + \gamma_u \frac{\partial \rho_{+,u}}{\partial x} = \mu_u \left(\rho_{-,u} - \rho_{+,u} \right) + \frac{1}{2} g_1(\rho_u, \rho_v) - f_1^-(\rho_u, \rho_v)\rho_{+,u},$$
$$(10.66a)$$

$$\frac{\partial \rho_{-,u}}{\partial t} - \gamma_u \frac{\partial \rho_{-,u}}{\partial x} = \mu_u \left(\rho_{+,u} - \rho_{-,u} \right) + \frac{1}{2} g_1(\rho_u, \rho_v) - f_1^-(\rho_u, \rho_v)\rho_{-,u},$$
$$(10.66b)$$

$$\frac{\partial \rho_{+,v}}{\partial t} + \gamma_v \frac{\partial \rho_{+,v}}{\partial x} = \mu_v \left(\rho_{-,v} - \rho_{+,v} \right) + \frac{1}{2} g_2(\rho_u, \rho_v) - f_2^-(\rho_u, \rho_v)\rho_{+,v},$$
$$(10.66c)$$

$$\frac{\partial \rho_{-,v}}{\partial t} - \gamma_v \frac{\partial \rho_{-,v}}{\partial x} = \mu_v \left(\rho_{+,v} - \rho_{-,v} \right) + \frac{1}{2} g_2(\rho_u, \rho_v) - f_2^-(\rho_u, \rho_v)\rho_{-,v},$$
$$(10.66d)$$

with impermeable (no-flow) boundaries, i.e., reflective boundary conditions, on $[0, L]$:

$$\rho_{+,u}(0, t) = \rho_{-,u}(0, t), \qquad \rho_{+,v}(0, t) = \rho_{-,v}(0, t), \qquad (10.67a)$$
$$\rho_{+,u}(L, t) = \rho_{-,u}(L, t), \qquad \rho_{+,v}(L, t) = \rho_{-,v}(L, t). \qquad (10.67b)$$

Equations (10.66) lead to the following evolution equations for the total densities $\rho_u(x, t) = \rho_{+,u}(x, t) + \rho_{-,u}(x, t)$, $\rho_v(x, t) = \rho_{+,v}(x, t) + \rho_{-,v}(x, t)$, and flows $j_u(x, t) = \rho_{+,u}(x, t) - \rho_{-,u}(x, t)$, $j_v(x, t) = \rho_{+,v}(x, t) - \rho_{-,v}(x, t)$:

$$\frac{\partial \rho_u}{\partial t} + \gamma_u \frac{\partial j_u}{\partial x} = g_1(\rho_u, \rho_v) - f_1^-(\rho_u, \rho_v)\rho_u, \qquad (10.68a)$$

$$\frac{\partial \rho_v}{\partial t} + \gamma_v \frac{\partial j_v}{\partial x} = g_2(\rho_u, \rho_v) - f_2^-(\rho_u, \rho_v)\rho_v, \qquad (10.68b)$$

$$\frac{\partial j_u}{\partial t} + \gamma_u \frac{\partial \rho_u}{\partial x} = -\left[2\mu_u + f_1^-(\rho_u, \rho_v) \right] j_u, \qquad (10.68c)$$

$$\frac{\partial j_v}{\partial t} + \gamma_v \frac{\partial \rho_v}{\partial x} = -\left[2\mu_v + f_2^-(\rho_u, \rho_v) \right] j_v. \qquad (10.68d)$$

Remark 10.2 These equations do not constitute a reaction-Cattaneo system because of the contribution of the intrinsic death rates $f_i^-(\rho_u, \rho_v)$, $i = 1, 2$, to the decay rate of the flows. Further, no reaction-telegraph equations can be derived for the total densities, unless the death rates $f_i^-(\rho_u, \rho_v)$ are constants.

The boundary conditions (10.67) become

$$j_u(0, t) = j_u(L, t) = 0, \tag{10.69a}$$

$$j_v(0, t) = j_v(L, t) = 0. \tag{10.69b}$$

The uniform steady state of (10.68) with boundary conditions (10.69) is given by

$$(\overline{\rho}_u(x), \overline{\rho}_v(x)) = (\overline{\rho}_u, \overline{\rho}_v), \quad (\overline{j}_u(x), \overline{j}_v(x)) = (0, 0), \tag{10.70}$$

and we assume that $(\overline{\rho}_u, \overline{\rho}_v)$ satisfies the stability conditions (10.23). To determine the stability of this state with respect to spatially nonuniform perturbations, we proceed similarly as for the reaction-Cattaneo case:

$$\rho_u(x, t) = \overline{\rho}_u + \delta\rho_u(x, t), \qquad \rho_v(x, t) = \overline{\rho}_v + \delta\rho_v(x, t), \tag{10.71a}$$

$$j_u(x, t) = \delta j_u(x, t), \qquad j_v(x, t) = \delta j_v(x, t). \tag{10.71b}$$

The linearized evolution equations for the DIRW are

$$\delta\dot{\rho}_u(x, t) + \gamma_u \delta j'_u(x, t) = J_{11}\delta\rho_u(x, t) + J_{12}\delta\rho_v(x, t), \tag{10.72a}$$

$$\delta\dot{\rho}_v(x, t) + \gamma_v \delta j'_v(x, t) = J_{21}\delta\rho_u(x, t) + J_{22}\delta\rho_v(x, t), \tag{10.72b}$$

$$\dot{j}_u(x, t) + \gamma_u \delta\rho'_u(x, t) = -[2\mu_u + f_1^-(\overline{\rho}_u, \overline{\rho}_v)]\delta j_u(x, t), \tag{10.72c}$$

$$\dot{j}_v(x, t) + \gamma_v \delta\rho'_v(x, t) = -[2\mu_v + f_2^-(\overline{\rho}_u, \overline{\rho}_v)]\delta j_v(x, t), \tag{10.72d}$$

where as usual the dot and the prime denote differentiation with respect to t and x, respectively. To shorten the notation, we set in the following

$$\mu = 2\mu_u + f_1^-(\overline{\rho}_u, \overline{\rho}_v), \ \nu = 2\mu_v + f_2^-(\overline{\rho}_u, \overline{\rho}_v), \ \gamma = \gamma_u, \ \chi = \gamma_v. \tag{10.73}$$

The boundary conditions (10.69) imply that the spatial modes for the flows are given by $\sin(kx)$ with $k = m\pi/L$, $m = 0, 1, 2, \ldots$. To obtain the appropriate spatial modes for the densities, we evaluate (10.68c) and (10.68d) at the boundaries $x = 0$ and $x = L$ and find

$$\frac{\partial\rho_u}{\partial x}(0, t) = \frac{\partial\rho_u}{\partial x}(L, t) = 0, \tag{10.74a}$$

$$\frac{\partial\rho_v}{\partial x}(0, t) = \frac{\partial\rho_v}{\partial x}(L, t) = 0. \tag{10.74b}$$

This implies that the spatial modes for the densities are given by $\cos(kx)$. We write the perturbations as

$$\delta\rho_u(x, t) = u_0 \cos(kx) \exp(\lambda_k t), \tag{10.75a}$$

$$\delta\rho_v(x, t) = v_0 \cos(kx) \exp(\lambda_k t), \tag{10.75b}$$

$$\delta j_u(x, t) = w_0 \sin(kx) \exp(\lambda_k t), \tag{10.75c}$$

$$\delta j_v(x, t) = z_0 \sin(kx) \exp(\lambda_k t), \tag{10.75d}$$

and the linearized equations (10.72) read

$$\lambda_k \delta \rho_u + \gamma \delta j_u' = J_{11} \delta \rho_u + J_{12} \delta \rho_v, \tag{10.76a}$$

$$\lambda_k \delta \rho_v + \chi \delta j_v' = J_{21} \delta \rho_u + J_{12} \delta \rho_v, \tag{10.76b}$$

$$\lambda_k \delta j_u + \gamma \delta \rho_u' = -\mu \delta j_u, \tag{10.76c}$$

$$\lambda_k \delta j_v + \chi \delta \rho_v' = -\nu \delta j_v. \tag{10.76d}$$

From (10.76c) and (10.76d) we obtain

$$\delta \rho_u' = -\frac{\lambda_k + \mu}{\gamma} \delta j_u, \tag{10.77a}$$

$$\delta \rho_v' = -\frac{\lambda_k + \nu}{\chi} \delta j_v. \tag{10.77b}$$

We differentiate (10.76a) and (10.76b) with respect to x and use (10.77) to eliminate $\delta \rho_u$ and $\delta \rho_v$ from the linearized evolution equations:

$$-\frac{\lambda_k + \mu}{\gamma} \lambda_k \delta j_u + \gamma \delta j_u'' = J_{11} \left(-\frac{\lambda_k + \mu}{\gamma} \right) \delta j_u + J_{12} \left(-\frac{\lambda_k + \nu}{\chi} \right) \delta j_v, \tag{10.78a}$$

$$-\frac{\lambda_k + \nu}{\chi} \lambda_k \delta j_v + \chi \delta j_v'' = J_{21} \left(-\frac{\lambda_k + \mu}{\gamma} \right) \delta j_u + J_{22} \left(-\frac{\lambda_k + \nu}{\chi} \right) \delta j_v. \tag{10.78b}$$

Since $\delta j_u'' = -k^2 \delta j_u$ and $\delta j_v'' = -k^2 \delta j_v$, these equations can be written after some simple algebra as

$$\begin{pmatrix} \chi \left[(\lambda_k + \mu)(J_{11} - \lambda_k) - k^2 \gamma^2 \right] & \gamma J_{12}(\lambda_k + \nu) \\ \chi J_{21}(\lambda_k + \mu) & \gamma \left[(\lambda_k + \nu)(J_{22} - \lambda_k) - k^2 \chi^2 \right] \end{pmatrix} \begin{pmatrix} \delta j_u \\ \delta j_v \end{pmatrix} = 0. \tag{10.79}$$

The characteristic equation is the determinant of the matrix in (10.79), and it is given by

$$\lambda_k^4 + c_1 \lambda_k^3 + c_2 \lambda_k^2 + c_3 \lambda_k + c_4 = 0, \tag{10.80}$$

with

$$c_1 = \mu + \nu - T, \tag{10.81}$$

$$c_2 = \Delta - T(\mu + \nu) + \mu\nu + (\chi^2 + \gamma^2)k^2, \tag{10.82}$$

$$c_3 = \Delta(\mu + \nu) - T\mu\nu - [\chi^2(J_{11} - \mu) + \gamma^2(J_{22} - \nu)]k^2, \tag{10.83}$$

$$c_4 = \Delta\mu\nu - [\mu\chi^2 J_{11} + \nu\gamma^2 J_{22}]k^2 + \gamma^2\chi^2 k^4. \tag{10.84}$$

The necessary condition for a Turing bifurcation, $c_4 = 0$, leads to

$$K^2 - \left(\frac{J_{11}}{\mathscr{D}_u} + \frac{J_{22}}{\mathscr{D}_v}\right) K + \frac{\Delta}{\mathscr{D}_u \mathscr{D}_v} = 0, \tag{10.85}$$

where we have set again $K = k^2$ and defined

$$\mathscr{D}_u = \frac{\gamma^2}{\mu}, \quad \mathscr{D}_v = \frac{\chi^2}{\nu}. \tag{10.86}$$

The Turing condition for two-variable DIRWs, (10.85), has the same form as the Turing condition for two-variable reaction–diffusion systems, (10.31). Consequently, the uniform steady state (10.70) of a DIRW undergoes a Turing bifurcation with critical wavenumber

$$k_{T,DIRW}^2 = \sqrt{\frac{\Delta}{\mathscr{D}_u \mathscr{D}_u}}, \tag{10.87}$$

for parameter values of the system such that

$$\mathscr{D}_v J_{11} + \mathscr{D}_u J_{22} = \sqrt{4\mathscr{D}_v \mathscr{D}_u \Delta}, \tag{10.88}$$

or equivalently at

$$\tilde{\theta}_{DIRW,c} = \left(\frac{\mathscr{D}_v}{\mathscr{D}_u}\right)_c = \left[\frac{1}{J_{11}}\left(\sqrt{\Delta} + \sqrt{-J_{12} J_{21}}\right)\right]^2. \tag{10.89}$$

Though (10.87), (10.88), and (10.89) have the same form as the corresponding expressions for reaction–diffusion systems, (10.42), (10.40) and (10.41), they are not identical. The $\mathscr{D}_i$ are "renormalized" and differ from the actual diffusion coefficients D_i:

$$\mathscr{D}_i = \frac{\gamma_i^2}{2\mu_i + f_i^-(\bar{\rho}_u, \bar{\rho}_v)} = D_i\left[1 + \frac{f_i^-(\bar{\rho}_u, \bar{\rho}_v)}{2\mu_i}\right]^{-1} = D_i\left[1 + \frac{f_i^-(\bar{\rho}_u, \bar{\rho}_v)}{\nu_i}\tau\right]^{-1}. \tag{10.90}$$

Here $D_i = \gamma_i^2/(2\mu_i)$, see (2.33), and we have set $2\mu_i = \nu_i/\tau$, where τ is the characteristic time of the transport process. One way to define this characteristic time is to choose the geometric mean of the correlation times of the particle turning processes, $\tau = \sqrt{\tau_u \tau_v}$, where $\tau_i = 1/(2\mu_i)$, see (2.32), and then $\nu_u = \sqrt{\mu_u/\mu_v}$ and

$v_v = v_u^{-1}$. Comparing expressions for the DIRW case and the reaction–diffusion case, we find

$$\theta_{\text{DIRW},c} = \left(\frac{D_v}{D_u}\right)_c = \frac{\mu_u}{\mu_v} \frac{2\mu_v + f_2^-(\bar{\rho}_u, \bar{\rho}_v)}{2\mu_u + f_1^-(\bar{\rho}_u, \bar{\rho}_v)} \theta_{\text{RD},c} \qquad (10.91)$$

$$= \frac{v_u}{v_v} \frac{v_v + \tau f_2^-(\bar{\rho}_u, \bar{\rho}_v)}{v_u + \tau f_1^-(\bar{\rho}_u, \bar{\rho}_v)} \theta_{\text{RD},c}, \qquad (10.92)$$

$$k_{\text{T,DIRW}}^2 = \sqrt{\frac{\Delta}{D_u D_v}} \sqrt{\frac{[2\mu_u + f_1^-(\bar{\rho}_u, \bar{\rho}_v)][2\mu_v + f_2^-(\bar{\rho}_u, \bar{\rho}_v)]}{4\mu_u \mu_v}} \qquad (10.93)$$

$$= k_{\text{T,RD}}^2 \sqrt{\frac{[2\mu_u + f_1^-(\bar{\rho}_u, \bar{\rho}_v)][2\mu_v + f_2^-(\bar{\rho}_u, \bar{\rho}_v)]}{4\mu_u \mu_v}} \qquad (10.94)$$

$$= k_{\text{T,RD}}^2 \sqrt{\frac{[v_u + \tau f_1^-(\bar{\rho}_u, \bar{\rho}_v)][v_v + \tau f_2^-(\bar{\rho}_u, \bar{\rho}_v)]}{v_u v_v}}. \qquad (10.95)$$

We draw several conclusions from these equations: (i) The Turing condition for persistent random walks with direction-independent kinetics depends on the parameters of the persistent random walk not only through the combination $D_i = \gamma_i^2/(2\mu_i)$ but also explicitly on the turning rates μ_i. (ii) The Turing bifurcation will be advanced or delayed compared to the reaction–diffusion case, depending if μ_u/μ_v is smaller or larger than $f_1^-(\bar{\rho}_u, \bar{\rho}_v)/f_2^-(\bar{\rho}_u, \bar{\rho}_v)$. (iii) The critical wavenumber is always shifted to larger values, or the intrinsic length of the Turing pattern to smaller values, compared with the reaction–diffusion system.

As for the reaction–diffusion case, Sect. 10.1.2, we use again the Brusselator to illustrate our results. For the Brusselator the loss rates of the activator and the inhibitor are

$$f_1^-(\rho_u, \rho_v) = b + 1, \quad f_2^-(\rho_u, \rho_v) = \rho_u^2. \qquad (10.96)$$

The uniform steady state of the Brusselator DIRW is $(\bar{\rho}_u, \bar{\rho}_v, \bar{j}_u, \bar{j}_v) = (a, b/a, 0, 0)$. The Turing condition (10.85) for the Brusselator DIRW reads

$$K^2 - \left[\frac{b-1}{\mathscr{D}_x} + \frac{-a^2}{\mathscr{D}_y}\right] K + \frac{a^2}{\mathscr{D}_x \mathscr{D}_y} = 0. \qquad (10.97)$$

The critical ratio of diffusion coefficients is given by

$$\theta_{\text{DIRW},c} = \left(\frac{D_v}{D_u}\right)_c = \frac{\mu_u}{\mu_v} \frac{2\mu_v + a^2}{2\mu_u + b + 1} \frac{a^2}{(b-1)^2} \left(1 + \sqrt{b}\right)^2 \qquad (10.98)$$

$$= \left(\frac{D_v}{D_u}\right)_c = \frac{\mu_u}{\mu_v}\frac{2\mu_v + a^2}{2\mu_u + b + 1}\theta_{RD,c} \tag{10.99}$$

and the critical wavenumber is given by

$$k^2_{T,DIRW} = \frac{a}{\sqrt{D_u D_v}}\sqrt{\frac{(2\mu_u + b + 1)(2\mu_v + a^2)}{4\mu_u \mu_v}} \tag{10.100}$$

$$= k^2_{T,RD}\sqrt{\frac{(2\mu_u + b + 1)(2\mu_v + a^2)}{4\mu_u \mu_v}}. \tag{10.101}$$

If we again consider b to be the control parameter, the explicit expression for the Turing threshold $b_{T,DIRW}$ can be obtained using computer algebra software such as MATHEMATICA. The result is many lines long and not enlightening at all. We therefore consider the Brusselator DIRW in the diffusive regime, τ small, to illustrate the effect of inertia in the transport process on the Turing threshold in terms of b. We write $b_{T,DIRW} = b_{0,DIRW} + b_{1,DIRW}\tau + \cdots$ and find

$$b_{0,DIRW} = b_{T,RD} = \left(1 + a\sqrt{\frac{D_u}{D_v}}\right)^2 \quad \text{[see (10.48)]}, \tag{10.102}$$

$$b_{1,DIRW} =$$
$$-\frac{a\sqrt{D_u}\left(a\sqrt{D_u} + \sqrt{D_v}\right)\left[2av_v\sqrt{D_u D_v} + 2v_v D_v + a^2\left(v_v D_u - v_u D_v\right)\right]}{v_u v_v D_v^2}. \tag{10.103}$$

The critical wavenumber in the diffusive regime is given by

$$k^2_{T,DIRW} =$$
$$\sqrt{\frac{a^2}{D_u D_v} + \frac{a^2\left[2av_v\sqrt{D_u D_v} + 2v_v D_v + a^2\left(v_u D_v + v_v D_u\right)\right]}{v_u v_v D_u D_v^2}\tau + \cdots}. \tag{10.104}$$

10.3.2 Spatial Hopf Instabilities in Direction-Independent Reaction Walks

Spatial Hopf bifurcations or wave bifurcations can never occur in two-variable reaction–diffusion systems, see Sect. 10.1.2. This is no longer the case for reaction–transport systems with inertia. As shown in Sects. 10.2.1 and 10.2.2, spatial Hopf bifurcations are in principle possible in two-variable hyperbolic reaction–diffusions

and two-variable reaction-Cattaneo systems. However, the general evaluation of the Hopf condition for those systems is an intractable task. It can be analyzed in the diffusive regime, i.e., small inertial effects, and no Hopf instability occurs. Persistent random walks offer an opportunity to analyze spatial Hopf or wave bifurcations in two-variable systems with inertia in a general way. According to (1.38), the uniform steady state (10.70) of the DIRW undergoes a spatial Hopf bifurcation if the Hurwitz determinant Δ_3 of the characteristic polynomial (10.80) vanishes for some $k_H \neq 0$:

$$\Delta_3 = c_3^2 - c_1 c_2 c_3 + c_4 c_1^2 = 0. \tag{10.105}$$

The Hopf frequency is given by

$$\omega_{H,DIRW} = \sqrt{\frac{c_3}{c_1}}. \tag{10.106}$$

Since T is negative according to the stability conditions (10.23), c_1 is always positive. The positivity of the Hurwitz determinant Δ_2 and c_4 at the Hopf bifurcation imply that $c_3 > 0$ there and that $\omega_{H,DIRW}$ is well defined [205]. Gathering terms of equal powers in k, we rewrite the Hopf condition as

$$a_0 k^4 + a_1 k^2 + a_2 = 0, \tag{10.107}$$

where, after some algebra,

$$a_0 = -\left(J_{11} - \mu\right)\left(J_{22} - \nu\right)\left(\chi^2 - \gamma^2\right)^2, \tag{10.108}$$

$$\begin{aligned} a_1 = {}&- 2\left(\Delta S - TM\right)B_1 - (S - T)\left(\Delta S - TM\right)\left(\chi^2 + \gamma^2\right) \\ &+ (S - T)B_1(\Delta - TS + M) - (S - T)^2 B_2, \end{aligned} \tag{10.109}$$

$$a_2 = TS\left[\Delta(\mu^2 + \nu^2) - TS(M + \Delta) + M^2 + \Delta^2 + T^2 M\right]. \tag{10.110}$$

Here

$$S = \mu + \nu, \quad M = \mu\nu, \tag{10.111}$$

$$B_1 = \chi^2(J_{11} - \mu) + \gamma^2(J_{22} - \nu), \tag{10.112}$$

and

$$B_2 = \mu\chi^2 J_{11} + \nu\gamma^2 J_{22}. \tag{10.113}$$

Since $\mu > 0$, $\nu > 0$, $\Delta > 0$, and $T < 0$, it follows that a_2 is always negative. Further, a_0 is negative if $\gamma \neq \chi$ and $\mu > J_{11}$. Lengthy calculations show that a_1 is negative if a_0 is negative [205]. Thus for $\mu > J_{11}$, (10.107) has no real roots, since

all coefficients are negative. In other words, a Hopf bifurcation can only occur if the characteristic time of the activator transport process is larger than the characteristic chemical time, $\tau_u = 1/(2\mu_u) > 1/J_{11} = \tau_{\text{chem}}$, i.e., the persistent random walk must be in the ballistic regime. If $\mu < J_{11}$ and $\gamma \neq \chi$, then a_0 is positive, and (10.107) has a positive root k_H. The existence of this Hopf bifurcation depends, however, on the kinetics. The Hopf condition reads

$$\mu < J_{11} \tag{10.114}$$

or

$$2\mu_u < J_{11} - f_1^-(\overline{\rho}_u, \overline{\rho}_v). \tag{10.115}$$

The uniform steady state of a DIRW can undergo a spatial Hopf or wave bifurcation only if the right-hand side of (10.115) is positive. In other words, the rate of activation must exceed the loss rate of the activator in the steady state. If a spatial Hopf instability occurs, then all spatial modes with wavenumbers bigger than k_H, the positive root of (10.107), are unstable.

Remark 10.3 The analysis of all three approaches to two-variable reaction–transport systems with inertia establishes that the Turing instability of reaction–diffusion systems is structurally stable. The threshold conditions are either the same, HRDEs and reaction-Cattaneo systems, or approach the reaction–diffusion Turing threshold smoothly as the inertia becomes smaller and smaller, $\tau \to 0$. Further, inertia effects induce no new spatial instabilities of the uniform steady state in the diffusive regime, τ small. A spatial Hopf bifurcation to standing wave patterns can only occur in the opposite regime, the ballistic regime.

We consider several model systems to explore if the spatial Hopf bifurcation does occur in DIRWs with commonly studied kinetics. We begin with the Brusselator. The spatial Hopf condition (10.114) reads

$$2\mu_u + b + 1 < b - 1 \tag{10.116}$$

or

$$\mu_u < -1, \tag{10.117}$$

which can never be satisfied, since the turning rate μ_u is of course always nonnegative.

For the Gierer–Meinhardt model, Sect. 1.4.6, the loss rates of the activator and inhibitor are

$$f_1^-(\rho_u, \rho_v) = 1, \quad f_2^-(\rho_u, \rho_v) = q, \tag{10.118}$$

and the spatial Hopf condition reads

$$2\mu_u + 1 < \frac{p-1}{p+1}, \tag{10.119}$$

$$\mu_u < -\frac{1}{p+1}, \tag{10.120}$$

which can never be true.

For the Schnakenberg model, Sect. 1.4.5, the loss rate of the activator is $f_1^- = 1$ and the right-hand side of the Hopf condition (10.115) is given by

$$J_{11} - f_1^- (\overline{\rho}_u, \overline{\rho}_v) = -\frac{2a}{a+b}. \tag{10.121}$$

For the Lengyel–Epstein model, Sect. 1.4.9, the loss rate of the activator is $\sigma f_1^- = 1 + 4\rho_v/(1 + \rho_u^2)$ and the right-hand side of the Hopf condition (10.115) is given by

$$J_{11} - f_1^- (\overline{\rho}_u, \overline{\rho}_v) = -\frac{2a^2 + 250}{\sigma(a^2 + 25)}. \tag{10.122}$$

For the Brusselator, the Gierer–Meinhardt model, the Schnakenberg model, and the Lengyel–Epstein model, the right-hand side of the Hopf condition (10.115) is always negative; the reaction kinetics suppresses the spatial Hopf instability in all these models. For the Oregonator, Sect. 1.4.8, the loss rate of the activator is $\epsilon f_1^- = \rho_u + h\rho_v/(\rho_u + q)$. The expression for $J_{11} - f_1^- (\overline{\rho}_u, \overline{\rho}_v)$ is lengthy and it is not obvious if it has a definite sign. Evaluating the expression numerically for a variety of chemically reasonable values for h and q, we find it to be negative in all cases. Again, the spatial Hopf bifurcation is suppressed in DIRWs with Oregonator kinetics.

For the Gray–Scott model, Sect. 1.4.7, the loss rate of the activator is $f_1^- = k_2 + q$ and the right-hand side of the Hopf condition (10.115) is given by

$$J_{11} - f_1^- (\overline{\rho}_u, \overline{\rho}_v) = 0. \tag{10.123}$$

Again the spatial Hopf bifurcation does not occur, but (10.123) shows that the Gray–Scott model represents a borderline case since $\mu_{u,H} = 0$. If this model is modified and the third-order autocatalysis replaced by a rather unrealistic fourth order, $F_1(\rho_u, \rho_v) = \rho_v \rho_u^3 - q\rho_u$, $F_2(\rho_u, \rho_v) = -\rho_v \rho_u^3 + q(1 - \rho_v)$, then for sufficiently small q the model has a nontrivial stable uniform steady state, for which $J_{11} - f_1^- (\overline{\rho}_u, \overline{\rho}_v) = q$. A spatial Hopf bifurcation occurs for $2\mu_u < q$. In conclusion, the existence of a spatial Hopf bifurcation for DIRWs in the ballistic regime is an interesting theoretical possibility, but studies of common models show that it is unlikely to occur for realistic kinetics.

10.3.3 Spatial Instabilities in One-Variable Systems

To shed further light on the occurrence of spatial Hopf bifurcations in DIRWs, it is instructive to study the stability properties of the uniform steady state in one-variable systems. Consider the one-variable reaction–diffusion system

$$\frac{\partial \rho}{\partial t} = D \frac{\partial^2 \rho}{\partial x^2} + F(\rho), \tag{10.124}$$

with no-flow boundary conditions on the interval $[0, L]$:

$$\frac{\partial \rho}{\partial x}(0, t) = \frac{\partial \rho}{\partial x}(L, t) = 0. \tag{10.125}$$

Let $\overline{\rho}$ be a stable steady state of the well-mixed system:

$$F(\overline{\rho}) = 0, \ \text{with} \ \frac{dF}{d\rho}(\overline{\rho}) \equiv \lambda_0 < 0. \tag{10.126}$$

The linearized evolution equation for small perturbations, $\rho(x, t) = \overline{\rho} + \delta\rho(x, t) = \overline{\rho} + \rho_0 \cos(kx) \exp(\lambda_k t)$, is

$$\lambda_k \delta\rho = -Dk^2 \delta\rho + \lambda_0 \delta\rho, \tag{10.127}$$

which yields the spectrum of "growth" rates, the dispersion relation,

$$\lambda_k = \lambda_0 - Dk^2. \tag{10.128}$$

For one-variable reaction–diffusion systems, diffusion is always stabilizing and no spatial instability of the uniform steady state can occur, explicitly confirming Corollary 10.1.

The evolution equations for the total density and flow of a one-variable DIRW are given by

$$\frac{\partial \rho}{\partial t} + \gamma \frac{\partial j}{\partial x} = g(\rho) - f^-(\rho)\rho = F(\rho), \tag{10.129a}$$

$$\frac{\partial j}{\partial t} + \gamma \frac{\partial \rho}{\partial x} = -[2\mu + f^-(\rho)]j. \tag{10.129b}$$

The uniform steady state is given by $(\overline{\rho}(x), \overline{j}(x)) = (\overline{\rho}, 0)$ and the linearized evolution equations are

$$\lambda_k \delta\rho(x, t) + \gamma \delta j'(x, t) = \lambda_0 \delta\rho(x, t), \tag{10.130a}$$

$$\lambda_k \delta j(x, t) + \gamma \delta\rho'(x, t) = -\tilde{\mu} \delta j(x, t), \tag{10.130b}$$

where

$$\tilde{\mu} = 2\mu + f^-(\overline{\rho}).$$ (10.131)

Eliminating $\delta\rho(x, t)$, we obtain

$$[(\lambda_k + \tilde{\mu})(\lambda_0 - \lambda_k) - \gamma^2 k^2]\delta j(x, t) = 0$$ (10.132)

or the characteristic equation

$$\lambda_k^2 + (\tilde{\mu} - \lambda_0)\lambda_k - \tilde{\mu}\lambda_0 + \gamma^2 k^2 = 0.$$ (10.133)

The spectrum of "growth" rates is given by

$$\lambda_{k,\pm} = \frac{1}{2}\left[\lambda_0 - \tilde{\mu} \pm \sqrt{(\lambda_0 + \tilde{\mu})^2 - 4\gamma^2 k^2}\right].$$ (10.134)

For

$$k < k_c = \frac{1}{2\gamma}\left|\lambda_0 + \tilde{\mu}\right|,$$ (10.135)

the "growth" rates are real and negative. At $k = k_c$, a double root occurs, $\lambda_{k_c} = \frac{1}{2}(\lambda_0 - \tilde{\mu})$, and for $k > k_c$, the "growth" rates become complex. The real part is equal to λ_{k_c} and negative. Perturbations with wavenumbers bigger than k_c exhibit damped oscillations. These perturbations decay with a rate that is the mean of the decay rate of the flow, $\tilde{\mu}$, and of the chemical decay rate $|\lambda_0|$. They oscillate with a frequency $\omega_k = \sqrt{\left|(\lambda_0 + \tilde{\mu})^2 - 4\gamma^2 k^2\right|}$. This behavior is qualitatively different from the reaction–diffusion system, where perturbations of all wavenumbers decay monotonically. As expected, k_c goes to infinity in the diffusive limit

$$k_c \to \frac{\mu}{\gamma} = \frac{\gamma}{2D} \to \infty,$$ (10.136)

as $\gamma \to \infty$, $\mu \to \infty$ with $D = \gamma^2/(2\mu)$. In the ballistic limit, $\mu \to 0$, the wavenumber k_c goes to

$$k_c = \frac{\left|\lambda_0 + f^-(\overline{\rho})\right|}{2\gamma}.$$ (10.137)

Note that if the decay rate of the flow, $\tilde{\mu} = 2\mu + f^-(\overline{\rho})$, coincides with chemical decay rate $|\lambda_0|$, i.e., $\tilde{\mu} = |\lambda_0|$, then $k_c = 0$, and perturbations with all wavenumbers

k exhibit damped oscillations. This phenomenon foreshadows the spatial Hopf condition for two-species DIRWs (10.114).

10.3.4 Turing Instabilities in Direction-Dependent Reaction Walks

The kinetic terms for DDRWs, see Sect. 5.6.2, depend on the details of the underlying mechanism of the reacting system, and it is impossible to write down a general form for them. We consider here the Brusselator model. In keeping with the spirit of the model, we consider two possible direction-dependent kinetic schemes, namely an activated U_2 complex or an activated UV complex, to investigate the effect of activation energy on the Turing instability [206].

10.3.4.1 Turing Instability in the Brusselator DDRW with Activated U Dimer

If the termolecular step in the Brusselator proceeds via an activated U_2 complex, we have the following kinetic scheme for the Brusselator DDRW:

$$A_\pm \xrightarrow{\kappa_1} U_\pm, \tag{10.138}$$

$$B_\pm + U_\mp \xrightarrow{\kappa_2} V_\mp + D_\pm, \tag{10.139}$$

$$U_+ + U_- + V_\pm \xrightarrow{\kappa_3} U_- + U_+ + U_\pm, \tag{10.140}$$

$$U_\pm \xrightarrow{\kappa_4} E_\pm. \tag{10.141}$$
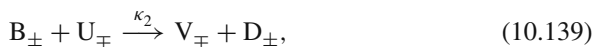
Here $\kappa_i = A_i = P_i Z_i$, and P_i is the steric factor and Z_i the collision frequency factor [350]. We consider only situations where the steric factor ensures that the kinetics are reaction-limited. We assume that the pool species A and B are in equilibrium, i.e., $\rho_{+,a} = \rho_{-,a} = \frac{1}{2}a$ and $\rho_{+,b} = \rho_{-,b} = \frac{1}{2}b$. Then the properly nondimensionalized evolution equations for the Brusselator DDRW with activated U dimer read

$$\frac{\partial \rho_{+,u}}{\partial t} + \gamma_u \frac{\partial \rho_{+,u}}{\partial x} = \mu_u \left(\rho_{-,u} - \rho_{+,u}\right) + \frac{1}{2}a - (b+1)\rho_{+,u} + 4\rho_{+,u}\rho_{-,u}\rho_{+,v},$$
$$\tag{10.142a}$$

$$\frac{\partial \rho_{-,u}}{\partial t} - \gamma_u \frac{\partial \rho_{-,u}}{\partial x} = \mu_u \left(\rho_{+,u} - \rho_{-,u}\right) + \frac{1}{2}a - (b+1)\rho_{-,u} + 4\rho_{+,u}\rho_{-,u}\rho_{-,v},$$
$$\tag{10.142b}$$

$$\frac{\partial \rho_{+,v}}{\partial t} + \gamma_v \frac{\partial \rho_{+,v}}{\partial x} = \mu_v \left(\rho_{-,v} - \rho_{+,v}\right) + b\rho_{+,u} - 4\rho_{+,u}\rho_{-,u}\rho_{+,v}, \tag{10.142c}$$

$$\frac{\partial \rho_{-,v}}{\partial t} - \gamma_v \frac{\partial \rho_{-,v}}{\partial x} = \mu_v \left(\rho_{+,v} - \rho_{-,v}\right) + b\rho_{-,u} - 4\rho_{+,u}\rho_{-,u}\rho_{-,v}. \tag{10.142d}$$

which lead to the following equations for the total densities and flows:

$$\frac{\partial \rho_u}{\partial t} + \gamma_u \frac{\partial j_u}{\partial x} = a - (b+1)\rho_u + (\rho_u^2 - j_v^2)\rho_v, \tag{10.143a}$$

$$\frac{\partial \rho_v}{\partial t} + \gamma_v \frac{\partial j_v}{\partial x} = b\rho_u - (\rho_u^2 - j_v^2)\rho_v, \tag{10.143b}$$

$$\frac{\partial j_u}{\partial t} + \gamma_u \frac{\partial \rho_u}{\partial x} = -2\mu_u j_u - (b+1)j_u + (\rho_u^2 - j_v^2)j_v, \tag{10.143c}$$

$$\frac{\partial j_v}{\partial t} + \gamma_v \frac{\partial \rho_v}{\partial x} = -2\mu_v j_v + bj_u - (\rho_u^2 - j_v^2)j_v. \tag{10.143d}$$

The uniform steady state of the Brusselator DDRW with activated U dimer with impermeable boundaries at $x = 0$ and $x = L$ is the same as for the Brusselator DIRW, namely $(\overline{\rho}_u, \overline{\rho}_v, \overline{j}_u, \overline{j}_v) = (a, b/a, 0, 0)$. A linear stability analysis leads to the characteristic equation $\det \widehat{J} = 0$, where

$$\widehat{J}_{11} = (\mu + \lambda_k)(b - 1 - \lambda_k) - (\gamma/\chi)a^2 b - k^2\gamma^2, \tag{10.144a}$$

$$\widehat{J}_{12} = -a^2(b - 1) + (\gamma/\chi)a^2(v + \lambda_k) + a^2\lambda_k, \tag{10.144b}$$

$$\widehat{J}_{21} = \lambda_k b - (\chi/\gamma)b(\mu + \lambda_k) + a^2 b, \tag{10.144c}$$

$$\widehat{J}_{22} = -(v + \lambda_k)(\lambda_k + a^2) + (\chi/\gamma)ba^2 - k^2\chi^2. \tag{10.144d}$$

Here μ, v, γ, and χ are defined by (10.73) and for the Brusselator are given by $\mu = 2\mu_u + b + 1$ and $v = 2\mu_v + a^2$.

The Turing condition, $c_4 = 0$, leads to ($K = k^2$)

$$K^2 - \left[\frac{b-1}{\mathscr{D}_u} + \frac{-a^2}{\mathscr{D}_v}\right]K + \frac{a^2}{\mathscr{D}_u\mathscr{D}_v} - \frac{a^4 b}{\mu v \mathscr{D}_u \mathscr{D}_v} = 0. \tag{10.145}$$

This equation is identical with the Turing condition for the Brusselator DIRW (10.97) except for the last term, which in the diffusive regime, small τ, is of order τ^2. The Turing threshold $b_{T,U2}$ for the Brusselator with activated U dimer coincides with the Turing threshold $b_{T,DIRW}$ for the Brusselator DIRW up to first order in τ; $b_{0,U2}$ and $b_{1,U2}$ are given by the same expressions as for $b_{0,DIRW}$ and $b_{1,DIRW}$, namely (10.102) and (10.103). In the Brusselator DDRW with activated U dimer, inertia and activation energy affect the locus of the Turing bifurcation at different orders. Inertia gives rise to a first-order effect, whereas the activation energy affects the Turing bifurcation only at a higher, namely second, order.

10.3.4.2   Turing Instability in the Brusselator DDRW with Activated UV Complex

To explore if the activation energy always affects the Turing bifurcation at a higher order than the inertia, we consider the kinetic scheme where the termolecular step in the Brusselator proceeds via an activated UV complex instead of an activated U dimer:

$$A_{\pm} \xrightarrow{\kappa_1} U_{\pm}, \tag{10.146}$$

$$B_{\pm} + U_{\mp} \xrightarrow{\kappa_2} V_{\mp} + D_{\pm}, \tag{10.147}$$

$$U_+ + V_- + U_{\pm} \xrightarrow{\kappa_3} U_- + U_+ + U_{\pm}, \tag{10.148}$$

$$U_- + V_+ + U_{\pm} \xrightarrow{\kappa_3} U_- + U_+ + U_{\pm}, \tag{10.149}$$

$$U_{\pm} \xrightarrow{\kappa_4} E_{\pm}. \tag{10.150}$$
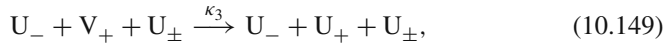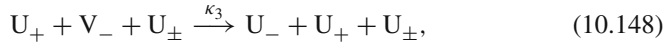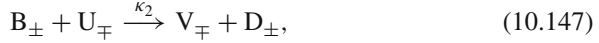
We assume again that the pool species A and B are in equilibrium. Then the properly nondimensionalized evolution equations for the Brusselator DDRW with activated UV complex read

$$\frac{\partial \rho_{+,u}}{\partial t} + \gamma_u \frac{\partial \rho_{+,u}}{\partial x} = \mu_u \left(\rho_{-,u} - \rho_{+,u} \right) + \frac{1}{2}a - (b+1)\rho_{+,u} + 2\rho_{-,u}\rho_{+,v}\rho_u, \tag{10.151a}$$

$$\frac{\partial \rho_{-,u}}{\partial t} - \gamma_u \frac{\partial \rho_{-,u}}{\partial x} = \mu_u \left(\rho_{+,u} - \rho_{-,u} \right) + \frac{1}{2}a - (b+1)\rho_{-,u} + 2\rho_{+,u}\rho_{-,v}\rho_u, \tag{10.151b}$$

$$\frac{\partial \rho_{+,v}}{\partial t} + \gamma_v \frac{\partial \rho_{+,v}}{\partial x} = \mu_v \left(\rho_{-,v} - \rho_{+,v} \right) + b\rho_{+,u} - 2\rho_{-,u}\rho_{+,v}\rho_u, \tag{10.151c}$$

$$\frac{\partial \rho_{-,v}}{\partial t} - \gamma_v \frac{\partial \rho_{-,v}}{\partial x} = \mu_v \left(\rho_{+,v} - \rho_{-,v} \right) + b\rho_{-,u} - 2\rho_{+,u}\rho_{-,v}\rho_u, \tag{10.151d}$$

which lead to the following equations for the total densities and flows:

$$\frac{\partial \rho_u}{\partial t} + \gamma_u \frac{\partial j_u}{\partial x} = a - (b+1)\rho_u + (\rho_u \rho_v - j_u j_v)\rho_u, \tag{10.152a}$$

$$\frac{\partial \rho_v}{\partial t} + \gamma_v \frac{\partial j_v}{\partial x} = b\rho_u - (\rho_u \rho_v - j_u j_v)\rho_u, \tag{10.152b}$$

$$\frac{\partial j_u}{\partial t} + \gamma_u \frac{\partial \rho_u}{\partial x} = -2\mu_u j_u - (b+1)j_u + (\rho_u j_v - \rho_v j_u)\rho_u, \tag{10.152c}$$

$$\frac{\partial j_v}{\partial t} + \gamma_v \frac{\partial \rho_v}{\partial x} = -2\mu_v j_v + b j_u - (\rho_u j_v - \rho_v j_u)\rho_u. \tag{10.152d}$$

The uniform steady state of the Brusselator DDRW with activated UV complex with impermeable boundaries at $x = 0$ and $x = L$ is again given by $(\bar{\rho}_u, \bar{\rho}_v, \bar{j}_u, \bar{j}_v) =$

$(a, b/a, 0, 0)$. A linear stability analysis leads to the characteristic equation $\det \widehat{J} = 0$, where

$$\widehat{J}_{11} = (\mu + b + \lambda_k)(b - 1 - \lambda_k) - (\gamma/\chi)2a^2b - k^2\gamma^2, \qquad (10.153a)$$

$$\widehat{J}_{12} = -a^2(b - 1) + (\gamma/\chi)a^2(v + \lambda_k) + a^2\lambda_k, \qquad (10.153b)$$

$$\widehat{J}_{21} = 2b\lambda_k - (\chi/\gamma)b(\mu + b + \lambda_k) + 2a^2b, \qquad (10.153c)$$

$$\widehat{J}_{22} = -(v + \lambda_k)(\lambda_k + a^2) + (\chi/\gamma)ba^2 - k^2\chi^2. \qquad (10.153d)$$

The Turing condition, $c_4 = 0$, leads to

$$K^2 - \left[\frac{b - 1}{\mathscr{D}_u} + \frac{-a^2}{\mathscr{D}_v} - \frac{b(1 - b)}{\mu\mathscr{D}_u} - \frac{a^2b}{\sqrt{\mu v \mathscr{D}_u \mathscr{D}_v}} \right] K$$
$$+ \frac{a^2}{\mathscr{D}_u \mathscr{D}_v} + \frac{a^2b}{\mu\mathscr{D}_u\mathscr{D}_v} - \frac{2a^2b}{\mu v \mathscr{D}_u\mathscr{D}_v} = 0. \qquad (10.154)$$

The coefficients of this equation differ from those of the corresponding equation for the Brusselator DIRW (10.97) by terms that are first order in τ, namely the terms with $1/\mu$ and $1/\sqrt{\mu v}$, and a term that is second order in τ, namely the term with $1/(\mu v)$. In the Brusselator DDRW with activated UV complex, inertia and activation energy both affect the threshold of the Turing bifurcation at first order, in contrast to the DDRW with activated U dimer. We find for the Turing threshold $b_{T,UV} = b_{0,UV} + b_{1,UV}\tau + \cdots$:

$$b_{0,UV} = \left(1 + a\sqrt{D_u/D_v}\right)^2, \qquad (10.155)$$

$$b_{1,UV} =$$
$$- \frac{a\sqrt{D_u}\left(a\sqrt{D_u} + \sqrt{D_v}\right)\left[4av_v\sqrt{D_uD_v} + 3v_vD_v + a^2(2v_vD_u - v_uD_v)\right]}{v_u v_v D_v^2}.$$
$$\qquad (10.156)$$

The critical wavenumber is given by

$$k_{T,UV}^2 = \sqrt{\frac{a^2}{D_uD_v} + \frac{a^2\left[4av_v\sqrt{D_uD_v} + 3v_vD_v + a^2(v_uD_v + 2v_vD_u)\right]}{v_u v_v D_u D_v^2}\tau + \cdots}.$$
$$\qquad (10.157)$$

10.4 Turing Instabilities in Reaction–Transport Systems with Anomalous Diffusion

As discussed in Sect. 2.3, the transport of particles or dispersal of individuals displays anomalous diffusive behavior in a variety of applications, and subdiffusion and superdiffusion are commonly modeled within a CTRW framework.

10.4.1 Turing Instabilities in Reaction–Subdiffusion Systems: Model B

In this section, we use Model B, see Sect. 3.4.2, to explore the effects of subdiffusion on the Turing instability. We consider the two-variable generalized reaction–diffusion equation [484],

$$
\frac{\partial \rho_u(x,t)}{\partial t} = F_1^+(\boldsymbol{\rho}(x,t)) - F_1^-(\boldsymbol{\rho}(x,t))
$$
$$
+ \frac{\sigma_u^2}{2} \nabla^2 \left[\int_0^t K_u(t-t') \rho_u(x,t') \exp\left[- \int_{t'}^t \frac{F_1^-(\boldsymbol{\rho}(x,t''))}{\rho_u(x,t'')} dt'' \right] dt' \right],
$$
$$(10.158a)$$

$$
\frac{\partial \rho_v(x,t)}{\partial t} = F_2^+(\boldsymbol{\rho}(x,t)) - F_2^-(\boldsymbol{\rho}(x,t))
$$
$$
+ \frac{\sigma_v^2}{2} \nabla^2 \left[\int_0^t K_v(t-t') \rho_v(x,t') \exp\left[- \int_{t'}^t \frac{F_2^-(\boldsymbol{\rho}(x,t''))}{\rho_v(x,t'')} dt'' \right] dt' \right],
$$
$$(10.158b)$$

for an infinite system. As pointed out in Remark 2.4, (10.158) is valid for arbitrary waiting time PDFs and has much wider applicability than subdiffusive transport. The uniform steady state of (10.158) is given by $(\overline{\rho}_u(x), \overline{\rho}_v(x)) = (\overline{\rho}_u, \overline{\rho}_v)$, and we assume, as in the preceding sections, that it satisfies the stability conditions (10.23). Linearizing (10.158) about the uniform steady state, we obtain the linearized evolution equations for $\delta\rho_u(x,t)$ and $\delta\rho_v(x,t)$:

$$
\frac{\partial \delta\rho_u(x,t)}{\partial t} = \frac{\sigma_u^2}{2} \nabla^2 \left\{ \overline{\rho}_u \int_0^t K_u(t-t') e^{-p_u(t-t')} \right.
$$
$$
\times \left[-A_{11} \int_{t'}^t \delta\rho_u(x,t'') dt'' - A_{12} \int_{t'}^t \delta\rho_v(x,t'') dt'' \right] dt' \right\}
$$
$$
+ \frac{\sigma_u^2}{2} \nabla^2 \int_0^t \delta\rho_u(x,t') K_u(t-t') e^{-p_u(t-t')} dt'
$$
$$
+ J_{11}(\overline{\rho}_u, \overline{\rho}_v) \delta\rho_u(x,t) + J_{12}(\overline{\rho}_u, \overline{\rho}_v) \delta\rho_v(x,t), \qquad (10.159a)
$$

$$\frac{\partial \delta\rho_v(x,t)}{\partial t} = \frac{\sigma_v^2}{2}\nabla^2\left\{\overline{\rho}_v\int_0^t K_v(t-t')e^{-p_v(t-t')}\right.$$

$$\times\left[-A_{21}\int_{t'}^t \delta\rho_u(x,t'')dt'' - A_{22}\int_{t'}^t \delta\rho_v(x,t'')dt''\right]dt'\right\}$$

$$+ \frac{\sigma_v^2}{2}\nabla^2\int_0^t \delta\rho_v(x,t')K_v(t-t')e^{-p_v(t-t')}dt'$$

$$+ J_{21}(\overline{\rho}_u,\overline{\rho}_v)\delta\rho_u(x,t) + J_{22}(\overline{\rho}_u,\overline{\rho}_v)\delta\rho_v(x,t). \qquad (10.159b)$$

Here $p_i = F_i^-(\overline{\rho}_u,\overline{\rho}_v)/\overline{\rho}_i$, and the matrix A is defined as

$$A_{ij} = \frac{\partial}{\partial\rho_j}\left[\frac{F_i^-(\rho)}{\rho_i}\right]_{(\overline{\rho}_u,\overline{\rho}_v)}. \qquad (10.160)$$

For the case of subdiffusive transport, the Laplace transforms of the waiting–time PDFs for the two species are given by $\hat{\phi}_u(s) \to 1 - (\tau_{0,u}s)^{\gamma_u}$ and $\hat{\phi}_v(s) \to 1 - (\tau_{0,v}s)^{\gamma_v}$. For rational values of γ_u and γ_v, we can Laplace and Fourier transform (10.159) and find [484]

$$s\widehat{\widetilde{\delta\rho}}_u(k,s) = \widehat{\widetilde{\delta\rho}}_u(k,t=0)$$

$$- \frac{\sigma_u^2 k^2\overline{\rho}_u[p_u\tau_{0,u}]^{1-\gamma_u}h_{\gamma_u}(s,p_u)}{2s\tau_{0,u}}\left[A_{11}\widehat{\widetilde{\delta\rho}}_u(k,s) + A_{12}\widehat{\widetilde{\delta\rho}}_v(k,s)\right]$$

$$- \frac{\sigma_u^2 k^2(s+p_u)^{1-\gamma_u}}{2\tau_{0,u}^{\gamma_u}}\widehat{\widetilde{\delta\rho}}_u(k,s)$$

$$+ J_{11}(\overline{\rho}_u,\overline{\rho}_v)\widehat{\widetilde{\delta\rho}}_u(k,s) + J_{12}(\overline{\rho}_u,\overline{\rho}_v)\widehat{\widetilde{\delta\rho}}_v(k,s), \qquad (10.161a)$$

$$s\widehat{\widetilde{\delta\rho}}_v(k,s) = \widehat{\widetilde{\delta\rho}}_v(k,t=0)$$

$$- \frac{\sigma_v^2 k^2\overline{\rho}_v[p_v\tau_{0,v}]^{1-\gamma_v}h_{\gamma_v}(s,p_v)}{2s\tau_{0,v}}\left[A_{21}\widehat{\widetilde{\delta\rho}}_u(k,s) + A_{22}\widehat{\widetilde{\delta\rho}}_v(k,s)\right]$$

$$- \frac{\sigma_v^2 k^2(s+p_u)^{1-\gamma_v}}{2\tau_{0,v}^{\gamma_v}}\widehat{\widetilde{\delta\rho}}_v(k,s)$$

$$+ J_{21}(\overline{\rho}_u,\overline{\rho}_v)\widehat{\widetilde{\delta\rho}}_u(k,s) + J_{22}(\overline{\rho}_u,\overline{\rho}_v)\widehat{\widetilde{\delta\rho}}_v(k,s), \qquad (10.161b)$$

where $h_{\gamma_i}(s,p_i) = 1 - p_i^{\gamma_i-1}(s+p_i)^{1-\gamma_i}$.

We determine the stability of the uniform steady state $(\overline{\rho}_u(x),\overline{\rho}_v(x)) = (\overline{\rho}_u,\overline{\rho}_v)$ of (10.158) and the conditions for the Turing instability by solving (10.161) for

$\widehat{\widetilde{\delta\rho}}_u(k, s)$ and $\widehat{\widetilde{\delta\rho}}_v(k, s)$, followed by taking an inverse Laplace transform. For simplicity, we assume that the species V undergoes normal diffusion, $\gamma_v = 1$, and we write $\gamma_u = \gamma$. Solving (10.161), we obtain

$$\widehat{\widetilde{\delta\rho}}_u(k, s) = \frac{\nu(s)}{\Delta(s)}, \tag{10.162}$$

where

$$\nu(s) = \left(s - J_{22} + \frac{\sigma_v^2 k^2}{2\tau_{0,v}}\right) \widehat{\delta\rho}_u(k, t = 0)$$

$$+ \left(J_{12} - \sigma_u^2 k^2 \overline{\rho}_u [p_u \tau_{0,u}]^{1-\gamma} \frac{h_\gamma(s, p_u)}{2s\tau_{0,u}}\right) \widehat{\delta\rho}_v(k, t = 0) \tag{10.163}$$

and

$$\Delta(s) = \left[s - J_{11} + \sigma_u^2 k^2 \frac{(s + p_u)^{1-\gamma}}{2\tau_{0,u}^\gamma}\right] \left[s - J_{22} + \frac{\sigma_v^2 k^2}{2\tau_{0,v}}\right] - J_{21} J_{12}$$

$$+ \sigma_u^2 k^2 \overline{\rho}_u [p_u \tau_{0,u}]^{1-\gamma} \frac{h_\gamma(s, p_u)}{2s\tau_{0,u}} \left(A_{12} J_{21} + A_{11}s - A_{11} J_{22} + A_{11} \frac{\sigma_v^2 k^2}{2\tau_{0,v}}\right). \tag{10.164}$$

We obtain a similar expression for $\widehat{\widetilde{\delta\rho}}_v(k, s)$, with the same denominator as in (10.162).

The inverse Laplace transform leads to

$$\widetilde{\delta\rho}_u(k, t) = \sum_i \zeta(s_i) e^{s_i t}, \tag{10.165}$$

where s_i are the zeros of the denominator $\Delta(s)$ on the right-hand side of (10.164), while $\zeta(s_i)$ are time-independent coefficients [484]. Equation (10.165) shows that the long-time asymptotic behavior of the perturbations is controlled only by the zeros of $\Delta(s)$. The perturbation $\widetilde{\delta\rho}_u(k, t)$ grows if at least one of the zeros s_i of $\Delta(s)$ has a positive real part, else it decays. This holds true for $\widetilde{\delta\rho}_v(k, t)$ as well, since the long-time asymptotics are controlled by the zeros of the same polynomial $\Delta(s)$. An instability occurs if all s_j have negative real parts except for s_{j_c} whose real part changes from negative to positive at the instability threshold as a control parameter of the system is varied. The Turing instability corresponds to a real zero crossing the imaginary axis, i.e., $\Delta(s_{j_T} \to 0) = 0$:

$$\left[\left(-J_{11} + \frac{\sigma_u^2 k^2 p_u^{1-\gamma}}{2\tau_{0,u}^\gamma}\right)\left(-J_{22} + \frac{\sigma_v^2 k^2}{2\tau_{0,v}}\right) - J_{21} J_{12}\right]$$

$$+ (\sigma_{\mathrm{u}}^2/2)k^2 \overline{\rho}_{\mathrm{u}} p_{\mathrm{u}}^{-\gamma} \tau_{0,\mathrm{u}}^{-\gamma} (\gamma - 1) \left(A_{12} J_{21} - A_{11} J_{22} + A_{11} \frac{\sigma_{\mathrm{v}}^2 k^2}{2\tau_{0,\mathrm{v}}} \right) = 0. \quad (10.166)$$

Using the generalized diffusion coefficient, see (2.54), $D_{\gamma;\mathrm{u}} = \sigma_{\mathrm{u}}^2/(2\tau_{0,\mathrm{u}}^\gamma)$, and the regular diffusion coefficient $D_{\mathrm{v}} = \sigma_{\mathrm{v}}^2/(2\tau_{0,\mathrm{v}})$, we write the Turing condition as

$$\left[\left(-J_{11} + D_{\gamma;\mathrm{u}} k^2 p_{\mathrm{u}}^{1-\gamma} \right) \left(-J_{22} + D_{\mathrm{v}} k^2 \right) - J_{21} J_{12} \right]$$
$$+ D_{\gamma;\mathrm{u}} k^2 \overline{\rho}_{\mathrm{u}} p_{\mathrm{u}}^{-\gamma} (\gamma - 1) \left(A_{12} J_{21} - A_{11} J_{22} + A_{11} D_{\mathrm{v}} k^2 \right) = 0. \quad (10.167)$$

Rewriting (10.167) in the form

$$k^4 + \hat{c}_2 k^2 + \hat{c}_4 = 0, \qquad (10.168)$$

with

$$\hat{c}_2 = \frac{-D_{\mathrm{v}} J_{11} p_{\mathrm{u}}^\gamma + (\gamma - 1) A_{12} J_{21} D_{\gamma;\mathrm{u}} \overline{\rho}_{\mathrm{u}} - J_{22} D_{\gamma;\mathrm{u}} [p_{\mathrm{u}} + (\gamma - 1) A_{11} \overline{\rho}_{\mathrm{u}}]}{D_{\mathrm{v}} D_{\gamma;\mathrm{u}} [p_{\mathrm{u}} + (\gamma - 1) A_{11} \overline{\rho}_{\mathrm{u}}]}$$
$$(10.169)$$

and

$$\hat{c}_4 = \frac{(J_{11} J_{22} - J_{12} J_{21}) p_{\mathrm{u}}^\gamma}{D_{\mathrm{v}} D_{\gamma;\mathrm{u}} [p_{\mathrm{u}} + (\gamma - 1) A_{11} \overline{\rho}_{\mathrm{u}}]}, \qquad (10.170)$$

furnishes the upper and lower cutoff of the band of unstable modes,

$$\frac{1}{2} \left(-\hat{c}_2 - \sqrt{\hat{c}_2^2 - 4\hat{c}_4} \right) < k^2 < \frac{1}{2} \left(-\hat{c}_2 + \sqrt{\hat{c}_2^2 - 4\hat{c}_4} \right), \qquad (10.171)$$

provided $\hat{c}_2 < 0$ and $\hat{c}_2^2 - 4\hat{c}_4 > 0$. At the Turing threshold, $\hat{c}_2^2 - 4\hat{c}_4 = 0$, and the critical wavenumber is $k_c^2 = -\hat{c}_2/2$.

Equation (10.167) is the general condition for the occurrence of a Turing instability in a two-component system when one of the components subdiffuses. By choosing $\gamma = 1$ in (10.167), we obtain the classical Turing condition, (10.30), for the case when both entities undergo normal diffusion:

$$\left(-J_{11} + D_{\mathrm{u}} k^2 \right) \left(-J_{22} + D_{\mathrm{v}} k^2 \right) - J_{21} J_{12} = 0, \qquad (10.172)$$

where $D_{\mathrm{u}} = D_{1;\mathrm{u}} = \sigma_{\mathrm{u}}^2/(2\tau_{0,\mathrm{u}})$.

To be able to compare directly a reaction–subdiffusing system with a standard reaction–diffusion system, we proceed in the following way. As shown in Sect. 10.1.2, a Turing instability can occur in a standard reaction–diffusion system only

if the activator diffuses slower than the inhibitor. This is expressed quantitatively by the critical ratio of diffusion coefficients $\theta_{RD,c}$ given by (10.41). The latter is equivalent to the ratio of the chemical length scales squared of the inhibitor and the activator. This observation points to the appropriate generalization of the ratio of diffusion coefficients for situations where the two species diffuse with a different characteristic exponent γ_i and the generalized diffusion coefficients $D_{\gamma_i;i}$ have different units. Define the effective diffusion constant for the subdiffusing species U by

$$\hat{D}_{\gamma;u} = D_{\gamma;u} p_u^{1-\gamma} = D_u (p_u \tau_{0,u})^{1-\gamma}, \tag{10.173}$$

which for normal diffusive behavior reduces to the standard diffusion constant D_u. Further, the mean squared chemical length of species i is given by $\langle x_i^2(\tau_{ch}) \rangle$. The chemical time scale τ_{ch} is determined by the characteristic lifetime of the activator, namely $\tau_{ch} = p_u^{-1}$. The mean squared displacement (MSD) for subdiffusing particles is given by (2.60):

$$\langle x_u^2(t) \rangle = \frac{2}{\Gamma(1+\gamma)} D_{\gamma;u} t^{\gamma}. \tag{10.174}$$

We obtain for the ratio of the mean squared chemical lengths of the inhibitor and the activator

$$\frac{\langle x_v^2(\tau_{ch}) \rangle}{\langle x_u^2(\tau_{ch}) \rangle} = \Gamma(1+\gamma) \frac{D_v}{\hat{D}_{\gamma;u}}. \tag{10.175}$$

Since the factor $\Gamma(1+\gamma)$ is close to 1 for $0 < \gamma \leq 1$, the result implies that the ratio $\theta_{c,\gamma'} = (D_v/\hat{D}_{\gamma;u})_c$, the ratio of the diffusion constant of the inhibitor and the effective diffusion constant of the activator at the Turing threshold, is the appropriate generalization of (10.41) to reaction–subdiffusion systems. We have set $\gamma' = 1 - \gamma$ for convenience, so that $\gamma' = 0$ corresponds to standard diffusion.

Introducing the effective diffusion constant for the activator into the Turing condition (10.167), we obtain

$$\left[\left(-J_{11} + \hat{D}_{\gamma;u} k^2 \right) \left(-J_{22} + D_v k^2 \right) - J_{21} J_{12} \right]$$
$$+ \hat{D}_{\gamma;u} k^2 \overline{\rho}_u p_u^{-1} (\gamma - 1) \left(A_{12} J_{21} - A_{11} J_{22} + A_{11} D_v k^2 \right) = 0. \tag{10.176}$$

When the subdiffusion exponent γ is close to one, (10.176) reduces to the condition

$$\left(-J_{11} + \hat{D}_{\gamma;u} k^2 \right) \left(-J_{22} + D_v k^2 \right) - J_{21} J_{12} = 0. \tag{10.177}$$

This is formally identical to the classical Turing condition with the effective diffusion coefficient of the subdiffusing species, $\hat{D}_{\gamma;u}$, in place of the original diffusion

constant D_u of the purely diffusive case. For small deviations from purely diffusive behavior into the subdiffusive regime, the memory of the transport shifts the Turing instability threshold and the characteristic wavenumber of the unstable mode at the threshold. This translates into a change in the characteristic size of the resulting pattern. Also, the upper and lower cutoffs of the band of unstable modes are shifted.

Equation (10.177) holds for all values of γ if the loss rate of the subdiffusing species U is linear, i.e., of the form $F_1^-(\rho_u, \rho_v) = p_u \rho_u$, since in this case $A_{11} = A_{12} = 0$. The Brusselator, see Sect. 1.4.4, $F_1(\rho_u, \rho_v) = a - (b+1)\rho_u + \rho_u^2 \rho_v$ and consequently $F_1^-(\rho_u, \rho_v) = (b+1)\rho_u$, the Gierer–Meinhardt model, see Sect. 1.4.6, $F_1(\rho_u, \rho_v) = 1 - \rho_u + a\rho_u^2/\rho_v$, i.e., $F_1^-(\rho_u, \rho_v) = \rho_u$, and the Schnakenberg model, see Sect. 1.4.5, $F_1(\rho_u, \rho_v) = a - \rho_u + \rho_u^2 \rho_v$, i.e., $F_1^-(\rho_u, \rho_v) = \rho_u$, belong to this class. For models with linear death rates it follows from (10.177) that the critical value of $\theta_{c,\gamma'}$ for a Turing instability to occur is given by

$$\theta_{c,\gamma'} = \theta_{\mathrm{RD},c} = \left[\frac{1}{J_{11}} \left(\sqrt{\Delta} + \sqrt{-J_{12}J_{21}} \right) \right]^2, \tag{10.178}$$

i.e., identical to the critical value of the ratio of diffusion coefficients for a Turing instability in a standard reaction–diffusion system (10.41). Therefore the diffusion coefficient of the normally diffusing inhibitor V must be larger than

$$D_{v,c} = \theta_{\mathrm{RD},c} \hat{D}_{\gamma;u} = \theta_{\mathrm{RD},c} D_u (p_u \tau_{0,u})^{1-\gamma} \tag{10.179}$$

for a Turing instability to occur if the activator displays subdiffusion with exponent γ.

If the loss rate of the activator is nonlinear, then we need to solve the Turing threshold condition $\hat{c}_2^2 - 4\hat{c}_4 = 0$, which provides two solutions for the ratio $\theta_{c,\gamma'}$. To choose the physically meaningful solution, we recall that for standard diffusion, $\gamma' = 0$, the ratio $\theta_{c,0} = (D_v/D_u)_{\mathrm{RD},c}$ must always be greater than one, see (10.35). This criterion leads to the choice

$$\begin{aligned}
\theta_{c,\gamma'} = \frac{1}{J_{11}^2 p_u^2} \Big\{ &-2J_{12}J_{21}p_u^2 + J_{11}J_{22}p_u^2 - A_{12}J_{11}J_{21}p_u\bar{\rho}_u\gamma' \\
&+2A_{11}J_{12}J_{21}p_u\bar{\rho}_u\gamma' - A_{11}J_{11}J_{22}p_u\bar{\rho}_u\gamma' \\
&+2\sqrt{J_{21}(-\Delta)p_u^2(p_u - A_{11}\bar{\rho}_u\gamma')[A_{12}J_{11}\bar{\rho}_u\gamma' + J_{12}(p_u - A_{11}\bar{\rho}_u\gamma')]} \Big\},
\end{aligned} \tag{10.180}$$

which reduces to $\theta_{c,0} = \theta_{\mathrm{RD},c}$, see (10.41), for $\gamma' = 0$.

We apply the result, (10.180), to the Oregonator model of the BZ reaction, see Sect. 1.4.8, and the Lengyel–Epstein model of the CDIMA reaction, see Sect. 1.4.9. Turing instabilities have been observed in experimental systems with normal diffusive behavior of the activator and inhibitor for both reactions. Equation (10.180) can

of course be evaluated explicitly for any kinetic scheme using symbolic computation software. However, the resulting expression for the Oregonator is very lengthy and not enlightening at all. It will therefore not be displayed here. We illustrate instead the behavior by choosing specific values for the kinetic parameters, namely $q = 0.005$, $h = 1.9$, and $\epsilon = 0.3$. For these values, the stability conditions (10.23) are fulfilled for the nontrivial steady state (1.132), and

$$\theta_{c,\gamma'} = 6.8012 + 6.1183\gamma' + 5.8167\sqrt{(0.98539 + \gamma')(1.3513 + \gamma')}. \quad (10.181)$$

A plot of this curve, $\theta_{c,\gamma'}$ vs γ', is shown in Fig. 10.1. The ratio of the diffusion constant of the inhibitor and the effective diffusion constant of the activator at the Turing threshold increases as the motion becomes more subdiffusive, $\gamma' \to 1$.
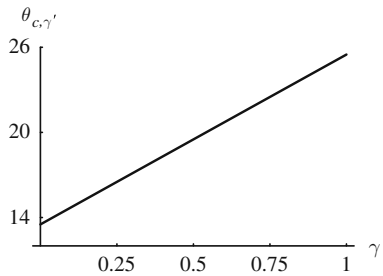
Fig. 10.1 Plot of $\theta_{c,\gamma'}$ for the Oregonator. The parameters are $q = 0.005$, $h = 1.9$, and $\epsilon = 0.3$. Reprinted with permission from [485]. Copyright 2008 by the American Physical Society

We are interested in the effect of subdiffusive motion of the activator on Turing instabilities. We focus on this mechanism exclusively and consider the LE model in its original form without a substrate, i.e., $\sigma = 1$ in (1.152) or (1.160). Equation (10.180) results in the following expression:

$$\theta_{c,\gamma'} = \frac{1}{(125 - 3a^2)^2}\left[625ab + 65a^3b + \frac{128a^5b\gamma'}{25 + a^2}\right.$$
$$\left. +4\sqrt{10}\sqrt{\frac{a^4b^2(125 + 5a^2 + 8a^2\gamma')(125 - 125\gamma' + 5a^2 + 11a^2\gamma')}{25 + a^2}}\right].$$
$$(10.182)$$

We again illustrate the behavior of the critical ratio $\theta_{c,\gamma'}$ by choosing specific values for the kinetic parameters, namely $a = 50.0$ and $b = 40.0$. For these values, the stability conditions (10.23) are fulfilled for the steady state (1.154), and

$$\theta_{c,\gamma'} = 5.9983 + 11.650\gamma' + 10.829\sqrt{(0.46119 + \gamma')(0.63125 + \gamma')}. \quad (10.183)$$

A plot of this curve is shown in Fig. 10.2. As for the Oregonator model, the ratio of the diffusion constant of the inhibitor and the effective diffusion constant of the activator at the Turing threshold increases as the motion becomes more subdiffusive, $\gamma' \to 1$.
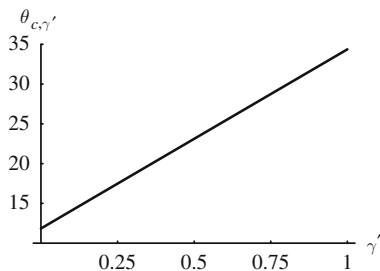
Fig. 10.2 Plot of $\theta_{c,\gamma'}$ for the Lengyel–Epstein model. The parameters are $a = 50.0$ and $b = 40.0$. Reprinted with permission from [485]. Copyright 2008 by the American Physical Society

It is worth noting that the nonlinear loss rate for the subdiffusing species, present in the two models analyzed above, is responsible for the increase of the ratio $\theta_{c,\gamma'}$ with an increase in γ'. The ratio $\theta_{c,\gamma'}$ remains unchanged on changing γ', if the subdiffusing species has a linear loss rate, see (10.178).

As shown in Sect. 10.1.2, Turing patterns arise from a competition between local activation and long-range inhibition. For the kinetic schemes studied in this section, the interaction between the nonlinear kinetics, especially the nonlinear death rate, and the memory effects of the transport, as explicitly displayed in the generalized reaction–diffusion equation (10.158) by the presence of both the kernel $K_i(t - t')$, related to the waiting time PDF of the CTRW, and the death rate $F_i^-(\rho(x,t))$ in the memory term, leads to an enhanced local activation. For the Oregonator and Lengyel–Epstein model and for the parameter values considered here, the specific loss rate of the activator, $F_1^-(\rho_u, \rho_v)/\rho_u$, decreases as the concentration ρ_u increases away from the steady state value. The increased survival rate in regions with positive fluctuations in the activator concentration, combined with the fact that subdiffusive activator particles stay longer in a given region than normally diffusing particles, leads to an increase of the local autocatalytic effect. This effect becomes more pronounced as the dispersion of the activator becomes more subdiffusive, $\gamma' \to 1$. A Turing instability can only occur, if the enhanced local autocatalytic effect is countered by a longer ranged inhibitory effect, and consequently $\theta_{c,\gamma'}$ increases as γ' increases.

Having examined the consequences of a subdiffusing activator on the Turing instability, we turn now to the opposite case of a subdiffusing inhibitor. We explore if the coupling between a nonlinear specific loss rate and subdiffusion can similarly enhance the inhibitory effect and result in conditions that are more favorable for the formation of Turing patterns. The Turing condition (10.167) is valid under the assumption that the first species, i.e., U, undergoes subdiffusion. Recall that we

denote the activator by U and the inhibitor by V, see Sect. 1.2.2. To be able to utilize (10.167) in studying the role of a subdiffusing inhibitor, we reverse the convention by setting the first species, U, as the inhibitor for activator–inhibitor models, (1.19) or (1.21), and the second species V as the activator. It is straightforward to show by symmetry arguments that the critical ratio of the effective diffusion constant for the subdiffusive inhibitor and the standard diffusion constant for the normally diffusing activator is given by

$$
\theta_{c,\gamma'} = \left(\frac{1}{J_{11}^2 p_u^2} \left\{ -2J_{12}J_{21}p_u^2 + J_{11}J_{22}p_u^2 - A_{12}J_{11}J_{21}p_u\bar{\rho}_u\gamma' \right. \right.
$$
$$
+2A_{11}J_{12}J_{21}p_u\bar{\rho}_u\gamma' - A_{11}J_{11}J_{22}p_u\bar{\rho}_u\gamma'
$$
$$
\left. \left. -2\sqrt{J_{21}(-\Delta)p_u^2(p_u - A_{11}\bar{\rho}_u\gamma')[A_{12}J_{11}\bar{\rho}_u\gamma' + J_{12}(p_u - A_{11}\bar{\rho}_u\gamma')]} \right\} \right)^{-1}.
$$

$$(10.184)$$

Previously, the physically meaningful solution branch for $\theta_{c,\gamma'}$, given by (10.180), was obtained by requiring that $\theta_{c,0} > 1$. Reversing the labels of the activator and inhibitor amounts to considering the inverse of the conjugate solution to 10.180, which is provided by 10.184.

The death rate of the inhibitor in the Oregonator is linear. Subdiffusive motion of this species leaves the critical ratio $\theta_{c,\gamma'}$ unchanged as γ' increases, $\theta_{c,\gamma'} = \theta_{c,0} = \theta_{RD,c}$, see (10.178). In the following we consider the Lengyel–Epstein model and the Schnakenberg model, Sect. 1.4.5, and the Gray–Scott model, Sect. 1.4.7. We will not display the explicit expression (10.184) for $\theta_{c,\gamma'}$ for each model, but rather illustrate the behavior by a plot of $\theta_{c,\gamma'}$ vs γ' for a typical set of parameter values. For the Lengyel–Epstein model with a subdiffusing inhibitor, a typical plot of $\theta_{c,\gamma'}$, obtained from (10.184), is shown in Fig. 10.3. In our reversed convention, the nonlinearities are given by

$$
F_1(\rho_u, \rho_v) = b\left[\rho_v - \frac{\rho_u\rho_v}{1 + \rho_v^2} \right], \tag{10.185a}
$$
$$
F_2(\rho_u, \rho_v) = a - \rho_v - 4\frac{\rho_u\rho_v}{1 + \rho_v^2}, \tag{10.185b}
$$

and the unique uniform steady state is $(\bar{\rho}_u, \bar{\rho}_v) = (1 + a^2/25, a/5)$.

Typical plots of $\theta_{c,\gamma'}$ for the Schnakenberg model with the kinetic terms

$$
F_1(\rho_u, \rho_v) = b - \rho_u\rho_v^2, \tag{10.186a}
$$
$$
F_2(\rho_u, \rho_v) = a - \rho_v + \rho_u\rho_v^2, \tag{10.186b}
$$
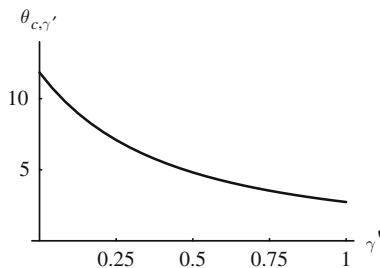
Fig. 10.3 Plot of $\theta_{c,\gamma'}$ for the Lengyel–Epstein model with a subdiffusing inhibitor. The parameters are $a = 50.0$ and $b = 40.0$. Reprinted with permission from [485]. Copyright 2008 by the American Physical Society

and steady state $(\overline{\rho}_u, \overline{\rho}_v) = (b/(a+b)^2, a+b)$ and for the Gray–Scott model with the kinetic terms

$$F_1(\rho_u, \rho_v) = -\rho_u \rho_v^2 + q(1 - \rho_u), \tag{10.187a}$$

$$F_2(\rho_u, \rho_v) = \rho_u \rho_v^2 - (k_2 + q)\rho_v, \tag{10.187b}$$

and steady state

$$(\overline{\rho}_u, \overline{\rho}_v) = \left(1 - \frac{(k_2 + q)\left(-q - \sqrt{-4k_2^2 q + q^2 - 8k_2 q^2 - 4q^3}\right)}{-2q(k_2 + q)}, \right.$$
$$\left. \frac{-q - \sqrt{-4k_2^2 q + q^2 - 8k_2 q^2 - 4q^3}}{-2q(k_2 + q)}\right), \tag{10.188}$$

are shown in Figs. 10.4 and 10.5, respectively.
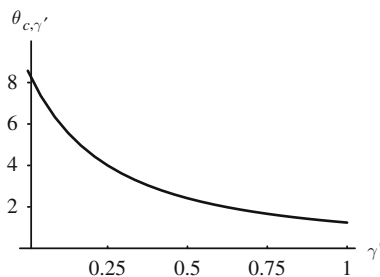
Fig. 10.4 Plot of $\theta_{c,\gamma'}$ for the Schnakenberg model with a subdiffusing inhibitor. The parameters are $a = 0.1$ and $b = 0.9$. Reprinted with permission from [485]. Copyright 2008 by the American Physical Society
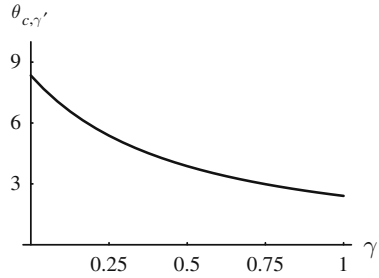
Fig. 10.5 Plot of $\theta_{c,\gamma'}$ for the Gray–Scott model with a subdiffusing inhibitor. The parameters are $q = 0.15$ and $k_2 = 0.03$. Reprinted with permission from [485]. Copyright 2008 by the American Physical Society

A subdiffusing inhibitor with a nonlinear loss term results in a decreasing $\theta_{c,\gamma'}$ as γ' increases, in contrast to the opposite case of a subdiffusing activator. Again, the interaction between the nonlinear kinetics, especially the nonlinear loss rate, and the memory effects of the transport enhances the effectiveness of the inhibitor. This effect becomes more pronounced as the dispersion of the activator becomes more subdiffusive, $\gamma' \to 1$, and makes it easier for a Turing instability to arise. Consequently $\theta_{c,\gamma'}$ decreases as γ' increases.

10.4.2 Turing Instabilities in Reaction–Subdiffusion Systems: Model A and Other Approaches

We have focused on Model B to investigate the effect of subdiffusive transport on the Turing instability, because it appears to have the broadest range of applicability. The assumptions inherent in the other CTRW models are quite restrictive. Model C, Sect. 3.4.3, corresponds to a pure birth process. Model A assumes that reactions do not change the waiting time PDF. As discussed in Sect. 3.4.1, in a chemical context this implies that reactive events do not destroy or create particles; they simply change the internal state of the reactant particles. It is not clear that actual chemical reactions meeting the requirements of Model A can display Turing instabilities. The situation appears to be more promising for ecological and other nonchemical systems. Experimental studies will of course be the ultimate arbiter of which model provides an adequate description for a specific system.

Nec and Nepomnyashchy have used Model A to investigate Turing instabilities in a two-variable activator–inhibitor subdiffusive system [317]. The analysis is quite involved, and the Turing condition is somewhat complicated. Since reactions do not change the waiting time PDF in model A, $\phi_u(t) = \phi_v(t) = \phi(t)$, the anomaly exponent is the same for both species. The authors find that the Turing condition is more restrictive than for standard RD systems. For anomaly exponents γ close to one, the critical ratio θ_c is larger than $\theta_{RD,c}$. Consequently, subdiffusion of the

activator and inhibitor with the same exponent γ has a stabilizing effect in Model A reaction–transport systems. Further, the growth rate of the most unstable mode decreases as γ decreases. Reducing γ for fixed θ will eventually stabilize the uniform steady state.

Numerical simulations of a subdiffusing activator–inhibitor system, namely the Schnakenberg model, see Sect. 1.4.5, have been conducted by Weiss [475] and Chiu and Chiam [76]. Weiss considers the case of a subdiffusing activator and a normally diffusing inhibitor. He observes a stabilization of Turing patterns due to subdiffusion and attributes it to subdiffusion mimicking the effects of a lower effective diffusion constant for the activator. Chiu and Chiam consider the case where the activator and the inhibitor have the same anomaly coefficient γ. They also find that subdiffusion has a stabilizing effect. As γ decreases, it becomes harder for Turing patterns to form. A direct quantitative comparison of the numerical observations with analytical results is not feasible. The models studied above are mean-field descriptions and neglect particle number fluctuations as discussed at the start of Chap. 3. In contrast, the simulations are stochastic in nature and the total number of particles, N, is relatively small. The largest N in Weiss's simulations is 5000, and in the simulations by Chiu and Chiam it is 6428. The reported results show that N is not large enough to neglect random fluctuations around the mean behavior. Particle number fluctuations have a strong effect in both numerical approaches and change the Turing conditions from those obtained for mean-field reaction–transport equations.

Several authors have considered reaction–transport equations, where the fractional time derivative operates both on the diffusion term and the nonlinear kinetic term [391, 490, 240, 235],

$$\frac{\partial \rho_i}{\partial t} = \mathcal{D}_t^{1-\gamma_i} \left[D_{\gamma_i;i} \frac{\partial^2 \rho_i}{\partial x^2} + F_i(\boldsymbol{\rho}) \right], \qquad (10.189)$$

or the equivalent form [147, 148],

$$\frac{\partial^{\gamma_i} \rho_i}{\partial t^{\gamma_i}} = D_{\gamma_i;i} \frac{\partial^2 \rho_i}{\partial x^2} + F_i(\boldsymbol{\rho}). \qquad (10.190)$$

These equations describe subdiffusion-limited chemical reactions. As stated in Chap. 2, such reactions are outside the scope of this monograph. For results on fronts and Turing instabilities in systems with subdiffusion-controlled chemical reactions, see for example [490, 240, 147, 148, 235, 318, 191].

10.4.3 Turing Instability in the Superdiffusive Brusselator

CTRWs with short–tailed waiting time PDFs and heavy-tailed jump length PDFs correspond to Lévy flights, which model superdiffusive processes, as discussed in Chap. 3. Lévy flights have been studied extensively [299, 74, 296] and have found

applications in subsurface hydrology [38, 42] and ecology [459, 20, 356, 24], though recent work questions the empirical evidence for Lévy flights in animal search patterns [108, 107]. The Lévy flight behavior is a good fit on length scales encountered in applications. From a fundamental viewpoint, however, the infinite variance of Lévy flights is problematic for particles or individuals, since it implies an unbounded velocity distribution [74, 24]. This feature leads to accelerating fronts for instance [90, 24].

Lévy flights are Markovian CTRWs, and we can therefore simply add a kinetic term to the RHS of (3.91),

$$\frac{\partial \rho_i(x,t)}{\partial t} = D_{\alpha_i;i} \frac{\partial^{\alpha_i} \rho_i(x,t)}{\partial |x|^{\alpha_i}} + F_i(\boldsymbol{\rho}), \tag{10.191}$$

with $1 < \alpha_i < 2$. This equation can also be obtained from the Master equation (3.138). Golovin and coworkers have investigated the Turing instability in the Brusselator model with superdiffusion [164],

$$\frac{\partial \rho_u}{\partial t} = D_{\alpha;u} \frac{\partial^{\alpha} \rho_u}{\partial |x|^{\alpha}} + a - (b+1)\rho_u + \rho_u^2 \rho_v, \tag{10.192a}$$

$$\frac{\partial \rho_v}{\partial t} = D_{\beta;v} \frac{\partial^{\beta} \rho_v}{\partial |x|^{\beta}} + b\rho_u - \rho_u^2 \rho_v, \tag{10.192b}$$

on $-\infty < x < \infty$. The authors write $(\rho_u(x,t), \rho_v(x,t)) = (\overline{\rho}_u + \delta\rho_u(x,t), \overline{\rho}_v + \delta\rho_v(x,t))$. They rescale the variables

$$\delta\rho_u = \sqrt{\theta_y}\rho_u^*, \quad \delta\rho_v = \left(1/\sqrt{\theta_y}\right)\rho_v^*, \quad x = \ell x^*, \tag{10.193}$$

where

$$\theta_y = \frac{D_{\beta;v}}{D_{\alpha;u}^{1/y}}, \quad y = \frac{\alpha}{\beta}, \quad \ell = D_{\alpha;u}^{1/\alpha}, \tag{10.194}$$

and obtain, dropping the $*$,

$$\frac{\partial \rho_u}{\partial t} = \frac{\partial^{\alpha} \rho_u}{\partial |x|^{\alpha}} + (b-1)\rho_u + q^2\rho_v + (b/q)\rho_u^2 + 2q\rho_u\rho_v + \rho_u^2\rho_v, \tag{10.195a}$$

$$\frac{1}{\theta_y}\frac{\partial \rho_v}{\partial t} = \frac{\partial^{\beta} \rho_v}{\partial |x|^{\beta}} - b\rho_u - q^2\rho_v - (b/q)\rho_u^2 - 2q\rho_u\rho_v - \rho_u^2\rho_v, \tag{10.195b}$$

with $q = a/\sqrt{\theta_y}$. A linear stability analysis of the uniform steady state $(\overline{\rho}_u(x), \overline{\rho}_v(x)) = (0,0)$ of (10.195) yields the dispersion relation

$$\lambda_k^2/\theta_y + c_1\lambda_k + c_2 = 0, \tag{10.196}$$

where

$$c_1 = q^2 + k^\beta - \left(b - 1 - k^\alpha\right)/\theta_y, \tag{10.197}$$

$$c_2 = ba^2 - \left(b - 1 - k^\alpha\right)\left(q^2 + k^\beta\right). \tag{10.198}$$

The locus of the stationary instability of mode k, i.e., $\lambda_k = 0$, can be written in the form

$$b(k) = \frac{1}{k^\beta}\left(1 + k^\alpha\right)\left(q^2 + k^\beta\right). \tag{10.199}$$

This curve has a single minimum, (k_T, b_T), which corresponds to the Turing instability of the uniform steady state. The Turing threshold b_T and the critical wavenumber k_T depend on q and read in parametric form

$$k_T = \zeta^{1/\alpha}, \quad b_T = \frac{(1 + \zeta)^2}{1 + (1 - y)\zeta}, \quad q^2 = \frac{y\zeta^{1+1/y}}{1 + (1 - y)\zeta}. \tag{10.200}$$

The parameter ζ varies over $(0, \infty)$ if $1/2 < y \leq 1$ and over $(0, 1/(y - 1))$ if $1 < y < 2$. Analysis shows that for $y = 1$, i.e., the activator and inhibitor have the same anomaly coefficient and which includes the case of standard diffusion, the conditions (10.200) reduce to those of the standard Brusselator RD system, see Sect. 10.1.3. If $y < 1$, the anomaly coefficient of the inhibitor is larger than that of the activator, and the tail of the jump length PDF of the inhibitor decreases faster than that of the activator, see (3.191). In other words, the activator has a longer range than the inhibitor, which prevents a Turing instability in a standard RD system. In contrast, a Turing bifurcation can occur in the superdiffusive Brusselator for such a situation, provided a is sufficiently large [164].

Exercises

10.1 Consider the model of Exercise 1.6 in a reaction–diffusion setting:

$$\frac{\partial \rho_u}{\partial t} = 1 - \rho_u \rho_v^h + D_u \frac{\partial^2 \rho_u}{\partial x^2}, \tag{10.201a}$$

$$\frac{\partial \rho_v}{\partial t} = \alpha \rho_u \rho_v^h - \alpha \rho_v + D_v \frac{\partial^2 \rho_v}{\partial x^2}. \tag{10.201b}$$

Can the uniform steady state of (10.201) undergo a Turing instability? If so, discuss the effect of increasing the Hill constant h.

10.2 Consider the modified Brusselator RD system,

$$\frac{\partial \rho_u}{\partial t} = a - (b+1)\rho_u + \rho_u^h \rho_v + D_u \frac{\partial^2 \rho_u}{\partial x^2}, \tag{10.202a}$$

$$\frac{\partial \rho_v}{\partial t} = b\rho_u - \rho_u^h \rho_v + D_v \frac{\partial^2 \rho_v}{\partial x^2}, \tag{10.202b}$$

with $h > 2$. Discuss the effect of increasing h on the Turing instability of the Brusselator.

10.3 Investigate the effect of cross-diffusion terms on the Turing instability in two-variable RD systems,

$$\frac{\partial \rho_u}{\partial t} = D_u \frac{\partial^2 \rho_u}{\partial x^2} + \frac{\partial}{\partial x} D_{uv}(\rho_u) \frac{\partial \rho_v}{\partial x} + F_1(\rho_u, \rho_v), \tag{10.203a}$$

$$\frac{\partial \rho_v}{\partial t} = D_v \frac{\partial^2 \rho_v}{\partial x^2} + \frac{\partial}{\partial x} D_{vu}(\rho_v) \frac{\partial \rho_u}{\partial x} + F_2(\rho_u, \rho_v), \tag{10.203b}$$

with no-flow boundary conditions on the interval $[0, L]$. The cross-diffusion coefficients D_{ij} must go to zero as ρ_i goes to zero, since there can be no flux of ρ_i if $\rho_i = 0$. Recall that in chemical systems, see Sect. 2.1.2, thermodynamics imposes the constraint that all eigenvalues of the diffusion matrix

$$\mathsf{D} = \begin{pmatrix} D_u & D_{uv} \\ D_{vu} & D_v \end{pmatrix} \tag{10.204}$$

must be real and positive, i.e., $\mathrm{tr}\,\mathsf{D} > 0$ and $\det \mathsf{D} > 0$.

Assume that

$$D_{uv}(\rho_u) = D_{uv} \frac{\rho_u}{\epsilon_u + \rho_u}, \tag{10.205}$$

$$D_{vu}(\rho_v) = D_{vu} \frac{\rho_v}{\epsilon_v + \rho_v}, \tag{10.206}$$

where ϵ_i is small. Then for $\rho_u \gg \epsilon_u$ and $\rho_v \gg \epsilon_v$, the cross-diffusion terms can be considered constant, and (10.203) reduces to

$$\frac{\partial \rho_u}{\partial t} = D_u \frac{\partial^2 \rho_u}{\partial x^2} + D_{uv} \frac{\partial^2 \rho_v}{\partial x^2} + F_1(\rho_u, \rho_v), \tag{10.207a}$$

$$\frac{\partial \rho_v}{\partial t} = D_v \frac{\partial^2 \rho_v}{\partial x^2} + D_{vu} \frac{\partial^2 \rho_u}{\partial x^2} + F_2(\rho_u, \rho_v). \tag{10.207b}$$

Investigate the spatial instabilities of (10.207). Assume that $D_u = 1$ and $D_v = d > 1$. The cross-diffusion terms can be positive or negative, but the constraint $\det \mathsf{D} > 0$ must be satisfied.

10.4 Discuss the spatial instabilities of the uniform steady states of the prey–predator system

$$\frac{\partial \rho_u}{\partial t} = \frac{\partial}{\partial x}\left(d_u + D_u\rho_u\right)\frac{\partial \rho_u}{\partial x} + \rho_u - \rho_u^2 - \rho_u\rho_v^2, \tag{10.208a}$$

$$\frac{\partial \rho_v}{\partial t} = \frac{\partial}{\partial x}\left(d_v + D_v\rho_u\right)\frac{\partial \rho_u}{\partial x} + \frac{\partial}{\partial x}D_v\rho_v\frac{\partial \rho_u}{\partial x} - \mu\rho_v + \alpha\rho_u\rho_v, \tag{10.208b}$$

with no-flow boundary conditions on the interval $[0, L]$. Here μ α, d_i, and D_i are positive quantities. For simplicity, consider the case $d_u = d_v = d$ and $D_u = D_v = D$.

10.5 Investigate the effect of a quiescent phase for the activator, i.e., an immobile unreactive phase, on the Turing instability of two-variable DIRWs,

$$\frac{\partial \rho_{+,u}}{\partial t} + \gamma_u\frac{\partial \rho_{+,u}}{\partial x} = \mu_u\left(\rho_{-,u} - \rho_{+,u}\right) + \frac{1}{2}\nu_2\rho_{0,u} - \nu_1\rho_{+,u}$$
$$+ \frac{1}{2}g_1(\rho_{+,u} + \rho_{-,u}, \rho_v) - f_1^-(\rho_{+,u} + \rho_{-,u}, \rho_v)\rho_{+,u}, \tag{10.209a}$$

$$\frac{\partial \rho_{-,u}}{\partial t} - \gamma_u\frac{\partial \rho_{-,u}}{\partial x} = \mu_u\left(\rho_{+,u} - \rho_{-,u}\right) + +\frac{1}{2}\nu_2\rho_{0,u} - \nu_1\rho_{-,u}$$
$$+ \frac{1}{2}g_1(\rho_{+,u} + \rho_{-,u}, \rho_v) - f_1^-(\rho_{+,u} + \rho_{-,u}, \rho_v)\rho_{-,u}, \tag{10.209b}$$

$$\frac{\partial \rho_{0,u}}{\partial t} = \nu_1(\rho_{+,u} + \rho_{-,u}) - \nu_2\rho_{0,u}, \tag{10.209c}$$

$$\frac{\partial \rho_{+,v}}{\partial t} + \gamma_v\frac{\partial \rho_{+,v}}{\partial x} = \mu_v\left(\rho_{-,v} - \rho_{+,v}\right) + \frac{1}{2}g_2(\rho_{+,u} + \rho_{-,u}, \rho_v)$$
$$- f_2^-(\rho_{+,u} + \rho_{-,u}, \rho_v)\rho_{+,v}, \tag{10.209d}$$

$$\frac{\partial \rho_{-,v}}{\partial t} - \gamma_v\frac{\partial \rho_{-,v}}{\partial x} = \mu_v\left(\rho_{+,v} - \rho_{-,v}\right) + \frac{1}{2}g_2(\rho_{+,u} + \rho_{-,u}, \rho_v)$$
$$- f_2^-(\rho_{+,u} + \rho_{-,u}, \rho_v)\rho_{-,v}, \tag{10.209e}$$

with impermeable boundaries. For simplicity, consider the case that $\nu_1 = \nu_2 = \nu$.

Chapter 11
Turing Instabilities in Reaction–Diffusion Systems with Temporally or Spatially Varying Parameters

In Chap. 10 we considered the Turing instability in systems where the kinetic parameters and the transport coefficients are constant in space and time. While the vast majority of theoretical work on Turing patterns deals with such systems, there are good reasons from applications in biology and ecology to account for the effect of spatial or temporal variations on the threshold of the Turing instability. Chemical or biological systems are rarely completely uniform. Pattern formation in the *Drosophila* egg, for example, occurs in the presence of maternally imposed gradients of gene products [106]. Experimental studies of Turing patterns in the CIMA and CDIMA reactions use continuously fed unstirred reactors (CFURs), see Chap. 12, which unavoidably exhibit gradients in the concentrations of the feed reactants. The problem of determining diffusion-driven instabilities in reacting systems with spatially or temporally varying parameters is in general a rather difficult one. The tools of the linear stability analysis employed in Chap. 10 cannot be extended to such systems, since they do not posses a uniform steady state in most cases. Reaction–diffusion systems with weak heterogeneities can be studied with perturbation techniques [19, 50, 92, 40, 341, 342]. Lengyel and coworkers [249] used an approximation of the reaction–diffusion equation to study the effect of the gradients in CFURs on the position and the possible three-dimensional character of the Turing structures. In general, numerical studies are required to address the problem of Turing patterns in heterogeneous systems, see for example [192, 433, 365, 394, 395, 55]. Voroney and coworkers carried out numerical simulations of the Sel'kov model with a complexing reaction [462]. They considered the case where the immobile complexing species is confined to disks or stripes. If the spatial distribution of the complexing agent varies on a scale small compared to the intrinsic length scales of the reaction–diffusion system, normal Turing pattern formation occurs. If the spatial scales are comparable, interactions between oscillatory behavior and Turing patterns generate spatiotemporal dynamics not observed in a homogeneous medium.

While in general the problem of pattern formation in heterogeneous media is a difficult one, the analysis is more manageable in situations where the spatial or temporal variations in parameters of the reaction–diffusion system do not compromise the existence of a uniform steady state. Such is the case for a varying diffusion

coefficient. In that situation, a uniform steady state exists, but the standard tools of bifurcation theory cannot be applied.

11.1 Turing Instability with Time-Varying Diffusivities

Ecological systems can display temporal oscillations in parameter values due to seasonal variations. The effects of time-varying diffusivities on the Turing instability were first considered by Timm and Okubo [436] in a predator–prey model describing the interaction between zooplankton and phytoplankton. Temporal variations in the horizontal diffusion coefficients arise from the interaction of vertical current shear with vertical mixing processes.

Consider the two-variable system

$$\frac{\partial \rho_u}{\partial t} = D_u \frac{\partial^2 \rho_u}{\partial x^2} + F_1(\rho_u, \rho_v), \tag{11.1a}$$

$$\frac{\partial \rho_v}{\partial t} = D_v(t) \frac{\partial^2 \rho_v}{\partial x^2} + F_2(\rho_u, \rho_v), \tag{11.1b}$$

with no-flow boundary conditions (10.20) on the interval $[0, L]$. For simplicity, we assume that only one of the diffusion coefficients is time-dependent, namely the diffusivity of the inhibitor,

$$D_v(t) = D_u[\theta + \epsilon \sin(\omega t)], \tag{11.2}$$

with

$$\theta > 1, \quad \theta > |\epsilon|. \tag{11.3}$$

We impose the first inequality in (11.3), since a Turing instability can occur in a two-variable reaction–diffusion system with constant parameters only if $\theta_{RD} > 1$. The second inequality ensures the positivity of $D_v(t)$. We assume that the system (11.1) possesses a uniform steady state, $(\overline{\rho}_u(x), \overline{\rho}_v(x)) = (\overline{\rho}_u, \overline{\rho}_v)$, with $F_1(\overline{\rho}_u, \overline{\rho}_v) = F_2(\overline{\rho}_u, \overline{\rho}_v) = 0$, which fulfills the stability conditions (10.23), and U is an activator and V an inhibitor.

To assess the stability of the uniform steady state, we carry out a linear stability analysis. We set

$$\rho_u(x, t) = \overline{\rho}_u + \delta_u(t) \cos(kx), \tag{11.4a}$$

$$\rho_v(x, t) = \overline{\rho}_v + \delta_v(t) \cos(kx), \tag{11.4b}$$

and obtain the linearized evolution equations

$$\frac{d\delta_u(t)}{dt} = [J_{11} - k^2 D_u]\delta_u(t) + J_{12}\delta_v(t), \tag{11.5a}$$

$$\frac{d\delta_v(t)}{dt} = J_{21}\delta_u(t) + [J_{22} - k^2 D_v(t)]\delta_v(t). \tag{11.5b}$$

We rescale time, $\tau \equiv \omega t$, and find

$$\frac{d\delta_u(\tau)}{d\tau} = \hat{J}_{11}\delta_u(\tau) + \hat{J}_{12}\delta_v(\tau), \tag{11.6a}$$

$$\frac{d\delta_v(\tau)}{d\tau} = \hat{J}_{21}\delta_u(\tau) + \hat{J}_{22}(\tau)\delta_v(\tau), \tag{11.6b}$$

with

$$\hat{J}_{11} = [J_{11} - k^2 D_u]\omega^{-1}, \tag{11.7a}$$

$$\hat{J}_{12} = J_{12}\omega^{-1}, \tag{11.7b}$$

$$\hat{J}_{21} = J_{21}\omega^{-1}, \tag{11.7c}$$

$$\hat{J}_{22}(\tau) = [J_{22} - k^2 D_u \theta]\omega^{-1} - (k^2 D_u \epsilon \omega^{-1}) \sin(\tau). \tag{11.7d}$$

From (11.6a) we obtain

$$\delta_v(\tau) = [d\delta_u(\tau)/d\tau - \hat{J}_{11}\delta_u(\tau)]/\hat{J}_{12}, \tag{11.8}$$

and substitution of this result into (11.6b) yields

$$\frac{d^2\delta_u(\tau)}{d\tau^2} - [\hat{J}_{11} + \hat{J}_{22}(\tau)]\frac{d\delta_u(\tau)}{d\tau} + [\hat{J}_{11}\hat{J}_{22}(\tau) - \hat{J}_{12}\hat{J}_{21}]\delta_u(\tau) = 0. \tag{11.9}$$

With the transformation

$$\delta_u(\tau) = \exp\left\{\frac{1}{2}\int^\tau \left[\hat{J}_{11} + \hat{J}_{22}(\tau')\right]d\tau'\right\}\hat{\delta}_u, \tag{11.10}$$

(11.9) turns into Hill's equation [259]

$$\frac{d^2\hat{\delta}_u}{d\tau^2} + Q(\tau)\hat{\delta}_u = 0, \tag{11.11}$$

where

$$Q(\tau) = \frac{1}{2}\frac{d\hat{J}_{22}(\tau)}{d\tau} - \frac{1}{4}[\hat{J}_{11} + \hat{J}_{22}(\tau)]^2 + [\hat{J}_{11}\hat{J}_{22}(\tau) - \hat{J}_{12}\hat{J}_{21}]. \tag{11.12}$$

If the corresponding system with constant parameters, i.e., $\epsilon = 0$, is at the Turing threshold, i.e., $\theta = \theta_{\mathrm{RD},c} = \left[J_{11}^{-1} \left(\sqrt{\Delta} + \sqrt{-J_{12}J_{21}} \right) \right]^2$, see (10.41), and if $k^2 = k_{\mathrm{T,RD}}^2 = \sqrt{\Delta/(D_{\mathrm{u}}D_{\mathrm{v}})}$, then a perturbation analysis of Hill's equation (11.11) shows that the uniform steady state of (11.1) with a temporally varying diffusion coefficient of the inhibitor is stable for sufficiently small oscillations, $\epsilon \ll 1$ [436]. In other words, small oscillations in the diffusion coefficient have a stabilizing effect; they delay the onset of the Turing instability.

Gourley and coworkers [168] have generalized Timm and Okubo's result and have applied perturbation theory to the system (11.1) with $D_i = D_i^{(0)} + \epsilon D_i^{(1)}(t)$ positive ($i = \mathrm{u, v}$), where ϵ small and the $D_i^{(1)}$ are periodic with period $\mathcal{T}$ and average zero. Choosing the system parameters again such that the corresponding system with constant parameters, i.e., $\epsilon = 0$, is at the Turing threshold, i.e., $\theta = \theta_{\mathrm{RD},c}$, and $k^2 = k_{\mathrm{T,RD}}^2$, they find that the uniform steady state is stable. In other words, all small-amplitude periodic perturbations with average zero in the diffusion coefficients delay the onset of the Turing instability. Further, if the periodic variations are $O(\epsilon)$, then the stabilizing effect is $O(\epsilon^2)$.

More general analytical results can be obtained if the periodic oscillations of the inhibitor diffusion coefficient are dichotomous or of "square-tooth" form [400]:

$$D_{\mathrm{v}}(t) = \begin{cases} D^+ & \text{on } n\mathcal{T} \leq t < (n+1/2)\mathcal{T}, \\ D^- & \text{on } (n+1/2)\mathcal{T} \leq t < (n+1)\mathcal{T}, \end{cases} \tag{11.13}$$

where $n \in \mathbb{Z}$. We assume $D^+ > D^- \geq 0$ and define $\overline{D} \equiv (D^+ + D^-)/2$ and $d \equiv (D^+ - D^-)/2$. For simplicity, we rescale x such that $D_{\mathrm{u}} = 1$:

$$\frac{\partial \rho_{\mathrm{u}}}{\partial t} = \frac{\partial^2 \rho_{\mathrm{u}}}{\partial x^2} + F_1(\rho_{\mathrm{u}}, \rho_{\mathrm{v}}), \tag{11.14a}$$

$$\frac{\partial \rho_{\mathrm{v}}}{\partial t} = D_{\mathrm{v}}(t) \frac{\partial^2 \rho_{\mathrm{v}}}{\partial x^2} + F_2(\rho_{\mathrm{u}}, \rho_{\mathrm{v}}). \tag{11.14b}$$

We assume again that (11.14) possesses a uniform steady state, $(\overline{\rho}_{\mathrm{u}}(x), \overline{\rho}_{\mathrm{v}}(x)) = (\overline{\rho}_{\mathrm{u}}, \overline{\rho}_{\mathrm{v}})$, with $F_1(\overline{\rho}_{\mathrm{u}}, \overline{\rho}_{\mathrm{v}}) = F_2(\overline{\rho}_{\mathrm{u}}, \overline{\rho}_{\mathrm{v}}) = 0$, which fulfills the stability condition (10.23), and that U is an activator and V an inhibitor.

With (11.4), the linearized evolution equations read

$$\frac{d\delta_{\mathrm{u}}(t)}{dt} = [J_{11} - k^2]\delta_{\mathrm{u}}(t) + J_{12}\delta_{\mathrm{v}}(t), \tag{11.15a}$$

$$\frac{d\delta_{\mathrm{v}}(t)}{dt} = J_{21}\delta_{\mathrm{u}}(t) + [J_{22} - k^2 D_{\mathrm{v}}(t)]\delta_{\mathrm{v}}(t). \tag{11.15b}$$

As is well known, any nth order homogeneous system of nonautonomous linear ordinary differential equations

$$\frac{d\mathbf{u}}{dt} = \mathsf{A}(t)\mathbf{u} \tag{11.16}$$

has n linearly independent solutions [458, 435]. We compose these n linearly independent solutions $\mathbf{u}_1(t), \ldots, \mathbf{u}_n(t)$ to a matrix $\Phi(t)$ with these solutions as columns, $\Phi(t) = (\mathbf{u}_1(t)\mathbf{u}_2(t) \ldots \mathbf{u}_n(t))$. Such a matrix is called a fundamental matrix of (11.16). The solution of (11.16) with the initial condition $\mathbf{u}(t_0) = \mathbf{u}_0$ is then given by

$$\mathbf{u}(t) = \Phi(t)\Phi(t_0)^{-1}\mathbf{u}_0. \tag{11.17}$$

If the linear equation (11.16) has periodically varying coefficients with period $\mathcal{T}$, $\mathsf{A}(t + \mathcal{T}) = \mathsf{A}(t)$, the Floquet theorem provides the fundamental result that the fundamental matrix of (11.16) can be written as the product of a $\mathcal{T}$-periodic matrix and a (generally) nonperiodic matrix [458, p. 80].

Theorem 11.1   *Suppose $\mathsf{A}(t)$ is periodic with period $\mathcal{T}$. Each fundamental matrix $\Phi(t)$ of (11.16) can be written as the product of two $n \times n$ matrices*

$$\Phi(t) = \mathsf{P}(t)\exp(\mathsf{B}t), \tag{11.18}$$

where $\mathsf{P}(t)$ is $\mathcal{T}$-periodic and B is a constant matrix.

Equation (11.18) implies that

$$\Phi(t + \mathcal{T}) = \Phi(t)\exp(\mathsf{B}\mathcal{T}) = \Phi(t)\mathsf{M}. \tag{11.19}$$

Remark 11.1 The matrix $\mathsf{M} = \exp(\mathsf{B}\mathcal{T})$ is called the monodromy matrix of $\dot{\mathbf{u}} = \mathsf{A}(t)\mathbf{u}$ [458].

Remark 11.2 The eigenvalues μ_i of M are known as *Floquet multipliers* or *characteristic multipliers* and the eigenvalues ν_i of B are known as the *Floquet exponents* or *characteristic exponents*. They are related by $\mu_i = \exp(\nu_i \mathcal{T})$ [435].

Theorem 11.2   *A periodic linear system is stable if all Floquet multipliers satisfy $|\mu_i| \leq 1$ (respectively all Floquet exponents satisfy $\mathrm{Re}\,\nu_i \leq 0$) and for all Floquet multipliers with $|\mu_i| = 1$ (respectively all Floquet exponents with $\mathrm{Re}\,\nu_i = 0$) the algebraic and geometric multiplicities are equal.*
A periodic linear system is asymptotically stable if all Floquet multipliers satisfy $|\mu_i| < 1$ (respectively all Floquet exponents satisfy $\mathrm{Re}\,\nu_i < 0$) [435].

Equation (11.19) implies that the monodromy matrix is given by $\mathsf{M} = \Phi(t_0)^{-1}\Phi(t_0 + \mathcal{T})$, independent of the choice of t_0. The main difficulty in applying Theorem 11.2 to a particular set of equations lies in obtaining a linearly independent set of solutions.

In the following we provide a summary of the stability analysis of (11.15) as carried out by Sherratt [400]. We write (11.15) in the form

$$\frac{d\delta}{dt} = \widehat{J}^+\delta \quad \text{on } nT \leq t < (n + 1/2)T, \tag{11.20a}$$

$$\frac{d\delta}{dt} = \widehat{J}^-\delta \quad \text{on } (n + 1/2)T \leq t < (n + 1)T, \tag{11.20b}$$

where

$$\delta(t) = \begin{pmatrix} \delta_u(t) \\ \delta_v(t) \end{pmatrix} \tag{11.21}$$

and

$$\widehat{J}^\pm = \begin{pmatrix} J_{11} - k^2 & J_{12} \\ J_{21} & J_{22} - k^2 D^\pm \end{pmatrix}. \tag{11.22}$$

We denote the eigenvalues and corresponding eigenvectors of $\widehat{J}^\pm$ by $\lambda_i^\pm$ and $z_i^\pm$ with $i = 1, 2$ and write $\Lambda^\pm(t) = \text{diag}(\exp(\lambda_1^\pm t), \exp(\lambda_2^\pm t))$. Let $Z^\pm$ be the matrix whose first and second columns are $z_1^\pm$ and $z_2^\pm$. Then any fundamental matrices $\Phi(t)$ of (11.20a) and (11.20b) have the form $Z^+\Lambda^+(t)C^+$ and $Z^-\Lambda^-(t)C^-$, respectively, where $C^\pm$ are matrices whose entries are constants of integration. Without loss of generality, we choose $C^+ = [\Lambda^+(T/2)]^{-1}$. Continuity at $t = T/2$ imposes that

$$C^- = [\Lambda^-(T/2)]^{-1}[Z^-]^{-1}Z^+ \tag{11.23}$$

and

$$M = [\Phi(0)]^{-1}\Phi(T) = [Z^+]^{-1}Z^-\Lambda^-(T/2)[Z^-]^{-1}Z^+\Lambda^+(T/2). \tag{11.24}$$

The eigenvalues μ of M, i.e., the Floquet multipliers are given by

$$\mu = \hat{\mu} \exp(-\Gamma T/4), \tag{11.25}$$

where

$$\hat{\mu}^2 - a_1\hat{\mu} + 1 = 0 \tag{11.26}$$

and $(K = k^2)$

$$\Gamma = 2[(1 + \overline{D})K - (J_{11} + J_{22})], \tag{11.27a}$$

$$a_1 = \frac{1}{2} \exp[(P^+ + P^-)\mathcal{T}/4]\left\{\left[1 + \exp(-P^+\mathcal{T}/2)\right]\left[1 + \exp(-P^-\mathcal{T}/2)\right]\right.$$
$$\left. + \frac{4J_{12}J_{21} + Q^+Q^-}{P^+ + P^-}\left[1 - \exp(-P^+\mathcal{T}/2)\right]\left[1 - \exp(-P^-\mathcal{T}/2)\right]\right\}, \tag{11.27b}$$

$$Q^{\pm} = KD^{\pm} - K + J_{11} - J_{22}, \tag{11.27c}$$

$$P^{\pm} = \sqrt{4J_{12}J_{21} + (Q^{\pm})^2}. \tag{11.27d}$$

We focus on the case, most relevant in applications, that the period $\mathcal{T}$ of $D_v(t)$ is much longer than the characteristic time scale of the kinetics, which implies that $\left|P^{\pm}\mathcal{T}\right| \gg 1$. Analysis of (11.25), (11.26), and (11.27) leads to the conclusion that there exists a $\mu > 1$, i.e., the uniform steady state is unstable to nonuniform perturbations if either (i) $P^+ > \Gamma$ or (ii) $[\Gamma + (P^+)^2 - (P^-)^2]^2 < 4\Gamma^2(P^+)^2$. Somewhat lengthy further calculations show that, to leading order for large $\mathcal{T}$, the uniform steady state will be driven unstable by diffusion if and only if either

$$\text{(i)} \quad 3J_{11} + J_{22} > 0, \tag{11.28a}$$

$$\frac{D^+ - 1}{D^- + 3} > \chi_c, \tag{11.28b}$$

or

$$\text{(ii)} \quad \overline{D}J_{11} + J_{22} > 0, \tag{11.29a}$$

$$[\overline{D}J_{11} + J_{22}]^2 > 4\overline{D}\Delta, \tag{11.29b}$$

$$d < d_c. \tag{11.29c}$$

Here, $\Delta = \det J = J_{11}J_{22} - J_{12}J_{21}$, and $\chi_c > 0$ is the larger root of

$$(3J_{11} + J_{22})^2\chi^2 + 2(3J_{11}^2 - 2J_{11}J_{22} - J_{22}^2 + 4J_{12}J_{21})\chi$$
$$+ J_{11}^2 - 2J_{11}J_{22} + 4J_{12}J_{21} + J_{22}^2 = 0. \tag{11.30}$$

Further, d_c is the unique value of d for which

$$F(K) = \overline{D}K^2 - (\overline{D}J_{11} + J_{22})K + \Delta + d^2\frac{K^2(J_{11} - K)(\overline{D}K - J_{22})}{[(1 + \overline{D})K - (J_{11} + J_{22})]^2} \tag{11.31}$$

touches the K-axis on $(0, J_{11})$.

The instability conditions (ii), (11.29), are an extension of the Turing instability conditions (10.43) when $D^+ = D^- = \overline{D}$. (Recall we rescaled space to set $D_u = 1$.) The first two inequalities, (11.29a) and (11.29b), are identical with the Turing instability condition (10.43) for the system (11.14) with a constant inhibitor diffusion coefficient $D_v(t) = \overline{D}$. It is therefore a necessary condition that the system with constant diffusion coefficients be Turing unstable, in order for condition (11.29) to be fulfilled. In that sense, square-tooth temporal oscillations in the diffusion coefficient of the inhibitor have a stabilizing effect, since an additional condition, namely (11.29c), needs to be satisfied. Further, it turns out that condition (i), (11.28), defines a region of diffusion-driven instability in parameter space that is separate from the unstable region defined by condition (ii), (11.29), only if d is sufficiently large, i.e., D^+ and D^- are sufficiently different. Then, if the system possesses parameter values that fall inside the region defined by condition (i), temporal variations in D_v can have destabilizing effect.

11.2 Turing Instability with Spatially Inhomogeneous Diffusivities

As discussed at the beginning of this chapter, biological and ecological systems are often spatially inhomogeneous, and consequently diffusion coefficients display spatial variations. In analogy to the case of temporally varying diffusivities, dealt with in Sect. 11.1, we study the simplest possible situation. Only the diffusion coefficient of the inhibitor varies spatially, and it is piece-wise constant, a step function in space with a single point of discontinuity. We consider the following two-variable system on the interval $[0, L]$ with no-flow boundary conditions:

$$\frac{\partial \rho_u}{\partial t} = \frac{\partial^2 \rho_u}{\partial x^2} + F_1(\rho_u, \rho_v), \tag{11.32a}$$

$$\frac{\partial \rho_v}{\partial t} = \frac{\partial}{\partial x}\left[D_v(x)\frac{\partial \rho_v}{\partial x}\right] + F_2(\rho_u, \rho_v), \tag{11.32b}$$

with

$$D_v(x) = \begin{cases} D^- & \text{on } 0 \le x < \xi L, \\ D^+ & \text{on } \xi L < x \le L, \end{cases} \tag{11.33}$$

$D^- > 0$, $D^+ > 0$, $D^- \neq D^+$, and $\xi \in (0, 1)$. We assume again that (11.32) possesses a uniform steady state, $(\overline{\rho}_u(x), \overline{\rho}_v(x)) = (\overline{\rho}_u, \overline{\rho}_v)$, with $F_1(\overline{\rho}_u, \overline{\rho}_v) = F_2(\overline{\rho}_u, \overline{\rho}_v) = 0$, which fulfills the stability condition (10.23), and that U is an activator and V an inhibitor.

The linear stability analysis of (11.32) was carried out by Maini and coworkers [263, 41], and we provide a summary of their work in the following. With

$$\rho_u(x, t) = \overline{\rho}_u + \delta_u(x) \exp(\lambda t), \tag{11.34a}$$

$$\rho_v(x, t) = \overline{\rho}_v + \delta_v(x) \exp(\lambda t), \tag{11.34b}$$

the linearized evolution equations read

$$\delta_u''(x) + [J_{11} - \lambda]\delta_u(x) + J_{12}\delta_v(x) = 0, \tag{11.35a}$$

$$[D_v(x)\delta_v'(x)]' + J_{21}\delta_u(x) + [J_{22} - \lambda]\delta_v(x) = 0, \tag{11.35b}$$

where the prime denotes d/dx. Since the system decomposes into parts, for each
of which the diffusion coefficient of the inhibitor is a constant, we consider (11.35)
separately on $[0, \xi L)$ and $(\xi L, L]$. For the first part, we multiply (11.35b) by s^-/D^-
and add it to (11.35a) to obtain

$$[\delta_u(x) + s^- \delta_v(x)]'' + \left[J_{11} - \lambda + \frac{J_{21}s^-}{D^-} \right]$$
$$\times \left[\delta_u(x) + \frac{J_{12} + (J_{22} - \lambda)s^-/D^-}{J_{11} - \lambda + J_{21}s^-/D^-} \delta_v(x) \right] = 0. \tag{11.36}$$

We choose s^- such that

$$\frac{J_{12} + (J_{22} - \lambda)s^-/D^-}{J_{11} - \lambda + J_{21}s^-/D^-} = s^-, \tag{11.37}$$

which is a quadratic equation:

$$J_{21}(s^-)^2 + [D^-(J_{11} - \lambda) - (J_{22} - \lambda)]s^- - J_{12}D^- = 0. \tag{11.38}$$

Let s_1^- and s_2^- be the roots of (11.38). Then (11.36) turns into two equations for the
quantity $\delta_j(x) \equiv \delta_u(x) + s_j^- \delta_v(x)$ for $j = 1, 2$:

$$\delta_1(x)'' + \left[J_{11} - \lambda + \frac{J_{21}s_1^-}{D^-} \right] \delta_1(x) = 0, \tag{11.39a}$$

$$\delta_2(x)'' + \left[J_{11} - \lambda + \frac{J_{21}s_2^-}{D^-} \right] \delta_2(x) = 0. \tag{11.39b}$$

The general solutions of (11.39) are given by

$$\delta_j(x) = C_j \cos(\alpha_j^- x) + \tilde{C}_j \sin(\alpha_j^- x), \tag{11.40}$$

where C_j and $\tilde{C}_j$ are constants of integration, and

$$\alpha_j^- = \sqrt{\frac{J_{11} - \lambda + J_{21}s_j^-}{D^-}}.$$ (11.41)

The no-flow boundary condition at $x = 0$ implies that the constants $\tilde{C}_j$ vanish. We express the constants C_j in terms of the values of $\delta_j(x)$ at $x = \xi L$ and solve for $\delta_u(x)$ and $\delta_v(x)$ on $[0, \xi L]$:

$$\delta_u(x) = \frac{1}{s_2^- - s_1^-}\left[\frac{\left(\Gamma_u + s_1^-\Gamma_v\right)s_2^-}{\cos(\alpha_1^-\xi L)}\cos(\alpha_1^- x) - \frac{\left(\Gamma_u + s_2^-\Gamma_v\right)s_1^-}{\cos(\alpha_2^-\xi L)}\cos(\alpha_2^- x)\right],$$

(11.42a)

$$\delta_v(x) = \frac{1}{s_2^- - s_1^-}\left[\frac{\left(\Gamma_u + s_2^-\Gamma_v\right)}{\cos(\alpha_2^-\xi L)}\cos(\alpha_2^- x) - \frac{\left(\Gamma_u + s_1^-\Gamma_v\right)}{\cos(\alpha_1^-\xi L)}\cos(\alpha_1^- x)\right],$$

(11.42b)

where $\Gamma_u = \delta_u(\xi L)$ and $\Gamma_v = \delta_v(\xi L)$. Proceeding similarly for the second part of the system, we obtain $\delta_u(x)$ and $\delta_v(x)$ on $(\xi L, L]$:

$$\delta_u(x) = \frac{1}{s_2^+ - s_1^+}\left[\frac{\left(\Gamma_u + s_1^+\Gamma_v\right)s_2^+}{\cos(\alpha_1^+(1-\xi)L)}\cos(\alpha_1^+(L-x))\right.$$
$$\left. - \frac{\left(\Gamma_u + s_2^+\Gamma_v\right)s_1^+}{\cos(\alpha_2^+(1-\xi)L)}\cos(\alpha_2^+(L-x))\right],$$ (11.43a)

$$\delta_v(x) = \frac{1}{s_2^+ - s_1^+}\left[\frac{\left(\Gamma_u + s_2^+\Gamma_v\right)}{\cos(\alpha_2^+(1-\xi)L)}\cos(\alpha_2^+(L-x))\right.$$
$$\left. - \frac{\left(\Gamma_u + s_1^+\Gamma_v\right)}{\cos(\alpha_1^+(1-\xi)L)}\cos(\alpha_1^+(L-x))\right].$$ (11.43b)

By construction, the solutions $\delta_u(x)$ and $\delta_v(x)$ of (11.35) given by (11.42) and (11.43) are continuous at $x = \xi L$. However, the solution must also satisfy continuity of flux at $x = \xi L$:

$$\lim_{x \to (\xi L)^-} \delta_u'(x) = \lim_{x \to (\xi L)^+} \delta_u'(x),$$ (11.44a)

$$\lim_{x \to (\xi L)^-} D^-\delta_v'(x) = \lim_{x \to (\xi L)^+} D^+\delta_v'(x).$$ (11.44b)

Substituting (11.42) and (11.43) into (11.44), we obtain

$$\begin{pmatrix} P(\lambda) & Q(\lambda) \\ R(\lambda) & S(\lambda) \end{pmatrix} \begin{pmatrix} \Gamma_u \\ \Gamma_v \end{pmatrix} = \begin{pmatrix} 0 \\ 0 \end{pmatrix}, \tag{11.45}$$

where

$$P(\lambda) = \frac{s_1^- T_2^- - s_2^- T_1^-}{s_2^- - s_1^-} + \frac{s_1^+ T_2^+ - s_2^+ T_1^+}{s_2^+ - s_1^+}, \tag{11.46a}$$

$$Q(\lambda) = \frac{s_1^- s_2^- (T_2^- - T_1^-)}{s_2^- - s_1^-} + \frac{s_1^+ s_2^+ (T_2^+ - T_1^+)}{s_2^+ - s_1^+}, \tag{11.46b}$$

$$R(\lambda) = \frac{D^- (T_1^- - T_2^-)}{s_2^- - s_1^-} + \frac{D^+ (T_1^+ - T_2^+)}{s_2^+ - s_1^+}, \tag{11.46c}$$

$$S(\lambda) = \frac{D^- (s_1^- T_1^- - s_2^- T_2^-)}{s_2^- - s_1^-} + \frac{D^+ (s_1^+ T_1^+ - s_2^+ T_2^+)}{s_2^+ - s_1^+}, \tag{11.46d}$$

with $T_j^- = \alpha_j^- \tan(\xi L \alpha_j^-)$ and $T_j^+ = \alpha_j^+ \tan((1 - \xi)L\alpha_j^+)$ for $j = 1, 2$. Here we assume that $s_1^\pm \neq s_2^\pm$, $\cos(\alpha_j^- \xi L) \neq 0$, and $\cos(\alpha_j^+ (1-\xi)L) \neq 0$ for $j = 1, 2$. From the solutions (11.42) and (11.43), $\Gamma_u = \Gamma_v = 0$ implies that $\delta_u(x) \equiv \delta_v(x) \equiv 0$. In order to obtain nontrivial solutions $\delta_u(x)$ and $\delta_v(x)$, the determinant of the matrix in (11.45) must vanish:

$$F(\lambda) \equiv P(\lambda)S(\lambda) - Q(\lambda)R(\lambda) = 0. \tag{11.47}$$

This is the dispersion relation for a two-variable reaction–diffusion system with a step-function diffusivity for V. It is the analog of (10.26) for homogeneous reaction–diffusion systems and relates the growth rates λ of spatial perturbations to the parameter values of the system. In contrast to the homogeneous case, the dispersion relation (11.47) is a complicated expression that cannot be solved analytically if $D^- \neq D^+$. A diffusion-driven instability of the uniform steady state of the system occurs if the stability condition (10.23) is satisfied and (11.47) has solutions with a positive real part.

Note that in deriving (11.47) we have assumed that $s_2^\pm - s_1^\pm$, $\cos(\alpha_j^- \xi L)$, and $\cos(\alpha_j^+ (1 - \xi)L)$ are all nonzero. The analysis can be carried out for those cases where one or more of these expressions are zero, but typically the solutions $\delta_u(x)$ and $\delta_v(x)$ cannot satisfy (11.44).

In general, the roots of the dispersion relation (11.47) will be complex valued. For homogeneous, two-variable reaction–diffusion systems, all complex solutions of the dispersion relation (10.26) have a negative real part. Extensive numerical simulations of the full nonlinear inhomogeneous system (11.32) by Maini and coworkers [263, 41] show that, if an instability occurs, the uniform steady state always evolves to a steady pattern and not a temporally oscillating solution. These observations suggest that the diffusion-driven instability is a Turing bifurcation, i.e., a real eigenvalue passes through zero. If λ is real, then $F(\lambda)$ is also real, and the dispersion relation

is amenable to simple numerical solution. The Turing condition that $F(\lambda) = 0$ has positive real solutions is far less enlightening than the Turing condition (10.43) for homogeneous systems. In particular, it is not immediately clear that the system must be either a pure activator–inhibitor scheme or a cross activator–inhibitor scheme. Numerical solutions of (11.47) suggest, however, as expected, that these requirements are still necessary for a diffusion-driven instability to occur in the system (11.32). Studies of chemical and biological models [263, 41], such as the Schnakenberg model, see Sect. 1.4.5, show that as expected the uniform steady state of (11.32) undergoes a Turing instability if $D^+ > D^- > \theta_{\mathrm{RD},c}$, where the latter is given by (10.41). A Turing bifurcation can occur for $D^- < \theta_{\mathrm{RD},c}$, if D^+ exceeds some critical value D_c^+, which depends on the system parameters, with $D_c^+ > \theta_{\mathrm{RD},c}$.

Exercise

11.1 Explore the dispersion relation (11.47) for the Brusselator.

Chapter 12
Chemical and Biological Applications of Turing Systems

Turing's paper on diffusion-driven instabilities in nonequilibrium reaction–diffusion systems as a means of biological pattern formation [440] attracted little attention for about two decades, as shown by the citation histogram in Fig. 12.1. One of the first scientists to be intrigued by Turing's ideas was Wardlaw, a botanist who thought about ways to test the mechanism experimentally [468, 470, 469]. By the early 1970s theoretical biologists and biomathematicians began to explore in earnest if Turing instabilities could explain spatial pattern formation in a variety of living systems and a considerable body of theoretical work was produced, see for example [157, 279, 231, 239, 182, 183, 264, 261, 308]. Morphogen-based pattern
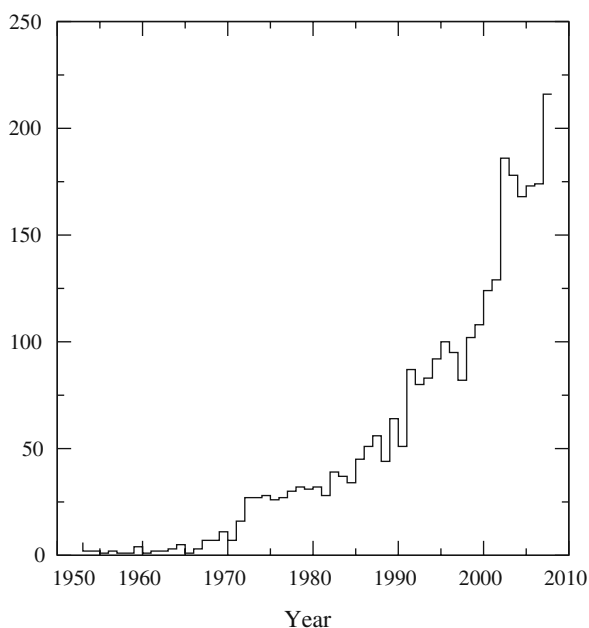
Fig. 12.1 Citation histogram for [440]: number of citations/year vs year. Figure courtesy of J. E. Pearson

formation, where the long-range influence of signaling molecules induces structure, is a well-established phenomenon in developmental biology [26]. However, definitive evidence for a Turing mechanism of pattern formation within a morphogen system is still lacking. Several promising candidate systems exist and are discussed in Sect. 12.2.

The first unambiguous observation of a Turing instability in any experimental system did not occur until 1990. That year, the Bordeaux group found convincing evidence for Turing patterns in an in vitro system, the CIMA reaction (see Sect. 1.4.9). The gap of almost 40 yr between Turing's theoretical prediction of diffusion-induced instabilities and the experimental realization of stationary chemical pattern was caused by two main factors.

12.1 Turing Patterns in the CIMA/CDIMA and BZ Reactions

Genuine Turing patterns are nonequilibrium structures and can occur only in open systems. This requirement represents the first obstacle on the way to an experimental realization of Turing patterns. Needed is an open reactor, an unstirred flow reactor, which can play the same role for spatial patterns that the CSTR plays for temporal patterns. This instrumentation problem was solved in the second half of the 1980s by the Austin group. They developed two types of open spatial reactors, the Couette reactor [433, 335, 456, 336] and the continuously fed unstirred reactor (CFUR) [322, 432, 431, 323]. The latter proved to be instrumental in the experimental realization of Turing patterns.

12.1.1 Continuously Fed Unstirred Chemical Reactor

A CFUR consists of a gel layer in contact with one or two well-stirred feed reservoirs. The main purpose of the gel is to prevent convective flows in the reactor, which would otherwise arise in an open reactor due to the feeds. The gel needs to be chemically inert and transparent, and it should have good mechanical properties. The first CFUR experiments with the BZ reaction used polyacrylamide. In the one-sided version of the CFUR, a thin gel disk sits on top of a CSTR. Reactants diffuse from the CSTR through a glass capillary array into the gel. This arrangement has the drawback that the reactants do already react in the feed reservoir. The two-sided CFUR can avoid this complication, and two configurations of this type of CFUR have been constructed, see Fig. 12.2. In the first version, the gel strip reactor, a thin gel slab is sandwiched between a white bottom plate and a Plexiglas cover. The assembly is oriented such that the two opposite thin long faces are in contact with two different chemical reservoirs A and B. The view of the spatial patterns in the gel layer is perpendicular to the direction of the feed gradients. In the second version, the disk reactor, a thin gel disk is sandwiched between two thin porous glass plates, such that the broad faces of the gel layer are in contact with the glass
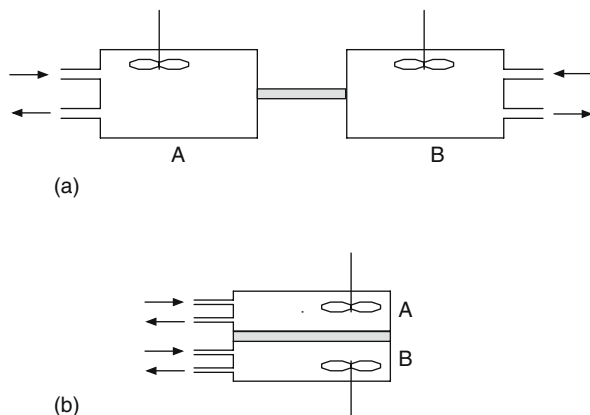
Fig. 12.2 Continuously fed unstirred reactor (CFUR). Sketch of (**a**) gel strip reactor and (**b**) disk reactor. The *grey rectangle* represents the gel and its support. Patterns are viewed from the top

plates, which in turn are in contact with two different chemical reservoirs A and B. The view of the spatial patterns in the gel layer is parallel to the direction of the feed gradients.

The reservoirs are CSTRs. Fresh reactants flow continuously at a fixed flow rate into these feed reservoirs, where they are vigorously stirred to ensure uniform and constant feed conditions. The reactants diffuse into the gel from the two reservoirs and generate counter gradients of the various reactants. The reactants are distributed in the reservoirs A and B in such a way that the pattern-forming reaction cannot occur in the reservoirs, in contrast to the one-sided CFUR.

The Austin group conducted extensive studies of the BZ reaction in one-sided and two-sided CFURs. They observed wave patterns [322, 432], but found no evidence of stationary chemical patterns. This failure is caused by the second obstacle on the way to an experimental realization of Turing patterns. According to Theorem 10.1, a Turing instability cannot occur if all the diffusion coefficients are the same. To be specific, the formation of Turing patterns requires that the diffusion coefficient of the inhibitor exceeds that of the activator, see (10.35). Unfortunately, diffusion coefficients of small molecules and ions in aqueous solution differ rarely by more than a factor 2. For typical conditions, a factor of 10 or even larger is necessary for a diffusion-driven instability [30, 111]. However, Theorems 10.2 and 10.3 indicate that a Turing instability can occur for special experimental conditions, namely when the system is sufficiently close to a Takens–Bogdanov point. The BZ reaction does display Takens–Bogdanov points. To explore the possibility of a Turing instability of the BZ reaction near these points, Pearson and Horsthemke employed the seven-variable Showalter–Noyes–Bar-Eli (SNB) model [408], which describes the inorganic part of the reaction in greater detail than the Oregonator. They found that, depending on the values of the rate constants, either Ce^{4+} or HOBr needs to diffuse slightly faster than Br^- for a Turing instability to occur [348]. Neither is likely to be true, and the BZ reaction is not a good candidate for the

experimental realization of Turing patterns, unless it is appropriately modified, see Sect. 12.1.5.

12.1.2 Turing Patterns in the CIMA and CDIMA Reactions: Experiments

The Bordeaux group found the first unambiguous evidence for Turing patterns in experiments with the CIMA reaction in a two-sided CFUR, a gel strip reactor [71]. Their set-up and findings are shown in Fig. 12.3. They first observed the formation of a series clear and dark bands parallel to the feed faces of the gel layer. These concentration patterns cannot be unambiguously identified as Turing patterns. They preserve the symmetry of the feed boundaries and could be caused by the concentration gradients in the reactor. However, for a well-defined range of malonic acid concentration in the reservoir B, all clear bands, except the one located closest to the B reservoir, break up into rows of periodic spots. This represents a genuine symmetry breaking in a direction perpendicular to the gradients imposed by the feeds. Further experiments showed that the wavelength, $\lambda \sim 0.2$ mm, is intrinsic, as it should be for a true Turing pattern. Ouyang and Swinney, using the second configuration of a two-sided CFUR, a disk reactor, confirmed the Bordeaux results and established beyond a doubt that the CIMA reaction displays Turing patterns [337, 338] (Fig. 12.4).
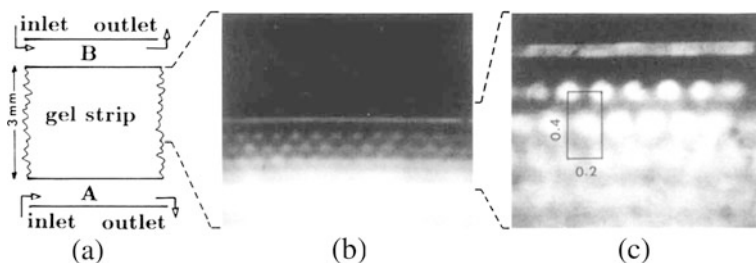
Fig. 12.3 (**a**) Sketch of the two-sided CFUR; dimensions of the gel slab: length $L = 20$ mm, width $w = 3$ mm, thickness $e = 1$ mm. (**b**) *Dark regions* of the gel correspond to reduced state, colored blue, and *clear regions* to the oxidized state. (**c**) An enlarged region of the pattern; dimensions are in mm. Reprinted with permission from [71]. Copyright 1990 by the American Physical Society

The ratio d of the diffusion coefficients of the inhibitor and the activator $d = D_{\mathrm{ClO_2^-}}/D_{\mathrm{I^-}}$ has a value very close to one. Typically a value of $d = 1.07$ is chosen in simulations, which appears to represent a situation rather unfavorable for the formation of Turing patterns. This view is too simple, however; it overlooks the role of starch in the reaction. As discussed in Sect. 1.4.9, the activator $\mathrm{I^-}$ reacts with iodine, I_2, to form triiodide ion I_3^-, which gets trapped by the starch molecules embedded in the gel or by iodide-binding sites of the gel. (Polyacrylamide binds polyiodide ions even in the absence of starch as does poly(vinyl alcohol), used as a
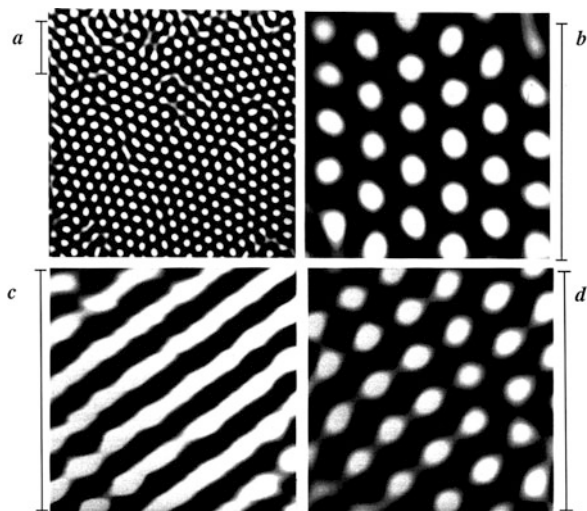
Fig. 12.4 Stationary patterns in the CIMA reaction in a CFUR. (**a**) and (**b**) hexagons, (**c**) stripes, (**d**) mixed state. The *bar* beside each picture represents 1 mm; the reactor is 25 mm in diameter. Reprinted with permission from Macmillan Publishers Ltd: *Nature* [337]. Copyright 1991

gel and color indicator in some experiments with the CDIMA reaction [86, 368].) Therefore the activator diffuses and reacts more slowly than in a medium without a substrate that binds triiodide ions. This slowing down effect of the reaction and transport process is captured in the LE model by the factor σ, see Sect. 1.4.9.

12.1.3 Theory of Turing Patterns in the CIMA and CDIMA Reactions: Lengyel–Epstein Model

The reaction–diffusion equations for the Lengyel–Epstein model,

$$\sigma \frac{\partial \rho_u(x,t)}{\partial t} = F_1(\rho_u, \rho_v) + \frac{\partial^2 \rho_u}{\partial x^2} = a - \rho_u - 4\frac{\rho_u \rho_v}{1 + \rho_u^2} + \frac{\partial^2 \rho_u}{\partial x^2}, \qquad (12.1a)$$

$$\frac{\partial \rho_v(x,t)}{\partial t} = F_2(\rho_u, \rho_v) + d\frac{\partial^2 \rho_v}{\partial x^2} = b\left(\rho_u - \frac{\rho_u \rho_v}{1 + \rho_u^2}\right) + d\frac{\partial^2 \rho_v}{\partial x^2}, \qquad (12.1b)$$

show that the effective ratio of the diffusion coefficients of the inhibitor and the activator is given by

$$\theta_{RD} = \sigma d, \qquad (12.2)$$

which can be made significantly larger than 1 by using a sufficiently large substrate concentration. For simplicity, x was rescaled such that $D_u = 1$. The LE reaction–diffusion system (12.1) has a unique uniform steady state,

$$\bar{\rho}_u(x) = \frac{a}{5}, \quad \bar{\rho}_v(x) = 1 + \frac{a^2}{25}, \tag{12.3}$$

which undergoes a Turing instability when condition (10.40) is satisfied. Solving the Turing condition for the control parameter b, we obtain an expression for the threshold of the Turing instability:

$$b_T = \frac{d}{5a}\left(13a^2 - 4\sqrt{10}a\sqrt{25 + a^2} + 125\right). \tag{12.4}$$

The critical wave number is given by (10.42) and reads for the LE system

$$k_T^2 = -5 + \frac{2\sqrt{10}a}{\sqrt{25 + a^2}}, \tag{12.5}$$

which is positive for $a > a^\circ = \sqrt{125/3}$, i.e., if iodide ion is indeed an activator, see (1.159). For experimentally reasonable values of the parameters, (12.5) yields an intrinsic wavelength of the order of 0.2 mm, which agrees with experimental observations. Note that both the Turing threshold and the critical wave number do not depend on σ. The uniform steady state is stable for large b, and it undergoes an instability as b is decreased, either a Hopf bifurcation to uniform oscillations at $b = b_H = (3a^2 - 125)/5a\sigma$, see (1.158), or a Turing bifurcation to a nonuniform steady state at $b = b_T$.

   This demonstrates the crucial role of the substrate for the formation of Turing patterns in the CIMA and CDIMA reactions. The critical value b_T for a bifurcation to stationary patterns is independent of σ, i.e., of the starch or substrate concentration, whereas the critical value b_H for a bifurcation to uniform oscillations is inversely proportional to σ. In order to observe the formation of steady chemical patterns, one must ensure that the Turing bifurcation is the primary bifurcation, i.e., it occurs before the Hopf bifurcation. In other words, the stability conditions (10.23) must be satisfied. For a given value of a, this can be achieved by using a sufficiently large concentration of complexing agent such that $\sigma > \sigma_c^*(a)$, where $\sigma_c^*(a)$ is given by $b_T = b_H$:

$$\sigma_c^*(a) = \frac{3a^2 - 125}{d\left(13a^2 - 4\sqrt{10}a\sqrt{25 + a^2} + 125\right)}, \tag{12.6}$$

which is positive for $a > a^\circ$.

12.1.4 Theory of Turing Patterns in the CIMA and CDIMA Reactions: "2+1" Model

The derivation of the LE model in Sect. 1.4.9 is based on two assumptions. The formation and dissociation of the iodide ion–substrate complex is in a fast equilibrium and the substrate concentration [S] can be considered constant. Then the three-variable activator–inhibitor–substrate system reduces to a two-variable activator–inhibitor system, where the kinetics and the diffusion coefficient of the activator are rescaled by a factor $1/\sigma$ [214, 246, 247]. We now explore these assumptions in greater detail. Consider the following well-stirred two-variable activator–inhibitor system

$$\frac{d\rho_u}{dt} = F_1(\rho_u, \rho_v), \qquad (12.7a)$$

$$\frac{d\rho_v}{dt} = F_2(\rho_u, \rho_v), \qquad (12.7b)$$

with a steady state $(\overline{\rho}_u, \overline{\rho}_v)$ given by

$$F_1(\overline{\rho}_u, \overline{\rho}_v, \mu) = F_2(\overline{\rho}_u, \overline{\rho}_v, \mu) = 0. \qquad (12.8)$$

Let $\mathbf{J}$ be the Jacobian of (12.7) at the steady state, see (1.18). Consider now the (2+1)-variable activator–inhibitor–substrate system by combining (12.7) with a complexation reaction between the substrate S and the activator U:

$$S + U \underset{k_r}{\overset{k_f}{\rightleftharpoons}} W. \qquad (12.9)$$

The rate equations for the well-stirred (2+1)-variable system can be written as

$$\frac{d\rho_u(t)}{dt} = F_1(\rho_u, \rho_v) - G(\rho_u, \rho_w), \qquad (12.10a)$$

$$\frac{d\rho_v(t)}{dt} = F_2(\rho_u, \rho_v), \qquad (12.10b)$$

$$\frac{d\rho_w(t)}{dt} = G(\rho_u, \rho_w), \qquad (12.10c)$$

where $G(\rho_u, \rho_w)$ is the reaction velocity of (12.9). As is clear from the structure of (12.10), the complexation reaction does not modify the steady values $(\overline{\rho}_u, \overline{\rho}_v)$. In the derivation of the LE model, Sect. 1.4.9, the reaction (12.9) obeys mass-action kinetics:

$$G(\rho_u, \rho_w) = k_f \rho_s \rho_u - k_r \rho_w. \qquad (12.11)$$

Note that in contrast to Sect. 1.4.9 we do not assume that [S] is constant, and we do not employ an effective rate coefficient for the forward reaction. The stoichiometry of (12.9) implies that $\rho_s + \rho_w = \rho_0$, where ρ_0 is the total substrate concentration, i.e., free plus bound substrate. The rate term can then be written as

$$G(\rho_u, \rho_w) = k_f(\rho_0 - \rho_w)\rho_u - k_r\rho_w. \tag{12.12}$$

If the equilibrium (12.9) is fast, we can eliminate ρ_w by setting its time derivative equal to zero and obtain

$$\rho_{w,eq} = \frac{k_f\rho_0\rho_u}{k_r + k_f\rho_u}. \tag{12.13}$$

Proceeding similarly as in Sect. 1.4.9, we add (12.10a) and (12.10c), substitute (12.13) into the resulting equation, and find that the scale factor σ is given by $\sigma = 1 + k_f\rho_0/k_r$. If ρ_s is to remain constant, $\rho_s \approx \rho_0$, then $\rho_{w,eq}$ must be small or

$$k_r \gg k_f\rho_u. \tag{12.14}$$

To obtain a decrease in the effective diffusion coefficient of the activator, $1/\sigma$, the complexation reaction must satisfy

$$k_f\rho_0/k_r > 1. \tag{12.15}$$

The time scale requirements amount to

$$k_f\rho_u \ll k_r < k_f\rho_0 \tag{12.16}$$

or

$$\tau_s \gg \tau_b > \tau_u. \tag{12.17}$$

Here $\tau_u = 1/k_f\rho_0$ is the time scale on which the activator is bound to the substrate, $\tau_b = 1/k_r$ the time scale on which the activator–substrate complex dissociates, and $\tau_s = 1/k_f\rho_u$ the time scale of substrate consumption, the time scale on which significant numbers of binding sites are used. The results show that the activator diffusion coefficient can be rescaled, if the dissociation time τ_b is much smaller than the substrate consumption time τ_s.

Pearson has analyzed the effect of an immobile species on the Turing instability in two-variable activator–inhibitor systems for more general conditions [346]. Consider the "2+1" species system described by the following reaction–diffusion equations:

$$\frac{\partial \rho_u(x, t)}{\partial t} = F_1(\rho_u, \rho_v) - G(\rho_u, \rho_w) + \frac{\partial^2 \rho_u}{\partial x^2}, \tag{12.18a}$$

$$\frac{\partial \rho_v(x, t)}{\partial t} = F_2(\rho_u, \rho_v) + d\frac{\partial^2 \rho_v}{\partial x^2}, \tag{12.18b}$$

$$\frac{\partial \rho_w(x, t)}{\partial t} = G(\rho_u, \rho_w). \tag{12.18c}$$

In the derivation of the LE model and above, we assumed that the complexation reaction obeys mass-action kinetics. That assumption is not needed here, and we consider a general form for the rate term $G(\rho_u, \rho_w)$. We postulate only that there exists a steady state $\overline{\rho}_w$, i.e., $G(\overline{\rho}_u, \overline{\rho}_w) = 0$, such that

$$\frac{\partial G(\rho_u, \rho_w)}{\partial \rho_u}(\overline{\rho}_u, \overline{\rho}_w) \equiv \bar{G}_u > 0, \quad \frac{\partial G(\rho_u, \rho_w)}{\partial \rho_w}(\overline{\rho}_u, \overline{\rho}_w) \equiv \bar{G}_w < 0. \tag{12.19}$$

The inequalities (12.19) are satisfied if (12.9) obeys simple mass-action kinetics. As is easily verified from (12.12) with (12.13), in that case

$$\bar{G}_u = \frac{k_f k_r \rho_0}{k_r + k_f \overline{\rho}_u} > 0, \quad \bar{G}_w = -k_r < 0. \tag{12.20}$$

System (12.18) possesses a uniform steady state $(\overline{\rho}_u(x), \overline{\rho}_v(x), \overline{\rho}_w(x)) = (\overline{\rho}_u, \overline{\rho}_v, \overline{\rho}_w)$. To assess its stability, we carry out as usual a linear stability analysis:

$$\rho_u(x, t) = \overline{\rho}_u + u_0 \cos(kx) \exp(\lambda_k t), \tag{12.21a}$$
$$\rho_v(x, t) = \overline{\rho}_v + v_0 \cos(kx) \exp(\lambda_k t), \tag{12.21b}$$
$$\rho_w(x, t) = \overline{\rho}_w + w_0 \cos(kx) \exp(\lambda_k t). \tag{12.21c}$$

The "growth rates" λ_k of the kth spatial mode are given by the eigenvalues of the Jacobian

$$J_3(k^2) = \begin{pmatrix} J_{11} - \bar{G}_u - k^2 & J_{12} & -\bar{G}_w \\ J_{21} & J_{22} - dk^2 & 0 \\ \bar{G}_u & 0 & \bar{G}_w \end{pmatrix}, \tag{12.22}$$

where $\mathbf{J} = (J_{ij})$ is the Jacobian of (12.7). Recall that a Turing instability occurs if a real eigenvalue λ_k with $k = k_T \neq 0$ goes through zero, while the $k = 0$ mode remains stable. The eigenvalues of the wavenumber zero mode are the roots of the characteristic polynomial

$$-\det(J_3(0) - \lambda_0 I_3) = \lambda_0^3 + c_1 \lambda_0^2 + c_2 \lambda_0 + c_3 = 0. \tag{12.23}$$

According to the Routh–Hurwitz Theorem 1.2, all roots of (12.23) have a negative real part if

$$\Delta_1 = c_1 > 0, \tag{12.24a}$$

$$\Delta_2 = c_1 c_2 - c_3 > 0, \tag{12.24b}$$

$$\Delta_3 = c_3 \left(c_1 c_2 - c_3 \right) > 0, \tag{12.24c}$$

$$c_3 > 0. \tag{12.24d}$$

Note that the inequality (12.24c) is satisfied if inequalities (12.24b) and (12.24d) are satisfied. The stability conditions for the wave number zero mode therefore read

$$c_1 = -T_3 > 0, \tag{12.25a}$$

$$c_3 = -\Delta_0 > 0, \tag{12.25b}$$

$$\Delta_2 = -T_3 \left(\bar{G}_{\mathrm{w}} T + \Delta - \bar{G}_{\mathrm{u}} J_{22} \right) + \Delta_0 > 0. \tag{12.25c}$$

Here $T_3 = \operatorname{tr} \mathsf{J}_3(0)$, $\Delta_0 = \det \mathsf{J}_3(0) = \bar{G}_{\mathrm{w}} \Delta$, $T = \operatorname{tr} \mathsf{J}$, and $\Delta = \det \mathsf{J}$.

A Turing instability corresponds to a degenerate root of $\det(\mathsf{J}_3(k^2)) \equiv \Delta(K) = 0$ ($K = k^2$):

$$\Delta(K) = \bar{G}_{\mathrm{w}} \left[dK^2 - \left(dJ_{11} + J_{22} \right) K + \Delta \right] = 0. \tag{12.26}$$

Note that $\Delta(K)$ does not depend on $\bar{G}_{\mathrm{u}}$ and that $\bar{G}_{\mathrm{w}}$ factors out; the complexation reaction has no effect on the Turing condition. The (2+1)-variable activator–inhibitor–substrate system has the same Turing threshold as the two-variable activator–inhibitor system without substrate. Equation (10.32),

$$dJ_{11} + J_{22} > 0, \tag{12.27}$$

is a necessary condition for a Turing bifurcation. The stable uniform steady state of the (2+1) system undergoes a Turing bifurcation for parameter values of the system such that (10.40) is satisfied, i.e.,

$$(dJ_{11} + J_{22})^2 = 4d\Delta, \tag{12.28}$$

provided the stability conditions (12.25) for the wave number zero mode are satisfied. The critical wavenumber is given by (10.42):

$$k_{\mathrm{T},3}^2 = \sqrt{\frac{\Delta}{d}}. \tag{12.29}$$

To understand the precise role of the substrate and the complexation reaction, consider the case $d = 1$, the case most unfavorable for a Turing bifurcation in

an activator–inhibitor system without substrate. Then the Turing condition (12.28) reads

$$T^2 = 4\Delta. \tag{12.30}$$

Equation (12.30) implies that when the full activator–inhibitor–substrate system is at the point of a Turing bifurcation, the corresponding well-stirred activator–inhibitor system without substrate is, in the generic case, at a transition from an unstable focus to an unstable node, see Fig. 1.1. (In the nongeneric case, the activator–inhibitor system without substrate is at a double-zero bifurcation point.) In other words, the wavenumber zero mode of the system would already be unstable in the absence of the substrate when the Turing bifurcation occurs. The uniform steady state would have undergone an instability to uniform oscillations before the stationary instability to Turing patterns occurs. In conclusion, the complexation reaction does not change the Turing threshold. Its only role is to ensure that the wavenumber zero mode is stable, i.e., the stability conditions (12.25) are satisfied. Conditions (12.19) ensure that the first condition (12.25a)

$$T_3 = J_{11} + J_{22} - \bar{G}_u + \bar{G}_w < 0 \tag{12.31}$$

is satisfied if the complexation reaction is sufficiently rapid. This is a less restrictive condition than the time scale requirement (12.17). The second stability condition (12.25b)

$$\Delta_0 = \bar{G}_w \Delta < 0 \tag{12.32}$$

is satisfied, since $\bar{G}_w < 0$ according to (12.19) and $\Delta > 0$ according to (12.30). If the complexation reaction is sufficiently fast, such that the J_{ij} can be neglected compared to $\bar{G}_u$ and $\bar{G}_w$, then the third stability condition (12.25c) simplifies to

$$\bar{G}_w T - \bar{G}_u J_{22} > 0. \tag{12.33}$$

Since $T > 0$ according to (12.27), $\bar{G}_w < 0$, $\bar{G}_u > 0$, and $J_{22} < 0$ and since V is an inhibitor, this stability condition requires that

$$\left| \bar{G}_u J_{22} \right| > \left| \bar{G}_w T \right|. \tag{12.34}$$

Note that the third stability condition corresponds to $\Delta_2 > 0$. According to (1.38), the wavenumber zero mode of the activator–inhibitor–substrate system undergoes a Hopf bifurcation if Δ_2 goes through 0. For mass-action kinetics, (12.20) implies that $\bar{G}_u \propto \rho_0$. Consequently, the third stability condition can fail, if the total substrate is too low. Then the Turing bifurcation ceases to be the primary instability, and a uniform Hopf bifurcation occurs first in the full system.

   The results for the (2+1)-system can be extended to $N + Q$ systems with N mobile species reacting with Q immobile species, provided the presence of the

immobile species does not change the steady states of the mobile species [347]. The theory has also been extended to the case where the reactions with the complexing agents are rapid, but the latter are no longer immobile [420].

12.1.5 Turing Patterns in the BZ-AOT Reaction: Experiments

The experimental results and theoretical insights for the CDIMA reaction suggest a strategy for designing systems that display Turing patterns [247]. Start with an oscillating reaction and find a complexing agent that binds reversibly to the activator. As the concentration of the complexing agent is increased, a transition from oscillations to a steady state should occur, providing a guideline for the appropriate concentration of the substrate in a CFUR. De Kepper and coworkers have elaborated these ideas [211]. They designed an experimental method to find chemical systems that display stationary patterns based on three steps: (i) Look for autocatalytic reactions that display spatial bistability in one-sided CFURs. (ii) Look for reactions where the major negative feedback is performed by a species that is not involved in the activation pathway. (iii) Induce space-scale separation of the activation and inhibition processes via a low-mobility complexing agent. Using this strategy, De Kepper and coworkers found stationary pH patterns in the thiourea–iodate–sulfite reaction.

The best known oscillating reaction is the BZ reaction. Unfortunately, no appropriate complexing agent exists for bromous acid, $HBrO_2$, the activator in the BZ reaction [453]. The Brandeis group has pioneered an alternative strategy to achieve the difference in diffusion coefficients needed to generate Turing patterns [450, 449, 453]. They employed a microheterogeneous medium, namely a water-in-oil AOT microemulsion. The surfactant sodium bis(2-ethylhexyl) sulfosuccinate, commonly known as aerosol OT (AOT), contains a small polar group and two long fat tails. When combined with water and oil (e.g., octane used in experiments by the Brandeis group), AOT can form a reverse microemulsion phase, which consists of nanometer-sized water droplets surrounded by a monolayer of AOT in oil. The polar group of AOT is hydrophilic and points toward the water core of the droplet, while the nonpolar tails are hydrophobic and are directed out into the oil.

All the initial reagents of the BZ reaction are hydrophilic and migrate into the water core of the droplets. Diffusion within single droplets plays no role in the pattern-forming mechanism of the BZ-AOT system, because of the small size of the droplets. Highly polar species are essentially confined to the water core of the droplets. Their diffusion coefficient is determined by the diffusion coefficient of the water droplets D_d, if the volume fraction of the droplets ϕ_d is less than the percolation threshold ϕ_p (around 0.5) of the microemulsion. The value of D_d depends on the radius of the droplets and on ϕ_d and is about one to two order of magnitude smaller than the diffusion coefficient of small molecules in octane. Typical values for D_d are approximately 10^{-7} cm^2/s [449]. Efficient mass exchange between droplets occurs via the collision–fusion–fission of two droplets.

Less polar or nonpolar intermediates of the BZ reaction, such as Br_2 or BrO_2, are octane-soluble and diffuse in the oil phase as single molecules with diffusion coefficients on the order of 10^{-5} cm^2/s [449]. Consequently, the radical BrO_2, which serves as a second activator, and Br_2, which serves as a second inhibitor, diffuse much faster than the water-soluble BZ reactants. For low values of the volume fraction ϕ_d, the inhibitor Br_2 is the dominant species in the oil phase. Since it diffuses ten to hundred times faster than the activator $HBrO_2$, confined to the slow-diffusing droplets, conditions should be favorable for the observation of Turing patterns.

The Brandeis group uses a batch reactor for experiments with the BZ-AOT system, similar to the gel-free gradient-free experiments with the CDIMA reaction [250, 248]. The reactive microemulsion is sandwiched between two flat optical windows. The reaction volume is a closed cylinder of radius 10 mm and height 0.1 mm, and the experiments are conducted at room temperature. Batch reactors have the advantage that no concentration gradients of the reactants occur in the reactor, in contrast to a CFUR. Batch reactors have the disadvantage that the patterns cannot be truly stationary, because the reactants are consumed. In the CDIMA system, the patterns remain "stationary" for 10–30 min. The BZ-AOT system displays a large variety of spatial structures, such as Turing patterns, standing waves, wave packets, target patterns, spirals, antispirals, accelerating waves, dash waves, segmented spiral, localized Turing patterns, and oscillons [450–452, 449, 453]. Patterns typically emerge after a few minutes, and their lifetime is a few hours [449, 453]. Turing patterns are observed for low values of ϕ_d, i.e., when Br_2 is the dominant species in the oil phase. At larger values of ϕ_d, BrO_2 replaces Br_2 as the dominant species in the oil phase. Instead of a fast-diffusing inhibitor, the system contains a fast-diffusing activator under these conditions, and the dynamics is changed. The Turing bifurcation is replaced by a wave bifurcation, which gives rise to standing waves. These patterns oscillate in time, but they posses, like Turing patterns, an intrinsic wavelength and the nodal points remain fixed.

12.1.6 Turing Patterns in the BZ-AOT Reaction: Theory

Vanag and Epstein have formulated a four-variable model to understand pattern formation in the BZ-AOT system [449, 453]. Their model builds on the Oregonator, see Sect. 1.4.8. It assumes that the chemistry within the water core of the droplets is well described by the two-variable Oregonator rate equations (1.131). It further assumes that the species in the oil phase are "inert," since they lack reaction partners, the key reactants all being confined to the aqueous core of the droplets. Consequently, only transfer reactions occur for the activator BrO_2 and inhibitor Br_2 in the oil phase. The rate terms for the two transfer reactions are added to the rate terms of the two-variable Oregonator model. The reaction–diffusion equations of the four-variable model of the BZ-AOT system are given in nondimensionalized form by

$$\frac{\partial \rho_u}{\partial t} = \frac{1}{\epsilon} \left[\rho_u - \rho_u^2 - h\rho_v \frac{\rho_u - q}{\rho_u + q} - \beta\rho_u + \rho_w \right] + d_u \frac{\partial^2 \rho_u}{\partial x^2}, \qquad (12.35a)$$

$$\frac{\partial \rho_v}{\partial t} = \rho_u - \rho_v - \alpha\rho_v + \gamma\rho_z + d_v \frac{\partial^2 \rho_v}{\partial x^2}, \qquad (12.35b)$$

$$\frac{\partial \rho_w}{\partial t} = \frac{1}{\epsilon_2} \left(\beta\rho_u - \rho_w + \chi\rho_z \right) + d_w \frac{\partial^2 \rho_w}{\partial x^2}, \qquad (12.35c)$$

$$\frac{\partial \rho_z}{\partial t} = \frac{1}{\epsilon_3} \left(\alpha\rho_v - \gamma\rho_z \right) + \frac{\partial^2 \rho_z}{\partial x^2}. \qquad (12.35d)$$

Here U = HBrO$_2$, V is the oxidized form of the catalyst, W = BrO$_2$ in the oil phase, and Z = Br$_2$ in the oil phase. The parameters ϵ, ϵ_2, ϵ_3, α, β, γ, χ, and q depend on the rate constants, the bromate concentration, and the droplet volume fraction ϕ_d; h is an adjustable stoichiometric parameter and ϵ, $\epsilon_3 \ll 1$. The diffusion coefficients have been scaled such that $D_z = 1$. The fact that species diffuse much faster in the oil phase implies $d_u = d_v \ll d_w \approx 1$.

The four-variable reaction–diffusion system (12.35) possesses a nontrivial uniform steady state given by

$$(\overline{\rho}_u(x), \overline{\rho}_v(x), \overline{\rho}_w(x), \overline{\rho}_z(x)) = (\overline{\rho}_u, \overline{\rho}_v, \overline{\rho}_w, \overline{\rho}_z), \qquad (12.36)$$

where

$$\overline{\rho}_u = \frac{B}{2} + \sqrt{\frac{B^2}{4} + q\left(1 + h + \chi\frac{\alpha}{\gamma}\right)}, \qquad (12.37a)$$

$$B = 1 + \chi\frac{\alpha}{\gamma} - h - q, \qquad (12.37b)$$

$$\overline{\rho}_v = \overline{\rho}_u, \qquad (12.37c)$$

$$\overline{\rho}_w = \left(\beta + \chi\frac{\alpha}{\gamma}\right)\overline{\rho}_u, \qquad (12.37d)$$

$$\overline{\rho}_z = \frac{\alpha}{\gamma}\overline{\rho}_u. \qquad (12.37e)$$

To assess the stability of the uniform steady state (12.36), we carry out again a linear stability analysis:

$$\rho_u(x, t) = \overline{\rho}_u + u_0 \cos(kx) \exp(\lambda_k t), \qquad (12.38a)$$
$$\rho_v(x, t) = \overline{\rho}_v + v_0 \cos(kx) \exp(\lambda_k t), \qquad (12.38b)$$
$$\rho_w(x, t) = \overline{\rho}_w + w_0 \cos(kx) \exp(\lambda_k t), \qquad (12.38c)$$
$$\rho_z(x, t) = \overline{\rho}_z + z_0 \cos(kx) \exp(\lambda_k t). \qquad (12.38d)$$

The "growth rates" λ_k of the kth spatial mode are given by the eigenvalues of the Jacobian ($K = k^2$)

$$
J(K) = \begin{pmatrix}
\frac{1}{\epsilon} A - d_u K & \frac{1}{\epsilon} \frac{h(q - \overline{\rho}_u)}{\overline{\rho}_u + q} & \frac{1}{\epsilon} & 0 \\
1 & -(1 + \alpha) - d_v K & 0 & \gamma \\
\frac{\beta}{\epsilon_2} & 0 & -\frac{1}{\epsilon_2} - d_w K & \frac{\chi}{\epsilon_2} \\
0 & \frac{\alpha}{\epsilon_3} & 0 & -\frac{\gamma}{\epsilon_3} - K
\end{pmatrix}, \tag{12.39}
$$

where

$$
A = 1 - \beta - 2\overline{\rho}_u - \frac{2hq\overline{\rho}_v}{(\overline{\rho}_u + q)^2}. \tag{12.40}
$$

To determine the stability of the kth mode, we conduct a Routh–Hurwitz analysis. All eigenvalues λ_k have a negative real part, if

$$
\Delta_1(K) = c_1(K) > 0, \tag{12.41a}
$$
$$
\Delta_2(K) = c_1(K)c_2(K) - c_3(K) > 0, \tag{12.41b}
$$
$$
\Delta_3(K) = c_1(K)c_2(K)c_3(K) - c_3(K)^2 - c_1(K)^2 c_4(K) > 0, \tag{12.41c}
$$
$$
c_4(K) = \det J(K) > 0. \tag{12.41d}
$$

The coefficients $c_i(K)$ of the characteristic polynomial $\det[J(k^2) - \lambda_k I_4] = 0$ and the Hurwitz determinants $\Delta_i(K)$ are easily obtained using computational algebra software such as MATHEMATICA (Wolfram Research, Inc., Champaign, IL) or MAPLE (Waterloo Maple Inc., Waterloo, Ontario). The kth mode undergoes a stationary bifurcation when condition (12.41d) is violated, namely $c_4(K) = 0$, as discussed in Sect. 1.2.3, see (1.36). In other words, a Turing bifurcation of the uniform steady state corresponds to $c_4(k_T^2) = 0$ with $k_T \neq 0$, while the stability conditions (12.41) are satisfied for all other modes with $k \neq k_T$. The kth mode undergoes an oscillatory bifurcation when condition (12.41c) is violated, namely $\Delta_3(K) = 0$, as discussed in Sect. 1.2.3, see (1.38). A wave bifurcation of the uniform steady state corresponds to $\Delta_3(k_W^2) = 0$ with $k_W \neq 0$, while the stability conditions (12.41) are satisfied for all other modes with $k \neq k_W$. As discussed in Sect. 10.1.2, see (10.29), a wave bifurcation cannot occur in a two-variable reaction–diffusion system.

Given the lengthy expressions for $c_i(K)$ and $\Delta_i(K)$, an exact general derivation of the Turing bifurcation and wave bifurcation thresholds is neither desirable nor analytically feasible for the latter, even with the help of symbolic computation software. Vanag and Epstein have carried out numerical evaluations of the eigenvalues

λ_k to obtain dispersion curves. They find that the four-variable model displays both Turing and wave bifurcations.

12.2 Turing Mechanism in Biological Pattern Formation

While the Turing instability has been observed in both the CIMA/CDIMA reaction and the BZ reaction, a definitive proof of a Turing mechanism in biological pattern formations is still lacking. An early favorite among model builders for the action of a diffusion-driven instability was the formation of the striped pattern of the pair-rule genes in the early *Drosophila* embryo. Unfortunately, a considerable amount of experimental evidence rules out a Turing instability as the origin of the striped pattern [3]. The main problem of validating Turing's idea in biological systems lies in the difficulties of identifying morphogens. During the last decade, progress has been made in this direction, and several strong candidates for a LALI reaction–diffusion mechanism have emerged, for example, TGF-β as the activator and an unknown inhibitor in limb bud morphogenesis [301]. While TGF-β is a strong candidate for the activator in a reaction–diffusion mechanism, it has been impossible so far to pin down the molecular identity of the inhibitor. Therefore Newman and Bhat consider an alternative to a diffusible inhibitor morphogen [319]. They propose that lateral inhibition is provided by local Notch-Delta juxtacrine signaling, followed by synchronization of a Notch-activated oscillatory state. It is the latter that converts the short-range juxtacrine signaling into long-range inhibition. The most compelling experimental evidence for a Turing morphogen system, a LALI reaction–diffusion system, has been found in the hair-follicle patterning and the left–right axis formation in mouse embryos. We briefly discuss these two systems below.

12.2.1 Hair-Follicle Patterning

Hair follicles form regular patterns, consisting of large primary follicles, which develop first, interspersed with smaller secondary follicles, which develop at a later stage. An explanation in terms of a Turing mechanism was first suggested by Nagorcka and Mooney [312, 313, 311]. The morphogens in their models were, however, entirely hypothetical, given that molecular biology had not yet identified the key players in the formation of epidermal appendages at that time. Sick et al. have studied hair-follicle patterning in developing murine skin [412]. They identified the proteins WNT and DKK as the primary determinants in this process. The WNT pathway is active from the earliest stages of follicular development, and WNT signaling is essential for the induction of hair and feather follicles. WNT plays the role of an activator; WNT receptor binding leads to the production of itself and DKK, which inhibits WNT. Both proteins are secreted into the extracellular space where they diffuse. Values for the diffusion coefficients are not available, but WNT proteins are about 20–60% larger than DKK proteins [412, supporting online

material]. Consequently, the activator WNT is expected to diffuse more slowly than the inhibitor DKK. The authors adopt a modified Gierer–Meinhardt system, see Sect. 1.4.6, to model the role of WNT and DKK in hair-follicle patterning:

$$\frac{\partial \rho_{\mathrm{u}}}{\partial t} = a_{\mathrm{u}} F(\rho_{\mathrm{u}}, \rho_{\mathrm{v}}) - b_{\mathrm{u}} \rho_{\mathrm{u}} + D_{\mathrm{u}} \nabla^2 \rho_{\mathrm{u}}, \tag{12.42a}$$

$$\frac{\partial \rho_{\mathrm{v}}}{\partial t} = a_{\mathrm{v}} F(\rho_{\mathrm{u}}, \rho_{\mathrm{v}}) - b_{\mathrm{v}} \rho_{\mathrm{v}} + D_{\mathrm{v}} \nabla^2 \rho_{\mathrm{v}}, \tag{12.42b}$$

where U = WNT and V = DKK. Since WNT binding leads to the production of both the activator and inhibitor, Sick et al. chose the production term F to be the same in both equations. The antagonistic action of DKK on WNT takes place at a particular receptor and is modeled by noncompetitive inhibition. Including a saturation term in F leads to the following form:

$$F(\rho_{\mathrm{u}}, \rho_{\mathrm{v}}) = \frac{\rho_{\mathrm{u}}^2}{(K_{\mathrm{v}} + \rho_{\mathrm{v}})\left(1 + c\rho_{\mathrm{u}}^2\right)}. \tag{12.43}$$

Equations (12.42) with (12.43) were integrated numerically on a square grid with no-flux boundary conditions, using the solver `d03rafe` from the NAG library, with $D_{\mathrm{u}} = 0.005$, $D_{\mathrm{v}} = 0.2$, $a_{\mathrm{u}} = 0.005$, $a_{\mathrm{v}} = 0.02$, $b_{\mathrm{u}} = 0.005$, $b_{\mathrm{v}} = 0.015$, $K_{\mathrm{v}} = 0.1$, and $c = 0.01$. These parameter values are arbitrary and not based on experimentally measured quantities. However, the authors found the system to be robust to parameter variations, and the qualitative behavior of the reaction–diffusion system is not affected by the actual parameter values. The initial conditions were randomly distributed around the uniform steady state values according to a Gaussian distribution. To model consecutive waves of follicle formation, the spots from the first simulation were fixed by adding a constant activator and inhibitor production at locations where the activator concentration ρ_{u} exceeds a threshold of 2. To account for embryo growth, the size of the system was doubled for the simulation of the second wave by stretching the coordinates.

The simulations predict that strong overexpression of the activator disrupts the patterning process, while moderate overexpression increases follicular density during the first or subsequent waves. Moderate overexpression of the inhibitor during the initial wave increases the spacing between follicles. During the secondary wave, increased expression of the inhibitor impedes the development of secondary follicles. The authors corroborated the predictions of their activator–inhibitor model in vivo using transgenic mice in which the expression of the gene *Dkk* is controlled by a promoter. The experimental confirmation of the theoretical predictions provides strong circumstantial evidence that "WNT and DKK determine hair-follicle spacing through a reaction-diffusion mechanism," to quote the title of the article by Sick et al. More experimental work is, however, necessary to elucidate further molecular details of the WNT–DKK interactions and to measure key parameters of

the system, such as diffusion coefficients, rates constants, in order to establish definitively that hair-follicle patterning does indeed occur via a Turing system [262, 419].

12.2.2 Left–Right Asymmetry in the Mouse Embryo

The vertebrate body plan has three axes: anterior–posterior (A-P), dorsal–ventral (D-V), and left–right (L-R) axes. The left–right asymmetry is established last [430]. Structures established by the formation of the A-P and D-V axes lead to a small initial breaking of the left–right symmetry. For example, in the mouse embryo, cilia protrude from cells located on the ventral side of the node. They rotate clockwise, viewed from the ventral side, and generate a leftward flow of the extraembryonic fluid in the node cavity, the so-called nodal flow [385]. The nodal flow leads to a small enhancement of the expression of *Nodal* on the left side. Though Nodal is a left-side determinant, experimental data suggest that the initial symmetry breaking due to the nodal flow, or other mechanisms in other vertebrates, alone does not generate a robust asymmetry [315, 429]. Nakamura and coworkers have provided compelling evidence that in the mouse embryo an activator–inhibitor reaction–diffusion system plays the key role in the formation of the L-R axis. The two morphogens involved are Nodal and Lefty. *Nodal*-related genes activate their own expression and Nodal signaling also promotes production of Lefty, which acts as a feedback inhibitor of Nodal activity [417, 315, 429]. Both Nodal and Lefty proteins move over long distances through tissues, but Lefty diffuses faster [417]. Nodal and Lefty fulfill Turing's requirement of local self-activation and long-range inhibition. Nakamura et al. have formulated a Nodal–Lefty reaction–diffusion model [315, supplemental data]:

$$\frac{\partial \rho_u}{\partial t} = F_1(z) - q_u \rho_u + D_u \frac{\partial^2 \rho_u}{\partial x^2} + E(x, t), \tag{12.44a}$$

$$\frac{\partial \rho_v}{\partial t} = F_2(z) - q_v \rho_v + D_v \frac{\partial^2 \rho_v}{\partial x^2}, \tag{12.44b}$$

where ρ_u and ρ_v denote the levels of Nodal and Lefty, respectively. The level of the net induction signal is given by

$$z = p_u \rho_u - p_v \rho_v. \tag{12.45}$$

The synthesis rates of Nodal and Lefty are given by $F_i(z)$; they are increasing functions of z, and thus increasing functions of ρ_u and decreasing functions of ρ_v. The rates are further assumed to be switching functions of z, i.e., $F_i(z)$ is close to 0 for z small, increases rapidly for z near the threshold value, and saturates for z large. The threshold values $z = T_u$ and $z = T_v$ are sufficiently large relative to the

degradation rates q_u and q_v. They are close in value, but experimental data indicate that $T_u < T_v$. For their numerical simulations, Nakamura and coworkers chose the following expressions for the synthesis rates $F_i(z)$:

$$F_1(z) = \frac{s_u}{1 + \exp\left[-\lambda_u\left(p_u\rho_u - p_v\rho_v - T_u\right)\right]}, \tag{12.46a}$$

$$F_2(z) = \frac{s_v}{1 + \exp\left[-\lambda_v\left(p_u\rho_u - p_v\rho_v - T_v\right)\right]}. \tag{12.46b}$$

The term $E(x, t)$ takes into account the small initial symmetry breaking due to the nodal flow. For all numerical simulations, the values of the various parameters are chosen such that the model without diffusion and nodal flow term shows "signal-dependent amplification." If the initial level of Nodal is large enough, the levels of both Nodal and Lefty increase transiently and then decrease and converge to zero. If the initial level of Nodal is small enough, the levels of both Nodal and Lefty converge to zero without a transient increase [315]. The model displays signal-dependent amplification, if q_u is sufficiently larger than q_v, and the Nodal self-activation rate is larger than its Lefty-mediated inhibition rate. The numerical values of the parameters are adjusted within these ranges to account for various mutant phenotypes. The model satisfactorily simulates experimental data on the expression patterns of *Nodal* and *Lefty* in various L-R mutants. Moreover, it provides an explanation for certain unexpected mutants, which are otherwise difficult to understand [315].

Exercises

12.1 Explore the spatial stability of the uniform steady state of a Brusselator RD system with a second fast-diffusing activator,

$$\frac{\partial \rho_u}{\partial t} = a - (b + 1)\rho_u + \rho_u^2\rho_v - c_1\rho_u + c_2\rho_w + d\frac{\partial^2 \rho_u}{\partial x^2}, \tag{12.47a}$$

$$\frac{\partial \rho_v}{\partial t} = b\rho_u - \rho_u^2\rho_v + d\frac{\partial^2 \rho_v}{\partial x^2}, \tag{12.47b}$$

$$\frac{\partial \rho_w}{\partial t} = c_1\rho_u - c_2\rho_w + D\frac{\partial^2 \rho_w}{\partial x^2}, \tag{12.47c}$$

with $D \gg d$.

12.2 Explore the spatial stability of the uniform steady state of a Brusselator RD system with a second fast-diffusing inhibitor,

$$\frac{\partial \rho_u}{\partial t} = a - (b+1)\rho_u + \rho_u^2 \rho_v + d\frac{\partial^2 \rho_u}{\partial x^2}, \tag{12.48a}$$

$$\frac{\partial \rho_v}{\partial t} = b\rho_u - \rho_u^2 \rho_v - c_1\rho_v + c_2\rho_w + d\frac{\partial^2 \rho_v}{\partial x^2}, \tag{12.48b}$$

$$\frac{\partial \rho_w}{\partial t} = c_1\rho_v - c_2\rho_w + D\frac{\partial^2 \rho_w}{\partial x^2}, \tag{12.48c}$$

with $D \gg d$.

12.3 Investigate the Turing instability of the hair-follicle patterning system (12.42).

12.4 Investigate the Turing instability of the Nodal–Lefty RD model (12.44) with $E(x, t) \equiv 0$.

12.5 Investigate the Turing instability of the following RD system:

$$\frac{\partial \rho_u}{\partial t} = a\frac{\rho_u^2 \rho_v}{1 + \kappa \rho_u^2} - e\rho_u + D_u\frac{\partial^2 \rho_u}{\partial x^2}, \tag{12.49a}$$

$$\frac{\partial \rho_v}{\partial t} = -b\frac{\rho_u^2 \rho_v}{1 + \kappa \rho_u^2} + c + D_v\frac{\partial^2 \rho_v}{\partial x^2}, \tag{12.49b}$$

which has been used to model the pattern on wings of ladybugs (*Coccinellidae*). Here a, b, c, e, and κ are nonnegative constants.

Chapter 13
Pattern Formation in Spatially Discrete Systems

The preceding chapters have dealt with the spatiotemporal behavior of spatially continuous systems. We now turn our attention to the dynamical behavior and stability properties of spatially discrete systems. A wide variety of phenomena in chemistry, biology, physics, and other fields involve the coupling between nonlinear, discrete units. Examples include arrays of Josephson junctions, chains of coupled diode resonators, coupled chemical or biochemical reactors, myelinated nerve fibers, neuronal networks, and patchy ecosystems. Such networks of coupled nonlinear units often combine dynamical and structural complexity [422]. Cells in living tissues, for example, are arranged in a variety of geometries. One-dimensional rings of cells were already considered by Turing [440]. Other types of lattices, such as open-ended linear arrays, tubes, rectangular and hexagonal arrays, and irregular arrangements in two or three dimensions are also found, see for example [5]. Cells interact with adjacent cells in various distinct ways. For example, signaling between cells may occur via diffusion through gap junctions [352, 230] or by membrane-bound proteins, juxtacrine signaling [339, 340, 471].

In specific applications, the number of discrete units involved can be quite large. However, insight into the dynamical behavior of coupled nonlinear elements can be gained already from the study of small arrays, consisting of as little as two units. The study of two coupled continuous-flow stirred tank reactors (CSTRs) has a history of more than 30 yr and has had considerable theoretical and practical impact, see for example [269, 145, 314, 423, 27, 54, 84, 83, 28, 245, 473, 97, 99, 202, 234, 488, 244, 198, 197, 499, 496]. In most studies, the reactors are coupled via passive diffusion-like mass transfer, though some have considered electrical coupling [84, 197, 198] and flow rate coupling [473, 202, 488]. Most theoretical and experimental investigations of coupled CSTRs have focused on coupled chemical oscillators, and many different types of dynamical behavior were observed. A few studies have considered the effect of coupled steady-state reactors. To study the relative stability of two steady states in a bistable system, Stuchl and Marek carried out a series of mixing experiments on two identical CSTRs with different steady states to determine the relative stability of the steady states [423]. Boukalouch and coworkers found that coupling two steady-state reactors, whose feed concentrations differ, may induce oscillations [54]. Laplante and Erneux considered the case of

bistable reactions. Specifically, they investigated propagation failure in a linear array of 16 cells [242, 241] and the coexistence of nonuniform steady states in linear and circular 16-cell arrays [241, 52].

The earliest studies of coupled chemical cells were theoretical investigations and focused on the diffusion-induced instability to nonuniform steady states [354, 443] in two coupled reactors. More recently, Epstein and Golubitsky investigated the Turing instability in linear and circular arrays of Brusselators [109]. Their approach makes use of underlying symmetry groups.

This chapter focuses on the stability properties of networks or arrays of coupled monostable units or cells. We consider two types of coupling, namely diffusive coupling and photochemical coupling. The two main concerns are how the topology of the network connectivity and how spatial inhomogeneities in the array affect instabilities. Spatially discrete systems or networks of coupled cells are described by sets of ordinary differential equations. Methods to determine the stability of stationary states of ODEs are well developed.

13.1　Linear Stability Analysis

For the sake of simplicity, we adopt the terminology of chemical kinetics in the following and use the term "reactor" instead of the general, but lengthy, term "discrete, nonlinear unit." We consider networks of coupled reactors such that the reactions in each reactor are the same and the dynamics is governed by

$$\frac{\mathrm{d}\boldsymbol{\rho}}{\mathrm{d}t} = \mathbf{F}(\boldsymbol{\rho}, \boldsymbol{\mu}), \tag{13.1}$$

where $\boldsymbol{\rho} \in \mathbb{R}^k$ and $\mathbf{F} : \mathbb{R}^k \to \mathbb{R}^k$. We assume that $\mathbf{F}$ depends on some fixed set of parameters $\boldsymbol{\mu}$ and that (13.1) has a steady state $\overline{\boldsymbol{\rho}}(\boldsymbol{\mu})$, i.e., $\mathbf{F}(\overline{\boldsymbol{\rho}}(\boldsymbol{\mu}), \boldsymbol{\mu}) = 0$. Networks of reactors can be described by graphs where the nodes correspond to the individual reactors and the edges represent connections between them. The graph $\mathcal{G}$, corresponding to a network of n reactors, has n nodes, $v_1, \ldots, v_n$, and (v_i, v_j), $i \neq j$, is an edge of $\mathcal{G}$ if and only if reactor i is coupled to reactor j. The sets of nodes and edges of $\mathcal{G}$ are denoted by $\mathcal{N}_{\mathcal{G}}$ and $\mathcal{E}_{\mathcal{G}}$, respectively. We assume in the following that $\mathcal{G}$ is connected and that the coupling is symmetric, i.e., $\mathcal{G}$ is a simple graph. The dynamics of the network is described by the set of ordinary differential equations

$$\frac{\mathrm{d}\boldsymbol{\rho}_i}{\mathrm{d}t} = \mathbf{F}(\boldsymbol{\rho}_i, \boldsymbol{\mu}_i) + \mathbf{G}_{\mathcal{G},i}(\boldsymbol{\rho}_1, \ldots, \boldsymbol{\rho}_n, \boldsymbol{\kappa}), \quad i = 1, \ldots, n. \tag{13.2}$$

The first term on the right-hand side describes the internal dynamics of each reactor. We allow for the possibility that the network is inhomogeneous, i.e., the set of parameters $\boldsymbol{\mu}$ can differ from reactor to reactor though the kinetic rate functions are identical for all reactors. The second term describes the dynamics due to the

coupling between reactors via the topology described by the graph $\mathcal{G}$, and κ is a set of parameters that characterizes the coupling between pairs of reactors. If the reactors are coupled by passive mass diffusion, then the coupling term is given by

$$\mathbf{G}_{\mathcal{G},i}(\boldsymbol{\rho}_1, \ldots, \boldsymbol{\rho}_n, \boldsymbol{\kappa}) = \sum_{j=1}^{n} a_{ij} \mathsf{D}(\boldsymbol{\rho}_j - \boldsymbol{\rho}_i), \quad i = 1, \ldots, n, \tag{13.3}$$

where $a_{ii} = 0$, a_{ij} can be either 0 or 1 for $i \neq j$ and $a_{ij} = a_{ji}$. The latter case, $a_{ij} = 1$, holds if and only if (v_i, v_j), $i \neq j$, is an edge of $\mathcal{G}$. The matrix D satisfies $\mathsf{D} = \kappa \operatorname{diag}(D_{11}, \ldots, D_{kk})$, where $\kappa > 0$, $D_{ll} > 0$, and $l = 1, \ldots, k$. The constant κ represents the coupling strength between reactors. Equations (13.2) and (13.3) can be rewritten as

$$\frac{d\boldsymbol{\rho}_i}{dt} = \mathbf{F}(\boldsymbol{\rho}_i, \boldsymbol{\mu}_i) + \sum_{j=1}^{n} L_{ij} \mathsf{D} \boldsymbol{\rho}_j, \quad i = 1, \ldots, n, \tag{13.4}$$

where $L_{ij} = a_{ij}$, $i \neq j$, and

$$L_{ii} = -\left(\sum_{j=1}^{i-1} a_{ij} + \sum_{j=i+1}^{n} a_{ij} \right), \quad i = 1, \ldots, n. \tag{13.5}$$

The corresponding matrix L is symmetric and is referred to as the Laplacian matrix of the graph $\mathcal{G}$. Note that some authors define the Laplacian to be the negative of our definition. The degree, or number of neighbors, of node i is $k_i = -L_{ii}$.

13.1.1 Routh–Hurwitz Analysis

It is convenient to rewrite (13.2) in the following compact form:

$$\frac{d\boldsymbol{\sigma}}{dt} = \mathbf{F}_{\mathcal{G}}(\boldsymbol{\sigma}), \tag{13.6}$$

with $\boldsymbol{\sigma} = (\rho_{1,1}, \rho_{2,1}, \ldots, \rho_{k,1}, \ldots, \rho_{1,n}, \ldots, \rho_{k,n})^T$. Let $\bar{\boldsymbol{\sigma}}$ be a stationary state of (13.6), i.e., $\mathbf{F}_{\mathcal{G}}(\bar{\boldsymbol{\sigma}}) = 0$. As discussed in Sect. 1.2, the stability of this steady state is given by the eigenvalues of the $m \times m$ Jacobian matrix $(m = kn)$

$$\mathsf{J}_{\mathcal{G}} = \left. \frac{\partial \mathbf{F}_{\mathcal{G}}}{\partial \boldsymbol{\sigma}} \right|_{\bar{\boldsymbol{\sigma}}}, \tag{13.7}$$

which are roots of the mth order characteristic polynomial, $(-1)^m \det(\mathsf{J}_{\mathcal{G}} - \lambda \mathsf{I}_m) = 0$:

$$\lambda^m + c_1\lambda^{m-1} + c_2\lambda^{m-2} + \cdots + c_{m-1}\lambda + c_m = 0. \tag{13.8}$$

The stationary state of the network of reactors is stable, if all roots λ of (13.8) have a negative real part. The necessary and sufficient conditions for this to hold are the Routh–Hurwitz conditions, see Theorem 1.2. The stationary state of the network, $\overline{\sigma}$, undergoes a stationary instability if $c_m = 0$, see (1.36), and an oscillatory instability if $\Delta_{m-1} = 0$, together with $c_m > 0$, $\Delta_l > 0$, $l = 1, \ldots, m - 2$, see (1.38). The Routh–Hurwitz analysis can be used to determine, in principle, the stability properties of the steady state of any network, even *inhomogeneous* networks. This advantage is, however, balanced by the fact that it is a computationally expensive task to evaluate all the coefficients c_l of the characteristic polynomial and the Hurwitz determinants Δ_l. In our studies of instabilities in arrays of coupled reactors, we used symbolic computation software, namely MATHEMATICA (Wolfram Research, Inc., Champaign, IL, 2002) and MAPLE (Waterloo Maple Inc., Waterloo, Ontario, 2002), to obtain exact, analytical expressions for the coefficients c_l of the characteristic polynomial (13.8) and the Hurwitz determinants Δ_l for arrays of up to six coupled reactors.

13.1.2 Structural Mode Analysis

The application of the Routh–Hurwitz analysis or the direct calculation of the eigenvalues and eigenvectors of the Jacobian $\mathsf{J}_\mathcal{G}$ of the network of reactors is a formidable task for moderate and large arrays of coupled reactors. There is an alternative approach, a spectral analysis of networks, that works for any size array of coupled reactors, as long as the array is *homogeneous*, i.e., $\boldsymbol{\mu}_i = \boldsymbol{\mu}$ for all i, $i = 1, \ldots, n$, and the coupling is diffusive. In this case, the system (13.4) has a uniform steady state:

$$\overline{\boldsymbol{\rho}}_i(\boldsymbol{\mu}) = \overline{\boldsymbol{\rho}}(\boldsymbol{\mu}), \quad i = 1, \ldots, n. \tag{13.9}$$

In the following we suppress the explicit dependence of the stationary state on the set of parameters $\boldsymbol{\mu}$ and write $\overline{\boldsymbol{\rho}}(\boldsymbol{\mu}) = \overline{\boldsymbol{\rho}}$. The Jacobian $\mathsf{J}_\mathcal{G}$ is given by

$$\mathsf{J}_\mathcal{G} = \mathsf{I}_n \otimes \mathsf{J} + \mathsf{L} \otimes \mathsf{D}, \tag{13.10}$$

where J is the Jacobian matrix of a single reactor,

$$J_{lm} \equiv \frac{\partial F_l}{\partial \rho_m}(\overline{\boldsymbol{\rho}}), \quad 1 \le l, m \le k, \tag{13.11}$$

and $\otimes$ denotes the Kronecker product, see Appendix A.

As we saw in Sect. 10.1, the stability properties of the uniform steady state of spatially continuous reaction–diffusion systems can be analyzed in terms of normal modes corresponding to the eigenfunctions of the Laplace operator. Othmer and

Scriven [334] showed that the stability of spatially discrete homogeneous reaction–diffusion systems can be analyzed in terms of the structural modes of the network, i.e., the eigenvectors of the Laplacian matrix L. We have extended that approach [305], and the eigenvalues and eigenvectors of the matrix

$$\widehat{\mathsf{J}}(r) \equiv \mathsf{J} - r\mathsf{D}, \tag{13.12}$$

with $r \geq 0$, play an important role in our linear stability analysis of the uniform steady state $\overline{\rho}$ of the homogeneous network $\mathcal{G}$. Equation (13.12) implies that

$$\widehat{\mathsf{J}}(r_1 + r_2) = \widehat{\mathsf{J}}(r_1) - r_2\mathsf{D}. \tag{13.13}$$

For simplicity we assume throughout this chapter the generic case that $\widehat{\mathsf{J}}(r)$ has a complete set of eigenvectors for all appropriate values of r. We extend the definition (13.12) to $\widehat{\mathsf{J}}_{\mathcal{G}}$:

$$\widehat{\mathsf{J}}_{\mathcal{G}}(r) \equiv \mathsf{J}_{\mathcal{G}} - r\mathsf{I}_n \otimes \mathsf{D}. \tag{13.14}$$

For simple networks, it is possible to obtain a complete description of the eigenvalues and eigenvectors of $\mathsf{J}_{\mathcal{G}}$ [334]. These include linear and circular arrays. A network of n reactors is said to be a linear array if

$$\mathcal{E}_{\mathcal{G}} = \cup_{i=1}^{n-1}\{(v_i, v_{i+1})\}. \tag{13.15}$$

The eigenvalues of $\mathsf{J}_{\mathcal{G}}$, associated with a linear array, are given by the eigenvalues of

$$\widehat{\mathsf{J}}\left(2 - 2\cos\left(j\pi/n\right)\right), \quad j = 0, 1, \ldots, n - 1. \tag{13.16}$$

The associated eigenvectors are given by

$$\mathbf{z}^j = (\alpha_{j1}\overline{\mathbf{z}}, \ldots, \alpha_{jn}\overline{\mathbf{z}})^T, \tag{13.17}$$

where $\overline{\mathbf{z}}$ is the associated eigenvector of (13.16), and

$$\alpha_{jl} = \begin{cases} \sqrt{1/n}, & j = 0, \\ \left[\sin(\frac{\pi jl}{n}) - \sin(\frac{\pi j(l-1)}{n})\right]/\sqrt{2n}\sin(\frac{\pi j}{2n}), & j > 0, \end{cases} \quad l = 1, \ldots, n. \tag{13.18}$$

A network is said to be a circular array if

$$\mathcal{E}_{\mathcal{G}} = \cup_{i=1}^{n-1}\{(v_i, v_{i+1})\} \cup (v_1, v_n). \tag{13.19}$$

In this case the eigenvalues of J_G are given by the eigenvalues of

$$\widehat{J}\,(2 - 2\cos(2j\pi/n))\,, \quad j = 0, 1, \ldots, n-1. \tag{13.20}$$

The associated eigenvectors have the form (13.17) but with $\bar{z}$ the associated eigenvector of (13.20) and

$$\alpha_{jl} = \sqrt{\frac{1}{n}}\,\exp\left(\frac{2\mathrm{i}j(l-1)\pi}{n}\right)\,, \quad \mathrm{i} = \sqrt{-1}, \quad l = 1, \ldots, n. \tag{13.21}$$

The linear stability analysis of the homogeneous steady state $\bar{\rho}_i = \bar{\rho}$ of arbitrary, homogenous networks

$$\frac{\mathrm{d}\rho_i}{\mathrm{d}t} = \mathbf{F}(\rho_i, \boldsymbol{\mu}) + \sum_{j=1}^{n} L_{ij} \mathsf{D}\rho_j, \quad i = 1, \ldots, n, \tag{13.22}$$

is enormously simplified by the fact that finding the eigenvalues and eigenvectors of $J_G(r)$ is equivalent to finding the eigenvalues and eigenvectors of the matrices L and $\widehat{J}(r)$ for appropriate values of r. This leads to much simpler problems, since L is symmetric and $\widehat{J}(r)$ is a $k \times k$ matrix with, typically, $k \ll n$. The foundation of our spectral analysis approach is the following theorems [305].

Theorem 13.1 *Consider a network of n reactors represented by a graph $\mathcal{G}$. Then λ is an eigenvalue of $\widehat{J}_G(r)$, $\lambda \in \sigma(\widehat{J}_G(r))$, if and only if $\lambda \in \sigma(\widehat{J}(-\beta + r))$, where $\beta \in \sigma(\mathsf{L})$. The associated eigenvectors $\mathbf{z}$ have the form*

$$\mathbf{z} = (\alpha_1 \bar{z}, \ldots, \alpha_n \bar{z})^T, \tag{13.23}$$

where $\bar{z}$ is the associated eigenvector of $\widehat{J}(-\beta + r)$ and $(\alpha_1, \ldots, \alpha_n)^T$ is the associated eigenvector of L.

Remark 13.1 The Laplacian matrix L is symmetric and therefore has real eigenvalues,

$$\beta_1 \geq \beta_2 \geq \cdots \geq \beta_n, \tag{13.24}$$

and a complete set of orthonormal eigenvectors $(\alpha_1, \ldots, \alpha_n)^T$, the so-called structural modes of the network $\mathcal{G}$ [334].

Theorem 13.2 *Consider a network of n reactors represented by a graph $\mathcal{G}$ and let $\lambda \in \sigma(\widehat{J}(r))$, i.e., $\beta = 0$, with eigenvector $\bar{z}$. Then $\lambda \in \sigma(\widehat{J}_G(r))$ with eigenvector $\mathbf{z} = (\bar{z}, \ldots, \bar{z})^T$.*

The remaining eigenvalues of $J_G(r)$ are associated with spatially nonuniform eigenvectors, and those eigenvectors share an additional property which is stated in the next theorem.

Theorem 13.3 *Consider a network of n reactors represented by a graph $\mathcal{G}$ and let $\lambda \in \sigma\left(\widehat{\mathbf{J}}_{\mathcal{G}}(r)\right)$ with eigenvector $\mathbf{z} = (\mathbf{z_1}, \ldots, \mathbf{z}_n)^T$, $\mathbf{z_i} \in \mathbb{R}^k$. Then if $\lambda \notin \sigma\left(\widehat{\mathbf{J}}(r)\right)$,*

$$\sum_{i=1}^{n} \mathbf{z}_i = 0. \tag{13.25}$$

This theorem complements the previous one. Uniform eigenvectors belong to eigenvalues of $\widehat{\mathbf{J}}_{\mathcal{G}}(r)$ that are also eigenvalues of $\widehat{\mathbf{J}}(r)$, whereas the nonuniform eigenvectors occur for eigenvalues of $\widehat{\mathbf{J}}_{\mathcal{G}}(r)$ that are *not* eigenvalues of $\widehat{\mathbf{J}}(r)$.

In the light of Theorem 13.1, information about the eigenvalues and eigenvectors of the Laplacian matrix L of the network $\mathcal{G}$ is important for the spectral method of linear stability analysis. Laplacian matrices appear in a variety of other contexts, and a survey of known results about their spectrum can be found in [293]. The following four theorems provide additional information about the eigenvalues of L, and in light of Theorem 13.1, on the eigenvalues of $\widehat{\mathbf{J}}_{\mathcal{G}}(r)$. The eigenvalue β_2, referred to as the algebraic connectivity of the graph [128], plays a critical role in determining the largest value of κ for which a Turing instability is possible.

Theorem 13.4 *For a network of n reactors represented by a graph $\mathcal{G}$ the Laplacian matrix L is negative semidefinite. Moreover, $\beta_1 = 0$, and*

$$\beta_n \geq 2 \min_{1 \leq i \leq n} L_{ii}. \tag{13.26}$$

Remark 13.2 For a circular array of n reactors it follows from (13.20) that as $n \to \infty$,

$$\beta_n \to -4 = 2 \min_{1 \leq i \leq n} L_{ii}. \tag{13.27}$$

The following Theorem addresses the question of how the eigenvalues of the Laplacian matrix change, when connections between reactors are removed or added in the network. It turns out that the eigenvalues of the smaller and the bigger graph interlace in an orderly arrangement.

Theorem 13.5 *Consider a network of n reactors, $n > 2$, represented by a graph $\mathcal{G}$ with Laplacian matrix $\mathsf{L}_{\mathcal{G}}$. Let $\mathcal{G}'$ be a connected subgraph of $\mathcal{G}$ such that $\mathcal{N}_{\mathcal{G}'} = \mathcal{N}_{\mathcal{G}}$ and for some $(v_l, v_m) \in \mathcal{E}_{\mathcal{G}}$, $\mathcal{E}_{\mathcal{G}'} = \mathcal{E}_{\mathcal{G}} \setminus (v_l, v_m)$. If $\mathsf{L}_{\mathcal{G}'}$ is the corresponding Laplacian matrix of $\mathcal{G}'$ with eigenvalues $\beta_1' \geq \beta_2' \geq \cdots \geq \beta_n'$ then*

$$0 = \beta_1' = \beta_1 > \beta_2' \geq \beta_2 \geq \cdots \geq \beta_n' \geq \beta_n. \tag{13.28}$$

A bound on β_2 can be found in terms of n and the diameter of $\mathcal{G}$, $d_{\mathcal{G}}$. The diameter of a graph is the maximum distance between any two nodes in the graph. Since the graph is connected, the distance between any two nodes v and v' is the length of the shortest path between them.

Theorem 13.6 *Consider a network of n reactors represented by a graph $\mathcal{G}$ with Laplacian matrix L, then*

$$\beta_2 \leq -\frac{4}{d_{\mathcal{G}}n}. \tag{13.29}$$

The following theorem establishes that the number of reactors in the network provides a lower bound for the spectrum of the Laplacian matrix of the network.

Theorem 13.7 *Consider a network of n reactors represented by a graph $\mathcal{G}$ with Laplacian matrix L. Then*

$$\beta_n \geq -n. \tag{13.30}$$

This result and Theorem 13.5 imply that the eigenvalues β of the Laplacian matrix L associated with the structural modes of the network $\mathcal{G}$ lie between 0 and $-n$, $0 \geq \beta \geq -n$. This narrows the search for eigenvalues leading to instabilities of the uniform steady state of the network to eigenvalues of $\widehat{\mathsf{J}}(r)$ with $0 \leq r \leq n$, with $r = -\beta$.

Theorem 13.8 *Consider a network of n reactors represented by a graph $\mathcal{G}$. If $\lambda \in \sigma(\widehat{\mathsf{J}}_{\mathcal{G}})$, then $\lambda \in \sigma(\widehat{\mathsf{J}}(r))$ where $0 \leq r \leq n$.*

13.2 Instabilities in Diffusively Coupled Reactor Networks

We use the results of the previous section to analyze the stability of the uniform steady state of homogeneous arrays of diffusively coupled reactors, whose internal dynamics can be described by the concentration of two species U and V:

$$\frac{d\rho_{ui}}{dt} = F_1(\rho_{ui}, \rho_{vi}, \mu) + \kappa D_u \sum_{j=1}^{n} L_{ij}\rho_{uj}, \quad i = 1, \ldots, n, \tag{13.31a}$$

$$\frac{d\rho_{vi}}{dt} = F_2(\rho_{ui}, \rho_{vi}, \mu) + \kappa D_v \sum_{j=1}^{n} L_{ij}\rho_{vj}, \quad i = 1, \ldots, n. \tag{13.31b}$$

As above, the kinetic rate functions F_1 and F_2 depend on a set of parameters. We display only one explicitly, namely the bifurcation parameter μ. The steady state $(\bar{\rho}_u, \bar{\rho}_v)$ of an isolated reactor is given by

$$F_1(\bar{\rho}_u, \bar{\rho}_v, \mu) = F_2(\bar{\rho}_u, \bar{\rho}_v, \mu) = 0, \tag{13.32}$$

and we assume that this steady state is stable in an isolated reactor, i.e., the trace $T = \operatorname{tr}\mathsf{J}$ of the Jacobian at the steady state is negative and the determinant $\Delta = \det\mathsf{J}$ is positive, see Sect. 1.2.2:

$$T = \text{tr}\, \mathsf{J} = J_{11} + J_{22} < 0, \tag{13.33a}$$

$$\Delta = \det \mathsf{J} = J_{11} J_{22} - J_{12} J_{21} > 0. \tag{13.33b}$$

The homogeneous network of reactors (13.31) has a uniform steady state (USS):

$$\left(\overline{\rho}_{\text{u}i}, \overline{\rho}_{\text{v}i}\right) = \left(\overline{\rho}_{\text{u}}, \overline{\rho}_{\text{v}}\right), \quad i = 1, \ldots, n. \tag{13.34}$$

According to the results of the previous section, the stability of the USS is determined by the eigenvalues of the matrix $\widehat{\mathsf{J}}(r)$,

$$\widehat{\mathsf{J}}(r) = \mathsf{J} - r\kappa \begin{pmatrix} D_{\text{u}} & 0 \\ 0 & D_{\text{v}} \end{pmatrix}, \tag{13.35}$$

with $r = -\beta_i$, where $\beta_i \in \sigma(\mathsf{L})$ and $i = 1, \ldots, n$. The uniform structural mode of the network $\mathcal{G}$ has the eigenvalue $\beta_1 = 0$:

$$\widehat{\mathsf{J}}(0) = \mathsf{J}. \tag{13.36}$$

According to our assumptions (13.33), the USS of the network is stable against uniform spatial perturbations. To analyze the stability of the USS against spatially nonuniform perturbations, we need to examine two possibilities for the structural modes associated with $\beta_i < 0$, $i = 2, \ldots, n$: (i) Can a pair of complex conjugate eigenvalues cross the imaginary axis, i.e., $\text{tr}\, \widehat{\mathsf{J}}(r) = 0$, which corresponds to an oscillatory or Hopf bifurcation of the structural mode? (ii) Can a real eigenvalue of $\widehat{\mathsf{J}}(r)$ pass through zero, i.e., $\det \widehat{\mathsf{J}}(r) = 0$, which corresponds to a stationary bifurcation of the structural mode?

The first possibility leads to

$$\text{tr}\, \widehat{\mathsf{J}}(r) = J_{11} + J_{22} - \kappa r(D_{\text{u}} + D_{\text{v}}) = T - \kappa r(D_{\text{u}} + D_{\text{v}}), \tag{13.37}$$

which is negative for all $r \geq 0$, since $T < 0$ and $D_{\text{u}} + D_{\text{v}} > 0$. As for spatially continuous systems, the USS of diffusively coupled reactor arrays cannot undergo an oscillatory spatial instability or wave bifurcation, if the kinetics depends only on two variables.

The second possibility, a stationary spatial or Turing instability, requires that $\det \widehat{\mathsf{J}}(r) = 0$,

$$(\kappa r)^2 - \kappa r(D_{\text{v}} J_{11} + D_{\text{u}} J_{22}) + J_{11} J_{22} - J_{12} J_{21} = 0, \tag{13.38}$$

or

$$(\kappa r)^2 - \kappa r(D_{\text{v}} J_{11} + D_{\text{u}} J_{22}) + \Delta = 0. \tag{13.39}$$

We can approach (13.38) or (13.39) from two viewpoints.

(i) We consider μ to be the bifurcation parameter and keep the coupling constant κ fixed. Then these equations determine the instability threshold for each structural mode, $\mu_c(\beta_i)$. The explicit form of the instability conditions depends on the particular internal kinetics, $\mathbf{F}$. The threshold of the Turing instability is given by $\mu_T = \min\{\mu_c(\beta_2), \ldots, \mu_c(\beta_n)\}$, if the USS becomes unstable as μ increases, or $\mu_T = \max\{\mu_c(\beta_2), \ldots, \mu_c(\beta_n)\}$, if the USS becomes unstable as μ decreases. We adopt this approach in Sect. 13.3 below.

(ii) We consider the coupling constant κ to be the bifurcation parameter and keep all other parameters fixed. For κ small, the reactors are only weakly coupled. Since each isolated reactor is stable, the USS of the network $\mathcal{G}$ will be stable for sufficiently small κ. For κ large, the array of coupled reactors behaves like one large CSTR. This is the "well-stirred" regime and no spatial patterns are possible. We expect that for moderate values of the coupling constant κ, the regime where the reaction terms and the coupling terms contribute equally to the evolution of the reactor network, stationary spatial instabilities can occur for a range of values of κ in an appropriate region of parameter space.

The roots of (13.39) have to be positive, since both $\kappa > 0$ and $r > 0$. As for the Turing instability in spatially continuous reaction–diffusion system, see Sect. 10.1.2,

$$D_v J_{11} + D_u J_{22} > 0 \tag{13.40}$$

is a necessary but not sufficient condition, since $\Delta > 0$ according to (13.33b). In light of (13.33a), a stationary spatial instability of the network can only occur if (i) the coefficients J_{11} and J_{22} do not have the same sign and (ii) if the diffusion coefficients are not equal; the same conditions that pertain to a Turing instability in reaction–diffusion systems, see Sect. 10.1.2. Again, we will assume that

$$J_{11} > 0, \quad J_{22} < 0, \tag{13.41}$$

and consequently $|J_{22}| > J_{11}$, since $T < 0$ and $J_{12} J_{21} < 0$ since $\Delta > 0$. The roots of (13.39) are given by

$$\kappa_{\pm} r = \frac{D_v J_{11} + D_u J_{22} \pm \sqrt{(D_v J_{11} + D_u J_{22})^2 - 4 D_u D_v \Delta}}{2 D_u D_v}. \tag{13.42}$$

The roots are positive if the discriminant is nonnegative

$$(D_v J_{11} + D_u J_{22})^2 \geq 4 D_u D_v \Delta. \tag{13.43}$$

The boundary of the instability region in parameter space occurs where (13.42) has a double root, i.e.,

$$D_v J_{11} + D_u J_{22} = \sqrt{4 D_u D_v \Delta}. \tag{13.44}$$

Inside the unstable region, i.e., $(D_v J_{11} + D_u J_{22})^2 > 4 D_u D_v \Delta$, the range of the coupling constant (κ_-, κ_+) in which the USS of $\mathcal{G}$ is unstable to the structural mode associated with β_i is given by

$$
\kappa_\pm = \frac{1}{-\beta_i} \frac{D_v J_{11} + D_u J_{22} \pm \sqrt{(D_v J_{11} + D_u J_{22})^2 - 4 D_u D_v \Delta}}{2 D_u D_v}, \quad i = 2, \ldots, n.
$$

$$\tag{13.45}$$

This implies that if we start with a network in the weak-coupling regime and then increase κ, the first structural mode to become unstable is the mode with the most negative eigenvalue, i.e., the eigenvector of the network Laplacian associated with β_n. For geometrically regular graphs, such as linear and circular arrays and pieces of rectangular two- and three-dimensional lattices with four and six nearest neighbors, respectively, this mode corresponds to a short-wavelength mode, and we will call this instability a "short-wavelength" instability for arbitrary networks $\mathcal{G}$.

If, on the other hand, we start with a network in the strong-coupling regime and then decrease κ, (13.45) implies that the first structural mode to become unstable is the mode with the least negative eigenvalue, i.e., the eigenvector of the network Laplacian associated with β_2. For geometrically regular graphs this mode corresponds to a long-wavelength mode, and we will call this instability a "long-wavelength" instability for arbitrary networks $\mathcal{G}$. Our results show that the stationary instability of the USS of $\mathcal{G}$ is reentrant, if the coupling strength κ is the bifurcation parameter.

13.3 Networks of Diffusively Coupled Reactors with Lengyel–Epstein Kinetics

We employ the tools of structural mode analysis to determine the instability threshold for Turing bifurcations to patterns in arrays of reactors that contain all the components of the CDIMA reaction, including the complexing agent. The reactors are linked by diffusive coupling via membranes that are impermeable to the complexing agent. In this section we consider the case that all reactors contain the same concentration of the complexing agent, i.e., the network is homogeneous. Arrays where the individual reactors are loaded with different concentrations of the substrate are discussed in Sect. 13.6.

13.3.1 Turing Threshold

As discussed in Sect. 1.4.9, the CDIMA reaction in a single CSTR is well described by the two-variable Lengyel–Epstein model. The evolution of a homogeneous network of n reactors with Lengyel–Epstein kinetics is governed by the set of ordinary differential equations

$$\frac{d\boldsymbol{\rho}_i}{dt} = \mathbf{F}(\boldsymbol{\rho}_i, \boldsymbol{\mu}_i) + \sum_{j=1}^{n} L_{ij} \mathsf{D} \boldsymbol{\rho}_j, \quad i = 1, \ldots, n, \tag{13.46}$$

where, $k = 2$,

$$\mathbf{F}(\boldsymbol{\rho}) = \begin{pmatrix} F_1(\rho_{\mathrm{u}}, \rho_{\mathrm{v}}) \\ F_2(\rho_{\mathrm{u}}, \rho_{\mathrm{v}}) \end{pmatrix} = \begin{pmatrix} \dfrac{1}{\sigma} \left(a - \rho_{\mathrm{u}} - 4 \dfrac{\rho_{\mathrm{u}} \rho_{\mathrm{v}}}{1 + \rho_u^2} \right) \\ b \left(\rho_{\mathrm{u}} - \dfrac{\rho_{\mathrm{u}} \rho_{\mathrm{v}}}{1 + \rho_u^2} \right) \end{pmatrix} \tag{13.47}$$

and

$$\mathsf{D} = \kappa \, \mathrm{diag}(1/\sigma, d), \tag{13.48}$$

with $a, b, d > 0$. The coupling strength κ corresponds to the mass transfer coefficient for the activator in the absence of the complexing agent. We allow for the possibility that the mass transfer coefficient of the inhibitor differs from that of the activator, and the ratio of the mass transfer coefficients of the two species is d. As discussed in Sect. 1.4.9, this system has a unique steady state in a single CSTR

$$\overline{\boldsymbol{\rho}} = (\overline{\rho}_{\mathrm{u}}, \overline{\rho}_{\mathrm{v}}) = \left(\frac{a}{5}, 1 + \frac{a^2}{25} \right), \tag{13.49}$$

which undergoes a Hopf bifurcation to oscillatory behavior as the parameter b is decreased at

$$b_{\mathrm{H}} = \frac{3a^2 - 125}{5a\sigma}. \tag{13.50}$$

We adopt here the first viewpoint discussed in the previous section. We keep the coupling constant κ fixed and consider b to be the bifurcation parameter. The parameter σ affects neither the stationary states of the network nor the stationary bifurcations, i.e., bifurcations corresponding to an eigenvalue of 0, as is clear from the structure of the right-hand side of (13.46). To observe the formation of Turing patterns, the Turing bifurcation must be the primary bifurcation, i.e., must occur before the Hopf bifurcation. The Turing threshold b_{T} must be larger than b_{H}. Since the Hopf threshold is inversely proportional to σ, one can ensure for a given value of a that any stationary bifurcation will occur before the Hopf bifurcation by choosing a sufficiently large concentration of complexing agent. If

$$\sigma > \sigma_{\mathrm{c}}^*(a), \tag{13.51}$$

where $\sigma_c^*(a)$ is given by $b_T = b_H$, then the stationary bifurcation occurs first.

The system (13.46) has a unique uniform steady state given by

$$\rho_i = \overline{\rho}. \tag{13.52}$$

To obtain the threshold condition for the Turing bifurcation of this USS, we need to determine all conditions for which the eigenvalues of J_G can vanish. According to Theorem 13.8, we need to determine the conditions such that

$$\widehat{J}(r) = \begin{pmatrix} \dfrac{1}{\sigma}\left(-5 + \dfrac{8a^2}{25 + a^2}\right) - \dfrac{r\kappa}{\sigma} & -\dfrac{1}{\sigma}\dfrac{20a}{25 + a^2} \\[2ex] b\dfrac{2a^2}{25 + a^2} & -b\dfrac{5a}{25 + a^2} - r\kappa d \end{pmatrix} \tag{13.53}$$

has a zero eigenvalue, i.e., that $\det \widehat{J}(r) = 0$, which yields

$$\frac{a^2 d\kappa r(-3 + \kappa r) + 5ab(5 + \kappa r) + 25 d\kappa r(5 + \kappa r)}{25 + a^2} = 0. \tag{13.54}$$

We obtain the following result:

Theorem 13.9 *If* $0 < \kappa r < 3$*, there exist a and d such that if* $b = b^* + \epsilon$ *and*

$$b^*(r) = \frac{d\kappa r\left[a^2(3 - \kappa r) - 25(5 + \kappa r)\right]}{5a(5 + \kappa r)}, \tag{13.55}$$

an eigenvalue of $\widehat{J}(r)$ *changes sign with* ϵ*, while for* $r = 0$ *or* $\kappa r \geq 3$ *the determinant is always positive.*

For a graph of $b^*(r)$ vs κr, see Fig. 13.1.

For b sufficiently large, the uniform steady state of $\mathcal{G}$, given by $\rho_i = \overline{\rho}$, is stable. As mentioned above, with σ large enough, the Turing bifurcation occurs before the Hopf bifurcation as b decreases. Define the set Γ as

$$\Gamma = \{r \,|\, r = -\beta, \beta \in \sigma(\mathsf{L}), 0 < \kappa r < 3\}, \tag{13.56}$$

i.e., the set of r such that the eigenvalues of $\widehat{J}(r)$ pass through zero with an appropriate choice of κ. Then it follows from (13.55) that the Turing threshold is given by

$$b_T = \max_{r \in \Gamma} b^*(r). \tag{13.57}$$

For $b > b_T$ the USS is stable, and for $b < b_T$ it is unstable to spatially nonuniform perturbations. Equation (13.55) implies that for a and d fixed, $b^*(r)$ is positive for
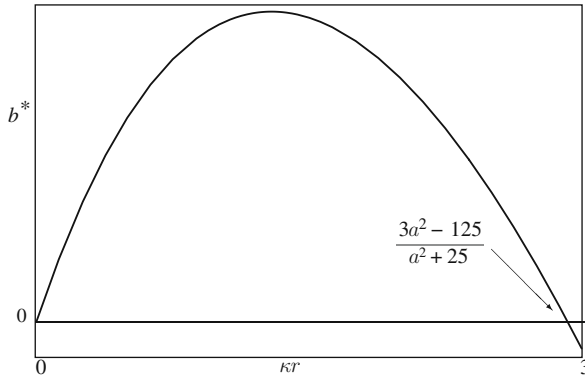
Fig. 13.1 b^* as function of κr for fixed a and d. Reprinted from [305]. Copyright 2005, with permission from Elsevier

$$0 < \kappa r < \frac{3a^2 - 125}{a^2 + 25}. \tag{13.58}$$

This implies that a Turing instability can occur only if a is larger than a°, see (1.159), i.e., the iodide ion must be an activator. Since $r = -\beta$ and $\beta_j \le \beta_2 < 0$, $j > 2$, the maximum value of κ for which a Turing instability can occur is

$$\kappa_{\max,\mathcal{G}} \equiv \frac{125 - 3a^2}{\beta_2(a^2 + 25)}. \tag{13.59}$$

This implies that if $\mathcal{G}'$ is a proper subgraph of $\mathcal{G}$ with the same number of nodes, a Turing instability of $\mathcal{G}$ can occur for no greater value of the coupling strength than the maximum value at which a Turing instability of $\mathcal{G}'$ occurs.

Theorem 13.10 *Consider a network of n LE reactors represented by a graph $\mathcal{G}$, and let $\mathcal{G}'$ be a connected subgraph of $\mathcal{G}$ such that $\mathcal{N}_{\mathcal{G}'} = \mathcal{N}_{\mathcal{G}}$ and $\mathcal{E}_{\mathcal{G}'} = \mathcal{E}_{\mathcal{G}} \backslash \{(v_i, v_j)\}$. Then $\kappa_{\max,\mathcal{G}} \le \kappa_{\max,\mathcal{G}'}$.*

Remark 13.3 For fixed n, Theorem 13.6 suggests that an ordering of $\kappa_{\max,\mathcal{G}}$ based on the diameter of $\mathcal{G}$ exists. A partial ordering based on graph diameter is observed when $n = 4$, as we show below [207].

13.3.2 Turing Instability in Small Arrays

We systematically survey the Turing threshold conditions and the structural mode that becomes unstable, for arrays of two, three, and four coupled reactors with Lengyel–Epstein kinetics. The results illustrate the importance of the value of the coupling strength on the occurrence of a Turing instability. They also provide the

first evidence of the effect of the network topology on the Turing threshold. The topology already plays a role in the occurrence of the Turing instability for the first nontrivial case, namely three coupled reactors.

13.3.2.1 Two Reactors

For two coupled reactors, the Laplacian matrix of the graph $\mathcal{G}$ reads

$$\mathsf{L}_2 = \begin{pmatrix} -1 & 1 \\ 1 & -1 \end{pmatrix}. \tag{13.60}$$

The structural modes and associated eigenvalues are

$$\left(\alpha_1^{(1)}, \alpha_2^{(1)}\right)^T = (1, 1)^T, \qquad\qquad \beta_1 = 0, \tag{13.61}$$

$$\left(\alpha_1^{(2)}, \alpha_2^{(2)}\right)^T = (-1, 1)^T, \qquad\qquad \beta_1 = -2. \tag{13.62}$$

There is only one nonuniform structural mode, and we obtain the Turing threshold by setting $r = 2$ in (13.55):

$$b_{\mathrm{T}} = \frac{2d\kappa \left(3a^2 - 2\kappa a^2 - 125 - 50\kappa\right)}{5a(5 + 2\kappa)}. \tag{13.63}$$

The mass-transfer coefficient κ must lie in the interval $(0, \kappa_{\max})$, see above, for Turing patterns to occur, where

$$\kappa_{\max} = \frac{3a^2 - 125}{2a^2 + 50}. \tag{13.64}$$

A strict upper bound for $\kappa_{\max}$ is given by $\kappa_{\sup} = 3/2$, the limit of $\kappa_{\max}$ as $a \to \infty$. No Turing instability occurs in two coupled reactors, if $\kappa > 3/2$. We illustrate our results for the specific case $\kappa = 1$, where contributions from reaction and diffusion terms are evenly balanced. For a and d, we choose $a = 50.0$ and $d = 1.07$. The latter value is the ratio of the diffusion coefficients of the activator and inhibitor in aqueous solution. We use these values in all examples in this section. For these conditions, $b_{\mathrm{T}} = 2.84314$, $\kappa_{\max} = 1.4604$, and $\sigma_c^* = 10.3758$.

13.3.2.2 Three Reactors

Two different network topologies are possible for three coupled reactors: (i) a linear array and (ii) a circular array. For three reactors, the latter coincides with global or all-to-all coupling. A linear array corresponds to the Laplacian matrix

$$L_{3lin} = \begin{pmatrix} -1 & 1 & 0 \\ 1 & -2 & 1 \\ 0 & 1 & -1 \end{pmatrix}. \tag{13.65}$$

The structural modes and associated eigenvalues are

$$\left(\alpha_1^{(1)}, \alpha_2^{(1)}, \alpha_3^{(1)}\right)^T = (1, 1, 1)^T, \qquad\qquad \beta_1 = 0, \tag{13.66}$$

$$\left(\alpha_1^{(2)}, \alpha_2^{(2)}, \alpha_3^{(2)}\right)^T = (-1, 0, 1)^T, \qquad\qquad \beta_2 = -1, \tag{13.67}$$

$$\left(\alpha_1^{(3)}, \alpha_2^{(3)}, \alpha_3^{(3)}\right)^T = (1, -2, 1)^T, \qquad\qquad \beta_3 = -3. \tag{13.68}$$

There are two nonuniform structural modes, one odd and one even, and we obtain the Turing threshold by setting $r = 1$ and $r = 3$ in (13.55). The USS is unstable to the structural mode $(-1, 0, 1)^T$ for values of b below

$$b^*(1) = \frac{d\kappa \left(3a^2 - \kappa a^2 - 25\kappa - 125\right)}{5a(5 + \kappa)}, \tag{13.69}$$

and the range for the coupling constant κ is $(0, \kappa_{1,\max})$ with

$$\kappa_{1,\max} = \frac{3a^2 - 125}{a^2 + 25}. \tag{13.70}$$

A strict upper bound for $\kappa_{1,\max}$ is given by $\kappa_{1,\sup} = 3$. Since this structural mode corresponds to the eigenvalue β_2 of the Laplacian matrix L_{3lin}, no Turing instability can occur in a linear three-reactor array if the mass-transfer coefficient κ exceeds the value 3 in accordance with (13.59).

The USS is unstable to the structural mode $(1, -2, 1)^T$ for values of b below

$$b^*(3) = \frac{d\kappa \left[9(1 - \kappa)a^2 - 225\kappa - 375\right]}{5a(5 + 3\kappa)}, \tag{13.71}$$

and the range for the coupling constant κ is $(0, \kappa_{3,\max})$ with

$$\kappa_{3,\max} = \frac{3a^2 - 125}{3a^2 + 75}. \tag{13.72}$$

A strict upper bound for $\kappa_{3,\max}$ is given by $\kappa_{3,\sup} = 1$. For a given value of the coupling constant κ, the instability thresholds of the two inhomogeneous structural modes coincide, i.e., the modes are degenerate, at

$$a_0(\kappa) = \frac{5\sqrt{25 + 20\kappa + 3\kappa^2}}{\sqrt{15 - 20\kappa - 3\kappa^2}}, \tag{13.73}$$

which is a real, positive number for $\kappa < (\sqrt{145} - 10)/3 = 0.680532$. For a given value of a, the two modes are degenerate at

$$\kappa_0(a) = \frac{\sqrt{5}\sqrt{3125 + 850a^2 + 29a^4} - 10a^2 - 250}{3(25 + a^2)}, \tag{13.74}$$

which is positive for $a > a^\circ$. These results imply that for $\kappa > \kappa_{3,\max}$ only the structural mode $(-1, 0, 1)^T$ can become unstable and

$$b_T = b^*(1) = \frac{d\kappa \left(3a^2 - \kappa a^2 - 225\kappa - 125\right)}{5a(5 + \kappa)}. \tag{13.75}$$

For $0.680532 < \kappa < \kappa_{3,\max}$, it represents the primary bifurcation, i.e., $b^*(1) > b^*(3)$. Therefore for fixed a, the Turing threshold b_T is given by (13.75) for coupling constants in the range $0.680532 < \kappa < \kappa_{1,\max}$. For $0 < \kappa < 0.680532$ we have that $b^*(3) > b^*(1)$ and

$$b_T = b^*(3) = \frac{d\kappa \left[9(1 - \kappa)a^2 - 225\kappa - 375\right]}{5a(5 + 3\kappa)}. \tag{13.76}$$

We illustrate our results for three specific values of the mass-transfer coefficient. We find that the two structural modes are degenerate at $\kappa_0(50.0) = 0.664053$. For $\kappa = 1$, only the eigenvalue of $\mathbf{J}_G$ associated with the structural mode $(-1, 0, 1)^T$, the odd mode, passes through zero and the Turing instability occurs at $b_T = 3.445967$. For $\kappa = 0.75$, the eigenvalues of $\mathbf{J}_G$ associated with the odd and the even nonuniform structural mode both pass through zero, the first one at $b^*(1) = 3.05997$ and the second one at $b^*(3) = 2.24977$. As expected, the primary bifurcation is still associated with the odd mode. For $k = 0.5$, the instability conditions for the two inhomogeneous structural modes correspond to $b^*(1) = 2.37832$ and $b^*(3) = 3.54335$ and thus $b_T = 3.54335$. It is now the even structural mode $(1, -2, 1)^T$ that goes unstable first. If we change the coupling strength κ in a linear three-reactor array from a value above $\kappa_0(a)$ to a value below $\kappa_0(a)$, then the Turing mode will change from an odd mode to an even mode.

A circular three-reactor array has the following Laplacian matrix:

$$\mathsf{L}_{3\text{circ}} = \begin{pmatrix} -2 & 1 & 1 \\ 1 & -2 & 1 \\ 1 & 1 & -2 \end{pmatrix}. \tag{13.77}$$

The structural modes and associated eigenvalues are

$$
\left(\alpha_1^{(1)}, \alpha_2^{(1)}, \alpha_3^{(1)}\right)^T = (1, 1, 1)^T, \qquad \beta_1 = 0, \qquad (13.78)
$$

$$
\left(\alpha_1^{(2)}, \alpha_2^{(2)}, \alpha_3^{(2)}\right)^T = (-1, 1, 0)^T, \qquad \beta_2 = -3, \qquad (13.79)
$$

$$
\left(\alpha_1^{(3)}, \alpha_2^{(3)}, \alpha_3^{(3)}\right)^T = (-1, 0, 1)^T, \qquad \beta_3 = -3. \qquad (13.80)
$$

The nonzero eigenvalue is doubly degenerate, and so is the eigenvalue of $J_{\mathcal{G}}$ that passes through zero. The Turing threshold is given by

$$
b_{\mathrm{T}} = b^*(3) = \frac{d\kappa \left[9(1 - \kappa)a^2 - 225\kappa - 375\right]}{5a(5 + 3\kappa)}, \qquad (13.81)
$$

and the USS of the array is unstable to any linear combination of the two nonuniform structural modes $(-1, 1, 0)^T$ and $(-1, 0, 1)^T$. The range for the coupling constant κ is $(0, \kappa_{3,\max})$.

The network topology affects the Turing instability already in a three-reactor array. Consider the case where the mass-transfer coefficient falls in the range $(\kappa_{3,\max}, \kappa_{1,\max})$, say for instance $\kappa = 1.5$. If we start with a circular array of three reactors, then the homogeneous steady state is stable against spatial perturbations. No Turing instability can occur in a circular three-reactor array for a coupling constant κ larger than $\kappa_{3,\max}$. When we sever the connection between the first and third reactors, i.e., we turn the circular array into a linear one, the uniform steady state can become unstable to nonuniform spatial perturbations and a stationary pattern can form, since κ is below the upper limit for a Turing instability in a linear three-reactor array given by (13.70).

13.3.2.3 Four Reactors

The six different network topologies that occur for arrays of four coupled reactors are shown in Fig. 13.2. The Laplacian matrix L of each network can be read off from Fig. 13.2 and is given below. We also list the structural modes of L and the corresponding eigenvalues.

(i) *Linear array*:

$$
\mathsf{L}_{4,\mathrm{i}} = \begin{pmatrix} -1 & 1 & 0 & 0 \\ 1 & -2 & 1 & 0 \\ 0 & 1 & -2 & 1 \\ 0 & 0 & 1 & -1 \end{pmatrix}. \qquad (13.82)
$$

The structural modes and associated eigenvalues are
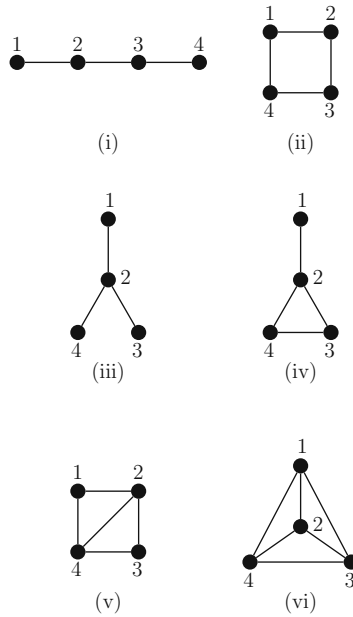
Fig. 13.2 Topologies for four coupled reactors: (*i*) linear; (*ii*) circular; (*iii*) star-shaped; (*iv*) triangle-plus-one; (*v*) circular-plus-diagonal; (*vi*) global or all-to-all coupling. Reprinted from [207]. Copyright 2004, with permission from Elsevier

$$\left(\alpha_1^{(1)}, \alpha_2^{(1)}, \alpha_3^{(1)}, \alpha_4^{(1)}\right)^T = (1, 1, 1, 1)^T, \qquad\qquad \beta_1 = 0, \qquad (13.83)$$

$$\left(\alpha_1^{(2)}, \alpha_2^{(2)}, \alpha_3^{(2)}, \alpha_4^{(2)}\right)^T = (-1, 1 - \sqrt{2}, -1 + \sqrt{2}, 1)^T, \quad \beta_2 = -2 + \sqrt{2}, \tag{13.84}$$

$$\left(\alpha_1^{(3)}, \alpha_2^{(3)}, \alpha_3^{(3)}, \alpha_4^{(3)}\right)^T = (1, -1, -1, 1)^T, \qquad\qquad \beta_3 = -2, \quad (13.85)$$

$$\left(\alpha_1^{(4)}, \alpha_2^{(4)}, \alpha_3^{(4)}, \alpha_4^{(4)}\right)^T = (-1, 1 + \sqrt{2}, -1 - \sqrt{2}, 1)^T, \quad \beta_2 = -2 - \sqrt{2}. \tag{13.86}$$

The eigenvalues of the three nonuniform structural modes, their instability thresholds, the maximum value of the coupling constant $\kappa_{\max}$, and its upper limit $\kappa_{\sup}$ as $a \to \infty$ are given in Table 13.1.

(ii) *Circular array*:

$$\mathsf{L}_{4,\mathrm{ii}} = \begin{pmatrix} -2 & 1 & 0 & 1 \\ 1 & -2 & 1 & 0 \\ 0 & 1 & -2 & 1 \\ 1 & 0 & 1 & -2 \end{pmatrix}. \tag{13.87}$$

Table 13.1 Instability threshold $b^*(r)$ for the nonuniform structural modes of four-reactor arrays. $r_\pm = \pm 2 + \sqrt{2}$, $t = 25 + 20\kappa + 2\kappa^2$, $n_\pm = \pm 25 r_\mp t + a^2[\mp 15 r_\mp \pm 4(\mp 6 + 5\sqrt{2}) - 2 r_\mp \kappa^2]$. Reprinted from [207]. Copyright 2004, with permission from Elsevier

β	$b^*(r)$	κ_{max}	κ_{sup}
(i) $-2+\sqrt{2}$	$\dfrac{d\kappa n_+}{5at}$	$\dfrac{3a^2-125}{-r_-(a^2+25)}$	5.12132
(i) -2	$\dfrac{d\kappa(6a^2-4\kappa a^2-100\kappa-250)}{a(25+10\kappa)}$	$\dfrac{3a^2-125}{2a^2+50}$	3/2
(i) $-2-\sqrt{2}$	$\dfrac{d\kappa n_-}{5at}$	$\dfrac{3a^2-125}{r_+(a^2+25)}$	0.87868
(ii) -2 (2×)	$\dfrac{d\kappa(6a^2-4\kappa a^2-100\kappa-250)}{a(25+10\kappa)}$	$\dfrac{3a^2-125}{2a^2+50}$	3/2
(ii) -4	$\dfrac{d\kappa(12a^2-16\kappa a^2-400\kappa-500)}{a(25+20\kappa)}$	$\dfrac{3a^2-125}{4a^2+100}$	3/4
(iii) -1 (2×)	$\dfrac{d\kappa(3a^2-\kappa a^2-25\kappa-125)}{a(25+5\kappa)}$	$\dfrac{3a^2-125}{a^2+25}$	3
(iii) -4	$\dfrac{d\kappa(12a^2-16\kappa a^2-400\kappa-500)}{a(25+20\kappa)}$	$\dfrac{3a^2-125}{4a^2+100}$	3/4
(iv) -1	$\dfrac{d\kappa(3a^2-\kappa a^2-25\kappa-125)}{a(25+5\kappa)}$	$\dfrac{3a^2-125}{a^2+25}$	3
(iv) -3	$\dfrac{d\kappa[9(1-\kappa)a^2-225\kappa-375]}{a(25+15\kappa)}$	$\dfrac{3a^2-125}{3a^2+75}$	1
(iv) -4	$\dfrac{d\kappa(12a^2-16\kappa a^2-400\kappa-500)}{a(25+20\kappa)}$	$\dfrac{3a^2-125}{4a^2+100}$	3/4
(v) -2	$\dfrac{d\kappa(6a^2-4\kappa a^2-100\kappa-250)}{a(25+10\kappa)}$	$\dfrac{3a^2-125}{2a^2+50}$	3/2
(v) -4 (2×)	$\dfrac{d\kappa(12a^2-16\kappa a^2-400\kappa-500)}{a(25+20\kappa)}$	$\dfrac{3a^2-125}{4a^2+100}$	3/4
(vi) -4 (3×)	$\dfrac{d\kappa(12a^2-16\kappa a^2-400\kappa-500)}{a(25+20\kappa)}$	$\dfrac{3a^2-125}{4a^2+100}$	3/4

The structural modes and associated eigenvalues are

$$\left(\alpha_1^{(1)}, \alpha_2^{(1)}, \alpha_3^{(1)}, \alpha_4^{(1)}\right)^T = (1, 1, 1, 1)^T, \qquad \beta_1 = 0, \qquad (13.88)$$

$$\left(\alpha_1^{(2)}, \alpha_2^{(2)}, \alpha_3^{(2)}, \alpha_4^{(2)}\right)^T = (-1, 0, 1, 0)^T, \qquad \beta_2 = -2, \qquad (13.89)$$

$$\left(\alpha_1^{(3)}, \alpha_2^{(3)}, \alpha_3^{(3)}, \alpha_4^{(3)}\right)^T = (0, -1, 0, 1)^T, \qquad \beta_3 = -2, \qquad (13.90)$$

$$\left(\alpha_1^{(4)}, \alpha_2^{(4)}, \alpha_3^{(4)}, \alpha_4^{(4)}\right)^T = (-1, 1, -1, 1)^T, \qquad \beta_2 = -4. \qquad (13.91)$$

The eigenvalues, and their multiplicity, of the three nonuniform structural modes, their instability thresholds, the maximum value of the coupling constant κ_{max}, and its upper limit κ_{sup} as $a \to \infty$ are given in Table 13.1.

(iii) *Star-shaped array*:

$$L_{4,iii} = \begin{pmatrix} -1 & 1 & 0 & 0 \\ 1 & -3 & 1 & 1 \\ 0 & 1 & -1 & 0 \\ 0 & 1 & 0 & -1 \end{pmatrix}. \qquad (13.92)$$

The structural modes and associated eigenvalues are

$$\left(\alpha_1^{(1)}, \alpha_2^{(1)}, \alpha_3^{(1)}, \alpha_4^{(1)}\right)^T = (1, 1, 1, 1)^T, \qquad \beta_1 = 0, \qquad (13.93)$$

$$\left(\alpha_1^{(2)}, \alpha_2^{(2)}, \alpha_3^{(2)}, \alpha_4^{(2)}\right)^T = (-1, 0, 1, 0)^T, \qquad \beta_2 = -1, \qquad (13.94)$$

$$\left(\alpha_1^{(3)}, \alpha_2^{(3)}, \alpha_3^{(3)}, \alpha_4^{(3)}\right)^T = (-1, 0, 0, 1)^T, \qquad \beta_3 = -1, \qquad (13.95)$$

$$\left(\alpha_1^{(4)}, \alpha_2^{(4)}, \alpha_3^{(4)}, \alpha_4^{(4)}\right)^T = (1, -3, 1, 1)^T, \qquad \beta_2 = -4. \qquad (13.96)$$

The eigenvalues, and their multiplicity, of the three nonuniform structural modes, their instability thresholds, the maximum value of the coupling constant κ_{max}, and its upper limit κ_{sup} as $a \to \infty$ are given in Table 13.1.

(iv) *Triangle-plus-one array*:

$$L_{4,iv} = \begin{pmatrix} -1 & 1 & 0 & 0 \\ 1 & -3 & 1 & 1 \\ 0 & 1 & -2 & 1 \\ 0 & 1 & 1 & -2 \end{pmatrix}. \qquad (13.97)$$

The structural modes and associated eigenvalues are

$$\left(\alpha_1^{(1)}, \alpha_2^{(1)}, \alpha_3^{(1)}, \alpha_4^{(1)}\right)^T = (1, 1, 1, 1)^T, \qquad \beta_1 = 0, \qquad (13.98)$$

$$\left(\alpha_1^{(2)}, \alpha_2^{(2)}, \alpha_3^{(2)}, \alpha_4^{(2)}\right)^T = (-2, 0, 1, 1)^T, \qquad \beta_2 = -1, \qquad (13.99)$$

$$\left(\alpha_1^{(3)}, \alpha_2^{(3)}, \alpha_3^{(3)}, \alpha_4^{(3)}\right)^T = (0, 0, -1, 1)^T, \qquad \beta_3 = -3, \qquad (13.100)$$

$$\left(\alpha_1^{(4)}, \alpha_2^{(4)}, \alpha_3^{(4)}, \alpha_4^{(4)}\right)^T = (1, -3, 1, 1)^T, \qquad \beta_2 = -4. \qquad (13.101)$$

The eigenvalues, and their multiplicity, of the three nonuniform structural modes, their instability thresholds, the maximum value of the coupling constant κ_{max}, and its upper limit κ_{sup} as $a \to \infty$ are given in Table 13.1.

(v) *Circular-plus-diagonal array*:

$$L_{4,v} = \begin{pmatrix} -2 & 1 & 0 & 1 \\ 1 & -3 & 1 & 1 \\ 0 & 1 & -2 & 1 \\ 1 & 1 & 1 & -3 \end{pmatrix}. \tag{13.102}$$

The structural modes and associated eigenvalues are

$$\left(\alpha_1^{(1)}, \alpha_2^{(1)}, \alpha_3^{(1)}, \alpha_4^{(1)}\right)^T = (1, 1, 1, 1)^T, \qquad \beta_1 = 0, \tag{13.103}$$

$$\left(\alpha_1^{(2)}, \alpha_2^{(2)}, \alpha_3^{(2)}, \alpha_4^{(2)}\right)^T = (-1, 0, 1, 0)^T, \qquad \beta_2 = -2, \tag{13.104}$$

$$\left(\alpha_1^{(3)}, \alpha_2^{(3)}, \alpha_3^{(3)}, \alpha_4^{(3)}\right)^T = (1, -2, 1, 0)^T, \qquad \beta_3 = -4, \tag{13.105}$$

$$\left(\alpha_1^{(4)}, \alpha_2^{(4)}, \alpha_3^{(4)}, \alpha_4^{(4)}\right)^T = (0, -1, 0, 1)^T, \qquad \beta_2 = -4. \tag{13.106}$$

The eigenvalues, and their multiplicity, of the three nonuniform structural modes, their instability thresholds, the maximum value of the coupling constant κ_{max}, and its upper limit κ_{sup} as $a \to \infty$ are given in Table 13.1.

(vi) *Array with global or all-to-all coupling*:

$$L_{4,vi} = \begin{pmatrix} -3 & 1 & 1 & 1 \\ 1 & -3 & 1 & 1 \\ 1 & 1 & -3 & 1 \\ 1 & 1 & 1 & -3 \end{pmatrix}. \tag{13.107}$$

The structural modes and associated eigenvalues are

$$\left(\alpha_1^{(1)}, \alpha_2^{(1)}, \alpha_3^{(1)}, \alpha_4^{(1)}\right)^T = (1, 1, 1, 1)^T, \qquad \beta_1 = 0, \tag{13.108}$$

$$\left(\alpha_1^{(2)}, \alpha_2^{(2)}, \alpha_3^{(2)}, \alpha_4^{(2)}\right)^T = (-1, 1, 0, 0)^T, \qquad \beta_2 = -4, \tag{13.109}$$

$$\left(\alpha_1^{(3)}, \alpha_2^{(3)}, \alpha_3^{(3)}, \alpha_4^{(3)}\right)^T = (-1, 0, 1, 0)^T, \qquad \beta_3 = -4, \tag{13.110}$$

$$\left(\alpha_1^{(4)}, \alpha_2^{(4)}, \alpha_3^{(4)}, \alpha_4^{(4)}\right)^T = (-1, 0, 0, 1)^T, \qquad \beta_2 = -4. \tag{13.111}$$

The eigenvalues, and their multiplicity, of the three nonuniform structural modes, their instability thresholds, the maximum value of the coupling constant κ_{max}, and its upper limit κ_{sup} as $a \to \infty$ are given in Table 13.1.

The effect of the network topology is evident from the values for κ_{sup}. A Turing instability occurs over the widest range of the coupling constant for the linear array. The array with global coupling has, as expected, the narrowest range. The six topologies can be grouped into four classes according to the largest κ_{sup}. Class one has the largest $\kappa_{\text{sup}} = 3/(2 - \sqrt{2}) = 5.12132$; it includes only the linear array. Arrays in class two have a largest κ_{sup} of 3 and include the star-shaped and the triangle-plus-one arrays. The circular array and the circular-plus-diagonal array belong to class three, where the largest κ_{sup} is 3/2. Class four comprises only the array with global coupling and has $\kappa_{\text{sup}} = 3/4$. If $\kappa > 3$, the uniform steady state can undergo a Turing bifurcation only in the linear array, and only one mode, an odd mode, is unstable. Note that arrays (iv) and (v) display localized Turing modes. In the second nonuniform structural mode of (iv), the array acts as a linear two-reactor array; only reactors 3 and 4 deviate from the steady state. In the first nonuniform structural mode of (v), the two most strongly coupled reactors, namely 2 and 4 with three connections each, do not participate in the pattern. We will present more general results on localized Turing patterns in the next section.

Our results for two coupled reactors, the circular three-reactor array, and the four-reactor array with all-to-all coupling suggest that κ_{sup} for arrays with global coupling is given by $\kappa_{\text{sup}} = 3/n$, which turns out to be indeed the case, see Theorem 13.13 and (13.59).

13.4 Localized Patterns in Homogeneous Networks of Diffusively Coupled Reactors

In the previous section, we found that some four-reactor arrays can display localized structural modes. We now investigate the conditions on network topology that lead to localized patterns, i.e., patterns that are constant over much of the network but vary on some connected portion of it. Such patterns are not unique to spatially discrete systems. They have been observed in spatially continuous reaction–diffusion systems, see for example [219]. The Turing bifurcation in a reaction–diffusion system with Lengyel–Epstein kinetics is subcritical. This implies that for a certain region in parameter space Turing patterns and the uniform steady state can coexist in a stable manner in different parts of the system. It is this pinning phenomenon that gives rise to a variety of localized patterns, for example, a Turing pattern surrounded by the uniform steady state. These localized patterns in the spatially continuous Lengyel–Epstein reaction–diffusion system result mainly from the kinetics, which causes the subcritical nature of the Turing bifurcation. As we saw above, networks of coupled reactors provide an alternative mechanism for the appearance of localized patterns. There localized structures can result from the transport and the network topology, which gives rise to localized structural modes of the graph $\mathcal{G}$.

To determine which network topologies give rise to localized stationary patterns, we need to investigate the conditions on the topology that lead to localized eigen-

vectors of J_G, i.e., eigenvectors that are zero over much of the network but vary on some portion of it.

Definition 13.1 Consider a graph G with two proper, connected subgraphs G' and G'' such that $\mathcal{N}_{G'} \cup \mathcal{N}_{G''} = \mathcal{N}_G$, $\mathcal{N}_{G'} \cap \mathcal{N}_{G''} = \emptyset$, and $(v', v'') \notin \mathcal{E}_{G'}, \mathcal{E}_{G''}$ whenever $v' \in \mathcal{N}_{G'}$ and $v'' \in \mathcal{N}_{G''}$. An eigenvector $\mathbf{z}$ is said to be *localized*, if the components of $\mathbf{z}$ corresponding to the nodes $\mathcal{N}_{G''}$ are zero.

Linear and circular arrays do not display localized eigenvectors, as shown by (13.17), (13.18), and (13.21). Localized eigenvectors also do not occur for topologies that correspond to pieces of two- or three-dimensional media, namely rectangular two- and three-dimensional lattices with four and six nearest neighbors, since their structural modes are obtained from tensor products of the one-dimensional structural modes [334]. Connectivity plays an important role for the existence of localized eigenvectors, and they occur for topologies with a higher degree of connectivity.

Definition 13.2 Consider a graph G and a proper, nonempty subset of its nodes $\bar{\mathcal{N}} \subset \mathcal{N}_G$. A nonempty subgraph G' is said to be *completely connected* with respect to $\bar{\mathcal{N}}$, if $\mathcal{N}_{G'} \cap \bar{\mathcal{N}} = \emptyset$, $(v', \bar{v}) \in \mathcal{E}_G$ whenever $v' \in \mathcal{N}_{G'}$ and $\bar{v} \in \bar{\mathcal{N}}$ and if $(v', v) \in \mathcal{E}_G$ and $v' \in \mathcal{N}_{G'}$ implies that $v \in \bar{\mathcal{N}} \cup \mathcal{N}_{G'}$.

The nodes $\bar{\mathcal{N}}$ form a barrier between G' and the rest of G. For this reason $\bar{\mathcal{N}}$ is referred to as a barrier set and is a special case of a separating set [95]. One important special case of a barrier set is the set of *complete* nodes of a graph, referred to henceforth as a complete barrier set.

Definition 13.3 A node $v \in \mathcal{N}_G$ is said to be *complete* if $(v, v') \in \mathcal{E}_G, \forall v' \in \mathcal{N}_G \backslash \{v\}$.

To illustrate the meaning of Definitions 13.2 and 13.3, we consider the four graphs shown in Fig. 13.3. The graph G_a is a star graph with 10 nodes. It has a degenerate (no edges) subgraph G'_a with nodes $\mathcal{N}_{G'_a} = \{v_2, \ldots, v_{10}\}$ that is completely connected with respect to $\bar{\mathcal{N}}_a = \{v_1\}$. Patterns on a reactor network G_a with Lengyel–Epstein kinetics are considered in Sect. 13.4.2.1.

Stationary patterns on the two graphs G_b and G_c are examined in Sect. 13.4.2.2. The graph G_b contains several completely connected subgraphs. With respect to $\bar{\mathcal{N}}_{b,1} = \{v_7, \ldots, v_{10}\}$, the subgraph $G'_{b,1}$ formed from the nodes $\mathcal{N}_{G'_{b,1}} = \{v_1, \ldots, v_6\}$ and edges connecting these nodes is a completely connected circular array. Similarly the degenerate subgraph $G'_{b,2}$ with $\mathcal{N}_{G'_{b,2}} = \{v_8, v_9\}$ and no edges is completely connected with respect to $\bar{\mathcal{N}}_{b,2} = \{v_1, \ldots, v_6, v_{12}\}$. Finally, the subgraph $G'_{b,3}$ with nodes $\mathcal{N}_{G'_{b,3}} = \{v_{13}, v_{15}\}$ and edge (v_{13}, v_{15}) is completely connected with respect to $\bar{\mathcal{N}}_{b,3} = \{v_7, v_{14}\}$.

Graph G_c is obtained from G_b by making nodes $v_7, \ldots, v_{10}$ complete. The subgraph $G'_{c,1} \equiv G'_{b,1}$ is still completely connected with respect to $\bar{\mathcal{N}}_{c,1} \equiv \bar{\mathcal{N}}_{b,1}$ but this barrier set is now complete. This is not true of the subgraph $G'_{b,2}$ since v_8 and v_9 are
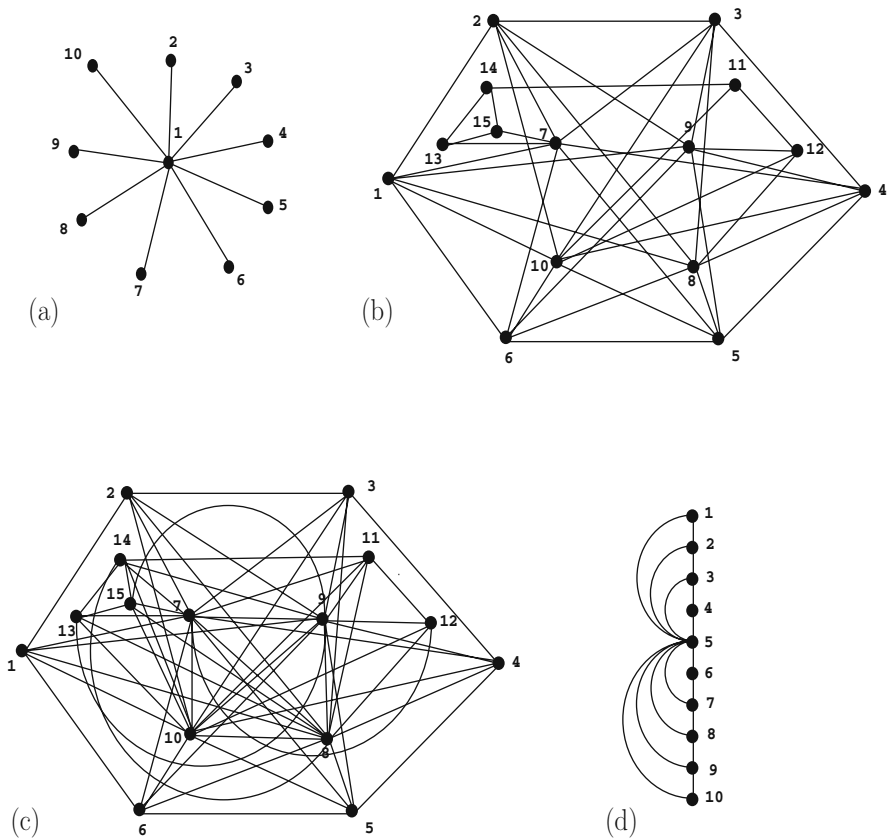
Fig. 13.3 Graphs of four networks: $\mathcal{G}_a$, $\mathcal{G}_b$, $\mathcal{G}_c$, and $\mathcal{G}_d$. Reprinted from [305]. Copyright 2005, with permission from Elsevier

complete nodes. The subgraph $\mathcal{G}'_{c,3} \equiv \mathcal{G}'_{b,3}$ is still completely connected but with respect to $\bar{\mathcal{N}}_{c,3} = \{v_7, \ldots, v_{10}, v_{14}\}$.

The graph $\mathcal{G}_d$ has two completely connected linear arrays, $\mathcal{G}'_{d,1}$ and $\mathcal{G}'_{d,2}$ with nodal sets $\mathcal{N}_{\mathcal{G}'_{d,1}} = \{v_1, \ldots, v_4\}$ and $\mathcal{N}_{\mathcal{G}'_{d,2}} = \{v_6, \ldots, v_{10}\}$, respectively, and appropriate edge sets with respect to the same complete barrier set $\bar{\mathcal{N}}_d = \{v_5\}$. We study patterns on these subgraphs in Sect. 13.4.2.3.

13.4.1 Theoretical Tools

In this section we present several results concerning the eigenvalues and eigenvectors of $\mathsf{J}_{\mathcal{G}}$ for graphs with complete nodes or completely connected subgraphs. See [305] for proofs of the following theorems.

Theorem 13.11 *Consider a network of n reactors represented by a graph $\mathcal{G}$ and let $v_i \in \mathcal{N}_{\mathcal{G}}$ be a complete node. If $\lambda \in \sigma(\widehat{\mathsf{J}}(n))$ with eigenvector $\bar{\mathbf{z}}$, then $\lambda \in \sigma(\mathsf{J}_{\mathcal{G}})$ with eigenvector $\mathbf{z}$ such that*

$$
\mathbf{z}_j = \begin{cases} \bar{\mathbf{z}}, & j \neq i, \\ -(n-1)\bar{\mathbf{z}}, & j = i. \end{cases} \tag{13.112}
$$

When $m < n$ complete nodes are present, the eigenvalues of $\widehat{\mathsf{J}}(n)$ are eigenvalues of $\mathsf{J}_{\mathcal{G}}$ of multiplicity m.

Theorem 13.12 *Consider a network of n reactors represented by a graph $\mathcal{G}$ and let*

$$
\mathcal{N}_0 = \{v | v \in \mathcal{N}_{\mathcal{G}}, \ v \text{ is a complete node}\} \neq \emptyset. \tag{13.113}
$$

If $m = |\mathcal{N}_0|$, $m < n$, and if $\lambda \in \sigma(\widehat{\mathsf{J}}(n))$, $\lambda \in \sigma(\mathsf{J}_{\mathcal{G}})$ of multiplicity at least m.

Together with Theorem 13.2, the two preceding theorems allow us to characterize completely the stability properties of an array of cells with all-to-all or global coupling. Such a network corresponds to a complete graph.

Theorem 13.13 *Consider a network of n reactors represented by a complete graph $\mathcal{G}$. Then the eigenvalues of $\mathsf{J}_{\mathcal{G}}$ are the eigenvalues of J of multiplicity 1 and the eigenvalues of $\widehat{\mathsf{J}}(n)$ of multiplicity $n-1$.*

We showed above that reactors that are coupled to all other reactors play a special role. In a similar way, the presence of completely connected subgraphs influences pattern formation in networks of diffusively coupled monostable elements. The following five theorems address the consequences of the presence of completely connected subgraphs with respect to a nonempty set of nodes $\bar{\mathcal{N}}$. In the latter three results, $\bar{\mathcal{N}}$ is a set of complete nodes. These results address the possibility of localized and "buffered" patterns in networks of diffusively coupled reactors. We demonstrate the existence of such patterns for networks with Lengyel–Epstein kinetics in Sect. 13.4.2.

Theorem 13.14 *Consider a network of n reactors represented by a graph $\mathcal{G}$ with nodes $\mathcal{N}_{\mathcal{G}} = \{v_1, \dots, v_n\}$. Suppose $\mathcal{G}$ has a completely connected subgraph $\mathcal{G}'$ with respect to $\bar{N} = \{v_1, \dots, v_{n_1}\}$ and $\mathcal{N}_{\mathcal{G}'} = \{v_{n_1+1}, \dots, v_{n_2}\}$. If $\lambda \in \sigma(\mathsf{J}_{\mathcal{G}'}(n_1))$ with eigenvector $\hat{\mathbf{z}}$ and $\lambda \notin \sigma(\widehat{\mathsf{J}}(n_1))$, then $\lambda \in \sigma(\mathsf{J}_{\mathcal{G}})$ with eigenvector $\mathbf{z} = (0, \hat{\mathbf{z}}, 0)^T$.*

Remark 13.4 For a related theorem for the Laplacian matrix see Merris [294].

From Theorem 13.1 it follows that the eigenvalues of $\mathsf{J}_{\mathcal{G}'}(n_1)$ depend on the topology of $\mathcal{G}'$ via the eigenvalues of the Laplacian matrix $\mathsf{L}_{\mathcal{G}'}$. If $|\mathcal{N}_{\mathcal{G}'}| \ll |\mathcal{N}_{\mathcal{G}}|$, then a significant reduction in the size of the eigenvalue problem for some of the eigenvalues of $\mathsf{J}_{\mathcal{G}}$ has been achieved.

The following theorem concerns the effect of adding or deleting a node from a completely connected subgraph. It suggests the existence of "buffered patterns," i.e., patterns that are not affected by changes in other parts of the network.

Theorem 13.15 *Consider a network of n reactors represented by a graph $\mathcal{G}$. Suppose that $\mathcal{N}_{\mathcal{G}}$ can be partitioned into two disjoint sets $\mathcal{N}_1 = \{v_1, v_2, \ldots, v_l\}$ and $\mathcal{N}_2 = \{v_{l+1}, \ldots, v_n\}$ such that $(v_i, v_j) \in \mathcal{E}_{\mathcal{G}}$ whenever $v_i \in \mathcal{N}_1$ and $v_j \in \mathcal{N}_2$. Let the graph $\mathcal{G}_i$ have nodes $\mathcal{N}_{\mathcal{G}_i} = \mathcal{N}_i$ and edges*

$$\mathcal{E}_{\mathcal{G}_i} = \{(v, v')|v, v' \in \mathcal{N}_i, \ (v, v') \in \mathcal{E}_{\mathcal{G}}\}, \tag{13.114}$$

for $i = 1, 2$. If $\lambda \in \sigma(\mathsf{J}_{\mathcal{G}_1}(n - l))$ with eigenvector $\bar{\mathbf{z}}$ and $\lambda \notin \sigma(\widehat{\mathsf{J}}(n - l))$, then $\lambda \in \sigma(\mathsf{J}_{\mathcal{G}})$ with eigenvector $\mathbf{z} = (\bar{\mathbf{z}}, \mathbf{0})^T$. Similarly if $\lambda \in \sigma(\mathsf{J}_{\mathcal{G}_2}(l))$ with eigenvector $\bar{\mathbf{z}}$ and $\lambda \notin \sigma(\widehat{\mathsf{J}}(l))$, then $\lambda \in \sigma(\mathsf{J}_{\mathcal{G}})$ with eigenvector $\mathbf{z} = (\mathbf{0}, \bar{\mathbf{z}})^T$.

Remark 13.5 The subgraph $\mathcal{G}_3$ given by $\mathcal{N}_{\mathcal{G}_3} = \mathcal{N}_{\mathcal{G}}$ and $\mathcal{E}_{\mathcal{G}_3} = \mathcal{E}_{\mathcal{G}}\backslash(\mathcal{E}_{\mathcal{G}_1} \cup \mathcal{E}_{\mathcal{G}_1})$ is a complete bipartite graph.

Theorem 13.15 implies that if an edge or node, which is not a complete node, is added to or deleted from $\mathcal{G}_1$, then the effect on the eigenvalues and eigenvectors will primarily be manifested only in $\mathcal{G}_1$.

If the barrier set $\bar{\mathcal{N}}$ is complete, a more thorough description of the eigenvalues and eigenvectors of $\mathsf{J}_{\mathcal{G}}$ than that of Theorem 13.14 is possible. Recall the simplifying assumption that for all $r, 0 \leq r \leq n, \widehat{\mathsf{J}}(r)$ has a complete set of eigenvectors.

Theorem 13.16 *Consider a network of n reactors represented by a graph $\mathcal{G}$ and assume there exists $\mathcal{N}_0$ defined by (13.113), such that $\mathcal{N}_0$ is a proper subset of $\mathcal{N}_{\mathcal{G}}$. Then there exist subgraphs $\mathcal{G}_i, i = 0, \ldots, l$, such that $\mathcal{N}_{\mathcal{G}_0} = \mathcal{N}_0; \mathcal{G}_i, i = 1, \ldots, l$, are completely connected with respect to $\mathcal{N}_0$;*

$$\mathcal{N}_{\mathcal{G}} = \mathcal{N}_0 \cup \left(\cup_{i=1}^l \mathcal{N}_{\mathcal{G}_i}\right) \equiv \{v_1, \ldots, v_{n_0}\} \cup \left(\cup_{i=1}^l \{v_{n_{i-1}+1}, \ldots, v_{n_i}\}\right); \tag{13.115}$$

$$\mathcal{E}_{\mathcal{G}} = \cup_{i=0}^l \mathcal{E}_{\mathcal{G}_i}. \tag{13.116}$$

Moreover the eigenvalues of $\mathsf{J}_{\mathcal{G}}$ include the eigenvalues of J of multiplicity at least 1; the eigenvalues of $\widehat{\mathsf{J}}(n)$ of multiplicity at least n_0; the eigenvalues of $\mathsf{J}_{\mathcal{G}_i}(n_0)$ that are not eigenvalues of $\widehat{\mathsf{J}}(n_0)$ of multiplicity at least one; and the eigenvalues of $\widehat{\mathsf{J}}(n_0)$ of multiplicity at least $l - 1$. The eigenvectors of $\mathsf{J}_{\mathcal{G}}$ have the form

$$\mathbf{z} = (\mathbf{z}_0, \ldots, \mathbf{z}_l)^T, \ \mathbf{z}_i \in \mathbb{R}^{kl_i}, \quad l_i = |\mathcal{G}_i| = \begin{cases} n_0, & i = 0, \\ n_i - n_{i-1}, & i = 1, \ldots, l. \end{cases} \tag{13.117}$$

Let $\bar{\mathbf{z}}_j^0, j = 1, \ldots, k$, be linearly independent eigenvectors of J. Then there are k corresponding linearly independent eigenvectors of $\mathsf{J}_{\mathcal{G}}$ given by Theorem 13.2. Let $\bar{\mathbf{z}}_j^n, j = 1, \ldots, k$, be linearly independent eigenvectors of $\widehat{\mathsf{J}}(n)$. Then there are $n_0 k$ corresponding linearly independent eigenvectors of $\mathsf{J}_{\mathcal{G}}$ given by Theorem 13.11. Let $\mathsf{L}_{\mathcal{G}_i}$ be the Laplacian matrix associated with $\mathcal{G}_i$ and let $\bar{\mathbf{z}}_i^j, j = 1, \ldots, l_i - 1$, be the $l_i - 1$ linearly independent eigenvectors of $\mathsf{L}_{\mathcal{G}_i}$ not associated with the

eigenvalue 0. Then there are $k(l_i - 1)$ linearly independent eigenvectors, $\mathbf{z}_i^j$, of $\mathbf{J}_{\mathcal{G}_i}(n_0)$, $i = 1, \ldots, l$, not associated with the eigenvalues of $\widehat{\mathbf{J}}(n_0)$, and thus $k(l_i - 1)$ corresponding linearly independent eigenvectors of $\mathbf{J}_{\mathcal{G}}$ such that

$$\mathbf{z}_m = \begin{cases} \mathbf{0}, & m \neq i, \\ \mathbf{z}_i^j, & m = i, \end{cases} \quad m = 0, \ldots, l. \tag{13.118}$$

Let $\bar{\mathbf{z}}_0^j$, $j = 1, \ldots, k$, be linearly independent eigenvectors of $\widehat{\mathbf{J}}(n_0)$. Then there are $k(l - 1)$ corresponding linearly independent eigenvectors of $\mathbf{J}_{\mathcal{G}}$ such that

$$\mathbf{z}_i = \begin{cases} \mathbf{0}, & i = 0, \\ \alpha_i (\bar{\mathbf{z}}_j^{n_0}, \ldots, \bar{\mathbf{z}}_j^{n_0})^T, & i = 1, \ldots, l, \end{cases} \tag{13.119}$$

where

$$\sum_{i=1}^{l} \alpha_i l_i = 0. \tag{13.120}$$

Remark 13.6 If for any $r_1 \neq r_2$ the eigenvalues of $\widehat{\mathbf{J}}(r_1)$ and $\widehat{\mathbf{J}}(r_2)$ are distinct, then the multiplicities of the eigenvalues in Theorem 13.16 of $\mathbf{J}$, $\widehat{\mathbf{J}}(n)$, and $\widehat{\mathbf{J}}(n_0)$ are precisely 1, n_0, and $l - 1$, respectively. If additionally the l_i, $i = 1, \ldots, l$, are distinct, then the same is true for the eigenvalues of $\mathbf{J}_{\mathcal{G}_i}(n_0)$. The eigenvalues of $\mathbf{J}_{\mathcal{G}}$ leading to Turing instabilities are the eigenvalues of $\widehat{\mathbf{J}}(r)$, $r \geq n_0$.

In principle, eigenvalues and eigenvectors of graphs with complete nodes can be found if eigenvalues and eigenvectors of appropriate subgraphs can be computed. In some cases it is possible to find all the eigenvalues and eigenvectors associated with such a network. The simplest case is that of a star graph (Fig. 13.3a) $\mathcal{G}$ of n nodes such that $\mathcal{E}_{\mathcal{G}} = \{(v_1, v_i) | i = 2, \ldots, n\}$.

Theorem 13.17 *Consider a network of n nodes represented by a star graph $\mathcal{G}$. Then the eigenvalues of $\mathbf{J}_{\mathcal{G}}$ are the eigenvalues of $\mathbf{J}$; the eigenvalues of $\widehat{\mathbf{J}}(1)$ of multiplicity $n - 2$; and the eigenvalues of $\widehat{\mathbf{J}}(n)$. The eigenvectors of $\mathbf{J}_{\mathcal{G}}$ associated with the eigenvalues of $\mathbf{J}$ are given by Theorem 13.16.*

Remark 13.7 If $\mathcal{G}$ is a complete or star graph, all the eigenvalues of its Laplacian are integers. A list of Laplacians with only integer eigenvalues is given in [173].

A second example where all the eigenvalues and eigenvectors associated with a network can be found is the following case. Since a complete description of the eigenvalues and eigenvectors associated with a linear array is available, networks built from linear arrays can be analyzed. In particular let $\mathcal{G}$ be a network formed from a linear array of n reactors by adding edges such that m nodes in $\mathcal{G}$ are complete (e.g., Fig. 13.3d with $m = 1$). Then a complete description of the eigenvalues and eigenvectors can be found.

Theorem 13.18 *Consider a network of n nodes represented by a graph $\mathcal{G}$ with $\mathcal{N}_{\mathcal{G}} = \{v_1, \ldots, v_n\}$ and*

$$\mathcal{E}_{\mathcal{G}} = \{(v_i, v_{i+1}) | i = 1, \ldots, n-1\} \cup \{(v, \bar{v}) \, | \forall \, \bar{v} \in \bar{\mathcal{N}}, \ v \in \mathcal{N}_{\mathcal{G}} \backslash \bar{v}\}, \quad (13.121)$$

where $\bar{\mathcal{N}} \subset \mathcal{N}_{\mathcal{G}} \backslash \{v_1, v_n\}$ such that $|\bar{\mathcal{N}}| = n_0$. Then there exist $\mathcal{G}_i$, $i = 1, \ldots, l$, and

$$\Lambda_j = \{\mathcal{G}_i | \, \big|\mathcal{N}_{\mathcal{G}_i}\big| = j, \ 1 \le i \le n\}, \quad j = 2, \ldots, n - n_0, \quad (13.122)$$

such that the eigenvalues of $\mathbf{J}_{\mathcal{G}}$ are the eigenvalues of $\mathbf{J}$; the eigenvalues of $\widehat{\mathbf{J}}(n)$ of multiplicity n_0; the eigenvalues of

$$\mathbf{J}\left(n_0 + 2\left(1 - \cos \frac{j\pi}{l_i}\right)\right), \quad j = 1, \ldots, l_i - 1, \quad (13.123)$$

of multiplicity $|\Lambda_j|$, where $l_i = \big|\mathcal{N}_{\mathcal{G}_i}\big|$; and the eigenvalues of $\widehat{\mathbf{J}}(n_0)$ of multiplicity $l - 1$. The eigenvectors of $\mathbf{J}_{\mathcal{G}}$ associated with the eigenvalues of $\mathbf{J}$, $\widehat{\mathbf{J}}(n)$, and $\widehat{\mathbf{J}}(n_0)$ are given by Theorem 13.16. The eigenvectors associated with the eigenvalues of (13.123) are given by (13.17) and Theorem 13.16.

13.4.2 Localized Pattern in Networks with Lengyel–Epstein Kinetics

Structural mode analysis is a linear stability analysis, while the stationary pattern of the network is the result of nonlinear dynamics. This raises the question if the pattern predicted by the linear analysis, i.e., the most unstable mode, is in qualitative agreement with the pattern finally selected. Jensen et al. [219] found in their study of the spatially continuous Lengyel–Epstein reaction–diffusion system that the stationary structures which finally appeared in the system showed good agreement with the prediction from linear analysis, provided the pattern developed from the uniform steady state. We investigate in this section if the same holds true for the Lengyel–Epstein model in networks of coupled reactors. We consider three examples of specific networks with particular parameter values to see if the results of Theorems 13.14, 13.17, and 13.18 carry over from the eigenvectors to the steady patterns. Figure 13.1 shows that the instability threshold $b^*(r)$ passes through a maximum, which occurs at

$$r_{\max} = \frac{4a^2\sqrt{10 + 250/a^2} - 10a^2 - 250}{2\kappa(a^2 + 25)}. \quad (13.124)$$

For our numerical simulations, we set $a = 50$, $d = 1.07$, and $\sigma = 20$. Then

$$r_{\max} = \frac{1.2932}{\kappa} \tag{13.125}$$

and $b_T = 3.6145$. (The Hopf threshold value is $b_H = 1.475$.) To obtain patterns associated with a specific $r \in \Gamma$, we choose κ so that (13.125) is satisfied with $r_{\max} = r$. Thus as κ changes, the value of $r_{\max}$ is shifted. Consequently, the first eigenvalue among the possible eigenvalues λ of $J_{\mathcal{G}}$ to pass through zero, i.e., the eigenvalue corresponding to the Turing condition, will vary, as will the associated structural mode to which the uniform steady state of $\mathcal{G}$ is unstable. As a result, we expect that the patterns will also change. For the numerical solutions we choose b slightly below the Turing threshold, namely $b = 3.5$, such that the uniform steady state is unstable and patterns form. The unique steady state is $(\overline{\rho}_u, \overline{\rho}_v) = (10, 101)$. To solve the system of ordinary differential equations (13.46) to steady state, we used the implicit multistep solver DASSL [58] with absolute and relative error tolerances of 10^{-8}, finite difference approximations for the Jacobian matrix and the dense matrix solver. The time interval used is $(0, 4 \times 10^7]$. All calculations are performed in double precision on a Compaq DS20 Alphastation. We represent the results by plotting the steady-state concentrations of the activator in the reactors, ρ_{ui}, $i = 1, \ldots, n$, where the horizontal axis corresponds to the reactor number. Plots of the concentrations of the inhibitor ρ_{vi} show the same qualitative behavior.

13.4.2.1 Star Graph

The simplest case of a network with a complete node is a star graph. We start our exploration of the nonlinear dynamical behavior of Lengyel–Epstein networks with a 10-node star graph, namely $\mathcal{G}_a$ of Fig. 13.3a. Theorem 13.17 implies that $\Gamma = \{1, 10\}$. Choosing $r = r_{\max} = 1$, we expect from (13.125) that a coupling strength of $\kappa = 1.2932$ will result in patterns on the 10-node star graph. We solve (13.46) with five initial conditions [$\boldsymbol{\rho} = (\rho_u, \rho_v)$]:

$(\boldsymbol{\rho}_1(0), \ldots, \boldsymbol{\rho}_{10}(0)) =$

$(10.2, 102, 9.96, 100.8, 10, 101, \ldots, 10, 101),$ \hfill (13.126)

$(10.2, 102, 9.96, 100.8, 10.2, 102, 9.96, 100.8, 10, 101, \ldots, 10, 101),$ \hfill (13.127)

$(10.2, 102, 9.96, 100.8, \ldots, 10.2, 102, 9.96, 100.8, 10, 101,$

$\quad 10, 101, 10, 101, 10, 101),$ \hfill (13.128)

$(10.2, 102, 9.96, 100.8, \ldots, 10.2, 102, 9.96, 100.8, 10, 101, 10, 101),$ \hfill (13.129)

$(10.2, 102, 9.96, 100.8, 10, 101, 10, 101, 10, 101, 10, 101, 10.2, 102,$

$\quad 9.96, 100.8, 10, 101, 10, 101).$ \hfill (13.130)

The resulting activator concentrations are shown in Fig. 13.4, from left to right, top to bottom. In all cases, the patterns are characterized by three constants, ρ_{u-},
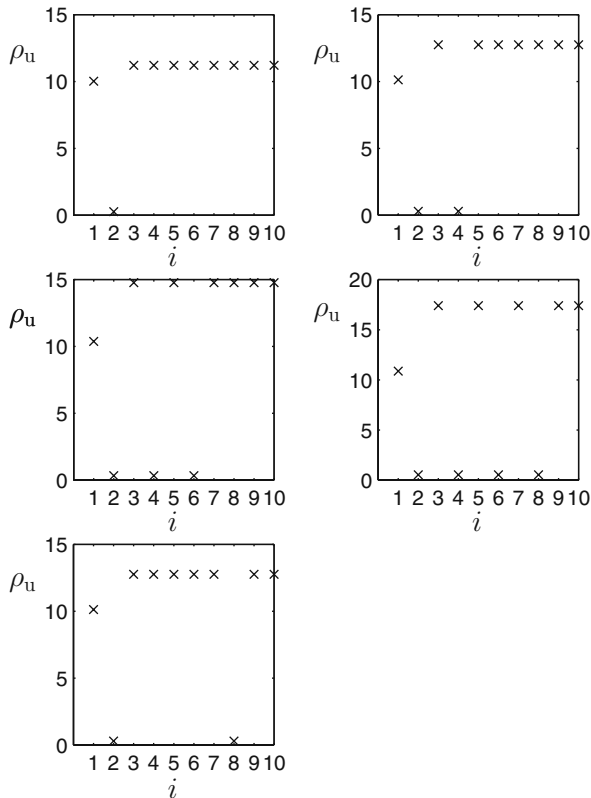
Fig. 13.4 Activator concentrations $\rho_{\mathrm{u}i}$ for the 10-node star graph, for initial conditions (13.126) (*top left*), (13.127), (13.128), (13.129), and (13.130) (*bottom left*). Reprinted from [305]. Copyright 2005, with permission from Elsevier

$\rho_{\mathrm{u}0}$, and $\rho_{\mathrm{u}+}$, where $\rho_{\mathrm{u}-} \approx 0$ and distinctly less than $\overline{\rho}_{\mathrm{u}}$, $\rho_{\mathrm{u}0} \approx \overline{\rho}_{\mathrm{u}}$, and $\rho_{\mathrm{u}+}$ distinctly larger than $\overline{\rho}_{\mathrm{u}}$. The actual value of the constants changes slightly as the number of nodes taking on those values varies. At the complete node ν_1, $\rho_{\mathrm{u}1} = \rho_{\mathrm{u}0}$. As the initial conditions change from (13.126) to (13.129), the number of nodes at which $\rho_{\mathrm{u}} = \rho_{\mathrm{u}-}$ increases from 1 to 4, while the number at which $\rho_{\mathrm{u}} = \rho_{\mathrm{u}+}$ decreases appropriately. Symmetry dictates that any permutation of a solution in the first four plots is also a solution. As an example, the solution in the last plot is a permutation of the solution in the second plot. The multiplicity of patterns for the same parameter values is due to the multiplicity of the root $r = 1$.

13.4.2.2 Completely Connected Circular Arrays

As a second example of the nonlinear dynamics of Lengyel–Epstein networks, we consider the graph $\mathcal{G}_b$ in Fig. 13.3b. As discussed above, this graph has three completely connected subgraphs, $\mathcal{G}'_{b,1}$, $\mathcal{G}'_{b,2}$, and $\mathcal{G}'_{b,3}$. For $\mathcal{G}'_{b,1}$, Theorem 13.14 and

(13.20) imply that if $\lambda \in \sigma(\widehat{\mathsf{J}}(6 - 2\cos(2j\pi/6)))$, $j = 1, 2, 3$, then $\lambda \in \sigma(\mathsf{J}_{\mathcal{G}_b})$. From Theorem 13.14 with $\mathcal{G}'_{b,2}$, the eigenvalues of $\widehat{\mathsf{J}}(7)$ are also eigenvalues of $\mathsf{J}_{\mathcal{G}_b}$. Finally with $\mathcal{G}'_{b,3}$, (13.16) and Theorem 13.14 imply that eigenvalues of $\widehat{\mathsf{J}}(4)$ are eigenvalues of $\mathsf{J}_{\mathcal{G}_b}$. From this we conclude that $\{4, 5, 7, 8\} \subset \Gamma$.

The values of κ corresponding to these values of r are 0.3233, 0.2586, 0.1847, and 0.1616. We obtain the stationary state of (13.46) numerically for the four values of κ and choose for all cases the initial conditions to be

$$(\boldsymbol{\rho}_1(0), \dots, \boldsymbol{\rho}_{15}(0)) =$$
$$(10.2, 102, 9.96, 100.8, 10, 101, \dots, 10, 101, 9.96, 100.8, 10.2, 102). \quad (13.131)$$

Steady state values of the activator for these four values of κ are shown in Fig. 13.5. When $\kappa = 0.3233$, the dominant eigenvalue and corresponding structural mode are associated with subgraph $\mathcal{G}'_{b,3}$. We therefore expect that the pattern will appear at only reactors 13 and 15. In fact the solution is constant on subgraphs $\mathcal{G}'_{b,1}$ and $\mathcal{G}'_{b,2}$ and varies on $\mathcal{G}'_{b,3}$ and on the remaining nodes. The constants are different, with neither constant being equal to $\overline{\rho}_\mathrm{u}$. The same is true when $\kappa = 0.2586$, except that the pattern appears on $\mathcal{G}'_{b,1}$, while the solution is constant (with different constants) on $\mathcal{G}'_{b,2}$ and $\mathcal{G}'_{b,3}$ and varies at the remaining nodes. Somewhat surprisingly the solution is not constant on the barrier set $\bar{\mathcal{N}}_{b,1}$. The pattern on $\mathcal{G}'_{b,1}$ is qualitatively the same as the associated structural mode $(1, 0, -1, -1, 0, 1)^T$. When $\kappa = 0.1847$, the pattern has moved to $\mathcal{G}'_{b,2}$ (the value $r = 7$ has multiplicity greater than one). The difference between the patterns for $\kappa = 0.1847$ and $\kappa = 0.1616$ is negligible and the pattern did not move back to $\mathcal{G}'_{b,1}$.

To investigate whether or not adding (or removing) an edge from a subgraph separated from another subgraph by a barrier set results in only local changes, we created a new graph $\hat{\mathcal{G}}_b$ by adding an edge between nodes ν_{12} and ν_{13} to $\mathcal{G}_b$. We expect that the solution behavior on $\mathcal{G}'_{b,1}$ should be only slightly affected. The steady state obtained when $\kappa = 0.2586$, seen on the left in Fig. 13.6, bears out this hypothesis, since the patterns on $\mathcal{G}'_{b,1}$ in both graphs (the upper right panel in Fig. 13.5 and the left panel in Fig. 13.6) are nearly identical while the symmetry on $\mathcal{G}'_{b,3}$ has been broken. Thus with complete connectivity coupled with a barrier set that is not complete we are able to obtain a "buffered" pattern, i.e., a pattern that is not affected by other parts of the graph, but not localized patterns.

To see if such localized patterns can appear, we consider $\mathcal{G}_c$ of Fig. 13.3c. Since $\mathcal{G}'_{c,1}$ and $\mathcal{G}'_{c,2}$ are completely connected subgraphs as described above, we have $\{5, 7, 8, 14\} \subset \Gamma$ and $4 \notin \Gamma$. Thus the largest value of κ is 0.2586. The corresponding steady state for the activator is shown on the right in Fig. 13.6. The solution is constant at the complete nodes and at the remaining nodes, but the constants are different. The constant at the complete nodes is approximately $\overline{\rho}_\mathrm{u}$. In this case the pattern is localized on $\mathcal{G}'_{c,1}$. Interestingly the pattern is also very close to the corresponding patterns on the two previous graphs (Fig. 13.5 upper right panel and Fig. 13.6 left panel).
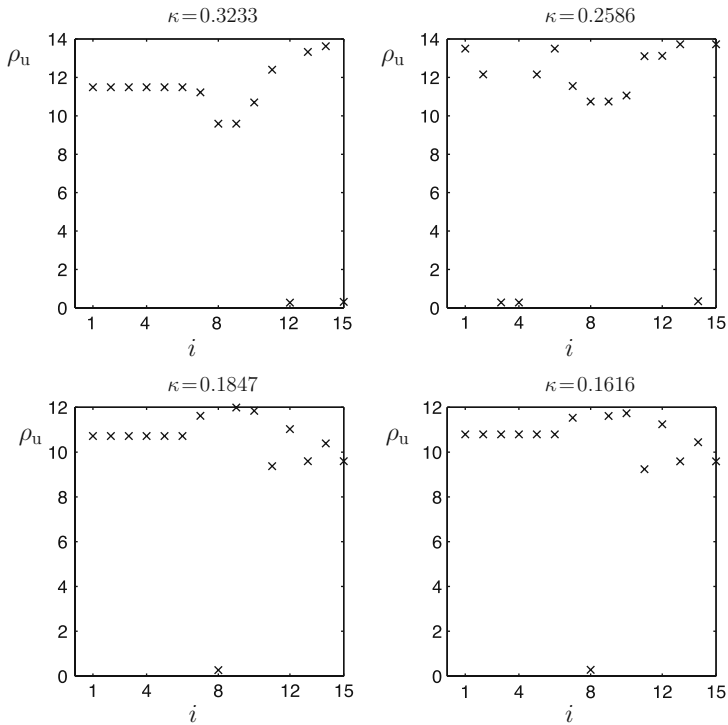
Fig. 13.5 Activator concentrations ρ_{ui} for the graph $\mathcal{G}_b$ for various values of κ. Reprinted from [305]. Copyright 2005, with permission from Elsevier
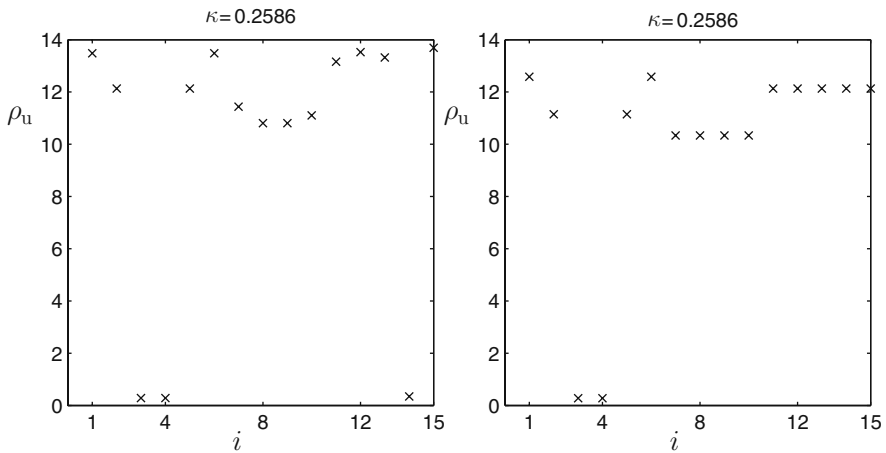
Fig. 13.6 Activator concentrations ρ_{ui} for $\kappa = 0.2586$ for the graph $\hat{\mathcal{G}}_b$ on the *left* and graph $\mathcal{G}_c$ on the *right*. Reprinted from [305]. Copyright 2005, with permission from Elsevier

13.4.2.3 Completely Connected Linear Arrays

In this example we investigate whether or not localized patterns exist for networks described in Theorem 13.18. We also examine the effect of varying κ on the type and location of observed patterns. If in Theorem 13.18 $n = 10$ and $\bar{\mathcal{N}} = \{v_5\}$, the result is $\mathcal{G}_d$ (see Fig. 13.3d). As discussed above, there are two completely connected linear arrays, $\mathcal{G}'_{d,1}$ and $\mathcal{G}'_{d,2}$, with four and six nodes, respectively. From Theorem 13.18 it follows that the eigenvalues of $\mathbf{J}_\mathcal{G}$ are the eigenvalues of: $\mathbf{J}$; $\widehat{\mathbf{J}}(10)$; $\widehat{\mathbf{J}}(1)$; $\widehat{\mathbf{J}}(3 - 2\cos(j\pi/4))$, $j = 1, 2, 3$; or $\widehat{\mathbf{J}}(3 - 2\cos(j\pi/5))$, $j = 1, \ldots, 4$. In this case

$$\Gamma = \{1, 1.3820, 1.5858, 2.3820, 3, 3.6180, 4.4142, 4.6180, 10\}. \qquad (13.132)$$

The values $r \in \Gamma$ between 1 and 10 alternate between $3 - 2\cos(j\pi/5)$, $j = 1, 2, 3$, and $3 - 2\cos(j\pi/4)$, $j = 1, 2$. Solutions are calculated using values of $\kappa = 1.2932$, $0.9357, 0.8155, 0.5429, 0.4311, 0.3574$, and 0.2930, corresponding to the first seven values in Γ, such that (13.125) holds. Additionally a solution is computed with $\kappa = 1.5$. The steady state activator concentrations for each of these cases are shown in Fig. 13.7, where the initial conditions are

$$(\boldsymbol{\rho}_1(0), \ldots, \boldsymbol{\rho}_{10}(0)) =$$
$$(10.2, 102, 9.96, 100.8, 10, 101, \ldots, 10, 101, 9.96, 100.8, 10.2, 102). \quad (13.133)$$

When $\kappa = 1.5$, the pattern corresponds to the structural mode associated with $r = 1$, and like the patterns in Sect. 13.4.2.1 it is characterized by three constants. With $\kappa = 1.2932$, a localized pattern emerges on $\mathcal{G}'_{d,2}$ corresponding to $r = 0.9357$ rather than $r = 1$ since $b < b_T$. The activator concentrations then alternate between localized patterns on $\mathcal{G}'_{d,2}$ and $\mathcal{G}'_{d,1}$. Patterns on $\mathcal{G}'_{d,2}$ are in good qualitative agreement with the structural modes but less so on $\mathcal{G}'_{d,1}$. Thus the eigenvectors have some predictive value. Since $l = 2$, only two constant values are attained on the nonpattern portion of the domain, one constant for the barrier set and the other for the remainder of the nodes. As in Sect. 13.4.2.2, at steady state, the constant values of ρ_u on the portion of the domain without a pattern are not equal to $\bar{\rho}_u$, while the value of the activator at the complete node, v_5, is close to $\bar{\rho}_u$. When $\kappa = 0.2930$, a pattern appears over the whole domain (the value of κ corresponding to $r = 4.6180$ is 0.2800) which is not constant on either $\mathcal{G}'_{d,1}$ or $\mathcal{G}'_{d,2}$, as opposed to the solution when $\kappa = 1.5$.

From Theorem 13.10 we expect that edge removal can lead to patterns at larger coupling strength. However, edge removal may also break up a subgraph leading to less robust localized patterns. To that end we consider a new graph $\hat{\mathcal{G}}_d$ obtained from $\mathcal{G}_d$ by removing the edge connecting nodes 7 and 8. Thus there are three subgraphs ($l = 3$) $\hat{\mathcal{G}}'_{d,1}$, $\hat{\mathcal{G}}'_{d,2}$ and $\hat{\mathcal{G}}'_{d,3}$ with nodes $\{v_1, \ldots, v_4\}$, $\{v_6, v_7\}$ and $\{v_8, v_9, v_{10}\}$, respectively, where $\hat{\mathcal{G}}'_{d,1} = \mathcal{G}'_{d,1}$. Now

$$\Gamma = \{1, 1.5858, 2, 3, 4, 4.4142, 10\}. \qquad (13.134)$$
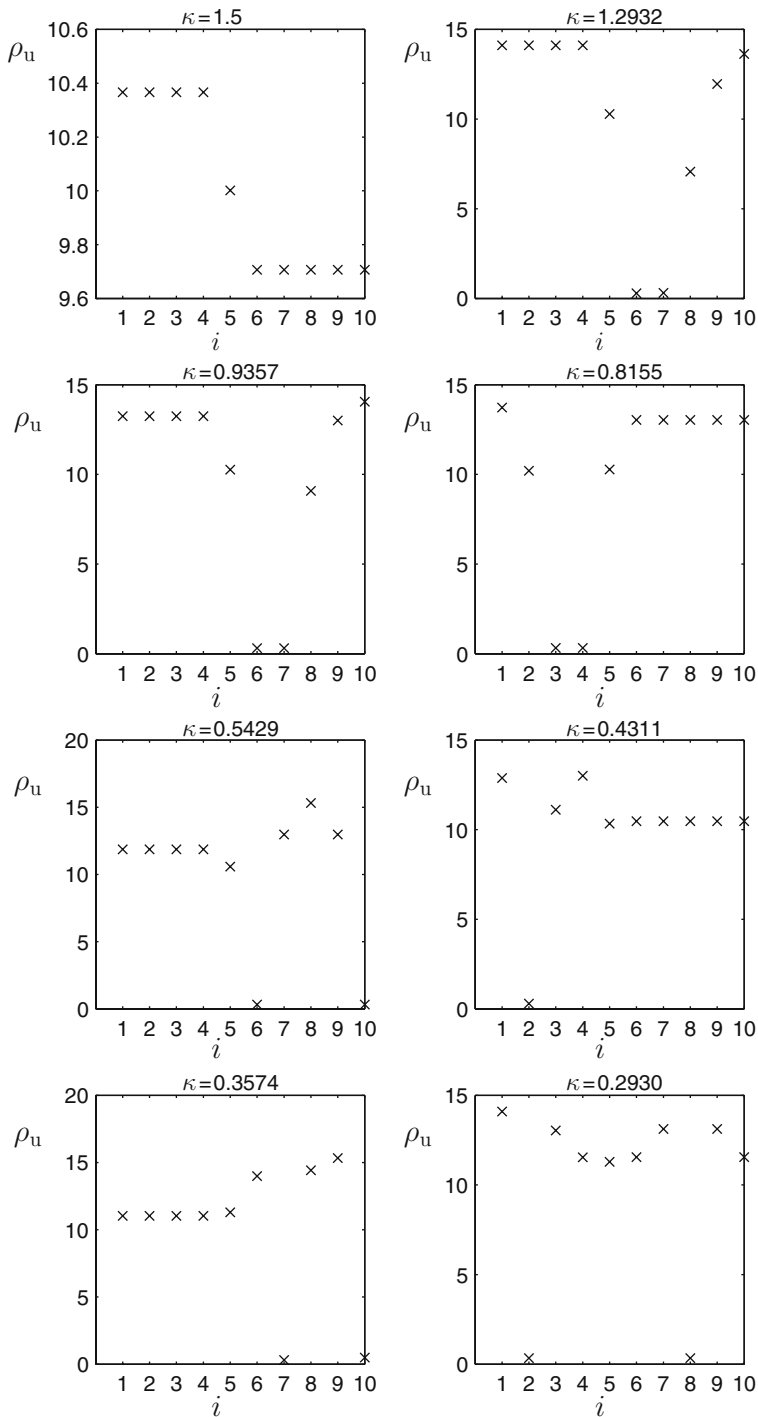
Fig. 13.7 Activator concentrations $\rho_{\mathrm{u}i}$ for various values of κ on $\mathcal{G}_d$. Reprinted from [305]. Copyright 2005, with permission from Elsevier

Activator concentrations computed with $\kappa = 1.2932, 0.9357, 0.8155, 0.6466,$ and 0.4311, which correspond to the first five values in Γ, and the initial conditions (13.133) are shown in the first five plots of Fig. 13.8. The activator concentration of a second solution, when $\kappa = 0.4311$, with initial conditions

$$(\boldsymbol{\rho}_1(0), \ldots, \boldsymbol{\rho}_{10}(0)) = (10, 101, 10, 101, 10, 101, 10, 101, 10, 101,$$
$$10.2, 102, 9.96, 100.8, 10, 101, \ldots, 10, 101), \quad (13.135)$$
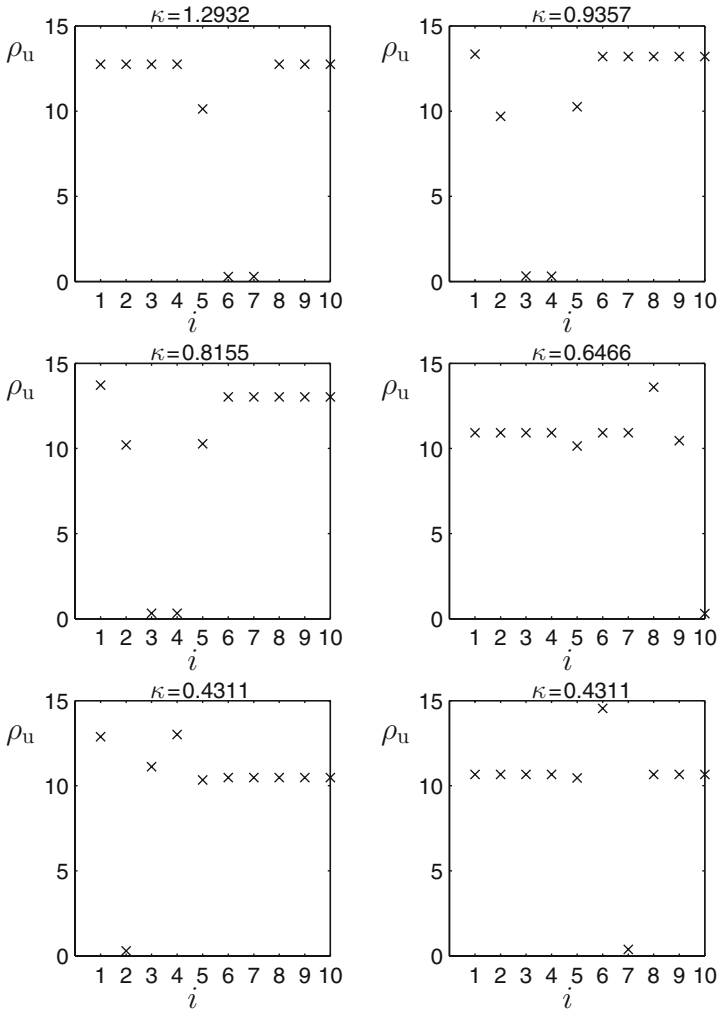
Fig. 13.8 Activator concentrations $\rho_{\mathrm{u}i}$ for various values of κ on $\hat{\mathcal{G}}_d$. Reprinted from [305]. Copyright 2005, with permission from Elsevier

is shown in the last plot of Fig. 13.8, since $r = 3$ is shared by both $\hat{\mathcal{G}}'_{d,1}$ and $\hat{\mathcal{G}}'_{d,2}$. The pattern corresponding to $r = 1$ (this time characterized by four constants since $l = 3$) is obtained when $\kappa = 1.2932$. Comparing the plots from both graphs when $\kappa = 1.2932$, we find that localized patterns do not appear until κ is smaller when the edge is removed. When $\kappa = 0.9357$ and 0.8155, the steady-state pattern is nearly identical to the one obtained on $\mathcal{G}_d$ as seen in Fig. 13.7. This supports the observation made earlier that adding or removing edges from the "non-pattern" portion of the graph does not affect the pattern. When $\kappa = 0.4311$, two different patterns are obtained from two different initial conditions, one a pattern on $\hat{\mathcal{G}}'_{d,1}$ and the second a pattern on $\hat{\mathcal{G}}'_{d,2}$. As in Sect. 13.4.2.1, when eigenvalues have multiplicity greater than one, multiple patterns are possible. In this case, however, both patterns are localized.

13.5 Turing Instability in Large Arrays

In the previous two sections we considered instabilities in networks of small and moderate sizes. Such networks are convenient to illustrate the analysis of arrays of diffusively coupled reactors, since the eigenvalues of the Laplacian matrix and the associated structural modes can be obtained with modest computational effort and patterns on such networks are easily visualized. We stress, however, that the structural mode analysis applies to networks of arbitrary size, even very large networks. Gaining complete knowledge of the Laplacian spectrum and the structural modes represents the main difficulty in the study of spatial instabilities of very large arrays of diffusively coupled reactors. Though complex networks have received tremendous interest, the spectrum and eigenvectors of the Laplacian matrix have received far less attention. The full spectrum and properties of the eigenvectors of the Laplacian have been investigated for random Erdös–Rényi networks [48] and small-world networks [302]. For a definition of Erdös–Rényi networks, small-world networks, and other types of networks, see for example [4]. McGraw and Menzinger examined numerically the eigenvalues and eigenvectors of the Laplacian for random Erdös–Rényi networks with Poisson degree distribution and Barabási–Albert networks with scale-free distribution [272]. They found that some of the structural modes of these networks are strongly localized. Increased clustering in the network, i.e., the tendency of neighbors of a given node to form links with each other, leads to more localized eigenvectors of the Laplacian. Zhang and coworkers have derived exact expressions for the eigenvalues and eigenvectors of the Laplacian for a family of growing tree-like networks [498].

Nakao and Mikhailov [316] performed numerical simulations of an activator–inhibitor model, namely the Mimura–Murray model, on a large array, namely a Barabási–Albert scale-free network with 1000 nodes and mean degree of 20:

$$\frac{d\boldsymbol{\rho}_i}{dt} = \mathbf{F}(\boldsymbol{\rho}_i, \boldsymbol{\mu}) + \sum_{j=1}^{n} L_{ij}\mathsf{D}\boldsymbol{\rho}_j, \quad i = 1, \ldots, n = 1000, \tag{13.136}$$

where

$$\mathbf{F}(\boldsymbol{\rho}) = \begin{pmatrix} F_1(\rho_u, \rho_v) \\ F_2(\rho_u, \rho_v) \end{pmatrix} = \begin{pmatrix} \left[\dfrac{1}{9}\left(35 + 16\rho_u - \rho_u^2\right) - \rho_v \right]\rho_u \\[2ex] \left[\rho_u - \left(1 + \dfrac{2}{5}\rho_v\right) \right]\rho_v \end{pmatrix} \qquad (13.137)$$

and

$$\mathsf{D} = \kappa\,\mathrm{diag}(1, \theta). \qquad (13.138)$$

The model has one nontrivial, physically acceptable uniform steady state, namely $(\overline{\rho}_u, \overline{\rho}_v)_i = (5, 10)$. The critical ratio of the diffusion coefficients necessary for a Turing instability is $\theta_c = 15.5$. The numerical simulations were performed for $\kappa = 0.12$ and $\theta = 15.6$. For these conditions, the critical structural mode is not localized. Starting from almost uniform initial conditions with very small perturbations, the activator concentration initially resembles closely the critical mode, but it develops into a quite different final pattern. The activator concentration for a large number of nodes, in particular for all nodes with a high degree, $k_i > 24$, remains close to, and mostly somewhat above, the USS value of 5. Nodes with a relatively small degree, $k_i < 24$, separate into two groups. In one group, the activator concentration is near, and mostly slightly above, the USS value of 5. In the other group, the activator concentration drops to lower values, in the vicinity of 2.5. The numerical simulations showed that the network displays multistability. Different patterns were observed for the same parameter values, and the final pattern depended sensitively on initial conditions. Increasing and decreasing the ratio θ revealed hysteresis effects between the various patterns. Numerical simulations with Brusselator kinetics and random Erdös–Rényi networks yielded similar results.

13.6 Turing Instability in Small Inhomogeneous Arrays

So far we have considered homogeneous networks with Lengyel–Epstein kinetics; all reactors were loaded with the same concentration of substrate. Since the substrate concentration plays a crucial role in ensuring the observability of Turing patterns, see (13.51), the question naturally arises how inhomogeneities affect the Turing threshold. The theory of Pearson and Bruno for systems where N mobile species react with Q immobile species [347] leads to the conclusion that $\sigma(x) > \sigma_c^*(a)$ everywhere is a sufficient condition for the Turing bifurcation to be the primary bifurcation of the uniform steady state in a reaction–diffusion system with Lengyel–Epstein kinetics. However, this is only a sufficient condition. We expect that as long as the regions where $\sigma(x) < \sigma_c^*(a)$ are sufficiently small or $\left|\sigma(x) - \sigma_c^*(a)\right|$ is not too large in those regions, the Turing bifurcation should still occur before the Hopf bifurcation. As discussed in Chap. 11, the analytical determination of the stability of spatially continuous reaction–diffusion systems with spatial nonuniformities is

difficult. The situation is much more favorable for networks of coupled reactors, since their evolution is governed by a set of ordinary differential equations. Structural mode analysis cannot be applied to inhomogeneous arrays of reactors, and we have to resort to the general method of linear stability analysis based on the Routh–Hurwitz criterion, see Sect. 13.1.1, for such systems.

We consider inhomogeneous networks with Lengyel–Epstein kinetics where the substrate concentration, i.e., the value of σ, can differ from reactor to reactor [208]. All other parameters are independent of the reactor number i. The evolution equations are

$$\mathsf{S}_i \frac{\mathrm{d}\boldsymbol{\rho}_i}{\mathrm{d}t} = \mathbf{F}(\boldsymbol{\rho}_i, \boldsymbol{\mu}) + \sum_{j=1}^{n} L_{ij} \mathsf{D} \boldsymbol{\rho}_j, \quad i = 1, \ldots, n, \tag{13.139}$$

where

$$\mathbf{F}(\boldsymbol{\rho}) = \begin{pmatrix} F_1(\rho_{\mathrm{u}}, \rho_{\mathrm{v}}) \\ F_2(\rho_{\mathrm{u}}, \rho_{\mathrm{v}}) \end{pmatrix} = \begin{pmatrix} a - \rho_{\mathrm{u}} - 4 \dfrac{\rho_{\mathrm{u}}\rho_{\mathrm{v}}}{1 + \rho_u^2} \\ b \left[\rho_{\mathrm{u}} - \dfrac{\rho_{\mathrm{u}}\rho_{\mathrm{v}}}{1 + \rho_u^2} \right] \end{pmatrix}, \tag{13.140}$$

$$\mathsf{S}_i = \begin{pmatrix} \sigma_i & 0 \\ 0 & 1 \end{pmatrix}, \tag{13.141}$$

and

$$\mathsf{D} = \kappa \operatorname{diag}(1, d), \tag{13.142}$$

with $a, b, d > 0$.

Generally, inhomogeneities in parameters of an array of reactors lead to nonuniform steady states. This is not the case for Lengyel–Epstein networks with inhomogeneities in the parameter σ, as is clear from the structure of (13.139). The network still has a unique uniform steady state given by (13.52). We use the Routh–Hurwitz criterion to determine the stability boundaries of this USS. Note that the Routh–Hurwitz analysis is general and can deal with the case where inhomogeneities in parameters lead to nonuniform steady states. Let

$$\lambda^m + c_1 \lambda^{m-1} + c_2 \lambda^{m-2} + \cdots + c_{m-1} \lambda + c_m = 0 \tag{13.143}$$

be the characteristic polynomial of the Jacobian matrix J_G of (13.139) evaluated at the steady state, $m = 2n$. As discussed in Sect. 1.2.3, a stationary bifurcation occurs if $c_m = 0$, see (1.36). We showed in Sect. 1.4.9 that a single CSTR with Lengyel–Epstein kinetics cannot undergo a stationary bifurcation. This implies that spatially homogeneous perturbations cannot have a vanishing real eigenvalue for the

array of CDIMA reactions, and $c_m = 0$, with $\Delta_l > 0$, is a necessary and sufficient condition for a Turing instability to occur. As discussed in Sect. 1.2.3, $\Delta_{m-1} = 0$, with $c_m > 0$, $\Delta_l > 0$, $l = 1, \ldots, m - 2$, is a necessary and sufficient condition for a conjugate pair of purely imaginary eigenvalues, i.e., for a Hopf bifurcation, see (1.38).

Therefore, the Turing bifurcation and the Hopf bifurcation occur together, if

$$c_m = 0 \quad \text{and} \quad \Delta_{m-1} = 0, \tag{13.144}$$

which determines the critical profile $\sigma_{i,c}(a)$. Since $\Delta_{m-1} = \Delta_{m-2} \cdot c_{m-1} - M_{m-2,m-1} \cdot c_m$, where $M_{i,j}$ is the minor of the (i, j)-element of the Hurwitz determinant Δ_{m-1}, (13.144) implies that $\Delta_{m-2} = 0$ also, if $c_{m-1} \neq 0$ which is the generic case. The Routh–Hurwitz stability analysis leads to a fully analytical criterion for the critical substrate concentration profile. This approach avoids time-consuming numerical searches of a large parameter space to determine the critical substrate concentration profile, i.e., the condition where the Turing bifurcation ceases to be the primary bifurcation.

We apply the Routh–Hurwitz analysis to linear inhomogeneous arrays of two, three, and four reactors. In the following we fix the coupling strength at $\kappa = 1$. Our results show that the Pearson and Bruno result, $\sigma_i > \sigma_c^*(a)$ for all reactors, is indeed only a sufficient condition for the Turing bifurcation to occur first. It is not a necessary condition. In fact, we find that for three and four coupled reactors, the Turing bifurcation will be the primary bifurcation, even if a reactor in the middle of the array contains no complexing agent at all, provided that a is low enough and σ high enough in those reactors that contain substrate.

13.6.1 Two Coupled Reactors

For two coupled reactors, the Jacobian $J_{\mathcal{G}}$ is given by

$$J_{\mathcal{G}} = \begin{pmatrix} R_1 & D_1 \\ D_2 & R_2 \end{pmatrix}, \tag{13.145}$$

where

$$R_i = \begin{pmatrix} (A_{11} - 1)/\sigma_i & A_{12}/\sigma_i \\ A_{21} & A_{22} - d \end{pmatrix} \tag{13.146}$$

and

$$D_i = \begin{pmatrix} 1/\sigma_i & 0 \\ 0 & d \end{pmatrix}. \tag{13.147}$$

The matrix A is given by (1.156).

The expressions for the coefficients c_m of the characteristic polynomial and the Hurwitz determinants Δ_l in terms of b, a, d, σ_1, and σ_2 are obtained using computational algebra software, such as MATHEMATICA (Wolfram Research, Inc., Champaign, IL, 2002) and MAPLE (Waterloo Maple Inc., Waterloo, Ontario, 2002). They are very lengthy already for only two coupled reactors and will not be displayed here. The condition $c_4 = 0$ yields the Turing threshold

$$b_{\mathrm{T}} = \frac{2d(a^2 - 175)}{35a}. \tag{13.148}$$

As expected, this expression is identical with the result (13.63) in Sect. 13.3.2.1 for $\kappa = 1$, since the parameter σ does not affect stationary bifurcations as discussed above. The Turing bifurcation exists if $a > a_{\min;2} = \sqrt{175} = 13.228756$. For a homogeneous array, i.e., $\sigma_1 = \sigma_2 = \sigma$, the Turing bifurcation occurs before the Hopf bifurcation if $\sigma > \sigma_c^*(a; 2)$ (the argument after the semicolon denotes the number of coupled reactors), where

$$\sigma_c^*(a; 2) = \frac{7(3a^2 - 125)}{2d(a^2 - 175)}. \tag{13.149}$$

For the inhomogeneous two-reactor array, let reactor 1 be the high-substrate reactor, $\sigma_1 > \sigma_c^*(a; 2)$, and reactor 2 the low-substrate reactor, $\sigma_2 < \sigma_c^*(a; 2)$. We vary σ_1 in reactor 1 and determine the critical concentration $\sigma_{2,\mathrm{c}}(\sigma_1, a, d)$ in reactor 2, as a function of σ_1. For $\sigma_2 > \sigma_{2,\mathrm{c}}(\sigma_1, a, d)$ the Turing bifurcation occurs first, whereas for $\sigma_2 < \sigma_{2,\mathrm{c}}(\sigma_1, a, d)$ the Hopf bifurcation is the primary bifurcation. We obtain the critical substrate concentration in reactor 2, $\sigma_{2,\mathrm{c}}(\sigma_1, a, d)$, by solving (13.144). We set $b = b_{\mathrm{T}}$, which ensures that the first condition of (13.144) holds, and use MATHEMATICA to solve $\Delta_3 = 0$ in terms of σ_2. The resulting expression for $\sigma_{2,\mathrm{c}}$ is very lengthy, about a dozen lines. It is not enlightening at all and will therefore not be displayed here. Instead we illustrate the behavior by choosing specific values for a and d and plot $\sigma_{2,\mathrm{c}}$ as a function of σ_1. As before, we choose $a = 50.0$ and $d = 1.07$ for all the arrays in this section. (The behavior is qualitatively similar for other values of these parameters. Below, we will no longer explicitly denote the dependence on d of quantities like $\sigma_{2,\mathrm{c}}$.) For these conditions, $b_{\mathrm{T}} = 2.84314$, and $\sigma_c^*(50; 2) = 10.3758$. If the concentration of substrate in reactor 1 is very large, i.e., $\sigma_1 \to \infty$, then the Turing instability occurs before the Hopf bifurcation if $\sigma_2 > \sigma_{2,\mathrm{c}}(\infty, 50) = 5.41038$. As σ_1 decreases, $\sigma_{2,\mathrm{c}}$ increases monotonically as can be seen from Fig. 13.9. As σ_1 approaches $\sigma_c^* = 10.3758$, so does $\sigma_{2,c}$.

These results lead to the conclusion that the USS of the array is more susceptible to the Hopf instability than to the Turing instability. If one reactor, i.e., half the system, contains no substrate, $\sigma_2 = 1$, then the Hopf bifurcation occurs first, no matter how large the substrate concentration σ_1 in the other reactor. In fact, for $a = 50.0$ the USS of the inhomogeneous two-reactor array will undergo a transition to oscillations first as b is decreased as long as $\sigma_2 < 5.41038$. Further, the
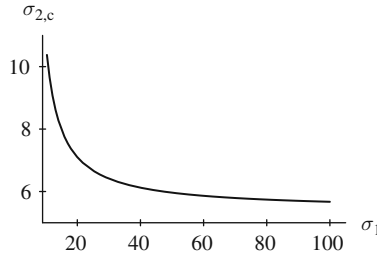
Fig. 13.9 Critical profile, $\sigma_{2,c}$ vs σ_1, for two coupled reactors with Lengyel–Epstein kinetics for $a = 50.0$, $d = 1.07$. Reprinted with permission from [208]. Copyright 2004, American Chemical Society

arithmetic mean of the critical profile, $\bar{\sigma}_c = \sigma_1 + \sigma_{2,c}(\sigma_1, a)$, and the geometric mean, $\hat{\sigma}_c = \sqrt{\sigma_1 \cdot \sigma_{2,c}(\sigma_1, a)}$, are larger than the critical value for a homogeneous array $\sigma_c^*(a; 2)$, which reinforces the conclusion that the USS is more vulnerable to an oscillatory instability than to a stationary instability.

13.6.2 Three Coupled Reactors

For three coupled reactors, the Jacobian is given by

$$J_{\mathcal{G}} = \begin{pmatrix} R_1 & D_1 & O \\ D_2 & \tilde{R}_2 & D_2 \\ O & D_3 & R_3 \end{pmatrix}, \tag{13.150}$$

where

$$\tilde{R}_i = \begin{pmatrix} (A_{11} - 2)/\sigma_i & A_{12}/\sigma_i \\ A_{21} & A_{22} - 2d \end{pmatrix} \quad \text{and} \quad O = \begin{pmatrix} 0 & 0 \\ 0 & 0 \end{pmatrix}. \tag{13.151}$$

The Turing condition corresponds to $c_6 = 0$ and again leads to the same threshold expression as (13.69) for $\kappa = 1$:

$$b_T = \frac{d(a^2 - 75)}{15a}. \tag{13.152}$$

A Turing bifurcation exists if $a > a_{\min;3} = \sqrt{75} = 8.660254$. For a homogeneous array, i.e., $\sigma_1 = \sigma_2 = \sigma_3 = \sigma$, the Turing bifurcation is the primary instability if $\sigma > \sigma_c^*(a; 3)$, where

$$\sigma_c^*(a; 3) = \frac{3(3a^2 - 125)}{d(a^2 - 75)}. \tag{13.153}$$

We consider two types of inhomogeneous substrate profiles, either an end reactor, say reactor 3, or the middle reactor has a different substrate concentration, i.e., (1) $\sigma_1 = \sigma_2 = \sigma > \sigma_3$ or (2) $\sigma_1 = \sigma_3 = \sigma > \sigma_2$. We determine the critical substrate profile, i.e., $\sigma_{3,c}(\sigma, a)$ in case 1 and $\sigma_{2,c}(\sigma, a)$ in case 2 by solving (13.144) with $n = 6$ for $\sigma > \sigma_c^*(a; 3)$. We proceed as for two coupled reactors and set $b = b_T$, which ensures that the first condition of (13.144) holds. We use MATHEMATICA to obtain Δ_5 in terms of σ_3 or σ_2, respectively. The solution of the second equation in (13.144), $\Delta_{m-1} = 0$, can no longer be found in closed, analytical form for three or more coupled reactors. The critical profile of the substrate concentration, $\sigma_{3,c}$ or $\sigma_{2,c}$, respectively, is obtained numerically. We emphasize that this is the only numerical step in the Routh–Hurwitz analysis. Analytical expressions are obtained for all other quantities and conditions. For $a = 50.0$ the Turing threshold is $b_T = 3.45967$ and $\sigma_c^*(50; 3) = 8.52683$. The critical profiles for case 1 and 2 are shown in Figs. 13.10 and 13.11, respectively. Again, $\sigma_{3,c}(\sigma, a)$ and $\sigma_{2,c}(\sigma, a)$ increase monotonically as σ decreases.
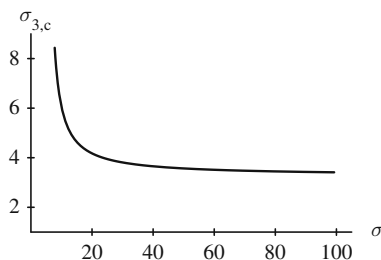
Fig. 13.10 Critical profile, $\sigma_{3,c}$ as a function of σ, for three coupled reactors with Lengyel–Epstein kinetics for case 1: $\sigma_1 = \sigma_2 = \sigma$; $a = 50.0$, $d = 1.07$. Reprinted with permission from [208]. Copyright 2004, American Chemical Society
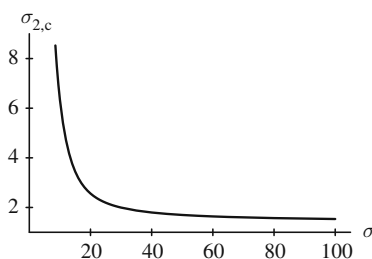
Fig. 13.11 Critical profile, $\sigma_{2,c}$ as a function of σ, for three coupled reactors with Lengyel–Epstein kinetics for case 2: $\sigma_1 = \sigma_3 = \sigma$; $a = 50.0$, $d = 1.07$. Reprinted with permission from [208]. Copyright 2004, American Chemical Society

The behavior of the critical profile is qualitatively the same in both cases and qualitatively the same as for two coupled reactors. A comparison of Figs. 13.10 and

13.11 with Fig. 13.9 shows that the critical values of the substrate concentration are lower for three coupled reactors than for two coupled reactors. This is due to the fact that Turing patterns are favored in two-thirds of the array for three coupled reactors, since two reactors have a substrate concentration above $\sigma_c^*(50; 3)$. For two coupled reactors, Turing patterns are favored only in half the array, explaining the higher critical value. For the three-reactor array, the critical substrate concentration is lower for case 2. Locating the reactor with a low substrate concentration at the end of the linear array, rather than in the middle, favors the Hopf bifurcation. The Hopf bifurcation always occurs first in both cases, if either $\sigma_3 = 1$ or $\sigma_2 = 1$, respectively, no matter how large σ is in the other two reactors. These results appear to strengthen the conclusion from the previous subsection that the Hopf bifurcation is more destabilizing than the Turing bifurcation in inhomogeneous Lengyel–Epstein networks. This is, however, not true, and the situation is more subtle for a three-reactor array. As a decreases, the critical profile retains the same qualitative form, but it shifts to lower values. For case 1, $\sigma_{3,c}(\sigma, a) > 1$ for $a > a_{\min;3}$, and if $\sigma_3 = 1$, then the Hopf instability occurs before the Turing bifurcation for all values of a and σ. The situation is different for case 2, where the reactor with the low substrate concentration is located in the middle. For a fixed value of $\sigma_1 = \sigma_3 = \sigma$, there exists an $a^* > a_{\min;3}$, such that for $a < a^*$ one finds $\sigma_{2,c}(\sigma, a) < 1$. The latter is physically unacceptable; experimentally σ cannot be smaller than one. The behavior of a^* as a function of σ is shown in Fig. 13.12. As σ increases, a^* increases and approaches an asymptotic value of 24.2072. For the largest experimentally acceptable value of the substrate concentration, $\sigma = 1000$, we find $a^* = 24.029$. For $a > 24.2072$, the Hopf bifurcation is the primary bifurcation, if $1 \leq \sigma_2 < \sigma_{2,c}(\sigma, a)$. For $a < 24.2072$ and σ sufficiently large, the Turing bifurcation always occurs first, even if the middle reactor contains no substrate. An inhomogeneous reactor array, where the reactor with the low substrate concentration is located in the middle, provides more favorable conditions for observing Turing patterns than an array where the reactor with the low substrate concentration is located at the end.
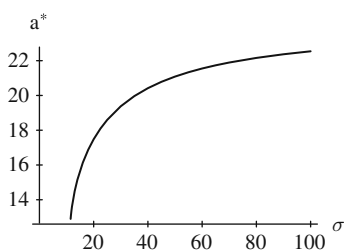
Fig. 13.12 Plot of a^* as a function of σ for three coupled reactors for case 2; $d = 1.07$. Reprinted with permission from [208]. Copyright 2004, American Chemical Society

13.6.3 Four Coupled Reactors

For four coupled reactors, the Jacobian is given by

$$J_{\mathcal{G}} = \begin{pmatrix} R_1 & D_1 & O & O \\ D_2 & \tilde{R}_2 & D_2 & O \\ O & D_3 & \tilde{R}_3 & D_3 \\ O & O & D_4 & R_4 \end{pmatrix}. \tag{13.154}$$

As shown in Sect. 13.3.2.3, see Table 13.1, two Turing instabilities can occur in a linear four-reactor array with $\kappa = 1$, namely

$$b_{\mathrm{T1}} = \frac{2d}{35a}(a^2 - 175), \tag{13.155}$$

with $a > a_{\mathrm{min};4(1)} = \sqrt{175} = 13.228756$, and

$$b_{\mathrm{T2}} = \frac{d}{235a}(2a^2 + 7\sqrt{2}a^2 - 2350 + 1175\sqrt{2}), \tag{13.156}$$

with $a > a_{\mathrm{min};4(2)} = 7.60544$. These two Turing bifurcations are degenerate at $a_{\mathrm{T0}} = 32.96566389$, and for $a \neq a_{\mathrm{T0}}$, the difference between b_{T1} and b_{T2} is small. For $a = 50.0$, the Turing instability corresponding to b_{T1} occurs first, $b_{\mathrm{T}} = b_{\mathrm{T1}} = 2.84314$, and $\sigma_c^*(50; 4) = 10.3758$. We have determined the critical substrate concentration profile for four cases following the same procedure as used for two and three coupled reactors: (1) $\sigma_1 = \sigma_2 = \sigma_3 = \sigma > \sigma_4$; (2) $\sigma_1 = \sigma_2 = \sigma_4 = \sigma > \sigma_3$; (3) $\sigma_1 = \sigma_2 = \sigma > \sigma_3 = \sigma_4$; (4) $\sigma_1 = \sigma_4 = \sigma > \sigma_2 = \sigma_3$.

The behavior of the critical substrate concentration is again qualitatively the same in all four cases and qualitatively the same as for two- and three-reactor arrays. Therefore we show only the two cases most favorable to Turing patterns, Figs. 13.13 and 13.14, which as expected are case 2 and case 4, where the low-substrate reactors are located in the interior of the array.

As for a linear array of three reactors, we find in case 2 that for a small enough and σ large enough, the Turing bifurcation always occurs first, even if the reactor
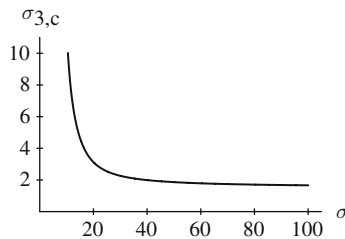
Fig. 13.13 Critical profile, $\sigma_{3,c}$ as a function of σ for four coupled reactors with Lengyel–Epstein kinetics for case 2: $\sigma_1 = \sigma_2 = \sigma_4 = \sigma$; $a = 50.0$, $d = 1.07$. Reprinted with permission from [208]. Copyright 2004, American Chemical Society
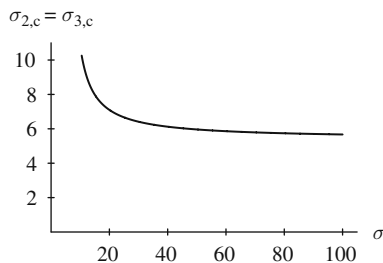
Fig. 13.14 Critical profile, $\sigma_{2,c} = \sigma_{3,c}$ as a function of σ, for four coupled reactors with Lengyel–Epstein kinetics for case 4: $\sigma_1 = \sigma_4 = \sigma$; $a = 50.0$, $d = 1.07$. Reprinted with permission from [208]. Copyright 2004, American Chemical Society

3 contains no substrate. We define, as for three coupled reactors, the critical value a^* by the condition that $\sigma_{3,c}(\sigma, a^*) = 1$. The behavior of a^* as function of σ is shown in Fig. 13.15. For $\sigma < 17.7$, two curves of Hopf bifurcation points approach each other, merge and vanish as a is decreased. This results in a jump of $\sigma_{3,c}$ from a value larger than 1 to a value smaller than 1, and the definition of a^* is no longer applicable.
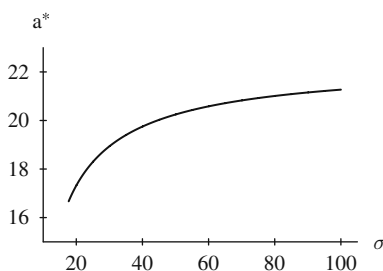
Fig. 13.15 Plot of a^* as a function of σ for four coupled reactors for case 2; $d = 1.07$. Reprinted with permission from [208]. Copyright 2004, American Chemical Society

13.7 Networks of Photochemically Coupled Reactors

In Sects. 13.3.2 and 13.4 we showed that the topology of the network strongly affects the stationary instability of the uniform steady state and the patterns which form on the network. A convenient way to implement complex network topologies is photochemical feedback coupling. Both the BZ reaction and the CDIMA reaction are photosensitive or exist in photosensitive variants [237, 210]. Photochemical coupling is implemented by measuring the concentration of one or more species, such as the activator or inhibitor. The concentration data are then fed into a computer algorithm to determine the light intensity that is projected onto each reactor in the network. This method of coupling was introduced by Showalter and coworkers in several experiments on the photosensitive BZ reaction [194, 193, 437].

We consider networks of coupled reactors such that in each CSTR the reactions are governed by

$$\frac{d\rho_u}{dt} = F_1(\rho_u, \rho_v, \phi) = \tilde{f}_1(\rho_u, \rho_v) + \phi \hat{f}_1(\rho_u, \rho_v), \tag{13.157a}$$

$$\frac{d\rho_v}{dt} = F_2(\rho_u, \rho_v, \phi) = \tilde{f}_2(\rho_u, \rho_v) + \phi \hat{f}_2(\rho_u, \rho_v). \tag{13.157b}$$

We consider only the case that the kinetic terms $F_1(\rho_u, \rho_v, \phi)$ and $F_2(\rho_u, \rho_v, \phi)$ depend linearly on the light intensity ϕ. This covers both the photosensitive BZ reaction and the CDIMA reaction, see Sect. 13.7.1. The influence of the projected light is additive if $\hat{f}_1$ and $\hat{f}_2$ are constants; otherwise it is multiplicative. We assume that the system (13.157) has a unique steady state $(\overline{\rho}_u(\phi), \overline{\rho}_v(\phi))$ which is stable. This requires that conditions (1.27) are satisfied, i.e., the trace of the Jacobian matrix

$$\mathsf{J}(\phi) = \begin{pmatrix} J_{11}(\phi) & J_{12}(\phi) \\ J_{21}(\phi) & J_{22}(\phi) \end{pmatrix} = \begin{pmatrix} \partial F_1/\partial \rho_u & \partial F_1/\partial \rho_v \\ \partial F_2/\partial \rho_u & \partial F_2/\partial \rho_v \end{pmatrix} \Bigg|_{(\overline{\rho}_u(\phi), \overline{\rho}_v(\phi))} \tag{13.158}$$

is negative,

$$T = \operatorname{tr} \mathsf{J}(\phi) = J_{11}(\phi) + J_{22}(\phi) < 0, \tag{13.159}$$

and the determinant is positive,

$$\Delta = \det \mathsf{J}(\phi) = J_{11}(\phi) J_{22}(\phi) - J_{12}(\phi) J_{21}(\phi) > 0. \tag{13.160}$$

13.7.1 Photosensitive BZ and CDIMA Reactions

As discussed in Sect. 1.4.8, the BZ reaction is well described by the two-variable Oregonator model (1.131). The BZ reaction is photosensitive if Ru(bpy)_3^{2+} is used as the catalyst. The effect of illumination can be modeled by a modification of (1.131) [237]:

$$F_1(\rho_u, \rho_v, \phi) = \frac{1}{\epsilon} \left\{ \rho_u - \rho_u^2 - [h\rho_v + \phi] \frac{\rho_u - q}{\rho_u + q} \right\}, \tag{13.161a}$$

$$F_2(\rho_u, \rho_v, \phi) = \rho_u - \rho_v. \tag{13.161b}$$

The steady states of an isolated reactor are given by $\overline{\rho}_v = \overline{\rho}_u$, where $\overline{\rho}_u$ is a root of the cubic equation:

$$\overline{\rho}_u^3 + \overline{\rho}_u^2 (h + q - 1) + \overline{\rho}_u (\phi - hq - q) - \phi q = 0. \tag{13.162}$$

Equation (13.162) has unique, physically acceptable solution if the stoichiometric parameter h is large enough.

The effect of illumination on the CDIMA reaction can be taken into account by a modified two-variable Lengyel–Epstein model [98]:

$$F_1(\rho_u, \rho_v, \phi) = a - \rho_u - 4\frac{\rho_u \rho_v}{1 + \rho_u^2} - \phi, \tag{13.163a}$$

$$F_2(\rho_u, \rho_v, \phi) = \sigma b \left[\rho_u - \frac{\rho_u \rho_v}{1 + \rho_u^2} + \phi \right]. \tag{13.163b}$$

The kinetic equations preserve positivity, see (1.2), if the light intensity satisfies

$$\phi \le a. \tag{13.164}$$

An isolated reactor has a unique steady state $(\overline{\rho}_u, \overline{\rho}_v)$ given by

$$\overline{\rho}_u = \frac{1}{5}a - \phi, \tag{13.165a}$$

$$\overline{\rho}_v = \frac{a(25 + a^2 - 10a\phi + 25\phi^2)}{25(a - 5\phi)}. \tag{13.165b}$$

A nonnegative steady state in an isolated reactor exists only if the light intensity satisfies a more stringent upper limit than (13.164), namely

$$\phi \le \frac{1}{5}a. \tag{13.166}$$

For $a/5 < \phi \le a$ the concentration of the inhibitor grows without bound as time goes to infinity in an isolated point reactor. In the following, we impose the bound given by (13.166).

13.7.2 Stability Analysis of Photochemically Coupled Reactors

A network of n photochemically coupled reactors is described by the following system of ordinary differential equations:

$$\frac{d\rho_{ui}}{dt} = F_1(\rho_{ui}, \rho_{vi}, \phi_i), \quad \frac{d\rho_{vi}}{dt} = F_2(\rho_{ui}, \rho_{vi}, \phi_i), \tag{13.167}$$

where

$$\phi_i = \frac{\phi_0}{2} \left\{ 1 + H\left[\kappa \sum_j L_{ij}(c_u \rho_{uj} + c_v \rho_{vj}) \right] \right\}. \tag{13.168}$$

Here $\phi_0/2$ is a reference level of illumination, the constant illumination experienced by a homogeneous state. The function $H(z)$ has the following properties: (i) H is monotonically increasing, (ii) $H(-\infty) = -1$, $H(0) = 0$, $H(+\infty) = 1$, and $H'(0) = 1$. A specific example is $H(z) = \tanh(z)$, which is used in the numerical simulation described below. The constant κ is the coupling strength and L is the Laplacian matrix of the network $\mathcal{G}$. If the coupling occurs only via the activator, $c_v = 0$, if only via the inhibitor, $c_u = 0$. The nature of the coupling, inhibitory or activatory, is characterized by the values ± 1 for c_u or c_v.

The system (13.167) with (13.168) has a uniform steady state $\bar{\rho}_{ui} = \bar{\rho}_u, \bar{\rho}_{vi} = \bar{\rho}_v, i = 1, \ldots, n$, with $\bar{\rho}_u = \bar{\rho}_u(\phi_0/2)$ and $\bar{\rho}_v = \bar{\rho}_v(\phi_0/2)$. The Jacobian matrix $\mathsf{J}_\mathcal{G}$ of the photochemically coupled array of reactors is given by

$$\mathsf{J}_\mathcal{G} = \mathsf{I}_n \otimes \mathsf{J}(\phi_0/2) + \mathsf{L} \otimes \kappa \mathsf{C}. \tag{13.169}$$

The coupling matrix C has entries

$$\mathsf{C} = \begin{pmatrix} C_{11} & C_{12} \\ C_{21} & C_{22} \end{pmatrix} = \begin{pmatrix} \frac{\phi_0}{2} c_u \hat{f}_1(\bar{\rho}_u, \bar{\rho}_v) & \frac{\phi_0}{2} c_v \hat{f}_1(\bar{\rho}_u, \bar{\rho}_v) \\ \frac{\phi_0}{2} c_u \hat{f}_2(\bar{\rho}_u, \bar{\rho}_v) & \frac{\phi_0}{2} c_v \hat{f}_2(\bar{\rho}_u, \bar{\rho}_v) \end{pmatrix} = \begin{pmatrix} c_u \overline{F} & c_v \overline{F} \\ c_u \overline{G} & c_v \overline{G} \end{pmatrix},$$

$$\tag{13.170}$$

where

$$\overline{F} \equiv \frac{\phi_0}{2} \hat{f}_1(\bar{\rho}_u, \bar{\rho}_v), \quad \overline{G} \equiv \frac{\phi_0}{2} \hat{f}_2(\bar{\rho}_u, \bar{\rho}_v). \tag{13.171}$$

As is clear from the structure of (13.169), the stability of the uniform steady state of a photochemically coupled network can be determined by structural mode analysis, as in the case of homogeneous diffusively coupled networks. According to Theorem 13.8, λ is an eigenvalue of $\mathsf{J}_\mathcal{G}$ if and only if λ is an eigenvalue of

$$\widehat{\mathsf{J}}(r) = \mathsf{J}(\phi_0/2) - r\kappa \mathsf{C}, \tag{13.172}$$

with $r = -\beta$, where β is any eigenvalue of L. The structural mode associated with $\beta_i, i = 1, \ldots, n$, undergoes a stationary instability if

$$\det \widehat{\mathsf{J}}(r) = 0, \tag{13.173}$$

and a Hopf instability if

$$\operatorname{tr} \widehat{\mathsf{J}}(r) = 0, \tag{13.174}$$

where $r = -\beta_i$.

13.7.3 Instability Thresholds

It is convenient to choose the coupling strength κ as the bifurcation parameter for photochemically coupled arrays of reactors. According to our assumptions (13.159) and (13.160) with $\phi = \phi_0/2$, the USS of the network is stable against uniform spatial perturbations. The nonuniform structural modes $i = 2, \ldots, n$ can undergo stationary or oscillatory instabilities. According to (13.173), the ith structural mode, $i > 1$, undergoes a stationary instability, as the coupling strength is increased, at the threshold value

$$\kappa_{st} = -\frac{\Delta}{[(c_v J_{11} - c_u J_{12})\overline{G} + (c_u J_{22} - c_v J_{21})\overline{F}]\beta_i}, \quad i > 1, \tag{13.175}$$

where $J_{lm} = J_{lm}(\phi_0/2)$. According to (13.174), the ith structural mode, $i > 1$, undergoes an oscillatory instability, as the coupling strength is increased, at the threshold value

$$\kappa_{osc} = -\frac{T}{(c_u \overline{F} + c_v \overline{G})\beta_i}, \quad i > 1. \tag{13.176}$$

The ith mode is stable if $\kappa < \min(\kappa_{st}, \kappa_{osc})$. Since the steady state of an isolated reactor is stable, i.e., $T < 0$ and $\Delta > 0$, see (13.159) and (13.160), it follows from (13.175) that the USS of the network can undergo a stationary bifurcation only if

$$(c_v J_{11} - c_u J_{12})\overline{G} + (c_u J_{22} - c_v J_{21})\overline{F} > 0. \tag{13.177}$$

Similarly, it follows from (13.176) that the USS can undergo a spatial Hopf bifurcation only if

$$c_u \overline{F} + c_v \overline{G} < 0. \tag{13.178}$$

The type of coupling that gives rise to either instability, i.e., inhibitory or activatory coupling, depends on the sign and value of the rate functions $\hat{f}_1$ and $\hat{f}_2$ at the uniform steady state.

The threshold conditions (13.175) and (13.176) imply that the first structural mode to become unstable is the mode with the most negative eigenvalue, i.e., the eigenvector of the network Laplacian associated with β_n. Increasing the coupling strength results in a "short-wavelength" instability as happens for diffusively coupled networks, see Sect. 13.2. There are, however, important differences between the instabilities in diffusively coupled networks and in photochemically coupled networks. (1) Diffusively coupled arrays of reactors cannot undergo an oscillatory spatial instability, if the kinetics depends only on two variables, see (13.37). (2) The USS becomes stable again as the coupling strength exceeds a maximum value $\kappa_+(\beta_i)$, see (13.45). (3) Adding edges to the graph has a stabilizing effect in diffusively coupled networks. As shown in Sect. 13.3.1, $\kappa_{max,G} \sim \beta_2^{-1}$. The

magnitude of β_2 typically increases with adding edges. Consequently, the maximum value of the coupling strength for which a Turing instability can occur in diffusively coupled Lengyel–Epstein networks decreases as the connectivity of the graph increases. Adding edges has a destabilizing effect for photochemically coupled networks. The threshold for a stationary or oscillatory instability of the USS is inversely proportional to β_n, whose magnitude also typically increases with adding edges thus lowering the instability threshold. For example, adding random long-range shortcuts to a circular array to generate small-world-like networks makes β_n more negative. To illustrate this, we consider a 10-node circular network which has $\beta_{10} = -4.000$, see Fig. 13.16c. A circular 10-node network with two extra edges between nodes 1 and 6 and nodes 4 and 9 has $\beta_{10} = -5.11491$, Fig. 13.16d. Networks with the lowest instability threshold belong to the class of graphs where the nth eigenvalue is equal to its lower bound, $\beta_n = -n$, see Theorem 13.7. Two members of this class are the complete graph of n nodes, corresponding to a network with all-to-all coupling, see Theorem 13.13, and the star graph of n nodes, see Theorem 13.17.
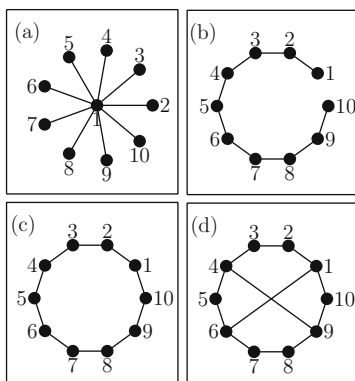
Fig. 13.16 Four 10-node graphs: (**a**) star graph, $\beta_{10} = -10$, (**b**) linear graph, $\beta_{10} = -3.90211$, (**c**) circular graph, $\beta_{10} = -4$, (**d**) small-world-like graph, $\beta_{10} = -5.11491$. Reprinted-rom [209]. Copyright 2006, with permission from Elsevier

13.7.4 Oregonator-Type Kinetics

For kinetic schemes with a structure similar to the Oregonator model, i.e., $\hat{f}_2(\rho_u, \rho_v) \equiv 0$, the expressions for the instability thresholds, (13.175) and (13.176), and for the instability conditions, (13.177) and (13.178), simplify to

$$\kappa_{st} = -\frac{\Delta}{(c_u J_{22} - c_v J_{21})\overline{F}\beta_n}, \tag{13.179}$$

$$\kappa_{osc} = -\frac{T}{c_u \overline{F}\beta_n}, \tag{13.180}$$

$$(c_u J_{22} - c_v J_{21})\overline{F} > 0, \tag{13.181}$$

$$c_u \overline{F} < 0. \tag{13.182}$$

If the coupling is via the inhibitor only, $c_u = 0$, then no Hopf instability can occur. The condition for a stationary instability to occur is given by

$$c_v J_{21} \overline{F} < 0. \tag{13.183}$$

For kinetic schemes that like the Oregonator model and pure activator–inhibitor schemes in general have $J_{21} > 0$, a stationary instability can occur only if c_v and $\overline{F}$ have opposite signs, i.e., if the coupling is inhibitory. The uniform steady state of an array of photochemically coupled Oregonator undergoes a stationary instability at

$$\kappa_{\mathrm{st}} = -\frac{2[-\phi_0 q + q^2(1 + h - 2\overline{\rho}_{\mathrm{u}}) - (2q\overline{\rho}_{\mathrm{u}} + \overline{\rho}_{\mathrm{u}}^2)(-1 + h + 2\overline{\rho}_{\mathrm{u}})]}{\phi_0(q^2 - \overline{\rho}_{\mathrm{u}}^2)\beta_n}, \tag{13.184}$$

for $c_v = 1$, which corresponds to inhibitory coupling for the following reason. Equation (13.161a) implies that an increase in the light intensity leads to a decrease in the production rate of the activator. If $c_v = 1$ and $v_j > v_i$, then reactor j increases the illumination on reactor i. Consequently, reactor j decreases the production of activator in reactor i; the coupling is inhibitory. If $c_v = -1$ and $v_j > v_i$, then reactor j decreases the illumination on reactor i. Consequently, reactor j increases the production of activator in reactor i; the coupling is activatory.

If the coupling is via the activator only, $c_v = 0$, the thresholds for the stationary and for the oscillatory instability are given by

$$\kappa_{\mathrm{st}} = -\frac{\Delta}{c_u \overline{F} J_{22} \beta_n}, \tag{13.185}$$

$$\kappa_{\mathrm{osc}} = -\frac{T}{c_u \overline{F} \beta_n}. \tag{13.186}$$

Since $T < 0$, an oscillatory instability of the uniform steady state of $\mathcal{G}$ occurs only for networks with inhibitory coupling, i.e., c_u and $\overline{F}$ have opposite signs. Interestingly, for kinetic schemes that like the Oregonator model and activator–inhibitor schemes in general have $J_{22} < 0$, a stationary instability also occurs only for networks with inhibitory coupling. If $|T| > |\Delta/J_{22}|$, the stationary instability is the primary instability; otherwise, the oscillatory instability occurs first.

13.7.5 Lengyel–Epstein-Type Kinetics

If the coupling is via the inhibitor only, $c_u = 0$, for kinetic schemes with a structure similar to the Lengyel–Epstein model, i.e., $\hat{f}_1(\rho_{\mathrm{u}}, \rho_{\mathrm{v}}) = -\mathrm{const}\, \hat{f}_2(\rho_{\mathrm{u}}, \rho_{\mathrm{v}})$, then the instability threshold expressions simplify:

$$\kappa_{\text{st}} = -\frac{\Delta}{c_v(J_{11}\overline{G} - J_{21}\overline{F})\beta_n},$$ (13.187)

$$\kappa_{\text{osc}} = -\frac{T}{c_v\overline{G}\beta_n}.$$ (13.188)

Equation (13.163) implies that an increase in the light intensity leads to a decrease in the production rate of the activator. Therefore $c_v = 1$ corresponds again to inhibitory coupling and $c_v = -1$ to activatory coupling.

The uniform steady state of $\mathcal{G}$ undergoes a Hopf instability only if $c_v\overline{G}$ is negative, i.e., for activatory coupling. The stationary instability can only occur if

$$c_v(J_{11}\overline{G} - J_{21}\overline{F}) > 0.$$ (13.189)

For pure activator–inhibitor schemes $J_{11} > 0$ and $J_{21} > 0$. These inequalities hold for the LE model if $a > a^\circ(\phi_0)$, which we assume to be the case in the following. The expression for $a^\circ(\phi_0)$ is rather cumbersome and not enlightening. For the following, only the lower bound $a^*(\phi_0) > 5 + 5\phi_0/2$ is needed. Since $\overline{G} > 0$ and $\overline{F} < 0$, a stationary instability cannot occur for LE networks with activatory coupling via v. On the other hand, in LE networks with inhibitory coupling via v, a Hopf instability is impossible and only the stationary instability can occur. Switching the nature of the coupling results in a change from an oscillatory instability of the network to a stationary instability, or vice versa.

The uniform steady state undergoes a stationary instability for inhibitory coupling at

$$\kappa_{\text{st}} = \frac{10\left(2a - 5\phi_0\right)^2}{a\phi_0\left[4a^2 - 20a\phi_0 + 25(\phi_0^2 - 4)\right]|\beta_n|},$$ (13.190)

and an oscillatory instability for activatory coupling at

$$\kappa_{\text{osc}} = \kappa_{\text{osc}}^* - \frac{2J_{11}}{\sigma b\phi_0|\beta_n|}.$$ (13.191)

Here

$$\kappa_{\text{osc}}^* = \frac{20\left(2a - 5\phi_0\right)}{\left[100 + (2a - 5\phi_0)^2\right]\phi_0\,|\beta_n|}$$ (13.192)

and

$$J_{11} = \frac{24a^3 - 100a^2\phi_0 + 50a\left(\phi_0^2 - 20\right) + 125\phi_0\left(\phi_0^2 + 4\right)}{(2a - 5\phi_0)\left[4a^2 - 20a\phi_0 + 25(\phi_0^2 + 4)\right]}.$$ (13.193)

As the concentration of the substrate is increased, the threshold of the oscillatory spatial instability increases and $\kappa_{\text{osc}} \to \kappa_{\text{osc}}^*$ as $\sigma \to \infty$. If

$$a < a_c(\phi_0) = \frac{5\left[4 + \phi_0^2 + 2\left(4 + \phi_0^2\right)^{1/2}\right]}{2\phi_0},$$ (13.194)

then $\kappa_{\text{osc}}^* < \kappa_{\text{st}}$ and a network with activatory coupling is always less stable than a network with the same topology and inhibitory coupling. If $a > a_c$, an inhibitory network is less stable than the corresponding activatory network for σ sufficiently large. Both κ_{st} and κ_{osc}^* approach $10/[a\phi_0\,|\beta_n|]$ for large a.

The behavior of networks photochemically coupled only via the inhibitor differs for networks of Oregonators and networks of reactors with LE kinetics. Switching from inhibitory to activatory coupling suppresses instabilities of the uniform steady state for Oregonator kinetics. For LE kinetics, switching from inhibitory to activatory coupling changes the instability of the uniform steady state from a stationary to an oscillatory instability without affecting the critical mode.

If the coupling occurs via the activator only, $c_v = 0$, then the instability conditions read

$$\kappa_{\text{st}} = -\frac{\Delta}{c_u(-J_{12}\overline{G} + J_{22}\overline{F})\beta_n},$$ (13.195)

$$\kappa_{\text{osc}} = -\frac{T}{c_u\overline{F}\beta_n}.$$ (13.196)

Since $\Delta > 0$, $J_{12} < 0$, $J_{22} < 0$, $\overline{F} < 0$, and $\overline{G} > 0$ for the LE model, $\mathcal{G}$ can undergo a stationary instability only if $c_u = 1$, i.e., for inhibitory coupling. Since $T < 0$ and $\overline{F} < 0$ for the LE model, $\mathcal{G}$ can undergo an oscillatory instability only if $c_u = 1$. If $|T/\overline{F}| > |\Delta/(-J_{12}\overline{G} + J_{22}\overline{F})|$, the stationary instability is the primary instability; otherwise, the oscillatory instability occurs first. In the case of photochemical coupling via the activator only, networks of Oregonators and networks of reactors with LE kinetics show the same behavior. Networks with activatory coupling are always stable, while networks with inhibitory coupling can display both a stationary and an oscillatory instability.

We have carried out some numerical studies to determine if the pattern predicted by the linear structural mode analysis is in qualitative agreement with the pattern finally selected by the photochemically coupled array. We have investigated the asymptotic states of LE networks with inhibitory coupling for the four graphs shown in Fig. 13.16, namely the linear 10-node graph, the circular 10-node graph, a circular 10-node graph with two extra edges (small-world-like graph), and the 10-node star graph.

The parameter values were $a = 10.0$, $\phi_0 = 0.1$, $\sigma = 1.0$, and $b = 5.0$. For these values, the uniform steady state $(\overline{\rho}_u(\phi_0/2), \overline{\rho}_v(\phi_0/2)) = (1.95, 4.92564)$ is stable and $a < a_c = 200.3749$. The stationary instability of the uniform state occurs

at $\kappa_{st} = 13.56824264/|\beta_{10}|$. (The threshold for the oscillatory instability in the corresponding networks with activatory coupling is $\kappa_{osc} = 2.54456146/|\beta_{10}|$.) In all cases, we have chosen the bifurcation parameter κ to be in the fully nonlinear regime, $\kappa = 23.56824264/|\beta_{10}|$, and a small perturbation of the uniform steady state as the initial condition. The system settles down to a steady pattern that resembles the structural mode associated with β_{10}, in good qualitative agreement with the linear analysis, see Fig. 13.17.
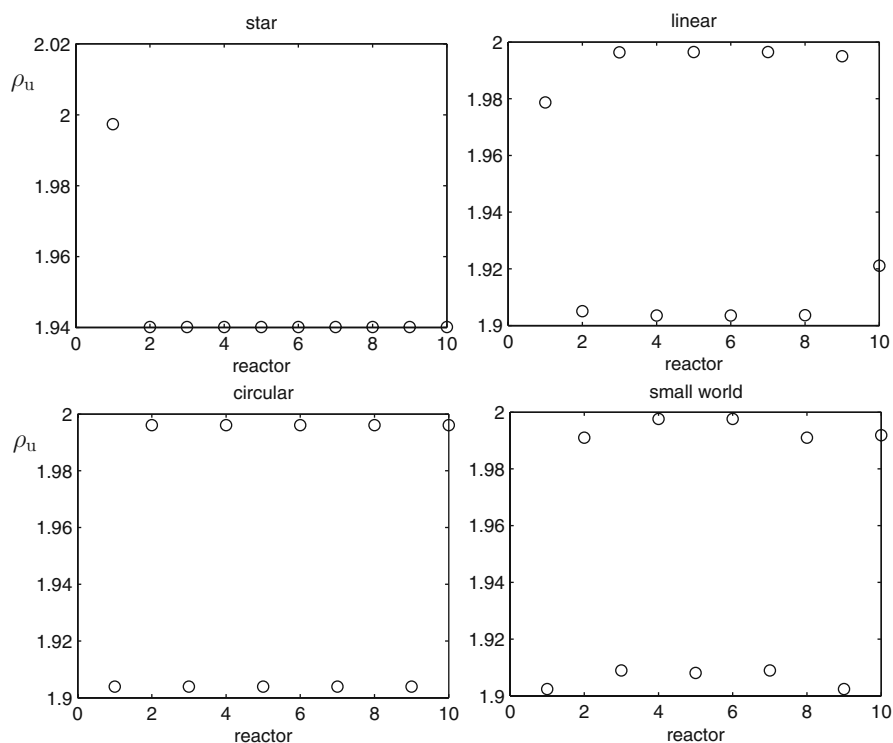
Fig. 13.17 Stationary pattern for the four graphs from Fig. 13.16 with inhibitory coupling and Lengyel–Epstein kinetics. The stationary value of the activator concentration ρ_u is plotted vs the reactor number. (The inhibitor concentration ρ_v shows qualitatively the same pattern.) Parameter values: $a = 10.0$, $\phi_0 = 0.1$, $\sigma = 1.0$, $b = 5.0$, and $\kappa = 23.56824264/|\beta_{10}|$. Reprinted from [209]. Copyright 2006, with permission from Elsevier

Figure 13.17 also illustrates the effects of the network topology. For example, the stationary pattern on the star graph is clearly imposed by the geometry of the reactor network. The value of ρ_u lies above $\overline{\rho}_u(\phi_0/2)$ for reactor 1, the central node, whereas all peripheral nodes have the same value, slightly below $\overline{\rho}_u(\phi_0/2)$. Also, a change from a circular graph to a small-world-like graph by adding two extra edges adds a small-amplitude modulation to the stationary pattern.

Exercises

13.1 Write the Laplacian for a five-node star graph. Let 1 be the central node and number the peripheral modes clockwise. Use computational algebra software or WolframAlpha (www.wolframalpha.com) to determine explicitly the eigenvalues β_i of the Laplacian to confirm Theorem 13.17. Also obtain the corresponding structural modes.

13.2 Add an edge between nodes 2 and 3 and between nodes 4 and 5 of the star graph in Exercise 13.1. Write the Laplacian and use computational algebra software or WolframAlpha (www.wolframalpha.com) to determine explicitly the eigenvalues β_i of the Laplacian and the corresponding structural modes.

13.3 Determine the Turing threshold for a linear three-reactor array, a circular three-reactor array, and a five-node star graph of Brusselators.

13.4 Determine the instability thresholds for "photochemically" coupled Brusselators, i.e., consider the system, $i = 1, \ldots, n$,

$$\frac{d\rho_{ui}}{dt} = a_i - (b + 1)\rho_{ui} + \rho_{ui}^2 \rho_{vi}, \qquad (13.197a)$$

$$\frac{d\rho_{vi}}{dt} = b\rho_{ui} - \rho_{ui}^2 \rho_v, \qquad (13.197b)$$

with

$$a_i = \frac{a_0}{2} \left\{ 1 + H\left[\kappa \sum_j L_{ij}(c_u \rho_{uj} + c_v \rho_{vj}) \right] \right\}. \qquad (13.198)$$

Appendix A
Kronecker Product

A.1 Definition

Let A be a $n \times n$ matrix (with entries a_{ij}) and let B be a $m \times m$ matrix. Then the *Kronecker product* of A and B is the $mn \times mn$ block matrix

$$A \otimes B = \begin{pmatrix} a_{11}B & \cdots & a_{1n}B \\ \vdots & \ddots & \vdots \\ a_{n1}B & \cdots & a_{nn}B \end{pmatrix}. \tag{A.1}$$

The Kronecker product is also known as the *direct product* or the *tensor product* [112, 345, 224].

$$\mathbf{z} = \mathbf{x} \otimes \mathbf{y} = (x_1 y_1, \ldots, x_1 y_m, \ldots, x_n y_1, \ldots, x_n y_m)^T, \tag{A.2}$$
$$(A \otimes B)\mathbf{z} = (A \otimes B)(\mathbf{x} \otimes \mathbf{y}) = (A\mathbf{x}) \otimes (B\mathbf{y}). \tag{A.3}$$

A.2 Fundamental Properties

1. The product is bilinear. If k is a scalar, and A, B, and C are square matrices, such that B and C are of the same dimension, then

$$A \otimes (B + C) = A \otimes B + A \otimes C, \tag{A.4}$$
$$(B + C) \otimes A = B \otimes A + C \otimes A, \tag{A.5}$$
$$k(A \otimes B) = (kA) \otimes B = A \otimes (kB). \tag{A.6}$$

2. If A, B, C, and D are square matrices such that the products AC and BD exist, then $(A \otimes B)(C \otimes D)$ exists and

$$(A \otimes B)(C \otimes D) = AC \otimes BD. \tag{A.7}$$

If A and B are invertible matrices, then

$$(A \otimes B)^{-1} = A^{-1} \otimes B^{-1}. \tag{A.8}$$

3. If A and B are square matrices, then for the transpose we have

$$(A \otimes B)^T = A^T \otimes B^T. \tag{A.9}$$

4. Let A and B be square matrices of dimensions n and m. If $\{\lambda_i | i = 1, \ldots, n\}$ are the eigenvalues of A and $\{\mu_j | j = 1, \ldots, m\}$ are the eigenvalues of B, then $\{\lambda_i \mu_j | i = 1, \ldots, n, \ j = 1, \ldots, m\}$ are the eigenvalues of $A \otimes B$. Also,

$$\det(A \otimes B) = (\det A)^m (\det B)^n, \tag{A.10}$$
$$\text{rank}(A \otimes B) = \text{rank} A \ \text{rank} B, \tag{A.11}$$
$$\text{tr}(A \otimes B) = \text{tr} A \ \text{tr} B. \tag{A.12}$$

References

1. Abedon, S.T., Culler, R.R.: Bacteriophage evolution given spatial constraint. J. Theor. Biol. **248**(1), 111–119 (2007). `http://dx.doi.org/10.1016/j.jtbi.2007.02.014`
2. Abedon, S.T., Culler, R.R.: Optimizing bacteriophage plaque fecundity. J. Theor. Biol. **249**(3), 582–592 (2007). `http://dx.doi.org/10.1016/j.jtbi.2007.08.006`
3. Akam, M.: Making stripes inelegantly. Nature **341**(6240), 282–283 (1989). `http://dx.doi.org/10.1038/341282a0`
4. Albert, R., Barabási, A.L.: Statistical mechanics of complex networks. Rev. Mod. Phys. **74**(1), 47–97 (2002). `http://dx.doi.org/10.1103/RevModPhys.74.47`
5. Alberts, B., Bray, D., Lewis, J., Raff, M., Roberts, K., Watson, J.D.: Molecular Biology of the Cell. Garland Publishing, Inc., New York (1994)
6. Al-Ghoul, M.: Generalized hydrodynamics of reaction–diffusion systems and dissipative structures. Philos. Trans. R. Soc. Lond. A **362**(1821), 1567–1581 (2004). `http://dx.doi.org/10.1098/rsta.2004.1396`
7. Al-Ghoul, M., Eu, B.C.: Hyperbolic reaction–diffusion equations and irreversible thermodynamics: cubic reversible reaction model. Physica D **90**(1–2), 119–153 (1996). `http://dx.doi.org/10.1016/0167-2789(95)00231-6`
8. Al-Ghoul, M., Eu, B.C.: Hyperbolic reaction–diffusion equations and irreversible thermodynamics: II. Two-dimensional patterns and dissipation of energy and matter. Physica D **97**(4), 531–562 (1996). `http://dx.doi.org/10.1016/0167-2789(96)00008-5`
9. Al-Ghoul, M., Eu, B.C.: Hyperbolic reaction–diffusion equations, patterns, and phase speeds for the Brusselator. J. Phys. Chem. **100**(49), 18900–18910 (1996). `http://dx.doi.org/10.1021/jp960865s`
10. Alroy, J.: A multispecies overkill simulation of the end-Pleistocene megafaunal mass extinction. Science **292**(5523), 1893–1896 (2001). `http://dx.doi.org/10.1126/science.1059342`
11. Ammelt, E., Astrov, Y.A., Purwins, H.G.: Stripe Turing structures in a two-dimensional gas discharge system. Phys. Rev. E **55**(6), 6731–6740 (1997). `http://dx.doi.org/10.1103/PhysRevE.55.6731`
12. Ammerman, A.J., Cavalli-Sforza, L.L.: Measuring the rate of spread of early farming in Europe. Man **6**(4), 674–688 (1971)
13. Ammerman, A.J., Cavalli-Sforza, L.L.: The Neolithic Transition and the Genetics of Populations in Europe. Princeton University Press, Princeton (1984)
14. Angelico, R., Ceglie, A., Olsson, U., Palazzo, G., Ambrosone, L.: Anomalous surfactant diffusion in a living polymer system. Phys. Rev. E **74**(3), 031403 (2006). `http://link.aps.org/abstract/PRE/v74/e031403`
15. Applebaum, D.: Lévy Processes and Stochastic Calculus. Cambridge Studies in Advanced Mathematics, vol. 93. Cambridge University Press, Cambridge, UK (2004)
16. Armero, J., Casademunt, J., Ramírez-Piscina, L., Sancho, J.M.: Ballistic and diffusive corrections to front propagation in the presence of multiplicative noise. Phys. Rev. E **58**(5), 5494–5500 (1998). `http://dx.doi.org/10.1103/PhysRevE.58.5494`

17. Armero, J., Sancho, J.M., Casademunt, J., Lacasta, A.M., Ramírez-Piscina, L., Sagués, F.: External fluctuations in front propagation. Phys. Rev. Lett. **76**(17), 3045–3048 (1996). `http://dx.doi.org/10.1103/PhysRevLett.76.3045`

18. Aronson, D.G., Weinberger, H.F.: Multidimensional nonlinear diffusion arising in population genetics. Adv. Math. **30**(1), 33–76 (1978). `http://dx.doi.org/10.1016/0001-8708(78)90130-5`

19. Auchmuty, J., Nicolis, G.: Bifurcation analysis of nonlinear reaction–diffusion equations—I. Evolution equations and the steady state solutions. Bull. Math. Biol. **37**(4), 323–365 (1975). `http://dx.doi.org/10.1007/BF02459519`

20. Austin, D., Bowen, W.D., McMillan, J.I.: Intraspecific variation in movement patterns: modeling individual behaviour in a large marine predator. Oikos **105**(1), 15–30 (2004). `http://dx.doi.org/10.1111/j.0030-1299.1999.12730.x`

21. Baer, S.M., Rinzel, J.: Propagation of dendritic spikes mediated by excitable spines: a continuum theory. J. Neurophysiol. **65**(4), 874–890 (1991). `http://jn.physiology.org/cgi/content/abstract/65/4/874`

22. Baeumer, B., Benson, D.A., Meerschaert, M.M.: Advection and dispersion in time and space. Physica A **350**(2–4), 245–262 (2005). `http://dx.doi.org/10.1016/j.physa.2004.11.008`

23. Baeumer, B., Benson, D.A., Meerschaert, M.M., Wheatcraft, S.W.: Subordinated advection-dispersion equation for contaminant transport. Water Resour. Res. **37**(6), 1543–1550 (2001). `http://www.agu.org/pubs/crossref/2001/2000WR900409.shtml`

24. Baeumer, B., Kovács, M., Meerschaert, M.: Fractional reproduction-dispersal equations and heavy tail dispersal kernels. Bull. Math. Biol. **69**(7), 2281–2297 (2007). `http://dx.doi.org/10.1007/s11538-007-9220-2`

25. Baeumer, B., Meerschaert, M.M.: Fractional diffusion with two time scales. Physica A **373**, 237–251 (2007). `http://dx.doi.org/10.1016/j.physa.2006.06.014`

26. Baker, R.E., Gaffney, E.A., Maini, P.K.: Partial differential equations for self-organization in cellular and developmental biology. Nonlinearity **21**(11), R251–R290 (2008). `http://dx.doi.org/10.1088/0951-7715/21/11/R05`

27. Bar-Eli, K.: Coupling of chemical oscillators. J. Phys. Chem. **88**(16), 3616–3622 (1984). `http://dx.doi.org/10.1021/j150660a048`

28. Bar-Eli, K.: Coupling of identical chemical oscillators. J. Phys. Chem. **94**(6), 2368–2374 (1990). `http://dx.doi.org/10.1021/j100369a033`

29. Barkai, E., Cheng, Y.C.: Aging continuous time random walks. J. Chem. Phys. **118**(14), 6167–6178 (2003). `http://dx.doi.org/10.1063/1.1559676`

30. Becker, P.K., Field, R.J.: Stationary concentration patterns in the Oregonator model of the Belousov–Zhabotinskii reaction. J. Phys. Chem. **89**(1), 118–128 (1985). `http://dx.doi.org/10.1021/j100247a028`

31. Bellomo, N., Preziosi, L.: Modelling and mathematical problems related to tumor evolution and its interaction with the immune system. Math. Comput. Model. **32**(3–4), 413–452 (2000). `http://dx.doi.org/10.1016/S0895-7177(00)00143-6`

32. Belousov, B.P.: A periodic reaction and its mechanism. In: Field, R.J., Burger, M., (eds.) Oscillations and Traveling Waves in Chemical Systems, pp. 605–613. Wiley, New York (1985)

33. ben Avraham, D., Havlin, S.: Diffusion and Reactions in Fractals and Disordered Systems. Cambridge University Press, Cambridge, UK (2000)

34. Benguria, R.D., Depassier, M.C.: Validity of the linear speed selection mechanism for fronts of the nonlinear diffusion equation. Phys. Rev. Lett. **73**(16), 2272–2274 (1994). `http://dx.doi.org/10.1103/PhysRevLett.73.2272`

35. Benguria, R.D., Depassier, M.C.: Variational principle for eigenvalue problems of Hamiltonian systems. Phys. Rev. Lett. **77**(14), 2847–2850 (1996). `http://dx.doi.org/10.1103/PhysRevLett.77.2847`

36. Benguria, R.D., Depassier, M.C.: Speed of pulled fronts with a cutoff. Phys. Rev. E **75**(5), 051106 (2007). `http://dx.doi.org/10.1103/PhysRevE.75.051106`

37. Ben-Jacob, E., Brand, H., Dee, G., Kramer, L., Langer, J.S.: Pattern propagation in nonlinear dissipative systems. Physica D **14**(3), 348–364 (1985). `http://dx.doi.org/10.1016/0167-2789(85)90094-6`

38. Benson, D.A., Schumer, R., Meerschaert, M.M., Wheatcraft, S.W.: Fractional dispersion, Lévy motion, and the MADE tracer tests. Transp. Porous Media **42**(1–2), 211–240 (2001). `http://dx.doi.org/10.1023/A:1006733002131`

39. Benson, D.A., Wheatcraft, S.W., Meerschaert, M.M.: The fractional-order governing equation of Lévy motion. Water Resour. Res. **36**(6), 1413–1424 (2000). `http://www.agu.org/pubs/crossref/2000/2000WR900032.shtml`

40. Benson, D.L., Maini, P.K., Sherratt, J.A.: Unravelling the Turing bifurcation using spatially varying diffusion coefficients. J. Math. Biol. **37**(5), 381–417 (1998). `http://dx.doi.org/10.1007/s002850050135`

41. Benson, D.L., Sherratt, J.A., Maini, P.K.: Diffusion driven instability in an inhomogeneous domain. Bull. Math. Biol. **55**(2), 365–384 (1993). `http://dx.doi.org/10.1007/BF02460888`

42. Berkowitz, B., Klafter, J., Metzler, R., Scher, H.: Physical pictures of transport in heterogeneous media: advection-dispersion, random-walk, and fractional derivative formulations. Water Resour. Res. **38**(10), 1191 (2002). `http://dx.doi.org/0.1029/2001WR001030`

43. Berkowitz, B., Scher, H.: Anomalous transport in random fracture networks. Phys. Rev. Lett. **79**(20), 4038–4041 (1997). `http://dx.doi.org/10.1103/PhysRevLett.79.4038`

44. Berloff, P.S., McWilliams, J.C., Bracco, A.: Material transport in oceanic gyres. Part I: Phenomenology. J. Phys. Oceanogr. **32**(3), 764–796 (2002). `http://dx.doi.org/10.1175/1520-0485(2002)032<0764:MTIOGP>2.0.CO;2`

45. Bernasconi, J., Alexander, S., Orbach, R.: Classical diffusion in one-dimensional disordered lattice. Phys. Rev. Lett. **41**(3), 185–187 (1978). `http://dx.doi.org/10.1103/PhysRevLett.41.185`

46. Bertuzzo, E., Maritan, A., Gatto, M., Rodriguez-Iturbe, I., Rinaldo, A.: River networks and ecological corridors: reactive transport on fractals, migration fronts, hydrochory. Water Resour. Res. **43**(4), W04419 (2007). `http://dx.doi.org/10.1029/2006WR005533`

47. Birdsell, J.P.: Some population problems involving Pleistocene man. Cold Spring Harbor Symp. Quant. Biol. **22**, 47–69 (1957). `http://library.cshl.edu/symposia/1957/contents.html`

48. Biroli, G., Monasson, R.: A single defect approximation for localized states on random lattices. J. Phys. A Math. Gen. **32**(24), L255–L261 (1999). `http://dx.doi.org/10.1088/0305-4470/32/24/101`

49. Bloodgood, B.L., Sabatini, B.L.: Neuronal activity regulates diffusion across the neck of dendritic spines. Science **310**(5749), 866–869 (2005). `http://dx.doi.org/10.1126/science.1114816`

50. Boa, J.A., Cohen, D.S.: Bifurcation of localized disturbances in a model biochemical reaction. SIAM J. Appl. Math. **30**(1), 123–135 (1976). `http://dx.doi.org/10.1137/0130015`

51. Bohr, T., Pikovsky, A.: Anomalous diffusion in the Kuramoto–Sivashinsky equation. Phys. Rev. Lett. **70**(19), 2892–2895 (1993). `http://dx.doi.org/10.1103/PhysRevLett.70.2892`

52. Booth, V., Erneux, T., Laplante, J.P.: Experimental and numerical study of weakly coupled bistable chemical reactions. J. Phys. Chem. **98**(26), 6537–6540 (1994). `http://dx.doi.org/10.1021/j100077a019`

53. Bouchaud, J.P., Georges, A.: Anomalous diffusion in disordered media: statistical mechanisms, models and physical applications. Phys. Rep. **195**(4–5), 127–293 (1990). `http://dx.doi.org/10.1016/0370-1573(90)90099-N`

54. Boukalouch, M., Elezgaray, J., Arneodo, A., Boissonade, J., De Kepper, P.: Oscillatory instability induced by mass interchange between two coupled steady-state reactors. J. Phys. Chem. **91**(23), 5843–5845 (1987). `http://dx.doi.org/10.1021/j100307a005`

55. Bouzat, S., Wio, H.S.: Pattern formation in inhomogeneous active media: a localized bistable domain immersed in an oscillatory medium. Phys. Lett. A **268**(4–6), 323–329 (2000). `http://dx.doi.org/10.1016/S0375-9601(00)00181-X`

56. Bramson, M., Lebowitz, J.L.: Asymptotic behavior of densities in diffusion-dominated annihilation reactions. Phys. Rev. Lett. **61**(21), 2397–2400 (1988). `http://dx.doi.org/10.1103/PhysRevLett.61.2397`

57. Bramson, M.D.: Maximal displacement of branching Brownian motion. Commun. Pure Appl. Math. **31**, 531–581 (1978). `http://dx.doi.org/10.1002/cpa.3160310502`

58. Brenan, K.E., Campbell, S.L., Petzold, L.R.: Numerical Solution of Initial-Value Problems in Differential-Algebraic Equations. SIAM, Philadelphia (1996)

59. Bressloff, P.C., Earnshaw, B.A.: Diffusion-trapping model of receptor trafficking in dendrites. Phys. Rev. E **75**(4), 041915 (2007). `http://dx.doi.org/10.1103/PhysRevE.75.041915`

60. Brockmann, D., Hufnagel, L.: Front propagation in reaction-superdiffusion dynamics: taming Lévy flights with fluctuations. Phys. Rev. Lett. **98**(17), 178301 (2007). `http://link.aps.org/abstract/PRL/v98/e178301`

61. Brunet, E., Derrida, B.: Shift in the velocity of a front due to a cutoff. Phys. Rev. E **56**(3), 2597–2604 (1997). `http://dx.doi.org/10.1103/PhysRevE.56.2597`

62. Bunde, A., Dräger, J.: Localization in disordered structures: breakdown of the self-averaging hypothesis. Phys. Rev. E **52**(1), 53–56 (1995). `http://dx.doi.org/10.1103/PhysRevE.52.53`

63. Campbell, G.S., Blackwell, P.G., Woodward, F.I.: Can landscape-scale characteristics be used to predict plant invasions along rivers? J. Biogeogr. **29**(4), 535–543 (2002). `http://dx.doi.org/10.1046/j.1365-2699.2002.00693.x`

64. Campos, D., Fort, J., Méndez, V.: Transport on fractal river networks: application to migration fronts. Theor. Popul. Biol. **69**(1), 88–93 (2006). `http://dx.doi.org/10.1016/j.tpb.2005.09.001`

65. Campos, D., Méndez, V.: A lattice-model representation of continuous-time random walks. J. Phys. A Math. Theor. **41**(8), 085101 (2008). `http://stacks.iop.org/1751-8121/41/085101`

66. Campos, D., Méndez, V., Fort, J.: Description of diffusive and propagative behavior on fractals. Phys. Rev. E **69**(3), 031115 (2004). `http://dx.doi.org/10.1103/PhysRevE.69.031115`

67. Campos, D., Méndez, V., Ortega-Cejas, V.: Lattice models for invasions through patchy environments. Bull. Math. Biol. **70**(7), 1937–1956 (2008). `http://dx.doi.org/10.1007/s11538-008-9333-2`

68. Capasso, V., Di Liddo, A.: Global attractivity for reaction–diffusion systems. The case of nondiagonal diffusion matrices. J. Math. Anal. Appl. **177**(2), 510–529 (1993). `http://dx.doi.org/10.1006/jmaa.1993.1274`

69. Capasso, V., Di Liddo, A.: Asymptotic behaviour of reaction–diffusion systems in population and epidemic models. J. Math. Biol. **32**(5), 453–463 (1994). `http://dx.doi.org/10.1007/BF00160168`

70. Caspi, A., Granek, R., Elbaum, M.: Enhanced diffusion in active intracellular transport. Phys. Rev. Lett. **85**(26), 5655–5658 (2000). `http://dx.doi.org/10.1103/PhysRevLett.85.5655`

71. Castets, V., Dulos, E., Boissonade, J., De Kepper, P.: Experimental evidence of a sustained standing Turing-type nonequilibrium chemical pattern. Phys. Rev. Lett. **64**(24), 2953–2956 (1990). `http://dx.doi.org/10.1103/PhysRevLett.64.2953`

72. Caswell, H.: Matrix Population Models: Construction, Analysis, and Interpretation. Sinauer Associates, Inc, Sunderland, MA (2001)

73. Cavalli-Sforza, L.L., Menozzi, P., Piazza, A.: Demic expansions and human evolution. Science **259**(5095), 639–646 (1993). `http://dx.doi.org/10.1126/science.8430313`

74. Chechkin, A.V., Gonchar, V.Y., Klafter, J., Metzler, R.: Fundamentals of Lévy flight processes. In: Kalmykov, Y.P., Coffey, W.T. (eds.) Fractals, Diffusion, and Relaxation in

Disordered Complex Systems. Part B, Advances in Chemical Physics, vol. 133B, pp. 439–496. Wiley, Hoboken (2006)

75. Chechkin, A.V., Gorenflo, R., Sokolov, I.M.: Fractional diffusion in inhomogeneous media. J. Phys. A Math. Gen. **38**(42), L679–L684 (2005). `http://dx.doi.org/10.1088/0305-4470/38/42/L03`

76. Chiu, J.W., Chiam, K.H.: Monte Carlo simulation and linear stability analysis of Turing pattern formation in reaction-subdiffusion systems. Phys. Rev. E **78**(5), 056708 (2008). `http://dx.doi.org/10.1103/PhysRevE.78.056708`

77. Chopard, B., Droz, M.: Cellular Automata Modeling of Physical Systems. Cambridge University Press, Cambridge, UK (1998)

78. Clark, J.S., Lewis, M., Horvath, L.: Invasion by extremes population spread with variation in dispersal and reproduction. Am. Nat. **157**(5), 537–554 (2001). `http://dx.doi.org/10.1086/319934`

79. Clark, J.S., Lewis, M., McLachlan, J.S., HilleRisLambers, J.: Estimating population spread: what can we forecast and how well? Ecology **84**(8), 1979–1988 (2003). `http://www.esajournals.org/doi/abs/10.1890/01-0618`

80. Colaiori, F., Flammini, A., Maritan, A., Banavar, J.R.: Analytical and numerical study of optimal channel networks. Phys. Rev. E **55**(2), 1298–1310 (1997). `http://dx.doi.org/10.1103/PhysRevE.55.1298`

81. Cox, D.R.: Renewal Theory. Methuen, London (1967)

82. Cross, M.C., Hohenberg, P.C.: Pattern formation outside of equilibrium. Rev. Mod. Phys. **65**(3), 851–1112 (1993). `http://dx.doi.org/10.1103/RevModPhys.65.851`

83. Crowley, M.F., Epstein, I.R.: Experimental and theoretical studies of a coupled chemical oscillator: phase death, multistability and in-phase and out-of-phase entrainment. J. Phys. Chem. **93**, 2496–2502 (1989). `http://dx.doi.org/10.1021/j100343a052`

84. Crowley, M.F., Field, R.J.: Electrically coupled Belousov–Zhabotinskii oscillators. 1. Experiments and simulations. J. Phys. Chem. **90**(9), 1907–1915 (1986). `http://dx.doi.org/10.1021/j100400a033`

85. Dagdug, L., Berezhkovskii, A.M., Makhnovskii, Y.A., Zitserman, V.Y.: Transient diffusion in a tube with dead ends. J. Chem. Phys. **127**(22), 224712 (2007). `http://link.aip.org/link/?JCP/127/224712/1`

86. Davies, P.W., Blanchedeau, P., Dulos, E., De Kepper, P.: Dividing blobs, chemical flowers, and patterned islands in a reaction–diffusion system. J. Phys. Chem. A **102**(43), 8236–8244 (1998). `http://dx.doi.org/10.1021/jp982034n`

87. Davison, K., Dolukhanov, P., Sarson, G.R., Shukurov, A.: The role of waterways in the spread of the Neolithic. J. Archaeol. Sci. **33**(5), 641–652 (2006). `http://dx.doi.org/10.1016/j.jas.2005.09.017`

88. De Kepper, P., Epstein, I.R., Kustin, K., Orban, M.: Systematic design of chemical oscillators. Part 8. Batch oscillations and spatial wave patterns in chlorite oscillating systems. J. Phys. Chem. **86**(2), 170–171 (1982). `http://dx.doi.org/10.1021/j100391a007`

89. del Castillo-Negrete, D.: Truncation effects in superdiffusive front propagation with Lévy flights. Phys. Rev. E **79**(3), 031120 (2009). `http://link.aps.org/abstract/PRE/v79/e031120`

90. del Castillo-Negrete, D., Carreras, B.A., Lynch, V.: Front dynamics in reaction–diffusion systems with Lévy flights: a fractional diffusion approach. Phys. Rev. Lett. **91**(1), 018302 (2003). `http://dx.doi.org/10.1103/PhysRevLett.91.018302`

91. Dentz, M., Cortis, A., Scher, H., Berkowitz, B.: Time behavior of solute transport in heterogeneous media: transition from anomalous to normal transport. Adv. Water Resour. **27**(2), 155–173 (2004). `http://dx.doi.org/10.1016/j.advwatres.2003.11.002`

92. Dewel, G., Borckmans, P.: Effects of slow spatial variations on dissipative structures. Phys. Lett. A **138**, 189–192 (1989). `http://dx.doi.org/10.1016/0375-9601(89)90025-X`

93. Dhar, P., Fischer, T.M., Wang, Y., Mallouk, T.E., Paxton, W.F., Sen, A.: Autonomously moving nanorods at a viscous interface. Nano Lett. **6**(1), 66–72 (2006). `http://dx.doi.org/10.1021/nl052027s`

94. Diamond, J.M.: The language steamrollers. Nature **389**(6651), 544–546 (1997). `http://dx.doi.org/10.1038/39184`

95. Diestel, R.: Graph Theory. Springer, New York (1997)

96. Doering, C.R., ben Avraham, D.: Diffusion-limited coagulation in the presence of particle input: exact results in one dimension. Phys. Rev. Lett. **62**(21), 2563–2566 (1989). `http://dx.doi.org/10.1103/PhysRevLett.62.2563`

97. Dolnik, M., Epstein, I.R.: A coupled chemical burster: the chlorine dioxide–iodide reaction in two flow reactors. J. Chem. Phys. **98**(2), 1149–1155 (1993). `http://dx.doi.org/10.1063/1.465081`

98. Dolnik, M., Zhabotinsky, A.M., Epstein, I.R.: Resonant suppression of Turing patterns by periodic illumination. Phys. Rev. E **63**(2), 026101 (2001). `http://dx.doi.org/10.1103/PhysRevE.63.026101`

99. Doumbouya, S.I., Münster, A.F., Doona, C.J., Schneider, F.W.: Deterministic chaos in serially coupled chemical oscillators. J. Phys. Chem. **97**(5), 1025–1031 (1993). `http://dx.doi.org/10.1021/j100107a009`

100. Drazer, G., Zanette, D.H.: Experimental evidence of power-law trapping-time distributions in porous media. Phys. Rev. E **60**(5), 5858–5864 (1999). `http://dx.doi.org/10.1103/PhysRevE.60.5858`

101. Dunbar, S.R.: A branching random evolution and a nonlinear hyperbolic equation. SIAM J. Appl. Math. **48**(6), 1510–1526 (1988). `http://locus.siam.org/SIAP/volume-48/art_0148094.html`

102. Ebeling, W., Sokolov, I.M.: Statistical Thermodynamics and Stochastic Theory of Nonequilibrium Systems. World Scientific, Singapore (2005)

103. Ebert, U., van Saarloos, W.: Universal algebraic relaxation of fronts propagating into an unstable state and implications for moving boundary approximations. Phys. Rev. Lett. **80**(8), 1650–1653 (1998). `http://dx.doi.org/10.1103/PhysRevLett.80.1650`

104. Ebert, U., van Saarloos, W.: Front propagation into unstable states: universal algebraic convergence towards uniformly translating pulled fronts. Physica D **146**(1–4), 1–99 (2000). `http://dx.doi.org/10.1016/S0167-2789(00)00068-3`

105. Edelstein-Keshet, L., Spiros, A.: Exploring the formation of Alzheimer's disease senile plaques *in silico*. J. Theor. Biol. **216**(3), 301–326 (2002). `http://dx.doi.org/10.1006/jtbi.2002.2540`

106. Edgar, B.A., Odell, G.M., Schubiger, G.: A genetic switch, based on negative regulation, sharpens stripes in *Drosophila* embryos. Dev. Genet. **10**(3), 124–142 (1989). `http://dx.doi.org/10.1002/dvg.1020100303`

107. Edwards, A.M.: Using likelihood to test for Lévy flight search patterns and for general power-law distributions in nature. J. Anim. Ecol. **77**(6), 1212–1222 (2008). `http://dx.doi.org/10.1111/j.1365-2656.2008.01428.x`

108. Edwards, A.M., Phillips, R.A., Watkins, N.W., Freeman, M.P., Murphy, E.J., Afanasyev, V., Buldyrev, S.V., da Luz, M.G.E., Raposo, E.P., Stanley, H.E., Viswanathan, G.M.: Revisiting Lévy flight search patterns of wandering albatrosses, bumblebees and deer. Nature **449**(7165), 1044–1048 (2007). `http://dx.doi.org/10.1038/nature06199`

109. Epstein, I.R., Golubitsky, M.: Symmetric patterns in linear arrays of coupled cells. Chaos **3**(1), 1–5 (1993). `http://dx.doi.org/10.1063/1.165974`

110. Epstein, I.R., Kustin, K., Kepper, P.D., Orban, M.: Oscillating chemical reactions. Sci. Am. **248**(3), 112–123 (1983)

111. Epstein, I.R., Pojman, J.A.: An Introduction to Nonlinear Chemical Dynamics. Oxford University Press, New York (1998)

112. Eves, H.: Elementary Matrix Theory. Dover Publications, Mineola (1980)

113. Faragher, J.M.: Women and Men on the Overland Trail. Yale University Press, New Haven (2001)

114. Fedotov, S.: Traveling waves in a reaction–diffusion system: diffusion with finite velocity and Kolmogorov–Petrovskii–Piskunov kinetics. Phys. Rev. E **58**(4), 5143–5145 (1998). `http://dx.doi.org/10.1103/PhysRevE.58.5143`

115. Fedotov, S.: Nonuniform reaction rate distribution for the generalized Fisher equation: ignition ahead of the reaction front. Phys. Rev. E **60**(4), 4958–4961 (1999). `http://dx.doi.org/10.1103/PhysRevE.60.4958`

116. Fedotov, S.: Wave front for a reaction–diffusion system and relativistic Hamilton–Jacobi dynamics. Phys. Rev. E **59**(5), 5040–5044 (1999). `http://dx.doi.org/10.1103/PhysRevE.59.5040`

117. Fedotov, S.: Front dynamics for an anisotropic reaction–diffusion equation. J. Phys. A Math. Gen. **33**(40), 7033–7042 (2000). `http://dx.doi.org/10.1088/0305-4470/33/40/302`

118. Fedotov, S.: Front propagation into an unstable state of reaction-transport systems. Phys. Rev. Lett. **86**(5), 926–929 (2001). `http://dx.doi.org/10.1103/PhysRevLett.86.926`

119. Fedotov, S., Iomin, A.: Migration and proliferation dichotomy in tumor-cell invasion. Phys. Rev. Lett. **98**(11), 118101 (2007). `http://dx.doi.org/10.1103/PhysRevLett.98.118101`

120. Fedotov, S., Iomin, A.: Probabilistic approach to a proliferation and migration dichotomy in tumor cell invasion. Phys. Rev. E **77**(3), 031911 (2008). `http://link.aps.org/abstract/PRE/v77/e031911`

121. Fedotov, S., Méndez, V.: Continuous-time random walks and traveling fronts. Phys. Rev. E **66**(3), 030102(R) (2002). `http://dx.doi.org/10.1103/PhysRevE.66.030102`

122. Fedotov, S., Méndez, V.: Non-Markovian model for transport and reactions of particles in spiny dendrites. Phys. Rev. Lett. **101**(21), 218102 (2008). `http://link.aps.org/abstract/PRL/v101/e218102`

123. Fedotov, S., Milstein, G.N., Tretyakov, M.V.: Superdiffusion of a random walk driven by an ergodic Markov process with switching. J. Phys. A Math. Theor. **40**(22), 5769–5782 (2007). `http://stacks.iop.org/1751-8121/40/5769`

124. Fedotov, S., Moss, D., Campos, D.: Stochastic model for population migration and the growth of human settlements during the Neolithic transition. Phys. Rev. E **78**(2), 026107 (2008). `http://link.aps.org/abstract/PRE/v78/e026107`

125. Fedotov, S., Okuda, Y.: Non-Markovian random processes and traveling fronts in a reaction-transport system with memory and long-range interactions. Phys. Rev. E **66**(2), 021113 (2002). `http://dx.doi.org/10.1103/PhysRevE.66.021113`

126. Feller, W.: An Introduction to Probability Theory and Its Applications, vol. 2. Wiley, New York (1971)

127. Ferrie, J.P.: A new sample of males linked from the public use microdata sample of the 1850 U.S. federal census of population to the 1860 U.S. federal census. Hist. Methods **29**, 141–156 (1996)

128. Fiedler, M.: Algebraic connectivity of graphs. Czechoslov. Math. J. **23**(98), 298–305 (1973)

129. Field, R.J., Burger, M. (eds.): Oscillations and Traveling Waves in Chemical Systems. Wiley, New York (1985)

130. Field, R.J., Körös, E., Noyes, R.M.: Oscillations in chemical systems. II. Thorough analysis of temporal oscillation in the bromate-cerium-malonic acid system. J. Am. Chem. Soc. **94**(25), 8649–8664 (1972). `http://dx.doi.org/10.1021/ja00780a001`

131. Field, R.J., Noyes, R.M.: Oscillations in chemical systems. IV. Limit cycle behavior in a model of a real chemical reaction. J. Chem. Phys. **60**(5), 1877–1884 (1974). `http://dx.doi.org/10.1063/1.1681288`

132. Fisher, R.A.: The wave of advance of advantageous genes. Ann. Eugenics **7**, 355–369 (1937). `http://digital.library.adelaide.edu.au/coll/special//fisher/152.pdf`

133. Flanders, S.A.: Atlas of American Migration. Facts on File, New York (1998)

134. Flores, J.C.: A mathematical model for Neanderthal extinction. J. Theor. Biol. **191**(3), 295–298 (1998). `http://dx.doi.org/10.1006/jtbi.1997.0581`

135. Fort, J.: Population expansion in the western Pacific (Austronesia): a wave of advance model. Antiquity **77**(297), 520–530 (2003). `http://copernic.udg.es/QuimFort/Antiquity.pdf`

136. Fort, J., Méndez, V.: Reaction–diffusion waves of advance in the transition to agricultural economics. Phys. Rev. E **60**(5), 5894–5901 (1999). `http://dx.doi.org/10.1103/PhysRevE.60.5894`

137. Fort, J., Méndez, V.: Time-delayed theory of the Neolithic transition in Europe. Phys. Rev. Lett. **82**(4), 867–870 (1999). `http://dx.doi.org/10.1103/PhysRevLett.82.867`

138. Fort, J., Méndez, V.: Time-delayed spread of viruses in growing plaques. Phys. Rev. Lett. **89**(17), 178101 (2002). `http://dx.doi.org/10.1103/PhysRevLett.89.178101`

139. Fort, J., Pujol, T.: Progress in front propagation research. Rep. Prog. Phys. **71**(8), 086001 (2008). `http://stacks.iop.org/0034-4885/71/086001`

140. Freidlin, M.: Geometric optics approach to reaction–diffusion equations. SIAM J. Appl. Math. **46**(2), 222–232 (1986). `http://dx.doi.org/10.1137/0146016`

141. Freidlin, M.I.: Functional Integration and Partial Differential Equations. Princeton University Press, Princeton (1985)

142. Freidlin, M.I., Wentzell, A.D.: Random Perturbations of Dynamical Systems. Springer, Berlin (1984)

143. Froemberg, D., Schmidt-Martens, H., Sokolov, I.M., Sagués, F.: Front propagation in $A + B \longrightarrow 2A$ reaction under subdiffusion. Phys. Rev. E **78**(1), 011128 (2008). `http://link.aps.org/abstract/PRE/v78/e011128`

144. Froemberg, D., Sokolov, I.M.: Stationary fronts in an $A + B \longrightarrow 0$ reaction under subdiffusion. Phys. Rev. Lett. **100**(10), 108304 (2008). `http://link.aps.org/abstract/PRL/v100/e108304`

145. Fuji, H., Sawada, Y.: Phase-difference locking of coupled oscillating chemical systems. J. Chem. Phys. **69**(8), 3830–3832 (1978). `http://dx.doi.org/10.1063/1.437048`

146. Fürth, R.: Die Brownsche Bewegung bei Berücksichtigung einer Persistenz der Bewegungsrichtung. Mit Anwendungen auf die Bewegung lebender Infusorien. Z. Phys. **2**, 244–256 (1920)

147. Gafiychuk, V.V., Datsko, B.Y.: Stability analysis and oscillatory structures in time-fractional reaction–diffusion systems. Phys. Rev. E **75**(5), 055201 (2007). `http://link.aps.org/abstract/PRE/v75/e055201`

148. Gafiychuk, V.V., Datsko, B.Y.: Spatiotemporal pattern formation in fractional reaction-diffusion systems with indices of different order. Phys. Rev. E **77**(6), 066210 (2008). `http://link.aps.org/abstract/PRE/v77/e066210`

149. Gallay, T., Raugel, R.: Stability of travelling waves for a damped hyperbolic equation. Z. Angew. Math. Phys. **48**(3), 451–479 (1997). `http://dx.doi.org/10.1007/s000330050043`

150. Gallay, T., Raugel, R.: Scaling variables and asymptotic expansions in damped wave equations. J. Differ. Equ. **150**(1), 42–97 (1998). `http://dx.doi.org/10.1006/jdeq.1998.3459`

151. Gallay, T., Raugel, R.: Scaling variables and stability of hyperbolic fronts. SIAM J. Math. Anal. **32**(1), 1–29 (2000). `http://dx.doi.org/10.1137/S0036141099351334`

152. Gallay, T., Raugel, R.: Stability of propagating fronts in damped hyperbolic equations. In: Necas, J., Jaeger, W., Stara, J., John, O., Najzar, K. (eds.) Partial Differential Equations: Theory and Numerical Solutions. Chapman & Hall Research Notes in Mathematics, vol. 406, pp. 130–146. Chapman & Hall/CRC Chapman, london (2000). `http://arxiv.org/abs/patt-sol/9809007`

153. Gantmacher, F.R.: The Theory of Matrices, vol. 2. AMS Chelsea, Providence (1959)

154. Gaspard, P., Klages, R.: Chaotic and fractal properties of deterministic diffusion–reaction processes. Chaos **8**(2), 409–423 (1998). `http://link.aip.org/link/?CHA/8/409/1`

155. Gatenby, R.A., Gawlinski, E.T.: A reaction–diffusion model of cancer invasion. Cancer Res. **56**(24), 5745–5753 (1996). `http://cancerres.aacrjournals.org/cgi/content/abstract/56/24/5745`

156. Gatenby, R.A., Maini, P.K., Gawlinski, E.T.: Analysis of tumor as an inverse problem provides a novel theoretical framework for understanding tumor biology and therapy.

Appl. Math. Lett. **15**(3), 339–345 (2002). `http://dx.doi.org/10.1016/S0893-9659(01)00141-0`

157. Gierer, A., Meinhardt, H.: A theory of biological pattern formation. Kybernetik **12**, 30–39 (1972). `http://www.eb.tuebingen.mpg.de/departments/former-departments/h-meinhardt/kyb.pdf`

158. Giese, A., Bjerkvig, R., Berens, M.E., Westphal, M.: Cost of migration: invasion of malignant gliomas and implications for treatment. J. Clin. Oncol. **21**(8), 1624–1636 (2003). `http://dx.doi.org/10.1200/JCO.2003.05.063`

159. Giese, A., Loo, M.A., Tran, N., Haskett, D., Coons, S.W., Berens, M.E.: Dichotomy of astrocytoma migration and proliferation. Int. J. Cancer **67**(2), 275–282 (1996). `http://dx.doi.org/10.1002/(SICI)1097-0215(19960717)67:2<275::AID-IJC20>3.0.CO;2-9`

160. Giese, A., Westphal, M.: Glioma invasion in the central nervous system. Neurosurgery **39**(2), 235–252 (1996). `http://journals.lww.com/neurosurgery/Fulltext/1996/08000/Glioma_Invasion_in_the_Central_Nervous_System.1.aspx`

161. Giona, M., Roman, E.H.: Fractional diffusion equation for transport phenomena in random media. Physica A **185**(1–4), 87–97 (1992). `http://dx.doi.org/10.1016/0378-4371(92)90441-R`

162. Golding, I., Cox, E.C.: Physical nature of bacterial cytoplasm. Phys. Rev. Lett. **96**(9), 098102 (2006). `http://dx.doi.org/10.1103/PhysRevLett.96.098102`

163. Goldstein, S.: On diffusion by discontinuous movements, and on the telegraph equation. Q. J. Mech. Appl. Math. **4**, 129–156 (1951)

164. Golovin, A.A., Matkowsky, B.J., Volpert, V.A.: Turing pattern formation in the Brusselator model with superdiffusion. SIAM J. Appl. Math. **69**(1), 251–272 (2008). `http://link.aip.org/link/?SMM/69/251/1`

165. Gonzalez, J.A., Oliveira, F.A.: Nucleation theory, the escaping processes, and nonlinear stability. Phys. Rev. B **59**(9), 6100–6105 (1999). `http://dx.doi.org/10.1103/PhysRevB.59.6100`

166. Gorenflo, R., Mainardi, F.: Random walk models for space-fractional diffusion processes. Fract. Calc. Appl. Anal. **1**, 167–191 (1998). `http://citeseerx.ist.psu.edu/viewdoc/download?doi=10.1.1.80.2691&rep=rep1&type=pdf`

167. Gourley, S.A.: Travelling fronts in the diffusive Nicholson's blowflies equation with distributed delays. Math. Comput. Model. **32**(7–8), 843–853 (2000). `http://dx.doi.org/10.1016/S0895-7177(00)00175-8`

168. Gourley, S.A., Britton, N.F., Chaplain, M.A.J., Byrne, H.M.: Mechanisms for stabilisation and destabilisation of systems of reaction–diffusion equations. J. Math. Biol. **34**(8), 857–877 (1996). `http://dx.doi.org/10.1007/BF01834823`

169. Gourley, S.A., So, J.W.H.: Extinction and wavefront propagation in a reaction-diffusion model of a structured population with distributed maturation delay. Proc. R. Soc. Edinb. Sect. A Math. **133**(3), 527–548 (2003). `http://dx.doi.org/10.1017/S0308210500002523`

170. Gray, P., Scott, S.K.: Sustained oscillations and other exotic patterns of behavior in isothermal reactions. J. Phys. Chem. **89**(1), 22–32 (1985). `http://dx.doi.org/10.1021/j100247a009`

171. Gray, P., Scott, S.K.: Chemical Oscillations and Instabilities. Clarendon Press, Oxford (1990)

172. Grigulis, K., Sheppard, A.W., Ash, J.E., Groves, R.H.: The comparative demography of the pasture weed *Echium plantagineum* between its native and invaded ranges. J. Appl. Ecol. **38**(2), 281–290 (2001). `http://dx.doi.org/10.1046/j.1365-2664.2001.00587.x`

173. Grone, R., Merris, R.: The Laplacian spectrum of a graph II. SIAM J. Disc. Math. **7**(2), 221–229 (1994). `http://link.aip.org/link/?SJD/7/221/1`

174. Gu, Q., Schiff, E.A., Grebner, S., Wang, F., Schwarz, R.: Non-Gaussian transport measurements and the Einstein relation in amorphous silicon. Phys. Rev. Lett. **76**(17), 3196–3199 (1996). `http://dx.doi.org/10.1103/PhysRevLett.76.3196`

175. Guckenheimer, J., Holmes, P.: Nonlinear Oscillations, Dynamical Systems, and Bifurcations of Vector Fields. Applied Mathematical Sciences, vol. 42. Springer, New York (1983)

176. Hadeler, K.P.: Travelling fronts for correlated random walks. Can. Appl. Math. Q. **2**(1), 27–43 (1994)

177. Hadeler, K.P.: Reaction telegraph equations and random walk systems. In: van Strien, S.J., Verduyn Lunel, S.M. (eds.) Stochastic and Spatial Structures of Dynamical Systems, pp. 133–161. North-Holland, Amsterdam (1996)

178. Hadeler, K.P.: Reaction transport systems in biological modelling. In: Diekmann, O., Durrett, R., Hadeler, K.P., Maini, P., Smith, H.L. (eds.) Mathematics Inspired by Biology, Lecture Notes in Mathematics, vol. 1714, pp. 95–150. Springer, Berlin (1999). `http://dx.doi.org/10.1007/BFb0092376`

179. Harris, K.M.: Structure, development, and plasticity of dendritic spines. Curr. Opin. Neurobiol. **9**(3), 343–348 (1999). `http://dx.doi.org/10.1016/S0959-4388(99)80050-6`

180. Harris, S.: An Introduction to the Theory of the Boltzmann Equation. Holt, Rinehart and Winston, New York (1971)

181. Harris, S.: Traveling waves with dispersive variability and time delay. Phys. Rev. E **68**(3), 031912 (2003). `http://dx.doi.org/10.1103/PhysRevE.68.031912`

182. Harrison, L.G.: Reaction–diffusion theory and intracellular differentiation. Int. J Plant Sci. **153**(s3), S76–S85 (1992). `http://dx.doi.org/10.1086/297065`

183. Harrison, L.G.: Kinetic Theory of Living Pattern. Cambridge University Press, New York (1993)

184. Hatzikirou, H., Deutsch, A., Schaller, C., Simon, M., Swanson, K.: Mathematical modelling of glioblastoma tumour development: a review. Math. Mod. Meth. Appl. Sci. **15**(11), 1779–1794 (2005). `http://dx.doi.org/10.1142/S0218202505000960`

185. Havlin, S., ben Avraham, D.: Diffusion in disordered media. Adv. Phys. **36**(6), 695–798 (1987). `http://dx.doi.org/10.1080/00018738700101072`

186. Henry, B.I, Langlands, T.A.M, Wearne, S.L.: Turing pattern formation in fractional activator–inhibitor systems. Phys. Rev. E **72**(2), 026101 (2005). `http://dx.doi.org/10.1103/PhysRevE.72.026101`

187. Henry, B.I., Langlands, T.A.M., Wearne, S.L.: Anomalous diffusion with linear reaction dynamics: from continuous time random walks to fractional reaction–diffusion equations. Phys. Rev. E **74**(3), 031116 (2006). `http://dx.doi.org/10.1103/PhysRevE.74.031116`

188. Henry, B.I., Wearne, S.L.: Fractional reaction–diffusion. Physica A **276**(3–4), 448–455 (2000). `http://dx.doi.org/10.1016/S0378-4371(99)00469-0`

189. Henry, B.I., Wearne, S.L.: Existence of Turing instabilities in a two-species fractional reaction–diffusion system. SIAM J. Appl. Math. **62**(3), 870–887 (2002). `http://dx.doi.org/10.1137/S0036139900375227`

190. Hentschel, H.G.E., Procaccia, I.: Relative diffusion in turbulent media: the fractal dimension of clouds. Phys. Rev. A **29**(3), 1461–1470 (1984). `http://link.aps.org/abstract/PRA/v29/p1461`

191. Hernández, D., Varea, C., Barrio, R.A.: Dynamics of reaction–diffusion systems in a subdiffusive regime. Phys. Rev. E **79**(2), 026109 (2009). `http://link.aps.org/abstract/PRE/v79/e026109`

192. Herschkowitz-Kaufman, M., Nicolis, G.: Localized spatial structures and nonlinear chemical waves in dissipative systems. J. Chem. Phys. **56**(5), 1890–1895 (1972). `http://dx.doi.org/10.1063/1.1677471`

193. Hildebrand, M., Cui, J., Mihaliuk, E., Wang, J., Showalter, K.: Synchronization of spatiotemporal patterns in locally coupled excitable media. Phys. Rev. E **68**(2), 026205 (2003). `http://dx.doi.org/10.1103/PhysRevE.68.026205`

194. Hildebrand, M., Skødt, H., Showalter, K.: Spatial symmetry breaking in the Belousov–Zhabotinsky reaction with light-induced remote communication. Phys. Rev. Lett. **87**(8), 088303 (2001). `http://dx.doi.org/10.1103/PhysRevLett.87.088303`

195. Hillen, T.: A Turing model with correlated random walk. J. Math. Biol. **35**(1), 49–72 (1996). `http://dx.doi.org/10.1007/s002850050042`

196. Hochachka, W.M., Dhondt, A.A.: Density-dependent decline of host abundance resulting from a new infectious disease. Proc. Natl Acad. Sci. USA **97**(10), 5303–5306 (2000). http://www.pnas.org/content/97/10/5303.abstract

197. Hohmann, W., Kraus, M., Schneider, F.W.: Pattern recognition by electrical coupling of eight chemical reactors. J. Phys. Chem. A **103**(38), 7606–7611 (1999). http://dx.doi.org/10.1021/jp991480n

198. Hohmann, W., Schinor, N., Kraus, M., Schneider, F.W.: Electrically coupled chemical oscillators and their action potentials. J. Phys. Chem. A **103**(29), 5742–5748 (1999). http://dx.doi.org/10.1021/jp991224a

199. Holcman, D., Marchewka, A., Schuss, Z.: Survival probability of diffusion with trapping in cellular neurobiology. Phys. Rev. E **72**(3), 031910 (2005). http://link.aps.org/doi/10.1103/PhysRevE.72.031910

200. Holcman, D., Schuss, Z.: Modeling calcium dynamics in dendritic spines. SIAM J. Appl. Math. **65**(3), 1006–1026 (2005). http://link.aip.org/link/?SMM/65/1006/1

201. Holmes, E.E.: Are diffusion models too simple? A comparison with telegraph models of invasion. Am. Nat. **142**(5), 779–795 (1993). http://dx.doi.org/10.1086/285572

202. Holz, R., Schneider, F.W.: Control of dynamic states with time delay between two mutually flow rate coupled reactors. J. Phys. Chem. **97**(47), 12239–12243 (1993). http://dx.doi.org/10.1021/j100149a024

203. Hornung, G., Berkowitz, B., Barkai, N.: Morphogen gradient formation in a complex environment: an anomalous diffusion model. Phys. Rev. E **72**(4), 041916 (2005). http://dx.doi.org/10.1103/PhysRevE.72.041916

204. Horsthemke, W.: Fisher waves in reaction random walks. Phys. Lett. A **263**(4–6), 285–292 (1999). http://dx.doi.org/10.1016/S0375-9601(99)00711-2

205. Horsthemke, W.: Spatial instabilities in reaction random walks with direction-independent kinetics. Phys. Rev. E **60**(3), 2651–2663 (1999). http://dx.doi.org/10.1103/PhysRevE.60.2651

206. Horsthemke, W.: Pattern formation in random walks with inertia. In: Kish, L.B., Lindenberg, K., Gingl, Z. (eds.) Noise in Complex Systems and Stochastic Dynamics III, *Proceedings of the SPIE*, vol. 5845, pp. 12–26. SPIE, Bellingham, WA (2005). http://dx.doi.org/10.1117/12.610253

207. Horsthemke, W., Lam, K., Moore, P.K.: Network topology and Turing instabilities in small arrays of diffusively coupled reactors. Phys. Lett. A **328**(6), 444–451 (2004). http://dx.doi.org/10.1016/j.physleta.2004.06.044

208. Horsthemke, W., Moore, P.K.: Turing instability in inhomogeneous arrays of diffusively coupled reactors. J. Phys. Chem. A **108**(12), 2225–2231 (2004). http://dx.doi.org/10.1021/jp037029k

209. Horsthemke, W., Zachary, C.E., Moore, P.K.: Instabilities in networks of reactors coupled by photochemical feedback. Chem. Phys. Lett. **432**(4–6), 457–461 (2006). http://dx.doi.org/10.1016/j.cplett.2006.10.121

210. Horváth, A.K., Dolnik, M., Zhabotinsky, A.M., Epstein, I.R.: Kinetics of photoresponse of the chlorine dioxide-iodine-malonic acid reaction. J. Phys. Chem. A **104**(24), 5766–5769 (2000). http://dx.doi.org/10.1021/jp000352s

211. Horvath, J., Szalai, I., De Kepper, P.: An experimental design method leading to chemical Turing patterns. Science **324**(5928), 772–775 (2009). http://dx.doi.org/10.1126/science.1169973

212. Hosking, J., Smith, J., Sheppard, A.W.: *Cytisus scoparius* L., Scotch Broom. In: Panetta, F.D., Groves, R.H., Shepherd, R.C.H. (eds.) The Biology of Australian Weeds, vol. 2, pp. 77–88. R.G. and F.J. Richardson, Melbourne (1998)

213. Hughes, B.D.: Random Walks and Random Environments: Volume 1: Random Walks. Oxford University Press, New York (1995)

214. Hunding, A., Sørensen, P.G.: Size adaptation of Turing prepatterns. J. Math. Biol. **26**(1), 27–39 (1988). http://dx.doi.org/10.1007/BF00280170

215. Hutchinson, G.E.: Circular causal systems in ecology. Ann. NY Acad. Sci. **50**, 221–246 (1948). http://www.wku.edu/~smithch/biogeog/HUTC1948.htm

216. Iomin, A.: Superdiffusion of cancer on a comb structure. J. Phys. Conf. Ser. **7**, 57–67 (2005). http://dx.doi.org/10.1088/1742-6596/7/1/005

217. Iomin, A.: Toy model of fractional transport of cancer cells due to self-entrapping. Phys. Rev. E **73**(6), 061918 (2006). http://link.aps.org/abstract/PRE/v73/e061918

218. Janssen, J., Manca, R.: Applied Semi-Markov Processes. Springer, New York (2006)

219. Jensen, O., Pannbacker, V.O., Mosekilde, E., Dewel, G., Borckmans, P.: Localized structures and front propagation in the Lengyel–Epstein model. Phys. Rev. E **50**(2), 736–749 (1994). http://dx.doi.org/10.1103/PhysRevE.50.736

220. Johansson, M.E., Nilsson, C.: Hydrochory, population dynamics and distribution of the clonal aquatic plant *Ranunculus lingua*. J. Ecol. **81**(1), 81–91 (1993). http://www.jstor.org/stable/2261226

221. Jongejans, E., Skarpaas, O., Tipping, P., Shea, K.: Establishment and spread of founding populations of an invasive thistle: the role of competition and seed limitation. Biol. Invasions **9**(3), 317–325 (2007). http://dx.doi.org/10.1007/s10530-006-9035-3

222. Joseph, D.D., Preziosi, L.: Heat waves. Rev. Mod. Phys. **61**(1), 41–73 (1989). http://dx.doi.org/10.1103/RevModPhys.61.41

223. Jou, D., Casas-Vázquez, J., Lebon, G.: Extended Irreversible Thermodynamics, 4th edn. Springer, New York (2010)

224. Kailath, T., Sayed, A.H., Hassibi, B.: Linear Estimation. Prentice Hall, Upper Saddle River (2000)

225. Keener, J.P.: Propagation of waves in an excitable medium with discrete release sites. SIAM J. Appl. Math. **61**(1), 317–334 (2000). http://www.siam.org/journals/siap/61-1/35081.html

226. Kenkre, V.M., Kuperman, M.N.: Applicability of the Fisher equation to bacterial population dynamics. Phys. Rev. E **67**(5), 051921 (2003). http://dx.doi.org/10.1103/PhysRevE.67.051921

227. Kessler, D.A., Ner, Z., Sander, L.M.: Front propagation: precursors, cutoffs, and structural stability. Phys. Rev. E **58**(1), 107–114 (1998). http://dx.doi.org/10.1103/PhysRevE.58.107

228. Kierstead, H., Slobodkin, L.B.: The size of water masses containing plankton blooms. J. Mar. Res. **12**, 141–147 (1953)

229. Klages, R., Radons, G., Sokolov, I.M. (eds.): Anomalous Transport: Foundations and Applications. Wiley-VCH Weinheim (2008)

230. Klein, C.T., Mayer, B.: A model for pattern formation in gap-junction coupled cells. J. Theor. Biol. **186**(1), 107–115 (1997). http://dx.doi.org/10.1006/jtbi.1996.0337

231. Koch, A.J., Meinhardt, H.: Biological pattern formation: from basic mechanisms to complex structures. Rev. Mod. Phys. **66**(4), 1481–1507 (1994). http://dx.doi.org/10.1103/RevModPhys.66.1481

232. Kolmogorov, A.N., Petrovskii, I.G., Piskunov, N.S.: Étude de l'équation de la diffusion avec croissance de la quantité de matière et son application à un problème biologique. Bull. Univ. Etat Moscou Ser. Int. Sect. A Math. et Mecan. **1**(6), 1–25 (1937)

233. Kopelman, R.: Fractal reaction kinetics. Science **241**(4873), 1620–1626 (1988). http://dx.doi.org/10.1126/science.241.4873.1620

234. Kosek, J., Marek, M.: Coupled excitable cells. J. Phys. Chem. **97**(1), 120–127 (1993). http://dx.doi.org/10.1021/j100103a022

235. Kosztołowicz, T., Lewandowska, K.D.: Time evolution of the reaction front in a subdiffusive system. Phys. Rev. E **78**(6), 066103 (2008). http://link.aps.org/abstract/PRE/v78/e066103

236. Krömker, S.: Wave bifurcation in models for heterogeneous catalysis. Acta Math. Univ. Comenianae **67**(1), 83–100 (1998). http://alf1.cii.fc.ul.pt/EMIS/journals/AMUC/_vol-67/_no_1/_kromker/kromker.html

237. Krug, H.J., Pohlmann, L., Kuhnert, L.: Analysis of the modified complete Oregonator accounting for oxygen sensitivity and photosensitivity of Belousov–Zhabotinskii systems. J. Phys. Chem. **94**(12), 4862–4866 (1990). http://dx.doi.org/10.1021/j100375a021

238. Kuzovkov, V., Kotomin, E.: Kinetics of bimolecular reactions in condensed media: critical phenomena and microscopic self-organisation. Rep. Prog. Phys. **51**(12), 1479–1523 (1988). http://stacks.iop.org/0034-4885/51/1479

239. Lacalli, T., Wilkinson, D., Harrison, L.: Theoretical aspects of stripe formation in relation to Drosophila segmentation. Development **104**(1), 105–113 (1988). http://dev.biologists.org/cgi/content/abstract/104/1/105

240. Langlands, T.A.M., Henry, B.I., Wearne, S.L.: Turing pattern formation with fractional diffusion and fractional reactions. J. Phys.: Condens. Matter **19**(6), 065115 (2007). http://dx.doi.org/10.1088/0953-8984/19/6/065115

241. Laplante, J.P., Erneux, T.: Propagation failure and multiple steady states in an array of diffusion coupled flow reactors. Physica A **188**, 89–98 (1992). http://dx.doi.org/10.1016/0378-4371(92)90256-P

242. Laplante, J.P., Erneux, T.: Propagation failure in arrays of coupled bistable chemical reactors. J. Phys. Chem. **96**(12), 4931–4934 (1992). http://dx.doi.org/10.1021/j100191a038

243. Lefever, R.: Dissipative structures in chemical systems. J. Chem. Phys. **49**(11), 4977–4978 (1968). http://dx.doi.org/10.1063/1.1669986

244. Lekebusch, A., Schneider, F.W.: Two biochemical oscillators coupled by mass exchange. J. Phys. Chem. B **101**(47), 9838–9843 (1997). http://dx.doi.org/10.1021/jp972257y

245. Lengyel, I., Epstein, I.R.: Diffusion-induced instability in chemically reacting systems: steady-state multiplicity, oscillation, and chaos. Chaos **1**(1), 69–76 (1991). http://dx.doi.org/10.1063/1.165819

246. Lengyel, I., Epstein, I.R.: Modeling of Turing structures in the chlorite-iodide-malonic acid-starch reaction system. Science **251**(4994), 650–652 (1991). http://dx.doi.org/10.1126/science.251.4994.650

247. Lengyel, I., Epstein, I.R.: A chemical approach to designing Turing patterns in reaction–diffusion systems. Proc. Natl Acad. Sci. USA **89**, 3977–3979 (1992). http://www.pnas.org/cgi/content/abstract/89/9/3977

248. Lengyel, I., Epstein, I.R.: The chemistry behind the first experimental chemical examples of Turing patterns. In: Kapral, R., Showalter, K. (eds.) Chemical Waves and Patterns, pp. 297–322. Kluwer Academic Publishers, Dordrecht (1995)

249. Lengyel, I., Kádár, S., Epstein, I.R.: Quasi-two-dimensional Turing patterns in an imposed gradient. Phys. Rev. Lett. **69**(18), 2729–2732 (1992). http://dx.doi.org/10.1103/PhysRevLett.69.2729

250. Lengyel, I., Kádár, S., Epstein, I.R.: Transient Turing structures in a gradient-free closed system. Science **259**(5094), 493–495 (1993). http://dx.doi.org/10.1126/science.259.5094.493

251. Lengyel, I., Rabai, G., Epstein, I.R.: Batch oscillation in the reaction of chlorine dioxide with iodine and malonic acid. J. Am. Chem. Soc. **112**(11), 4606–4607 (1990). http://dx.doi.org/10.1021/ja00167a103

252. Lengyel, I., Rabai, G., Epstein, I.R.: Experimental and modeling study of oscillations in the chlorine dioxide-iodine-malonic acid reaction. J. Am. Chem. Soc. **112**(25), 9104–9110 (1990). http://dx.doi.org/10.1021/ja00181a011

253. Lévy, P.: Processus semi-markoviens. Proc. Int. Cong. Math. (Amsterdam) **3**, 416–426 (1954)

254. Lim, S.C., Muniandy, S.V.: Generalized Ornstein–Uhlenbeck processes and associated self-similar processes. J. Phys. A: Math. Gen. **36**(14), 3961–3982 (2003). http://dx.doi.org/10.1088/0305-4470/36/14/303

255. Lindenberg, K., West, B.J., Kopelman, R.: Steady-state segregation in diffusion-limited reactions. Phys. Rev. Lett. **60**(18), 1777–1780 (1988). http://dx.doi.org/10.1103/PhysRevLett.60.1777

256. Lotka, A.J.: Elements of Mathematical Biology. Dover, New York (1956)
257. Ludwig, D., Aronson, D.G., Weinberger, H.F.: Spatial patterning of the spruce budworm. J. Math. Biol. **8**(3), 217–258 (1979). http://dx.doi.org/10.1007/BF00276310
258. Lutz, E.: Fractional Langevin equation. Phys. Rev. E **64**(5), 051106 (2001). http://dx.doi.org/10.1103/PhysRevE.64.051106
259. Magnus, W., Winkler, S.: Hill's Equation. Dover, New York (1979)
260. Mainardi, F., Luchko, Y., Pagnini, G.: The fundamental solution of the space-time fractional diffusion equation. Fract. Calc. Appl. Anal. **4**(2), 153–192 (2001). http://pamina.bo.infn.it/people_web_pages/mainardi/download/lumapa.pdf
261. Maini, P.K.: Mathematical models in morphogenesis. In: Diekmann, O., Durrett, R., Hadeler, K.P., Maini, P., Smith, H.L. (eds.) Mathematics Inspired by Biology. Lecture Notes in Mathematics, vol. 1714, pp. 151–189. Springer, Berlin (1999). http://dx.doi.org/10.1007/BFb0092377
262. Maini, P.K., Baker, R.E., Chuong, C.M.: Developmental biology: the Turing model comes of molecular age. Science **314**(5804), 1397–1398 (2006). http://dx.doi.org/10.1126/science.1136396
263. Maini, P.K., Benson, D.L., Sherratt, J.A.: Pattern formation in reaction-diffusion models with spatially inhomogeneous coefficients. IMA J. Math. Appl. Med. Biol. **9**, 197–213 (1992). http://dx.doi.org/10.1093/imammb/9.3.197
264. Maini, P.K., Painter, K.J., Chau, H.N.P.: Spatial pattern formation in chemical and biological systems. J. Chem. Soc. Faraday Trans. **93**(20), 3601–3610 (1997). http://dx.doi.org/10.1039/a702602a
265. Mancinelli, R., Vergni, D., Vulpiani, A.: Superfast front propagation in reactive systems with non-Gaussian diffusion. Europhys. Lett. **60**(4), 532–538 (2002). http://dx.doi.org/10.1209/epl/i2002-00251-7
266. Mandelbrot, B.B., Van Ness, J.W.: Fractional Brownian motions, fractional noises and applications. SIAM Rev. **10**(4), 422–437 (1968). http://dx.doi.org/10.1137/1010093
267. Mansury, Y., Deisboeck, T.S.: Simulating 'structure-function' patterns of malignant brain tumors. Physica A **331**(1–2), 219–232 (2004). http://dx.doi.org/10.1016/j.physa.2003.09.013
268. Mansury, Y., Deisboeck, T.S.: Simulating the time series of a selected gene expression profile in an agent-based tumor model. Physica D **196**(1–2), 193–204 (2004). http://dx.doi.org/10.1016/j.physd.2004.04.008
269. Marek, M., Stuchl, I.: Synchronization in two interacting oscillatory systems. Biophys. Chem. **3**(3), 241–248 (1975). http://dx.doi.org/10.1016/0301-4622(75)80016-0
270. Marro, J., Dickman, R.: Nonequilibrium Phase Transitions in Lattice Models. Cambridge University Press, Cambridge, UK (1999)
271. Mátyás, L., Gaspard, P.: Entropy production in diffusion–reaction systems: the reactive random Lorentz gas. Phys. Rev. E **71**(3), 036147 (2005). http://link.aps.org/abstract/PRE/v71/e036147
272. McGraw, P.N., Menzinger, M.: Laplacian spectra as a diagnostic tool for network structure and dynamics. Phys. Rev. E **77**(3), 031102 (2008). http://link.aps.org/abstract/PRE/v77/e031102
273. McKean, H.P.: Chapman–Enskog–Hilbert expansion for a class of solutions of the telegraph equation. J. Math. Phys. **8**(3), 547–552 (1967). http://dx.doi.org/10.1063/1.1705230
274. McKean, H.P.: Nagumo's equation. Adv. Math. **4**(3), 209–223 (1970). http://dx.doi.org/10.1016/0001-8708(70)90023-X
275. Meerschaert, M.M., Benson, D.A., Baeumer, B.: Operator Lévy motion and multiscaling anomalous diffusion. Phys. Rev. E **63**(2), 021112 (2001). http://dx.doi.org/10.1103/PhysRevE.63.021112
276. Meerschaert, M.M., Benson, D.A., Scheffler, H.P., Baeumer, B.: Stochastic solution of space-time fractional diffusion equations. Phys. Rev. E **65**(4), 041103 (2002). http://dx.doi.org/10.1103/PhysRevE.65.041103

277. Meerschaert, M.M., Benson, D.A., Scheffler, H.P., Becker-Kern, P.: Governing equations and solutions of anomalous random walk limits. Phys. Rev. E **66**(6), 060102 (2002). `http://dx.doi.org/10.1103/PhysRevE.66.060102`

278. Meerschaert, M.M., Scheffler, H.P.: Limit theorems for continuous-time random walks with infinite mean waiting times. J. Appl. Probab. **41**(3), 623–638 (2004). `http://dx.doi.org/10.1239/jap/1091543414`

279. Meinhardt, H.: Models of Biological Pattern Formation. Academic, London (1982)

280. Meinhardt, H., Gierer, A.: Pattern formation by local self-activation and lateral inhibition. BioEssays **22**(8), 753–760 (2000). `http://dx.doi.org/10.1002/1521-1878(200008)22:8<753::AID-BIES9>3.0.CO;2-Z`

281. Méndez, V.: Variational principles for nonlinear dynamical systems. J. Math. Phys. **39**(2), 954–966 (1998). `http://dx.doi.org/10.1063/1.532363`

282. Méndez, V., Camacho, J.: Dynamics and thermodynamics of delayed population growth. Phys. Rev. E **55**(6), 6476–6482 (1997). `http://dx.doi.org/10.1103/PhysRevE.55.6476`

283. Méndez, V., Campos, D., Fedotov, S.: Analysis of fronts in reaction-dispersal processes. Phys. Rev. E **70**(6), 066129 (2004). `http://dx.doi.org/10.1103/PhysRevE.70.066129`

284. Méndez, V., Campos, D., Zemskov, E.P.: Variational principles and the shift in the front speed due to a cutoff. Phys. Rev. E **72**(5), 056113 (2005). `http://dx.doi.org/10.1103/PhysRevE.72.056113`

285. Méndez, V., Compte, A.: Wavefronts in bistable hyperbolic reaction–diffusion systems. Physica A **260**(1–2), 90–98 (1998). `http://dx.doi.org/10.1016/S0378-4371(98)00281-7`

286. Méndez, V., Fedotov, S., Campos, D., Horsthemke, W.: Biased random walks and propagation failure. Phys. Rev. E **75**(1), 011118 (2007). `http://dx.doi.org/10.1103/PhysRevE.75.011118`

287. Méndez, V., Fedotov, S., Horsthemke, W.: Effect of memory kernels on the speed of reaction–diffusion fronts. Europhys. Lett. **77**(5), 58006 (2007). `http://dx.doi.org/10.1209/0295-5075/77/58006`

288. Méndez, V., Fort, J., Farjas, J.: Speed of wave-front solutions to hyperbolic reaction–diffusion equations. Phys. Rev. E **60**(5), 5231–5243 (1999). `http://dx.doi.org/10.1103/PhysRevE.60.5231`

289. Méndez, V., Fort, J., Pujol, T.: The speed of reaction–diffusion wavefronts in nonsteady media. J. Phys. A Math. Gen. **36**(14), 3983–3993 (2003). `http://dx.doi.org/10.1088/0305-4470/36/14/304`

290. Méndez, V., Fort, J., Rotstein, H.G., Fedotov, S.: Speed of reaction–diffusion fronts in spatially heterogeneous media. Phys. Rev. E **68**(4), 041105 (2003). `http://dx.doi.org/10.1103/PhysRevE.68.041105`

291. Méndez, V., Llebot, J.E.: Hyperbolic reaction–diffusion equations for a forest fire model. Phys. Rev. E **56**(6), 6557–6563 (1997). `http://dx.doi.org/10.1103/PhysRevE.56.6557`

292. Méndez, V., Ortega-Cejas, V., Campos, D.: Front propagation in population dynamics with dispersive variability and delayed growth. Physica A **367**, 283–292 (2006). `http://dx.doi.org/10.1016/j.physa.2005.11.005`

293. Merris, R.: Laplacian matrices of graphs: a survey. Linear Alg. Appl. **197–198**, 143–176 (1994). `http://dx.doi.org/10.1016/0024-3795(94)90486-3`

294. Merris, R.: Laplacian graph eigenvectors. Linear Alg. Appl. **278**(1–3), 221–236 (1998). `http://dx.doi.org/10.1016/S0024-3795(97)10080-5`

295. Metz, J.A.J., Diekman, O. (eds.): The Dynamics of Physiologically Structured Populations Lecture Notes in Biomathematics, vol. 68. Springer, Berlin (1986)

296. Metzler, R., Chechkin, A.V., Gonchar, V.Y., Klafter, J.: Some fundamental aspects of Lévy flights. Chaos Solitons Fractals **34**(1), 129–142 (2007). `http://dx.doi.org/10.1016/j.chaos.2007.01.055`

297. Metzler, R., Glöckle, W.G., Nonnenmacher, T.F.: Fractional model equation for anomalous diffusion. Physica A **211**(1), 13–24 (1994). `http://dx.doi.org/10.1016/0378-4371(94)90064-7`

298. Metzler, R., Klafter, J.: The random walk's guide to anomalous diffusion: a fractional dynamics approach. Phys. Rep. **339**(1), 1–77 (2000). `http://dx.doi.org/10.1016/S0370-1573(00)00070-3`

299. Metzler, R., Klafter, J.: The restaurant at the end of the random walk: recent developments in the description of anomalous transport by fractional dynamics. J. Phys. A Math. Gen. **37**, R161–R208 (2004). `http://dx.doi.org/10.1088/0305-4470/37/31/R01`

300. Milstein, G.N., Tretyakov, M.V.: Stochastic Numerics for Mathematical Physics. Springer, New York (2004)

301. Miura, T., Shiota, K., Morriss-Kay, G., Maini, P.K.: Mixed-mode pattern in *Doublefoot* mutant mouse limb – Turing reaction–diffusion model on a growing domain during limb development. J. Theor. Biol. **240**(4), 562–573 (2006). `http://dx.doi.org/10.1016/j.jtbi.2005.10.016`

302. Monasson, R.: Diffusion, localization and dispersion relations on "small-world" lattices. Eur. Phys. J. B **12**(4), 555–567 (1999). `http:/dx.doi.org/10.1007/s100510051038`

303. Monin, A.S., Yaglom, A.M.: Statistical Fluid Mechanics. The MIT Press, Cambridge (1971)

304. Montroll, E.W., Shlesinger, M.F.: On the wonderful world of random walks. In: Lebowitz, J.L., Montroll, E.W. (eds.) Nonequilibrium Phenomena II: From Stochastics to Hydrodynamics, pp. 1–121. Elsevier Science Publishers BV, Amsterdam (1984)

305. Moore, P.K., Horsthemke, W.: Localized patterns in homogeneous networks of diffusively coupled reactors. Physica D **206**(1–2), 121–144 (2005). `http://dx.doi.org/10.1016/j.physd.2005.05.002`

306. Mosco, U.: Invariant field metrics and dynamical scalings on fractals. Phys. Rev. Lett. **79**(21), 4067–4070 (1997). `http://link.aps.org/abstract/PRL/v79/p4067`

307. Müller, H.P., Kimmich, R., Weis, J.: NMR flow velocity mapping in random percolation model objects: evidence for a power-law dependence of the volume-averaged velocity on the probe-volume radius. Phys. Rev. E **54**(5), 5278–5285 (1996). `http://dx.doi.org/10.1103/PhysRevE.54.5278`

308. Murray, J.D.: On pattern formation mechanisms for lepidopteran wing patterns and mammalian coat markings. Philos. Trans. R. Soc. Lond. B **295**(1078), 473–496 (1981). `http://dx.doi.org/10.1098/rstb.1981.0155`

309. Murray, J.D.: Mathematical Biology I: An Introduction. Interdisciplinary Applied Mathematics, vol. 17, 3rd edn. Springer, New York (2002). `http://dx.doi.org/10.1007/b98868`

310. Murray, J.D.: Mathematical Biology II: Spatial Models and Biomedical Applications. Interdisciplinary Applied Mathematics, vol. 18, 3rd edn. Springer, New York (2003). `http://dx.doi.org/10.1007/b98869`

311. Nagorcka, B.: The role of a reaction–diffusion system in the initiation of skin organ primordia. I. The first wave of initiation. J. Theor. Biol. **121**(4), 449–475 (1986). `http://dx.doi.org/10.1016/S0022-5193(86)80102-3`

312. Nagorcka, B.N., Mooney, J.R.: The role of a reaction–diffusion system in the formation of hair fibres. J. Theor. Biol. **98**(4), 575–607 (1982). `http://dx.doi.org/10.1016/0022-5193(82)90139-4`

313. Nagorcka, B.N., Mooney, J.R.: The role of a reaction–diffusion system in the initiation of primary hair follicles. J. Theor. Biol. **114**(2), 243–272 (1985). `http://dx.doi.org/10.1016/S0022-5193(85)80106-5`

314. Nakajima, K., Sawada, Y.: Experimental studies on the weak coupling of oscillatory chemical reaction systems. J. Chem. Phys. **72**(4), 2231–2234 (1980). `http://dx.doi.org/10.1063/1.439466`

315. Nakamura, T., Mine, N., Nakaguchi, E., Mochizuki, A., Yamamoto, M., Yashiro, K., Meno, C., Hamada, H.: Generation of robust left–right asymmetry in the mouse embryo requires a self-enhancement and lateral-inhibition system. Dev. Cell **11**(4), 495–504 (2006). `http://dx.doi.org/10.1016/j.devcel.2006.08.002`

316. Nakao, H., Mikhailov, A.S.: Turing patterns on networks. arXiv:0807.1230v1 [nlin.PS] (2008). `http://arxiv.org/abs/0807.1230`

317. Nec, Y., Nepomnyashchy, A.A.: Turing instability in sub-diffusive reaction–diffusion systems. J. Phys. A Math. Theor. **40**(49), 14687–14702 (2007). `http://stacks.iop.org/1751-8121/40/14687`

318. Nec, Y., Nepomnyashchy, A.A.: Turing instability of anomalous reaction-anomalous diffusion systems. Eur. J. Appl. Math. **19**(3), 329–349 (2008). `http://dx.doi.org/10.1017/S0956792508007389`

319. Newman, S.A., Bhat, R.: Activator-inhibitor dynamics of vertebrate limb pattern formation. Birth Defects Res. C **81**(4), 305–319 (2007). `http://dx.doi.org/10.1002/bdrc.20112`

320. Nielsen, S., Kapral, R.: Coloring a Lorentz gas. J. Chem. Phys. **109**(15), 6460–6468 (1998). `http://link.aip.org/link/?JCP/109/6460/1`

321. Nimchinsky, E.A., Sabatini, B.L., Svoboda, K.: Structure and function of dendritic spines. Annu. Rev. Physiol. **64**(1), 313–353 (2002). `http://dx.doi.org/10.1146/annurev.physiol.64.081501.160008`

322. Noszticzius, Z., Horsthemke, W., McCormick, W.D., Swinney, H.L., Tam, W.Y.: Sustained chemical waves in an annular gel reactor: a chemical pinwheel. Nature **329**, 619–620 (1987). `http://dx.doi.org/10.1038/329619a0`

323. Noszticzius, Z., Horsthemke, W., McCormick, W.D., Swinney, H.L., Tam, W.Y.: Annular gel reactor for chemical pattern formation. US Patent 4,968,484, 1990

324. Novikov, E.A.: Functionals and the random-force method in turbulence theory. Sov. Phys. JETP **20**(5), 1290–1294 (1965)

325. Noyes, R.M., Field, R.J.: Mechanisms of chemical oscillators: experimental examples. Acc. Chem. Res. **10**(8), 273–280 (1977). `http://dx.doi.org/10.1021/ar50116a001`

326. Noyes, R.M., Field, R.J., Körös, E.: Oscillations in chemical systems. I. Detailed mechanism in a system showing temporal oscillations. J. Am. Chem. Soc. **94**(4), 1394–1395 (1972). `http://dx.doi.org/10.1021/ja00759a080`

327. Okubo, A.: Dynamical aspects of animal grouping: swarms, schools, flocks, and herds. Adv. Biophys. **22**, 1–94 (1986). `http://dx.doi.org/10.1016/0065-227X(86)90003-1`

328. Okubo, A., Levin, S.A.: Diffusion and Ecological Problems. Springer, New York (2001)

329. Ortega-Cejas, V., Fort, J., Méndez, V.: The role of the delay time in the modeling of biological range expansions. Ecology **85**(1), 258–264 (2004). `http://dx.doi.org/10.1890/02-0606`

330. Ortega-Cejas, V., Fort, J., Méndez, V., Campos, D.: Approximate solution to the speed of spreading viruses. Phys. Rev. E **69**(3), 031909 (2004). `http://dx.doi.org/10.1103/PhysRevE.69.031909`

331. O'Shaughnessy, B., Procaccia, I.: Analytical solutions for diffusion on fractal objects. Phys. Rev. Lett. **54**(5), 455–458 (1985). `http://link.aps.org/abstract/PRL/v54/p455`

332. Oster, G.F.: Lateral inhibition models of developmental processes. Math. Biosci. **90**(1–2), 265–286 (1988). `http://dx.doi.org/10.1016/0025-5564(88)90070-3`

333. Othmer, H.G., Dunbar, S.R., Alt, W.: Models of dispersal in biological systems. J. Math. Biol. **26**(3), 263–298 (1988). `http://dx.doi.org/10.1007/BF00277392`

334. Othmer, H.G., Scriven, L.E.: Instability and dynamic patterns in cellular networks. J. Theor. Biol. **32**, 507–537 (1971). `http://dx.doi.org/10.1016/0022-5193(71)90154-8`

335. Ouyang, Q., Boissonade, J., Roux, J.C., De Kepper, P.: Sustained reaction-diffusion structures in an open reactor. Phys. Lett. A **134**(5), 282–286 (1989). `http://dx.doi.org/10.1016/0375-9601(89)90637-3`

336. Ouyang, Q., Castets, V., Boissonade, J., Roux, J.C., De Kepper, P., Swinney, H.L.: Sustained patterns in chlorite-iodide reactions in a one-dimensional reactor. J. Chem. Phys. **95**(1), 351–360 (1991). `http://dx.doi.org/10.1063/1.461490`

337. Ouyang, Q., Swinney, H.L.: Transition from a uniform state to hexagonal and striped Turing patterns. Nature **352**, 610–612 (1991). `http://dx.doi.org/10.1038/352610a0`

338. Ouyang, Q., Swinney, H.L.: Transition to chemical turbulence. Chaos **1**(4), 411–420 (1991). `http://dx.doi.org/10.1063/1.165851`

339. Owen, M.R., Sherratt, J.A.: Mathematical modelling of juxtacrine cell signalling. Math. Biosci. **153**(2), 125–150 (1998). `http://dx.doi.org/10.1016/S0025-5564(98)10034-2`

340. Owen, M.R., Sherratt, J.A., Wearing, H.J.: Lateral induction by juxtacrine signaling is a new mechanism for pattern formation. Dev. Biol. **217**(1), 54–61 (2000). `http://dx.doi.org/10.1006/dbio.1999.9536`

341. Page, K., Maini, P.K., Monk, N.A.M.: Pattern formation in spatially heterogeneous Turing reaction–diffusion models. Physica D **181**(1–2), 80–101 (2003). `http://dx.doi.org/10.1016/S0167-2789(03)00068-X`

342. Page, K., Maini, P.K., Monk, N.A.M.: Complex pattern formation in reaction–diffusion systems with spatially varying parameters. Physica D **202**(1–2), 95–115 (2005). `http://dx.doi.org/10.1016/j.physd.2005.01.022`

343. Painter, K.J., Maini, P.K., Othmer, H.G.: Stripe formation in juvenile *Pomacanthus* explained by a generalized Turing mechanism with chemotaxis. Proc. Natl Acad. Sci. USA **96**(10), 5549–5554 (1999). `http://www.pnas.org/cgi/content/abstract/96/10/5549`

344. Paynter, Q., Fowler, S.V., Memmott, J., Sheppard, A.W.: Factors affecting the establishment of *Cytisus scoparius* in southern France: implications for managing both native and exotic populations. J. Appl. Ecol. **35**(4), 582–595 (1998). `http://dx.doi.org/10.1046/j.1365-2664.1998.3540582.x`

345. Pearson, C.E.: Handbook of Applied Mathematics. Van Nostrand Reinhold, New York (1990)

346. Pearson, J.E.: Pattern formation in a (2+1)-species activator-inhibitor-immobilizer system. Physica A **188**, 178–189 (1992). `http://dx.doi.org/10.1016/0378-4371(92)90264-Q`

347. Pearson, J.E., Bruno, W.J.: Pattern formation in an $N + Q$ component reaction–diffusion system. Chaos **2**(4), 513–524 (1992). `http://dx.doi.org/10.1063/1.165893`

348. Pearson, J.E., Horsthemke, W.: Turing instabilities with nearly equal diffusion coefficients. J. Chem. Phys. **90**(3), 1588–1599 (1989). `http://dx.doi.org/10.1063/1.456051`

349. Perumpanani, A.J., Sherratt, J.A., Norbury, J.: Mathematical modelling of capsule formation and multinodularity in benign tumour growth. Nonlinearity **10**(6), 1599 (1997). `http://dx.doi.org/10.1088/0951-7715/10/6/009`

350. Pilling, M.J., Seakins, P.W.: Reaction Kinetics. Oxford University Press, Oxford (1995)

351. Pinhasi, R., Fort, J., Ammerman, A.J.: Tracing the origin and spread of agriculture in Europe. PLoS Biol. **3**(12), 2220–2228 (2005). `http://dx.doi.org/10.1371/journal.pbio.0030410`

352. Pitts, J.D., Finbow, M.E.: The gap junction. J. Cell Sci. Suppl. **4**, 239–266 (1986)

353. Podlubny, I.: Fractional Differential Equations. Mathematics in Science and Engineering, vol. 198. Academic, San Diego (1999)

354. Prigogine, I., Lefever, R.: Symmetry breaking instabilities in dissipative systems. II. J. Chem. Phys. **48**(4), 1695–1700 (1968). `http://dx.doi.org/10.1063/1.1668896`

355. Quintero, N.R., Sánchez, A.: Anomalous resonance phenomena of solitary waves with internal modes. Phys. Rev. Lett. **84**(5), 871–874 (2000). `http://dx.doi.org/10.1103/PhysRevLett.84.871`

356. Ramos-Fernández, G., Mateos, J.L., Miramontes, O., Cocho, G., Larralde, H., Ayala-Orozco, B.: Lévy walk patterns in the foraging movements of spider monkeys (*Ateles geoffroyi*). Behav. Ecol. Sociobiol. **55**(3), 223–230 (2004). `http://dx.doi.org/10.1007/s00265-003-0700-6`

357. Rendine, S., Piazza, A., Cavalli-Sforza, L.L.: Simulation and separation by principal components of multiple demic expansions in Europe. Am. Nat. **128**(5), 681 (1986). `http://dx.doi.org/10.1086/284597`

358. Renfrew, C.: The origins of Indo-European languages. Sci. Am. **261**, 82–90 (1989)

359. Résibois, P.M.V., De Leener, M.: Classical Kinetic Theory of Fluids. Wiley, New York (1977)

360. Rinaldo, A., Rodriguez-Iturbe, I., Rigon, R., Ijjasz-Vasquez, E., Bras, R.L.: Self-organized fractal river networks. Phys. Rev. Lett. **70**(6), 822–825 (1993). `http://link.aps.org/abstract/PRL/v70/p822`

361. Riordan, J., Doering, C.R., ben Avraham, D.: Fluctuations and stability of Fisher waves. Phys. Rev. Lett. **75**(3), 565–568 (1995). `http://dx.doi.org/10.1103/PhysRevLett.75.565`

362. Rodriguez, A., Ehlenberger, D.B., Dickstein, D.L., Hof, P.R., Wearne, S.L.: Automated three-dimensional detection and shape classification of dendritic spines from fluorescence microscopy images. PLoS ONE **3**(4), e1997 (2008). `http://dx.doi.org/10.1371/journal.pone.0001997`

363. Rodríguez-Iturbe, I., Rinaldo, A.: Fractal River Basins: Chance and Self-Organization. Cambridge University Press, Cambridge (1997)

364. Rodríguez-Iturbe, I., Rinaldo, A., Rigon, R., Bras, R.L., Marani, A., Ijjász-Vásquez, E.: Energy dissipation, runoff production, and the three-dimensional structure of river basins. Water Resour. Res. **28**(4), 1095–1103 (1992). `http://www.agu.org/pubs/crossref/1992/91WR03034.shtml`

365. Röhricht, B., Horsthemke, W.: A bifurcation sequence to stationary spatial patterns in a nonuniform chemical model system with equal diffusion coefficients. J. Chem. Phys. **94**(6), 4421–4426 (1991). `http://dx.doi.org/10.1063/1.460703`

366. Rotstein, H.G., Nepomnyashchy, A.A.: Dynamics of kinks in two-dimensional hyperbolic models. Physica D **136**(3–4), 245–265 (2000). `http://dx.doi.org/10.1016/S0167-2789(99)00160-8`

367. Rotstein, H.G., Zhabotinsky, A.M., Epstein, I.R.: Dynamics of one- and two-dimensional kinks in bistable reaction–diffusion equations with quasi-discrete sources of reaction. Chaos **11**(4), 833–842 (2001). `http://dx.doi.org/10.1063/1.1418459`

368. Rudovics, B., Barillot, E., Davies, P.W., Dulos, E., Boissonade, J., De Kepper, P.: Experimental studies and quantitative modeling of Turing patterns in the (chlorine dioxide, iodine, malonic acid) reaction. J. Phys. Chem. A **103**, 1790–1800 (1999). `http://dx.doi.org/10.1021/jp983210v`

369. Ruiz-Lorenzo, J.J., Yuste, S.B., Lindenberg, K.: Simulations for trapping reactions with subdiffusive traps and subdiffusive particles. J. Phys. Condens. Matter **19**(6), 065120 (2007). `http://dx.doi.org/10.1088/0953-8984/19/6/065120`

370. Sabatini, B.L., Maravall, M., Svoboda, K.: Ca^{2+} signaling in dendritic spines. Curr. Opin. Neurobiol. **11**(3), 349–356 (2001). `http://dx.doi.org/10.1016/S0959-4388(00)00218-X`

371. Saichev, A.I., Zaslavsky, G.M.: Fractional kinetic equations: solutions and applications. Chaos **7**(4), 753–764 (1997). `http://link.aip.org/link/?CHA/7/753/1`

372. Samko, S.G., Kilbas, A.A., Marichev, O.I.: Fractional Integrals and Derivatives: Theory and Applications. Gordon and Breach, London (1993)

373. Samorodnitsky, G., Taqqu, M.S.: Stable Non-Gaussian Random Processes: Stochastic Models with Infinite Variance. Chapman and Hall, New York (1994)

374. Sancho, J.M., Sánchez, A.: Selection, shape, and relaxation fronts: a numerical study of the effects of inertia. Phys. Rev. E **63**(5), 056608 (2001). `http://dx.doi.org/10.1103/PhysRevE.63.056608`

375. Santamaria, F., Wils, S., De Schutter, E., Augustine, G.J.: Anomalous diffusion in Purkinje cell dendrites caused by spines. Neuron **52**(4), 635–648 (2006). `http://dx.doi.org/10.1016/j.neuron.2006.10.025`

376. Santos, M.A., Sancho, J.M.: Noise-induced fronts. Phys. Rev. E **59**(1), 98–102 (1999). `http://dx.doi.org/10.1103/PhysRevE.59.98`

377. Santos, M.A., Sancho, J.M.: Front dynamics in the presence of spatiotemporal structured noises. Phys. Rev. E **64**(1), 016129 (2001). `http://dx.doi.org/10.1103/PhysRevE.64.016129`

378. Sato, K.i.: Lévy Processes and Infinitely Divisible Distributions. Cambridge Studies in Advanced Mathematics, vol. 68. Cambridge University Press, Cambridge (1999)

379. Saxton, M.J.: Anomalous diffusion due to binding: a Monte Carlo study. Biophys. J. **70**(3), 1250–1262 (1996). `http://www.biophysj.org/cgi/content/abstract/70/3/1250`

380. Saxton, M.J.: Anomalous subdiffusion in fluorescence photobleaching recovery: a Monte Carlo study. Biophys. J. **81**(4), 2226–2240 (2001). `http://www.biophysj.org/cgi/content/abstract/81/4/2226`

381. Scalas, E., Gorenflo, R., Mainardi, F.: Uncoupled continuous-time random walks: solution and limiting behavior of the master equation. Phys. Rev. E **69**(1), 011107 (2004). `http://dx.doi.org/10.1103/PhysRevE.69.011107`

382. Scher, H., Margolin, G., Metzler, R., Klafter, J., Berkowitz, B.: The dynamical foundation of fractal stream chemistry: the origin of extremely long retention times. Geophys. Res. Lett. **29**(5), 5 (2002). `http://dx.doi.org/10.1029/2001GL014123`

383. Scher, H., Montroll, E.W.: Anomalous transit-time dispersion in amorphous solids. Phys. Rev. B **12**(6), 2455–2477 (1975). `http://dx.doi.org/10.1103/PhysRevB.12.2455`

384. Schlögl, F.: Chemical reaction models for non-equilibrium phase transitions. Z. Phys. **253**(2), 147–161 (1972). `http://dx.doi.org/0.1007/BF01379769`

385. Schlueter, J., Brand, T.: Left–right axis development: examples of similar and divergent strategies to generate asymmetric morphogenesis in chick and mouse embryos. Cytogenet. Genome Res. **117**(1–4), 256–267 (2007). `http://www.karger.com/DOI/10.1159/000103187`

386. Schuss, Z., Singer, A., Holcman, D.: The narrow escape problem for diffusion in cellular microdomains. Proc. Natl. Acad. Sci. USA **104**(41), 16098–16103 (2007). `http://www.pnas.org/cgi/content/abstract/104/41/16098`

387. Schwille, P., Korlach, J., Webb, W.W.: Fluorescence correlation spectroscopy with single-molecule sensitivity on cell and model membranes. Cytometry **36**(3), 176–182 (1999). `http://dx.doi.org/10.1002/(SICI)1097-0320(19990701)36:3<176::AID-CYTO5>3.0.CO;2-F;36(99)176`

388. Segel, L.A.: Modeling Dynamic Phenomena in Molecular and Cellular Biology. Cambridge University Press, Cambridge (1984)

389. Seki, K., Bagchi, B., Tachiya, M.: Dynamics of barrierless and activated chemical reactions in a dispersive medium within the fractional diffusion equation approach. J. Phys. Chem. B **112**(19), 6107–6113 (2008). `http://dx.doi.org/10.1021/jp076753q`

390. Seki, K., Shushin, A.I., Wojcik, M., Tachiya, M.: Specific features of the kinetics of fractional-diffusion assisted geminate reactions. J. Phys. Condens. Matter **19**(6), 065117 (2007). `http://dx.doi.org/10.1088/0953-8984/19/6/065117`

391. Seki, K., Wojcik, M., Tachiya, M.: Fractional reaction–diffusion equation. J. Chem. Phys. **119**(4), 2165–2170 (2003). `http://dx.doi.org/10.1063/1.1587126`

392. Seki, K., Wojcik, M., Tachiya, M.: Recombination kinetics in subdiffusive media. J. Chem. Phys. **119**(14), 7525–7533 (2003). `http://dx.doi.org/10.1063/1.1605946`

393. Sekimura, T., Madzvamuse, A., Wathen, A.J., Maini, P.K.: A model for colour pattern formation in the butterfly wing of *Papilio dardanus*. Proc. R. Soc. Lond. B **267**(1446), 851–859 (2000). `http://dx.doi.org/10.1098/rspb.2000.1081`

394. Setayeshgar, S., Cross, M.C.: Turing instability in a boundary-fed system. Phys. Rev. E **58**(4), 4485–4500 (1998). `http://dx.doi.org/10.1103/PhysRevE.58.4485`

395. Setayeshgar, S., Cross, M.C.: Numerical bifurcation diagram for the two-dimensional boundary-fed chlorine-dioxide–iodine–malonic-acid system. Phys. Rev. E **59**(4), 4258–4264 (1999). `http://dx.doi.org/10.1103/PhysRevE.59.4258`

396. Sheppard, A.W., Cullen, J.M., Aeschlimann, J.P.: Predispersal seed predation on *Carduus nutans (Asteraceae)* in southern Europe. Acta Oecol. **15**(5), 529–541 (1994)

397. Sheppard, A.W., Cullen, J.M., Aeschlimann, J.P., Sagliocco, J.L., Vitou, J.: The importance of insect herbivores relative to other limiting factors on weed population dynamics: a case study of *Carduus nutans*. In: Delfosse, E.S. (ed) Proceedings of the VII International Symposium on Biological Control of Weeds, Rome, Italy, pp. 211–220. MAF, Rome, Italy (1990)

398. Sheppard, A.W., Hodge, P., Paynter, Q., Rees, M.: Factors affecting invasion and persistence of broom *Cytisus scoparius* in Australia. J. Appl. Ecol. **39**(5), 721–734 (2002). `http://dx.doi.org/10.1046/j.1365-2664.2002.00750.x`

399. Sherratt, J.A.: Cellular growth control and travelling waves of cancer. SIAM J. Appl. Math. **53**(6), 1713–1730 (1993). `http://link.aip.org/link/?SMM/53/1713/1`

400. Sherratt, J.A.: Turing bifurcations with a temporally varying diffusion coefficient. J. Math. Biol. **33**(3), 295–308 (1995). http://dx.doi.org/10.1007/BF00169566

401. Sherratt, J.A.: Traveling wave solutions of a mathematical model for tumor encapsulation. SIAM J. Appl. Math. **60**(2), 392–407 (1999). http://dx.doi.org/10.1137/S0036139998345355

402. Sherratt, J.A.: Wavefront propagation in a competition equation with a new motility term modelling contact inhibition between cell populations. Proc. R. Soc. Lond. A **456**(2002), 2365–2386 (2000). http://dx.doi.org/10.1098/rspa.2000.0616

403. Shigesada, N., Kawasaki, K.: Biological Invasions: Theory and Practice. Oxford University Press, Oxford (1997)

404. Shigesada, N., Kawasaki, K., Teramoto, E.: Spatial segregation of interacting species. J. Theor. Biol. **79**(1), 83–99 (1979). http://dx.doi.org/10.1016/0022-5193(79)90258-3

405. Shigesada, N., Kawasaki, K., Teramoto, E.: Traveling periodic waves in heterogeneous environments. Theor. Popul. Biol. **30**(1), 143–160 (1986). http://dx.doi.org/10.1016/0040-5809(86)90029-8

406. Shishido, K., Watarai, A., Naito, S., Ando, T.: Action of bleomycin on the bacterio-phage T7 infection. J. Antibiot. (Tokyo) **28**(9), 676–680 (1975). http://www.journalarchive.jst.go.jp/english/jnlabstract_en.php?cdjournal=antibiotics1968&cdvol=28&noiss-ue=9&startpage=676

407. Shlesinger, M.F., West, B.J., Klafter, J.: Lévy dynamics of enhanced diffusion: application to turbulence. Phys. Rev. Lett. **58**(11), 1100–1103 (1987). http://dx.doi.org/10.1103/PhysRevLett.58.1100

408. Showalter, K., Noyes, R.M., Bar-Eli, K.: A modified Oregonator model exhibiting complicated limit cycle behavior in a flow system. J. Chem. Phys. **69**(6), 2514–2524 (1978). http://dx.doi.org/10.1063/1.436894

409. Shushin, A.I.: Anomalous features of the kinetics of subdiffusion-assisted bimolecular reactions. J. Chem. Phys. **122**(15), 154504 (2005). http://dx.doi.org/10.1063/1.1883164

410. Shushin, A.I.: Kinetics of subdiffusion-assisted reactions: non-Markovian stochastic Liouville equation approach. New J. Phys. **7**, 21 (2005). http://dx.doi.org/10.1088/1367-2630/7/1/021

411. Shushin, A.I.: Effect of interparticle interaction on kinetics of geminate recombination of subdiffusing particles. J. Chem. Phys. **129**(11), 114509 (2008). http://link.aip.org/link/?JCP/129/114509/1

412. Sick, S., Reinker, S., Timmer, J., Schlake, T.: WNT and DKK determine hair follicle spacing through a reaction–diffusion mechanism. Science **314**(5804), 1447–1450 (2006). http://dx.doi.org/10.1126/science.1130088

413. Skarpaas, O., Shea, K.: Dispersal patterns, dispersal mechanisms, and invasion wave speeds for invasive thistles. Am. Nat. **170**(3), 421–430 (2007). http://www.journals.uchicago.edu/doi/abs/10.1086/519854

414. Skellam, J.G.: Random dispersal in theoretical populations. Biometrika **38**(1–2), 196–218 (1951). http://www.jstor.org/stable/2332328

415. Smith, W.L.: Regenerative stochastic processes. Proc. R. Soc. Lond. A **232**(1188), 6–31 (1955). http://rspa.royalsocietypublishing.org/content/232/1188/6.abstract

416. Sokolov, I.M., Schmidt, M.G.W., Sagués, F.: Reaction–subdiffusion equations. Phys. Rev. E **73**(3), 031102 (2006). http://dx.doi.org/10.1103/PhysRevE.73.031102

417. Solnica-Krezel, L.: Vertebrate development: taming the nodal waves. Curr. Biol. **13**(1), R7–R9 (2003). http://dx.doi.org/10.1016/S0960-9822(02)01378-7

418. Solomon, T.H., Weeks, E.R., Swinney, H.L.: Observation of anomalous diffusion and Lévy flights in a two-dimensional rotating flow. Phys. Rev. Lett. **71**(24), 3975–3978 (1993). http://dx.doi.org/10.1103/PhysRevLett.71.3975

419. Stark, J., Andl, T., Millar, S.E.: Hairy math: insights into hair-follicle spacing and orientation. Cell **128**(1), 17–20 (2007). http://dx.doi.org/10.1016/j.cell.2006.12.020

420. Strier, D.E., Ponce Dawson, S.: Role of complexing agents in the appearance of Turing patterns. Phys. Rev. E **69**(6), 066207 (2004). `http://dx.doi.org/10.1103/PhysRevE.69.066207`

421. Strogatz, S.H.: Nonlinear Dynamics and Chaos. Addison-Wesley, Reading (1994)

422. Strogatz, S.H.: Exploring complex networks. Nature **410**, 268–276 (2001). `http://dx.doi.org.10.1038/35065725`

423. Stuchl, I., Marek, M.: Dissipative structures in coupled cells: experiments. J. Chem. Phys. **77**(6), 2956–2963 (1982). `http://dx.doi.org/10.1063/1.444217`

424. Stucki, J.W.: Stability analysis of biochemical systems—a practical guide. Prog. Biophys. Mol. Biol. **33**, 99–187 (1979). `http://dx.doi.org/10.1016/0079-6107(79)90027-0`

425. Sullivan, J.H.: Mechanism of the "bimolecular" hydrogen–iodine reaction. J. Chem. Phys. **46**(1), 73–78 (1967). `http://dx.doi.org/10.1063/1.1840433`

426. Svoboda, K., Tank, D.W., Denk, W.: Direct measurement of coupling between dendritic spines and shafts. Science **272**(5262), 716–719 (1996). `http://dx.doi.org/10.1126/science.272.5262.716`

427. Swanson, K.R., Alvord, E.C., Jr., Murray, J.D.: A quantitative model for differential motility of gliomas in grey and white matter. Cell Prolif. **33**(5), 317–329 (2000). `http://www.amath.washington.edu/~swanson/cellprolif.pdf`

428. Swanson, K.R., Bridge, C., Murray, J.D., Alvord, E.C., Jr.: Virtual and real brain tumors: using mathematical modeling to quantify glioma growth and invasion. J. Neurol. Sci. **216**(1), 1–10 (2003). `http://dx.doi.org/10.1016/j.jns.2003.06.001`

429. Tabin, C.J.: The key to left–right asymmetry. Cell **127**(1), 27–32 (2006). `http://dx.doi.org/10.1016/j.cell.2006.09.018`

430. Takaoka, K., Yamamoto, M., Hamada, H.: Origin of body axes in the mouse embryo. Curr. Opin. Genet. Dev. **17**(4), 344–350 (2007). `http://dx.doi.org/10.1016/j.gde.2007.06.001`

431. Tam, W.Y., Horsthemke, W., McCormick, W.D., Swinney, H.L.: Two-dimensional uniformly fed unstirred chemical reactor. US Patent 4,832,914, 1989

432. Tam, W.Y., Horsthemke, W., Noszticzius, Z., Swinney, H.L.: Sustained spiral waves in a continuously fed unstirred chemical reactor. J. Chem. Phys. **88**(5), 3395–3396 (1988). `http://dx.doi.org/10.1063/1.453935`

433. Tam, W.Y., Vastano, J.A., Swinney, H.L., Horsthemke, W.: Regular and chaotic chemical spatiotemporal patterns. Phys. Rev. Lett. **61**(19), 2163–2166 (1988). `http://dx.doi.org/10.1103/PhysRevLett.61.2163`

434. Taylor, G.I.: Diffusion by continuous movements. Proc. Lond. Math. Soc. Ser. 2 **20**, 196–212 (1921)

435. Teschl, G.: Ordinary Differential Equations and Dynamical Systems. Universität Wien, Wien (2008). `http://www.mat.univie.ac.at/~gerald/ftp/book-ode/`

436. Timm, U., Okubo, A.: Diffusion-driven instability in a predator–prey system with time-varying diffusivities. J. Math. Biol. **30**(3), 307–320 (1992). `http://dx.doi.org/10.1007/BF00176153`

437. Tinsley, M., Cui, J., Chirila, F.V., Taylor, A., Zhong, S., Showalter, K.: Spatiotemporal networks in addressable excitable media. Phys. Rev. Lett. **95**(3), 038306 (2005). `http://dx.doi.org/10.1103/PhysRevLett.95.038306`

438. Tolić-Nørrelykke, I.M., Munteanu, E.L., Thon, G., Oddershede, L., Berg-Sørensen, K.: Anomalous diffusion in living yeast cells. Phys. Rev. Lett. **93**(7), 078102 (2004). `http://dx.doi.org/10.1103/PhysRevLett.93.078102`

439. Tracqui, P., Cruywagen, G.C., Woodward, D.E., Bartoo, G.T., Murray, J.D., Alvord, E.C., Jr.: A mathematical model of glioma growth: the effect of chemotherapy on spatio-temporal growth. Cell Prolif. **28**(1), 17–31 (1995). `http://dx.doi.org/10.1111/j.1365-2184.1995.tb00036.x`

440. Turing, A.M.: The chemical basis of morphogenesis. Philos. Trans. R. Soc. Lond. B **237**(641), 37–72 (1952). `http://rstb.royalsocietypublishing.org/content/237/641/37`

441. Tyson, J.J.: Some further studies of nonlinear oscillations in chemical systems. J. Chem. Phys. **58**(9), 3919–3930 (1973). http://dx.doi.org/10.1063/1.1679748

442. Tyson, J.J., Fife, P.C.: Target patterns in a realistic model of the Belousov–Zhabotinskii reaction. J. Chem. Phys. **73**(5), 2224–2237 (1980). http://dx.doi.org/10.1063/1.440418

443. Tyson, J.J., Kauffman, S.A.: Control of mitosis by a continuous biochemical oscillation: synchronization; spatially inhomogeneous oscillations. J. Math. Biol. **1**(4), 289–310 (1975). http://dx.doi.org/10.1007/BF00279848

444. Uchaikin, V.V., Zolotarev, V.M.: Chance and Stability. Stable Distributions and Their Applications. VSP, Utrecht (1999)

445. van den Bosch, F., Metz, J.A.J., Diekmann, O.: The velocity of spatial population expansion. J. Math. Biol. **28**(5), 529–565 (1990). http://dx.doi.org/10.1007/BF00164162

446. Van den Broeck, C.: Waiting times for random walks on regular and fractal lattices. Phys. Rev. Lett. **62**(13), 1421–1424 (1989). http://link.aps.org/abstract/PRL/v62/p1421

447. von Foerster, H.: Some remarks on changing populations. In: Stohlman, F., Jr. (ed.) The Kinetics of Cellular Proliferation, pp. 382–407. Grune and Stratton, New York (1959)

448. van Saarloos, W.: Front propagation into unstable states. Phys. Rep. **386**(2–6), 29–222 (2003). http://dx.doi.org/10.1016/j.physrep.2003.08.001

449. Vanag, V.K.: Waves and patterns in reaction–diffusion systems. Belousov–Zhabotinsky reaction in water-in-oil microemulsions. Phys. Usp. **47**(9), 923–941 (2004). http://dx.doi.org/10.1070/PU2004v047n09ABEH001742

450. Vanag, V.K., Epstein, I.R.: Pattern formation in a tunable medium: the Belousov–Zhabotinsky reaction in an aerosol ot microemulsion. Phys. Rev. Lett. **87**(22), 228301 (2001). http://dx.doi.org/10.1103/PhysRevLett.87.228301

451. Vanag, V.K., Epstein, I.R.: Packet waves in a reaction–diffusion system. Phys. Rev. Lett. **88**(8), 088303 (2002). http://dx.doi.org/10.1103/PhysRevLett.88.088303

452. Vanag, V.K., Epstein, I.R.: Stationary and oscillatory localized patterns, and subcritical bifurcations. Phys. Rev. Lett. **92**, 128301 (2004). http://dx.doi.org/10.1103/PhysRevlett.92.128301

453. Vanag, V.K., Epstein, I.R.: Patterns of nanodroplets: The Belousov-Zhabotinsky-aerosol OT-microemulsion system. In: Al-Shamery, K., Parisi, J. (eds.) Self-Organized Morphology in Nanostructured Materials. Springer Series in Materials Science, vol. 99, pp. 89–113. Springer, Heidelberg (2008). http://dx.doi.org/10.1007/978-3-540-72675-3_5

454. Vanag, V.K., Epstein, I.R.: Cross-diffusion and pattern formation in reaction-diffusion systems. Phys. Chem. Chem. Phys. **11**(6), 897–912 (2009). http://dx.doi.org/10.1039/b813825g

455. Vastano, J.A., Pearson, J.E., Horsthemke, W., Swinney, H.L.: Chemical pattern formation with equal diffusion coefficients. Phys. Lett. A **124**(6–7), 320–324 (1987). http://dx.doi.org/10.1016/0375-9601(87)90019-3

456. Vastano, J.A., Russo, T., Swinney, H.L.: Bifurcation to spatially induced chaos in a reaction-diffusion system. Physica D **46**(1), 23–42 (1990). http://dx.doi.org/10.1016/0167-2789(90)90111-2

457. Veit, R.R., Lewis, M.A.: Dispersals, population growth, and the Allee effect: dynamics of the house finch invasion of eastern North America. Am. Nat. **148**(2), 255–274 (1996). http://dx.doi.org/10.1086/285924

458. Verhulst, F.: Nonlinear Differential Equations and Dynamical Systems. Springer, Berlin (1990)

459. Viswanathan, G.M., Afanasyev, V., Buldyrev, S.V., Murphy, E.J., Prince, P.A., Stanley, H.E.: Lévy flight search patterns of wandering albatrosses. Nature **381**, 413–415 (1996). http://dx.doi.org/10.1038/381413a0

460. Vlad, M.O.: Age distributions in physical systems. J. Phys. A: Math. Gen. **20**(11), 3367–3380 (1987). http://dx.doi.org/10.1088/0305-4470/20/11/039

461. Vlad, M.O., Ross, J.: Systematic derivation of reaction–diffusion equations with distributed delays and relations to fractional reaction–diffusion equations and hyperbolic transport

equations: application to the theory of Neolithic transition. Phys. Rev. E **66**(6), 061908 (2002). `http://dx.doi.org/10.1103/PhysRevE.66.061908`

462. Voroney, J.P., Lawniczak, A.T., Kapral, R.: Turing pattern formation in heterogeneous media. Physica D **99**(2–3), 303–317 (1996). `http://dx.doi.org/10.1016/S0167-2789(96)00132-7`

463. Wachsmuth, M., Waldeck, W., Langowski, J.: Anomalous diffusion of fluorescent probes inside living cell nuclei investigated by spatially-resolved fluorescence correlation spectroscopy. J. Mol. Biol. **298**(4), 677–689 (2000). `http://dx.doi.org/10.1006/jmbi.2000.3692`

464. Walgraef, D.: Spatio–Temporal Pattern Formation. Springer, New York (1996)

465. Wang, K.G.: Long-time-correlation effects and biased anomalous diffusion. Phys. Rev. A **45**, 833–837 (1992). `http://dx.doi.org/10.1103/PhysRevA.45.833`

466. Wang, K.G., Dong, L.K., Wu, X.F., Zhu, F.W., Ko, T.: Correlation effects, generalized Brownian motion and anomalous diffusion. Physica A **203**(1), 53–60 (1994). `http://dx.doi.org/10.1016/0378-4371(94)90031-0`

467. Wang, K.G., Tokuyama, M.: Nonequilibrium statistical description of anomalous diffusion. Physica A **265**(3–4), 341–351 (1999). `http://dx.doi.org/10.1016/S0378-4371(98)00644-X`

468. Wardlaw, C.W.: A commentary on Turing's diffusion–reaction theory of morphogenesis. New Phytol. **52**(1), 40–47 (1953). `http://www.jstor.org/stable/2429242`

469. Wardlaw, C.W.: The chemical concept of organization in plants. New Phytol. **54**(3), 302–310 (1955). `http://www.jstor.org/stable/2429313`

470. Wardlaw, C.W.: Evidence relating to the diffusion–reaction theory of morphogenesis. New Phytol. **54**(1), 39–48 (1955). `http://www.jstor.org/stable/2429448`

471. Wearing, H.J., Sherratt, J.A.: Nonlinear analysis of juxtacrine patterns. SIAM J. Appl. Math. **62**(1), 283–309 (2001). `http://dx.doi.org/10.1137/S003613990037220X`

472. Weeks, E.R., Swinney, H.L.: Anomalous diffusion resulting from strongly asymmetric random walks. Phys. Rev. E **57**(5), 4915–4920 (1998). `http://dx.doi.org/10.1103/PhysRevE.57.4915`

473. Weiner, J., Holz, R., Schneider, F.W., Bar-Eli, K.: Mutually coupled oscillators with time delay. J. Phys. Chem. **96**(22), 8915–8919 (1992). `http://dx.doi.org/10.1021/j100201a041`

474. Weiss, G.H.: Aspects and Applications of the Random Walk. North-Holland, Amsterdam (1994)

475. Weiss, M.: Stabilizing Turing patterns with subdiffusion in systems with low particle numbers. Phys. Rev. E **68**(3), 036213 (2003). `http://dx.doi.org/10.1103/PhysRevE.68.036213`

476. Weiss, M., Elsner, M., Kartberg, F., Nilsson, T.: Anomalous subdiffusion is a measure for cytoplasmic crowding in living cells. Biophys. J. **87**(5), 3518–3524 (2004). `http://dx.doi.org/10.1529/biophysj.104.044263`

477. Weiss, M., Hashimoto, H., Nilsson, T.: Anomalous protein diffusion in living cells as seen by fluorescence correlation spectroscopy. Biophys. J. **84**(6), 4043–4052 (2003). `http://www.biophysj.org/cgi/content/abstract/84/6/4043`

478. Wells, A.: EGF receptor. Int. J. Biochem. Cell Biol. **31**(6), 637–643 (1999). `http://dx.doi.org/10.1016/S1357-2725(99)00015-1`

479. Woodburn, T.L., Sheppard, A.W.: The demography of *Carduus nutans* as a native and an alien weed. Plant Prot. Q. **11**, 236–238 (1996)

480. Woodward, D.E., Cook, J., Tracqui, P., Cruywagen, G.C., Murray, J.D., Alvord, E.C., Jr.: A mathematical model of glioma growth: the effect of extent of surgical resection. Cell Prolif. **29**(6), 269–288 (1996). `http://dx.doi.org/10.1111/j.1365-2184.1996.tb01580.x`

481. Wu, H.Y., Baer, S.M.: Analysis of an excitable dendritic spine with an activity-dependent stem conductance. J. Math. Biol. **36**(6), 569–592 (1998). `http://dx.doi.org/10.1007/s002850050115`

482. Wu, J., Zou, X.: Traveling wave fronts of reaction–diffusion systems with delay. J. Dyn. Diff. Eq. **13**(3), 651–687 (2001). `http://dx.doi.org/10.1023/A:1016690424892`

483. Xin, J.: Front propagation in heterogeneous media. SIAM Rev. **42**(2), 161–230 (2000). `http://www.siam.org/journals/sirev/42-2/36429.html`

484. Yadav, A., Horsthemke, W.: Kinetic equations for reaction–subdiffusion systems: derivation and stability analysis. Phys. Rev. E **74**(6), 066118 (2006). `http://dx.doi.org/10.1103/PhysRevE.74.066118`

485. Yadav, A., Milu, S.M., Horsthemke, W.: Turing instability in reaction–subdiffusion systems. Phys. Rev. E **78**(2), 026116 (2008). `http://link.aps.org/abstract/PRE/v78/e026116`

486. Yin, J.: Evolution of bacteriophage T7 in a growing plaque. J. Bacteriol. **175**(5), 1272–1277 (1993). `http://jb.asm.org/cgi/content/abstract/175/5/1272`

487. Yin, J., McCaskill, J.: Replication of viruses in a growing plaque: a reaction–diffusion model. Biophys. J. **61**(6), 1540–1549 (1992). `http://dx.doi.org/10.1016/S0006-3495(92)81958-6`

488. Yoshimoto, M., Yoshikawa, K., Mori, Y.: Coupling among three chemical oscillators: synchronization, phase death, and frustration. Phys. Rev. E **47**(2), 864–874 (1993). `http://dx.doi.org/10.1103/PhysRevE.47.864`

489. You, L., Yin, J.: Amplification and spread of viruses in a growing plaque. J. Theor. Biol. **200**(4), 365–373 (1999). `http://dx.doi.org/10.1006/jtbi.1999.1001`

490. Yuste, S.B., Acedo, L., Lindenberg, K.: Reaction front in an $A + B \longrightarrow C$ reaction–subdiffusion process. Phys. Rev. E **69**(3), 036126 (2004). `http://dx.doi.org/10.1103/PhysRevE.69.036126`

491. Yuste, S.B., Lindenberg, K.: Subdiffusion-limited $A + A$ reactions. Phys. Rev. Lett. **87**(11), 118301 (2001). `http://dx.doi.org/10.1103/PhysRevLett.87.118301`

492. Yuste, S.B., Lindenberg, K.: Subdiffusion-limited reactions. Chem. Phys. **284**(1–2), 169–180 (2002). `http://dx.doi.org/10.1016/S0301-0104(02)00546-3`

493. Yuste, S.B., Lindenberg, K.: Trapping reactions with subdiffusive traps and particles characterized by different anomalous diffusion exponents. Phys. Rev. E **72**(6), 061103 (2005). `http://dx.doi.org/10.1103/PhysRevE.72.061103`

494. Zauderer, E.: Partial Differential Equations of Applied Mathematics. Wiley, New York (1989)

495. Zemskov, E.P., Méndez, V.: Speed shift in reaction–diffusion equations with cutoff. Physica A **376**, 208–214 (2007). `http://dx.doi.org/10.1016/j.physa.2006.10.057`

496. Zeyer, K.P., Mangold, M., Gilles, E.D.: Experimentally coupled thermokinetic oscillators: phase death and rhythmogenesis. J. Phys. Chem. A **105**, 7216–7224 (2001). `http://dx.doi.org/10.1021/jp0041454`

497. Zhabotinsky, A.M.: A history of chemical oscillations and waves. Chaos **1**(4), 379–386 (1991). `http://dx.doi.org/10.1063/1.165848`

498. Zhang, Z., Qi, Y., Zhou, S., Lin, Y., Guan, J.: Recursive solutions for Laplacian spectra and eigenvectors of a class of growing treelike networks. Phys. Rev. E **80**(1), 016104 (2009). `http://link.aps.org/abstract/PRE/v80/e016104`

499. Zhong, S., Xin, H.: Effects of noise and coupling on the spatiotemporal dynamics in a linear array of coupled chemical reactors. J. Phys. Chem. A **105**, 410–415 (2001). `http://dx.doi.org/10.1021/jp002600q`

Index

**Temporal Disorder
in Human Oscillatory Systems**
Editors: L. Rensing, U. an der Heiden,
M. C. Mackey

The Physics of Structure Formation
Theory and Simulation
Editors: W. Güttinger, G. Dangelmayr

**Computational Systems – Natural and
Artificial** Editor: H. Haken

**From Chemical to Biological
Organization** Editors: M. Markus,
S. C. Müller, G. Nicolis

Information and Self-Organization
A Macroscopic Approach to Complex
Systems 2nd Edition By H. Haken

**Propagation in Systems Far from
Equilibrium** Editors: J. E. Wesfreid,
H. R. Brand, P. Manneville, G. Albinet,
N. Boccara

Neural and Synergetic Computers
Editor: H. Haken

**Cooperative Dynamics in Complex
Physical Systems** Editor: H. Takayama

**Optimal Structures in Heterogeneous
Reaction Systems** Editor: P. J. Plath

Synergetics of Cognition
Editors: H. Haken, M. Stadler

Theories of Immune Networks
Editors: H. Atlan, I. R. Cohen

Relative Information Theories
and Applications By G. Jumarie

**Dissipative Structures in Transport
Processes and Combustion**
Editor: D. Meinköhn

Neuronal Cooperativity
Editor: J. Krüger

Synergetic Computers and Cognition
A Top-Down Approach to Neural Nets
2nd edition By H. Haken

Foundations of Synergetics I
Distributed Active Systems 2nd Edition
By A. S. Mikhailov

Foundations of Synergetics II
Complex Patterns 2nd Edition
By A. S. Mikhailov, A. Yu. Loskutov

Synergetic Economics By W.-B. Zhang

Quantum Signatures of Chaos
2nd Edition By F. Haake

Rhythms in Physiological Systems
Editors: H. Haken, H. P. Koepchen

Quantum Noise 3rd Edition
By C.W. Gardiner, P. Zoller

**Nonlinear Nonequilibrium
Thermodynamics I** Linear and Nonlinear
Fluctuation-Dissipation Theorems
By R. Stratonovich

**Self-organization and Clinical
Psychology** Empirical Approaches
to Synergetics in Psychology
Editors: W. Tschacher, G. Schiepek,
E. J. Brunner

**Nonlinear Nonequilibrium
Thermodynamics II** Advanced Theory
By R. Stratonovich

Limits of Predictability
Editor: Yu. A. Kravtsov

On Self-Organization
An Interdisciplinary Search
for a Unifying Principle
Editors: R. K. Mishra, D. Maaß, E. Zwierlein

**Interdisciplinary Approaches
to Nonlinear Complex Systems**
Editors: H. Haken, A. Mikhailov

Inside Versus Outside
Endo- and Exo-Concepts of Observation
and Knowledge in Physics, Philosophy
and Cognitive Science
Editors: H. Atmanspacher, G. J. Dalenoort

**Ambiguity in Mind and Nature
Multistable Cognitive Phenomena**
Editors: P. Kruse, M. Stadler

**Modelling the Dynamics
of Biological Systems**
Editors: E. Mosekilde, O. G. Mouritsen

**Self-Organization in Optical Systems
and Applications in Information**
Technology 2nd Edition
Editors: M. A. Vorontsov, W. B. Miller

**Principles of Brain Functioning
A Synergetic Approach to Brain Activity,
Behavior and Cognition**
By H. Haken

**Synergetics of Measurement, Prediction
and Control** By I. Grabec, W. Sachse

Predictability of Complex Dynamical Systems
By Yu.A. Kravtsov, J. B. Kadtke